The Effect of HDAC Inhibitor MI192 on Stem Cell Behaviour – The Potential of Utilising MI192 for Bone Tissue Engineering

Liam Michael Lawlor

Submitted in accordance with the requirements for the degree of
Doctor of Philosophy

The University of Leeds
Faculty of Engineering
School of Mechanical Engineering

January 2016

The candidate confirms that the work submitted is his own and that appropriate credit has been given where reference has been made to the work of others.

Acknowledgements

First and foremost, I would like to thank my supervisor Dr. Xuebin Yang for the ideas, support and advice throughout my PhD. You have been a fantastic mentor and I am immensely grateful for everything you have taught me. I would also like to thank my secondary supervisor Professor Ron Grigg for all of your guidance.

Thank you to the EPSRC Doctoral Training Centre in Tissue Engineering and Regenerative Medicine (DTC TERM), and especially to Professor Joanne Tipper, for the great opportunity and the funding to carry out this work.

The work in this thesis wouldn't have been possible without the help of many brilliant people, so my thanks to all of you. To name a few... Jackie Hudson for all of the technical support and for keeping the laboratory running (and moving it!). Dr. Matthew Tomlinson for the help with the teeth and the FACs. Dr Adam Mitchell and Dr. Sarah Churchman for teaching me all about PCR. Sue Keat and Dr. Sushmita Saha for teaching me the joys of immunos. Dr El Mostafa Raif, Dr Hugh Russell and Dr. Mehrnoosh Rezapour for all of the cell culture support. Claire Godfrey, Greg Baugh, Adam Steel, Julie McDermott and Ruth Kayman for all of the administrative support. Thank you to all members of the department of oral biology, past and present, for teaching me so much and creating such a great working environment. Thanks to (the soon to be) Dr. Nikoletta Pechlivani, Dr. Sarah Myers, Shabnum Rashid, Rachel Howard and Hanaa Alkharobi for being such great office mates, the bisQuits (!), and keeping me sane. Finally, thanks also to everybody who was willing to go the pub on a Friday for a moan, there are too many of you6 to mention.

Thankyou to all of my friends outside of work who have supported me throughout my PhD. Especially to my friends from Sheffield University who must be sick of me moaning about university by now, to the Roslin Roaders and all affiliated, to everybody from the DTC for making conferences something to look forward to, and to Fashion Forward (Marcus, Reiss and Sinead) for seeing me through the dark science times.

I am forever grateful to my parents for their love and support (both financial and not!!) throughout this process. Thank you for instilling in me the drive and determination to achieve this. Thank you also to my sister Erin for being there when needed, and to the rest of my family for their love and encouragement.

Finally, to Nima, thank you for all of your love, patience and enduring support, especially throughout the hard times. I am eternally grateful.Without you, I wouldn’t have made it through in one piece.

Abstract

Controlling lineage specific differentiation of stem cells is crucial for functional tissue engineering, and current methods have drawbacks and limitations. Histone deacetlyase (HDAC) proteins are key to cellular epigenetics, and a number of studies have shown that their inhibitors (HDACis) can control stem cell fate. The aim of this study was to investigate the effect of a novel HDAC2 and HDAC3 selective inhibitor, MI192, on human adipose derived stem cells (ADSCs), exploring the potential of utilising MI192 in controlling the osteogenic differentiation of ADSCs, with the long term goal of improving the efficacy of bone tissue engineering. MI192 was synthesised in house and characterised with NMR analysis. The effect of MI192 was explored on commercially (Life Technologies) available ADSCs. It was found that 1 µM to 100 µM MI192 was cytotoxic and reduced ADSC viability, with a dose response observed. Using propidium iodide staining, it was demonstrated that MI192 halted the cell cycle in the G2M phase. FACs analysis showed that MI192 altered the stem cell marker expression profile of ADSCs; increasing expression of some markers (CD34 and CD146) and decreasing some (CD29, CD44, CD73, CD105, CD166). When utilised in a pre-treatment strategy in 2D models, MI192 improved the osteogenic differentiation of ADSCs, strongly increasing production of alkaline phosphatase protein, with 2 days of 30 µM pre-treatment being the optimal concentration and treatment length. MI192 pre-treatment also increased ADSC mineralisation (calcium accumulation stained with Alizarin Red and mineral nodule formation stained with Von Kossa) and increased osteogenic gene expression (*BMP2, RUNX2, COL1* and *ALP*). The adipogenic differentiation of the ADSCs was inhibited by MI192 pre-treatment, with reduced lipid droplet accumulation (stained with Oil Red O) and adipogenic gene (*PPARγ* and *ADIPOQ*) expression seen. Increased osteogenic differentiation was further demonstrated in 3D models, using Am silk scaffolds. Cell attachment was assessed with live cell labelling, and collagen production, mineralisation and protein production analysed with histology and immunohistochemistry. Finally, TaqMan® Gene Expression Array Cards were utilised to investigate how two days of MI192 treatment altered the expression of 96 different genes. Some key Wnt related genes, as well as other key osteogenic genes such as *BMP2* were up-regulated, providing some mechanistic explanation for the increase in osteogenic differentiation potential seen with MI192 pre-treatment. This thesis demonstrates the potential of utilising MI192 to improve bone tissue engineering strategies.

Table of Contents

Acknowledgements **3**
Abstract **5**
Table of Contents **6**
List of Figures **13**
List of Tables **24**
Chapter 1: Literature Review **26**
1.1 Background 26
1.2 Epigenetics 28
1.2.1 Introduction to Epigenetics 28
1.2.2 Human DNA 29
1.2.3 Acetylation 31
1.2.4 HDACs and HATs 33
1.2.5 Non-histone acetylation 33
1.2.6 HDAC isoforms 34
1.2.7 HDAC structure and mechanism of deacetylation 39
1.2.8 The effects of histone acetylation levels on chromatin 41
1.3 HDAC Inhibitors 42
1.3.1 Mechanism of HDAC inhibition 43
1.3.2 Specific HDACis compared to panHDACis 43
1.3.3 Design of HDACis 44
1.4 The Effect of HDACis on Cancerous and Normal Cells 49
1.4.1 Cell Death and Related Responses to HDACis 50
1.4.2 DNA Alteration and its Effects on Mitosis 57
1.5 Tissue Engineering of Bone 59
1.5.1 The Clinical Need and Current Practices 59
1.5.2 The Biology of Bone 60
1.5.3 Stem Cells 63
1.5.4 Epigenetics and HDACis as Tools in Tissue Engineering 70
1.5.5 HDACis and Bone tissue Engineering 71
1.6 Introduction Synopsis 75
1.7 Thesis Aims and Objectives 76

Chapter 2: General Materials and Methods 77

2.1 General reagents 77

2.2 MI192 77

2.3 Cell Culture 78

2.3.1 Cell detachment and seeding 78

2.3.2 Cell Counting 78

2.3.3 Human Adipose Derived Stem Cells 79

2.3.4 *In vitro* expansion of ADSCs 79

2.3.5 Osteogenic Induction Culture 79

2.3.6 Adipogenic Induction Culture 80

2.3.7 Chondrogenic Induction Culture 80

2.4 Biochemical assays 81

2.4.1 PicoGreen® DNA quantification assay 81

2.4.2 Alkaline Phosphatase (ALP) Quantitative Assay 82

2.4.3 Alkaline Phosphatase Specific Activity (ALPSA) Calculation 82

2.5 Histological Staining 83

2.5.1 Alkaline Phosphatase Staining 83

2.5.2 Alizarin Red Staining for Calcium Accumulation 83

2.5.3 Von Kossa Staining for Mineral Nodule Formation 83

2.5.4 Oil Red O Stain for Lipid Droplets 84

2.6 Histology of 3D samples 84

2.6.1 Paraffin Embedding and Sectioning 84

2.6.2 Taking Slides to Water 84

2.6.3 Haematoxylin and Eosin (H+E) Staining 85

2.6.4 Weigert's Haematoxylin, Picrosirius Red and/or Alcian Blue Staining 85

2.7 Polymerase chain reaction (PCR) 86

2.7.1 RNA Isolation 86

2.7.2 Reverse Transcription 87

2.7.3 qRT-PCR 87

2.7.4 Generation of standard curves 88

2.7.5 Optimisation of Housekeeping Genes 88

Chapter 3: The Chemical Synthesis of MI192 90

3.1 Introduction 90

3.2 Materials and Methods 94

3.2.1 Synthesis scheme of 4-(4,6-Dimethoxy-1,3,5-triazin-2-yl)-4-methylmorpholinium tetrafluoroborate (compound 1)..... 94

3.2.2 Synthesis of 4-((Tert-butoxycarbonylamino)methyl)benzoic acid (compound 2)..... 95

3.2.3 Synthesis of *tert*-Butyl 4-(2-aminophenylcarbamoyl)benzylcarbamate (compound 3)..... 96

3.2.4 Synthesis scheme of 4-(Aminomethyl)-*N*-(2-aminophenyl)benzamide (compound 4)..... 96

3.2.5 Synthesis of MI192..... 97

3.3 Results..... 98

3.4 Discussion..... 99

Chapter 4: The General Effects of MI192 on Adipose Derived Stem Cells Cultured in Monolayer..... 101

4.1 Introduction..... 101

4.2 Materials and Methods..... 103

4.2.1 Assessment of Cell Morphology..... 103

4.2.2 Effect of MI192 on ADSC DNA quantity (as an indicator of cell number)..... 103

4.2.3 Cytotoxic effect of MI192 on ADSCs..... 103

4.2.4 Effect of MI192 on ADSCs viability..... 104

4.2.5 Effect of MI192 on the HDAC specific activity of ADSCs..... 104

4.2.6 Effect of MI192 on ADSC Cell Cycle..... 105

4.2.7 Effect of MI192 on ADSC Stem cell Markers..... 107

4.2.8 Statistical Analysis..... 111

4.3 Results..... 112

4.3.1 Effect of MI192 on ADSC Morphology..... 112

4.3.2 Effect of MI192 on ADSC DNA quantity (as an indicator of cell number)..... 117

4.3.3 Cytotoxic effect of MI192 on ADSCs..... 119

4.3.4 Effect of MI192 on ADSCs viability..... 120

4.3.5 Effect of MI192 on the HDAC specific activity of ADSCs..... 122

4.3.6 Effect of MI192 on ADSC Cell Cycle..... 123

4.3.7 Effect of MI192 on ADSC Stem Cell Markers..... 126

4.4 Discussion..... 133

Chapter 5: The Effects of MI192 on the Differentiation of Adipose Derived Stem Cells in 2D..... 140

5.1 Introduction..... 140

5.2 Materials and methods..... 143

5.2.1 The effect of MI192 on the early osteogenic differentiation of ADSCs....143

5.2.2 Assessment of the effect of MI192 pre-treatment on the osteogenic gene expression of ADSCs....147

5.2.3 The effect of MI192 pre-treatment on the calcium accumulation and mineralisation of ADSCs....148

5.2.4 The effect of MI192 pre-treatment on the Oil Red O staining (adipogenic differentiation) of ADSCs....149

5.2.5 Assessment of the effect of MI192 pre-treatment on the adipogenic gene expression of ADSCs....149

5.2.6 Statistical Analysis....150

5.3 Results....151

5.3.1 The effect of MI192 pre-treatment on the alkaline phosphatase staining levels of ADSCs....151

5.3.2 The effect of MI192 pre-treatment dose and time period on the ALPSA of ADSCs....153

5.3.3 The effect of MI192 pre-treatment on the ALPSA of ADSCs across multiple time points and with two different osteogenic media....161

5.3.4 Assessment of the effect of MI192 pre-treatment on the osteogenic gene expression of ADSCs....164

5.3.5 The effect of MI192 pre-treatment on the calcium accumulation and osteogenic mineralisation of ADSCs....171

5.3.6 The effect of MI192 pre-treatment on the Oil Red O staining (adipogenic differentiation) of ADSCs....176

5.3.7 Assessment of the effect of MI192 pre-treatment on the adipogenic gene expression of ADSCs....179

5.4 Discussion....182

Chapter 6: The Effects of MI192 on Bone Tissue Engineering using Adipose Derived Stem Cells and Three Dimensional *In Vitro* Models...194

6.1 Introduction....194

6.2 Materials and Methods....200

6.2.1 Silk protein fibroin extraction and 3D scaffold production....200

6.2.2 Scaffold preparation before experiments....200

6.2.3 Dynamic seeding of cells on 3D silk scaffolds....200

6.2.4 Live and dead cell Labelling....203

6.2.5 ADSCs seeded onto 3D silk scaffolds prior to MI192 treatment (Expt 1)....203

6.2.6 ADSCs treated with MI192 followed by 7 days of osteogenic induction prior to seeding on 3D silk scaffolds (Expt 2)....204

6.2.7 ADSCs treated with MI192 prior to seeding on 3D silk scaffolds (Expt 3) 205

6.2.8 Immunohistochemical staining..... 205

6.3 Results..... 207

6.3.2 The effect of MI192 on ADSCs seeded onto 3D silk scaffolds prior to MI192 treatment (Expt 1)..... 207

6.3.3 The effect of MI192 treatment on ADSCs, which underwent osteogenic induction prior to seeding on 3D silk scaffolds (Expt 2) ……...213

6.3.4 The effect of MI192 treatment on ADSCs treated with MI192 prior to seeding on 3D silk scaffolds and osteogenic induction (Expt 3) 223

6.3.5 Immunohistochemical staining..... 226

6.4 Discussion 241

Chapter 7: The effect of MI192 treatment on ADSC gene expression 248

7.1 Introduction 248

7.2 Materials and Methods..... 249

7.2.1 MI192 treatment of ADSCs..... 249

7.2.2 Isolation of RNA/DNA/Protein..... 250

7.2.3 Reverse Transcription 250

7.2.4 qRT-PCR 250

7.2.5 Ct Value Calculations 255

7.2.6 Statistical Analysis..... 256

7.2.7 Data Presentation..... 256

7.3 Results..... 257

7.3.2 The effect of MI192 treatment on the expression of early cartilage and bone related transcripts in ADSCs 260

7.3.3 The effect of MI192 treatment on the expression of bone related transcripts in ADSCs 263

7.3.4 The effect of MI192 treatment on the expression of early stage cartilage, and cartilage and bone extracellular matrix related transcripts in ADSCs 265

7.3.5 The effect of MI192 treatment on the expression of stromal related transcripts in ADSCs 270

7.3.6 The effect of MI192 treatment on the expression of Neural/nerve related transcripts in ADSCs 274

7.3.7 The effect of MI192 treatment on the expression of miscellaneous transcripts in ADSCs..... 275

7.3.8 Genes that were flagged due to potentially erroneous results or non-expression..... 276

7.4 Discussion 280

7.4.1 The effect of MI192 treatment on the expression of Wnt related transcripts in ADSCs 280

7.4.2 The effect of MI192 treatment on the expression of early cartilage and bone related transcripts in ADSCs 283

7.4.3 The effect of MI192 treatment on the expression of later stage bone related transcripts in ADSCs 287

7.4.4 The effect of MI192 treatment on the expression of cartilage and bone extracellular matrix formation related transcripts in ADSCs 290

7.4.5 The effect of MI192 treatment on the expression of adipogenic transcripts in ADSCs 292

7.4.6 The effect of MI192 treatment on the expression of stromal related transcripts in ADSCs 293

7.4.7 The effect of MI192 treatment on the expression of Neural/nerve related transcripts in ADSCs 297

7.4.8 The effect of MI192 treatment on the expression of *NGFR* (CD271) in ADSCs and a comparison of the transcription profile to CD271+ cells 298

7.4.9 The effect of MI192 treatment on the expression of miscellaneous transcripts in ADSCs 300

7.4.10 Discussion summary 301

Chapter 8: General Discussion, Conclusions and Future Work 304

8.1 General Discussion 304

8.1.1 Summary 311

8.2 Conclusion 313

8.3 Future Work 313

Bibliography i

List of Abbreviations xxxiii

Appendix A Supplementary Lab Data xxxvi

A.1 - NMR Spectra xxxvi

A2 - Confirmation of tri-linage differentiation potential of ADSCs xlii

A3 - Investigation of the effect off 1% – 0.01% DMSO has on ADSC cell number and viability xliv

A4 - Effect of MI192 on ADSC Stem Cell Markers: FACs plots and autofluorescence comparison histograms xlvii

A5 – qRT-PCR choice of housekeeping gene and standard curves lii

A5.1 - Choice of Housekeeping Gene for qRT-PCR Assays lii

A5.2 - Standard Curves for qRT-PCR Assays liv

Appendix B List of conference presentations and publications lvi

B.1 Oral Presentations lvi

B.2 Poster Presentations lvi

B.3 Book Chapter lvii

Appendix C Rights Permissions for Figures from Journal Articles lviii

List of Figures

Figure 1.1 - The crystal structure of the nucleosome-core-particle. The 146 base pair DNA ribbon structure is in brown and turquoise. It is wrapped around the eight histone protein backbone chains (H3 is blue, H4 green, H2A yellow and H2B red). The left view is down the DNA superhelix axis, and perpendicular to the axis on the right. . Reprinted with permission from (Luger et al. 1997)..... 30

Figure 1.2 – Diagram showing how DNA wraps around the histone proteins, then the formation of a chromosome particle. Reprinted with permission from (Zaidi et al. 2010)..... 30

Figure 1.3 - An Acetyl group, a chemical group with the chemical formula $COCH_3$. A small chemical motif consisting of a methyl group single boned to a carbonyl group, which is a carbon and an oxygen joined by a double bond. It is sometimes shortened to 'Ac'. 32

Figure 1.4 – Space filling diagram. A 'space filling' representation of HDACi TSA bound in the active site, (a sock shaped cavity), of HDLP. Reprinted with permission from (Finnin et al. 1999). 39

Figure 1.5 – Mechanism of action. The relevant residues and molecules involved in a proposed HDAC1 active site of HDLP, along with a proposed mechanism for the deacetylation of an acetylated lysine residue. Adapted from (Finnin et al. 1999). 40

Figure 1.6 - Structures of HDACis commonly found in the literature. Clockwise from top left – Sodium butyrate, Valproic Acid, Trichostatin A, Romidepsin, Entinostat (MS-275) and Vorinostat (SAHA). 44

Figure 1.7 – Molecular pharmacophore of HDACis. SAHA is given as an example, adapted from (Pontiki & Hadjipavlou-Litina 2011). 46

Figure 1.8 - Chemical phylogenetic analysis of HDACs; the binding affinity of HDACis for different HDAC isoforms. a) Hierarchical clustering of HDACs with a representative panel of HDACi compounds binding affinity for different HDAC isoforms, with an indication of inhibitor potency (K_i); b) and c) Dendrogram representative diagrams, with the chemical structure and enzymatic selectivity profiles of MS-275 (b) and SAHA (c), overlaying molecular phylogeny. The circles are representative of K_i on a logarithmic scale. Reprinted with permission from (Bradner et al. 2010)..... 48

Figure 1.9 – A schematic showing the standard properties of a tumour cell blocked by treatment with a HDACi. Tumour cells can undergo many processes under normal physiological conditions, and this diagram shows some of the processes that HDACis are known to stop, with red lines through the arrows. Apoptosis is typically favoured, hence the green arrow. Adapted from (New et al. 2012)..... 50

Figure 1.10 – Effects of HDACi on the cell cycle. When treated with a low concentration of a HDACi, normal cells continue the normal cell cycle and pass the G2M checkpoint to survive the treatment. When treated with a HDACi, during the late G1 and S phase, tumour cells undergo aberrant mitosis and a rapid apoptotic effect results. When treated during the G1 phase, there is a G1 arrest, and a delayed but eventual apoptosis. Adapted from (Burgess et al. 2004; Johnstone 2002) 56

Figure 1.11 – The four key pillars of tissue engineering. From left to right: Cells, Environmental Stimuli. Chemical cues and scaffolds, with examples listed, and pictures of each. All pictures are the author's own. 58

Figure 1.12 – The structure of a typical long bone. Adapted from (Pocock & Richards 2006). 62

Figure 1.13 – Schematic summary of cells decreasing in differentiation potential. 'The hills of differentiation potential'. As cells fall down to lower hills they lose their differentiation potential, becoming less stem cell like. 66

Figure 1.14 - Hematopoietic stem cell nice. A diagram of hematopoietic stem cells in the bone marrow niche they can be found. Adapted from (Moore & Lemischka 2006; Wang & Wagers 2011). 68

Figure 3.1 – The complete synthesis scheme of MI192. Compound 1 - 4-(4,6-Dimethoxy-1,3,5-triazin-2-yl)-4-methylmorpholinium tetrafluoroborate, compound 2 - 4-((Tert-butoxycarbonylamino)methyl)benzoic acid, compound 3 - *tert*-Butyl 4-(2-aminophenylcarbamoyl)benzylcarbamate, compound 4 - 4-(Aminomethyl)-*N*-(2-aminophenyl)benzamide. 93

Figure 3.2 – Synthesis scheme of 4-(4,6-Dimethoxy-1,3,5-triazin-2-yl)-4-methylmorpholinium tetrafluoroborate (compound 1). 94

Figure 3.3 - Synthesis scheme of 4-((Tert-butoxycarbonylamino)methyl)benzoic acid (compound 2). 95

Figure 3.4 – Synthesis scheme of tert-Butyl 4-(2-aminophenylcarbamoyl)benzylcarbamate (compound 3). 96

Figure 3.5 - Synthesis of 4-(Aminomethyl)-N-(2-aminophenyl)benzamide (compound 4). 96

Figure 3.6- Synthesis scheme of MI192. 97

Figure 4.1 – Gates created in flow cytometry analysis of ADSCs stained with PI for cell cycle analysis. Representative gates shown, which were created in ModFit software to account for intact cells (Gate 1), material related to intact nuclei (Gate 2) and for single cells (Gate 3). . 107

Figure 4.2 – Representative pictures of gates created in Kaluza software. Gate 1 - to account for intact cells. Gate 2 - to count the percentage of intact cells marked positive with FITC and PE. 108

Figure 4.3 - Phase contrast images of ADSCs treated with MI192 for 12 (A) and 24 (B) hours. Cells dosed with MI192 (5 μM, 30 μM and 50 μM) and compared to a basal control with no MI192 dose. Scale bars = 100 μM. 114

Figure 4.4 - Phase contrast images of ADSCs treated with MI192 for 48 (A) and 72 (B) hours. Cells dosed with MI192 (5 μM, 30 μM and 50 μM) and compared to a basal control with no MI192 dose. Scale bars = 100 μM. 115

Figure 4.5 - Phase contrast images of ADSCs treated with MI192 for 96 hours (A) and ADSCs treated with TSA for a range of time points (B). A - Cells dosed with MI192 (5μM, 30 μM and 50 μM) and compared to a basal control with no MI192 dose. B – Cells dosed at the same time but with 10μM TSA for the same time points. Scale bars = 100 μM. 116

Figure 4.6 - Quant-iT™ PicoGreen® analysis of ADSCs treated for 1 day, 2 days and 3 days with a range of doses of MI192. Results expressed as mean ± SD (n=3). A selected sample of significance levels are shown, * = P ≤ 0.05, ** = P ≤ 0.01 and **** = P ≤ 0.0001 118

Figure 4.7 - CytoTox-Fluor™ analysis of ADSCs treated with a range of MI192 doses (50 μM, 40 μM, 30 μM, 20 μM, 10 μM and 1 μM) for 1 day, 2 days and 3 days. Results expressed as mean ± SD (n=3) Significance levels shown are the sample compared to the basal control for that time point, i.e. A 40 μM dose for 2 days compared to basal control at 2 days. * = p ≤ 0.05, ** = p ≤ 0.01 and *** = p ≤ 0.001. .. 121

Figure 4.8 - CellTiter-Glo® analysis of ADSCs treated with a range of MI192 doses (50 μM, 40 μM, 30 μM, 20 μM, 10 μM and 1 μM) for 1 day, 2 days and 3 days. Results expressed as mean ± SD (n=3). Significance levels shown are the sample compared to the basal control for that time point, i.e. A 40 μM dose for 2 days compared to basal control at 2 days. * = P ≤ 0.05, ** = P ≤ 0.01 and *** = P ≤ 0.001… 121

Figure 4.9 – HDAC activity of ADSCs treated for 1 day and 2 days two of doses of MI192. Results expressed as mean ± SD (n=3), ** = P ≤ 0.01 . 122

Figure 4.10 – Representative histograms of the flow cytometry analysis of the cell cycle distribution for ADSCs dosed with 30 μM and 10 μM MI192 and 10 μM TSA with untreated controls, for 12, 24 and 48 hours. Representative histograms from each time point and test group shown, the experiment was carried out in biological triplicate, and histograms are representative of at least 2000 events. The first large peak represents the population of cells in the G0/G1 phase, the second small peak the population of cells in the G2/M phase, with the area in between the S Phase. 124

Figure 4.11 - Representative histograms showing flow cytometric analysis of PI staining of MI192 treated ADSCs. A – Gate 1, gating for intact cells, B – Gate 2 (box D on the plot) – gating for the subpopulation of cells, C – size analysis of the subpopulation of cells from Gate 2 (D on the plot). D – Statistical analysis of the gates. 128

Figure 4.12 – CD29, CD34 and CD44. Representative histograms and graphical representation of flow cytometric analysis of stem cell markers in MI192 treated compared to untreated ADSCs. A – CD29, B – CD34, C – CD44. Untreated ADSCs (red colour) compared to MI192 treated (green colour). Note the y axis is a different scale for each graph. 129

Figure 4.13 – CD45, CD73 and CD90. Representative histograms and graphical representation of flow cytometric analysis of stem cell markers in MI192 treated compared to untreated ADSCs. A – CD45, B – CD73, C – CD90. Untreated ADSCs (red colour) compared to MI192 treated (green colour). Note the y axis is a different scale for each graph. 130

Figure 4.14 – CD105, CD146 and CD166. Representative histograms and graphical representation of flow cytometric analysis of stem cell markers in MI192 treated compared to untreated ADSCs. A – CD105, B – CD146, C – CD166. Untreated ADSCs (red colour) compared to MI192 treated (green colour). Note the y axis is a different scale for each graph. 131

Figure 5.1 – ALP Staining of ADSCs treated with MI192 then cultured in osteogenic induction medium. A – Basal medium control; B – Osteogenic medium control; C – 100 µM pre-treatment for 2 days with MI192 then 7 days in osteogenic medium; D – 30 µM pre-treatment for 2 days with MI192 then 7 days in osteogenic medium. Cells stained blue for ALP. Macro image of the well of the plate shown, as well as phase contrast and bright field images showing detailed cell staining. Scale bars = 100 µM. 152

Figure 5.2 – ALPSA of ADSCs pre-treated with MI192 then cultured in osteogenic induction medium. ADSCs were pre-treated with 50 µM, 40 µM, 30 µM and 20 µM MI192 for one and 2 days, before culture in osteogenic induction medium for 7 days, with basal medium and osteogenic medium controls. Results expressed as mean ± SD (n=3). Statistical significance was determined using a one-way ANOVA. * = P ≤ 0.05, ** = P ≤ 0.01 and *** = P ≤ 0.001. 154

Figure 5.3 - PicoGreen® DNA quantification (A) and ALPSA (B) of ADSCs pre-treated with MI192 then cultured in osteogenic induction medium, compared to ADSCs treated continuously with MI192 in osteogenic medium. A – Total DNA content of ADSCs pre-treated with 30 µM - 750 nM MI192 and cultured in osteogenic induction medium, compared to the DNA content of cells cultured in osteogenic induction medium containing 10 µM - 750 nM MI192 continuously; B – ALPSA of the same ADSCs. For both, significance level shown is compared to osteogenic control, along with a selection of other values. Results expressed as mean ± SD (n=3). Statistical significance was determined using a one-way ANOVA. * = P ≤ 0.05 and *** = P ≤ 0.001. 156

Figure 5.4 – ALPSA of ADSCs pre-treated with two different batches of MI192 then cultured in osteogenic induction medium and basal medium. The specific ALP activity of cells pre-treated with 30 µM of MI192 for 2 days, before culture in osteogenic induction, or basal medium for 7 days, with basal medium and osteogenic medium controls. Results expressed as mean ± SD (n=3). Statistical significance was determined using a one-way ANOVA. *** = P ≤ 0.001. 158

Figure 5.5 - ALPSA of ADSCs pre-treated with MI192 and TSA. The specific ALP activity of cells pre-treated with MI192 and TSA for 2 days. Significance level for every group compared to osteogenic control shown above the bar. Results expressed as mean ± SD (n=3). Statistical significance was determined using a one-way ANOVA. *** = P ≤ 0.001. 160

Figure 5.6 – ALPSA of ADSCs from 4 different donors pre-treated with MI192. The specific ALP activity of cells pre-treated with 30 µM and 10 µM MI192 for 2 days. Results expressed as mean ± SD (n=3). Statistical significance was determined using a one-way ANOVA. * = P ≤ 0.05 and *** = P ≤ 0.001 160

Figure 5.8 - ALPSA of ADSCs, pre-treated with MI192, across 4 time points, with the osteogenic induction (A) and osteogenic mineralisation (B) media. The ALPSA of cells pre-treated with 30 µM for 2 days, before culture in osteogenic mineralisation or osteogenic induction media for 3, 5, 7 and 9 days, with basal medium and osteogenic medium for both. Results expressed as mean ± SD (n=3). Statistical significance was determined using a one-way ANOVA. * = P ≤ 0.05, ** = P ≤ 0.01 and *** = P ≤ 0.001. 163

Figure 5.9 – Quantitative expression of *RUNX2* (A) and *BMP2* (B) in ADSCs. Cells were pre-treated with 30 µM MI192 for 2 days, then cultured in osteogenic medium. Gene expression was analysed at day 3, day 5, day 7, day 14 and day 21. Results expressed as mean ± SD (n=3). Statistical significance was determined using a one-way ANOVA. Only the significance levels between the conditions at each time point shown. * = P ≤ 0.05, ** = P ≤ 0.01 and *** = P ≤ 0.001… 168

Figure 5.10 – Quantitative expression of *ALP* (A) and *COL1* (B) in ADSCs. Cells were pre-treated with 30 μM MI192 for 2 days, then cultured in osteogenic medium. Gene expression was analysed at day 3, day 5, day 7, day 14 and day 21. Results expressed as mean ± SD (n=3). Statistical significance was determined using a one-way ANOVA. Only the significance levels between the conditions at each time point shown. * = P ≤ 0.05, ** = P ≤ 0.01 and *** = P ≤ 0.001. 169

Figure 5.11 – Quantitative expression of *OCN/BGLAP* (A) and *SPP1* (B) in ADSCs. Cells were pre-treated with 30 μM MI192 for 2 days, then cultured in osteogenic medium. Gene expression was analysed at day 3, day 5, day 7, day 14 and day 21. Results expressed as mean ± SD (n=3). Statistical significance was determined using a one-way ANOVA. Only the significance levels between the conditions at each time point shown. * = P ≤ 0.05, ** = P ≤ 0.01 and *** = P ≤ 0.001.... 170

Figure 5.12 - ADSCs treated with MI192 then cultured in osteogenic mineralisation medium, before staining for calcium with Alizarin Red staining. A – Basal medium control, B – Osteogenic medium control, C – 30 μM pre-treatment for 2 days with MI192, D – 10 μM pre-treatment for 2 days with TSA. Red staining indicates calcium accumulation. Macro image of the well of the plate shown, as well as two phase contrast images showing detailed cell staining. Scale bars = 100 μM. 173

Figure 5.13 – Quantitative measurement of Alizarin Red stain. Stain destained from ADSCs pre-treated with MI192 then cultured in osteogenic medium, before staining for calcium with Alizarin Red staining. Stain was destained and quantified from a basal medium control, an osteogenic medium control, cells pre-treated with 30 μM of MI192 and 10 μM TSA (same cells as pictures in (Figure 5.11). Average absorbance of readings taken 550 nm. Results expressed as mean ± SD (n=3). Statistical significance was determined using a one-way ANOVA. Only the significance levels between compared to the osteogenic control shown. * = P ≤ 0.05. 174

Figure 5.14 - ADSCs pre-treated with MI192 then cultured in osteogenic mineralisation medium, before staining for mineralisation with Von Kossa staining. A – Basal medium control, B – Osteogenic medium control, C – 30 μM pre-treatment for 2 days with MI192 then 28 days in osteogenic medium, D – 10 μM pre-treatment for 2 days with TSA then 28 days in osteogenic medium. Brown and black staining indicates calcium accumulation, black being a stronger stain. Macro image of the well of the plate shown, as well as two phase contrast images showing detailed cell staining. Scale bars = 100 μM. 175

Figure 5.15 - ADSCs pre-treated with MI192 then cultured in adipogenic medium, before staining for lipid droplet accumulation with an Oil Red O stain. A – Basal medium control; B – Adipogenic medium control; C, D, E, F, G – Cells pre-treated with HDACis MI192 and TSA then cultured in adipogenic medium for 14 days. Cells pre-treated with C: 10 μM MI192; D: 20 μM MI192; E: 50 μM MI192; F: 10 μM TSA; G: 20 μM TSA. Red staining indicates lipid droplets. Macro image of the well of the plate shown, as well as two phase contrast images showing detailed cell staining. Scale bars = 100 μM. 177

Figure 5.16 - Quantitative measurement of Oil Red O stain, destained from ADSCs pre-treated with MI192 then cultured in adipogenic medium, before staining for lipid droplet accumulation with an Oil Red O stain. The stain was quantified from a basal medium control, an adipogenic medium control, cells pre-treated with 50 μM, 30 μM and 10 μM of MI192 and 20 μM TSA and 10 μM TSA (same cells as pictures in (Figure 5.14). Average absorbance of readings taken 500 nm. Results expressed as mean ± SD (n=3). Statistical significance was determined using a one-way ANOVA. Only the significance levels between compared to the adipogenic control shown. *** = P ≤ 0.001. 178

Figure 5.17 - Quantitative expression of *PPRγ* (A) and *ADIPOQ* (B) in ADSCs pre-treated with 40 μM, 30 μM and 20 μM of MI192 for 2 days, then cultured in adipogenic medium for 14 days. Gene expression was analysed at day 3 and, day 14. Results expressed as mean ± SD (n=3). For ADIPOQ (B) the graph is on a log scale and undetermined genes were set at an expression value of 1, where the Day 3 Basal *ADIPOQ* value was undetermined. Statistical significance was determined using a one-way ANOVA. Only the significance levels between the conditions at each time point shown. * = P ≤ 0.05, ** = P ≤ 0.01 and *** = P ≤ 0.001. 181

Figure 6.1 – Depictions of cells in 2D and 3D culture systems. An illustration of the difference in cell morphology, and therefore adhesive, topographical, mechanical and soluble cues between 2D and 3D culture systems. Reprinted with permission from (Baker & Chen 2012). 195

Figure 6.2- Schematic representing the three different experimental designs for the scaffold studies covered in this chapter. Design 1: Where the cells were pre-treated with MI192 once seeded onto the scaffolds. Design 2: Where the cells were pre-treated with MI192 in monolayer, had a 7 day osteogenic induction period in monolayer, then seeded onto the scaffold for further osteogenic induction. Design 3: Where the cells were pre-treated with MI192 in monolayer and seeded straight onto the scaffold. 199

Figure 6.3 – Photographs of the in house dynamic cell seeding device. A – Unloaded device. Arrows indicate the black bars which rotate when the device is turned on, which causes the seeding device to rotate. B – Empty seeding device loaded onto the cell seeder. C – Seeding device with an empty tube in, indicating how tubes sit in the device. 202

Figure 6.4 – Live/Dead cell dye test. Fluorescent imaging of viable ADSCs (green colour) on Am silk scaffolds labelled with both the live (CFMDA) and the dead (EthD-1) markers 1 day after seeding. A – Live marker alone; B – dead marker alone; C – superimposed images A and B. Scale bars = 100 µM. Yellow arrows indicate live cells growing aligned with the fibres of the scaffold. 209

Figure 6.5 - Fluorescent imaging of viable ADSCs (green colour) on Am silk scaffolds 6 weeks after seeding, in Expt 1. A + B – Osteogenic control; C + D – pre-treated with 30 µM MI192. Scale bars = 100µM.....210

Figure 6.6 - Fluorescent imaging of viable ADSCs (green colour) on Am silk scaffolds 9 weeks after seeding, in Expt 1. A + B – Osteogenic control; C + D – pre-treated with 30 µM MI192. Scale bars = 100 µM.....210

Figure 6.7 – Van Gieson's Stain of sections from ADSC-silk scaffold constructs after 9 weeks of *in vitro* culture (Exp1). A – C – Osteogenic control; D – F – Constructs treated with 30 µM MI192. Silk scaffold stained a yellow colour and the tissues were stained a pink colour. Arrows indicate the scaffold architecture. Scale bars = 100 µM. 211

Figure 6.8 - Fluorescent imaging of viable ADSCs (green colour) on Am silk scaffolds 24 hours after seeding, in Expt 2. A + B – osteogenic control; C + D – ADSCs pre-treated with 10 µM MI192; E + F – ADSCs pre-treated with 30 µM MI192. Scale bars = 100 µM. 215

Figure 6.9 - Fluorescent imaging of viable ADSCs (green colour) on Am silk scaffolds 6 weeks after seeding, in Expt 2. A + B – osteogenic control; C + D – ADSCs pre-treated with 10 µM MI192; E + F – ADSCs pre-treated with 30 µM MI192. Scale bars = 100 µM. 216

Figure 6.10 - Van Gieson's, Picrosirius red and Von Kossa stain of sections from ADSC-silk scaffold constructs after 6 weeks of *in vitro* culture (Expt 2). Example stains of samples where there was poor tissue formation, where cells and scaffold were not visible. A – Van Gieson's stain of osteogenic control; B – Van Gieson's stain of ADSCs pre-treated with 10 µM MI192; C – Picrosirius red stain Osteogenic control, A; D – Von Kossa stain of osteogenic control. Scale bars = 100 µM. 217

Figure 6.11 - Van Gieson's stain of sections from ADSC-silk scaffold constructs after 6 weeks of *in vitro* culture (Expt 2). A + B – Osteogenic control; D – F – ADSCs pre-treated with 10 µM MI192; E + F – ADSCs pre-treated with 30 µM MI192. Silk scaffold stained a yellow/pink colour and the tissues were stained a darker pink colour. Arrows indicate the scaffold architecture. Scale bars = 100 µM. 218

Figure 6.12 – Picrosirius red stain, with Weigert's haematoxylin nuclei counterstain, of sections from ADSC-silk scaffold constructs after 6 weeks of *in vitro* culture (Expt 2). A + B – Osteogenic control; C + D – ADSCs pre-treated with 10 μM MI192; E + F – ADSCs pre-treated with 30 μM MI192. Silk scaffold stained a yellow/grey colour, the tissues were stained red if collagen was present and the nuclei were stained black. Arrows indicate the scaffold architecture. Scale bars = 100 μM. 220

Figure 6.13 – Von Kossa staining, with a weak Van Gieson's counter stain for tissue, of sections from ADSC-silk scaffold constructs after 6 weeks of *in vitro* culture (Expt 2). A + B – Osteogenic control; C + D – ADSCs pre-treated with 10 μM MI192; E + F – ADSCs pre-treated with 30 μM MI192. Mineral nodules stained black/dark brown, silk scaffold stained a pink/brown colour and the cell tissue stained pink. Arrows indicate strong areas of mineralisation in each scaffold. Scale bars = 100 μM. 221

Figure 6.14 – Fluorescent imaging of viable ADSCs (green colour) on Am silk scaffolds 24 hours after seeding, in Exp3. A + B – Untreated ADSCs, seeded onto the scaffolds; C + D – ADSCs pre-treated with 10 μM MI192; E + F – ADSCs pre-treated with 30 μM MI192. Scale bars = 100 μM. 228

Figure 6.15 – Fluorescent imaging of viable ADSCs (green colour) on Am silk scaffolds 6 weeks after seeding, in Exp3. A + B – basal medium control; C + D – osteogenic control; E + F – ADSCs pre-treated with 10 μM MI192; G + H – ADSCs pre-treated with 30 μM. Scale bars = 100 μM. 229

Figure 6.16 - SEM images of ADSCs on Am silk scaffolds 6 weeks after seeding, in Exp3. Low magnification images on the left, high magnification images on the right. A + B – Unseeded control scaffolds; C + D – basal control; E + F – osteogenic control; G + H – ADSCs pre-treated with 30 μM MI192; I + J – ADSCs pre-treated with 10 μM MI192. Arrows indicate some of the mineralisation. Magnification and scale indicated on the image. 230

Figure 6.17 - SEM images, with environmental EDS SEM images, of ADSCs on Am silk scaffolds 6 weeks after seeding, Exp3. In EDS images: Red = carbon, green = calcium and blue = phosphorus. A + B – basal control; C + D – osteogenic control; E + F – ADSCs pre-treated with 10 μM MI192; G + H – ADSCs pre-treated with 30 μM MI192. Magnification and scale indicated on the image. 231

Figure 6.18 – Histograms showing elemental mapping of the elements present in the experimental Design 3 scaffolds. Maps taken at a low magnification to give indication of overall mineralisation levels. Labelled peaks show the Phosphorous and Calcium peaks. 232

Figure 6.19 – Van Gieson's stain of sections from ADSC-silk scaffold constructs after 6 weeks of *in vitro* culture (Exp3). A + B – basal control; C + D – osteogenic control; E - H – ADSCs pre-treated with 10 µM MI192; I - L – ADSCs pre-treated with 30 µM MI192. Silk scaffold stained a yellow/pink colour and the tissues were stained a darker pink colour. Scale bars = 100 µM. 233

Figure 6.20 – Picrosirius Red stain, with Weigert's haematoxylin nuclei stain, of sections from ADSC-silk scaffold constructs after 6 weeks of *in vitro* culture (Exp3). All samples labelling (A – L) same as Figure 6.19. Silk scaffold stained a yellow/grey colour, the tissues were stained red if collagen was present, with the nuclei counterstained black. Scale bars = 100 µM.....235

Figure 6.21 – Von Kossa staining, with a weak Van Gieson's counter stain for tissue, of sections from ADSC-silk scaffold constructs after 6 weeks of *in vitro* culture (Exp3). All samples labelling (A – L) same as Figure 6.19. Mineral nodules stained black/dark brown, silk scaffold stained a pink/brown colour and the cell tissue stained pink. Arrows indicate some strong areas of mineralisation in each scaffold. Scale bars = 100 µM. 236

Figure 6.22 – Run2 immunohistochemistry. Low magnification Runx2 immunohistochemical staining (brown), with a weak Harris haematoxylin counter stain (purple) for tissue, of sections from ADSC-silk scaffold constructs after 6 weeks of *in vitro* culture (Exp3). A – basal control; B – osteogenic control; C – ADSCs pre-treated with 10 µM MI192; D – ADSCs pre-treated with 30 µM MI192. Arrows indicate some of the Runx2 staining. Scale bars = 100 µM. 238

Figure 6.23 – Collagen 1 immunohistochemistry. High and low magnification collagen 1 immunohistochemical staining (brown), with a weak Harris haematoxylin counter stain (purple) for tissue, of sections from ADSC-silk scaffold constructs after 6 weeks of *in vitro* culture (Exp3). A + B – basal control; C + D – osteogenic control; E + F – ADSCs pre-treated with 10 µM MI192; H + G – ADSCs pre-treated with 30 µM MI192. Arrows indicate some of the collagen 1 staining. Scale bars = 100 µM. 239

Figure 6.24 – Ocn immunohistochemistry. Low magnification Ocn immunohistochemical staining (brown), with a weak Harris haematoxylin counter stain (purple) for tissue, of sections from ADSC-silk scaffold constructs after 6 weeks of *in vitro* culture (Exp3). A – basal control; B – osteogenic control; C – ADSCs pre-treated with 10 µM MI192; D – ADSCs pre-treated with 30 µM MI192 for two days. Arrows indicate Ocn staining. Scale bars = 100 µM. 240

Figure 7.1 - Graphical depictions of gene expression changes between treated and untreated cells in Wnt pathway related transcripts. Graphs on a logarithmic scale and results expressed as fold changes (n=6). * = P ≤ 0.05 259

Figure 7.2 - Figure 7.3 - Graphical depictions of gene expression changes between treated and untreated cells in early cartilage and bone related transcripts. Graphs on a logarithmic scale and results expressed as fold changes (n=6). * = P ≤ 0.05..... 262

Figure 7.4 - Graphical depictions of gene expression changes between treated and untreated cells in later stage bone related transcripts. Graphs on a logarithmic scale and results expressed as fold changes (n=6). * = P ≤ 0.05. 264

Figure 7.5 - Graphical depictions of gene expression changes between treated and untreated cells in cartilage and bone extracellular matrix related transcripts. Graphs on a logarithmic scale and results expressed as fold changes (n=6). * = P ≤ 0.05. 267

Figure 7.6 - Graphical depictions of gene expression changes between treated and untreated cells in adipogenic transcripts. Graphs on a logarithmic scale and results expressed as fold changes (n=6). * = P ≤ 0.05..... 269

Figure 7.7 - Graphical depictions of gene expression changes between treated and untreated cells in half of the stromal related transcripts. Graphs on a logarithmic scale and results expressed as fold changes (n=6). * = P ≤ 0.05 271

Figure 7.8 - Graphical depictions of gene expression changes between treated and untreated cells in the other half of the stromal related transcripts. Graphs on a logarithmic scale and results expressed as fold changes (n=6). * = P ≤ 0.05..... 272

Figure 7.9 - Graphical depictions of gene expression changes between treated and untreated cells in neural/nerve related transcripts. Graphs on a logarithmic scale and results expressed as fold changes (n=6). * = P ≤ 0.05. 274

Figure 7.10 - Graphical depictions of gene expression changes between treated and untreated cells in miscellaneous transcripts. Graphs on a logarithmic scale and results expressed as fold changes (n=6). * = P ≤ 0.05..... 276

Figure 7.11 – Upregulated fold changes grouped. Graph indicating the average fold change for every upregulated transcript with MI192 treatment. HPRT reference gene is set to 1. A number greater than 1 indicates an up-regulation. Statistical significant (P ≤ 0.05) indicated on the graph with a *. Any gene with a donor number less than 4, or with abnormal amplification curves were removed from the graph. 278

Figure 7.12- Downregulated fold changes grouped. Graph indicating the average fold change for every down-regulated transcript with MI192 treatment. HPRT reference gene is set to 1. A number less than 1 indicates a down-regulation. Statistical significant (P ≤ 0.05) indicated on the graph with a *. Any gene with a donor number less than 4, or with abnormal amplification curves were removed from the graph..... 279

List of Tables

Table 1-1 - A summary of the zinc dependent HDAC isoforms. 35

Table 3-1 - The inhibition of HDAC activity in HeLa cell nuclear extracts by MI192, MS-275 and TSA (Boissinot et al. 2012).....92

Table 3-2 – HDAC isoform specificity information for HDACis MI192, TSA, MS-275 and MGCD0103, for HDAC isoforms HDAC1, HDAC2, HDAC3, HDAC8, HDAC4, HDAC6 and HDAC7 (Boissinot et al. 2012). 92

Table 4-1 - Cell surface markers used in analysis of ADSCs. Each marker is detailed with alternative names, distribution, a summary of understanding of function, relevant references and conjugate and catalogue number. 109

Table 4-2 – Table of data for the flow cytometry analysis of the cell cycle distribution for ADSCs. Cells were dosed with 30 µM and 10 µM MI192, 10 µM TSA and untreated controls, for 12, 24 and 48 hours. Average percentage of cells for each of the three calculated phases of the cell cycle shown, with the standard deviation (SD) for each. 125

Table 4-3 – The percentage of untreated and MI192 treated ADSCs positive for stem cell markers CD29, CD34, CD44, CD45, CD73, CD90, CD105, CD146 and CD166. The percentage change on treatment was calculated. 132

Table 5-1 – ADSC donor information.....147

Table 5-2 - TaqMan gene expression assays used in 5.2.2, the assessment of the effect of MI192 pre-treatment on the osteogenic gene expression of ADSCs 148

Table 5-3 - TaqMan gene expression assays used in 5.2.5, the assessment of the effect of MI192 pre-treatment on the adipogenic gene expression of ADSCs 150

Table 5-4 – Summary of pre-treatment strategies in the literature with HDACis and MSCs 183

Table 6-1 – Antibodies for immunohistochemical staining and the conditions they were used in.....206

Table 6-2 - Element analysis of Design 3 scaffolds using EDS (% w.t.).....232

Table 7-1 - donor and passage information for the 6 batches of ADSCs.....249

Table 7-2 - Assay identification for microfluidic card. 251

Table 7-3 – Fold changes in expression of Wnt related transcripts in ADSCs treated with MI192 for 2 days 258

Table 7-4 - Fold changes in expression of early cartilage and bone related transcripts in ADSCs treated with MI192 for 2 days 261

Table 7-5 – Fold changes in expression of markers of osteogenic differentiation in ADSCs treated with MI192 for 2 days.....263

Table 7-6 – Fold changes in expression of cartilage and bone extracellular matrix related transcripts in ADSCs treated with MI192 for 2 days 266

Table 7-7 – Fold changes in expression of adipogenic transcripts in ADSCs treated with MI192 for 2 days 269

Table 7-8 – Fold changes in expression of stromal related transcripts in ADSCs treated with MI192 for 2 days 273

Table 7-9 - Fold changes in expression of neural/nerve related transcripts in ADSCs treated with MI192 for 2 days 274

Table 7-10 – Fold change in expression of miscellaneous transcripts in ADSCs treated with MI192 for 2 days 275

Table 7-11 - Genes that were flagged due to potentially erroneous results. No transcripts were significantly up or down-regulated..... 277

Chapter 1: Literature Review

This chapter reviews the literature relevant to this thesis, providing an introduction to the relevant topics. The review firstly provides an explanation of epigenetics and the role of HDAC enzymes in the human body. This is followed by an introduction to HDAC inhibitor compounds, the design of these inhibitors and their current uses. Further discussion focuses on the potential of these inhibitors in tissue engineering, more specifically bone tissue engineering, as well as introducing the current approaches and state of play in these fields. It finishes with thoughts on potential future directions for the field.

1.1 Background

There is a largely unmet clinical need for the repair and regeneration of human tissues and organs. In 2011, the total healthcare expenditure in the UK alone was £142.8 billion (Payne 2013). Due to the limitations of conventional clinical therapies, tissue engineering, a multidisciplinary area of research, has come to the fore. Tissue engineering aims to produce functional tissue and organs, essentially by the delivery of cells onto biomaterials, in a three dimensional (3D) structure, along with the necessary stimulus (be that chemical, mechanical or environmental) (Naderi et al. 2011) to generate the tissue/organ of interest. Some early successes have been achieved by transplanting relatively simple tissues or organs such as the trachea (Orlando et al. 2011) and the bladder (Atala et al. 2006). The excitement accompanying these early accomplishments demonstrates the huge potential of using tissue engineering approaches to restore tissue and organ function, although much more research is needed, especially for transplants to be fully functional, and for more complicated organs and tissues to be generated (Dai et al. 2012; Evans 2011; Bertino & Otterson 2011).

Stem cells are a key cell source for tissue engineering purposes, with the potential to be differentiated into the specific lineages required for the repair and restoration of functional tissues. Increased reporting of the limitations of current methods of using stem cells in tissue engineering has galvanised research investigating new methods of controlling stem cell fate (Vater et al. 2011; Wilson 2009; Reya et al. 2001).

Environmental stimuli and chemicals/growth factors/proteins etc that stem cells come into contact with can affect their fate (Vunjak-Novakovic et al. 2010; Baker & Chen 2012). Researchers currently have many options to utilise growth factors, bioactive molecules and genetic modifications/therapies to control the differentiation of stem cells for tissue engineering purposes (Hochedlinger & Plath 2009). A review collating examples of different culture conditions utilised to influence the *in vitro* differentiation of mesenchymal stem cells down multiple lineages (including osteogenic, chondrogenic and adipogenic) is an excellent source for understanding how wide the range of conditions available is (Vater et al. 2011). However, current protocols for effectively controlling stem cell proliferation and differentiation are ill defined, challenging, have side effects and can be very time consuming, expensive and unreproducible on the large scale.

It is well documented that both a cell's genetic and epigenetic make-up can affect how it behaves. For many years, research was primarily focused on genetics (Tollervey & Lunyak 2012), but more recently it has become apparent that '*epigenetics'* plays a massive role in cell fate and controlling the cell's properties. More specifically, research has discovered that modifications to the histone proteins in a cell, such as those by histone deacetylation enzymes, affect chromatin structure, and thus stem cell properties like potency and differentiation potential (Tollervey & Lunyak 2012; Hochedlinger & Plath 2009; Kretsovali et al. 2012a). Knowledge and understanding of this may be crucial for improving tissue engineering and cell-based therapies. Work on the inhibition of histone deacetylase enzymes as a tool for affecting cell properties technically began in the late 1970s, when Sodium Butyrate (NaB) was found to affect leukaemia cells. However, work only really took off in the late 1990s, and since then, two small molecular inhibitors of histone deacetylase enzymes (HDACis), Vorinostat and Romidepsin, have found FDA approval for the treatment of T-cell lymphoma (Marks & Breslow 2007; Bertino & Otterson 2011). In 2015, Panobinostat (Farydak) was approved by the FDA for the treatment of multiple myeloma (U.S. Food and Drug Administration n.d.).

While the main focus of work with HDACis remains in cancer therapeutics, work has begun to investigate these elsewhere, such as in HIV therapeutics (Barton et al. 2014), in inflammatory diseases such as rheumatoid arthritis (Gillespie et al. 2012), as drugs to treat or prevent cardiac diseases (McKinsey 2011) and key to this thesis, in combination with stem to improve tissue engineering. For example, inhibition of

histone deacetylation enzymes has been utilised to improve *in vitro* expansion methods of human hematopoietic stem cells (Elizalde et al. 2012), to improve the differentiation of stem cells into bone cells (Boer et al. 2006), to increase the efficiency of generation of induced pluripotent stem cells (iPSCs) (Hochedlinger & Plath 2009), and to increase efficiency of cellular therapies (Lee et al. 2007).

1.2 Epigenetics

1.2.1 Introduction to Epigenetics

Genetics is the study of the primary structure of nucleic acids, deoxyribonucleic acid (DNA), the information they code for and how this information is utilised and transferred from one generation of cells to the next. Epigenetics describes the post-genetic modifications made to the DNA sequence; the chemical functional groups such as methyl or acetyl on DNA, the protein scaffolds that DNA is wrapped around, or other proteins involved with DNA in the cell. These post-genetic modifications made to the DNA sequence are in the form of chemical functional groups, such as methyl or acetyl. The actual base genomic code remains unchanged with the epigenetic modifications. These epigenetic changes are potentially heritable and can be passed down to daughter cells during cell division, which is potentially important when considering stem cell fates. Although it is questionable whether epigenetic modifications are always heritable, and whether heritability is a defining property of epigenetics. A number of different definitions of epigenetics exist; for example, in a key early paper it was described as “the structural adaptation of chromosomal regions so as to register, signal or perpetuate altered activity states” (Tollervey & Lunyak 2012; Bird 2007).

Epigenetic modifications include, but aren’t limited to, methylation, acetylation, phosphorylation, ubiquitination, sumoylation, citrullination and Adenosine diphosphate ribosylation (Spivakov & Fisher 2007). Research has demonstrated that external environmental influences can alter the levels of these modifications in human cells. For example, alterations have been seen as a result of microbial infection (Minárovits 2009), pollution (Silveyra & Floros 2012), alcohol consumption (Agudelo et al. 2012), smoking (Hillemacher et al. 2008) and diet (Burdge et al. 2012). How these changes come about, and how they influence DNA, cells and the overall effects on the human body, is the subject of much investigation. This is of

particular interest to medical researchers, because a cell's epigenome is the key cellular level influencing factor behind a number of diseases, perhaps most notably cancers (Ropero & Esteller 2007) and inflammatory diseases (Shakespear et al. 2011), although it has become apparent that many other diseases also have epigenetics as a key mediator (Dinarello et al. 2011).

1.2.2 Human DNA

DNA in its most basic form exists as the famous double helix. DNA can be packed into further assembly levels (Figure 1.1) where charge, polarities and structural interactions are controlled in complicated and highly regulated processes (Verreault 2000). This DNA packing results in tight, but flexible assemblies; the flexibility allowing the structures to be altered constantly, resulting in the correct parts of the DNA being utilised in DNA transcription, replication or repair (Hondele & Ladurner 2011). The hierarchical order of DNA assemblies, from small to large, is DNA → Chromatin → Nucleosome-core particles → Nucleosomes → Chromosomes.

Chromatin is the term for the complex of DNA and the proteins which form the nucleosomes in eukaryotic cells. Nucleosomes are the repeating units of chromatin, and the main genetic component of cell nuclei. These nucleosome structures are formed from DNA when the 145-147 base unit structures wrap twice around two copies of each type of histone protein – H2A, H2B, H3 and H4 (Shahbazian & Grunstein 2007). A whole single unit is known as the nucleosome-core particle (Figure 1.1), and these particles are further assembled into chromosomes (Figure 1.2).

Histone proteins are highly abundant proteins in cell nuclei and under normal physiological conditions contain a high proportion of amino acids with positively charged, basic, side chains. It is these positive charges and their ionic interaction with the negative regions of the DNA backbone that account for the ease of assembly of DNA. Other interactions, such as hydrogen bonding, account for the remainder of the bonding energy between histones and DNA (Hondele & Ladurner 2011).

Figure 1.1 - The crystal structure of the nucleosome-core-particle. The 146 base pair DNA ribbon structure is in brown and turquoise. It is wrapped around the eight histone protein backbone chains (H3 is blue, H4 green, H2A yellow and H2B red). The left view is down the DNA superhelix axis, and perpendicular to the axis on the right. Reprinted with permission from (Luger et al. 1997)**.**

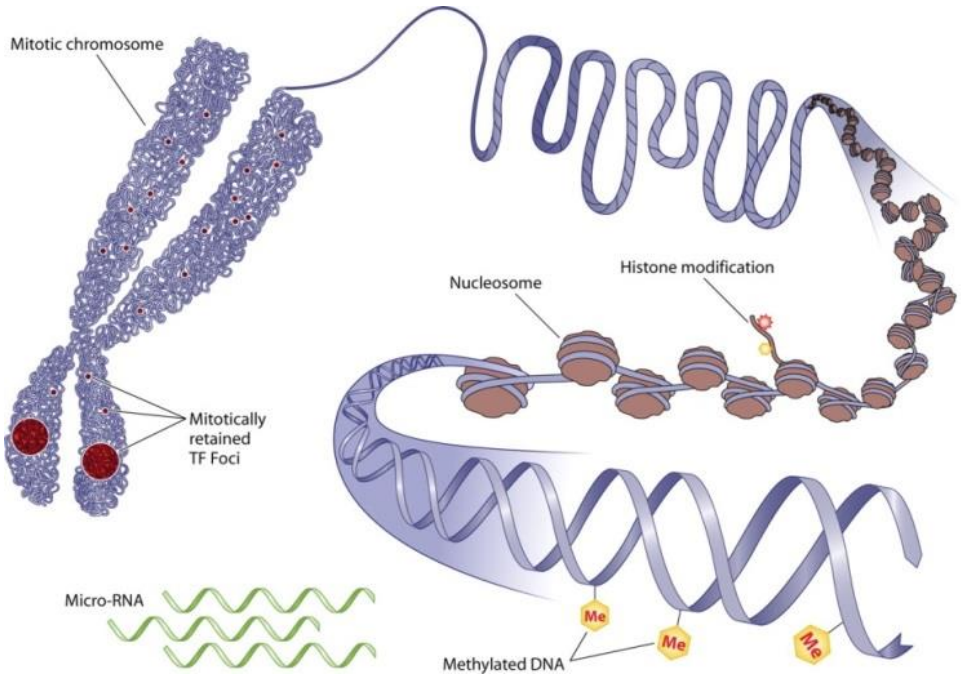

Figure 1.2 – Diagram showing how DNA wraps around the histone proteins, then the formation of a chromosome particle. Reprinted with permission from (Zaidi et al. 2010).

Chromatin's higher order structure, i.e. how the chromatin is folded, is governed by interactions between nucleosomal histones, DNA, neighbouring nucleosomes and other non-histone proteins. In the cell, the structure of the chromatin is dependent on cell-cycle, the level of gene activity and the region of the chromosome involved. Post translational modifications (PTMs) made to the histone are key controlling factors. PTMs are modifications made to the DNA or related proteins after it has been synthesised/translated, and epigenetic modifications are an example of PTMs. The majority of PTMs have been shown to be reversible (Tollervey & Lunyak 2012).

The epigenetic makeup of the cell affects this chromatin higher-order structure (Jones 2012). Chromatin states are dynamic, but when simplified, chromatin can transition between an open and relaxed, or a compact and folded form. The compaction level affects the accessibility of the DNA, which has wide reaching cellular consequence. The epigenetic makeup affects three key chromatin properties: 1) The positioning of specific nucleosomes, 2) The higher order structure of chromatin, 3) The compartmentalisation of the chromatin sections. These can subsequently affect how the DNA is read and translated, and thus how genes are expressed in cells, with wide ranging consequences (Eberharter & Becker 2002).

Furthermore, epigenetics has an impact on the chromatin assembly processes, which take place in the S phase of the cell cycle (Verreault 2000). Due to the potential for large numbers of unwanted interactions between different parts of DNA, the histone proteins themselves, and other specialist proteins known as histone chaperones, control the assembly of DNA onto the histones. The full mechanism by which histones and histone chaperones assemble the nucleosome is not fully understood, but it is believed that epigenetic modifications to the histones, which alter the charges on the DNA, histone proteins and assembly proteins, may play a role. Consequently, epigenetics may affect how histone chaperones assemble the cell's DNA in the first place, as well as how the DNA is read (Shahbazian & Grunstein 2007).

1.2.3 Acetylation

Two especially critical epigenetic modifications are the addition (acetylation) or removal (deacetylation) of acetyl groups to chromatin's histone lysine residue(s). This is one of the most abundant post translational modifications and genome wide

analysis of cells has shown that acetylation is a modification at least as frequent as phosphorylation (Filippakopoulos & Knapp 2012; Kretsovali et al. 2012a). Acetylation is a key epigenetic modification, with levels affecting processes such as the previously mentioned chromatin folding and the assembly of the nucleosome by histone-chaperones.

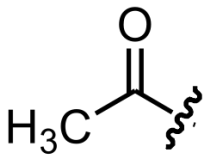

Figure 1.3 - An Acetyl group, a chemical group with the chemical formula $COCH_3$. A small chemical motif consisting of a methyl group single bonded to a carbonyl group, which is a carbon and an oxygen joined by a double bond. It is sometimes shortened to 'Ac'.

In biochemical terms, there are two key ways in which the addition of an acetyl group (Figure 1.3) to a histone tail alters the properties of the tail. Firstly, the acetyl group neutralises the positive charge that was previously present on the lysine residue, potentially resulting in the electrostatic interactions of the nucleosomes with anionic DNA (or anything else it is interacting with) being weakened, leading to a more open chromatin structure (Uciechowska et al. 2009). Secondly, the acetyl group prevents further epigenetic modifications, blocking the site and effectively chemically locking them from further/alternative epigenetic modifications (Sadoul et al. 2008). This change is only temporary as these groups can also be removed.

It has been shown that the acetylation of lysine residues allows them to act as docking sites for the binding of other regulatory ‘reader’ proteins where the acetyl group is essential for this interaction. These reader proteins can measure and ‘read out’ the histones acetylation level, potentially mediating transcription and any other chromatin dependent processes. As this is a board remit, by definition, the enzymes controlling acetylation levels are classified as both co-activators and co-repressors (Reichert et al. 2012). A class of proteins called bromodomains are currently the only known interaction modules that *specifically* recognise and read the acetylation of the N-terminal of histone lysine residues (Dhalluin et al. 1999), playing a key epigenetic role and may be interesting therapeutic targets (Filippakopoulos & Knapp 2012).

However, they fall outside the scope of this review due to their entirely different mechanism of action to HDACs and different inhibitor/activator compounds/mechanisms.

1.2.4 HDACs and HATs

While the histone code can be “read” by proteins such as bromodomains, it can also be written and erased. The acylation levels of histone proteins are predominantly controlled by two groups of cellular enzymes; classified as histone deacetylases (HDACs) and histone acetyltransferases (HATs). If proteins such as bromodomains are the acetylation ‘readers’, HATs are the ‘writers’, and HDACs the ‘erasers’ (Filippakopoulos & Knapp 2012). HATs mediate the transfer of acetyl groups onto the lysine residues, and the actions of HDACs remove those acetyl groups. HDAC inhibitor (HDACi) compounds inhibit the action of HDACs, generally resulting in increased acetylation levels of proteins.

1.2.5 Non-histone acetylation

Lysine amino acid residues are found in many cellular proteins, not just as part of histones. HATs and HDACs have multiple targets, they don’t just simply modify the acetylation level of histone proteins (Martínez-Balbás et al. 2000). Evolutionary studies suggest that HDAC enzymes actually pre-date the evolution of histone proteins themselves. Some functions of these enzymes are not even related to histones; for example, HDAC6 interacts with tubulin proteins and HDAC1 on transcription factors such as the tumour suppressor p53 (Gregoretti et al. 2004). Despite containing histone in their names, non-histone proteins may actually constitute the majority of substrates affected by HATs and HDACs (Choudhary et al. 2009). This huge range of targets results in the wide-ranging cellular consequences of altering or affecting the HAT and HDAC proteins, and why they are considered so important (Duncan et al. 2011; Buchwald et al. 2009; Spange et al. 2009; Sadoul et al. 2008).

With this in mind, Balasubramanian et al. have argued it is actually technically incorrect to name these classes of enzymes/proteins HATs and HDACs. It may be more accurate to refer to them as lysine acetylases/deacetylases, or the more commonly referenced alternative protein acetylases/deacetylases (LATs and LDACs, or ATs and DACs, with corresponding inhibitors as LDACis and DACis)

(Balasubramanian et al. 2009). Another review states that HDACs should be named KDACs (Reichert et al. 2012). While the huge range of targets of these compounds must be understood, the nomenclature convention of HATs, HDACs and HDACis will be adhered to here, as this is the standard in the majority of the literature (Spange et al. 2009).

1.2.6 HDAC isoforms

There are 18 distinct human enzymes known to have deacetylation activity, conventionally numbered 1–18 (for example, HDAC8). Based on molecular phylogenetic analysis of protein primary structures, and their homology to yeast enzymes, these 18 HDACs are grouped into two categories – classical and sirtuins (Bertrand 2010), which can be further subdivided into four classes (Bradner et al. 2010): classes I, II and IV are classical HDACs and class III are sirtuins. The activity of the classical HDACs depends on zinc (Zn^{2+}) ions, whereas the sirtuin class utilise nicotinamide adenine dinucleotide: NAD^{+} - a phosphate linked dinucleotide coenzyme. As they have entirely different mechanisms of action, structure and inhibitors, sirtuins fall outside the scope of this review (Uciechowska et al. 2009).

Different HDAC enzymes can have highly specific functions; often two or more isoforms can function together in unison, and some isoforms have overlapping functions. While the full physiological roles of each individual HDAC isoform are not known, studies inhibiting individual isoforms, or knock out studies of specific isoforms have provided some insight to their function (Kretsovali et al. 2012a). Summaries of such mouse development studies can be found elsewhere (Witt et al. 2009; Reichert et al. 2012). Table 1-1 contains summary of the known cellular location of, tissue distribution and biological functions of HDACs.

Table 1-1 - A summary of the zinc dependent HDAC isoforms.

	HDAC	Cellular Location	Tissue Distribution	Known Biological Functions
Class I	**HDAC1**	Nucleus (de Ruijter et al. 2003)	Ubiquitous (Yang et al. 1997).	Cellular proliferation (Lagger et al. 2002; Zupkovitz et al. 2010). Cell cycle regulation and haematopoiesis (Wilting et al. 2010; Yamaguchi et al. 2010). DNA damage response (Miller et al. 2010). Cardiac development (Montgomery et al. 2007; D.-F. Lu et al. 2014). Oligodendrocyte, glial cell, synapse and neuronal cell development and function (Montgomery et al. 2009; Ye et al. 2009; MacDonald & Roskams 2008; D. Kim et al. 2008; Akhtar et al. 2009; Humphrey et al. 2008). Regulating Schwann cells (Jacob et al. 2011; Chen et al. 2011). Osteogenic and skeletal muscle development (Maroni et al. 2012; Moresi et al. 2012). Modulating T Cell response (Grausenburger et al. 2010). Epidermal formation (Leboeuf et al. 2010). Adipogenesis (Haberland et al. 2010). Cartilage formation (Hong et al. 2009).
	HDAC2	Nucleus (de Ruijter et al. 2003)	Ubiquitous (Yang et al. 1997).	Cell cycle regulation (Yamaguchi et al. 2010). Cardiac development (Montgomery et al. 2007; Trivedi et al. 2007). DNA damage response (Miller et al. 2010). Oligodendrocyte, glial cell, synapse and neuronal cell development and function

				(Montgomery et al. 2009; Ye et al. 2009; MacDonald & Roskams 2008; Guan et al. 2009; Jawerka et al. 2010; Akhtar et al. 2009; Humphrey et al. 2008).Regulating Schwann cells (Jacob et al. 2011; Bai et al. 2005). Skeletal muscle development (Moresi et al. 2012). Epidermal formation (Leboeuf et al. 2010). Adipogenesis (Haberland et al. 2010). Regulating cartilage structure (Hong et al. 2009).
Class I	**HDAC3**	Nucleus and cytoplasm (de Ruijter et al. 2003)	Ubiquitous (Yang et al. 1997).	Cell cycle regulation (Bhaskara et al. 2009; Jiang & Hsieh 2014). Osteogenic development (Maroni et al. 2012; Schroeder et al. 2004; Hesse et al. 2010; Lamour et al. 2007). Liver function (Knutson et al. 2008; Feng et al. 2011). Cardiac function (Trivedi et al. 2008; Montgomery et al. 2008) Bone mass and formation,(McGee-Lawrence et al. 2013; Razidlo et al. 2010; Hesse et al. 2010; Maroni et al. 2012; Schroeder et al. 2004) including osteoclast suppression (Pham et al. 2011). Chondroprogenitor differentiation to cartilage (Razidlo et al. 2010). Brain memory function (McQuown et al. 2011). Neural stem cell proliferation and differentiation (Jiang & Hsieh 2014; Sun et al. 2007). Hematopoietic stem cell growth (Elizalde et al. 2012).
	HDAC8	Nucleus and cytoplasm (de Ruijter et al. 2003)	Ubiquitous (Yang et al. 1997).	Craniofacial and skull bone in embryonic development (Haberland et al. 2009). Mediates the osteogenic differentiation of stem cells (Fu et al. 2014).

Class IIa	**HDAC4**	Nucleus and cytoplasm (de Ruijter et al. 2003)	Brain, heart and skeletal muscle (Verdin et al. 2003; Zhao et al. 2001), prehypertrophic chondrocytes (Vega et al. 2004) retina (Chen & Cepko 2009), neurons (Bolger & Yao 2005; Bolger et al. 2007; Chawla et al. 2003).	Myofibroblast development (Glenisson et al. 2007). Chondrocyte hypertrophy and endochondral ossification (Vega et al. 2004). Retinal neuronal function (Chen & Cepko 2009). Regulates neuronal activity, cell death and survival (Bolger & Yao 2005; Bolger et al. 2007). Muscle differentiation (Zhao et al. 2001).
	HDAC5	Nucleus and cytoplasm (de Ruijter et al. 2003)	Heart, skeletal muscle and brain (Verdin et al. 2003; Mckinsey et al. 2000), neurons (Chawla et al. 2003).	Myocardial and endothelial functions (Mckinsey et al. 2000). Differentiation of neural stem cells (Sun et al. 2007) and neuronal activity (Chawla et al. 2003). Memory function (Agis-Balboa et al. 2013).
	HDAC7	Nucleus and cytoplasm (de Ruijter et al. 2003)	Thymus (Dequiedt et al. 2003), heart, muscle and lung (Verdin et al. 2003).	In embryonic development found in endothelial cells of developing heart, blood vessels, and mesenchyme and myocardial layers of heart and in lung tissue (Chang et al. 2006). Role in developing thymocytes (Dequiedt et al. 2003; Ji et al. 2010). Osteoclast activity (Pham et al. 2011). Inflammatory macrophages (Shakespear et al. 2013).
	HDAC9	Nucleus and cytoplasm (de Ruijter et al. 2003)	Heart, skeletal muscle and brain (Verdin et al. 2003; Zhou et al. 2001).	Redundant role in heart development (Chang & McKinsey 2004). Motor innervation in muscles (Méjat et al. 2005).

Class IIb	**HDAC6**	Mainly the cytoplasm (de Ruijter et al. 2003)	Muscle (Balasubramanian et al. 2014), brain (d'Ydewalle et al. 2012) heart (Zhang et al. 2014), liver (Gradilone et al. 2014), kidneys (Liu et al. 2012), testes (Zhang et al. 2008).	Involved in Cellular response to stress (Boyault et al. 2007; Kwon et al. 2007) and macro-autophagy (J.-Y. Lee et al. 2010). Muscle differentiation (Balasubramanian et al. 2014). Tubulin acetylation, minor role in bone mass regulation and immune response modulation (Zhang et al. 2008). Neuroprotective and neurodegenerative functions (d'Ydewalle et al. 2012). Arterial modelling (Zhang et al. 2014). Platelet activation (Sadoul et al. 2015).
	HDAC10	Nucleus and cytoplasm (de Ruijter et al. 2003)	Liver, spleen and kidney (Kao et al. 2002), skin (Lai et al. 2010).	Promotes autophagy-mediated cell survival in neuroblastoma cells (Oehme et al. 2013). Role in melanin production in the skin (Lai et al. 2010).
Class IV	**HDAC11**	Nucleus and cytoplasm (de Ruijter et al. 2003)	Brain (Liu et al. 2008), heart, skeletal muscle, and kidneys (Gao et al. 2002).	Influences immune activation versus immune tolerance (Villagra et al. 2008). Expressed in the developing brain within neural oligodendrocyte cells (Liu et al. 2008).

1.2.7 HDAC structure and mechanism of deacetylation

Each HDAC isoform has a (sometimes subtly) different structure. However, full structural data on HDACs is limited; X-ray crystal structures are very difficult to obtain and only a few HDAC enzymes have been isolated, typically by co-crystallisation with an inhibitor or a signalling molecule, giving an indicator of how the enzyme potentially forms complexes, or its enzymatic function, in the cell. To date, the structures of HDAC7, HDAC4, HDAC3, HDAC2 and HDAC1 have been established, and HDAC8 has been characterised most prolifically (Wagner et al. 2013).

It was pioneering work by Finnin et al. (1999) that lead to the first description of a histone-deacetlyase-like protein (HDLP, Protein Data Bank code 1C3P) (Figure 3) (Finnin et al. 1999). HDLP was isolated from the bacterium *Aquifex aeolicus*, and today this is still considered a good HDAC structural model, with a 35% homology to HDAC1. While, HDLP is only a homologue of human HDAC enzymes, it still provides a framework for further research into the mechanisms of catalytic activity and inhibition. As well as this structure, Finnin and co-workers also suggested a mechanism of action of HDAC enzymes (Summarised in Figure 1.5), and while a number of mechanisms of deacetylation by the HDAC active site have since been proposed (Vanommeslaeghe, De Proft, et al. 2005; Corminboeuf et al. 2006), this is still considered possibly accurate today.

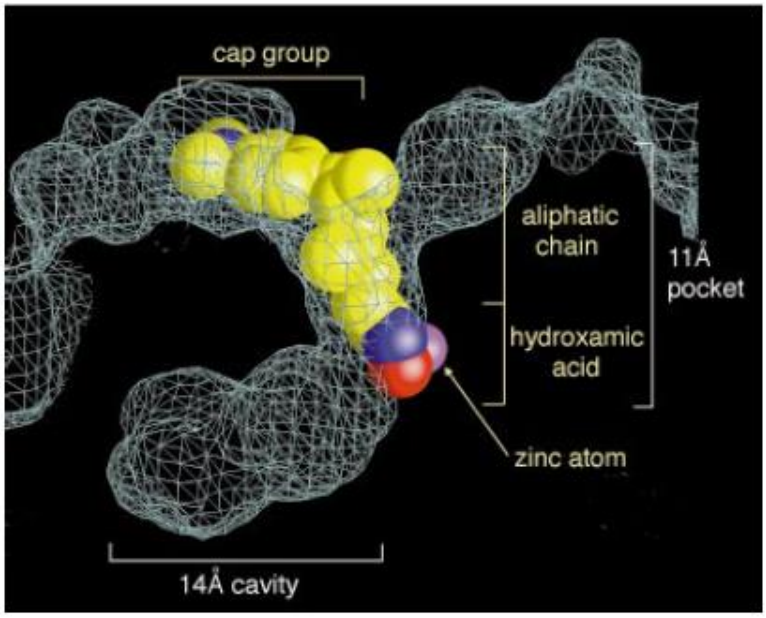

Figure 1.4 – Space filling diagram. A ‘space filling’ representation of HDACi TSA bound in the active site, (a sock shaped cavity), of HDLP. Reprinted with permission from (Finnin et al. 1999).

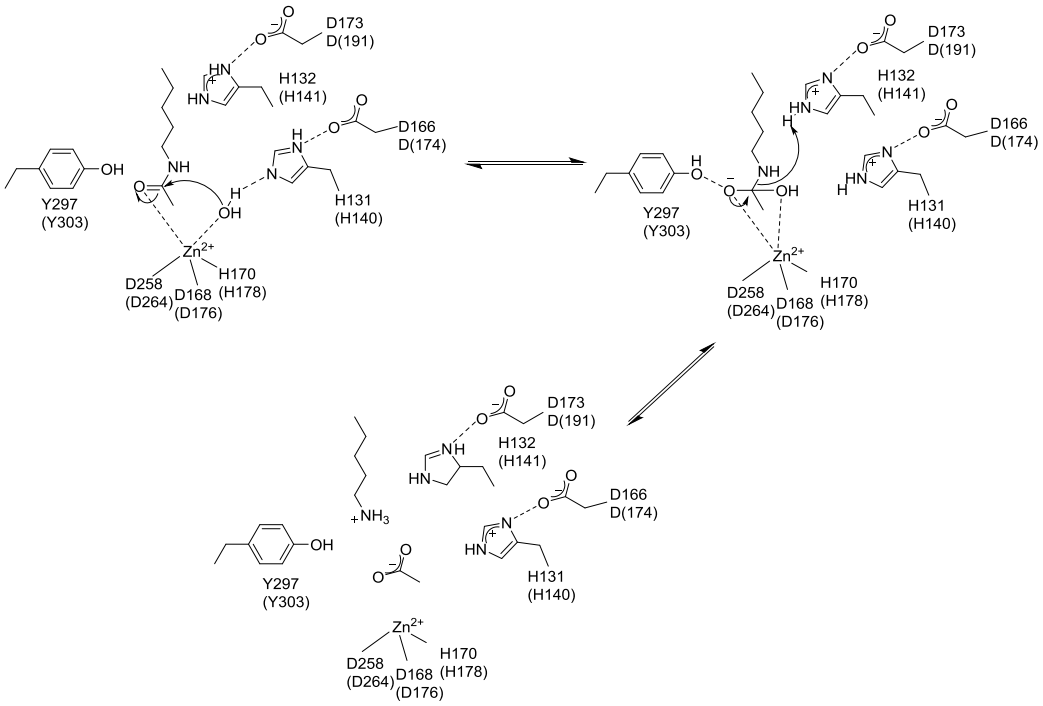

Figure 1.5 – Mechanism of action. The relevant residues and molecules involved in a proposed HDAC1 active site of HDLP, along with a proposed mechanism for the deacetylation of an acetylated lysine residue**.** Adapted from (Finnin et al. 1999).

The active site of this HDLP consists of an 11 A°-deep sock-shaped cavity or tunnel, comprising of around 390 amino acids. In this, a Zn^{2+} ion sits bound at the 'heel' of the sock. The internal cavity walls are hydrophobic, consisting of lipophilic amino acids that differ depending on the class of HDAC. While there may be differences in residues and pocket shape between HDAC classes, this catalytic zinc ion is common to all zinc dependent HDAC proteins (Jones 2012), and researchers are confident this is essential to the deacetylation process.

Until 2004/5, the HDLP model was the only source of structural information about the active sites of HDAC enzymes. This changed when X-Ray structures of human HDAC8 with an inhibitor bound in the catalytic pocket were published, proving that the catalytic site was in fact very similar to that of HDLP (Somoza et al. 2004; Vannini et al. 2004). As of 2015, 29 different crystallographic structures of human zinc-dependent HDACs have been logged in the Protein Data Bank. However, crystal structures are only a snapshot of the structure of a protein. When in solution (as they

are naturally in the cell), the structure could be very different, as well as being dynamic and constantly changing. This is problematic for researchers attempting to design compounds to bind to proteins, as they have to work from potentially inaccurate crystal structures (Deschamps et al. 2015).

Much important work is ongoing in the field of structural determination, as these studies can reveal the structural relation between the enzymes and their higher-order complex partners, the role of potential signalling molecules on complex formation and enzymatic function, and how inhibitor compounds actually bind and cause a loss of enzymatic function (Silvestri et al. 2012; Deschamps et al. 2015). While the full enzyme structures are not known, researchers can still utilise what they know in design of inhibitors of these enzymes.

1.2.8 The effects of histone acetylation levels on chromatin

The way in which chromatin is organised and read affects all nuclear processes involving DNA. This in turn has an effect on gene expression, with far reaching consequences. With regards to stem cells, important properties such as pluripotency, differentiation and reprogramming are all affected by the "epigenetic landscape" (Tollervey & Lunyak 2012).

Generally, histone acetylation results in a more open and more transcriptionally active chromatin; acetylation reduces interactions between the nucleosomes and the histone tails are released from the linker DNA, causing it to open up. Deacetylation leads to a more condensed and transcriptionally silenced chromatin, increasing the number of possible interactions as less sites are blocked by acetyl groups, and resulting in a repression of transcription (Grunstein 1997). However, this is a simplification, and it is not always productive to talk in simplified terms of acetylation causing more transcriptionally active chromatin and vice versa. It is often not just a case of on or off, open or closed, active or inactive, permissive or repressive chromatin structures. In some cases epigenetic modifications can silence some sections of the chromatin, while simultaneously causing the area to actually become more transcriptionally active. In the literature, these silent but transcriptionally available sections of chromatin are sometimes referred to as bivalent domains, a third, "poised" state (Mikkelsen et al., 2007). It was originally thought that these bivalent markers were a feature of only pluripotent stem cells. However, these

regions also exist in several different animal cell populations (Tollervey & Lunyak 2012; Mikkelsen et al. 2007).

1.3 HDAC Inhibitors

HDACis are typically small molecular compounds that can bind to and block the action of HDAC enzymes. They can be isolated from natural sources, such as Trichostatin A (TSA, isolated from antifungal bacteria) (Tsuji et al. 1976), or designed using medicinal chemistry tools and synthesised in a laboratory (Hahnen et al. 2008). Interestingly, the HDACi valproic acid (VPA) has been used in psychiatry and neurology for several decades, and its mechanism of action was only discovered to be inhibition of HDACs in 2001 (Phiel et al. 2001; Göttlicher et al. 2001; Hahnen et al. 2008).

High levels of deacetylation activity can be linked to tumour pathology. These high levels deacetylation activity repress the activity of certain genes, which are in turn known to repress cancer cells (Bertrand 2010). Due to this, and other mechanisms of action, to date, HDACis have primarily been associated with cancer therapeutics (Ropero & Esteller 2007). Three HDACis have achieved FDA approval for use in cancer treatments; Vorinostat, also known as Suberoylanilide Hydroxamic Acid (SAHA) or Zolinza (Richardson et al. 2008), Romidepsin (Bertino & Otterson 2011) and Panobinostat (Prince & Bishton 2009). At the end of 2012, a review found that at least 20 structurally different HDACis were found in various stages of anti-cancer clinical trials, as either monotherapies or in combination with other anti-cancer agents (Nebbioso et al. 2012). Typically they have been applied to the treatment of haematological malignancies, as the response of solid tumours to HDACis doesn't appear to be translatable, athough they are being explored in a number of combination therapies (West & Johnstone 2014).

More recently, research has diversified, and HDACis have been discovered as potential tools in many different therapeutic areas, such as inflammatory diseases (Bode & Dalpke 2011), diabetes (Christensen et al. 2011), arthritis (Buckland 2011; Gillespie et al. 2012) and tissue engineering (Boer et al. 2006).

Different papers characterise current HDACis differently. However some major categories are common to most reviews (Nebbioso et al. 2012). These major categories are hydroxamic acids, natural cyclic peptides, short-chain and aromatic fatty acids, benzamide based and electrophilic ketones and thiols. Very few HDACis don't fit into one of these categories, although occasionally an 'other HDACis' category is used to account for these.

1.3.1 Mechanism of HDAC inhibition

Hydroxamic HDACis block the HDAC active site, with the zinc ion coordinating to the two oxygen atoms of the hydroxamic acid section of the HDACi. There are potentially other disrupting interactions, such as the active site changing shape, which can account for the inhibition action. These all depend on the structure of the HDACi. The aliphatic chain region of the HDACi occupies the channel, where hydrophobic interactions strengthen the binding energy between the HDACi and the enzyme. The capping group, often an aromatic ring, blocks access to the pocket, reducing the potential for any competitive binding. The rim of the catalytic pocket is usually where the structural differences between HDAC isoforms can be found, so it is often here that efforts are often focussed when designing isoform specific inhibitors (Deschamps et al. 2015).

1.3.2 Specific HDACis compared to panHDACis

To date, research has largely focused on non-specific/unselective HDACi compounds (panHDACis), which are broad spectrum HDACis that target multiple HDAC isoforms at once (Balasubramanian et al. 2009). Most first generation HDACis, such as SAHA and Romidepsin (Bertino & Otterson 2011; Richardson et al. 2008), are relatively unselective (Jones 2012). However, conflicting findings have been reported, for example Bradner et al. (2010) have demonstrated that some such HDACis can be selective to certain HDAC isoforms. Discrepancies in this field can arise due to a lack of knowledge of HDAC structure and problems with currently utilised screening techniques, such as the isolated enzymes mentioned previously, which can have different structures to the enzymes naturally (Bradner et al. 2010; Madsen & Olsen 2012). The chemical structures of some of the key HDACis in the field can be seen in Figure 1.6.

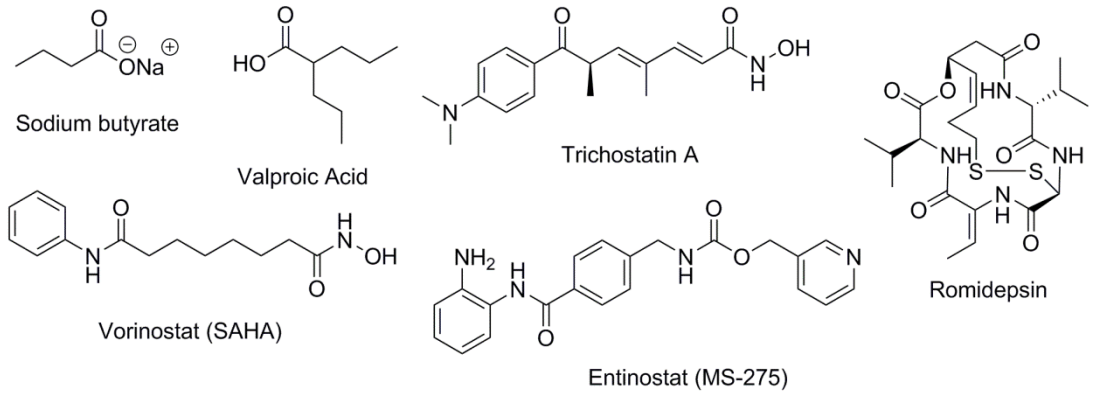

Figure 1.6 - Structures of HDACis commonly found in the literature. Clockwise from top left – Sodium butyrate, Valproic Acid, Trichostatin A, Romidepsin, Entinostat (MS-275) and Vorinostat (SAHA).

While some panHDACis have proven to be effective drugs (Richardson et al. 2008; Bertino & Otterson 2011), research is beginning to move away from this unselective approach, to explore isoform selective inhibitors. The broad spectrum of targets of the panHDACis means that it is hard to fathom the mechanism of action of the HDACi, and leads to a greater potential for side effects. It has been be argued that targeting specific HDACs is key to the development of future HDAC therapeutics (Balasubramanian et al. 2009; Jones 2012; Witt et al. 2009). This is easier said than done, as the structural differences between different HDAC isoforms are often subtle, with most of the features of the enzyme catalytic pocket being conserved between isoforms (Deschamps et al. 2015).

1.3.3 Design of HDACis

Computational studies can be undertaken to aid in the design of HDACis, where researchers can model the binding sites of inhibitors on HDAC enzymes. These binding pockets can then have libraries of compounds virtually docked into the binding site, modelling how well different chemicals bind into the catalytic pockets. Known HDACis or ligands for the enzymes can also be bound, so benchmark values can be generated to validate the models. Interactions such as hydrogen bonds, Van Der Waals interactions and metal chelation forces are taken into account. Quantitative structure activity relationship models have been developed for HDACs and HDACis, which relate the chemical structure of compounds to their biological activity (Nair et al. 2012). This is just one illustrative example of potential

computational models for compound design, it is a very broad subject (Wang 2009; Pontiki & Hadjipavlou-Litina 2011).

Computational designers can produce whole libraries of potentially useful compounds (Xiang et al. 2012; Tang et al. 2009), or individual design motifs of HDACis, such as the zinc binding group, can be investigated (Vanommeslaeghe, Loverix, et al. 2005). Chemical libraries are collections of chemical compounds that have been grouped for a purpose. Only a very limited number of HDACi compound libraries have been reported so far, and thus there is a highlighted need for further development in this field (Nair et al. 2012). However, this work relies on improvements to the detailed structural knowledge of HDACis.

1.3.3.1 The HDACi Design Pharmacophore

Computational studies have led to a set of design principles being adopted for HDACis, which typically result in them having three key domains. When designing compounds, this is known as the pharmacophore (Figure 1.7, where SAHA is given as an example). The International Union of Pure and Applied Chemistry (IUPAC) defines a pharmacophore to be “an ensemble of steric and electronic features that is necessary to ensure the optimal supramolecular interaction with a specific biological target and to trigger or block its biological response” (Wermuth et al. 1998).

The following three components make up the most common HDACi design pharmacophore (Pontiki & Hadjipavlou-Litina 2011; Sternson et al. 2001):

1) A metal binging group, which interacts with the zinc ion in active site at the heel of the HDAC pocket.
2) A linking domain, which occupies the majority of the HDAC pocket. This can be cyclic or chain like, and links the metal binder and the capping domain.
3) A surface recognition or capping domain, which typically interacts with residues on the rim of the HDAC tunnel.

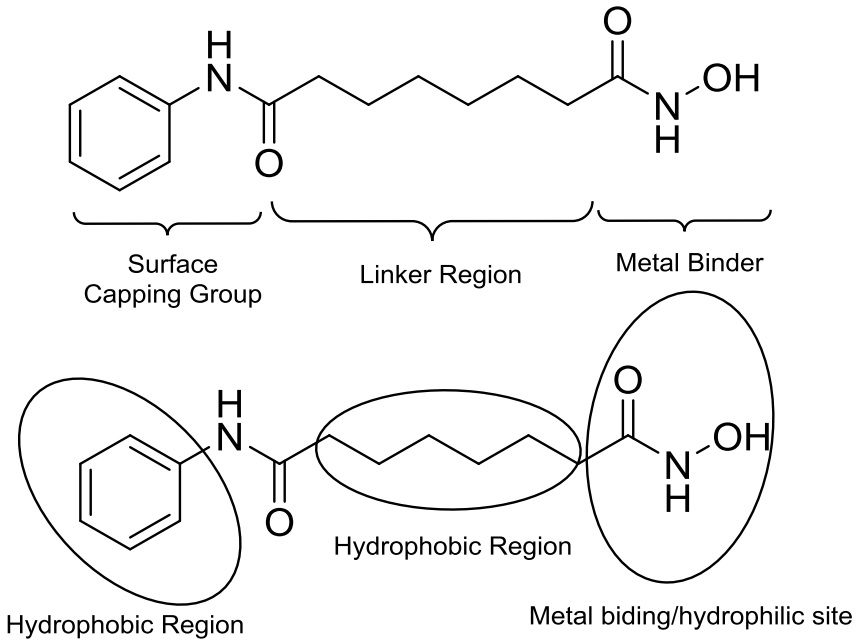

Figure 1.7 – Molecular pharmacophore of HDACis. SAHA is given as an example, adapted from (Pontiki & Hadjipavlou-Litina 2011).

Within each of these three major pharmacophore components, there is much scope for chemical diversity, and each component can have its own set of design rules (Bertrand 2010). This pharmacophore has developed because the three domains are known to either interact with, or facilitate other parts of the compound to interact with the previously described catalytic pocket or tunnel of the HDAC enzyme. X-Ray crystallography studies of HDACis interacting with HDAC catalytic pockets, such as the previously mentioned by Finnin et al. lead to these deductions (Finnin et al. 1999). These can be represented by space filling diagrams, where computational modelling has predicted the size and shape of the catalytic pocket, and the space can be filled by a chemical molecule (Figure 1.4).

1.3.3.2 Isoform Specific HDACis and their design

Considering the advanced stage of research and trials that some of these HDACis have reached, it is remarkable how little is known about selectivity and the mechanism of action of HDACis. The previously mentioned report of HDACi selectivity are conflicting and Bradner et al. demonstrated that a large proportion of the well investigated compounds widely perceived as non-selective, panHDACis, actually had an unexpectedly high level of selectivity for certain HDAC isoforms, most usually HDAC1 and HDAC2 (Bradner et al. 2010). A summary of their findings can be

seen in Figure 1.8. For example, SAHA, which has been reported elsewhere to be selective for HDAC7 in 14 different cell types (Dokmanovic et al. 2007), was found to be selective only for HDAC1, HDAC2, HDAC3 and HDAC6 (Bradner et al. 2010).

Therefore, research is moving towards the design of selective HDACis, creating a so called ‘second generation’ of HDACis. The development of these second generation HDACis may have advantages for some applications, but it is worth noting there are still advantages with panHDACis, especially considering that from a regulatory perspective, many of these are close to reaching FDA approval (Jones 2012; Balasubramanian et al. 2009; Bieliauskas & Pflum 2009).

While cancer is still the main focus of research in this area, the rise of HDAC specific enzymes (especially driven by the fact that specific HDACs may be highly expressed in certain cancers (Balasubramanian et al. 2009) is helping push the field of HDACis in new directions (McKinsey 2011).

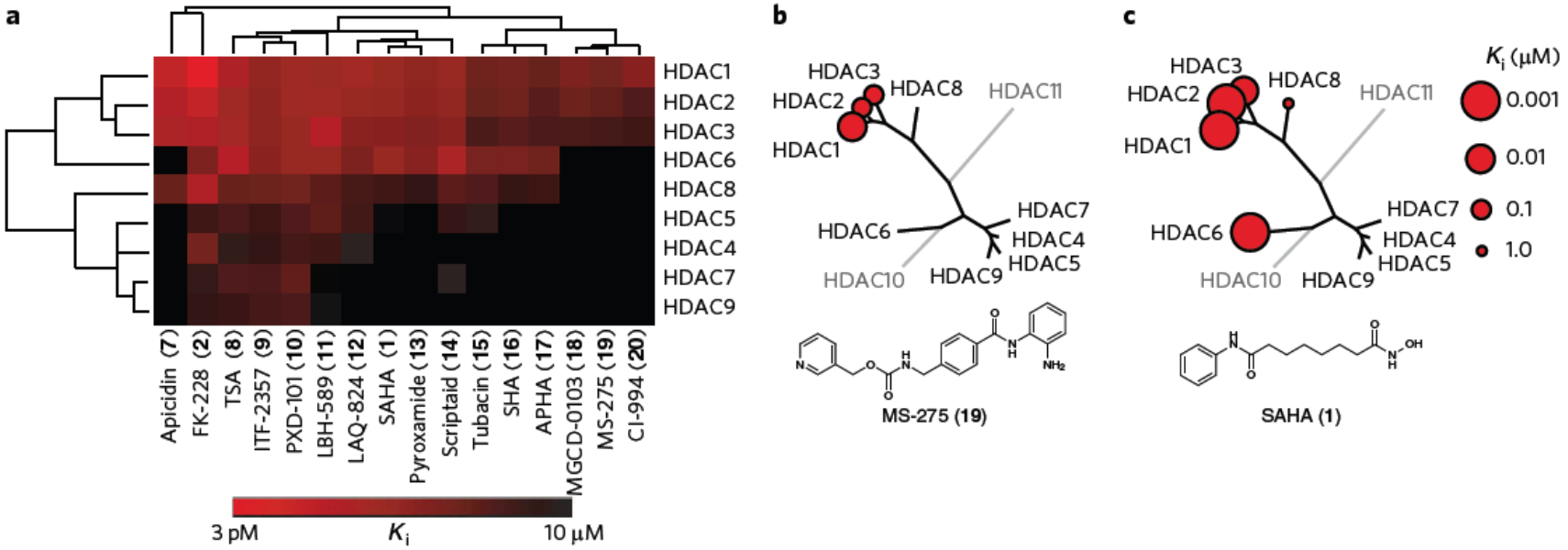

Figure 1.8 - Chemical phylogenetic analysis of HDACs; the binding affinity of HDACis for different HDAC isoforms. a) Hierarchical clustering of HDACs with a representative panel of HDACi compounds binding affinity for different HDAC isoforms, with an indication of inhibitor potency (K_i); b) and c) Dendrogram representative diagrams, with the chemical structure and enzymatic selectivity profiles of MS-275 (b) and SAHA (c), overlaying molecular phylogeny. The circles are representative of K_i on a logarithmic scale. Reprinted with permission from (Bradner et al. 2010).

1.4 The Effect of HDACis on Cancerous and Normal Cells

Cancerous cells are understood to have an abnormal epigenetic make up, compared to normal cells in the human body (Tsaniras et al. 2014; Reya et al. 2001). It has been reported that HDACi compounds can kill or damage cancerous cells, while leaving normal cells relatively unharmed (Qiu et al. 2000; Bose et al. 2014). This is especially advantageous when compared to other cancer treatments, such as chemotherapy and radiotherapy, which are known to be very damaging to normal cells. This specificity for cancerous tissue is a major advantage for HDACis in cancer therapeutics.

HDACis are found to be selective for tumour cells over normal cells (that are often reported as resistant to the effects of HDACis) at clinically utilised concentrations (Nebbioso et al. 2005; Dokmanovic et al. 2007). This can be through several possible mechanisms. For example, on HDACi treatment, normal cells experience an increase in the levels of thioredoxin, a protein that acts to resistance to reactive oxygen species (ROS) accumulation. This increase in thioredoxin is not seen in cancerous cells and the high levels of ROS can cause the death of cancer cells (Ungerstedt et al. 2005). Interestingly, some of the effects of HDACis have been observed to be reversible (J. H. Lee et al. 2010), thus it is vital researchers reach a better understanding of how HDACis affect normal cells.

HDACis can have wide ranging effects on both normal and cancerous cells, causing alterations to the cell-cycle, differentiation potential, proliferation, gene expression, reactive oxygen species accumulation and normal cell death pathways. The effects of HDACis on cancerous cells are depicted pictorially in Figure 1.9. The effects are dependent on the cell type, choice of HDACi and application factors such as exposure time and concentration of inhibitor (Xu et al. 2007). For example, SAHA has been found to have negative effects on normal cells in mouse *in vivo* models (McGee-Lawrence et al. 2011). The full range of individual mechanisms related to each of these effects are difficult to isolate and describe, and the effects are often happening in synergy with each other.

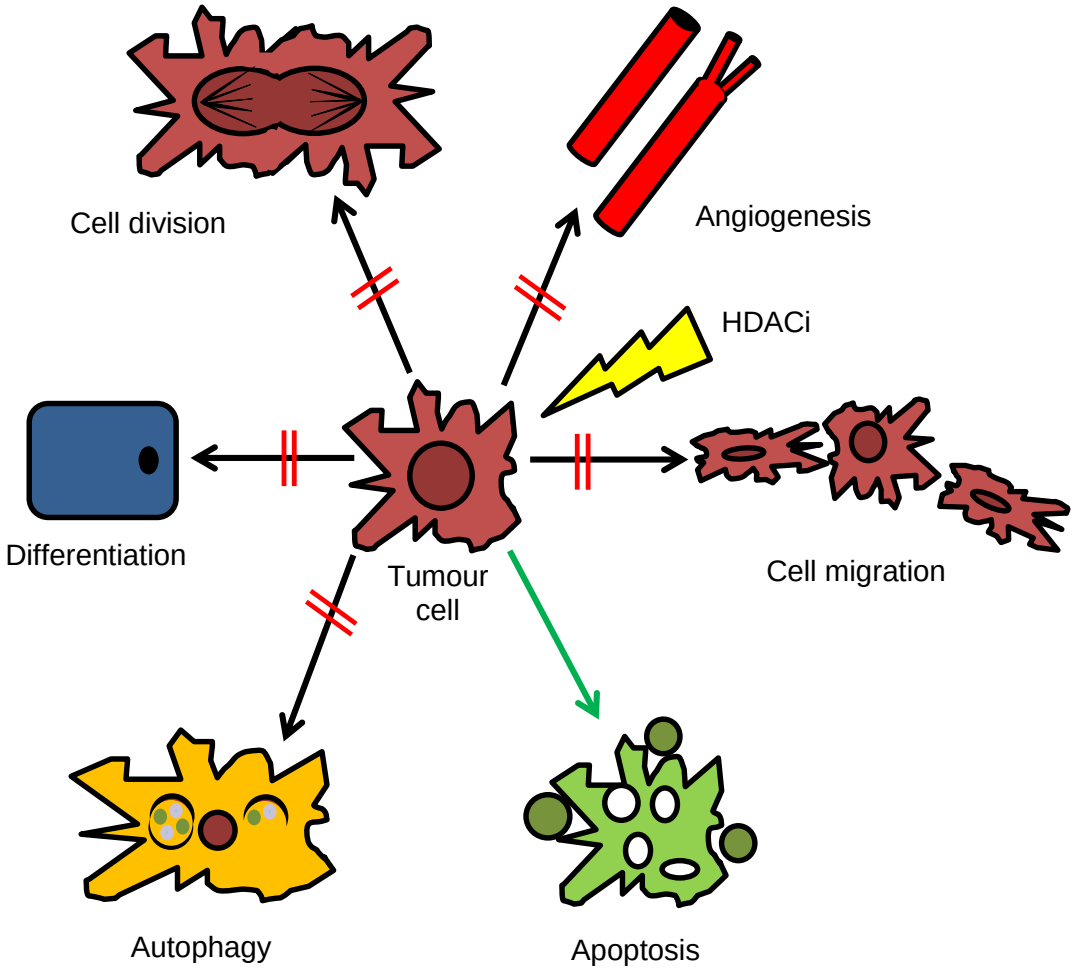

Figure 1.9 – A schematic showing the standard properties of a tumour cell blocked by treatment with a HDACi. Tumour cells can undergo many processes under normal physiological conditions, and this diagram shows some of the processes that HDACis are known to stop, with red lines through the arrows. Apoptosis is typically favoured, hence the green arrow. Adapted from (New et al. 2012).

1.4.1 Cell Death and Related Responses to HDACis

As it is typically the aim of the therapy, the effects of HDACis on cell death in cancerous cells is well explored. How these translate into normal cells is of much interest to researchers looking to explore the side effects of HDACis, or utilise them elsewhere.

1.4.1.1 Apoptosis, Necrosis, Necroptosis and Autophagic Cell Death

Apoptosis is the controlled, programmed cell death that occurs without outside stimulus,resulting in minimal inflammation. It is the most studied and evolutionarily conserved form of programmed cell death, and alternations in this can lead to cancerous cells developing. In contrast, necrosis is passive cell death occurring due to a stimulus from the outside environment, resulting in the release of inflammatory cellular contents (Fink et al. 2005). Necroptosis is another form of non-apoptotic cell death, usually occurring when the caspase proteins triggering apoptosis are inhibited. Autophagic cell death usually takes place as a result of stress conditions, and is often linked to other cell death pathways. It is a lysosome-dependent process utilised normally in the cell to degrade unnecessary or dysfunctional cellular components, but can also be part of a programmed cell death pathway. However, there is a debate as to whether autophagy is simply as a result of other cell death pathways, or separate in its own right. Cells can die via other caspase-dependent death pathways such as pyroptosis, and also caspase-independent cell death pathways (Tait et al. 2014).

Many different death resulting phenotypes can form as a result of HDACi treatment (Xu et al. 2007), including apoptotic pathway activation (Frew et al. 2009), autophagic cell death (Shao et al. 2004; Robert et al. 2011) and mitotic cell death (Atadja et al. 2004; Dowling et al. 2005). Cancerous cells have abnormal cell death pathways, which is one of the key reasons uncontrolled tumour growth can occur. HDACi treatment of cancerous cells results in an increase in pro-apoptotic and a decrease in anti-apoptotic proteins (Xu et al. 2007; Dell'Aversana et al. 2012; Bose et al. 2014).

Most of the work related to the effect of HDACis on cell death has been carried out on cancerous cells. Despite reports of normal cells being resistant to HDACis, it is incorrect to assume that normal cells are not going to suffer cell death from HDACi treatment. A study undertaken in 2009 showed that at clinical concentrations, SAHA activates the mitochondrial apoptosis pathway in normal cells. The cells resisted the apoptotic effect of SAHA for 24 hours, but 60% of cells had died after 72 hours of exposure (Brodska et al. 2009). This is despite having received clinical approval, with strong claims that normal cells are not affected (Richardson et al. 2008). Furthermore, necrosis and apoptosis have been observed in normal peripheral blood lymphocytes (as well as in a cancerous lymphocyte line) when treated with

SAHA (and NaB) (Brodská & Holoubek 2011). In another study, SAHA has been shown to induced apoptotic cell death in normal human lymphocytes (Kuzelová et al. 2010), and SAHA and MS-275 increased apoptotic pathways in bone marrow derived stem cells (Di Bernardo et al. 2009). This just serves to highlight some examples of SAHA's potential to cause cell death. Due to its clinical approval, it is one of the more explored compounds in this field.

1.4.1.2 Reactive Oxygen Species Accumulation

As well as the above cell death pathways, HDACis are also known to cause cell death through the disruption of mitochondrial membrane proteins, resulting in increased levels of reactive oxygen species (ROS) in the cell (Ruefli et al. 2001; Rosato et al. 2003). It has been reported that normal cells have a resistance to this effect (Qiu et al. 1999; Atadja et al. 2004; Kelly et al. 2003). However, that isn't to say that researchers utilising HDACis shouldn't be aware and monitor this, especially as there is evidence of this happening in normal human cells (Brodská & Holoubek 2011).

1.4.1.3 HDACi Effect on the Cell Cycle, DNA Damage Response, Proliferation and Mitotic Cell Death

The cell cycle is the name given to the normal series of events that a cell will go through to prepare for and undergo cell division prior to the processes of proliferation and differentiation. In normal cells this is monitored with checkpoints in between phases, which can be activated to halt the cell cycle, and in turn cell division, when needed (Majdzadeh et al. 2008; Jiang & Hsieh 2014). When the DNA is damaged, the spindles on that DNA is damage or not aligned correctly, or the previous cell cycle does not finish correctly, and so checkpoints will be activated and prevent the progression of the cell cycle. If possible DNA will be repaired and the cycle will continue as normal. This prevents the transmission of a mutated genome to future generations of the cell. Any loss or damage to the cell cycle checkpoints, such as is common in tumour cells, results in a growth advantage for tumour cells and a loss in protective mechanisms. A halt in the cell cycle also halts the proliferation of the cells, and a lack of this halting is what causes uncontrolled cell division in cancers (Bose et al. 2014; Qiu et al. 2000).

Cancerous cells have disrupted cell cycle checkpoints, but on treatment with HDACis, cell cycles in cancerous cells can be halted at the either G1 or the G2 phase of the cell cycle. Halting these cells at the cell cycle checkpoints can then result in the cell's normal apoptotic mechanism being activated (Johnstone 2002). The lack of cell cycle arrest at the G1 phase in cancerous cells has been linked to a specific gene – $p21^{WAF1}$ (Chen et al. 2004). When the acetylation of histones associated with $p21^{WAF1}$ increased with HDACi treatment, there was a resulting drop in HDAC1 bound to the $p21^{WAF1}$ promoter region, and consequential cell-cycle arrest at the G1 point (Gui et al. 2003). This is a slow cell death pathway. Cells can also arrest at the G2 checkpoint and undergo an aberrant mitosis (Qiu et al. 2000; Burgess et al. 2004).

Alterations in cell cycle is one of the key anti-cancer mechanism of HDACis, and a key factor in determining the specificity of HDACis for normal cells (Burgess et al. 2004; Qiu et al. 2000), and is an effect observed utilising HDACIs with many types of cancers, for example in colon cancer (Wilson et al. 2006; Jackson & Evers 2009; Gum et al. 1997).

As with many of the effects of HDACis on cells, the effects of HDACis on the cell-cycle are found to be less for normal cells than transformed cells. The cell-cycle is still affected in normal cells, but because normal cells have intact cell-cycle checkpoints, the effects are less pronounced (Schroeder & Westendorf 2005). Normal cells have fully functioning cell-cycle arrest points, typically not possessed by cancerous cells (Qiu et al. 2000). Studies on normal cells such as osteoblasts found the cell cycle of such cells to be uninterrupted on treatment with HDACis (Schroeder & Westendorf 2005). However, the opposite has been found in other cell types, such as epithelial cells (Davis et al. 2000). Human bone marrow MSCs treated with HDACis MS-275 and SAHA were arrested at the G1 phase of the cell cycle. With the MS-275 treated cells, there was a reduction in the S phase, which was not seen in the SAHA treated cells. In the SAHA treated cells, a G2/M reduction was observed, which was not seen in the MS-275 cells (Di Bernardo et al. 2009). This may be due to the inhibitors acting upon different HDAC isoforms.

HDACis can also induce a forced cellular senescence (Xu et al. 2005). Although it has been reported that normal cells treated with HDACis showed no evidence of

senescence (Xu et al. 2005), this contrasts with a study with human MSCs and the MS-275 and SAHA, where different effects on senescence and death pathways were observed (Di Bernardo et al. 2009).

A number of studies have shown that the effect of HDACis on the cell cycle in turn affects the proliferation capacity of the cells. HDACis can halt proliferation of the cancerous cells and subsequent cell death, but importantly cancerous cells that are not proliferating are also targeted and die; although the death effect takes longer to begin. In contrast, the cell cycle and proliferation of normal cells are stopped by HDACis, but it is reported that they do not die as a consequence of this (Qiu et al. 2000; Burgess et al. 2004). A summary of this can be seen in Figure 1.10.

Investigating specific HDAC isoforms linked to the cell cycle, HDAC1 and HDAC2 are known to be of particular importance. In several studies, it was found that inhibiting HDAC1 induced a partial G1/S cell-cycle arrest, resulting in reduced cell proliferation (Lagger et al. 2002; Zupkovitz et al. 2010). The complete deletion of HDAC1 has no effect on proliferation; however, deletion of both HDAC1 and HDAC2 leads to a stronger G1 cell cycle arrest. It is known that both HDAC1 and HDAC2 (that have overlapping effects), and the p21 and p57 genes, are key to the regulation of the G1-to-S-phase transition in a normal cell cycle (Yamaguchi et al. 2010; Wilting et al. 2010). It appears, when HDAC1 is deleted, HDAC2 can compensate, probably due to overlapping functions. HDAC1 and HDAC2 were found to be key to the cell cycle progression of renal fibroblast cells (Pang et al. 2011). Silencing of HDAC2, but not HDAC1 resulted in an increased protein level of p27, a negative cell cycle regulator. It was also found that the down-regulation of HDAC1 and HDAC2 both had an effect on the signal transducer and activator of transcription 3 (STAT3) signalling pathway. HDAC1 and HDAC2 are essential to the activation of these pathways, which affect the proliferation of these cells (Pang et al. 2011). Finally, in the previously mentioned study, the HDAC1, HDAC2 and HDAC3 specific MS-275 was found halt the cell cycle at the G1 checkpoint, and a reduction of cells in the S phase of the cell cycle (Di Bernardo et al. 2009). This is cell type dependent; however, with variance found between different cell lines (Senese et al. 2007).

As well as HDAC1 and HDAC2, HDAC3 has also been found to play a role in the progression of cell cycle. In a study with HeLa cells, a cancerous cell line, researchers found that a HDAC3 complex is essential in the regulation of cellular spindle function and microtubule attachment during mitosis (Ishii et al. 2008). When HDAC3 was deleted in a mouse model, Bhaskara et al. found it resulted in early embryonic lethality. This lead them to examine cells derived from the HDAC3 deficient mouse embryos, finding the cells died by an apoptotic pathway. However, unlike the mitotic catastrophe effect of a halted cell cycle, this was due to DNA damage and inefficient repair of the DNA double strand breaks. In transformed and cancerous cells, HDAC3 inhibition/deletion results in mitotic catastrophe apoptosis, which is likely because it's combined with these DNA damaging effects. In normal cells, these DNA damage effects are repairable, so HDAC3 inhibition does not result in cell death (Bhaskara et al. 2009).

For even greater detail in this area, reviews have been undertaken into the exact pathways and ways by which different HDACs affect the cell cycle and cellular proliferation (Reichert et al. 2012; Gabrielli et al. 2011).

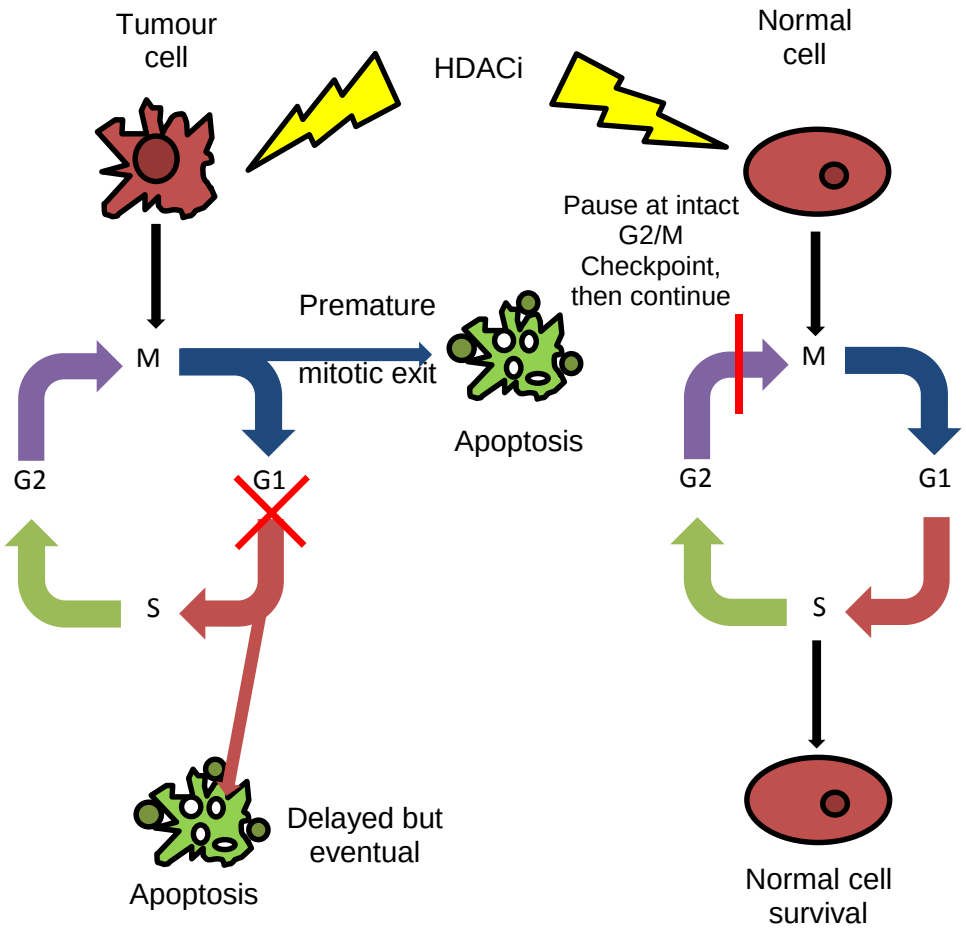

Figure 1.10 – Effects of HDACi on the cell cycle. When treated with a low concentration of a HDACi, normal cells continue the normal cell cycle and pass the G2/M checkpoint to survive the treatment. When treated with a HDACi, during the late G1 and S phase, tumour cells undergo aberrant mitosis and a rapid apoptotic effect results. When treated during the G1 phase, there is a G1 arrest, and a delayed but eventual apoptosis. Adapted from (Burgess et al. 2004; Johnstone 2002)

1.4.2 DNA Alteration and its Effects on Mitosis

Another way HDACis can affect cells, which is different to, but related to the effects on the cell cycle, is by altering the cell's DNA. This can be either by causing direct damage or by targeting the cell's mitotic DNA replication processes (Eot-Houllier et al. 2009). Some researchers believe this induced genomic instability is often overlooked in clinical trials (Eot-Houllier et al. 2009). For example, HDACis such as SAHA can directly damage DNA (Petruccelli et al. 2011). To make matters worse, HDACis, by multiple mechanisms, can also inhibit DNA repair mechanisms (Bose et al. 2014). HDACis can also effect the centromere (the central linking part of the chromosome), which can lead to catastrophic cell death (Zhang et al. 2010).

Lee at al. (2010) found that SAHA caused damage to the DNA of both cancerous and normal cells; however, this was found to be reversible in normal cells (J. H. Lee et al. 2010). This is not always the case, as when treated with SAHA, VPA, MS-275 and NaB, normal human fibroblast cells demonstrated a reduced double strand break repair capacity (Purrucker et al. 2010). This effect on DNA often reported as not relevant in normal cells, and that damage may be reversible, but there as this evidence suggests, this is not always the case.

While the majority of studies in the past have focused on the effects of HDACis on cancerous cells, an increasing number investigate the effects of HDACis on normal cells. It is not only the proliferative capacity, cell cycle and DNA damage response of the cell that is altered by HDACi treatment; the differentiation capacity can also be altered. The ability of compounds such as HDACis to alter, and potentially control, stem cell fate is a very attractive prospect for researchers. Stem cells therapies and their applications, such as tissue engineering, may benefit greatly from this increased control.

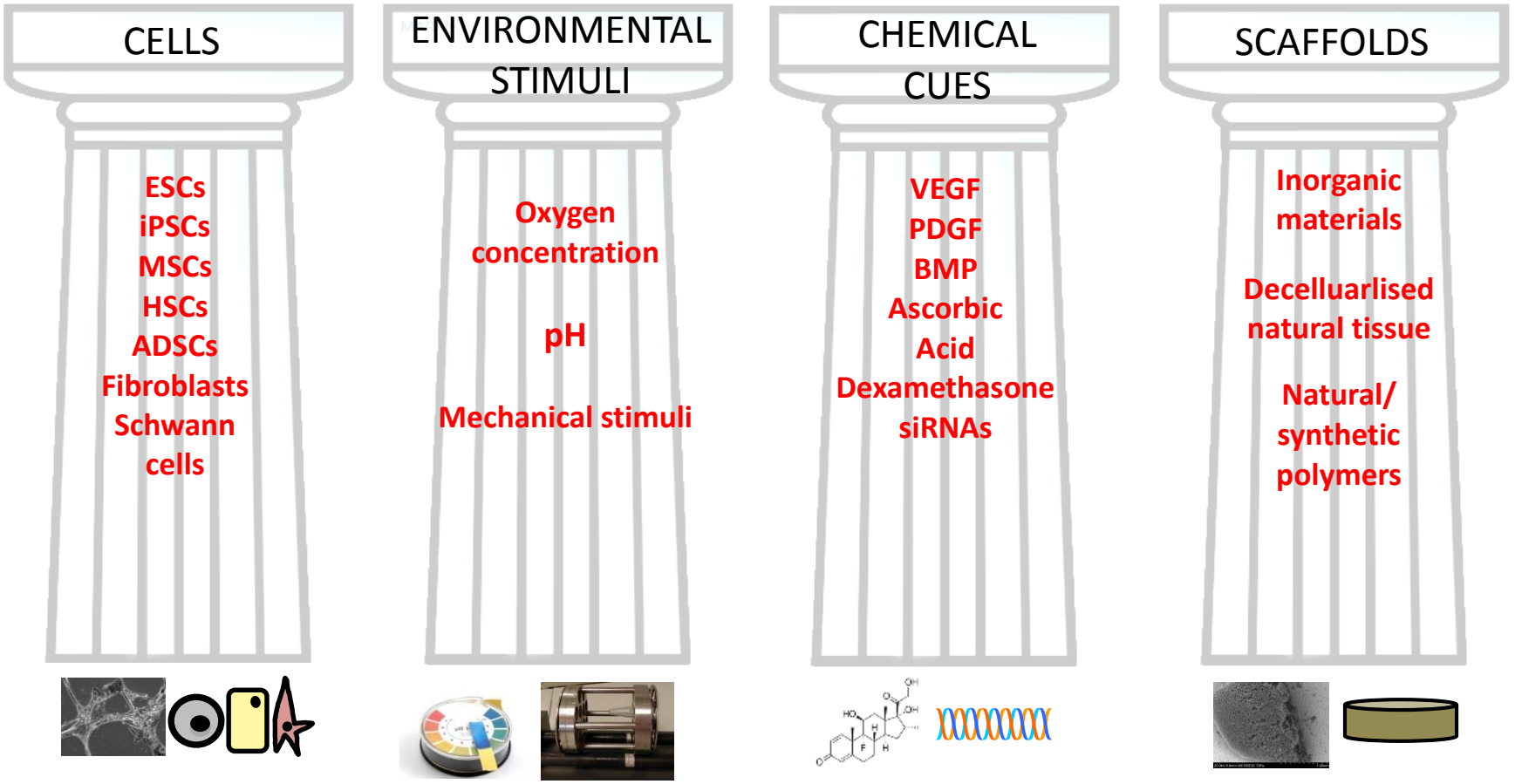

Figure 1.11 – The four key pillars of tissue engineering. From left to right: Cells, Environmental Stimuli. Chemical cues and scaffolds, with examples listed, and pictures of each. All pictures are the author's own.

1.5 Tissue Engineering of Bone

Tissue engineering comprises of four (sometimes simplified to three) key pillars: cells, scaffolds, growth factors/bioactive molecules and environmental/mechanical stimulation (Figure 1.11) (Kessler & Grande 2008).

1.5.1 The Clinical Need and Current Practices

There is a major clinical need to regenerate tissues and organs (Naderi et al. 2011; Payne 2013). In developed countries, such as the United States, the expenditure on functional bone grafts is expected to double between 2012 and 2020, to meet the increased and aging population. Expenditure was over $2.5 billion annually in 2012. Tissue engineered bone grafts are needed for fracture repair and the restoration of bone lost due to injury, congenital disorders and degenerative diseases. There is the potential for tissue engineering to provide some solutions to this; however, the field is still currently struggling to produce actual *functional* tissue regeneration (Amini et al. 2012).

Tissue engineered devices should mimic the natural biology of the bone, allowing for ingrowth of bone (osteoconduction), or the promotion of new bone formation (osteoinduction and osteogenesis). For this to take place successfully, implants should be able to integrate into the natural environment, allowing for diffusion of cells, natural growth factors, chemicals and signals that will promote osteoconduction/osteoinduction. In bone, these processes involve extracellular matrix deposition, mineralisation, vascularisation and a controlled and minimal inflammatory response to the newly implanted material. The implant should ideally degrade at the same rate new bone is being deposited. As all bones in the body have a structural, supportive function, the mechanical integrity of any tissue engineered material is also key (Ericka M. Bueno & Glowacki 2011; McMahon et al. 2013; Xiadou Wang et al. 2010).

Currently, allografts and autografts are used in the clinic for bone tissue repair. Allografts of bone from sources such as cadavers do not have a good integration with the host tissue, as well as having a relatively high risk of infection. Furthermore, the tissue quality harvested for these grafts can be very variable.

Autografts, which are currently considered the gold standard, have superior integration in the site, primarily due to them being fully vascularised on transplantation. However, with autografts, the tissue source is much more limited and there are associated complications with donor site morbidity (McMahon et al. 2013; Xiadou Wang et al. 2010).

Theoretically, tissue engineered constructs could be transplanted in patients to replace the need for autografts and allografts. There has been limited exploration of these in the clinic, with the majority of reports being a single component of cells, scaffolds or growth factors, not a combination of two or three. Therefore, currently, there is much scope to develop combined approaches for bone tissue engineering, utilising cells, scaffolds growth factors and environmental stimuli (Liu et al. 2013).

1.5.2 The Biology of Bone

1.5.2.1 Bone function

Bone has four main functions in the human body (Pocock & Richards 2006):

1) Protection and support for the body, through supporting tissues such as muscle, tendons and ligaments.
2) Supporting movement of the body by being able to articulate at the joints.
3) A homeostatic role providing a mineral deposit for the body.
4) Storage of bone marrow, thus playing a role in repair and regeneration of other tissues in the body, such as through haematopoietic stem cells forming blood and immune system cells.

1.5.2.2 The Structural Constituents of Bone

Bone is often crudely thought of as simply a rigid, inert, mass of hard tissue. However, on closer inspection bone is actually much more complicated than this. Bone is a living, dynamic structure, a specialist connective tissue, which will respond to the conditions that it is subjected to (Pocock & Richards 2006; D.L. Bartel et al. 2006). Bone is a very complex structure, with several quite distinct hierarchical levels. In the main skeleton, (i.e. not craniofacial bone that can have a different structure), there are two types of bone; cortical and trabecular. At a lower level, both are comprised of a composite of mineralized collagen matrixes.

Cortical bone is mainly located on the outside of long bone structures, forming a shell. Trabecular bone is found towards the centre of the cortical bone shells and towards the end of joints, where its more elastic properties aid in it acting in a load absorbing capacity. The articulating ends of the bone are covered in growth cartilage, a flexible but strong tissue that allows for bone growth (covered later) (Mackie et al. 2008). The outer layer of the bone is covered in the periosteum, a tough fibrous connective tissue with an inner layer capable of forming bone tissue. Long bones also contain a marrow cavity, where fatty yellow marrow is located, which is typically not involved in haematopoiesis. Haematopoiesis takes place in the red marrow, which is found in small, flat, irregular bones such as the sternum and ilium. A diagram of a typical long bone can be seen in Figure 1.12 (Pocock & Richards 2006).

When studying the material properties of bone, at the underlying hierarchical material level (0.5 – 1 mm scale), cortical and trabecular bone actually have similar structures. Both are made of lamellar bone structures. Lamellar bone is formed from a regular, highly organised, pattern of the collagen fibres. At a micrometre scale, cortical bone is comprised of many sheets of lamellar bone formed around the Haversian Canals. These canals provide the essential blood supply to the bone, necessary for essential functions such as nutrition supply and waste disposal. In contrast, trabecular bone (sometimes called spongy bone) at the micrometre scale is a more highly porous bone structure, in which the lamellar are arranged in less well organised packets than in cortical bone. Trabecular bone consists of rods and plates with irregular geometries, giving it a more porous structure than cortical bone (Donald L. Bartel et al. 2006; Pocock & Richards 2006).

A key difference between cortical and trabecular bone is the increased levels of new bone formation and bone remodelling in trabecular bone. This newly formed bone is less mineralised than the older cortical bone. Although, this may not always be the case, as trabecular bone has a more varied structure than cortical bone, which is largely dependent on the anatomical site as bone structure varies a lot between different anatomical sites. The age, lifestyle and medical history of the individual person from which the bone is being studied must also be considered (Donald L. Bartel et al. 2006).

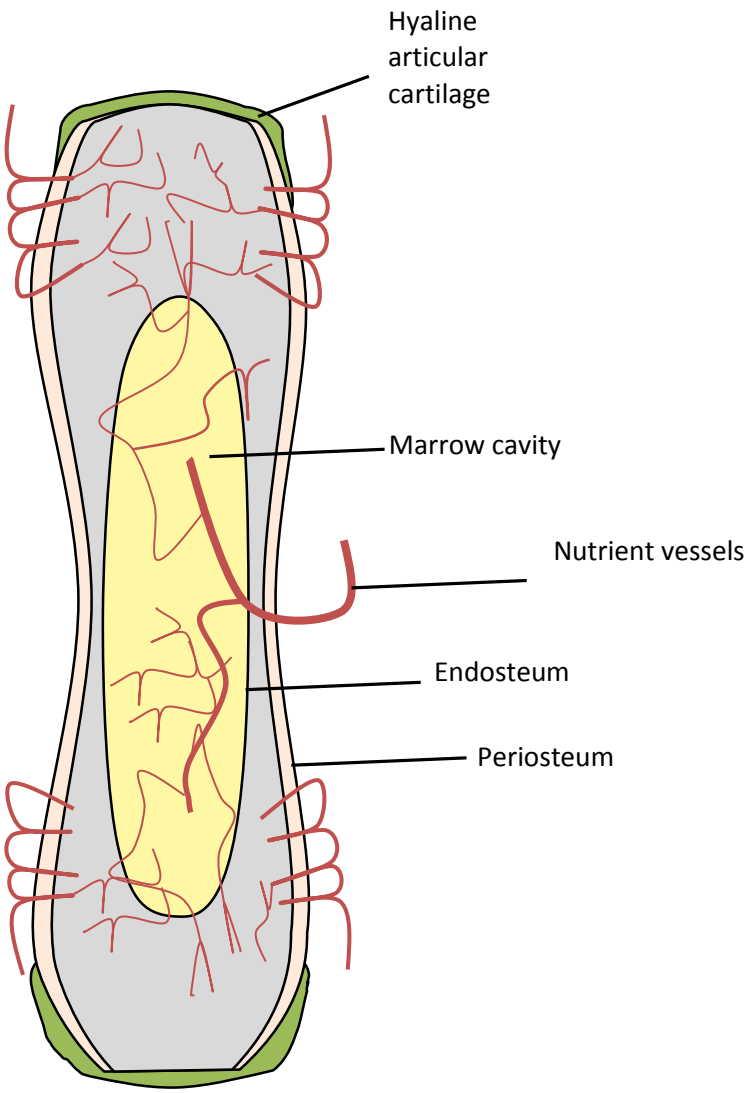

Figure 1.12 – The structure of a typical long bone. Adapted from (Pocock & Richards 2006).

1.5.2.3 The Cellular Constituents of Bone

There are three major cell types in bone: osteoblasts, osteoclasts and osteocytes (Pocock & Richards 2006; Gilbert 2000):

Osteoblasts – Located primarily on the bone surface and lining marrow cavities. These cells are responsible for bone formation, secreting bone constituents such as collagen, glycol proteins and also mineralise the newly formed bone by calcifying it. Calcification occurs when osteoblasts secrete a collagen-proteoglycan matrix. This is able to bind calcium and calcium salts, calcifying the osteoid bone matrix. In

tissue engineering, creating osteoclast-like cells is often the goal of researcher, due to the bone forming ability of these cells.

Osteocytes – Mature bone cells, which are terminally differentiated osteoblasts. They are trapped in lacunae, small spaces in-between the laid down mineralised bone matrix. They are responsible for movement of calcium through the bone, via tiny channels linking osteocyte cells to each other (canaliculi).

Osteoclasts – Larger than the other bone cells, they are responsible for bone resorption during bone growth and remodelling. They are found near bone surfaces where bone erosion is occurring.

1.5.2.4 Bone formation

Bone forms from two different processes, endochondral ossification and intramembrane ossification. Long bones are formed from endochondral ossification, which is via a cartilage intermediate. Flat bones form by intramembrane ossification, where cells condense to form bone directly, without a cartilage intermediate (Chen et al. 2012). How and when these processes take place depends on the physical environment of the site of formation and the biochemical cues present. Mesenchymal stem cells (MSCs) and/or other progenitor cells are key, as they can form a number of cells necessary to these processes, most importantly osteoblasts and chondrocytes. These formation processes are regulated by a number of complicated signalling pathways, including bone morphogenetic protein (BMP), Transforming growth factor beta (TGF-β), Indian hedgehog and Wnt signalling pathways (Chen et al. 2012; Mackie et al. 2008; Zhang et al. 2013).

1.5.3 Stem Cells

Stem cells, such as MSCs, are a key cell source for tissue engineering with the potential to be controlled, resulting in cells of the specific lineages required for creating and/or regenerating functional tissues, such as bone. Theoretically, stem cells will respond to virtually any stimuli they are subjected to, whether that be from scaffolds, growth factors, mechanical stimulation or any other external factors (Drummond-Barbosa 2008).

Control of the key pathways of stem cells to bone cells, such as the Wnt or BMP signalling pathways, could lead to improved osteogenic differentiation protocols, mimicking the environment in the body where bone is formed. Currently, chemicals such as dexamethasone, ascorbic acid and phosphate sources (El-Gendy & Yang 2012; Saha et al. 2013) are utilised, as well as osteogenic growth factors such as BMPs, to stimulate osteogenic differentiation of stem cells toward bone forming cells (Yang et al. 2003). These MSC derived, osteoblast-like cells can produce collagen matrix and modulate matrix mineralization and maturation (Vater et al. 2011). However, the current technologies either have limited efficacy, financial restrictions, ill-defined protocols or detrimental associated side effects, resulting in the search for additional or alternative approaches to enhance bone tissue engineering (Liu et al. 2013; Ericka M. Bueno & Glowacki 2011; Tollervey & Lunyak 2012).

1.5.3.1 What are Stem Cells?

Stem cells are a type of cell found in niches in the human body, capable of differentiating into other cell types. Differentiation is the process by which stem cells move down a cell lineage or derivation pathway, to progenitor-like cells, and finally to adult (somatic) cells. This more differentiated a cell is, the more limited the number of potential future cell divisions it has. The key, *defining*, property of stem cells is their ability to self-renew. Self-renewal is asymmetric cell division, where one of the resulting daughter cells is an identical copy of the original stem cell, while the other is a more differentiated cell (Gronthos et al. 2002; Hochedlinger & Plath 2009; Tollervey & Lunyak 2012).

It is important to understand the different classifications used for stem cells. One method of classification is related to cell potency; the ability of the stem cell to differentiate into different tissue types (Preynat-Seauve & Krause 2011). In order of most differentiation potential, to the least, cells can be classified as omni/totipotent, pluripotent, multipotent or unipotent. Totipotent cells, such as zygote cells, can differentiate to form every cell type in an organism. Embryonic stem cells are classified as pluripotent, because they can form all cells from the embryo, and consequently all adult tissues (just not the embryonic tissues). Multipotent cells are less potent and can give rise to usually just one lineage of cells; most adult stem

cells are classified as multipotent. Finally, unipotent cells can only maintain one cell type or lineage, and are considered terminally differentiated (Hochedlinger & Plath 2009). A schematic representation of stem cells losing their potency can be seen in Figure 1.13, whereas the stem cells move down the hills, they lose their potency and differentiate into other cell types.

Stem cells can also be categorised according to their origin, most simply either ‘embryonic’ or ‘adult’. However, the more recently discovered induced pluripotent stem cells are considered as a third major category (Takahashi et al. 2007; Park et al. 2008). Also to be considered is the emerging category of ‘neonatal’ stem cells, as well as all the populations associated with germ cells (Turnpenny et al. 2006). Furthermore, within the category of ‘adult stem cells’, further classification terms such as mesenchymal or hematopoietic can be used. These usually depend on the origin of the cells, or lineage that can result from them. Classifications such as totipotent and multipotent are not mutually exclusive; for example, hematopoietic stem cells are classified as multipotent stem cells. Poor characterisation of stem cell biochemical and molecular characteristics makes the classification of stem cells a difficult and constantly evolving process, and researchers are often at odds about how to classify them. In particular, the property of ‘stemness’, or differentiation potential, is difficult to describe and characterise. The indicator genes, biomarkers etc. responsible for this potential are not consistent across different stem cell populations. For example, compounding the problem, even the methods of determining stem cell genes and overlapping gene populations are not consistent (Ramalho-Santos et al. 2002). The exact definition of stem cells is often bought into question, as some researchers even question the property of self-renewal truly being a defining property of stem cells (Grafi & Avivi 2004). Epigenetic analysis and further understanding of epigenetics may hold some of the solutions to these difficulties.

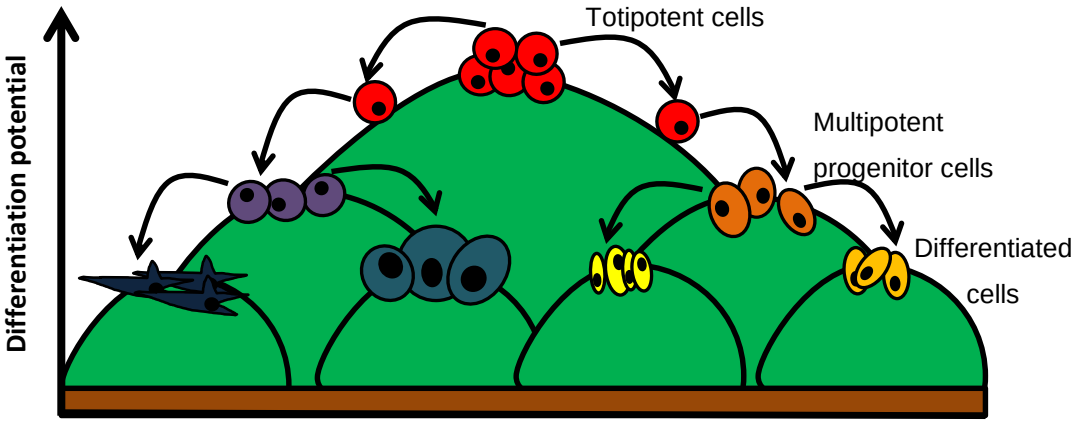

Figure 1.13 – Schematic summary of cells decreasing in differentiation potential. ‘The hills of differentiation potential’. As cells fall down to lower hills they lose their differentiation potential, becoming less stem cell like**.**

1.5.3.2 Mesenchymal Stem cells

The term ‘mesenchymal stem cell’ (MSC) is used to collectively describe multipotential stromal cells that can differentiate into a number of different tissues. However, the term is a confusing one, sometimes, particularly historically, used solely to describe bone marrow stem/stromal cells, the cells isolated only from bone marrow. However, the term has also evolved to be used to describe a variety of multipotential cells from different tissues, for example adipose (Zuk et al. 2001), synovial membrane (De Bari et al. 2001), skeletal muscle (Zammit & Beauchamp 2001) and dental pulp (Gronthos et al. 2000; Gronthos et al. 2002; Tomlinson et al. 2015). The multipotential of such cells has been demonstrated by generating a number of different tissue types, including those of the classic tri-lineage differentiation potential test; bone, cartilage and adipose tissues (Jones & Yang 2011; Lindner et al. 2010; Dudakovic et al. 2015). These cells don’t just differentiate into cells of the mesoderm; however, there has been work to demonstrate their differentiation into other lineages derived from other embryonic layers, such as neuronal (Zhao et al. 2002) and lung tissue (Ortiz et al. 2003), demonstrating the wider potential of these cells. However, there are limited examples of this, often with a lack of *in vivo* validation, along with a lack of evidence of these cells demonstrating lifelong self-renewal *in vivo* (Bianco et al. 2009). For these reasons, researchers are still debating if it is correct to name these cells multipotential cells, or perhaps even stem cells.

It is useful to compare MSCs to other stem cell populations for context. ESCs can differentiate into all embryonic tissues (of the endoderm, mesoderm and ectoderm), are relatively easily isolated from embryos, and have been extensively characterised with *in vivo* testing to prove their plasticity. However, there are a plethora of ethical and legal issues associated with ESCs. Hematopoietic stem cells can be found in a well-defined niche (a simple schematic of this can be seen in Figure 1.14) in the bone marrow, and their differentiation into all blood cell types has been demonstrated (Moore & Lemischka 2006; Keller 2005). Whereas cells currently classified as MSCs can be found in multiple different tissues/organs, and their niches are undefined in comparison.

These different cell populations are often collectively referred to as MSCs due to their ability to adhere to plastic (a property exploited in the routine tissue culture experiments carried out in laboratories), and their fibroblast like morphology. There have been attempts to find common surface markers among different MSC populations, and to fully characterise these, but there is still a lack of consensus this. This is why sometimes in the literature, these cells are referred to by other names, such as ‘multipotent adult progenitor cells’ (Lindner et al. 2010; Jacobs et al. 2013).

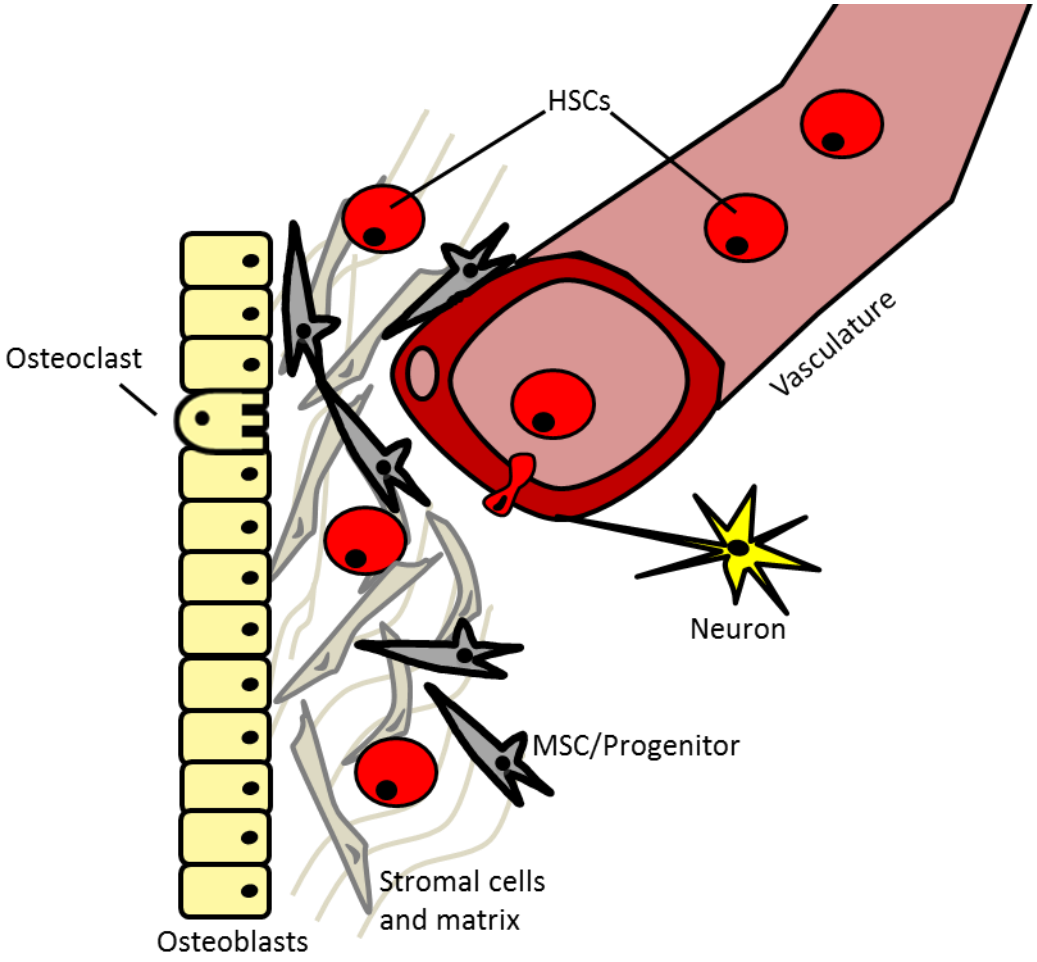

Figure 1.14 - Hematopoietic stem cell nice. A diagram of hematopoietic stem cells in the bone marrow niche they can be found. Adapted from (Moore & Lemischka 2006; Wang & Wagers 2011).

1.5.3.3 Adipose Derived MSCs

Human adipose derived stem cells (ADSCs) were discovered in subcutaneous fat, and isolated as a by-product of liposuction surgery (hence they were originally Processed Lipoaspirate Cells, or PLA cells) cells. Their multi-lineage potential was demonstrated *in vitro* (Zuk et al. 2001). Since then, ADSCs have been identified as one of the most promising sources of MSCs, largely due to their ease of harvesting compared to other MSCs from other sources such as bone marrow. ADSCs can also be isolated from alternative fat sources to subcutaneous fat (Dragoo et al. 2003), and have shown multilineage differentiation potential comparable to the current gold standard of bone marrow MSCs, with ADSCs being able to differentiate

into bone (Levi & Longaker 2011), cartilage (Erickson et al. 2002), nerve (Golipoor et al. 2010), endothelial (Planat-Benard et al. 2004) and cardiac (Lee & Kemp 2006) lineages. Controlling and improving upon these differentiation protocols is the focus of much research today, due to their huge potential for both autologous and allogenic treatments.

1.5.3.4 Epigenetics Markers and Stem Cells

There are strong links between epigenetic markers and the differentiation properties of stem cells. Epigenetics plays a key role in the differentiation potential of stem cells, and its role has been described elsewhere as “staggeringly complicated” (Tollervey & Lunyak 2012). Until relatively recently, when stem cells were analysed and discussed, it was usual for only the transcriptional regulation and factor networks to be focused upon. However, it has become apparent that the differentiation states and the potency of stem cells are linked to the cell’s “epigenetic landscape”. Epigenetics is key to defining the molecular base of pluripotency, reprogramming and early human development (Tollervey & Lunyak 2012; Teven et al. 2011). Different genes are switched on or off as cell potency changes, which is controlled by expression of different transcription factors and also processes linked to epigenetic control, such as chromatin remodelling. The fact that epigenetic modifications are heritable allows for the potential for modifications to early stage stem cells to have long lasting effects, and to possibly be utilised control stem cell lineages all the way from pluripotent cells to terminally differentiated adult cells.

Tollervey et al. define three classic cornerstones of epigenetics that orchestrate gene activity and pluripotency as (Tollervey & Lunyak 2012):

1. Chromatin remodelling and chromatin modifications.
2. DNA methylation of CpG dinucleotide (a cytosine nucleotide occurring next to a guanine nucleotide) regions of DNA.
3. The activity of non-coding RNA.

The effect of compounds such as HDACis directly and indirectly on chromatin modelling, one of the three key pillars, is therefore of interest to those looking to control stem cells. Studies have shown that as cells become less potent, they typically become more transcriptionally restrained, due to condensation of the

chromatin and an increase in heterochromatin levels. Levels of, and specific epigenetic markers can actually be used to assess potency of stem cells (Tollervey & Lunyak 2012; Stancheva 2011).

The vast and complicated pattern of epigenetic modifications has a role to play in stem cell pluripotency, differentiation and reprograming (Tollervey & Lunyak 2012; Kretsovali et al. 2012b; Liang et al. 2010). As more and more research is conducted into stem cells with the aim of producing cellular therapies, disease models and in tissue regeneration and creation, the fundamentals of stem cells need to be better understood. If this research is to be recreated on a larger, commercial scale, or improved to make more of an impact on the clinic, tools such as epigenetics need to be harnessed.

1.5.4 Epigenetics and HDACis as Tools in Tissue Engineering

HDACis can have a wide range of effects on cells, some desirable but some undesirable, as discussed previously. In theory, HDACis may be able to alter the differentiation properties of stem cells, allowing greater control of their fate. The advance of some HDACis to cancerous clinical trials has led to research investigating the side-effects of HDACis on naturally occurring stem cell populations that reside in the body, such as MSCs. For example, SAHA and MS-275 were found to reduce the stem cell like properties of human MSCS, as well as the previously mentioned effects of inducing cell cycle arrest, an increase in apoptotic death pathways and increased cellular senescence (Di Bernardo et al. 2009). These findings may not necessarily be a bad thing; a reduction in the differentiation potential, combined with the movement of a cell down a single lineage, may be beneficial.

From a translational research perspective, a number of alternative properties of HDACis on cells may make them a promising tool for the translation of tissue engineering. Potentially useful effects of HDACis include pain relief (Li et al. 2012; Naguib et al. 2012; Denk & McMahon 2012; Chiechio et al. 2009; Z. Zhang et al. 2011), anti-microbial (Steinmann et al. 2009), immune response modulatory (Schildberg et al. 2010; Kinugasa et al. 2008; Reddy et al. 2004; Choi & Reddy 2011), and anti-inflammatory properties (Shakespear et al. 2011; Bhavsar et al. 2008; Choi & Reddy 2011; T.-I. Kim et al. 2013).

Recently, more and more studies have emerged exploring the use of HDACis in bone tissue engineering. As well as bone, which will be covered in detail in the following sections, work has begun attempting to utilise HDACis for the regeneration of different tissues, such as cardiac (Ohtani & Dimmeler 2011), neural/nervous (Hsieh et al. 2004), adipose (Catalioto et al. 2009), dental (Duncan et al. 2011; Duncan et al. 2012), liver (Niki et al. 1999; Snykers et al. 2009; Knutson et al. 2008; Kurinna & Barton 2011), skin (Glenisson et al. 2007), pancreatic (Avrahami & Kaestner 2012), muscle (M.-S. Kim et al. 2008) and cartilage (Hong et al. 2009).

1.5.5 HDACis and Bone tissue Engineering

1.5.5.1 A brief history

Research into the effect of HDACis on bone really first began in the 1990s, when NaB was found to promote bone formation by osteoblast cells (Iwami & Moriyama 1993). Due to initial concerns about the side-effects of HDACis utilised in cancer therapies on bone tissue, several early studies also investigated the effect of HDACis on bone densities (Nissen-Meyer et al. 2007; Senn et al. 2010; McGee-Lawrence et al. 2011; Pratap et al. 2010). SAHA was found to have a number of worrying effects on bone cells in animal models, including the reduction of osteoblast numbers, harmful effects on mature osteoblasts, DNA damage and an overall loss of bone mass in animal models (McGee-Lawrence et al. 2011; Pratap et al. 2010). Similar concerns were held with VPA (Nissen-Meyer et al. 2007; Senn et al. 2010).

However, allaying the fears of some clinicians, a study published in 2013 found that while SAHA inhibited the proliferation of bone related cell populations, such as human bone marrow MSCs, it also increased their osteogenic differentiation potential *in vitro*. This indicates that perhaps SAHA didn't have a negative effect on bone cells, and that it could be a promising tool for both oncological and tissue engineering applications (Xu et al. 2013). However, problems can arise using animal models to draw conclusions about the effect of HDACis, as some species may be affected by HDACis in different ways (Senn et al. 2010). The exposure dose and length are also key factors when studying HDACis, therefore human clinical trials are needed to closely monitor the potential side effects.

1.5.5.2 HDAC isoforms and their links with bone cells

High levels of HDAC acetylation were found to block vitamin D stimulation of osteocalcin production and thus osteoblast differentiation (Montecino et al. 1999). It has been suggested that several specific HDAC isoforms are linked to osteoblast activity. In particular, HDAC3 is thought to be closely linked to bone tissue formation (Schroeder & Westendorf 2005; Schroeder et al. 2004; Razidlo et al. 2010; McGee-Lawrence et al. 2013). HDAC3 interacts with Runx2, supressing osteocalcin production and regulating progenitors differentiation into osteoblasts (Schroeder et al. 2004; Hesse et al. 2010; Lamour et al. 2007). During the differentiation of osteoblasts, HDAC3 activity is reduced, resulting in acetylation of histones 3 and 4. This balance of acetylation can be altered in cells by over or under expressing Nuclear Factor of Activated T Cells (NFAT) signalling (Choo et al. 2009). *In vivo* HDAC3 knockout reduced osteoblast levels and increased fatty deposits in bone marrow, seriously compromising skeletal health in mice (Razidlo et al. 2010). Another study found HDAC3 to be essential for bone maintenance during aging; when knocked down the mouse bone mass was reduced (McGee-Lawrence et al. 2013).

Of the other class 1 HDAC isoforms, similarly, HDAC1 is downregulated during differentiation of osteoblasts, making it another potentially interesting bone linked HDAC isoform to specifically target with inhibitors to induce osteoblast differentiation (Lee et al. 2006). Often overlooked as a class 1 HDAC, there has been a recent investigation into the role of HDAC8 in osteogenic differentiation, where it was discovered HDAC8 suppressed osteogenic-related genes expression, and inhibition of this with VPA promoted osteogenic expression of rat bone marrow stromal cells (Fu et al. 2014).

Jointly HDAC4 and HDAC5 have been found to play a role in osteoblast differentiation (Kang et al. 2005; Jeon et al. 2006). HDAC4 also specifically controls chondrocyte hypertrophy, which is involved in endochondral ossification during bone formation (Vega et al. 2004). Moreover, HDAC6 is linked to the differentiation of mesenchymal stem cells into osteogenic lineages (Huang et al. 2012).

Moving on from osteoblasts linked effects, both class I and class II HDAC isoforms are required for osteoclast differentiation (Cantley et al. 2011), and Romidepsin,

which preferentially inhibits class 1 HDACs, inhibits osteoclastogenesis (Nakamura et al. 2005). HDAC3 and HDAC7 appear to have opposite effects: suppression of HDAC7 accelerates osteoclast differentiation, while suppression of HDAC3 inhibits osteoclast differentiation (Pham et al. 2011). Similarly, other researchers have suggested that HDAC5 and HDAC6 activity will reduce osteoclast differentiation (J. H. Kim et al. 2011).

1.5.5.3 Current status of the potential of HDACis in *in vitro* bone tissue engineering

Although the specificity of different HDACis are questionable (Bradner et al. 2010), it is clear that there are obvious differences in effects between different HDACis on bone related cells. Lee et al. (2006) demonstrated that both NaB and TSA can increase osteogenic activity in rat cell lines, including upregulation of osteoblast marker genes (Lee et al. 2006). It has also been reported that NaB can also promote osteogenic differentiation of periodontal ligament fibroblasts (with the added benefit of modulating inflammatory reactions) (T.-I. Kim et al. 2013). Similarly, TSA, MS-275 and VPA have been shown to upregulate pre-osteoblasts osteogenic gene expression (Schroeder et al. 2007). However, others suggest that TSA may not actually induce osteoblasts maturation (Schroeder & Westendorf 2005; Iwami & Moriyama 1993). Other studies have found that HDAC1, HDAC2 and HDAC3 specific MS-275 stimulates bone regeneration both *in vitro* and *in vivo* (H.-N. Kim et al. 2011; Kim et al. 2012). Another HDACi, Largazole, was found to increase the *in vitro* osteogenic potential of C2C12 cell line cells, believed to be due to an increased expression of RUNX2 and BMPs (Lee et al. 2011). Thus, reports are conflicting, and the effects of HDACis on bone tissue engineering are still unclear and require further study.

It is clear that the choice of HDACi, delivery system and the length of time that cells are exposed to the HDACis may be vital (Jung et al. 2010). Several *in vitro* studies demonstrate the importance of controlling the length of time cells are exposed to the HDACis, often developing pre-treatment strategies to effect differentiation (Maroni et al. 2012; Xu et al. 2009; Cho et al. 2005).

1.5.5.4 Current status of the effect of HDACis on Osteoclasts

HDACis, such as Trichostatin A (TSA) and NaB, inhibit osteoclast differentiation (Iwami & Moriyama 1993; Rahman et al. 2003; Takada et al. 2006). In 2007, Yi e al. reported that TSA can actually cause osteoclast death (Yi & Baek 2007), and Kim et al. (2012) suggested that HDAC1, HDAC2 and HDAC3 specific inhibitor (MS-275) can reduce bone absorption by having a negative impact on osteoclast differentiation (Kim et al. 2012). These inhibitory effects on osteoclasts could be utilised to prevent bone loss in inflammatory disease (Cantley et al. 2012). Although, contradictorily, it has also been shown that TSA promoted the expression of RANKL, a ligand integral to osteoclast formation, function and survival (Fan et al. 2004).

1.5.5.5 Current status of the potential of HDACis in *in vivo* bone tissue engineering

In one of the key first studies utilising HDACis in bone tissue engineering, it was reported that the panHDACis TSA and NaB increased osteogenic differentiation of MSCs *in vitro* and *ex vivo* (Cho et al. 2005). However, these results could not be recreated in *in vivo* conditions (Boer et al. 2006).

In 2010, Hung HM et al observed an increased osteoblast differentiation over controls, when the α-calcium scaffolds loaded with TSA and NaB were placed in rat bone defect models (Jung et al. 2010). Elsewhere NaB and VPA have been used in combination with reduced oxygen environments and ADSCs to achieve the regeneration of bone tissue both *in vitro* and *in vivo* (Xu et al. 2009). Similarly Lee et al. demonstrated that collagen scaffolds soaked in Largazole solution could improve mouse bone formation in two models (Lee et al. 2011).

1.6 Introduction Synopsis

The actions of histone deacetylases (HDACs) remove the acetyl groups from lysine residues, leading to the formation of a condensed and transcriptionally silenced chromatin. HDACis block the action of HDACs, resulting in hyperacetylation of histones, thereby affecting gene expression. The use of these compounds has so far mostly been limited to cancer treatments, due to their profound effect on cancer cells while usually leaving normal cells unaffected.

However, research has begun to explore their use in other applications, such as tissue engineering. Different HDAC isoforms can be linked to different tissue types, such as bone. There is a highlighted clinical need to improve bone tissue engineering, leading to some research into how HDACis affect formation of bone and with the potential to utilise this in bone tissue engineering

1.7 Thesis Aims and Objectives

The **aim** of this study was to investigate the effect of HDACi MI192 on the behaviour of adipose derived stem cells, with the long term goal of improving the efficacy of bone tissue engineering.

The main **objectives** of the study:

1) To synthesise and characterise MI192.
2) To investigate the effect of MI192 on the general properties of ADSCs.
3) To investigate the effect of MI192 on the differentiation (osteogenic and adipogenic) of ADSCs, in 2D.
4) To investigate the effect of MI192 on *in vitro* 3D models of bone tissue engineering.
5) To investigate the effect of MI192 on the gene expression of ADSCs, without any induction of differentiation.

Chapter 2: General Materials and Methods

This chapter describes all of the general materials and methods that apply to the subsequent chapters. Those individual chapters also have methods specific to those chapters where relevant.

2.1 General reagents

All reagents (e.g. hydrochloric acid (HCl), dimethyl sulfoxide (DMSO) and ethanol (EtOH)) were purchased from Sigma-Aldrich, unless otherwise stated.

Tissue culture flasks and plates were purchased from Corning. General reagents used for cell culture were phosphate buffered saline (1x PBS, pH 7.4 without Ca or Mg, Lonza, Cat. no: BE17-516F), Alpha minimal essential medium (α-MEM, without L-Glutamine, Lonza, Cat. no: BE12-169F), fetal calf serum (FCS, Sigma, Cat. no: F9665), penicillin-streptomycin (P/S, Sigma Cat. no: P4333), L-glutamine (L-G, Sigma, Cat. no: G7513) and 0.25 % (w/v) trypsin-EDTA (Ethylenediaminetetraacetic acid) solution (T/E, Sigma-Aldrich, Cat. no: T4049). 'Basal medium' refers to α-MEM supplemented with 10 % FCS, 1 % P/S (10,000 units/mL penicillin, 10 mg/mL streptomycin) and 1 % L-G (200 µM).

2.2 MI192

Unless otherwise stated, MI192 used was the batch synthesised in Chapter 3: The Chemical Synthesis of MI192. HDACi MI192 was dissolved in DMSO to make a 10 mM stock solution (3.8148 mg in 1 mL DMSO). The stock was then added directly to culture medium to make the desired concentration. All media containing MI192 were made fresh to use, never stored, to avoid any MI192 degradation in solution. The concentration of DMSO in cell culture was always below 0.5 %, so as to have a minimal cytotoxic effect on cells. The effect of DMSO on ADSCs was investigated to ensure that the concentrations used in this thesis were not having an adverse effect on the ADSCs. The results can be seen in the Appendix (A3 - Investigation of the effect off 1% – 0.01% DMSO has on ADSC cell number and viability).

2.3 Cell Culture

All cell incubations were carried out in an incubator at 37 °C, 5 % CO_2 and greater than 90 % humidity. All cell culture experiments were carried out aseptically in a class II biological safety laminar flow hood.

2.3.1 Cell detachment and seeding

To detach cells, medium was aspirated and cells were washed twice with 1x PBS prior to being incubated in T/E for 5-10 minutes, until complete cell detachment was observed (confirmed under a light microscope). The resulting cell suspension was centrifuged at 1100 RPM for 5 minutes, the supernatant was aspirated and the cell pellet was re-suspended in the appropriate culture media. Cells were counted and seeded at different densities according to experimental design.

2.3.2 Cell Counting

To determined cell numbers, a mixture of a 40 μl cell suspension with equal volume of trypan blue (Sigma-Aldrich, Cat. no: T8154) was added in both sides of a haemocytometer, and the cell number was manually counted under a light microscope. Any cells stained dark blue were determined dead or not viable, and were not counted. The total viable cells in 4 corner squares (of the 9 squares in one side's full grid) were counted and from the average cell number in 1 square was calculated. This was undertaken for both sides of the haemocytometer and the average of these was used for the cell count. Each square was 1 mm x 1 mm so the total area was 1 mm^2. The depth of each square was 0.1 mm, so the final volume of each square was 100 nL. The total number of cells could then be calculated by multiplying the cell count by the trypan blue dilution factor, then by 10,000 and finally by the total volume of cell suspension:

$$Total\ cells = average\ cell\ number\ x\ dilution\ factor\ x\ 10{,}000\ x\ total\ suspension\ volume$$

2.3.3 Human Adipose Derived Stem Cells

Unless otherwise stated, human adipose derived stem cells were purchased from Life Technologies (STEMPRO® Human Adipose Derived Stem Cells, Cat. no: R7788-110/R7788-115)[1]. The cells are isolated from human adipose tissue collected during liposuction procedures and cryopreserved from primary cultures. Before cryopreservation, the ADSCs were expanded for one passage in MesenPRO RS™ Medium. Each lot of ADSCs originates from a single donor of human lipoaspirate tissue. Cells are prepared from low-passage (passage 1) adherent human adipose-derived primary cell cultures. Cells express a flow-cytometry cell-surface protein profile positive for CD29, CD44, CD73, CD90, CD105, and CD166 (> 95 %), and negative for CD14, CD31, CD45, and Lin1 (< 2 %). Unless otherwise stated, cells from 1 donor (Lot: 2118, cells isolated from the Abdomen of a 45 year old female) were used for all experiments.

2.3.4 *In vitro* expansion of ADSCs

All ADSCs were expanded in an 'expansion medium', MesenPRO RS™ Basal Medium (Life Technologies, reduced serum medium for long term culture of MSCs, Cat. no: 12746-012) supplemented with 1 % P/S. This was recommended for ADSC expansion by Life Technologies. The medium was changed every 3-4 days. Cells were passaged when approaching 90 % confluency. Cells of passage 5 were used for all experiments. To prove their multi-differentiation potential, P5 ADSCs from this donor underwent tri-lineage differentiation (osteogenic, adipogenic and chondrogenic). A summary of this can be seen in the appendix (A2 - Confirmation of tri-linage differentiation potential of ADSCs).

2.3.5 Osteogenic Induction Culture

Two different media were used for the osteogenic differentiation of ADSCs. Both media were changed every 3 – 4 days.

---

[1] Manufacturer's information for these cells can be found at http://tools.lifetechnologies.com/content/sfs/brochures/stempro-adsc-manual.pdf.

‘Osteogenic induction medium’ was used for short term induction experiments (1 - 10 days) to induce the early osteogenic differentiation of cells. This was ‘Basal medium’, as above, supplemented with 100 μM L-Ascorbic acid 2-phosphate sesquimagnesium salt hydrate (Sigma-Aldrich, Cat. no: A8960) and 10 nM dexamethasone (Sigma-Aldrich, Cat. no: D4902). It contained no mineral additional source.

‘Mineralisation medium’ (commercial name: StemPro® Osteogenesis Differentiation Media, Life Technologies, Cat. no: A10072-01) was used for long term induction experiments (over 10 days), to induce extracellular matrix mineralisation. The full contents are not disclosed by the manufacturer, but it presumably contains a mineral source. Manufacturer’s information states it contains a low glucose level, GlutaMAX™ glutamine source, standard serum level (10 %), no phenol red or HEPES buffer and sodium phosphate inorganic salts.

2.3.6 Adipogenic Induction Culture

To induce adipogenic lineage differentiation, the Zen Bio adipogenic culture protocol was followed, where two media were used sequentially. Firstly, cells were cultured in ‘adipogenic induction medium’ (Zen Bio, Cat. no: DM-2) for 7 days. After this, according to the protocol, a fixed amount (e.g. for a 12 well plate, 1.2 mL of the 2 mL total medium) of this induction medium was removed, then a fixed amount of ‘adipocyte maintenance medium’ (Zen Bio, Cat. no: AM-1) was added (e.g. for a 12 well plate, 1.6 mL was added). Cells were then cultured for a further 7 days before assessment.

2.3.7 Chondrogenic Induction Culture

For chondrogenic differentiation, cell pellets (2.5 x 10^5 cells per pellet) were cultured in chondrogenic induction media, which is serum free α-MEM supplemented with 1 % L-G, 1 % P/S, 0.1 μM dexamethasone, 10 ng/mL Human TGF-β-3 Recombinant Protein (Cambridge Bioscience, Cat. no: GFH109-2), 50 μg/mL L-Ascorbic acid 2-phosphate sesquimagnesium salt hydrate (Sigma Aldrich, Cat. no: A8960) and 1 % 100x insulin transferrin selenium solution (ITS–G, Life Technologies, Cat. no: 41400045), for 3 weeks. The medium was changed every 3 days.

2.4 Biochemical assays

Cells for biochemical assays were washed twice with 1x PBS and stored in a –80 °C freezer in a fixed volume per well of 0.1 % Triton X-100 (Fisher Scientific, Cat. no: BPE151-500) for a maximum of two weeks until needed. Cells were lysed when undergoing three freeze-thaw cycles of –80 °C and 37 °C, with scraping in-between.

2.4.1 PicoGreen® DNA quantification assay

After the cells were lysed in Triton X-100, DNA quantity was then assessed by Quant-iT™ PicoGreen® (Invitrogen, Life Technologies, Cat. no: P7581) DNA quantification assay. PicoGreen® reagent is an ultrasensitive fluorescent nucleic acid stain, which detects double stranded DNA in solution.

A 10 mg/mL DNA stock standard was prepared by adding 10.47 mg of DNA sodium salt from herring testes (Sigma-Aldrich, Cat. no: D6898) to 1047 µL of 1x Tris-EDTA (1x TE, Sigma-Aldrich, Cat. no: 93302) buffer and incubating for 60 minutes at 37 ºC on a shaker. The DNA concentration was checked on a Thermo Scientific ND1000 Nanodrop spectrophotometer. DNA standards were then prepared by adding this to 1x TE buffer; prepared standards ranged from 1 ng/mL to 1 µg/mL.

For the assay, 10 µL – 30 µL of cell lysate solution (prepared as above) was added to 70 µL – 90 µL of 1x TE buffer (giving a total volume of 100 µL). 100 µL of PicoGreen® reagent (a 1:200 dilution in 1x TE buffer) was then added to every sample and each standard, and was incubated at 37 ºC in the dark for 5 minutes. Three technical repeats of each biological repeat were performed. Blank reading wells of 100 µL of TE buffer, with addition of 100 µL of the PicoGreen® reagent, were also created, for background readings. The fluorescence was then measured in a Varioskan Flash Multimode Microplate Reader (Model 3001, Thermo Scientific) by exciting the samples at 480 nm, with emission reading set at 520 nm. The unknown value of DNA was then calculated using the standard curve generated, to give the ng of DNA. The total µg of DNA per well was calculated from the ng DNA per mL calculated and Triton X-100 harvest volume from each well.

2.4.2 Alkaline Phosphatase (ALP) Quantitative Assay

ALP quantity was assessed using the 4-nitrophenyl colourmetric phosphate liquid system. Standards (100 µM – 5 µM) for the ALP activity assay were prepared by a serial dilution of 4-nitrophenyl (10 mM solution, Sigma-Aldrich, Cat. no: N7660) in an assay buffer solution (60 µL 2 % aq. solution of Tergitol® type NP-40, Sigma-Aldrich, Cat. no: NP40S, in 10 mL 1.5 M alkaline buffer solution, Sigma-Aldrich, Cat. no: A9226, and 20 mL dH_2O). 10 µL of cell lysate solution was incubated in a 96 well plate with 90 µL of 4-nitrophenol phosphate liquid system (Sigma-Aldrich, Cat. no: 4264-83-9), along with the standards, for 45 - 60 minutes at 37 °C. Blank wells of 10 µL of cell lysis solution, with no cells, and the 4-nitrophenol phosphate liquid system were also set up, for background readings. Three technical repeats of each biological repeat and standard were performed. The reaction was stopped by addition of 100 µL of 1 M NaOH, (including addition to the standards), and the absorbance was read at 405 nm. The unknown value of ALP was then calculated using the generated standard curve, to give the mmol of ALP. The net (nmol/hour/well) ALP activity was then calculated from the mmol ALP multiplied by 1000, total Triton X-100 harvest volume, assay volume and time length of the ALP reaction (incubation time):

$$net\ ALPactivity = \frac{\left(\frac{(mmol\ ALP\ x\ 1000) x\ total\ Triton\ X - 100\ harvest\ volume}{incubation\ time}\right)}{assay\ volume}$$

2.4.3 Alkaline Phosphatase Specific Activity (ALPSA) Calculation

Alkaline phosphatase specific activity (ALPSA) for each well was calculated using the total ALP quantity divided by the total DNA content of the same well (nmol ALP/hour/µg of DNA):

$$ALPSA = \frac{Total\ ALP\ per\ hour\ per\ well\ (nmol)}{total\ DNA\ content\ per\ well\ (\mu g)}$$

2.5 2D Histological Staining

2.5.1 Alkaline Phosphatase Staining

Samples were washed twice in 1x PBS, fixed in 10 % neutral buffered formalin (NBF, Cellpath, Cat. no: BAF-0010-01A) for 60 seconds and washed with three washes of distilled water (dH_2O). The sample was then stained for ALP using the SIGMAFAST™ BCIP®/NBT kit (Sigma-Aldrich, Cat. no: B5655). One tablet from the kit was dissolved in 10 mL of dH_2O, and the cells stained with this solution for 30 minutes to 1 hour 37 °C in darkness. Cells were then washed with dH_2O, left to air dry and observed under a Leica DMI6000 B inverted microscope. A blue coloured stain indicates ALP protein.

2.5.2 Alizarin Red Staining for Calcium Accumulation

Samples were washed twice with 1x PBS, fixed in 10 % NBF for 1 hour and then washed three times with dH_2O. The samples were then incubated with Alizarin Red solution (40 mM at pH 4.1 +/- 0.1, Millipore (UK) Limited, Cat. no: TMS-008-C) for 15 minutes at room temperature, followed by three washes of dH_2O and one further 1 hour wash in dH_2O on a rocking device. Cells were then air dried and observed under a Leica DMI6000 B inverted microscope. A red coloured stain indicates calcium deposition. The stain was then destained by adding 1 mL of 10 % cetylpyridinium chloride (Sigma, Cat. No: C0732) in 0.1 M phosphate buffer (pH 7.0) to each well and placing the plate on a rocking device for 1 hour, allowing the stain to dissolve into the solution. 10 µL extracts from each well were diluted with 90 µL dH_2O, and the absorbance was read on a plate reader at 550 nm. Blanks were prepared from 10 µL 10 % cetylpyridinium chloride and 90 µL dH_2O.

2.5.3 Von Kossa Staining for Mineral Nodule Formation

Samples were washed twice with 1x PBS, fixed in 10 % NBF for 1 hour and then washed three times with dH_2O. The samples were then incubated with a 1 % aq. silver nitrate (Sigma-Aldrich, Cat. no: S6506) solution at room temperature in a U.V. light box for 15 minutes. This was followed by three dH_2O washes and one wash with 5 % sodium thiosulfate (Sigma-Aldrich, Cat. no: S7026). Cells were then air dried and

observed under a Leica DMI6000 B inverted microscope. A brown/black colour stain indicates mineral deposition.

2.5.4 Oil Red O Stain for Lipid Droplets

Samples were washed twice with 1x PBS, fixed in 10 % NBF for 1 hour, washed three times with dH_2O, and then washed once with 60 % i-propanol (Sigma-Aldrich, Cat. no: 190764). The samples were then incubated with an Oil Red O Stain (20 µM pore filtered 0.3 % weight in 60 % i-propanol Oil Red O powder stain, Sigma-Aldrich, Cat. no: O0625) for 15 minutes. Cells were then washed with 60 % i-Propanol and then three washes of dH_2O. Cells were then air dried and observed under a Leica DMI6000 B inverted microscope. Red colour stain indicates lipid droplet accumulation. The stain was then destained by adding 500 µL of 100 % i-Propanol to each well and placing the plate on a rocking device for 1 hour, allowing the stain to dissolve into the solution. The absorbance at 500 nm of 100 µL extracts from each well were read on a plate reader. Blanks were made from 100 µL 100 % i-Propanol.

2.6 Histology of 3D samples

2.6.1 Paraffin Embedding and Sectioning

All 3D samples for histological analysis were processed in a VIP Tissue processor (Sakura) through 70 % EtOH, 90 % EtOH, 4 changes of 100 % EtOH, 3 changes of 100 % xylene and 3 changes of wax, prior to be embedded in paraffin. 5 µM sections were cut using a Leitz rotary microtome and mounted on glass slides using a 40 °C water bath. Slides used for histological staining were Superfrost™ Plus Microscope Slides (Fisherbrand™, Cat. no: 12-550-15) and slides used for immunohistochemical staining were Silane Adhesion Whitecoat slides (CellPath, Cat. no: MDC-0102-54A).

2.6.2 Taking Slides to Water

Prior to any histological staining or immunohistochemistry, paraffin sections on slides were ‘taken to water’ to remove the wax and hydrate the sections. This was done by immersing the slides in a bath of 100 % xylene (VWR, Cat. no: VWRC28975) for 5

minutes, two 100% EtOH baths for 5 minutes each and washing in running tap water bath for 5 minutes.

2.6.3 Haematoxylin and Eosin (H+E) Staining

After being taken to water, slides were stained with Harris's Haematoxylin (Shandon, Cat. no: 6765002) for 3 minutes, washed in a running tap water bath for 2 minutes, developed in Scott's tap water (Leica Microsystems, Cat. no: 02901) for 3 minutes, washed in a running tap water bath for 2 minutes and stained with 1 % aq. eosin (Leica Microsystems, Cat. no: 01592E) for two minutes. The slides were then immersed in a running tap water bath for 5 minutes, and two 100 % EtOH baths, for 5 minutes each, and in xylene for 2 minutes before mounting in DPX (p-xylene-bis (N-pyridinium bromide), Agar Scientific Cat. No: R1340). The stains were then observed under an Olympus BX50 microscope.

2.6.4 Weigert's Haematoxylin, Picrosirius Red and/or Alcian Blue Staining

After being taken to water, slides were then stained with Weigert's haematoxylin (an equal part mix of Haematoxylin Weigert's Solution A and Haematoxylin Weigert's Solution B, TCS Biosciences, Cat. nos: HS375-500 and HS380-500) for 15 minutes, then washed in a tap water bath for 10 minutes. Then the slides were (if required) stained with Alcian Blue (1 % w/v in 3 % acetic acid, TCS Biosciences, Cat. no: HS116-500) for 10 minutes, washed in a tap water bath prior to staining with a Picrosirius Red Stain Kit (Polysciences, Inc, Cat. no: 24901), following the manufacturer's instructions. Slides were immersed in solution A for two minutes, washed in tap water for 1 minute, immersed in solution B for 60 minutes and finally in solution C for 1 minute. Slides were then blotted dry, washed in two 100 % EtOH baths, for 5 minutes each, and washed in 100 % xylene for 2 minutes before mounting in DPX (p-Xylene-bis (N-pyridinium bromide), Agar Scientific Cat. No: R1340). The stains were then observed under an Olympus BX50 microscope.

2.6.5 Van Gieson Staining

After being taken to water, slides were then stained with Van Gieson Stain (Thermo Scientific Cat. no: 12688636) for 5 minutes, then washed in a tap water bath for 5 minutes. Slides were then washed, mounted and observed as in 2.6.4: Weigert's Haematoxylin, Picrosirius Red and/or Alcian Blue Staining.

2.6.6 Von Kossa Staining

After being taken to water, slides were then placed in a U.V. light box and stained with 1% silver nitrate (Sigma Aldrich Cat no: 209139) in dH_2O for 10 minutes. Slides were then washed in 5% Sodium Thiosulfate: (Sigma Aldrich Cat no: 217263) for 5 minutes, before washing in running tap water for 10 minutes, and counter staining in Van Gieson Stain for 1 minute. Slides were then washed, mounted and observed as in 2.6.4: Weigert's Haematoxylin, Picrosirius Red and/or Alcian Blue Staining.

2.7 Polymerase chain reaction (PCR)

Prior to quantitative real-time polymerase chain reaction (qRT-PCR), Ribonucleic acid (RNA) was isolated from cultured cells and reverse transcribed into complementary DNA (cDNA).

2.7.1 RNA Isolation

To extract RNA, cells were lysed by incubation for 10 minutes at room temperature with 600 µL per well (for a 12 well plate) of Trizol® reagent (Life Technologies Cat. no: 15596-026). Lysates were stored at -80 °C for a maximum of 14 days before RNA was extracted using an RNAase mini kit with an additional DNase digestion step (Qiagen, Cat. nos: 74104 and 79254) following the manufacturer's instructions. Briefly, the kit utilises a silica gel membrane column to bind RNA in the presence of high concentrations of salts. The RNA is loaded onto the column, where it attaches. The RNA attached to the column then goes through multiple wash steps, any genomic DNA contaminate is digested by the DNAse kit, and the RNA is finally eluted using UltraPure™ DNase/RNase-Free Distilled Water (Life Technologies, Cat. no: 10977035).

RNA quality and concentration was measured at 260 nm using a Thermo Scientific ND1000 Nanodrop spectrophotometer, and the purity calculated and checked using the 260:280 nm ratio. Ratios above 1.8 were considered of good purity, any below were treated with caution. RNA was frozen and stored at -80 °C until required.

2.7.2 Reverse Transcription

200 ng of RNA was then was transcribed to cDNA using a high capacity RNA-to-cDNA Kit (Applied Biosystems, Cat. no: 4387406), following the manufacturer's instructions. Briefly 200 ng of the RNA dissolved in water, 1 µL enzyme and 10 µL of 10x buffer were made to a total volume of 20 µL with nuclease-free water, and then reactions performed on a F. Hoffmann-La Roche Ltd. MJ Research PTC-100 ThermoCycler at 37 °C for 1 hour, followed by an enzyme denaturing step at 95 °C for 5 minutes. cDNA was stored at - 20 °C (for a maximum of 3 months) before use. Based on the manufacturer's recommendations, it was assumed that the reverse transcription reaction was 100 % efficient, so cDNA synthesised was the same amount as the RNA inputted.

2.7.3 qRT-PCR

Expression levels of different genes were determined by qRT-PCR using TaqMan gene expression assays. All reactions were carried out in 96 well semi-skirted PCR plates for a Roche LightCycler (Starlab Cat. no: I1402-9909), in TaqMan® Gene Expression Master Mix (Life Technologies Cat. no: 4369016) and UltraPure™ DNase/RNase-Free Distilled Water. The TaqMan® Assays have been optimised to be 100 % efficient by the manufacturer. Amplification curves were obtained using a LightCycler 480 real time QPCR system. All samples underwent a 10 minute 95 °C pre-incubation step, followed by 45 cycles of 10 seconds at 95 °C, 30 seconds at 60 °C and 1 second at 72 °C. Samples were cooled to 40 °C at the end of the 45 cycles. The cycle threshold (Ct) value was generated for each sample and the comparative Ct method ($2^{-\Delta\Delta Ct}$) was used to quantify gene expression levels, relative to a housekeeping gene.

2.7.4 Generation of standard curves

Optimal cDNA concentration for assays, and probe efficiency was investigated by plotting standard curves for each probe using known cDNA concentrations. The details and the standard curves can be found in A5.2 - Standard Curves for qRT-PCR Assays. Serial dilutions of cDNA were run with each primer/probe set to produce the standard curves. Values were generated from a day 0 sample of cells, against resulting Ct values for reactions where all other variables (water, master mix and probe used) all stayed the same. No template controls were also run to check for unwanted reactions. All reactions were run in triplicate and the average Ct value for each Log_{10} concentration of cDNA was plotted, to give the standard curve. cDNA concentration was determined suitable at 5 ng/reaction and all probes were found to be of sufficient efficiency for experiments.

2.7.5 Optimisation of Housekeeping Genes

For all experiments, it is standard practice to use an endogenous control housekeeping gene in qRT-PCR analysis, to normalise the expression of target genes. This housekeeping gene should expressed at a constant level in all samples, and is essential to act as a reference, reducing error in cDNA concentrations or reaction volumes (Rubie et al. 2005; Ragni et al. 2013). The more stable the housekeeping gene, the better for determining the change in expression of other genes. Glyceraldehyde-3-phosphate (*GAPDH*) is a commonly utilised housekeeping gene; however, it is believed that there are more stable genes available. Previous work in the department, and a journal article on the topic (Ragni et al. 2013), suggested that tyrosine 3-monooxygenase/tryptophan 5-monooxygenase activation protein (*YWHAZ*) may be a more stable gene, especially in differentiation protocols.

To assess this, a comparative study between *GAPDH* and *YWHAZ* was undertaken to determine the most stable housekeeping gene. For four different conditions from the adipogenic differentiation experiment outlined in Chapter 5: (5.2.5: Assessment of the effect of MI192 pre-treatment on the adipogenic gene expression of ADSCs) the expression of the two genes was calculated, in biological triplicate and with three technical repeats for a total of n = 18 for each condition. Graphs of the mean ± SE was plotted and the statistical significance was determined by Kruskal-Wallis 1 way ANOVA test of variance, using Graphpad Version 5. The graphs and statistical

analysis can be found in the Appendix (A5.1 - Choice of Housekeeping Gene for qRT-PCR Assays). There was a lower variance with the *YWHAZ* housekeeping gene between samples that resulted in this being selected for all qRT-PCR experiments.

Chapter 3: The Chemical Synthesis of MI192

This chapter introduces the key HDACi utilised in this thesis, MI192. The key property of MI192 is its selective for HDAC isoforms HDAC2 and HDAC3. The design of the compound is briefly discussed, along with the work undertaken involving the synthesis and characterisation of MI192 by the author in the Department of Chemistry, University of Leeds.

3.1 Introduction

MI192 was the most potent inhibitor found in a library of HDACis designed to be class 1 HDAC specific. It was discovered by the Grigg group in 2008 as part of a series of tetrahydroisoquinolines created by Martin Inham. MI192 was designed by M. Inham *in silico* in Accelrys Accord. Libraries of designed inhibitors were screened and then docked of the inhibitors into HDAC homology models, based on known HDAC structures, in AutoDock docking program (Zhu et al. 2010). Docking and enzyme binding was evaluated in SPROUT 6.2 (Morris et al. 1998).

MI192 has low molecular weight, microsomal stability and CYP450 inhibition, meaning it should have excellent drug like properties (Ogu & Maxa 2000). It is believed that MI192 is a slow binding HDACi (Boissinot et al. 2012). Boissinot et al. (2012) undertook an experiment to determine the inhibition activity of MI192 for all HDAC isoforms, in HeLa cell nuclear extracts (Table 3-1) (Boissinot et al. 2012). The IC_{50} value is the half maximal inhibitory concentration, and is a measure of the effectiveness of the compounds in the assay. This technique is commonly used to investigate how the strength of HDAC inhibition by HDACis (Sebaugh 2011).

The overall HDACi inhibition with HeLa cell extracts showed that TSA is a stronger HDAC inhibitor when considering all HDAC isoforms (Table 3-1). MI192 had comparable HDAC inhibition levels to MS-275.

Also undertaken was recombinant human HDAC isoform specificity profiling, as part of a collaborative effort with Cancer Research Technology (http://www.cancertechnology.co.uk/), undertaken by Amphora Discovery Corp, NC, USA (http://www.tekprotocol.com/amphora/#hdac), now part of Caliper Life Sciences (http://www.caliperls.com). The results generated from this give an indicator of the specificity of MI192, compared to some commercial inhibitors (Table 3-1).

The results from the HDAC isoform screen (Table 3-2) demonstrated the key characteristic of MI192, that it is specific for HDAC2 and HDAC3. The inhibition of HDAC3 by MI192 is ~60-140 fold stronger than MS-275 and Mocetinostat (MGCD0103). The inhibition of HDAC2 by MI192 is 40 fold more effective than MS275 and is comparable to that of MGCD0103. However, MI192 has ~26-140 less strength of binding to HDAC1 than MS-275 and MGCD0103. Therefore they found that MI192 is selective for HDAC2 and HDAC3, in contrast to commercial HDACis MGCD0103, TSA and MS-275 (Boissinot et al. 2012).

To date, there only two papers focusing on MI192, related to rheumatoid arthritis and leukaemia research (Gillespie et al. 2012; Boissinot et al. 2012). MI192 was found to be a very effective potential compound in both of these fields. These successes lead to further research avenues being explored for MI192, resulting in the collaboration between Leeds School of Dentistry and Department of Chemistry, exploring the effect of MI192 on stem cell differentiation.

The synthesis of MI192 has yet to be published; however, the route was established by the Grigg group, and a schematic of this approach can be seen in Figure 3.1. The synthesis of MI192 was undertaken by the author; the full synthesis route is explained in the materials and methods. The compound synthesised was characterised by NMR, compared to control batches of the compound and deemed pure, for biological experiments.

Table 3-1 - The inhibition of HDAC activity in HeLa cell nuclear extracts by MI192, MS-275 and TSA (Boissinot et al. 2012)**.**

Compound	HDAC inhibition (IC_{50} μM)
TSA	0.005 ± 0.0005
MS-275[a]	3.0 ± 0.2
MI192	1.5 ± 0.5

Table 3-2 – HDAC isoform specificity information for HDACis MI192, TSA, MS-275 and MGCD0103, for HDAC isoforms HDAC1, HDAC2, HDAC3, HDAC8, HDAC4, HDAC6 and HDAC7 (Boissinot et al. 2012)**.**

HDAC	TSA	MS-275[a]	MGCD0103[a]	MI192
HDAC1	0.0047	0.18 ± 0.06	0.034 ± 0.017	4.8
HDAC2	0.0084	1.2 ± 0.13	0.034 ± 0.008	0.030
HDAC3	0.0023	2.3 ± 0.80	0.998 ± 0.431	0.016
HDAC8	1.3	> 10	> 10	> 10
HDAC4-CAT	0.0074	> 10	> 10	5.0
HDAC6	0.0036	> 10	> 10	> 10
HDAC7	0.0057	> 10	> 10	4.1

[a] Values for MS-275 and MGCD0103 taken from the literature (Khan et al. 2008).

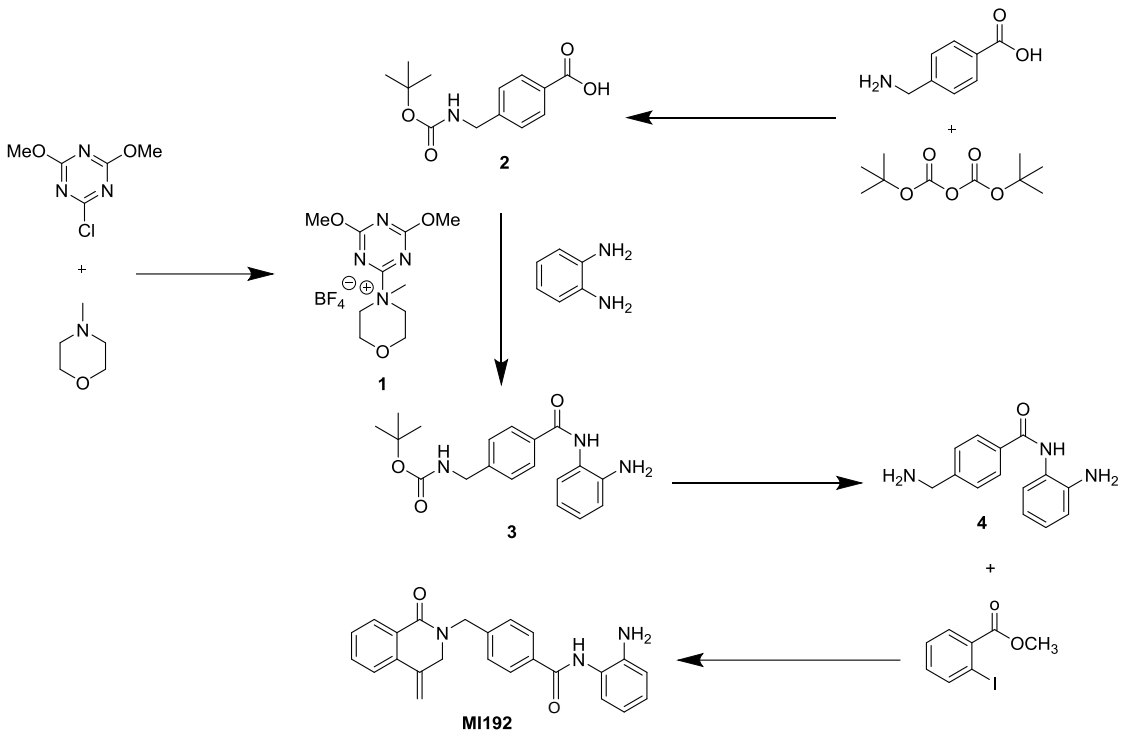

Figure 3.1 – The complete synthesis scheme of MI192. Compound **1** - 4-(4,6-Dimethoxy-1,3,5-triazin-2-yl)-4-methylmorpholinium tetrafluoroborate, compound **2** - 4-((Tert-butoxycarbonylamino)methyl)benzoic acid, compound **3** - *tert*-Butyl 4-(2-aminophenylcarbamoyl)benzylcarbamate, compound **4** - 4-(Aminomethyl)-*N*-(2-aminophenyl)benzamide.

3.2 Materials and Methods

All chemicals were obtained from Sigma Aldrich. ^{1}H NMR spectra were recorded at 300 Mhz on a Bruker DPX300 instrument. The deuterated solvents used for each compounds were recorded with the spectra. Chemical shifts are given in parts per million (δ) downfield from tetramethylsilane (0.00 δ). The following abbreviations are used: s – singlet; d – doublet; dd – double doublet; m – multiplet (n > 6). Column chromatograpghy was performed on silica gel 60 (Merck, 230-400 mesh). Full NMR spectra can be found in the Appendix (A.1 - NMR Spectra).

All reaction steps, except the final MI192 synthesis step, were first undertaken on a small, ~100 mg, pilot scale, to test and optimise the synthesis, before the large scale reactions were undertaken.

3.2.1 Synthesis scheme of 4-(4,6-Dimethoxy-1,3,5-triazin-2-yl)-4-methylmorpholinium tetrafluoroborate (compound 1)

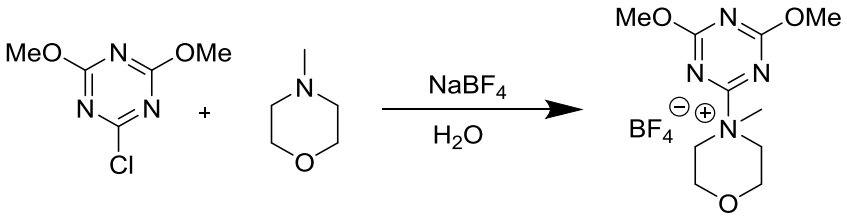

1

Figure 3.2 – Synthesis scheme of 4-(4,6-Dimethoxy-1,3,5-triazin-2-yl)-4-methylmorpholinium tetrafluoroborate (compound 1).

To a stirred suspension of 7.39g of 2-chloro-4,6-dimethoxy-1,3,5-triazine in 100 mL of water (1 eq., 41.4 mmol) was added 5 mL N-methylmorpholine (1.1 eq., 45.6 mmol). After stirring for 25 mins at room temperature the solid had dissolved to give a colourless solution. Then, 5.57 g of sodium tetrafluoroborate (1.2 eq., 49.7 mmol) dissolved in water (150 mL) was added dropwise over 5 minutes, causing a white precipitate to form. The resulting suspension was stirred for 1 hour further. The precipitate was collected by vacuum filtration and washed sequentially with water (two washes of 20 mL) and methanol (1 wash of 40 mL). The material was dried *in*

vacuo to give compound **1**, 4-(4,6-Dimethoxy-1,3,5-triazin-2-yl)-4-methylmorpholinium tetrafluoroborate, (Figure 3.2), as a colourless solid (11 g, 81%).

3.2.2 Synthesis of 4-((Tert-butoxycarbonylamino)methyl)benzoic acid (compound 2)

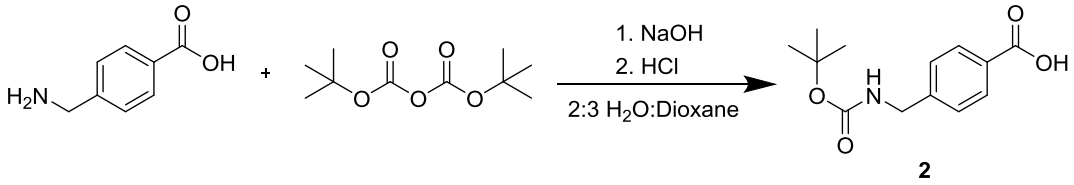

Figure 3.3 - Synthesis scheme of 4-((Tert-butoxycarbonylamino)methyl)benzoic acid (compound 2).

6.04 g 4-Aminomethybenzoic acid (1 eq., 40 mmol) and 17.4 g di-tert-butyl dicarbonate (2 eq., 80 mmol) were stirred in a mixture of dioxane (200 mL) and water (132 mL). The mixture was adjusted to pH 9 by drop wise addition of sodium hydroxide solution (10%). The resulting colourless solution was stirred for 1.5 hours at room temperature and then reduced to 1/3 volume *in vacuo* by removing 2/3 of the organic solvent. The residue was acidified to pH 3, at 0 °C, with drop wise addition of HCl (37%). The resulting colourless precipitate was collected by vacuum filtration and dried *in vacuo* at 80 °C overnight to give compound **2**, 4-((Tert-butoxycarbonylamino)methyl)benzoic acid (Figure 3.3), as a colourless solid (8.23 g, 81.85%).

3.2.3 Synthesis of *tert*-Butyl 4-(2-aminophenylcarbamoyl)benzylcarbamate (compound 3)

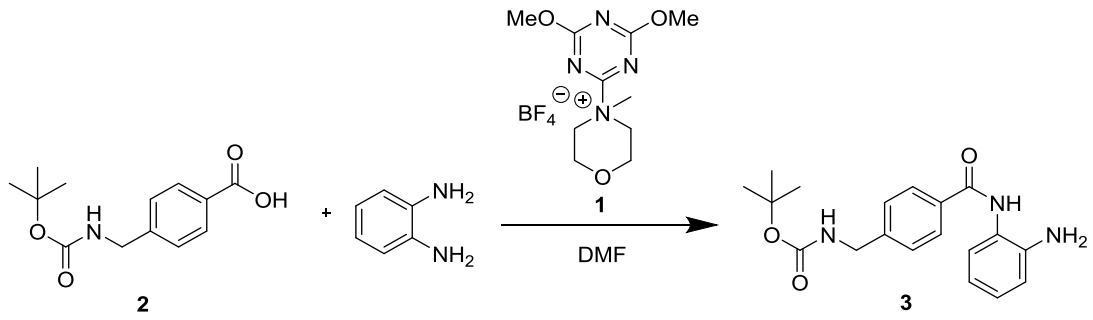

Figure 3.4 – Synthesis scheme of tert-Butyl 4-(2-aminophenylcarbamoyl)benzylcarbamate (compound 3).

To a stirred solution of 7.306g of compound **1** (1 eq., 22.3 mmol) and 5.591g of compound **2** (1 eq., 22.2 mmol) in 66 mL DMF, 2.887g of *o*-phenylenediamine (1.2 eq., 26.7 mmol) was added. The solution turned from yellow to green in five minutes and was stirred for 4 hours at room temperature. The mixture was then diluted with 200 mL of water, extracted with two changes of EtOAc (30 mL each), the combined organics were washed with H_2O (one wash of 20 mL), filtered and concentrated *in vacuo*. The thick, oily orange residue was triturated with 50 mL of Et_2O for 1 hour at a time, three times. The resulting precipitated titrates were combined, vacuum filtered and dried overnight *in vacuo* to give compound **3**, tert-Butyl 4-(2-aminophenylcarbamoyl)benzylcarbamate (Figure 3.4), as a yellow solid (5.46 g, 71.3%).

3.2.4 Synthesis scheme of 4-(Aminomethyl)-*N*-(2-aminophenyl)benzamide (compound 4)

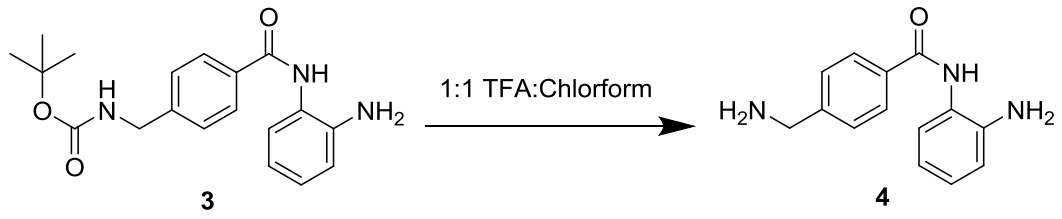

Figure 3.5 - Synthesis of 4-(Aminomethyl)-N-(2-aminophenyl)benzamide (compound 4).

1 g of compound **3** (3 mmol) was stirred in a 1:1 mixture of TFA (10 mL) and chloroform (10 mL) for 2 hours. The mixture was then concentrated *in vacuo*, taken up in EtOAc (20 mL), then sequentially washed with 10% sodium hydroxide (two washes of 20 mL), followed by saturated sodium chloride solution (20 mL) and concentrated *in vacuo*, to give compound **4** (4-(Aminomethyl)-N-(2-aminophenyl)benzamide (Figure 3.5), as a solid yellow product (453 mg, 64%).

3.2.5 Synthesis of MI192

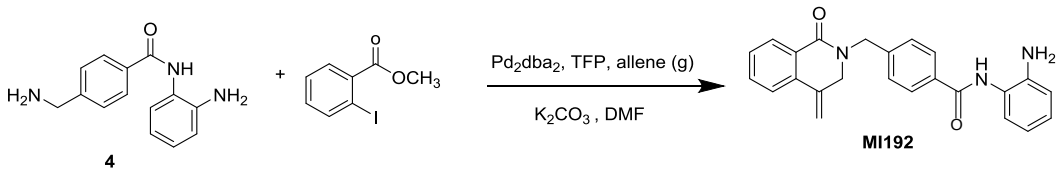

Figure 3.6- Synthesis scheme of MI192.

Methyl 2-iodobenzoate (1.0 mol eq.), compound **4**, (1.1 mol eq.), Pd_2dba_2 (0.025 mol eq.), tri-2-furylphosphine (0.1 mol eq.), K_2CO_3 (2.0 mol eq.) and DMF (10 mL / mmol) were combined in a Schlenk tube with a stirrer bar, subjected to three liquid nitrogen freeze-pump-thaw cycles and charged under pressure with allene gas (0.5 bar). This was then allowed to thaw to room temperature and stirred at 80 °C for 24 hours. The reaction was then cooled to room temperature, diluted with H_2O (20 mL) and extracted with EtOAc (3 x 20 mL), dried with $MgSO_4$, gravity filtered and concentrated *in vacuo*. The resulting orange oil was purified by column chromatography (12.5 g silica, gradient of 10% EtOAc in hexane to 70% EtOAc:Hexane) to yield **MI192** as an orange powder. Two reactions of 133 mg of compound **4** yielded 177 mg of product, 46.2 %.

3.3 Results

All compounds in the scheme were synthesised and satisfactory yields were obtained. Yields were at least comparable to, or better than previously described (unpublished data from lab books). All compounds were characterised by NMR, confirming the expected products had been obtained. The NMRs can be found in the Appendix (A.1 - NMR Spectra) and the peak descriptions can be seen below, describing each compound:

Compound **1**, 4-(4,6-Dimethoxy-1,3,5-triazin-2-yl)-4-methylmorpholinium tetrafluoroborate (Figure 3.2) : ^{1}H NMR (300 MHz; DMSO) δ_H 3.45 (3H, s, N-C*H*$_3$), 3.75-4.35 (2H, m, N-C*H*$_2$-C*H*$_2$-O), 4.1 (6H, s, O-C*H*$_3$).

Compound **2**, 4-((Tert-butoxycarbonylamino)methyl)benzoic acid (Figure 3.3): ^{1}H NMR (300 MHz; DMSO) δ_H 1.3 (9H, s, C-C*H*$_3$ Boc group), 4.2 (2H, d, NH-C*H*$_2$), 7.3 (2H, d, aromatic C*H*), 7.55 (1H, t, N*H*), 7.9 (2H, d, aromatic C*H*).

Compound **3**, tert-Butyl 4-(2-aminophenylcarbamoyl)benzylcarbamate (Figure 3.4): ^{1}H NMR (300 MHz; DMSO) δ_H 1.4 (9H, s, C-C*H*$_3$ Boc group), 4.2 (2H, d, NH-C*H*$_2$), 4.8 (2H, d, NH$_2$), 6.6 (1H, dd, aromatic C*H*), 6.8 (1H, d, aromatic C*H*), 6.95 (1H, dd, aromatic C*H*), 7.25 (1H, d, aromatic C*H*), 7.35 (2H, d, aromatic C*H*), 7.5 (1H, t, CH$_2$-NH), 7.95 (2H, d, aromatic C*H*), 9.65 (1H, s, O=C-N*H*).

Compound **4**, 4-(Aminomethyl)-N-(2-aminophenyl)benzamide (Figure 3.5): ^{1}H NMR (300 MHz; MeOD) δ_H 3.65 (2H, d, NH$_2$-C*H*$_2$), 6.8 (1H, dd, aromatic C*H*), 6.9 (1H, d, aromatic C*H*), 7.1 (1H, dd, aromatic C*H*), 7.2 (1H, d, aromatic C*H*), 7.5 (2H, d, aromatic C*H*), 7.95 (2H, d, aromatic C*H*).

MI192 (Figure 3.6): ^{1}H NMR (300 MHz; $CDCl_3$) δ_H 3.75 (2H, broad s, C-N*H*$_2$), 4.15 (1H, s, N-C*H*$_2$), 4.8 (2H, s, N-C*H*$_2$), 5.15 (1H, s, C=C*H*), 5.6 (1H, s, C=C*H*), 6.85 (2H, m, aromatic C*H*), 7.1 (1H, dd, aromatic C*H*), 7.35 (1H, d, aromatic C*H*), 7.5 (5H, m, aromatic C*H*), 7.8 (3H, m, aromatic C*H* and O=C-N*H*), 8.2 (1H, d, aromatic O=C-C*H*).

3.4 Discussion

The Grigg group has a history of utilising allene gas in neat and effective chemical synthesis reactions (Elboray et al. 2012). Without the use of the gas, the synthesis of MI192 would be many more steps and a very laborious process. The already optimised route was adhered to for the synthesis of MI192, with improvements made where possible.

The first step, Figure 3.2, consists of forming the coupling reagent, for use in the third reaction step. 2-chloro-4,6-dimethoxy-1,3,5-triazine and N-methylmorpholine reacted to give the coupling reagent, which was then stabilised with addition of sodium tetrafluoroborate salt, allowing the reagent to be stored and used in subsequent reactions (Kamiński et al. 2005). The yield was high, at 81% on a gram scale.

Secondly, the tert-butyl carbamate (boc) protection of a primary amide was undertaken, Figure 3.3. Without protection the free amine may interfere in the second step, a coupling reaction. Once the pilot study was successful, the boc protection took place on a gram scale with a 82% yield, which were comparable to the work being followed (80%).

Thirdly, Figure 3.4, the coupling reaction was undertaken. This reaction was the first step where some optimisation of the methods was necessary. The trituration wasn't successful on a small scale, and the product did not precipitate out on the first attempt. A more vigorous stirring technique and the use of less Et_2O resulted in some successful product isolation. A second trituration also yielded some product; however, on a small 1 mmol starting material scale the yield was only 50.6%. Because the starting materials were cheap and a large amount of them had been synthesised, a larger scale coupling was undertaken anyway, despite the poor yield. On an 11 mmol starting material scale (10 x the pilot) the yield improved to 63.9% and on doubling the scale again (the scale reported in the materials and methods) the yield was 71.3%. Either the reaction or the work up process is improved on a larger scale. In the optimised work the expected yield was 70%, so this was another slight improvement.

In the Boc deprotection step, Figure 3.5, the supplied method used addition of 36% HCl (aq.) to the product stirred in water. The work up process involved use of hot THF, which appeared to react with the product, resulting in a loss of product and a low yield of 41%. On a gram scale this yield of 41% was deemed unsatisfactory, so an alternative deprotection method from the literature was attempted (Hooker et al. 2010). On a 100 mg scale a 1:1 mixture of TFA and chloroform gave a 73.2% yield, and on a larger scale a 64% yield. While not as good as the 87% yield expected from the optimised work, this was more acceptable than the 41% yield obtained when this was repeated. Enough compound was synthesised when optimising the step, so further optimisation work was not undertaken.

Problems were also encountered with the synthesis of MI192, Figure 3.6. Due to the expense of the gas, at least £100 per reaction, optimisation of this reaction was limited by cost, not time or availability of the reagents. Initially a method using caesium carbonate as the base was followed; however, on several repetitions, including with different batches of starting materials and meticulous degassing of the reaction mixture using liquid nitrogen freeze thaw cycles, no product was even seen in crude reaction NMR spectra. On switching to potassium carbonate as a base two parallel reactions were successful. MI192 was produced in a 46.2% yield. This yield was below that reported previously (~ 60%); however, enough product was obtained from these two reactions, and due to the cost of the gas, further optimisation or reactions were not undertaken. The NMR spectra for the MI192 synthesised was compared to a batch synthesied in the group previously, as well as a batch obtained as part of a collaboration with Cancer Research Technology UK (http://www.cancertechnology.co.uk/) as part of a separate collaborative project.

This MI192 synthesised was sufficient for a large number of biological testing experiments, due to the very low amounts of compound used. The compound was stored in the dark in a -20 °C freezer and used as needed.

Chapter 4: The General Effects of MI192 on Adipose Derived Stem Cells Cultured in Monolayer

The aim of this chapter is to investigate the general, non-differentiation related effects of MI192 on ADSC cells in monolayer. The objectives are to investigate the effects of MI192 on ADSC morphology, cell number, cytotoxic effects and if the ADSC viability changes over while treated with MI192. Also investigated was the effect of MI192 treatment on the cell cycle, HDAC activity and stem cell markers of ADSCs.

4.1 Introduction

HDACis are small molecular compounds that inhibit the deacetylation action of HDAC enzymes in the cell. Since acetylation/deacetylation is a key epigenetic process, and stem cell fate is closely linked to a cell epigenetic landscape, HDACis can potentially drastically affect stem cell fate (Tollervey & Lunyak 2012). Researchers have explored the prospect of using HDACis such as NaB (Iwami & Moriyama 1993), TSA (Boer et al. 2006), VPA, (Schroeder et al. 2007) and MS-275 (H.-N. Kim et al. 2011) to improve the osteogenic potential of cells.

There are 18 HDAC isoforms in the human cell, and, to date, most inhibitors target a large number of these. However, to try and narrow down side effects and control the functions of HDACis more carefully, researchers are looking to utilise HDACis to target specific HDAC isoforms. For example, as described in Chapter 3: The Chemical Synthesis of MI192, MS-275 is a HDACi that specifically targets HDAC1, HDAC2 and HDAC3 (Bradner et al. 2010). The inhibitor this study is focused upon is MI192, which is specific for HDAC2 and HDAC3, and believed to be the only one of its kind in the world. This ability to target just these isoforms is an exciting prospect.

As discussed in depth in the literature review, HDAC3 in particular is an important isoform when considering bone tissue, it is key to bone formation (Schroeder & Westendorf 2005; Schroeder et al. 2004; Razidlo et al. 2010; McGee-Lawrence et al.

2013; Hesse et al. 2010; Lamour et al. 2007; Choo et al. 2009; Shen et al. 2002). In comparison, there are less links with HDAC2 and bone.

Adipose tissue is an abundant, very promising source for easily isolatable MSCs (Zuk et al. 2001; Zuk et al. 2002). ADSCs are commercially available from a number of sources, and are known to have the potential to differentiate into multiple lineages (Levi & Longaker 2011; Erickson et al. 2002; Planat-Benard et al. 2004; Golipoor et al. 2010). However, many of these methods of inducing differentiation are not very effective, thus researchers are seeking ways to improve protocols. Therefore HDACis, with their ability to affect stem cell fate, could help researchers in achieving this goal.

However, before looking at how the differentiation potential of these cells is altered, it is very important and interesting to investigate firstly the more general effects of MI192 on ADSC properties, such as viability and function.

4.2 Materials and Methods

4.2.1 Assessment of Cell Morphology

ADSCs were seeded in two 12 well plates (1 x 10^5 cells per well) and cultured in basal medium for 24 hours. The medium was then replaced with medium containing different concentrations of MI192 (50 µM, 30 µM and 5 µM in 1 mL basal medium) and TSA (10 µM in 1 mL basal medium). Basal medium alone (untreated wells) was used as a control. The sample size was three (n=3) for all groups. Cells were observed under a Leica DMI6000 B inverted microscope at 12, 24, 48 and 72 hour time points and cell morphology was assessed. Plates were not washed before observation to prevent cells being washed away.

4.2.2 Effect of MI192 on ADSC DNA quantity (as an indicator of cell number)

ADSCs were seeded in three 24 well plates (5 x 10^4 cells per well) and cultured in basal medium for 24 hours. The medium was then replaced with medium containing different concentrations of MI192 (10 µM – 100 µM in 500 µL basal medium). Basal medium alone (untreated wells) was used as a control. The sample size was three (n=3) for all groups. At 24, 48 and 72 hour time points, one plate of cells was washed with twice 1x PBS (to wash away dead/detached cells), lysed in 0.1 % Triton-X 100 and then stored in a –80 °C freezer for DNA quantification by a PicoGreen® assay.

4.2.3 Cytotoxic effect of MI192 on ADSCs

ADSCs were seeded in three 96 well plates (1 x 10^4 cells per well) and cultured in basal medium for 24 hours. The medium was then replaced with medium containing different concentrations of MI192 (10 µM – 100 µM in 100 µL basal medium). Basal medium alone (untreated wells) was used as a control. The sample size was three (n=3) for all groups. At 24, 48 and 72 hour time points, one of the plates was stopped for a cytotoxicity assay. The CytoTox 96® Non-Radioactive Cytotoxicity Assay (Promega, Cat. no: G9260) was used according to the manufacturer's instructions. Briefly, the prepared reagent (100 µL per well) is added directly to the medium of the plate, with addition also to controls containing no cells for blank background readings. The plate was then incubated for 30 minutes at 37 °C and the fluorescence was then

measured in a Varioskan Flash Multimode Microplate Reader (Model 3001, Thermo Scientific), by exciting the samples at 488 nm with emission reading set at 520 nm.

The CytoTox-Fluor Assay is a single-reagent addition assay that measures the relative number of dead cells in a cell population. A fluorogenic peptide substrate (bis-alanyl-alanyl-phenylalanyl-rhodamine 110) reacts with proteases that have been released from the dead cells in the population. The peptide cannot penetrate the membrane of live cells so no signal is generated from these.

4.2.4 Effect of MI192 on ADSCs viability

ADSCs were seeded in three 96 well plates (1 x 10^4 cells per well) and cultured in basal medium for 24 hours. The medium was then replaced with medium containing different concentrations of MI192 (10 µM – 100 µM in 100 µL basal medium). Basal medium alone (untreated wells) was used as a control. The sample size was three (n=3) for all groups. At 24, 48 and 72 hour time points, one of the plates was stopped for a cell viability assay. The CellTiter-Glo Luminescent Cell Viability Assay (Promega, Cat. no: G7570) was used according to the manufacturer's instructions. Briefly, the plates were equilibrated to room temperature for 30 minutes, prepared reagent (100 µL per well) was added directly to the medium of the plate, with addition also to controls containing no cells, for blank background readings. The plate was then mixed on a rocker for 2 minutes and then incubated for 10 minutes at room temperature to stabilise the luminescent signal. The luminescence was then measured on a Varioskan Flash Multimode Microplate Reader (Model 3001, Thermo Scientific).

The CellTiter-Glo assay determines the number of viable cells in a population based on quantification of the ATP levels present, as ATP activity is a sign of metabolically active cells. The assay reagent lyses the cells and the presence of ATP catalyses a reaction involving a thermostable luciferase (Ultra-Glo™ Recombinant Luciferase) to generate a luminescent signal.

4.2.5 Effect of MI192 on the HDAC specific activity of ADSCs

ADSCs were seeded in two 24 well plates (5 x 10^4 cells per well) and cultured in basal medium for 24 hours. The medium was then replaced with MI192 containing

medium (30 µM and 10 µM in 500 µL basal medium). Basal medium alone (untreated wells) was used as a control. The sample size was three (n=3) for all groups. At 24 and 48 hour time points the HDAC activity of the cells was measured using an *in situ* HDAC activity fluorometric assay kit (Biovision Cat. no: K339-100), according to the manufacturer's instructions. Briefly, the cells were lysed with scraping and two freeze-thaw cycles of –80 °C and 37 °C. To ensure no protein degradation, the assay was carried out straight away.

20 µL of cell lysate was added to 65 µL of UltraPure™ DNase/RNase-Free distilled water and 10 µL of the supplied 10x Assay buffer (giving a total volume of 95 µL). As well as the test groups, a series of standards from a provided deacetylated sample were also plated. A positive control of provided HeLa nuclear extract was tested, along with a negative control of provided TSA added to nuclear extracts of untreated ADSCs. For the reaction, 5 µL of the fluorometric substrate was added and the plate was mixed on a rocker for 2 minutes, prior to incubation at 37 °C for 30 minutes. Then, 10 µL of the lysine developer was added and the plate incubated for a further 30 minutes at 37 °C. The fluorescence was measured in a Varioskan Flash Multimode Microplate Reader (Model 3001, Thermo Scientific) by exciting the samples at 368 nm with emission reading set at 442 nm. Total DNA content in the same samples was quantified with a PicoGreen® assay. The unknown value of HDAC activity was then calculated using the generated standard curve to give the µg HDAC activity, and the value per well was calculated from Triton X-100 harvest volume and volume of lysate used for the assay. The µg of DNA per well was calculated in the same way, and the HDAC specific activity per well was calculated by dividing the µg HDAC activity by the total DNA content in the same well.

The HDAC activity assay measures the deacetylation ability of the HDAC enzymes in cells. The substrate contains an acetylated lysine side chain that HDAC enzymes will deacetlyase. A developer is then added that produces the fluorophore from deacetylated HDAC substrate, with a greater reading indicating a larger HDAC enzyme activity in cells.

4.2.6 Effect of MI192 on ADSC Cell Cycle

ADSCs were seeded in three 6 well plates (1 x 10^5 cells per well) and cultured in basal medium for 72 hours, to ensure normal cell cycle function was initiated. The

medium was then replaced with medium containing MI192 (30 µM and 10 µM in 2mL basal medium), and TSA (10 µM in 1 mL basal medium). Basal medium alone (untreated wells) was used as a control. The sample size was three (n=3) for all groups. At 12, 24 and 48 hour time points the cells were harvested; the medium was aspirated, cells washed 3 times with 1x PBS and then detached with T/E for 5 - 10 minutes. The resulting cell suspensions were centrifuged at 1100 RPM for 5 minutes, the supernatant was removed and 500 µL ice cold 70 % (v/v) ethanol/PBS was added drop wise, with gentle vortexing. Cells were then stored at -80 °C for no more than one week.

For propidium iodide staining, the cells were centrifuged at 1100 RPM for 5 minutes, the supernatant carefully decanted, the cells washed in 500 µL 4 °C FACS buffer (1x PBS with addition of 0.1 % (w/v) bovine serum albumin (Sigma-Aldrich Cat. no: A2058) and 0.1 % TWEEN-20 (Sigma-Aldrich Cat. no: P9416)) and then centrifuged at 1100 RPM for 5 minutes. The supernatant was decanted and the cells re-suspended with gentle pipetting in 500 µL of freshly made staining solution, 20 µg/mL propidium iodide (Sigma-Aldrich, Cat. no: P4170) and 200 µg Ribonuclease A (Sigma-Aldrich Cat. no: R6513). Cells were incubated at room temperature for 20 minutes, placed on ice and events were collected with a 2 laser (blue and violet) Attune NxT Flow Cytometer (Life Technologies). Ideally at least 5000 events for each sample was logged, (although for the smaller cell counts 2000 events was logged), then samples were analysed with the standard procedures for cell cycle analysis using the ModFitLT software version 3 (Becton Dickinson).

Briefly, events were gated to account only for intact cells (gate 1 – by forward scatter against side scatter), then to account only for material related to intact nuclei (gate 2 – by BL3 area against forward scatter area) and finally to remove any doublets or abnormal cells, i.e. diploid cells (gate 3 – by BL3 height against BL3 area) (Figure 4.1). Gates were then applied to all samples and histograms of the BL3 area against count were created, with two distinct peaks representing the G0/G1 phase and the G2/M phase, with the area in between the S Phase of the cell cycle. The area under the peaks was then measured to give the percentage of events in each cycle, with a confidence value. All confidence values were between 3.48 and 7.78, with the majority falling below 5.5, indicating a good confidence in the data.

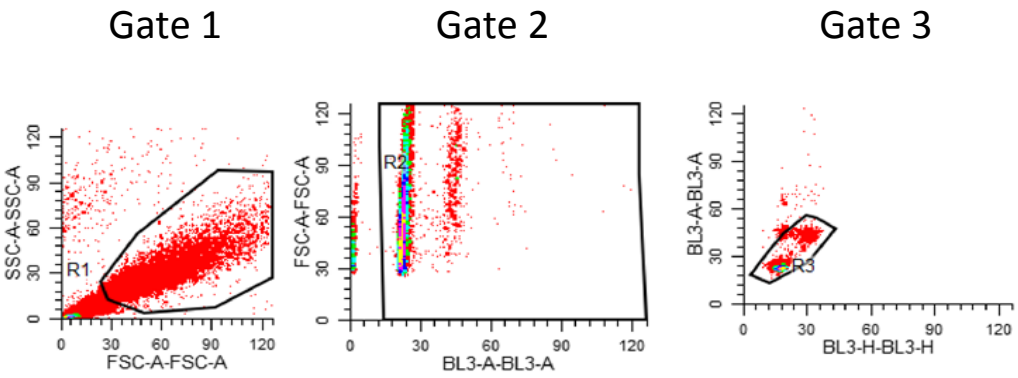

Figure 4.1 – Gates created in flow cytometry analysis of ADSCs stained with PI for cell cycle analysis. Representative gates shown, which were created in ModFit software to account for intact cells (Gate 1), material related to intact nuclei (Gate 2) and for single cells (Gate 3).

4.2.7 Effect of MI192 on ADSC Stem cell Markers

The cell culture was carried out by the author, cell labelling and flow cytometry analysis was carried out by Dr. Matthew Tomlinson (Leeds School of Dentistry) and data analysis jointly by Dr. Tomlinson and the author.

ADSCs were seeded in two T75 flasks (1 x 10^6 cells per flask) and cultured in basal medium for 24 hours. The medium in one flask was then replaced with MI192 containing medium (30 µM in 10 mL basal medium) with an un-treated control flask, where the medium was changed to 10 mL of basal medium. At 48 hours the cells were harvested by aspiration of the medium, 3x washes in 1x PBS and detached with T/E for 5 - 10 minutes. The resulting cell suspension was centrifuged at 1100 RPM for 5 minutes to give a pellet. Cells were then resuspended in 1x PBS and 10 µL Fc receptor blocking solution (Miltenyi Biotec Cat. No: 130-059-901) before incubation with various antibodies (5 µL per 1×10^6 cells unless stated) in a total volume of 100 µL for 20 min at room temperature in the dark. Following labelling, 900 µL of PBS was added to each sample before centrifugation at 1100 RPM and resuspension in 500 µL 1x PBS. For each marker, untreated and treated cells were labelled three times (n=3), for three technical repeats. Samples were analysed using a BD LSRII flow cytometer (BD Biosciences) running BD FACSDiva 8 software and subsequent data analysis was performed using Kaluza (Beckman Coulter Inc.).

Antibodies used were as follows: CD29-Alexa Fluor 488, CD34-FITC, CD44-FITC (10 µL per 1×10^6 cells), CD45-PE, CD73-PE (2 µL per 1×10^6 cells), CD90-APC, CD105-PE, CD146-Alexa Fluor 488 and CD166-PE (10 µL per 1×10^6 cells). All antibodies were purchased from Biolegend (Cat. nos: See Table 4-1). Propidium iodide (Miltenyi Biotec, Cat. no: 130-093-233) was used as a viability dye.

All threshold values for flow cytometry were obtained by analysing both autofluorescence of non-labelled ADSCs and reactivity of isotype matched controls. Events were gated based on forward and side scatter, to account only for intact cells (Gate 1, an example of which is shown below in Figure 4.2 –). Colour compensation was performed for each panel and applied equally to all markers. The intact cell events were then grid gated so that the percentage of positive and negative cells could be counted for each marker (Gate 2, an example of which is shown below in Figure 4.2). Histograms were produced showing cell count for each marker for both untreated and treated cells, compared to a negative control. Comparative histograms were also produced comparing the untreated and treated cell populations. The percentage of labelled cells for each technical repeat was also recorded.

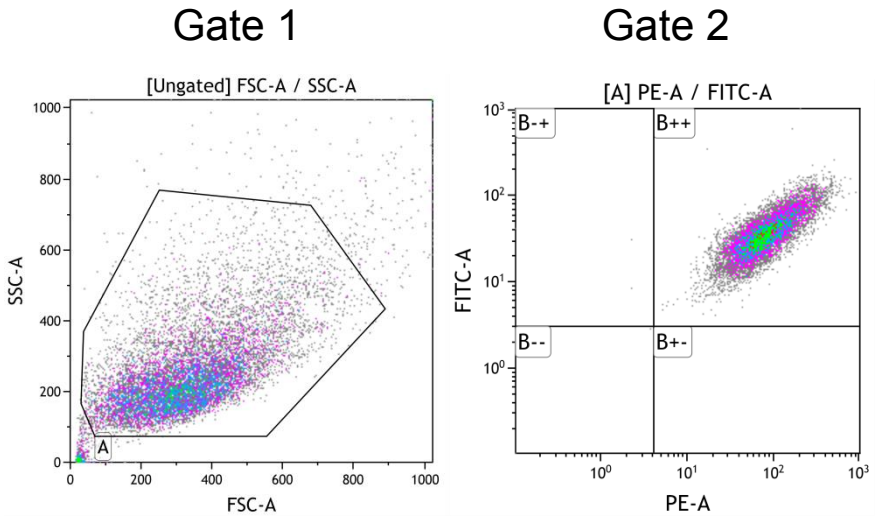

Figure 4.2 – Representative pictures of gates created in Kaluza software. Gate 1 - to account for intact cells. Gate 2 - to count the percentage of intact cells marked positive with FITC and PE. Intact cells marked positive with both FITC and PE shown in the top right quadrant, B++.

Table 4-1 - Cell surface markers used in analysis of ADSCs. Each marker is detailed with alternative names, distribution, a summary of understanding of function, relevant references and conjugate and catalogue number.

Marker	Distribution and function	References	Conjugate (Biolegend Catalogue number)
CD29 / Integrin β1	Involved in cell-cell and cell-matrix, tissue repair and immune response. Used as part of haematopoietic and stromal MSC marker panels.	(Hynes 1992; Tomlinson et al. 2015; Baboolal et al. 2014)	CD29-Alexa Fluor 488 (303016)
CD34 / Platelet endothelial cell adhesion molecule-1 (PECAM-1)	Function is not fully understood, potentially enhances proliferation and halts the differentiation of progenitor cells. Also possibly promotes the adhesion of lymphocytes to the vascular endothelium in lymphoid tissues. Used as a marker of hematopoietic stem cells (HSCs) to isolate them for bone-marrow transplantation. Also been employed as a marker to identify other stem cells.	(Nielsen & McNagny 2008)	CD34-FITC (350006)
CD44	Cell adhesion protein involved in matrix-dependent migration, which binds hyaluronan and other matrix proteins. Involved in many cellular processes, including the regulation of growth, survival, differentiation and cell motility.	(Baboolal et al. 2014; Ponta et al. 2003)	CD44-FITC (103022)

CD45 / Leukocyte Common Antigen (LCA)	Expressed highly in hematopoietic cells, is an essential regulator of T- and B-cell antigen receptor signalling. Present on all leukocytes, therefore it can be used to separate HSCs from MSCs	(Trowbridge & Thomas 1994)	CD45-FITC (304038)
CD73 / Ecto-5'-nucleotidase	Expressed on epithelial and stromal cells and bone marrow MSCs. It hydrolyses extracellular nucleoside monophosphates into bioactive nucleoside intermediates. Involved in angiogenesis, hypoxic response, endothelial tissue barrier function. Especially used as a positive marker for bone marrow MSCs.	(Baboolal et al. 2014; Battula et al. 2009; Lv et al. 2014; Colgan et al. 2006)	CD73-PE (344004)
CD90 / Thy-1	Glycoprotein involved in signal transduction, found on hematopoietic and bone marrow stem cells, neurons, all thymocytes, and peripheral T-cells, but not on B-cells. It is involved in lymphocyte activation, and proliferation, inflammatory responses and differentiation of hematopoietic stem cells.	(Baboolal et al. 2014; Mayani & Lansdorp 1994; Kisselbach et al. 2009)	CD90-APC (328114)
CD105 / Endoglin	High expressed in angiogenic endothelial cells and in the blood vessels of tumour tissues. Associated with proliferation of endothelial cells and hypoxic conditions. Receptor for transforming growth factor (TGF) -1 and -3 and modulates TGF- signalling.	(Duff et al. 2003)	CD105-PE (323206)
CD146 / Melanoma	Highly expressed in blood vessels, smooth muscles and pericytes,	(Robey 2011; Covas et al. 2008)	CD146-Alexa Fluor 488

Cell Adhesion Molecule (MCAM)	although its function is not well understood. It is thought to be involved in interactions of MSCs and other cells with endothelial cells. It is a commonly used marker of multipotent mesenchymal stromal cells.		(342008)
CD166 / Activated Leukocyte Cell Adhesion Molecule (LCAM)	Mediates both heterophilic and homophilic cell-cell interactions. Expressed in MSCs, growing or migrating dynamic tissues, including neural, organ development, haematopoiesis and immune responses, namely T-cells.	(Swart 2002)	CD166-PE (343904)

4.2.8 Statistical Analysis

All statistical analysis undertaken with Graphpad Prism 5. Method used: ANOVA multiple comparisons test with Tukey modification. For all graphs: ns = $P > 0.05$, * = ≤ 0.05, ** = $P \leq 0.01$ *** = $P \leq 0.001$ and **** = $P \leq 0.0001$.

4.3 Results

4.3.1 Effect of MI192 on ADSC Morphology

Representative *in situ* pictures were taken at 12, 24, 48, 72 and 96 hours of cells cultured with 5 µM, 30 µM and 50 µM of MI192, 10 µM of TSA and a basal control group (Figure 4.3, Figure 4.4 and Figure 4.5).

At the 12 hour time point (the earliest time point), the cells in basal medium culture group are showing a typical phenotype for these stem cells (fibroblast like) (Figure 4.3 A, top left image). The cells in the 5 µM MI192 pre-treated group have become clearly smaller and more circular (Figure 4.3 A, top right image), and the cells in the 30 µM and 50 µM MI192 pre-treated groups are clumping together in clusters with distinctive bridges between the clusters (Figure 4.3 A, bottom two images), when compared with the untreated basal medium controls. A morphological change is especially clear in the picture of the cells in the lowest dose (5 µM), where more cells are visible, due to less cell detachment.

At the 24 hour time point, the cells in the basal medium culture group are showing a higher cell density, with cells beginning to grow to over confluency, and demonstrating a continuation of the fibroblast like morphology (Figure 4.3 B, top left image). The cells in the 5 µM MI192 pre-treated group are showing an increase in cell density over the previous time point, although less than the basal group, indicating the cell proliferation may have slower or halted. They have the same smaller and more circular morphology as at 12 hours (Figure 4.3 B, top right image) when compared to the basal control. The photographs of cells in the 30 µM and 50 µM MI192 pre-treated group show some small white dots (Figure 4.3 B, bottom two images), which indicates cell death/detachment compared to that in the 5 µM MI192 concentration and the basal medium control groups. The cells are also showing a lower cell density.

At the 48 hour time point, there is little change in the cells in the basal medium culture group, as they have reached over confluency and have nowhere to grow (Figure 4.4 A, top left image). The cells in the 5 µM MI192 pre-treated group have the same smaller and more circular morphology as at 12 and 24 hours (Figure 4.4 A, top right image), along with a similar cell density (indicating a lack of proliferation) to the 5 µM

MI192 cells at other two time points. Some cell death is visible, indicated by small white dots. The photographs of cells in the 30 µM and 50 µM MI192 pre-treated group have a large number of small white dots (Figure 4.4 A, bottom two images), which indicates higher cell death/detachment compared to that in the 5 µM MI192 concentration and the basal medium control groups.

At the 72 hour time point, the basal group remains unchanged (Figure 4.4 B, top left image). A similar level of cell death/detachment in the 5 µM MI192 pre-treated group (Figure 4.4 B, top right image), to the 48 hour time points visible There is a high level of cell death/detachment visible in the 30 µM and 50 µM MI192 pre-treated groups (Figure 4.4 B, bottom two images). The 30 µM group has a higher cell density than the 50 µM treated group, indicating a lower loss of cells.

At the 96 hour time point, the basal group remains unchanged (Figure 4.5 A, top left image). A higher level of cell death is visible in the 5 µM MI192 pre-treated group (Figure 4.5 A, top right image) than in the previous time points, indicating MI192 may now be having a cytotoxic effect. There are very few attached cells in the 30 µM and 50 µM MI192 dosed groups (Figure 4.5 A, bottom two images), indicating the well is approaching 100 % cell death.

Culture with 5 µM TSA has a different effect on the cells (Figure 4.5 B). Compared to the 5 µM MI192 pre-treated cells, the 5 µM TSA dosed cells have become more elongated, with a fibroblast-like morphology. There is very minimal cell death observed throughout the time points and the pattern of cells is similar to that of the basal controls.

A:

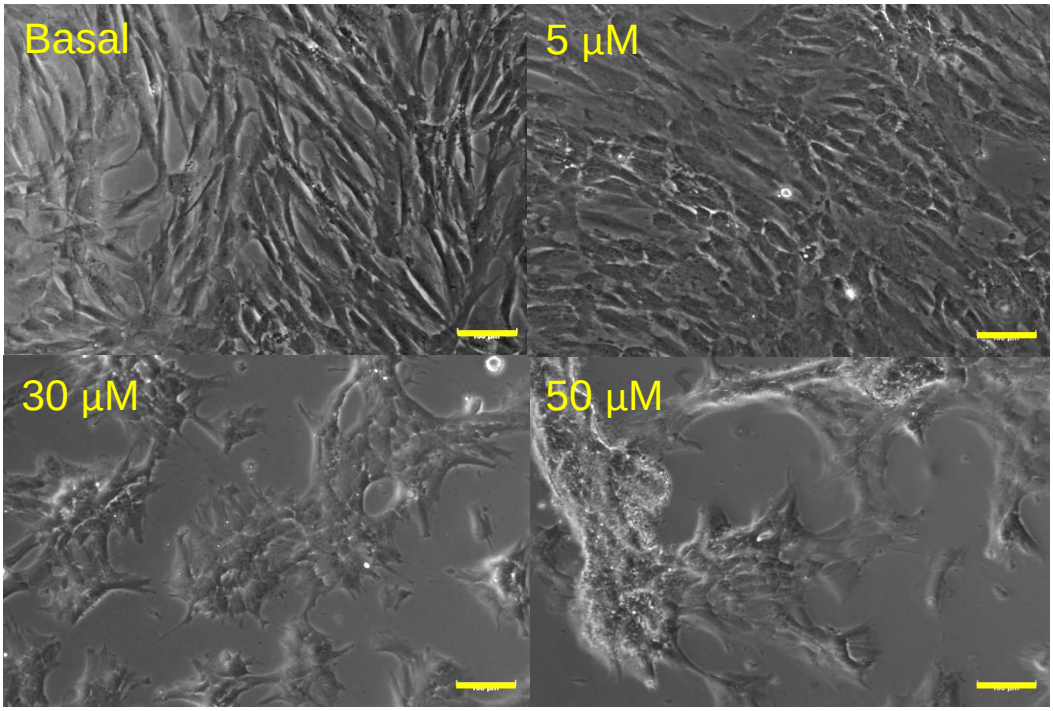

B:

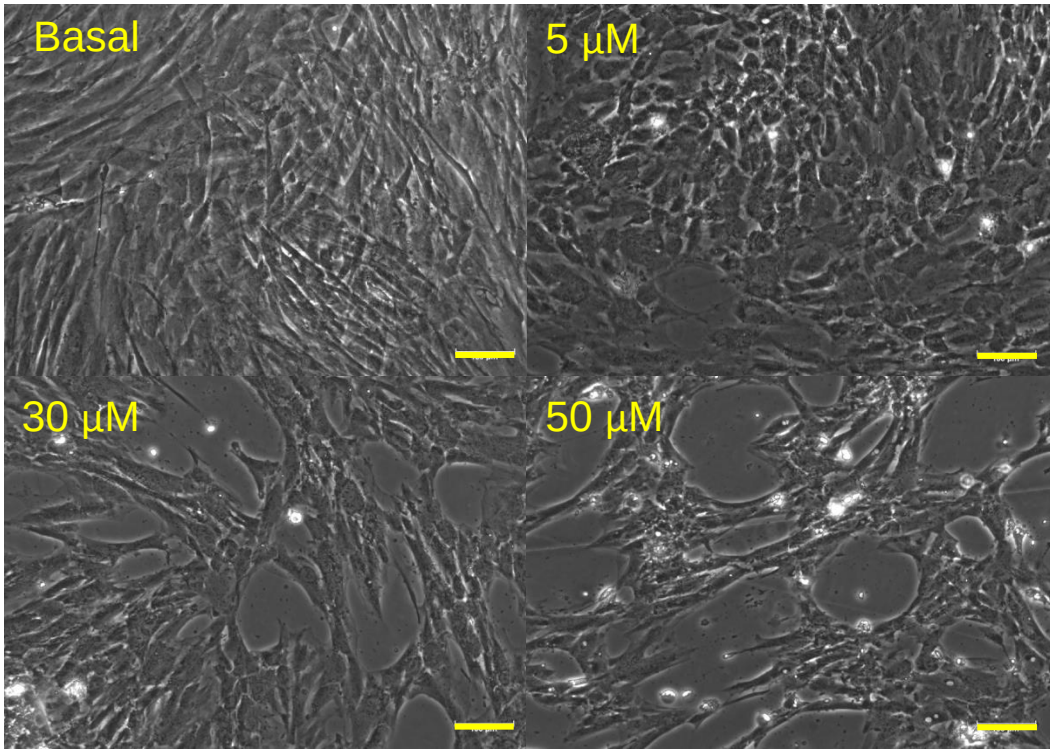

Figure 4.3 - Phase contrast images of ADSCs treated with MI192 for 12 (A) and 24 (B) hours. Cells dosed with MI192 (5 µM, 30 µM and 50 µM) and compared to a basal control with no MI192 dose. Scale bars = 100 µM.

A:

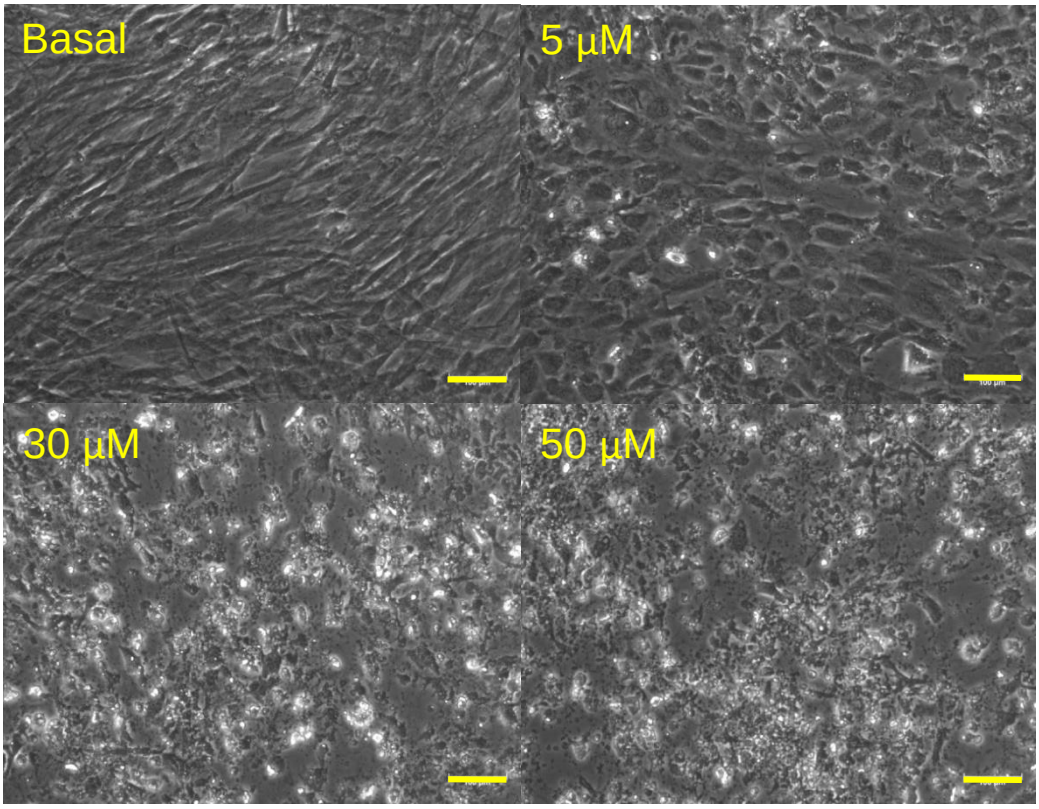

B:

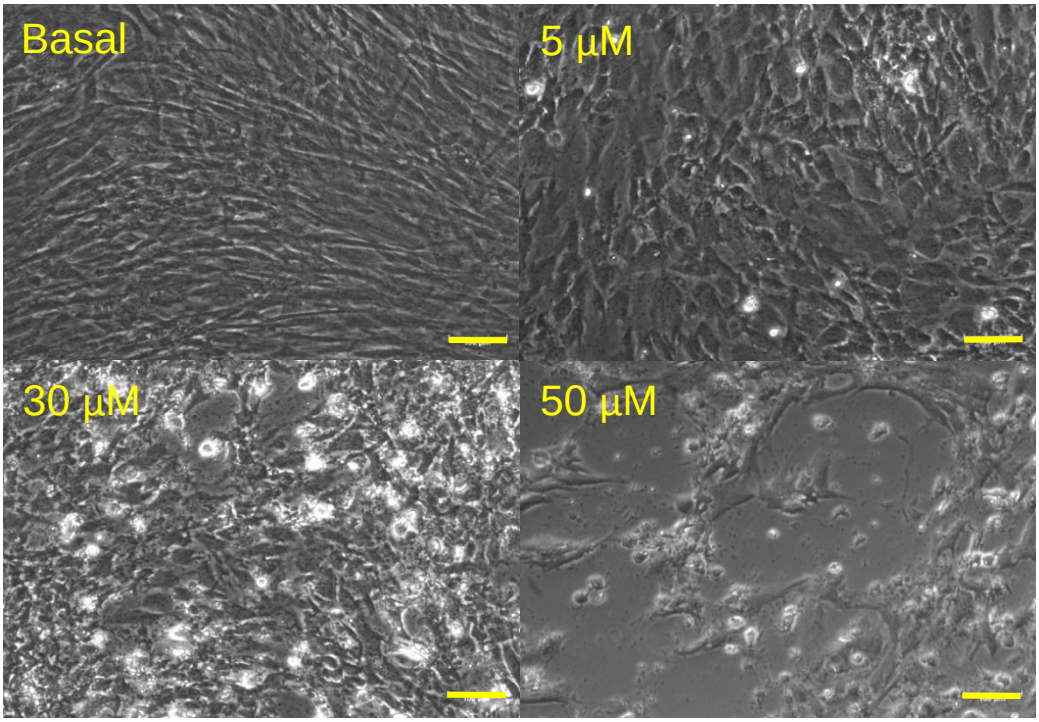

Figure 4.4 - Phase contrast images of ADSCs treated with MI192 for 48 (A) and 72 (B) hours. Cells dosed with MI192 (5 µM, 30 µM and 50 µM) and compared to a basal control with no MI192 dose. Scale bars = 100 µM.

A:

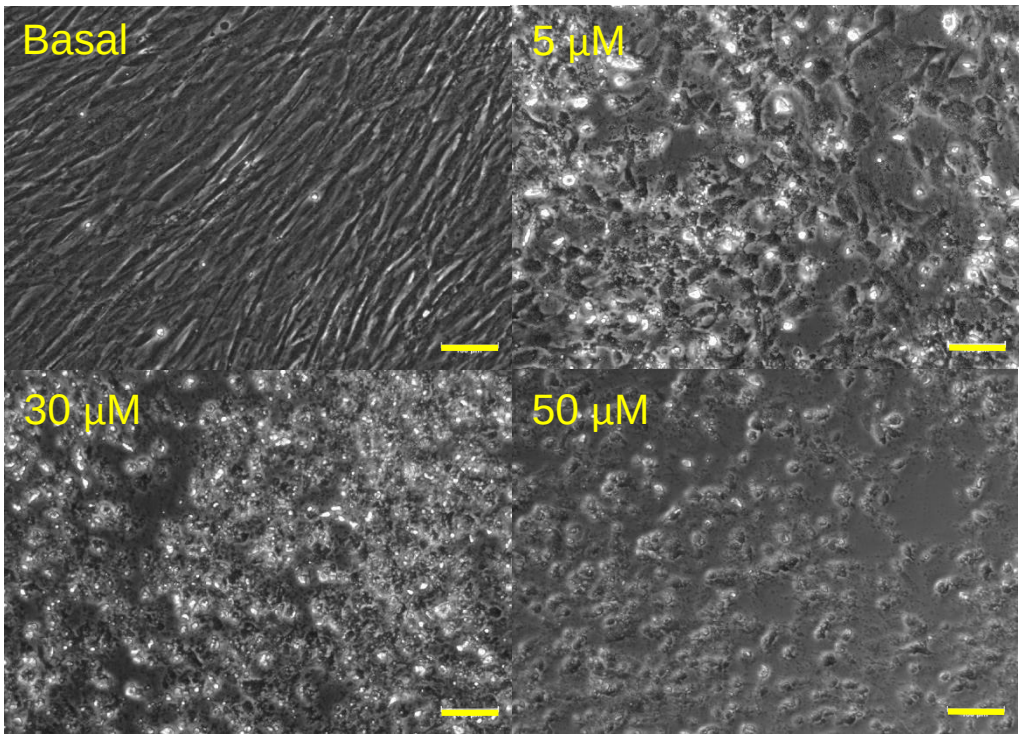

B:

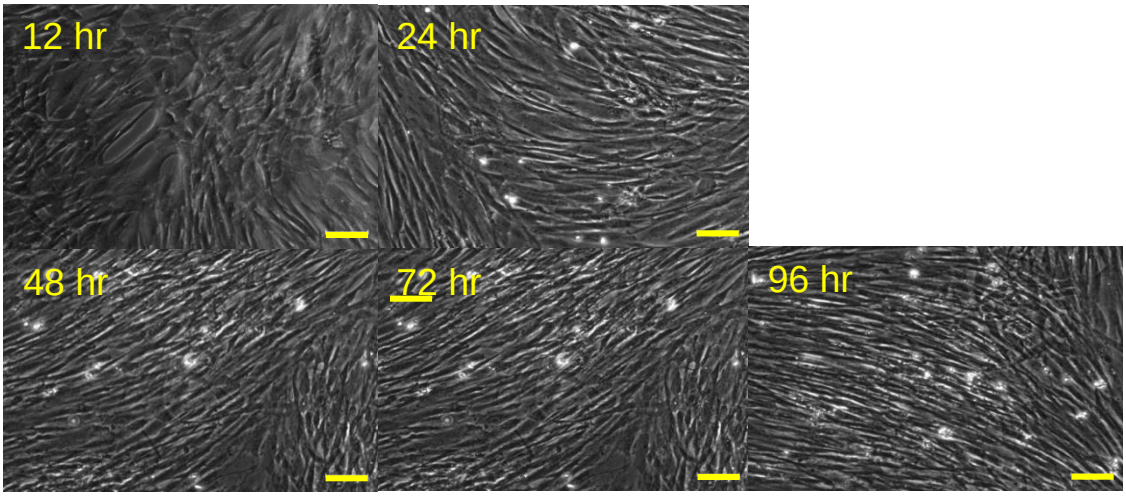

Figure 4.5 - Phase contrast images of ADSCs treated with MI192 for 96 hours (A) and ADSCs treated with TSA for a range of time points (B). A - Cells dosed with MI192 (5µM, 30 µM and 50 µM) and compared to a basal control with no MI192 dose. **B** – Cells dosed at the same time but with 10µM TSA for the same time points. Scale bars = 100 µM.

4.3.2 Effect of MI192 on ADSC DNA quantity (as an indicator of cell number)

After 1 day of treatment with different concentrations of MI192 (10 µM - 100 µM), only the ADSCs treated with the lowest concentration of MI192 (10 µM) showed no statistically significant ($P > 0.05$) reduction in total DNA content, comparted to the untreated basal medium control (Figure 4.6). There was a statistically significant ($P \leq 0.05$) reduction in the total DNA content in the higher concentration (20 µM - 100 µM) groups compared to the basal medium control. There was no significant difference in the total DNA content between the higher concentration of MI192 groups, compared to each other ($P > 0.05$).

After 2 days, there was an increase in cell number (although not statistically significant, $P > 0.05$) in the untreated basal medium control compared to the day 1 samples. In contrast, in all concentrations of MI192 (10 µM - 100 µM) there was a statistically significant ($P \leq 0.001$) reduction in total DNA content, compared to the untreated basal medium control. The reduction was down to a similar level to that seen in the day 1 treated group. It could be result showing cellular proliferation halting. There was a statistically significant reduction in the 100 µM group compared to 10 µM group ($P \leq 0.05$), with no statistical significant ($P > 0.05$) difference between the other groups.

After 3 days, there was another increase in cell number (although not statistically significant, $P > 0.05$) in the untreated basal medium control compared to the day 1 and day 2 samples. In all concentrations of MI192 there was a reduction in total DNA content, compared to the untreated basal medium control. Except in the 10 µM MI192 treated cells, this reduction was lower than the previous time points, indicating cell death or detachment, as the cell numbers are reducing over time. The reduction compared to the untreated basal medium control was highly significant in all groups ($P \leq 0.001$). Comparing the 10 µM MI192 and 100 µM MI192 treated cells, there was a highly significant difference ($P \leq 0.001$), and a dose response (although not statistically significant, $P > 0.05$) between the doses of MI192, indicating a higher concentration results in a lower total DNA content. The total DNA content for the 10 µM MI192 treated cells stayed similar across all three time points. These results indicate that MI192 has a cytotoxic, and/or proliferation halting effect on ADSCs, at all concentrations, with a dose response visible.

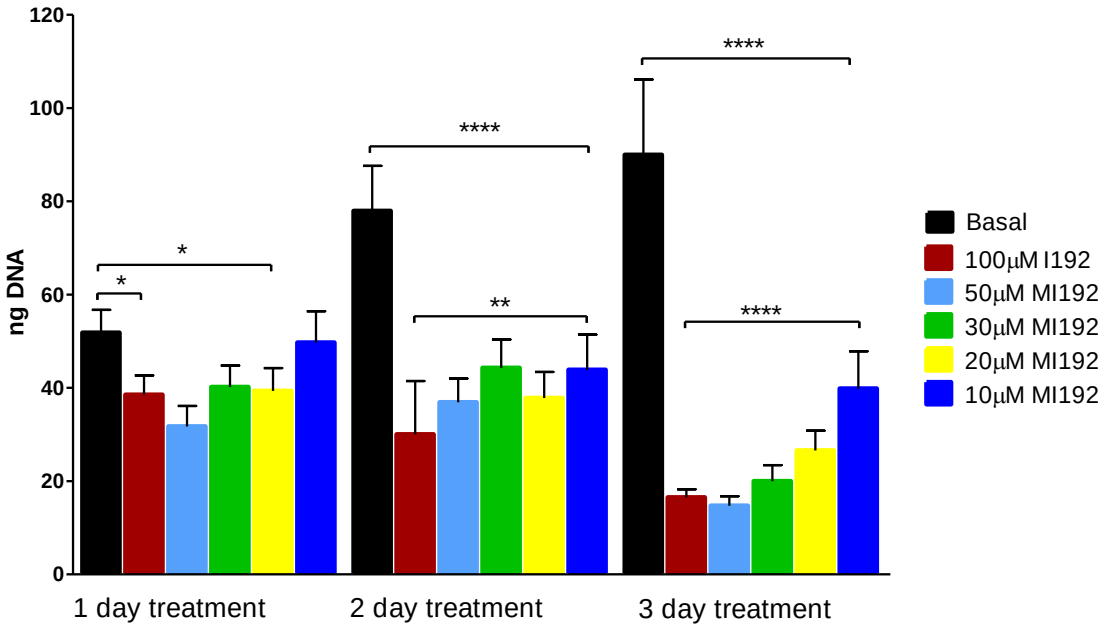

Figure 4.6 - Quant-iT™ PicoGreen® analysis of ADSCs treated for 1 day, 2 days and 3 days with a range of doses of MI192. Results expressed as mean ± SD (n=3). A selected sample of significance levels are shown, * = P ≤ 0.05, ** = P ≤ 0.01 and **** = P ≤ 0.0001

4.3.3 Cytotoxic effect of MI192 on ADSCs

After 1 day of treatment with different concentrations of MI192 (1 µM - 50 µM), no statistically significant ($P > 0.05$) cytotoxic effect of MI192 was seen in the test groups compared to the untreated basal control group (Figure 4.7).

After 2 days of treatment with MI192, the 50 µM and 100 µM groups showed extremely statistically significant ($P \leq 0.001$) cytotoxic marker release compared to the untreated basal control group. There were also statistically significant cytotoxicity markers measured in the lower concentrations, with 30 µM ($P \leq 0.01$), 20 µM ($P \leq 0.05$) and 10 µM ($P \leq 0.05$) all showing a measured cytotoxic effect compared untreated basal control group. However, there was no statistical significant difference between the 1 µM group and the untreated basal control group ($P \geq 0.05$). The cytotoxic effect was not statistically significant different between most groups ($P > 0.05$); however, there was a dose response visible, with a higher cytotoxic effect visible in the higher doses of MI192.

After 3 days of treatment with MI192, all groups showed an increase in the cytotoxic marker release compared to the untreated basal control group. 1 µM MI192 showed a statistically significant cytotoxic marker release ($P \leq 0.01$) and all other groups (10 µM - 100 µM) had an extremely high difference compared to the control ($P \leq 0.001$). There was a lower cytotoxic effect seen in the lower MI192 doses (1 µM and 10 µM), with the higher doses (20 µM - 50 µM) all having a comparable cytotoxic effect.

MI192 was found to have a cytotoxic effect on ADSCs, which was suggested previously by the reduction in cell number (Figure 4.6). At all treatment concentrations of MI192, the cytotoxic effect of MI192 can be seen in the release of cytotoxicity markers, with an increase in treatment length and dose size.

4.3.4 Effect of MI192 on ADSCs viability

After 1 day of treatment with different concentrations of MI192 (1 µM - 50 µM), a statistically significant reduction ($P \leq 0.001$) in cell viability was observed in all treatment groups ($P \leq 0.001$), except at 1 µM, which had no statistically significant ($P \geq 0.05$) reduction, compared to the untreated basal control group (Figure 4.8). The reduction was to a similar level in all groups.

After 2 days of treatment with MI192, all MI192 treatment groups showed a statistically significant reduction in cell viability ($P \leq 0.001$) compared to the untreated basal control group. The higher doses (40 µM and 50 µM) showed the greatest reduction in cell viability compared to the untreated basal control group. There was a clear dose response, with the lower doses showing the least reduction in cell viability compared untreated basal control group.

After 3 days of treatment with MI192 all groups showed a statistically significant reduction ($P \leq 0.001$ for all treatment groups except 1 µM, which was $P \leq 0.01$) in cell viability, compared to the untreated basal control group. A dose response was visible; in the higher doses (50 µM, 40 µM and 30 µM) the cell viability was near 0, with the lower doses (20 µM, 10 µM and 1 µM) having higher overall level of viable cells.

MI192 was found to have an effect on the viability of ADSCs, at all doses and dose lengths, except 1 day of 1 µM MI192. At all doses, except 1 µM, a reduction in cell viability was seen with increasing dosage time. 1 µM showed a reduction after 2 days of treatment, with the same level of reduction seen at 3 days, compared to the untreated basal controls.

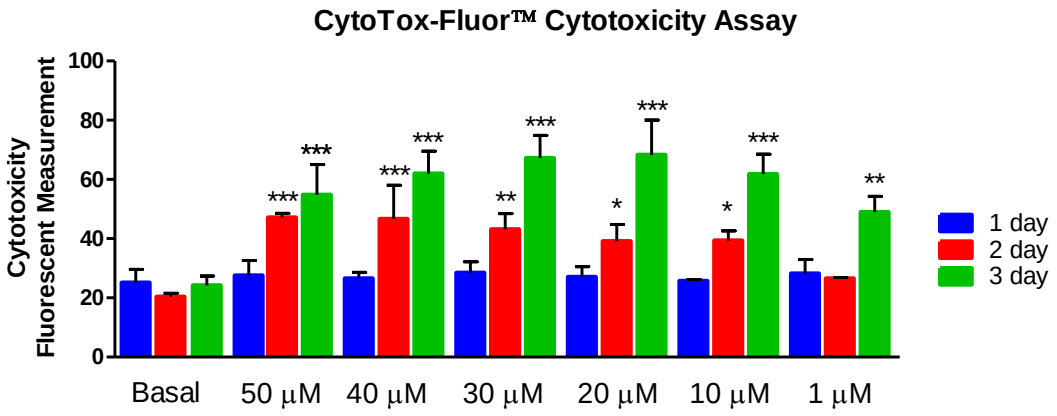

Figure 4.7 - CytoTox-Fluor™ analysis of ADSCs treated with a range of MI192 doses (50 µM, 40 µM, 30 µM, 20 µM, 10 µM and 1 µM) for 1 day, 2 days and 3 days. Results expressed as mean ± SD (n=3) Significance levels shown are the sample compared to the basal control for that time point, i.e. A 40 µM dose for 2 days compared to basal control at 2 days. * = p ≤ 0.05, ** = p ≤ 0.01 and *** = p ≤ 0.001.

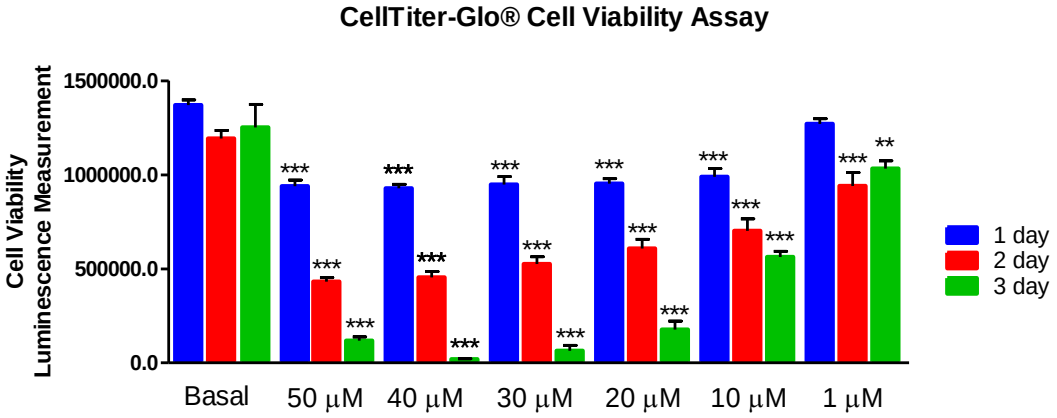

Figure 4.8 - CellTiter-Glo® analysis of ADSCs treated with a range of MI192 doses (50 µM, 40 µM, 30 µM, 20 µM, 10 µM and 1 µM) for 1 day, 2 days and 3 days. Results expressed as mean ± SD (n=3). Significance levels shown are the sample compared to the basal control for that time point, i.e. A 40 µM dose for 2 days compared to basal control at 2 days. * = P ≤ 0.05, ** = P ≤ 0.01 and *** = P ≤ 0.001.

4.3.5 Effect of MI192 on the HDAC specific activity of ADSCs

Treatment of ADSCs for both one and two days with two doses of MI192 (30 µM and 10 µM) lead to a statistically significant (P ≤ 0.01) reduction in the HDAC specific activity of the cells, compared to untreated controls (Figure 4.9). There was no observable difference between the two different doses at both time points.

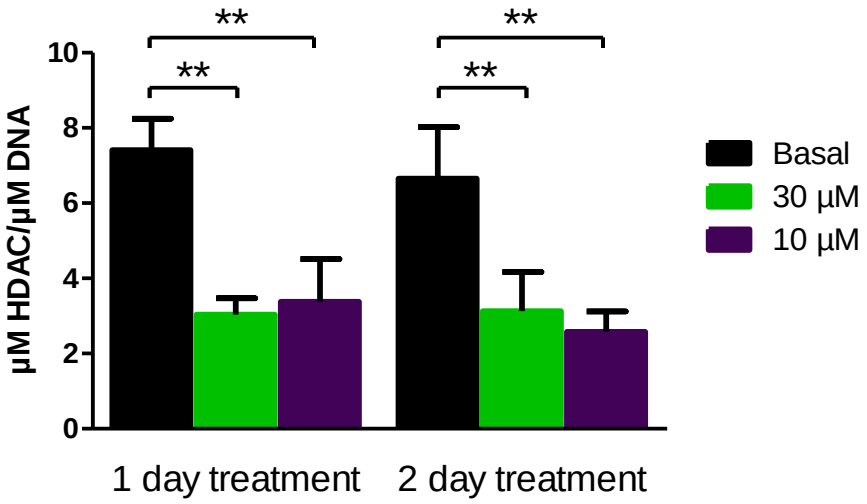

Figure 4.9 – HDAC activity of ADSCs treated for 1 day and 2 days two of doses of MI192. Results expressed as mean ± SD (n=3), ** = P ≤ 0.01

4.3.6 Effect of MI192 on ADSC Cell Cycle

Representative histograms show the number of cells in different stages of the cell cycle (Figure 4.10). The average exact % of each group was calculated (Table 4-2).

After 12 hours, 92.05 % of the cells in untreated basal medium group were in the G0/G1 phase, 3.25 % of the cells were in G2/M phase and 4.76 % of the cells were in S phase. In contrast, both MI192 treatment groups showed an increase in the G2/M phase (11.32 % for 30 µM and 7.03 % for 10 µM) compared to that of the basal control (3.25 %). There is also an increase in the S phase in the treated groups (9.22 % for 30 µM and 6.39 % for 10 µM) compared to that of the basal control (4.76 %). The 10 µM TSA group showed a similar increase at G2/M phase (8.96 %), but a slight drop in the S phase (2.68 %) compared to the basal controls.

After 24 hours, 68.65 % of the cells in basal medium group were in the G0/G1 phase, 17.13 % of the cells were in G2/M phase and 14.22 % of the cells were in S phase. Again, both MI192 treatment groups showed an increase in the G2/M phase (23.56 % for 30 µM and 21.98 % for 10 µM) compared to that of the basal control (17.13 %). There were less cells found in the S phase of the cell cycle in the treated groups (7.30 % for 30 µM and 8.51 % for 10 µM), compared to the basal medium group (14.22 %). The 10 µM TSA group also showed a increase G2/M phase (23.47 %), but a higher percentage of cells in the S phase (12.65 %) than the MI192 treated groups.

After 48 hours, 56.3 % of the cells in untreated basal medium group were in the G0/G1 phase, 9.46 % of the cells were in G2/M phase and 40.86 % of the cells were in S phase. Again, both MI192 treatment groups showed an increase in the G2/M phase (11.97 % for 30 µM and 18.59 % for 10 µM) compared to that of the untreated basal medium group (9.46 %). In the S phase the MI192 treated groups had a lower percentage of cells (33.81 % for 30 µM and 8.153 % for 10 µM) than the untreated basal medium group (40.86 %). The 10 µM TSA group showed a similar increase at G2/M phase (18.72 %), and a lower percentage of cells in the S phase (10.43 %) than the basal control, with a level comparable to the 10 µM MI192 treated group.

MI192 treatment was found to increase halting of the ADSC cell cycle of in the G2/M phase, with the results showing a similar trend with TSA treatment.

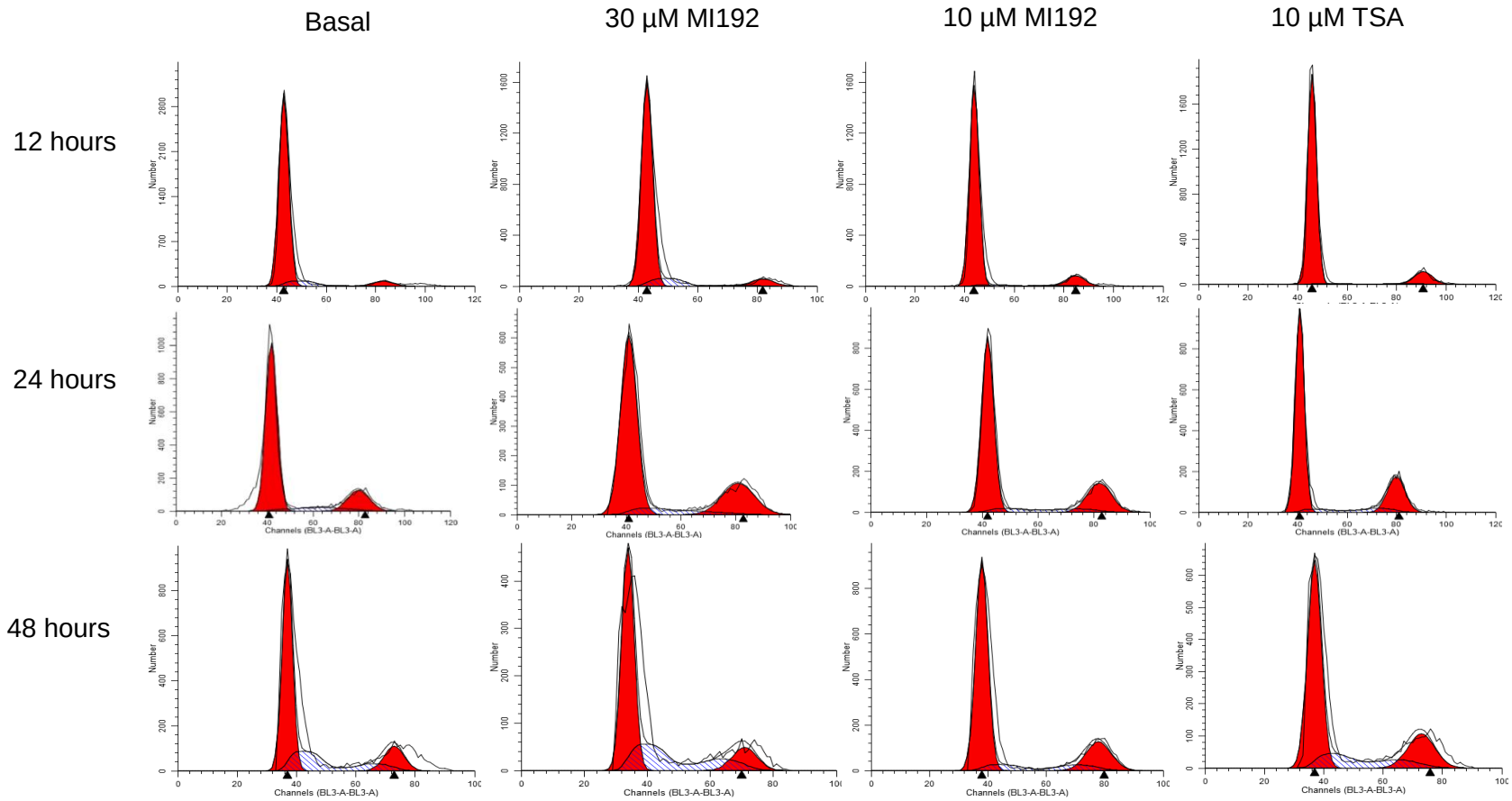

Figure 4.10 – Representative histograms of the flow cytometry analysis of the cell cycle distribution for ADSCs dosed with 30 µM and 10 µM MI192 and 10 µM TSA with untreated controls, for 12, 24 and 48 hours. Representative histograms from each time point and test group shown, the experiment was carried out in biological triplicate, and histograms are representative of at least 2000 events. The first large peak represents the population of cells in the G0/G1 phase, the second small peak the population of cells in the G2/M phase, with the area in between the S Phase.

Table 4-2 – Table of data for the flow cytometry analysis of the cell cycle distribution for ADSCs. Cells were dosed with 30 µM and 10 µM MI192, 10 µM TSA and untreated controls, for 12, 24 and 48 hours. Average percentage of cells for each of the three calculated phases of the cell cycle shown, with the standard deviation (SD) for each.

		G0/G1Phase Mean %	SD	G2/M Phase Mean %	SD	S Phase Mean %	SD
12 hours	**Basal**	92.05	2.74	3.25	1.14	4.76	1.68
	30 µM MI192	79.46	6.47	11.32	2.07	9.22	2.07
	10 µM MI192	86.61	1.91	7.03	1.24	6.39	2.95
	10 µM TSA	88.36	0.39	8.96	1.53	2.68	1.22
24 hours	**Basal**	68.65	7.81	17.13	0.96	14.22	8.75
	30 µM MI192	69.15	1.44	23.56	1.09	7.30	1.10
	10 µM MI192	69.50	3.38	21.98	0.44	8.51	3.05
	10 µM TSA	63.88	4.91	23.47	1.02	12.65	4.04
48 hours	**Basal**	56.3	5.42	9.46	3.94	40.86	9.36
	30 µM MI192	54.22	3.62	11.97	0.40	33.81	4.01
	10 µM MI192	73.26	3.25	18.59	0.49	8.153	2.87
	10 µM TSA	70.86	6.88	18.72	1.09	10.43	5.81

4.3.7 Effect of MI192 on ADSC Stem Cell Markers

The expression of 9 commonly used stem cell markers (see Table 4-1 for full details) was investigated in ADSCs treated with 30 µM MI192 for 2 days, compared to untreated basal medium controls. Markers were assessed as a group of three (CD29/CD73/CD90) and three groups of two (CD34/CD45, CD44/CD166 and CD146/CD105). Representative dot plots of the events (after gating for intact cells) were produced for the groups of markers for both the untreated ADSCs and are shown in the Appendix (A4 - Effect of MI192 on ADSC Stem Cell Markers: FACs plots and autofluorescence comparison histograms). Also produced and shown in the Appendix were histograms showing the expression of the marker compared to the negative autofluorescence readings for the cells, for both untreated and MI192 treated ADSCs. This was to account autofluorescence when analysing the markers, and to ensure there was no overlap with the expressing populations.

The events in the treated cells were more spread than in the untreated controls, so to understand if the spread of data was just due to a size alteration on the death of the cells, a propidium iodide stain of the MI192 treated cells was analysed (Figure 4.11). The cells were washed several times before detachment and labelling, so cells that were already dead should not have been labelled. However, the PI staining indicates that only 84.25 % of the cells labelled were alive, so some cells labelled will be close to death and likely did not just detach with the wash. These dead cells were gated out when analysing the stem cell markers. The PI staining indicates two populations of cells, so these were gated (Figure 4.11 D) and then the spread of these cells was re-assessed. Figure 4.11 C shows that the cells in this sub-population had a spread of size similar to that of the whole population (Figure 4.11 A). This showed that the sub population of cells that has appeared is not solely due to the cells being a different size, or dying, the population appears to be a distinct one, of live cells.

To show the difference in stem cell marker expression in cells treated with MI192, compared to untreated controls, representative histograms were produced (Figure 4.12, Figure 4.13 and Figure 4.14), along with a table illustrating the average percentage (of the three technical repeats) of the total population of cells labelled with the marker, for the untreated and MI192 treated cells (Table 4-3). The treatment of ADSCs with MI192 clearly causes an increase in expression of CD34 and CD146

(Figure 4.12 B and Figure 4.14 B), when compared to the untreated controls. This was a +35.46 % increase for CD34 and an increase of +35.02 % for CD146. After MI192 treatment, cells with lower expression of CD29, CD44, CD73, CD90, CD105 and CD166 can be seen when compared to the controls (Figure 4.12 A and C, Figure 4.13 B and C and Figure 4.14 A and C). For some markers, there was a large decrease; -20.61 % for CD29, -7.94 % for CD73, and -40.29 % for CD105 (Figure 4.12 A, Figure 4.13 B and Figure 4.14 A). There was only a smaller decrease in CD44 (-2.84 %) and CD166 (-4.53 %) (Figure 4.12 C and Figure 4.14 C). In contrast, and virtually no change in the expression level of CD45 and CD90 (Figure 4.13 A and C) remained similar level compare to the untreated group (+0.66 % and -0.12 % respectively).

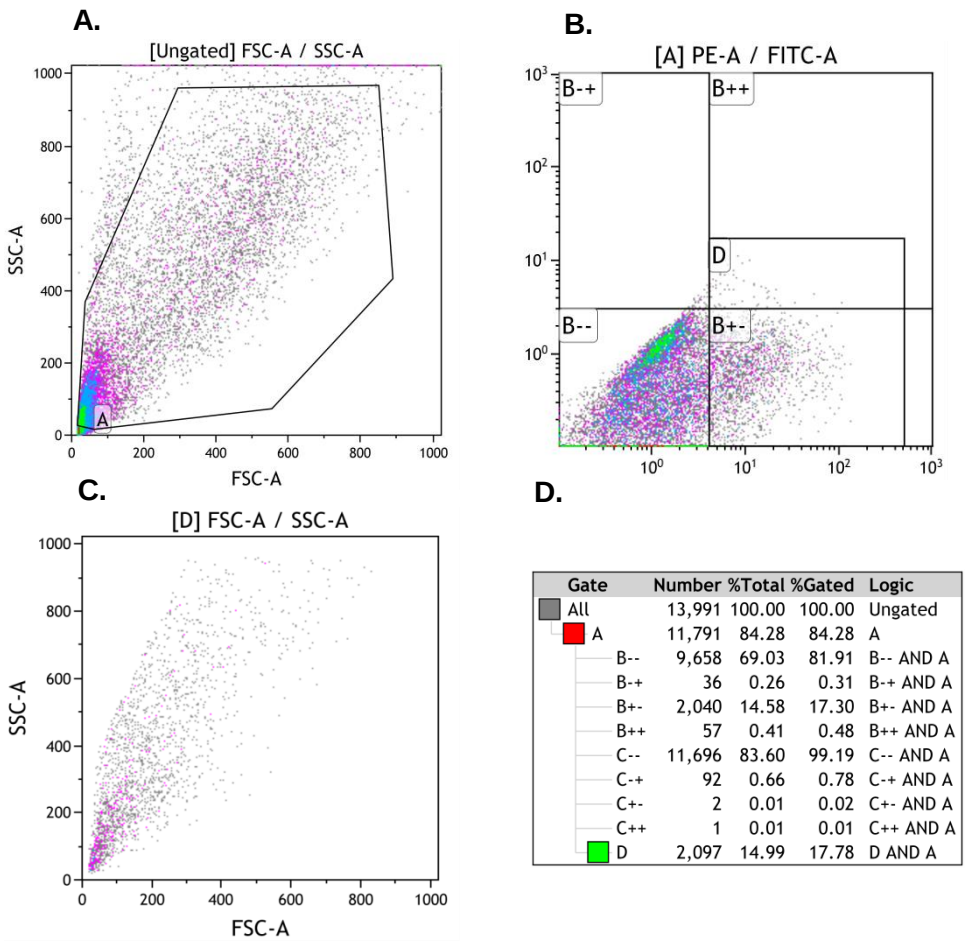

Figure 4.11 - Representative histograms showing flow cytometric analysis of PI staining of MI192 treated ADSCs. A – Gate 1, gating for intact cells, **B** – Gate 2 (box D on the plot) – gating for the subpopulation of cells, **C** – size analysis of the subpopulation of cells from Gate 2 (D on the plot). **D** – Statistical analysis of the gates.

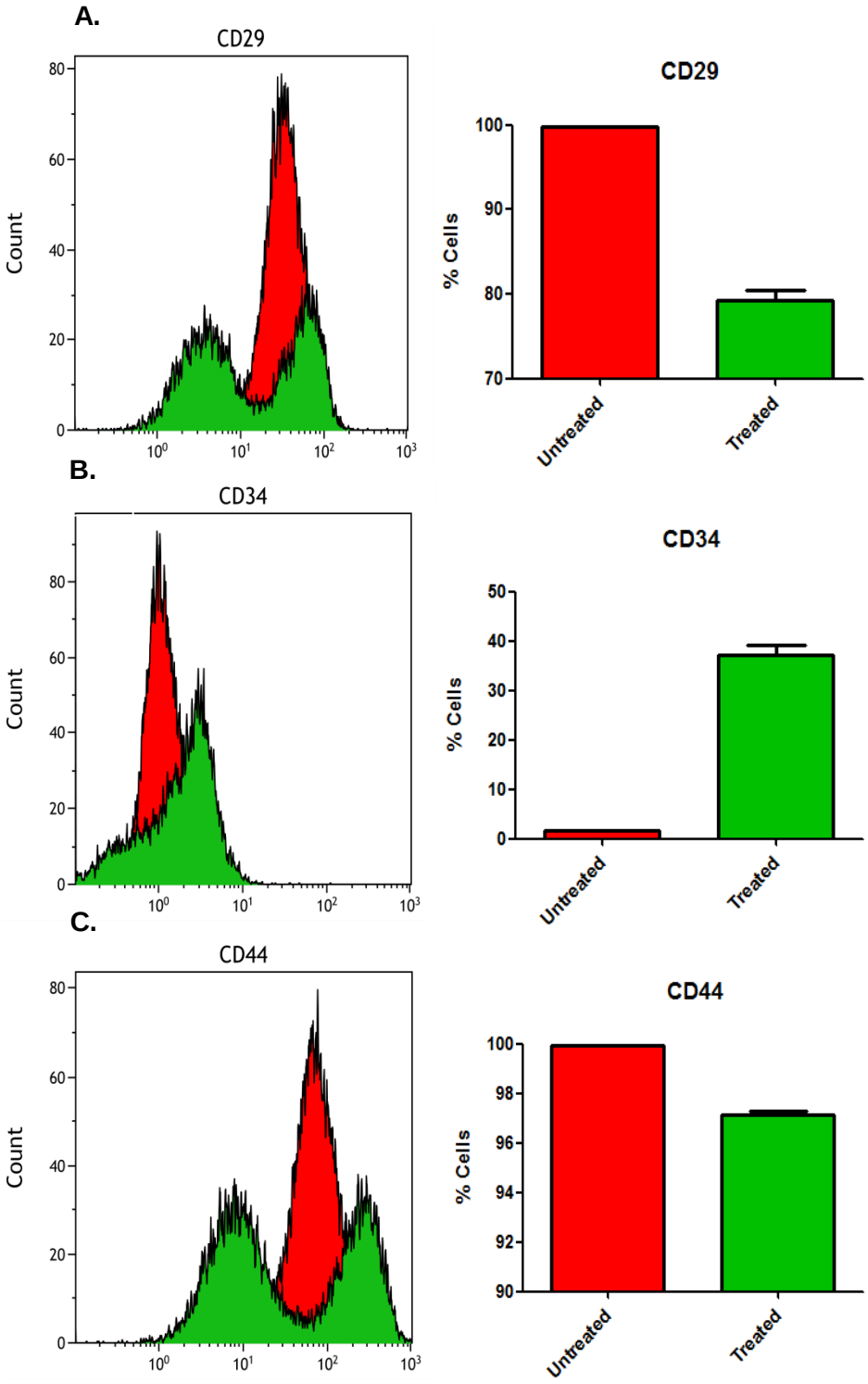

Figure 4.12 – CD29, CD34 and CD44. Representative histograms and graphical representation of flow cytometric analysis of stem cell markers in MI192 treated compared to untreated ADSCs. Error bars represent SD of technical repeats (n = 3). **A** – CD29, **B** – CD34, **C** – CD44. Untreated ADSCs (red colour) compared to MI192 treated (green colour). Note the y axis is a different scale for each graph.

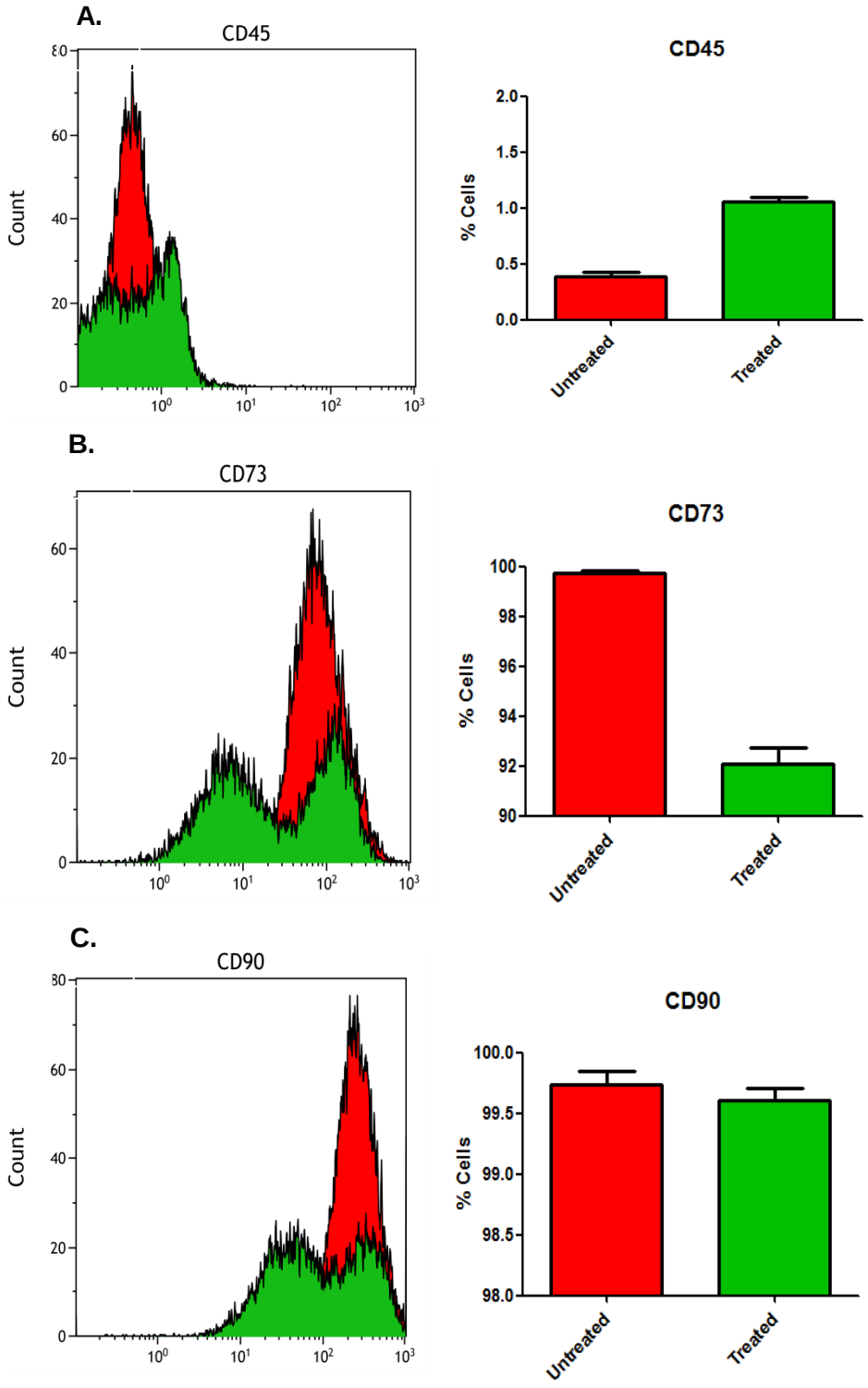

Figure 4.13 – CD45, CD73 and CD90. Representative histograms and graphical representation of flow cytometric analysis of stem cell markers in MI192 treated compared to untreated ADSCs. Error bars represent SD of technical repeats (n = 3). **A** – CD45, **B** – CD73, **C** – CD90. Untreated ADSCs (red colour) compared to MI192 treated (green colour). Note the y axis is a different scale for each graph.

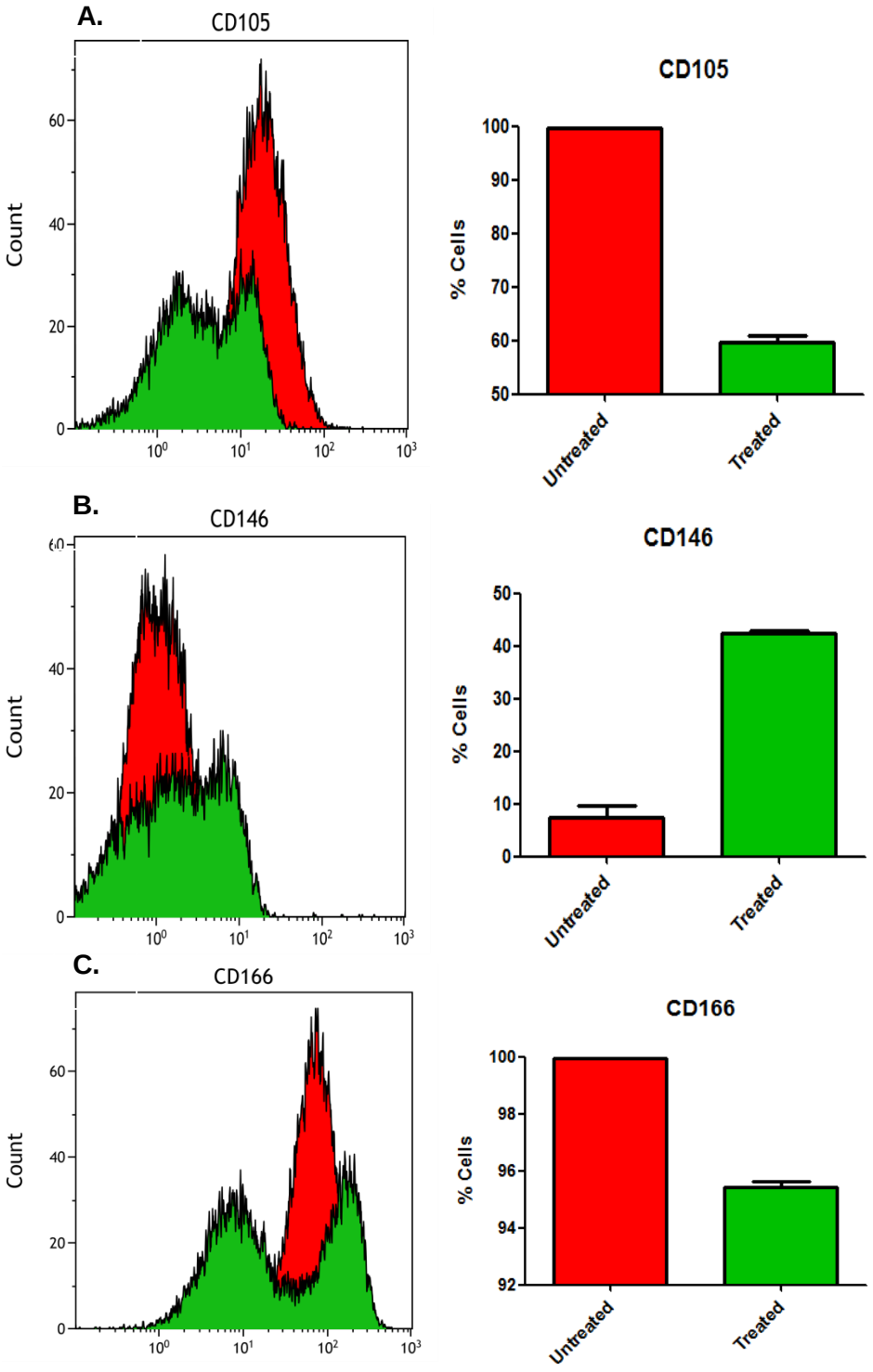

Figure 4.14 – CD105, CD146 and CD166. Representative histograms and graphical representation of flow cytometric analysis of stem cell markers in MI192 treated compared to untreated ADSCs. Error bars represent SD of technical repeats (n = 3). **A** – CD105, **B** – CD146, **C** – CD166. Untreated ADSCs (red colour) compared to MI192 treated (green colour). Note the y axis is a different scale for each graph.

Table 4-3 – The percentage of untreated and MI192 treated ADSCs positive for stem cell markers CD29, CD34, CD44, CD45, CD73, CD90, CD105, CD146 and CD166. The percentage change on treatment was calculated.

Marker	Untreated	Treated	Change
CD29	99.84 %	79.23 %	- 20.61 %
CD34	1.66 %	37.12 %	+ 35.46 %
CD44	99.96 %	97.12 %	- 2.84 %
CD45	0.39 %	1.05 %	+ 0.66 %
CD73	99.74 %	92.10 %	- 7.94 %
CD90	99.73 %	99.61 %	- 0.12 %
CD105	99.69 %	59.67 %	- 40.29 %
CD146	7.42 %	42.44 %	+ 35.02 %
CD166	99.96 %	95.43 %	- 4.53 %

4.4 Discussion

In recent years, the possibility of utilising HDACi compounds to control the osteogenic potential of cells for tissue engineering applications has been explored (Iwami & Moriyama 1993; Schroeder et al. 2007; H.-N. Kim et al. 2011). In many publications exciting findings such as improvements to differentiation protocols (Maroni et al. 2012; Boer et al. 2006), are reported, but often avoid the reporting of side effects to using the HDACis, such as cytotoxicity or proliferative halting effects.

Thus, it is important to gain an understanding of the effect of HDAC2 and HDAC3 selective MI192 on general cellular properties before looking at its effects on differentiation. Cytotoxic effects and alterations to cell properties such as changing the cell cycle or stem cell marker expression may have implications for how these compounds are utilised.

It has been reported in the literature that HDACis halt the proliferation of cells (Khan et al. 2008), particularly MSCs (Lee et al. 2009; Kurihara & Suzuki 2014). While it has been reported that low doses of TSA (10 nM – 100 nM) stimulate the proliferation of dental pulp derived MSCs (Jin et al. 2013), another paper reported that TSA halted the proliferation of murine dental pulp cells (Duncan et al. 2012). This is likely due to HDACis halting the cell cycle, but this is discussed later. This proliferation halting effect may be being observed in the images taken throughout MI192 treatment (Figure 4.3, Figure 4.4 and Figure 4.5). These show that cells treated with MI192 become smaller and more rounded, which can be seen as early as 12 hours, and most clearly in the lower, 5 µM MI192 doses (Figure 4.3 A). Cells will often clump together in clusters, sometime detaching as clusters (Figure 4.3 A). It is clear that MI192 has an effect on the cell phenotype, with cell death also visible at higher doses. This is in contrast to TSA, where cell death is not visible, and the cells have a different, although still distinct morphological change. When treated with TSA, the cells become more elongated. This cell morphology change may be due to the TSA dosage halting proliferation of the ADSCs, potentially causing the cells to become more elongated rather than pushing against each other as in the basal controls. Also relevant, and although no data is shown, when seeding cells, MI192 clearly inhibited cell attachment and caused high levels of cell death.

Assessment of the total DNA content, indicating cell numbers, gave a quantitative measurement of the cell death or proliferative halting effect observed previously. As dead cells were washed away, the total DNA content correlates to the total number of live cells. The total DNA content is reduced over 1, 2 and 3 days when cells are treated with MI192 (Figure 4.6). This could be a combination of, or one of, cellular proliferation being halted or cell death. At least some of this must be due to cell death, as the DNA content, especially in the groups with the higher doses (30 µM – 50 µM), drops below the initial basal level of cells (if it was purely a proliferation halting effect, the DNA content would be the same as at seeding). A dose response can also be seen, with the lower doses having the lowest reduction in DNA content. It is clear that the longer the treatment time, the more cell death.

It is important to know if any compound utilised with cells is going to have a cytotoxic effect, or an effect on cell viability, as this may have implications for how (or if at all) the compound is utilised. This is especially important given the drop in cell numbers observed previously. In the literature, HDACis are often utilised at low concentrations, and are often reported not to be cytotoxic to normal cells, or affect cell viability (for example in Duncan et al. 2012; Paino et al. 2014; Xu et al. 2013). This is the opposite of typical reports with cancer cells, where the aim is usually to utilise HDACis to kill cancerous cells (Frew et al. 2009). The results in this chapter (Figure 4.7) show that after two days of treatment, high concentrations of MI192 had a cytotoxic effect on ADSCs. The effect was dose dependent, and it was even more pronounced after three days of treatment.

A simple one reagent addition ATP assay was chosen to show the effect of MI192 on cell viability (Figure 4.8), as this is the most widely used assay for high throughput screening and is regarded as being a fast and reliable method of determining cell viability (Riss et al. 2004). In the literature, this method has been utilised to assess the effect of SAHA on leukaemia cells (Petruccelli et al. 2011).

There was a visible loss in cell viability after just one day of treatment with MI192. This effect was dose and time dependent. By day 3, there was very few (5 % – 20 % of the basal control) viable cells in the 50 µM – 20 µM groups. It is worth noting that the cell viability assay only measures ATP activity in cells, which is associated with

cell viability, but does not measure if the cells are able to recover to a viable state. The assay works on the principle that when dying cells lose membrane integrity their ability to synthesise ATP will cease and endogenous ATPases will remove any ATP present in the cells. However, if all of the cells not generating viable ATP signals were dead in this assay, a much larger reduction in cell number (total DNA content) would be observed previously in these cells with MI192 treatment (Figure 4.8). More than 5 % of cells remained after 3 days of treatment with 30 µM MI192, and therefore not all can be dying. It may be that the alteration of the epigenetic makeup of the cell may affect the cell's ability to produce ATP, which may not have any other adverse or long term effects. Indeed, there are established links between ATP fuelled transporters and HDAC enzymes and inhibition, and this may be a side effect of that (Ni et al. 2015).

An alternative viability assessment method was also undertaken with propidium iodide, in combination with the assessment of stem cell makers. It is a commonly used tool for assessment of cell viability, for example used in the literature to assess peripheral blood lymphocytes treated with SAHA (Brodská & Holoubek 2011). PI staining confirmed that 84.25 % cells remained viable after two days of 30 µM MI192 treatment, although this didn't measure include dead cells that had been washed away prior to staining.

These results all together indicate that ADSCs should not be exposed to MI192 for longer than 2 days and/or to high doses of MI192 (over 10 µM), at least without appreciating there will be a loss of cell number and/or viability.

It is important to explore the effect of MI192 on the HDAC activity of the ADSCs. As discussed in Chapter 3: The Chemical Synthesis of MI192, it has been reported that MI192 reduces the activity of HeLa cells, to a comparable or better level than other HDACis (Boissinot et al. 2012). Elsewhere, a fluorometric assay sold by Biovision has been used to show that HDACis (e.g. MS-275) reduce the HDAC activity of cells (Kim et al. 2014; Zhang et al. 2012). The assay contains a substrate with an acetylated lysine side chain, which HDAC enzymes will deacetylate, resulting in a product that can be developed with a developer to produce a fluorescence signal.

In this study, the same assay was used to demonstrate that MI192 reduces the HDAC activity of ADSCs. After 1 and 2 days treatment, both doses of MI192 (30µM and 10 µM) reduced ADSC HDAC activity. These reductions were similar in both doses of MI192 and at both time points. It is known that MI192 is specific for HDAC2 and HDAC3, and has a much lower inhibition of other HDAC isoforms (Boissinot et al. 2012). Therefore, uninhibited HDAC enzymes could still act to deacetylate the substrate and some activity should still be observed in cells. This study confirmed that MI192 has a HDAC inhibitory effect function after 24 hours. The fact that the two doses are showing the similar levels of HDAC activity indicates that both doses of MI192 will reduce HDAC activity, and that the differences in effects, such as cytotoxicity, may be due to other effects of MI192. Alternatively, cells may metabolise MI192, or it may unbind, and in the higher concentrations there is more opportunity for MI192 to rebind, having a longer period affecting cells. Also, MI192 may have a short half-life in the medium, and a higher concentration of MI192 results in there being a greater amount of MI192 available over time.

In a normal functioning cell, the cell cycle is the sequence of events that takes place leading to cell division, and it is essential to normal cell function and the processes of proliferation and differentiation (Majdzadeh et al. 2008; Jiang & Hsieh 2014). A number of studies show that HDAC2 and HDAC3 are both involved in the regulation of the cell cycle (Yamaguchi et al. 2010; Bhaskara et al. 2009; Jiang & Hsieh 2014). Thus, disrupting their action could have an effect on the cell cycle that in turn could help to control cell function. It has been reported that SAHA reduced the number of MSCs in the G2/M phase, MS-275 reduced the number of MSCs in the S phase, and both of them halted the cells in the G1 phase of the cell cycle (Di Bernardo et al. 2009).

In this study, MI192 was shown to reduce cell numbers in the S phase of the cell cycle, but it increased numbers in the G2/M phase (Table 4-2 and Figure 4.10), which doesn't mirror the results seen with MS-275 or SAHA (Di Bernardo et al. 2009). A similar effect was also seen in the TSA treated group, where the cells halted the cell cycle in the G2/M phase. This indicates that MI192 and TSA may have a different mechanism of action compared to MS-275 and SAHA. The standard deviation of the S phase was especially high, at later time points, and the histograms show the fact that the software had a harder time picking the peaks at the later time points. This is

likely due to a greater spread in the cell cycle as a mixed stromal population of cells diverges from a set point (i.e. when they are seeded) more over a longer period of time.

Although reports can vary, MS-275 is thought to be relatively HDAC1, HDAC2 and HDAC3 selective (Bradner et al. 2010; Khan et al. 2008; Boissinot et al. 2012). Jiang et al. (2014) demonstrated that in HDAC3 mouse knock down models, cells cannot progress through the G2/M phase of the cell cycle (Jiang & Hsieh 2014); HDAC3 controls this progression through stabilisation of the G2/M cyclin dependent kinase 1 (CDK1). Therefore, the inhibition of HDAC3 may result in an induction of cycle arrest in G2/M, an effect seen in this study. The G2/M cell cycle check point is where the cell checks for DNA damage. Some HDACis are known to cause damage to DNA (McGee-Lawrence et al. 2011; Petruccelli et al. 2011), therefore it may be that the high level of cells at the G2/M checkpoint is in response to this DNA damage, and that cells are halting here and exiting the cell cycle via controlled apoptosis. This could explain the high level of cell death observed in the MI192 treated cells.

Stem cell markers are a general term, referring to genes or proteins that can be utilised to isolate and/or identify stem cells (Baer & Geiger 2012; Churchman et al. 2012; Nielsen & McNagny 2008). The effect of HDACis on these markers may reflect on their role in stem cell fate. HDACis have the potential to promote stem cell self-renewal or increase the stem cell properties of cells (Kretsovali et al. 2012). In mouse ES cells, it has been shown that HDACis (such as VPA, NaB and TSA) improved transfection protocols and had no effect on stem cell markers (pluripotency marker Oct4, was tested) (Y. Kim et al. 2013), although these were different markers to those tested here. There is very little literature precedent for this work, and no studies test the stem cell markers before and after HDAC treatment. The ADSCs used in this thesis were sorted by the manufacturer (Life Technologies) to be positive for CD29, CD44, CD73, CD90, CD105 and CD166, and negative for CD45. The results demonstrate that at passage 5, the cells are still maintaining their stem cell markers.

Treatment of cells with MI192 may have resulted in a subpopulation of cells forming, with a different stem cell marker profile was observed. The testing of the cells with propidium iodide, which will only penetrate cells when they are dead, demonstrated

that this sub-population of cells that has formed was not just due to cell death, and when the size of the cells in the sub-population of cells was investigated, the sub-population was not just due to a change in the cell size (which is observed in the cell phenotype changing with MI192 treatment). The sub-population of cells had a large increase of expression of CD34 and CD146, with a decrease in expression of CD29, CD44, CD73, CD105, CD166, with no change in the expression of CD45 and CD90.

Regarding the markers that were up-regulated with MI192 treatment, CD34 is a commonly utilised marker of HSCs, and can be used to separate these cells from bone marrow MSCs (Trowbridge & Thomas 1994; Tomlinson et al. 2015; Nielsen & McNagny 2008). CD146 is highly expressed in blood vessels and pericytes, structural cells of the vascular system. While CD34 is classified as a marker of hematopoietic lineage, it is expressed in early ADSCs, and is lost with increased cell culture time. CD146 is also reported to decrease with culture time, but is expressed in CD34 negative cells, and not in CD34 positive cells (Mitchell et al. 2006; Baer & Geiger 2012). The increased expression of both of these on treatment with MI192 is very interesting.

It has been suggested that HSCs may actually be progenitor cells for ADSCs (Sera et al. 2010), so the increase of these stem cell markers may indicate the ADSCs, which survive the treatment with MI192, are more immature. This may mean that they have greater differentiation potential. Alternatively, they may be primed to differentiate down the lineages that HSCs are specialist for, such as the blood, lymphatic and immune systems. The treatment of ADSCs with MI192 may be priming these cells to behave like HSCs, or may just be making the cells more “stem cell like” and/or immature ADSC like. Although the topic is controversial and conclusions are not fully drawn. Reportedly, CD34 positive cells have greater colony forming ability and proliferative capacity, but less ability to differentiate into osteogenic and adipogenic lineages (Suga et al. 2009). This could have implications for the differentiation potential of the MI192 treated ADSCs.

The down-regulation of the CD29, CD44, CD73, CD105 and CD166 could have a wide range of consequences. Markers such as CD29 are also markers of HSCs, while others, e.g. CD73 was more used as bone marrow MSC markers. The

reduction in these was quite small, in the range of (3 % - 8%, and the cells still expressed these markers to a reasonably high percentage (except CD105 which had a 40 % reduction). It is well known that CD105 is highly expressed in angiogenic endothelial cells and in the blood vessels of tumour tissues, which means that these cells may be losing angiogenic potential (Duff et al. 2003). However, CD34 is also a marker of angiogenesis, and expression was increased on MI192 treatment, so picture is a slightly confusing one. The alteration of these markers could have implication for their applications, as vascularisation of tissues is becoming more of a highlighted issue for generating functional tissue as tissue engineering evolves (Liu et al. 2013).

Chapter 5: The Effects of MI192 on the Differentiation of Adipose Derived Stem Cells in 2D

The aim of this chapter is to investigate effects of MI192 on the differentiation of ADSCs, and primarily to address how the osteogenic differentiation potential of these cells is affected. The objectives are to investigate how MI192 pre-treatment and treatment for the whole experiment affects the alkaline phosphatase (ALP) activity of ADSCs, how the pre-treatment with MI192 affects the ALPSA of ADSCs compared to TSA, the effect of MI192 on ALP activity in cells from four different donors and with two different batches of MI192, and how the effect of pre-treatment with MI192 with two different osteogenic mediums affects ALP production over time. Further objectives are to investigate the effect of MI192 pre-treatment on osteogenic gene expression, and mineralisation through Alizarin Red and Von Kossa staining. Finally, the effect of MI192 pre-treatment on the adipogenic potential of the ADSCs was investigated, through Oil Red O staining and assessment of adipogenic gene expression.

5.1 Introduction

The clinical need for bone tissue engineering could be met by the appropriate combination of stem cells, scaffolds, suitable mechanical stimuli and optimal growth factors. Cells can be taken either from the patient, or obtained from an allogenic source, engineered to differentiate down an osteogenic lineage and implanted into the patient. The potential for using ADSCs in bone tissue engineering has been well documented both *in vitro* and *in vivo* (Levi & Longaker 2011; Halvorsen et al. 2001; Zheng et al. 2006; Colnot 2011).

Reports of HDACis being utilised in bone related research primarily began with studies into the side-effects of HDACis being utilised in cancer therapies (Witt et al. 2009). SAHA and VPA have been reported to have a negative impact on bone density in patients, as well as a damaging effect on osteoblasts (McGee-Lawrence et al. 2011; Pratap et al. 2010). For example, VPA has been found to increase the neurogenic differentiation capacity of canine ADSCs, while reducing the late stages of adipogenic and osteogenic potential of these cells (Kurihara & Suzuki 2014).

SAHA was found to decrease osteoblastic gene expression, induce cell cycle arrest and cause DNA damage in *in vitro* tests with mouse bone marrow MSCs. Interestingly, mature osteoblast cells were not affected (McGee-Lawrence et al. 2011).

In contrast, Dudakovic et al. (2015) reported that SAHA enhanced ADSC expression of some key stem cell pluripotency markers (*NANOG*, *OCT4/POU5F1*, and *SOX2*), which may indicate that SAHA induces a more immature pluripotent state in ADSCs (Dudakovic et al. 2015). Also, Xu et al (2013) suggested that while high doses of SAHA are toxic to human bone marrow MSCs, lower doses will increase the osteogenic potential of these cells (increasing ALP activity, mRNA expression of osteogenic markers, and matrix mineralisation). Furthermore, it has been shown that when mice were dosed with clinically relevant doses of SAHA, there was no sign of loss in bone density (Xu et al. 2013). This study highlights the importance of dose optimisation when using compounds such as SAHA, with potentially very harmful side effects, as this can be the crucial to find a balance between negative and positive effects.

As well as investigating the side effects of HDACis on cells within cancer therapeutics, researchers have begun to investigate their effect on stem cells, for tissue engineering purposes. Early successes with mouse derived bone marrow MSCs (Cho et al. 2005; Schroeder & Westendorf 2005) preceded similar findings with human bone marrow MSCs, where TSA was found to improve their osteogenic differentiation (Boer et al. 2006). Similarly, SAHA and VPA have been shown to increase the osteogenic potential of human bone marrow MSCs, with no negative effect on bone in mouse animal models (Xu et al. 2013). There are other studies also demonstrating the potential of HDACis to increase the osteogenic potential of other cell populations, such as human periodontal ligament fibroblasts (T.-I. Kim et al. 2013) and mouse dental pulp-derived cells (Duncan et al. 2012).

More specifically regarding this study, researchers have also investigated the effect of HDACis on ADSCs. However, the picture can be a confusing one, as there is evidence to suggest that HDACis can both increase and reduce the osteogenic differentiation potential of ADSCs. The majority of findings in field support the potential for HDACis to have a positive impact on the osteogenic potential of

ADSCs. At varying oxygen concentrations, both VPA and NaB have been found to increase the osteogenic potential of mouse adipose derived stem cells, promoting gene expression, Alizarin Red staining and ALP activity, while also decreasing the adipogenic potential of the cells (Xu et al. 2009). Also, TSA and NaB can enhance rat ADSCs osteogenic gene expression, ALP activity and mineralisation levels of the cells (Hu et al. 2014; Hu et al. 2013).

Isoform specificity is becoming particularly interesting to researchers, as outlined in depth in the introduction of Chapter 4: The General Effects of MI192 on Adipose Derived Stem Cells Cultured in Monolayer. In 2012, Maroni et al. investigated the effect of blocking HDAC1 and HDAC3 on the differentiation potential of ADSCs, and suggested that specific targeting of HDAC isoforms may improve the differentiation potential. Pre-treatment of cells with TSA before osteogenic induction increased the osteogenic potential of the ADSCs (assessed by measurement of ALP activity, Alizarin Red staining and assessment collagen production) (Maroni et al. 2012). This is in line with the aforementioned study by Boer et al. (2006), where it was reported that TSA increased the osteogenic potential of human bone marrow MSCs (Boer et al. 2006). Maroni et al. also found that the genetic blocking of HDAC1 and HDAC3 with small interfering RNAs (siRNAs) activated the osteogenic differentiation pathway of the ADSCs, with increased *RUNX2* and decreased *PPARγ* expression (respectively the osteogenic and adipogenic master transcription factors) (Maroni et al. 2012). siRNAs have also been utilised to block HDAC6, which was found to activate the osteogenic differentiation pathway of human ADSCs, by increasing *RUNX2* and decreasing *PPARγ* expression (Huang et al. 2012). Aside from ADSCs, MS-275, allegedly a HDACi specific to HDAC1 HDAC2 and HDAC3 improved the osteogenic differentiation potential of mouse primary osteoblast precursor cells (Kim et al. 2012; H.-N. Kim et al. 2011).

MI192 is an isoform specific HDACi, specifically targeting HDAC isoforms HDAC2 and HDAC3. The aim of this study was to investigate the effects of MI192 on the differentiation potential of ADSCs, with particular attention paid to the effect on the osteogenic differentiation potential of the cells.

5.2 Materials and methods

5.2.1 The effect of MI192 on the early osteogenic differentiation of ADSCs

Alkaline phosphatase activity can be stained histologically or measured in a biochemical assay and normalised to total DNA content of the cells, giving the quantitative alkaline phosphatase specific activity (ALPSA) of the cells. See 2.4: Biochemical assays for the ALPSA methods. ALP is a useful marker for measuring early stage osteogenic differentiation of cells. They were used in a number of experiments investigating MI192 and its effect on the osteogenic differentiation potential of ADSCs.

5.2.1.1 The effect of MI192 pre-treatment on the alkaline phosphatase staining levels of ADSCs

ADSCs were seeded in a 12 well plate (1 x 10^5 cells per well) and cultured in basal medium for 24 hours. The medium was then replaced with MI192 containing medium (100 µM and 30 µM in 1 mL basal medium). Basal medium alone (untreated wells) was used as the negative control group. After 48 hours of pre-treatment, the cells in all groups were washed twice with 1x PBS. The medium for the test groups (MI192 pre-treated cells) and the osteogenic positive control group was changed to osteogenic induction medium, and the negative basal control group changed to fresh basal medium. n=3 for all groups. After 7 days of culture, the cells were washed twice with 1x PBS, stained for alkaline phosphatase, observed under a Leica DMI6000 B inverted microscope and photographed using a macro camera (HTC One Mini 2 Phone camera).

5.2.1.2 The effect of MI192 pre-treatment dose and time period on the ALPSA of ADSCs

ADSCs were seeded in three 24 well plates (5 x 10^4 cells per well) and cultured in basal medium for 24 hours. The medium was then replaced with MI192 containing medium (50 µM, 40 µM, 30 µM, 20 µM and 10 µM in 500 µL basal medium), with untreated cells as the controls. After 24, 48 and 72 hours of pre-treatment, the cells in all groups on one plate at each time point were washed twice with 1x PBS. The

medium for the test groups (MI192 pre-treated cells) and the osteogenic positive control groups was changed to osteogenic induction medium, and the negative basal control group changed to fresh basal medium. n=3 for all groups. The cells were cultured for 7 days. The cells were then washed twice with 1x PBS, lysed in 200 µL of Triton X-100 per well then stored at –80 °C for a quantitative alkaline phosphatase specific activity (ALPSA) assay.

5.2.1.3 A comparison of MI192 pre-treatment and continuous treatment on the ALPSA of ADSCs

ADSCs were seeded in two 24 well plates (5 x 10^4 cells per well) and cultured in basal medium for 24 hours.

For one plate, the medium was then replaced with MI192 containing medium (30 µM, 20 µM, 10 µM, 5 µM, 1 µM and 750 nm MI192 in 500 µL basal medium), with untreated cells as the controls. After 48 hours of pre-treatment, the cells in all groups on this plate were washed twice with 1x PBS. The medium for the test groups (MI192 pre-treated cells) and the osteogenic positive control groups was changed to osteogenic induction medium, and the negative basal control group changed to fresh basal medium. n=3 for all groups. The cells were cultured for 7 days. The cells were then washed twice with 1x PBS, lysed in 200 µL of Triton X-100 per well then stored at –80 °C for an ALPSA assay.

For the other plate, the medium in the test group was replaced with MI192 containing medium (10 µM, 7.5 µM, 5 µM, 2.5 µM, 1 µM and 750 nm MI192 in 500 µL osteogenic induction medium). The medium in the untreated positive controls group was replaced with fresh osteogenic induction medium and that in the untreated negative controls was replaced with basal medium. The cells were cultured for 7 days. The cells were then washed twice with 1x PBS, lysed in 200 µL of Triton X-100 per well then stored at –80 °C for a quantitative alkaline phosphatase specific activity assay.

5.2.1.4 A comparison of pre-treatment with two different batches of MI192 on the ALPSA of ADSCs

MI192 from two different batches was used in this experiment. 'Batch 1' was the MI192 synthesised in Chapter 3: The Chemical Synthesis of MI192, which was used for all other experiments in the thesis, and 'Batch 2' was synthesised by Cancer Research Technology UK (http://www.cancertechnology.co.uk/) as part of a separate collaborative project.

ADSCs were seeded in two 6 well plates (5 x 10^5 cells per well) and cultured in basal medium for 24 hours. The medium was then replaced with two separate mediums containing the two different batches of MI192 (30 µM in 2 mL basal medium), with untreated cells as the controls. After 48 hours of pre-treatment, the cells in all groups were washed twice with 1x PBS. The medium for the test groups (MI192 pre-treated cells) and the osteogenic positive control groups was changed to osteogenic induction medium. The medium in one of the groups of the batch 1 MI192 pre-treated cells and the negative basal control group were changed to fresh basal medium. n=3 for all groups. The cells were cultured for 7 days. The cells were then washed twice with 1x PBS, lysed in 200 µL of Triton X-100 per well then stored at –80 °C for an ALPSA assay.

5.2.1.5 A comparison of pre-treatments with either MI192 or TSA on the ALPSA of ADSCs

ADSCs were seeded in two 24 well plates (5 x 10^4 cells per well) and cultured in basal medium for 24 hours. The medium was then replaced with MI192 containing medium (50 µM, 40 µM 30 µM, 20 µM, 10 µM, 5 µM MI192 and 10 µM, 5 µM 1 µM TSA in 500 µL basal medium), with untreated cells as the controls. After 48 hours of pre-treatment, the cells in all groups were washed twice with 1x PBS. The medium for the test groups (MI192 and TSA pre-treated cells) and the osteogenic positive control groups was changed to osteogenic induction medium, and the negative basal control group changed to fresh basal medium. n=3 for all groups. The cells were cultured for 7 days. The cells were then washed twice with 1x PBS, lysed in 200 µL of Triton X-100 per well then stored at –80 °C for an ALPSA assay.

5.2.1.6 A comparison of MI192 pre-treatment on the ALPSA of ADSCs from four donors

ADSCs from 4 different donors (Information in Table 5-1) were seeded in four 24 well plates (5 x 10^4 cells per well) and cultured in basal medium for 24 hours. For every donor, the medium was then replaced with MI192 containing medium (30 µM, and 10 µM in 500 µL basal medium), with untreated cells as the controls. After 48 hours of pre-treatment, the cells in all groups were washed twice with 1x PBS. The medium for the test groups (MI192 pre-treated cells) and the osteogenic positive control groups was changed to osteogenic induction medium, and the medium in the negative basal control group was changed to fresh basal medium. n=3 for all groups, for each donor. The cells were cultured for 7 days. The cells were then washed twice with 1x PBS, lysed in 200 µL of Triton X-100 per well then stored at –80 °C for an ALPSA assay.

5.2.1.7 The effect of MI192 pre-treatment on the ALPSA of ADSCs across multiple time points and with two different osteogenic media

ADSCs were seeded in four 24 well plates (5 x 10^4 cells per well) and cultured in basal medium for 24 hours. For a plate for each time point, the medium was then replaced with MI192 containing medium (30 µM in 500 µL basal medium), with untreated cells as the controls, with two groups of each condition on each plate. After 48 hours of pre-treatment, the cells in all groups were washed twice with 1x PBS. The medium in the MI192 pre-treated cells and the osteogenic positive control groups was changed to osteogenic induction medium and osteogenic mineralisation medium, with a MI192 pre-treated group and a osteogenic positive control for each media type, and the medium in the negative basal control group was changed to fresh basal medium. n=3 for all groups, for each media at each time point. The cells were cultured for 3, 5, 7 and 9 days. At each time point, one plate of cells was washed twice with 1x PBS, cells were lysed in 200 µL of Triton X-100 per well then stored at –80 °C for an ALPSA assay.

Table 5-1 – ADSC donor information.

Donor	Company (Catalogue number)	Manufacturer donor / lot number	Donor(s) age / Sex / Tissue location
1	Life Technologies (R7788110)	2118	45/Female/Abdomen
2	Life Technologies (R7788110)	2117	49/Female/Abdomen
3	Life Technologies (R7788110)	2033	63/Male/Breast and Abdomen
4	Lonza (PT-5006)	407088	46/Female/Abdomen (assumed)

5.2.2 Assessment of the effect of MI192 pre-treatment on the osteogenic gene expression of ADSCs

ADSCs were seeded in five 12 well plates (1 x 10^5 cells per well) and cultured in basal medium for 24 hours. The media was then replaced with MI192 containing medium (30 µM in 1 mL basal medium), with untreated cells as the controls. After 48 hours of pre-treatment, the cells in all groups were washed twice with 1x PBS. The medium for the test groups (MI192 pre-treated cells) and the osteogenic positive control groups was changed to StemPro® Osteogenesis Differentiation Medium, and the negative basal control group changed to MesenPRO RS™ growth medium. The medium was changed every 4 days. n=3 for all groups. Cells were cultured for 3, 5, 7, 14 and 21 days, with one plate stopped at every time point by harvesting in Trizol® reagent. RNA isolation and cDNA conversions were carried out according to the methods described in Chapter 2: General Materials and Methods.

qRT-PCR was utilised to analyse gene expression of commonly utilised osteogenic markers, according to the methods described in Chapter 2: General Materials and Methods. qRT-PCR was performed using TaqMan gene expression assays (Life Technologies) and the full list of genes and assays can be found in Table 5-2**.** Standard curves for each gene can be found in the Appendix (A5.2 - Standard Curves for qRT-PCR Assays). Gene expression level was normalised to

housekeeping gene *YWHAZ*, statistical analysis undertaken, and then further normalised to the gene expression of the basal sample of the respective time point.

Table 5-2 - TaqMan gene expression assays used in 5.2.2, the assessment of the effect of MI192 pre-treatment on the osteogenic gene expression of ADSCs

Gene symbol	Description	TaqMan assay identification
YWHAZ	tyrosine 3-monooxygenase/tryptophan 5-monooxygenase activation protein	Hs00237047_m1
	Housekeeping gene	
RUNX2	Runt-related transcription factor 2	Hs00298328_s1
BMP2	Bone morphogenetic protein 2	Hs00154192_m1
ALPL	Alkaline phosphatase	Hs01029144_m1
COL1A1	Collagen, type I	Hs00164004_m1
OCN/BGLAP	Osteocalcin / PMF-bone gamma-carboxyglutamate (gla) protein	Hs00609452_g1
SPP1/OPN	Osteopontin / secreted phosphoprotein 1/ bone sialoprotein I	Hs00959010_m1

5.2.3 The effect of MI192 pre-treatment on the calcium accumulation and mineralisation of ADSCs

ADSCs were seeded in two 12 well plates (1 x 10^5 cells per well) and cultured in basal medium for 24 hours. The medium was then replaced with MI192 containing medium (30 µM in 1 mL basal medium), TSA containing medium (10 µM in 1 mL basal medium) with untreated cells as the controls. After 48 hours of pre-treatment,

the cells in all groups were washed twice with 1x PBS. The medium for the test groups (MI192 and TSA pre-treated cells) and the osteogenic positive control groups was changed to osteogenic mineralisation medium and the negative basal control group was changed to MesenPRO RS™ growth medium. n=3 for all groups. The cells were cultured for 28 days, with the medium being changed every 4 - 5 days. Cells were then fixed in 10% NBF for 1 hour, washed in dH_2O three times and stained for calcium accumulation with Alizarin Red staining or mineral nodule formation with Von Kossa staining according to the methods described Chapter 2: General Materials and Methods.

5.2.4 The effect of MI192 pre-treatment on the Oil Red O staining (adipogenic differentiation) of ADSCs

ADSCs were seeded in a 12 well plate (1 x 10^5 cells per well) and cultured in basal medium for 24 hours. The medium was then replaced with MI192 containing medium (30 µM and 50 µM in 1 mL basal medium), with untreated controls. After 48 hours of pre-treatment, the cells in all groups were washed twice with 1x PBS. The medium for the test groups (MI192 pre-treated cells) and the adipogenic positive control groups was changed to adipogenic induction medium and the adipogenic differentiation protocol (2.3.6: Adipogenic Induction Culture) was followed. The negative basal control group medium was changed to fresh basal medium. n=3 for all groups. The cells were cultured for 14 days. The cells were then washed with 1x PBS and stained for lipid droplets with Oil Red O Stain.

5.2.5 Assessment of the effect of MI192 pre-treatment on the adipogenic gene expression of ADSCs

ADSCs were seeded in four 12 well plates (1 x 10^5 cells per well) and cultured in basal medium for 24 hours. The medium was then replaced with MI192 containing medium (40 µM, 30 µM and 20 µM in basal medium), with untreated cells as the controls. After 48 hours of pre-treatment, the cells in all groups were washed twice with 1x PBS. The medium for the test groups (MI192 pre-treated cells) and the adipogenic positive control groups was changed to adipogenic induction medium, and the negative basal control group changed to MesenPRO RS™ growth medium. n=3 for all groups. Cells were cultured for 5 and 14 days, following the adipogenic induction protocol, with two plates stopped at each time point. At each time point

cells were harvested in Trizol® reagent for RNA isolation and cDNA conversions according to the methods described in Chapter 2: General Materials and Methods.

qRT-PCR was used to analyse gene expression of cells for commonly used adipogenic markers, according to the methods described in Chapter 2: General Materials and Methods. qRT-PCR was performed using TaqMan gene expression assays (Life Technologies) and the full list of genes and assays can be found in Table 5-3**.** Standard curves for each gene can be found in the Appendix (A5.2 - Standard Curves for qRT-PCR Assays). Gene expression level was normalised to housekeeping gene *YWHAZ*, statistical analysis undertaken, and then further normalised to the gene expression of a day 0 sample.

Table 5-3 - TaqMan gene expression assays used in 5.2.5, the assessment of the effect of MI192 pre-treatment on the adipogenic gene expression of ADSCs

Gene symbol	Description	TaqMan assay identification
YWHAZ	tyrosine 3-monooxygenase/tryptophan 5-monooxygenase activation protein	Hs00237047_m1
	Housekeeping gene	
PPARγ	Peroxisome proliferator-activated receptor gamma	Hs01115513_m1
ADIPOQ	Adiponectin	Hs00605917_m1

5.2.6 Statistical Analysis

All statistical analysis undertaken with Graphpad Prism 5. Method used: ANOVA multiple comparisons test with Tukey modification. For all graphs: ns = P > 0.05, * = ≤ 0.05, ** = P ≤ 0.01 *** = P ≤ 0.001 and **** = P ≤ 0.0001.

5.3 Results

5.3.1 The effect of MI192 pre-treatment on the alkaline phosphatase staining levels of ADSCs

ALP was stained in ADSCs pre-treated with 100 µM and 30 µM of MI192 for 2 days.

After 2 days pre-treatment with MI192 followed by a further 7 days of culture in osteogenic induction medium, the ALP levels of ADSCs were measured with ALP staining (Figure 5.1). The positive control group (osteogenic medium alone, Figure 5.1B) had stronger blue ALP staining than the negative control group (basal medium alone, Figure 5.1A). The cells pre-treated with 100 µM MI192 (Figure 5.1C) had very low ALP staining, levels comparable to the other groups. The cells pre-treated with 30 µM MI192 had the strongest ALP staining (Figure 5.1D). The cell density was lower in both of the MI192 pre-treated groups, with the lowest in the 100 µM MI192 pre-treated group. Cells treated with M192 also showed a different morphology to that of the basal and osteogenic controls.

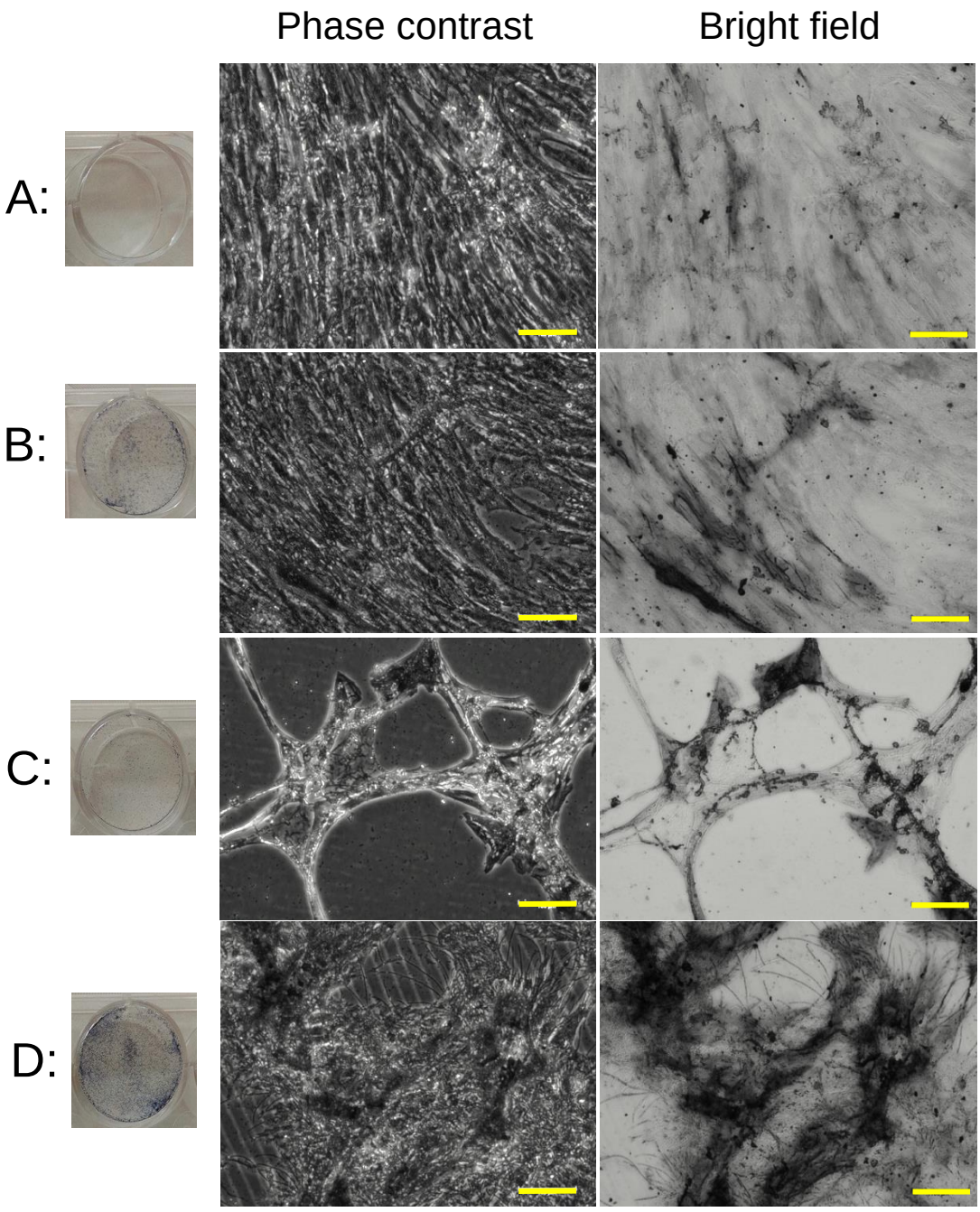

Figure 5.1 – ALP Staining of ADSCs treated with MI192 then cultured in osteogenic induction medium. A – Basal medium control; **B** – Osteogenic medium control; **C** – 100 µM pre-treatment for 2 days with MI192 then 7 days in osteogenic medium; **D** – 30 µM pre-treatment for 2 days with MI192 then 7 days in osteogenic medium. Cells stained blue for ALP. Macro image of the well of the plate shown, as well as phase contrast and bright field images showing detailed cell staining. Scale bars = 100 µM.

5.3.2 The effect of MI192 pre-treatment dose and time period on the ALPSA of ADSCs

The Alkaline Phosphatase (ALP) levels in ADSCs pre-treated with a range (50 μM – 20 μM) of MI192 doses for different treatment periods (1 - 2 days) was assessed with a biochemical assay, and normalised to DNA content, giving the ALP specific activity (ALPSA) (Figure 5.2). The total DNA content is not shown as the same trend as in Chapter 3:The Chemical Synthesis of MI192 was seen.

In the 1 day pre-treatment groups, the osteogenic medium positive control group showed a statistically significant increase ($P \leq 0.05$) in ALPSA over the basal medium negative control group (Figure 5.2). However, there was no significant difference between the MI192 pre-treated groups and the osteogenic medium positive control, or between the different doses ($P > 0.05$) in the 1 day pre-treatment groups. After two days of pre-treatment, all MI192 pre-treated cells have a statistically significant increase of ALPSA over the osteogenic medium positive control (40 μM $P \leq 0.05$, 30 μM $P \leq 0.001$ and 20 μM $P \leq 0.01$). 30 μM of MI192 pre-treatment for two days had the highest level of ALPSA of all groups, and was statistically significantly higher than the other groups in one day pre-treatment ($P \leq 0.01$), most notably the same dose. However, there were no significant difference ($P > 0.05$) between 30 μM and 40 μM, 20 μM pre-treated for two days cells, but the highest ALPSA was seen in the 30 μM group.

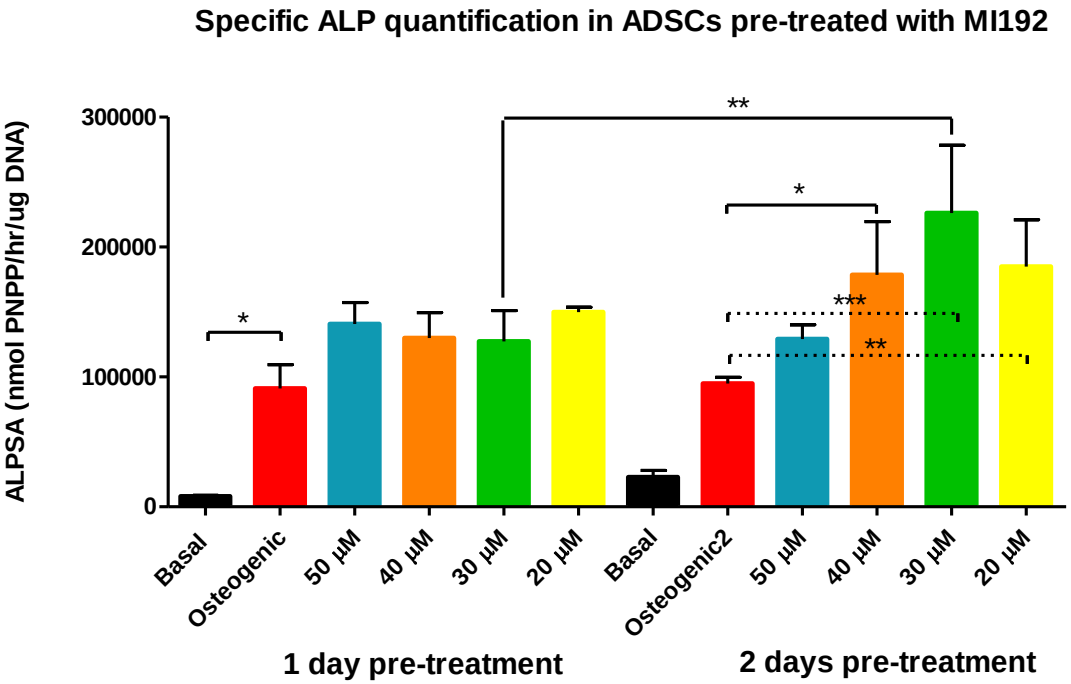

Figure 5.2 – ALPSA of ADSCs pre-treated with MI192 then cultured in osteogenic induction medium. ADSCs were pre-treated with 50 µM, 40 µM, 30 µM and 20 µM MI192 for one and 2 days, before culture in osteogenic induction medium for 7 days, with basal medium and osteogenic medium controls. Results expressed as mean ± SD (n=3). Statistical significance was determined using a one-way ANOVA. * = P ≤ 0.05, ** = P ≤ 0.01 and *** = P ≤ 0.001.

5.3.2.1 A comparison of MI192 pre-treatment and continuous treatment on the ALPSA of ADSCs

ADSCs were either pre-treated with a range (30 µM – 750 nM) of MI192 doses for two days, or treated with MI192 (10 µM – 750 nM) for the whole culture period, of the same total length.

5.3.2.2 Total DNA content

The DNA quantification (Figure 5.3 A) showed that there was a reduction in the DNA, and therefore cell numbers, in all groups compared to basal medium negative control group (Figure 5.3 A). The osteogenic medium positive control group reduced total DNA content compared to the basal control, although not significantly ($P > 0.05$). The MI192 pre-treated groups showed a dose dependent trend in reduction of total DNA content, although no results were statistically significantly lower than the controls ($P > 0.05$). With the continuous MI192 treatment, the higher doses (10 µM, 7.5 µM, 5 µM MI192 and 2.5 µM) significantly reduced total DNA content compared with the osteogenic medium control group ($P \leq 0.001$, $P \leq 0.001$, $P \leq 0.001$ and $P \leq 0.05$ respectively). There was no significant difference between the lower doses (1 µM and 750 nm MI192) groups and the osteogenic medium control group ($P > 0.05$).

5.3.2.3 ALPSA

For the continuous treatment with MI192, all doses showed an increase in the ALPSA compared to the controls (Figure 5.3 B). The increase was statistically significantly higher ($P \leq 0.05$) for the 10 µM and 7.5 µM whole time groups. The increase in ALPSA in the pre-treated cells was much higher, and with a similar trend seen in Figure 5.2. The 30 µM and 20 µM pre-treated groups showed the greatest increase over the osteogenic medium positive control group ($P \leq 0.001$). The lower doses of pre-treatment (1 µM and 750 nM) had a much smaller increase in specific ALP activity than the higher doses (not statistically significant and $P \leq 0.05$ respectively).

A

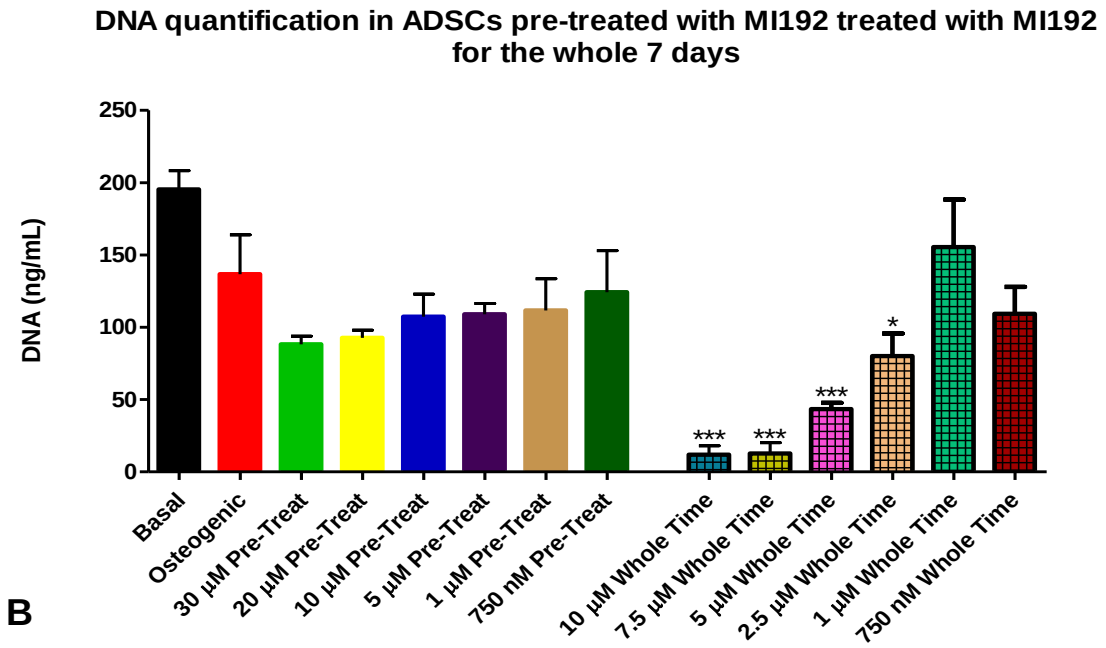

B

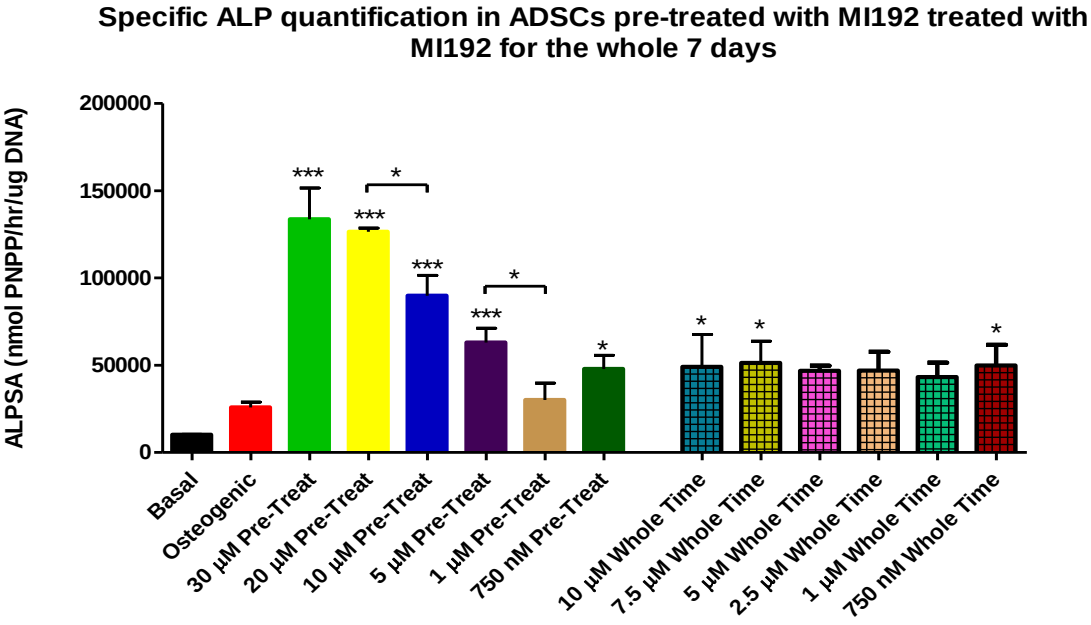

Figure 5.3 - PicoGreen® DNA quantification (A) and ALPSA (B) of ADSCs pre-treated with MI192 then cultured in osteogenic induction medium, compared to ADSCs treated continuously with MI192 in osteogenic medium. A – Total DNA content of ADSCs pre-treated with 30 µM - 750 nM MI192 and cultured in osteogenic induction medium, compared to the DNA content of cells cultured in osteogenic induction medium containing 10 µM - 750 nM MI192 continuously; **B** – ALPSA of the same ADSCs. For both, significance level shown is compared to osteogenic control, along with a selection of other values. Results expressed as mean ± SD (n=3). Statistical significance was determined using a one-way ANOVA. * = $P \leq 0.05$ and *** = $P \leq 0.001$.

5.3.2.4 A comparison of pre-treatment with two different batches of MI192 on the ALPSA of ADSCs

The difference between the ALPSA of ADSCs pre-treated with two different compound batches of MI192 for two days was investigated. In this experiment a group where ADSCs were pre-treated with MI192 and then cultured in basal medium negative control was also included, to investigate if this lead to a rise in ALPSA (Figure 5.4).

After two days of pre-treatment with two batches of MI192 (30 µM) followed by culture in osteogenic medium positive control group for one week, both pre-treated groups significantly enhanced ALPSA compared to the osteogenic control ($P < 0.01$ and $P < 0.001$ respectively) and the basal control ($P \leq 0.01$ and $P \leq 0.001$ respectively, not shown on the graph). There was no significant difference between the two batches, and the error bars overlapped.

The basal medium ADSCs treated with MI192 showed an enhancement of ALPSA; however, there was no significant difference compared to the positive control and basal medium control groups ($P > 0.05$) (Figure 5.4).

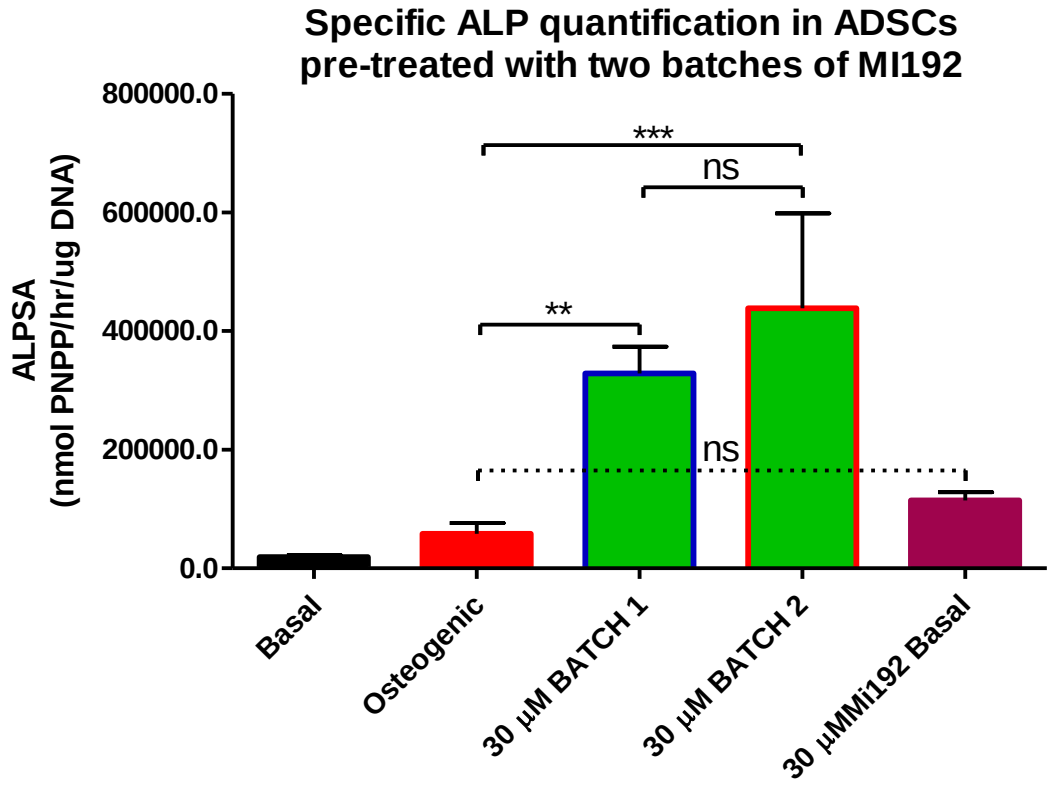

Figure 5.4 – ALPSA of ADSCs pre-treated with two different batches of MI192 then cultured in osteogenic induction medium and basal medium. The specific ALP activity of cells pre-treated with 30 µM of MI192 for 2 days, before culture in osteogenic induction, or basal medium for 7 days, with basal medium and osteogenic medium controls. Results expressed as mean ± SD (n=3). Statistical significance was determined using a one-way ANOVA. *** = $P \leq 0.001$.

5.3.2.5 A comparison of pre-treatments with either MI192 or TSA on the ALPSA of ADSCs

The ALPSA of ADSCs pre-treated with a range (50 µM – 10 µM) of MI192 doses for two days was compared to the ALPSA of ADSCs pre-treated with a commercially available HDACi TSA (10 µM – 1 µM) (Figure 5.5).

The osteogenic medium positive control group showed an increase in ALPSA over the basal medium negative control group, although this was not statistically significant. This was similar to the results from other experiments as described earlier (e.g. Figure 5.2 and Figure 5.3 B). 10 µM and 5 µM TSA pre-treatment group showed enhanced ALPSA compared to that of the basal and osteogenic control groups, however this was not significant ($P > 0.05$). The ALPSA was much higher in all of the MI192 pre-treated groups. When comparing the 10 µM MI192 pre-treatment group and the 10 µM TSA pre-treatment group, the ALPSA was strongly and statistically significantly higher ($P \leq 0.001$).

5.3.2.6 A comparison of MI192 pre-treatment on the ALPSA of ADSCs from four donors

To test for donor variability, the ALPSA levels of ADSCs from 4 different donors were compared after pre-treatment with two doses of MI192 (30 µM and 10 µM) (Figure 5.6) In all four donors the osteogenic medium positive control group had higher ALPSA than the basal medium negative controls of the same donor. However, there was only one donor with a significantly higher ALPSA ($P \leq 0.05$). Four 30 µM and two 10 µM MI192 pre-treatment groups showed an extremely significant increase in the ALPSA compared to both basal and osteogenic controls of the same donor ($P \leq 0.001$). In two out of four donors, 30 µM MI192 pre-treatment groups had significant higher ALPSA compared to that of 10 µM MI192 pre-treated groups in the same donor, as seen in the previous experiments, with the same donor (in 5.3.2) The other two donors had comparable ALPSA levels in both the 30 µM MI192 and 10 µM MI192 pre-treatment groups ($P > 0.05$).

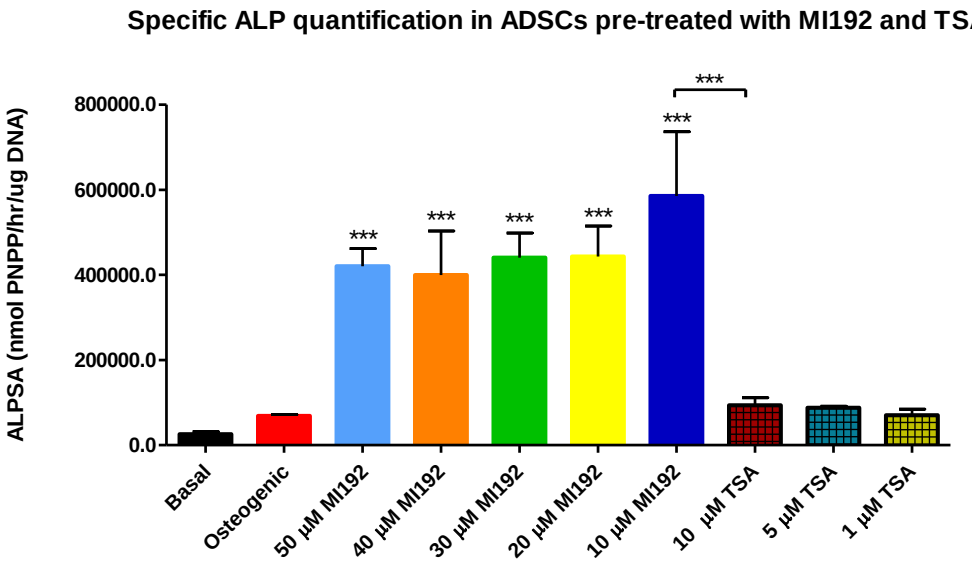

Figure 5.5 - ALPSA of ADSCs pre-treated with MI192 and TSA. The specific ALP activity of cells pre-treated with MI192 and TSA for 2 days. Significance level for every group compared to osteogenic control shown above the bar. Results expressed as mean ± SD (n=3). Statistical significance was determined using a one-way ANOVA. *** = P ≤ 0.001.

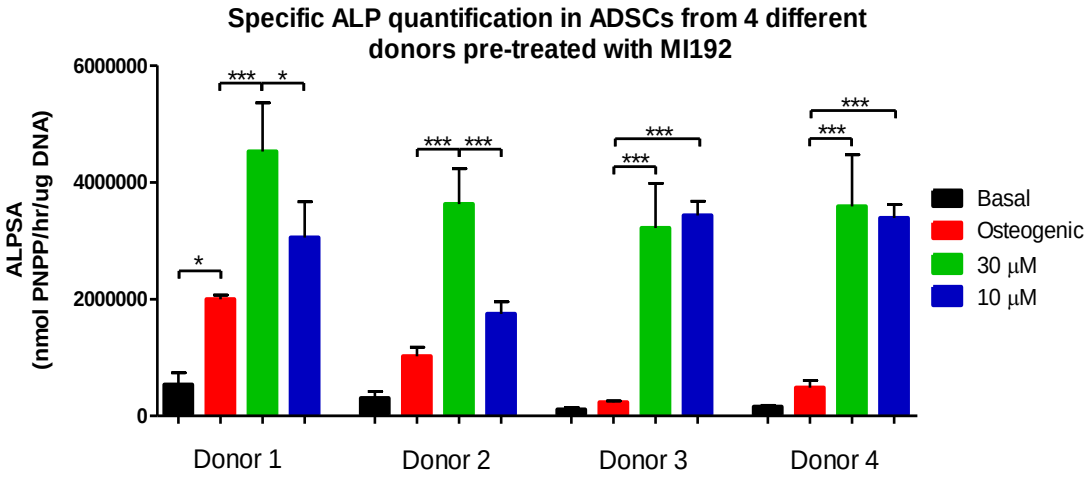

Figure 5.6 – ALPSA of ADSCs from 4 different donors pre-treated with MI192. The specific ALP activity of cells pre-treated with 30 µM and 10 µM MI192 for 2 days. Results expressed as mean ± SD (n=3). Statistical significance was determined using a one-way ANOVA. * = P ≤ 0.05 and *** = P ≤ 0.001

5.3.3 The effect of MI192 pre-treatment on the ALPSA of ADSCs across multiple time points and with two different osteogenic media

Two different osteogenic media were used in this thesis. The ‘osteogenic induction medium’ was used for all previous osteogenic differentiation experiments in this chapter, and contains no additional mineral source(s). But, to ensure maximum osteogenic differentiation, StemPro® Osteogenesis Differentiation Medium, which contains additional mineral sources, and is recommended for use with these cells, was used in long term experiments, where mineralisation, or gene expression linked to mineralisation, was measured. This is the ‘osteogenic mineralisation medium’. This was not used initially in optimisation experiments due to the massive increased cost (£85 for 100 mL) of the StemPro® Osteogenesis Differentiation Medium.

Firstly, the two media was compared, to ensure that the effect of MI192 was seen with the osteogenic mineralisation medium’ as well as the ‘osteogenic induction medium’. Discussion of the content of both media can be found in this chapter’s discussion. The ALPSA of ADSCs pre-treated with MI192, across 4 time points, with both osteogenic media – the osteogenic induction medium (Figure 5.7 A) and the osteogenic mineralisation medium (Figure 5.7 B) was assessed. This study aims to compare the effect these two osteogenic media on the ADSCs ALPSA over time and their effect of cell response to MI192 pre-treatment.

The ‘osteogenic induction medium’ significantly increased the ALPSA of the osteogenic positive controls ADSCs at day 5, day 7 and day 9, although not statistically significantly ($P > 0.05$), when compared to that of the basal medium negative control group at the same time points. There was a trend of increasing ALPSA over the time points. For all time points, there was a statistically significant increase in the ALPSA in the 30 µM MI192 pre-treated group compared to that of the osteogenic induction medium group at the same time point (day 3: $P \leq 0.01$, day 5: $P \leq 0.001$, day 7: $P \leq 0.001$ and day 9 $P \leq 0.05$). The highest ALPSA levels in the MI192 pre-treated groups was at day 7.

The ‘osteogenic mineralisation medium’ significantly increased the ALPSA of the osteogenic control ADSCs at day 3, day 5, day 7 and day 9, although not statistically significantly ($P > 0.05$), when compared to that in the basal controls at the same time points. There was a trend of increasing over the time points. For all time points, there was an increase in the ALPSA in the 30 µM MI192 pre-treated group compared to that of the osteogenic induction medium group at the same time point (day 3: $P \leq 0.01$, day 5: $P \leq 0.001$, day 7: $P \leq 0.05$ and day 9 $P > 0.05$). The highest ALPSA levels in the MI192 pre-treated groups was at day 5.

With the osteogenic mineralisation medium (Figure 5.7 B) a similar trend to the osteogenic induction medium was seen (Figure 5.7 A). In both media, at all time points there was an increase in the ALP levels of the positive osteogenic control over the basal control. For the 30 µM MI192 pre-treated group, there was an increase in ALP at every time point, with the osteogenic induction medium having peak ALPSA at day 7 and the osteogenic mineralisation medium at day 5. The increase in ALP result was successfully repeated with the osteogenic mineralisation medium, so it was utilised for all subsequent experiments.

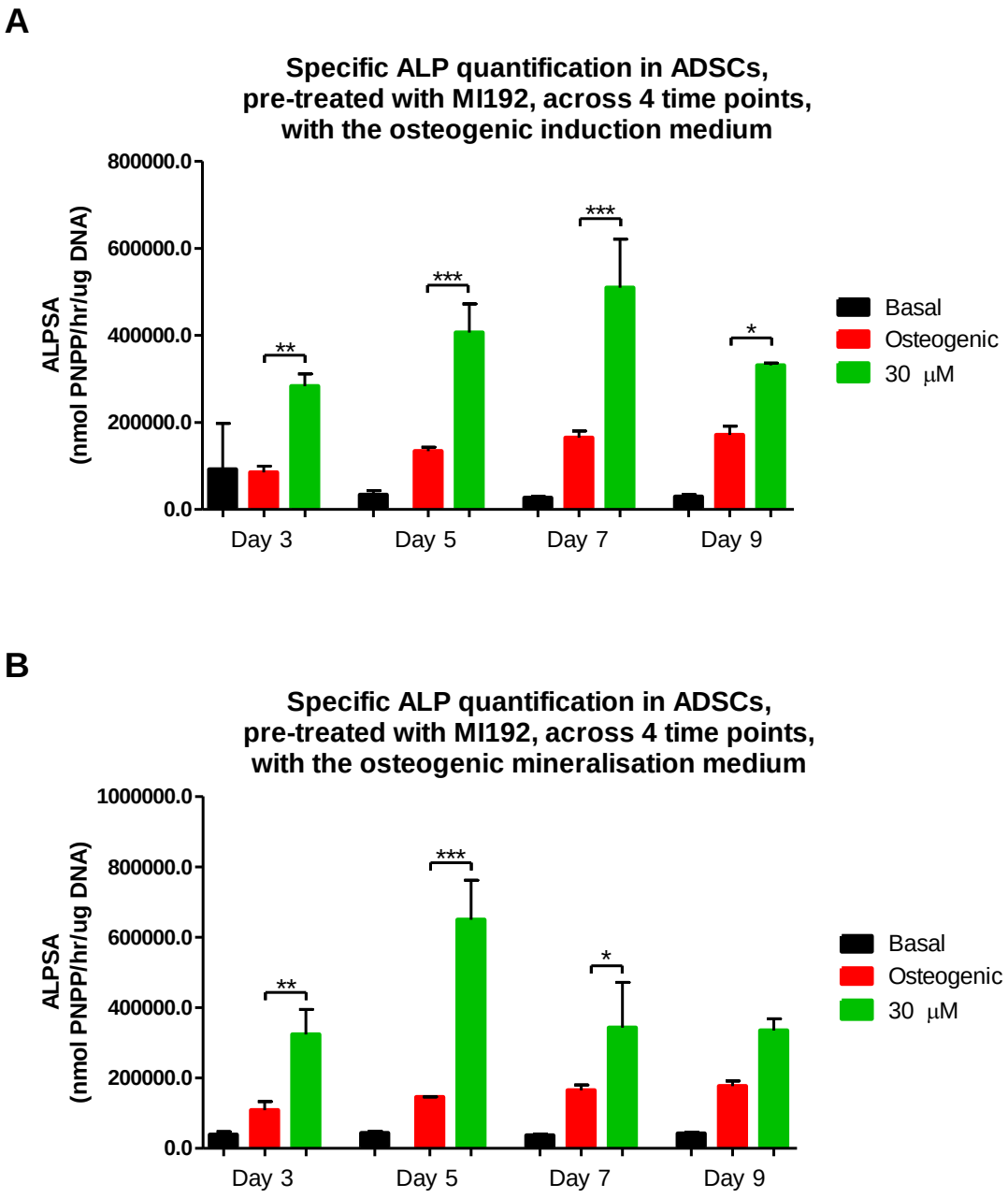

Figure 5.7 - ALPSA of ADSCs, pre-treated with MI192, across 4 time points, with the osteogenic induction (A) and osteogenic mineralisation (B) media. The ALPSA of cells pre-treated with 30 µM for 2 days, before culture in osteogenic mineralisation or osteogenic induction media for 3, 5, 7 and 9 days, with basal medium and osteogenic medium for both. Results expressed as mean ± SD (n=3). Statistical significance was determined using a one-way ANOVA. * = $P \leq 0.05$, ** = $P \leq 0.01$ and *** = $P \leq 0.001$.

5.3.4 Assessment of the effect of MI192 pre-treatment on the osteogenic gene expression of ADSCs

To better understand the mechanism by which MI192 affects the osteogenic differentiation of ADSCs, the expression of osteogenic marker genes at multiple time points (3 days, 5 days, 7 days, 14 days and 21 days) was assessed by qRT-PCR (Figure 5.8, Figure 5.9 and Figure 5.10).

5.3.4.1 *RUNX2*

The expression of *RUNX2* in the osteogenic medium positive control group was consistently statistically significantly higher ($P \leq 0.001$) than the basal medium negative control group in the same group at all time points (Figure 5.8 A). Initially, at day 3, the *RUNX2* expression in the MI192 pre-treated cells was at basal levels, and statistically significantly lower than the osteogenic control ($P \leq 0.001$). At day 5, the *RUNX2* expression of MI192 pre-treated cells was similar to that of the osteogenic control ($P > 0.05$), and statistically significantly ($P \leq 0.001$) higher than the basal control. However, there was extremely significantly higher *RUNX2* expression in the MI192 pre-treated cells compared to the osteogenic control at days 7 and 14 ($P \leq 0.001$). At day 21, the *RUNX2* expression level drops back down in both osteogenic control and the test group although there was still a significant difference compared to the basal control ($P \leq 0.001$ and $P \leq 0.05$ respectively). However, there was no significant difference between the MI192 pre-treated group and the osteogenic control ($P > 0.05$) at day 21.

5.3.4.2 *BMP2*

The expression of *BMP2* in the osteogenic medium positive control group was 1.3 – 2.2 times higher compared to that of the basal medium negative control group of the same day at every time point except day 5 (where expression was at the basal level), although this was never statistically significant ($P > 0.05$) (Figure 5.8 B).

The expression of *BMP2* in the MI192 pre-treated cells was highest at day 3, which was statistically significant higher than the basal control ($P \leq 0.001$); however, not statistically significantly higher than the osteogenic control ($P > 0.05$). This may due to a huge standard deviation (and when extra technical repeats were undertaken independently, the results of which are not included, here n still equals 3, the results

were the same). Similarly, *BMP2* expression in the MI192 pre-treated cells was higher than the osteogenic control at day 5 and at day 7 ($P > 0.05$). At days 14 and 21, the *BMP2* expression level in the MI192 pre-treated cells was lower, and the same level as the osteogenic control ($P > 0.05$).

5.3.4.3 *ALP*

ALP expression in the osteogenic medium positive control group increases steadily over the time points (Figure 5.9 A). Initially, expression is only 3 times greater than basal medium negative control group, and not statistically significant ($P > 0.05$), but this rises to 10 times greater by day 14 and day 21, becoming statistically significantly different ($P \leq 0.001$).

ALP expression in the MI192 pre-treated cells was initially slightly lower than the osteogenic control, at day 3 (although not statistically significantly, $P > 0.05$). But at day 5 there is a huge spike and expression is much higher than the osteogenic control, statistically significantly ($P \leq 0.001$). The expression in the MI192 pre-treated cells remains higher than the osteogenic control at day 7, although there was no statistical significance ($P > 0.05$), before dropping down to basal levels at day 14 and 21. The expression level is down as low as it was at day 3, and at day 14 and day 21 is not statistically significantly higher than the basal controls. The osteogenic control has *ALP* expression much higher, statistically significantly ($P \leq 0.001$) than the MI192 pre-treated cells at day 14 and day 21.

5.3.4.4 *COL1*

COL1 expression in the basal medium negative control group increased steadily with culture, with high levels by day 21. It is still normalised to 1 for the graph (Figure 5.9 B). Compared to the basal control, there was a spike expression of *COL1* at day 3 and day 7 in the osteogenic medium positive control group, both statistically significantly ($P \leq 0.001$). In the osteogenic control, the expression at day 5 and 14 was comparable to the basal control, with no statistically significant difference ($P > 0.05$) and at day 21 it was statistically significantly lower than the basal control ($P \leq 0.001$).

The MI192 pre-treated cells had *COL1* expression levels lower than basal and osteogenic control at day 3 (both statistically significantly, P ≤ 0.001). At day 5 the expression levels in all three groups were comparable. At day 7 the MI192 pre-treated cells had a huge peak in *COL1* expression, with statistically significant (P ≤ 0.001) increase over the osteogenic control (which also had a peak in expression, albeit lower than the MI192 pre-treated group) and basal control. The expression of *COL1* drops off in the MI192 pre-treated cells and is statistically significantly (P ≤ 0.01) lower than the basal at day 14 and statistically significantly (P ≤ 0.001) lower than both the basal and osteogenic controls at day 21.

5.3.4.5 *OCN/BGLAP*

OCN/BGLAP expression was relatively low in all samples, with only small peaks in the osteogenic medium positive control groups compared to the basal medium negative control groups at day 3 (not statistically significantly, P > 0.05) and day 14 (statistically significantly, P ≤ 0.01) (Figure 5.10 A). The expression in the osteogenic control was lower than the basal control at day 5, the same at day 7 and only slightly higher at day 21.

In the MI192 pre-treated cells the expression of *OCN/BGLAP* was actually statistically significantly (P ≤ 0.001) below the basal controls at day 3 and day 5, indicating MI192 may be inhibiting *OCN/BGLAP* expression. At day 7 the expression in the pre-treated cells was slightly higher than the osteogenic control, although not statistically significantly (P > 005). In the MI192 pre-treated cells, the expression was higher in the basal control at day 14, although below the osteogenic control (although not statistically significantly, P > 0.05) and expression was lower than the basal and osteogenic control at day 21 (also not statistically significantly, P > 0>05).

5.3.4.6 SPP1/OPN

Expression of *SPP1/OPN* was highest in the basal medium negative control groups at every time point (the highest levels were at day 5 and day 7). The expression of *SPP1/OPN* in the osteogenic medium positive control group was consistently statistically significantly (P ≤ 0.001) lower than the basal control, except at day 14 when a small peak in expression was observed, and there was still a reduced

expression compared to the basal control (although it was not statistically significant, ($P > 0.05$), unlike at every other time point).

In the MI192 pre-treated cells, there was a consistently lower expression of *SPP1/OPN* than the basal control ($P \leq 0.001$ at every time point) and the osteogenic control ($P \leq 0.001$ at day 3, day 5 and day 14, $P \leq 0.01$ at day 7 and not significantly, $P > 0.05$ at day 21) indicating that MI192 is actually inhibiting the expression of *SPP1/OPN*, even more so than the osteogenic control.

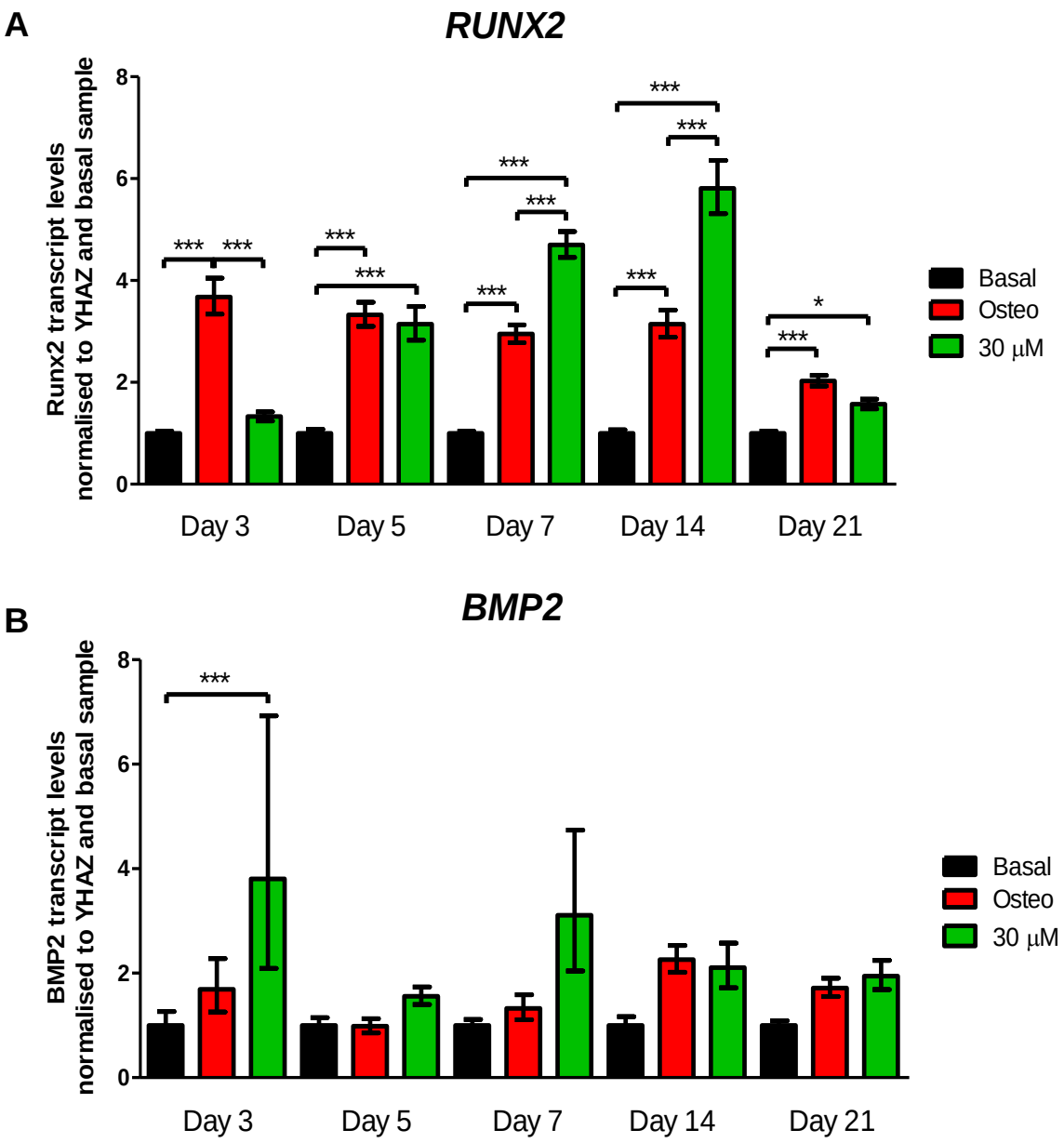

Figure 5.8 – Quantitative expression of *RUNX2* (A) and *BMP2* (B) in ADSCs. Cells were pre-treated with 30 μM MI192 for 2 days, then cultured in osteogenic medium. Gene expression was analysed at day 3, day 5, day 7, day 14 and day 21. Results expressed as mean ± SD (n=3). Statistical significance was determined using a one-way ANOVA. Only the significance levels between the conditions at each time point shown. * = P ≤ 0.05, ** = P ≤ 0.01 and *** = P ≤ 0.001.

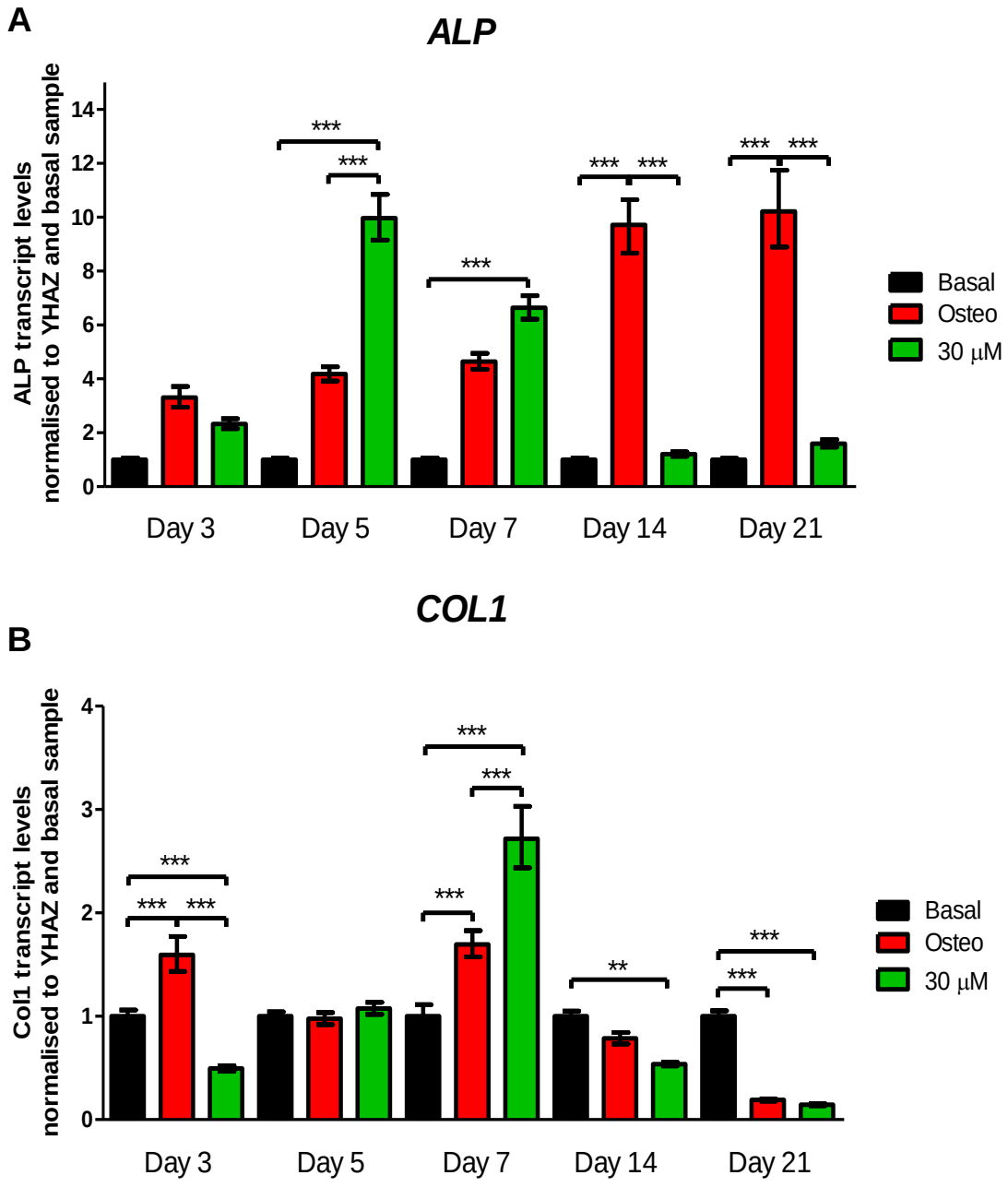

Figure 5.9 – Quantitative expression of *ALP* (A) and *COL1* (B) in ADSCs. Cells were pre-treated with 30 μM MI192 for 2 days, then cultured in osteogenic medium. Gene expression was analysed at day 3, day 5, day 7, day 14 and day 21. Results expressed as mean ± SD (n=3). Statistical significance was determined using a one-way ANOVA. Only the significance levels between the conditions at each time point shown. * = P ≤ 0.05, ** = P ≤ 0.01 and *** = P ≤ 0.001.

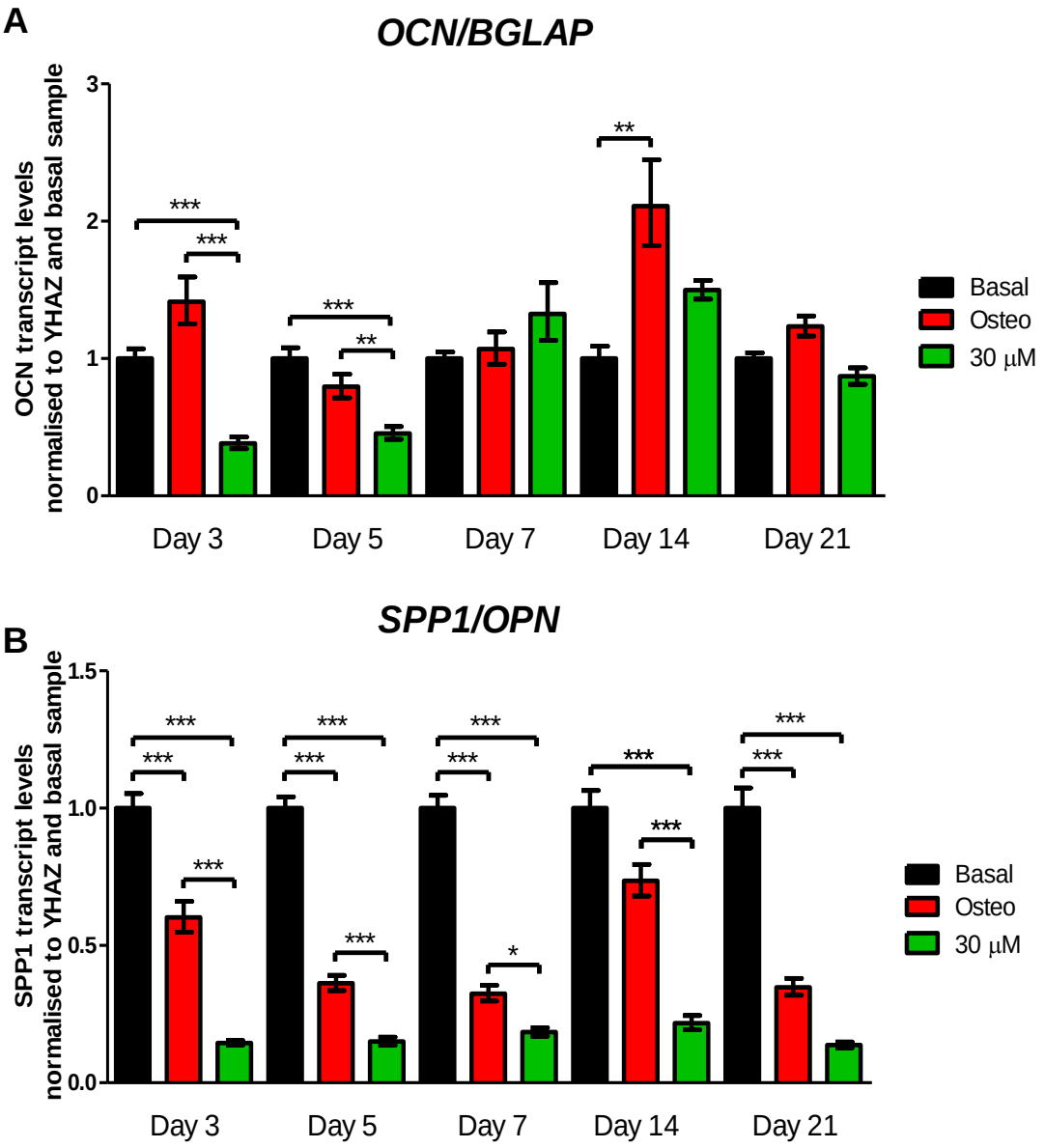

Figure 5.10 – Quantitative expression of *OCN/BGLAP* (A) and *SPP1* (B) in ADSCs. Cells were pre-treated with 30 μM MI192 for 2 days, then cultured in osteogenic medium. Gene expression was analysed at day 3, day 5, day 7, day 14 and day 21. Results expressed as mean ± SD (n=3). Statistical significance was determined using a one-way ANOVA. Only the significance levels between the conditions at each time point shown. * = $P \leq 0.05$, ** = $P \leq 0.01$ and *** = $P \leq 0.001$.

5.3.5 The effect of MI192 pre-treatment on the calcium accumulation and osteogenic mineralisation of ADSCs

The effect of 30 µM MI192 pre-treatment on the mineralisation levels of ADSCs, compared to pre-treatment with 10 µM of TSA, was assessed with an Alizarin Red stain for calcium (Figure 5.11) and a Von Kossa stain for mineral nodule formation (Figure 5.13).

5.3.5.1 Alizarin Red Staining

A red stain indicates calcium deposition. After 2 days pre-treatment with MI192 or TSA followed by 28 days of culture in osteogenic mineralisation medium. Alizarin Red staining showed negative staining in the basal medium negative control group (Figure 5.11 A). In contrast, the osteogenic positive control had a much stronger red coloured Alizarin Red positive staining (Figure 5.11 B) than the basal negative control. The overall staining level in the 30 µM MI192 treated group (Figure 5.11 C) was lower than the osteogenic control (Figure 5.11 B). However, in the MI192 pre-treated group, the staining was more indicative of mineral nodule formation, where large clumps of mineralisation had occurred, not just a low level staining of lots of cells as seen in the osteogenic control. Also, in the MI192 pre-treated group, there were very few areas without staining (the white areas being where there were no cells), which is a similar trend to the ALP staining (Figure 5.1). The osteogenic control had large areas of cells not stained, and thus not all cells were accumulating calcium. The TSA pre-treated group (Figure 5.11 D) had overall weaker staining levels than the osteogenic control.

The stain was destained using a 10% cetylpyridinium chloride solution, to give a quantitative reading for each group (Figure 5.12). This supported the qualitative observations of the staining intensity. The basal control group had a lower reading than all other groups, and the osteogenic control had the highest staining. The MI192 pre-treated group had a higher staining level than the basal control, although lower than the osteogenic control. The TSA pre-treated group had a small increase in staining level compared to the MI192 pre-treated group, although it was still lower than the osteogenic control.

5.3.5.2 Von Kossa Staining

Von Kossa staining is utilised to stain not just the calcium accumulated in the cell, but functional mineral nodules, by acting to replace the calcium in mineral nodules with silver nitrate that binds to an anion such as phosphate or carbonate. Therefore a positive Von Kossa stain indicates functional mineral nodules, containing other anions bound to calcium, not just the pure calcium that may have accumulated in the cell. Black/brown staining indicates mineral nodule formation.

The strongly stained nodules only show up as small black dots, which are hard to visualise in the macro photos. There was no positive staining in the basal control group (Figure 5.13 A). Phase contrast images show a low level of brown staining in the osteogenic control (Figure 5.13 B), with spots of black, when compared to the basal control, which is a sign of a low level of mineralisation in nodules. The 30 µM MI192 pre-treated group (Figure 5.13 C) has several large areas of intense black, positive Von Kossa staining. The staining is clearer and there are more and larger mineral nodules observed in the MI192 pre-treated cells, indicating that more functional mineralisation is taking place. The TSA pre-treated group had a higher level of brown staining than the osteogenic control, with evidence of some small black stained nodules. This was weaker than that in the 30 µM MI192 pre-treated group.

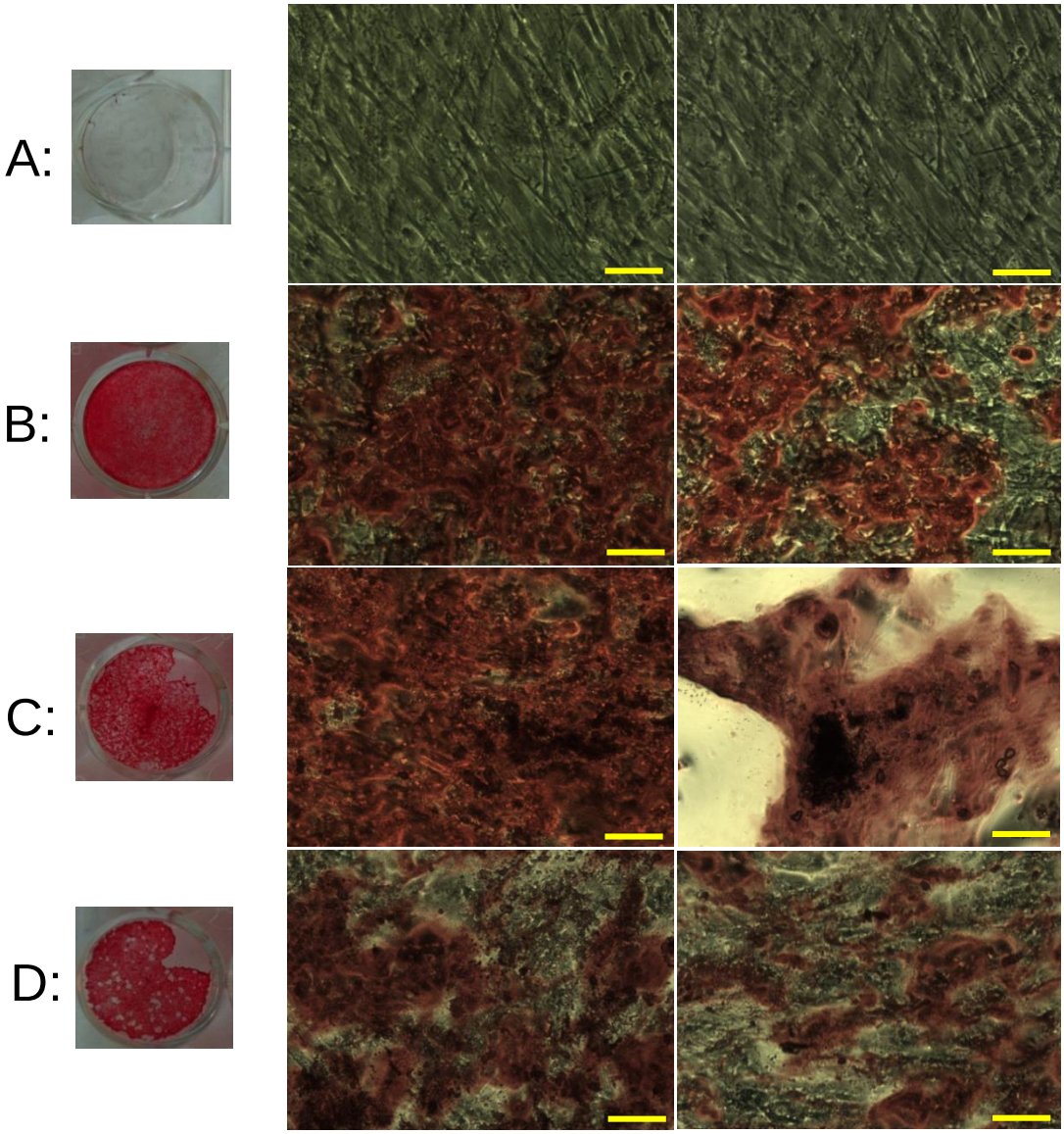

Figure 5.11 - ADSCs treated with MI192 then cultured in osteogenic mineralisation medium, before staining for calcium with Alizarin Red staining. A – Basal medium control, **B** – Osteogenic medium control, **C** – 30 µM pre-treatment for 2 days with MI192, **D** – 10 µM pre-treatment for 2 days with TSA. Red staining indicates calcium accumulation. Macro image of the well of the plate shown, as well as two phase contrast images showing detailed cell staining. Scale bars = 100 µM.

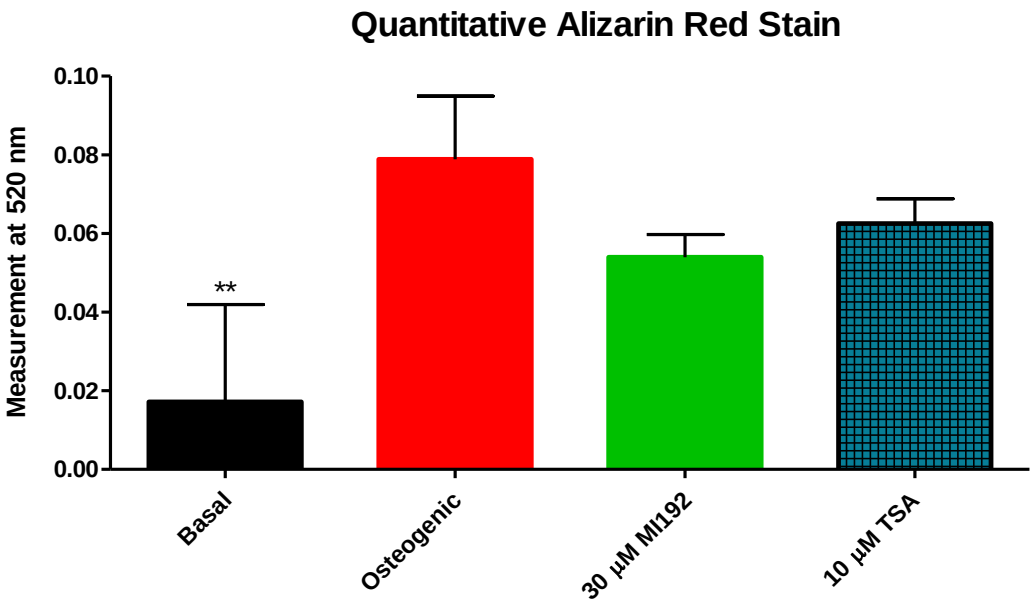

Figure 5.12 – Quantitative measurement of Alizarin Red stain. Stain destained from ADSCs pre-treated with MI192 then cultured in osteogenic medium, before staining for calcium with Alizarin Red staining. Stain was destained and quantified from a basal medium control, an osteogenic medium control, cells pre-treated with 30 µM of MI192 and 10 µM TSA (same cells as pictures in Figure 5.11). Average absorbance of readings taken 550 nm. Results expressed as mean ± SD (n=3). Statistical significance was determined using a one-way ANOVA. Only the significance levels between compared to the osteogenic control shown. * = $P \leq 0.05$.

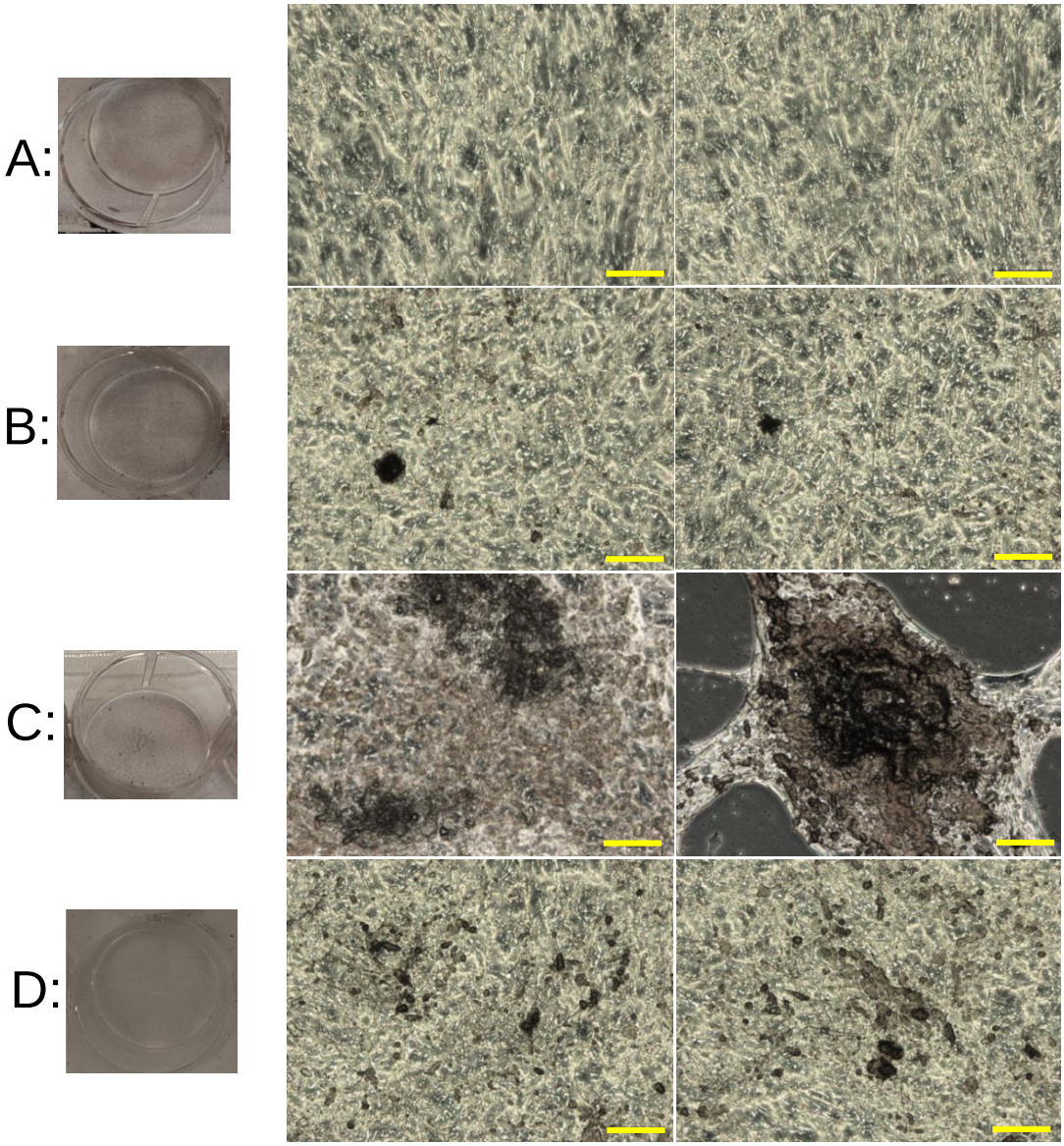

Figure 5.13 - ADSCs pre-treated with MI192 then cultured in osteogenic mineralisation medium, before staining for mineralisation with Von Kossa staining. A – Basal medium control, **B** – Osteogenic medium control, **C** – 30 µM pre-treatment for 2 days with MI192 then 28 days in osteogenic medium, **D** – 10 µM pre-treatment for 2 days with TSA then 28 days in osteogenic medium. Brown and black staining indicates calcium accumulation, black being a stronger stain. Macro image of the well of the plate shown, as well as two phase contrast images showing detailed cell staining. Scale bars = 100 µM.

5.3.6 The effect of MI192 pre-treatment on the Oil Red O staining (adipogenic differentiation) of ADSCs

To investigate the effect of MI192 pre-treatment on the adipogenic differentiation of ADSCs, the lipid accumulation in ADSCs were assessed by an Oil Red O staining for lipid droplets (Figure 5.14).

There was no positive Oil Red O stain in the basal medium negative control group (Figure 5.14 A). In contrast, the positive adipogenic control group (Figure 5.14B) showed an increased level of red staining.

The Oil Red O staining in cells pre-treated with 10 µM, 20 µM and 50 µM of MI192 (Figure 5.14 C, D and E) and 10 µM and 20 µM of TSA (Figure 5.14 F and G) followed by culture in adipogenic differentiation medium showed a weaker positive staining for Oil Red O compared to that of the positive adipogenic control (Figure 5.14 B). Lower concentration of the pre-treatment (10 µM MI192 and 10 µM TSA, Figure 5.14 C and F) groups showed slightly stronger positive staining than the basal control, although the staining is much lower than the positive adipogenic control (Figure 5.14 B). The staining was much weaker in the higher doses of MI192 and TSA groups.

The stain was destained using 100% isopropanol, to give a quantitative reading for each group (Figure 5.15). The results were similar to the qualitative analysis of the stain made by eye. Staining intensity was higher in the adipogenic control than the basal control. The MI192 pre-treated groups had lower staining level than the adipogenic control ($P \leq 0.001$), although all groups were slightly higher than the basal control. The TSA pre-treated groups had a slightly lower staining level than the MI192 pre-treated groups, also much lower than the adipogenic control $P \leq 0.001$).

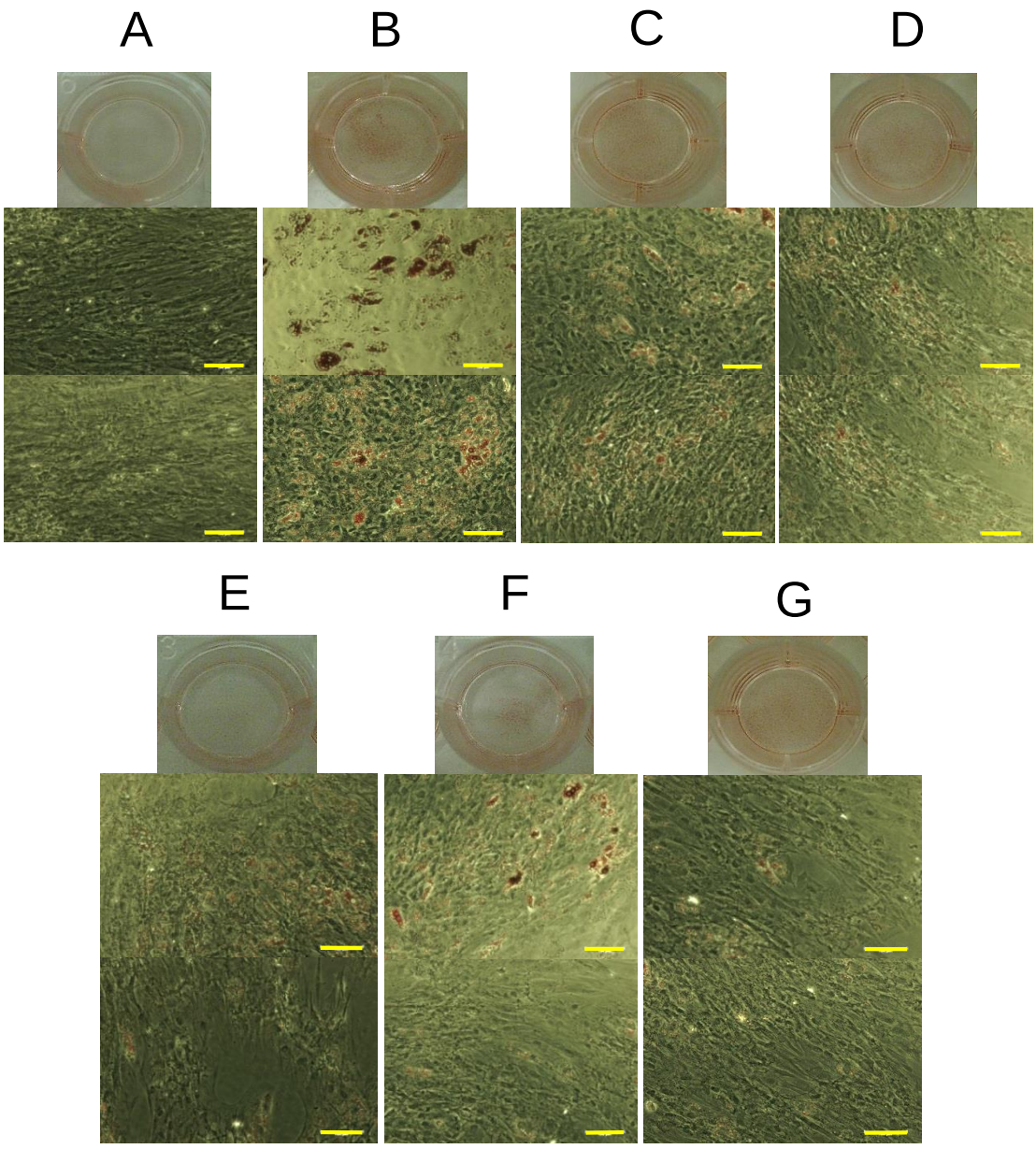

Figure 5.14 - ADSCs pre-treated with MI192 then cultured in adipogenic medium, before staining for lipid droplet accumulation with an Oil Red O stain. A – Basal medium control; **B** – Adipogenic medium control; **C, D, E, F, G** – Cells pre-treated with HDACis MI192 and TSA then cultured in adipogenic medium for 14 days. Cells pre-treated with **C:** 10 µM MI192; **D:** 20 µM MI192; **E:** 50 µM MI192; **F:** 10 µM TSA; **G:** 20 µM TSA. Red staining indicates lipid droplets. Macro image of the well of the plate shown, as well as two phase contrast images showing detailed cell staining. Scale bars = 100 µM.

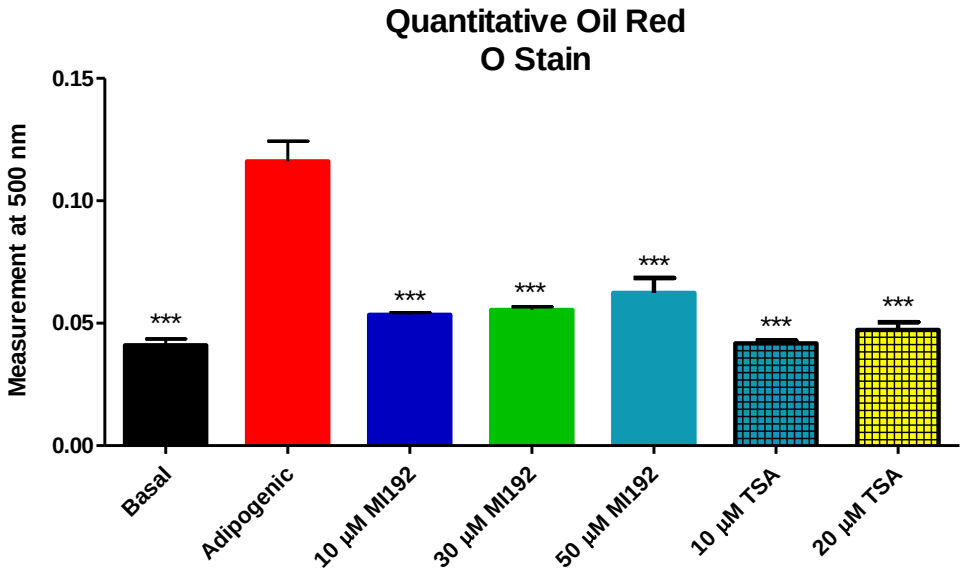

Figure 5.15 - Quantitative measurement of Oil Red O stain, destained from ADSCs pre-treated with MI192 then cultured in adipogenic medium, before staining for lipid droplet accumulation with an Oil Red O stain. The stain was quantified from a basal medium control, an adipogenic medium control, cells pre-treated with 50 µM, 30 µM and 10 µM of MI192 and 20 µM TSA and 10 µM TSA (same cells as pictures in (Figure 5.14). Average absorbance of readings taken 500 nm. Results expressed as mean ± SD (n=3). Statistical significance was determined using a one-way ANOVA. Only the significance levels between compared to the adipogenic control shown. *** = $P \leq 0.001$.

5.3.7 Assessment of the effect of MI192 pre-treatment on the adipogenic gene expression of ADSCs

To better understand the mechanism by which MI192 affects the adipogenic differentiation of ADSCs, cells were pre-treated with 3 doses (40 µM, 30 µM and 20 µM) of MI192 for two days, cultured in adipogenic induction medium for 3 days and 14 days. Gene expression was assessed by qRT-PCR (Figure 5.16).

5.3.7.1 *PPARγ*

The expression of *PPARγ* was over 5 fold, statistically significantly ($P \leq 0.001$), up-regulated in ADSCs in the adipogenic control group compared to the basal medium negative control group at day 3. At day 14 it was over 9 fold greater ($P \leq 0.001$). Comparing the two time points, in the adipogenic culture groups, the *PPARγ* expression level in ADSCs at day 14 was significantly higher than at day 3 ($P \leq 0.001$)

At day 3, *PPARγ* transcript levels for the ADSCs pre-treated with MI192 (20 µM - 40 µM) were the same as the basal controls. This expression was statistically significantly lower than the adipogenic medium control group ($P \leq 0.001$). At day 14, the *PPARγ* expression level in the three MI192 pre-treated groups were higher than the basal control group ($P \leq 0.001$), but still lower than the adipogenic control. There was a dose response visible for *PPARγ* expression in the MI192 pre-treated groups, where the higher doses inhibited the *PPARγ* transcription the most. The *PPARγ* expression level in the 40 µM and 30 µM MI192 pre-treated groups were significantly lower than that of adipogenic control group ($P \leq 0.001$). The expression of *PPARγ* was statistically significantly up-regulated in the 20 µM MI192 pre-treated group, compared to the higher concentrations of MI192 pre-treatment (40 µM : $P \leq 0.001$ and 30 µM : $P \leq 0.05$) and was similar to that of the adipogenic control group.

5.3.7.2 *ADIPOQ*

Expression of *ADIPOQ* was undetected in the basal medium negative control group at both time points, which was expected given that when attempting to generate a standard curve for *ADIPOQ* it was undetected at all concentrations of cDNA. However, this shows that it was detected once adipogenic differentiation was

induced in the cells. At both day 3 and day 14 the expression of *ADIPOQ* was higher in the adipogenic positive controls (statistically significantly, $P \leq 0.001$).

At day 3, the pre-treatment of the cells with MI192 supressed expression of *ADIPOQ*. Only a very small amount of *ADIPOQ* was expressed in the 20 µM MI192 pre-treated cells, and it was statistically significantly lower than the adipogenic control cells ($P \leq 0.001$). At the 14 day time point some expression was seen in the MI192 pre-treated cells, which was a similar level in all groups ($P > 0.05$). However, the expression in the MI192 pre-treated groups was statistically significantly lower than the adipogenic medium controls ($P \leq 0.001$ for the cells pre-treated with 40 µM and 20 µM MI192, and $P \leq 0.01$ for the cells pre-treated with 30 µM MI192).

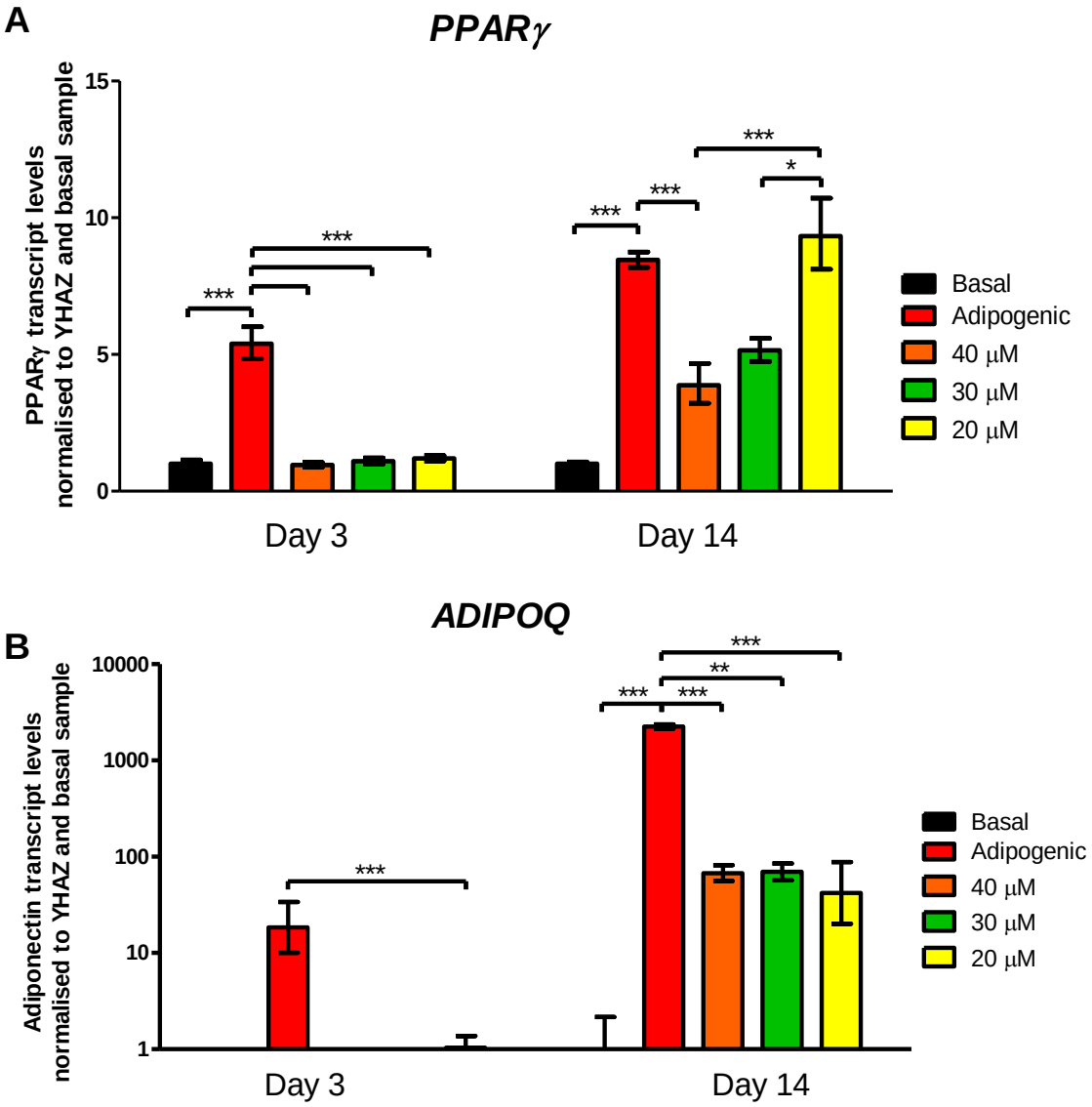

Figure 5.16 - Quantitative expression of *PPRγ* (A) and *ADIPOQ* (B) in ADSCs pre-treated with 40 μM, 30 μM and 20 μM of MI192 for 2 days, then cultured in adipogenic medium for 14 days. Gene expression was analysed at day 3 and, day 14. Results expressed as mean ± SD (n=3). For ADIPOQ (**B**) the graph is on a log scale and undetermined genes were set at an expression value of 1, where the Day 3 Basal *ADIPOQ* value was undetermined. Statistical significance was determined using a one-way ANOVA. Only the significance levels between the conditions at each time point shown. * = P ≤ 0.05, ** = P ≤ 0.01 and *** = P ≤ 0.001.

5.4 Discussion

The effect of MI192 on the osteogenic and adipogenic differentiation of ADSCs was explored in this chapter. HDAC inhibitors can be broadly placed into one of two categories; panHDACis, which target all zinc ion dependent HDAC isoforms (those being the class I isoforms HDAC1, HDAC2, HDAC3 and HDAC8, and class II isoforms HDAC4, HDAC5, HDAC6, HDAC7, HDAC9 and HDAC10, and Class IV isform HDAC11), and isoform specific HDACis, which target only one, or a small number, of HDAC isoforms. The use of isoform specific HDACis holds great potential for researchers, whether they are applied to cancer therapeutics (Balasubramanian et al. 2009) or other fields such as nerve tissue engineering (Rivieccio et al. 2009). While panHDACis, such as SAHA and NaB, have demonstrated potential to be applied to bone tissue engineering scenarios (Xu et al. 2013; Xu et al. 2009), researchers are beginning to look to more isoform selective HDACis, to address clinical needs.

To date, studies exploring the potential of isoform specific HDACis in bone tissue engineering are limited. MS-275 is an important HDACi, and specifically inhibits HDAC1, HDAC2 and HDAC3. It has shown the potential to improve the osteogenic potential of mouse primary osteoblast precursor cells (Kim et al. 2012; H.-N. Kim et al. 2011). It is particularly interesting that MS-275 is a specific HDAC, with a demonstrated potential for improving bone tissue engineering. Although there are some reports it also targets HDAC9 (Balasubramanian et al. 2009), it is still relatively specific compared to panHDACis and most studies find it certainly targets HDAC1, HDAC2 and HDAC3. The improvements made to the differentiation potential may be due to its HDAC3 specificity.

HDAC3 is an important HDAC isoform when considering bone tissue, as it is involved in bone formation (Schroeder & Westendorf 2005; Schroeder et al. 2004; Razidlo et al. 2010; McGee-Lawrence et al. 2013; Hesse et al. 2010; Lamour et al. 2007; Choo et al. 2009; Shen et al. 2002). Interestingly, inhibition of HDAC3 (along with HDAC1) with siRNAs in ADSCs resulted in an increase in osteogenic differentiation in the cells (Maroni et al. 2012). Comparatively, there are only minimal links with HDAC2 and bone. A specific link between HDAC2 and bone was made in 2014, when the silencing of HDAC2 in human dental pulp stem cells was found to increase *OPN* expression and bone sialoprotein levels, while decreasing

OCN expression. Separately, but in the same cells, VPA was found to decrease *OCN* expression, believed to be as a result of the inhibition of HDAC2 (Paino et al. 2014). Therefore, the effect on the differentiation potential of cells when treated with a HDACi specific to HDAC2 and HDAC3 in combination, such as MI192, would be interesting.

The results from Chapter 4: The General Effects of MI192 on Adipose Derived Stem Cells Cultured in Monolayer indicate that long exposure to MI192 results in high levels of cell death, so the possibility of a pre-treatment strategy was explored. Cells would be pre-treated, or primed, with MI192, before undergoing differentiation. This pre-treatment with HDACi strategy has been used in the literature (see Table 5-4) (Xu et al. 2009; Cho et al. 2005). TSA is known to improve the osteogenic differentiation of MSCs. Therefore, it was used as a control in some relevant experiments (Hu et al. 2014; Hu et al. 2013). Maroni et al. (2012) utilised a pre-treatment strategy (similar to that employed in this chapter) pre-treating ADSCs with 1 – 2.5 µM of TSA for 2 days. Therefore lower concentrations (1 µM – 20 µM) of TSA than MI192 were typically employed as a control; similar to levels utilised in the literature (Maroni et al. 2012).

Table 5-4 – Summary of pre-treatment strategies in the literature with HDACis and MSCs

Paper	HDACi(s)	Cells/aim	Strategy
Maroni et al. 2012	TSA	ADSCs / investigating bone and adipogenic differentiation potential	Pre-treatment of cells for 2 days with 1 µM TSA
Xu et al. 2009	NaB and VPA	Mouse ADSCs / osteogenic differentiation	Pre-treatment of cells for 2 days with NaB and VPA
Cho et al. 2005	VPA	Bone marrow MSCs and ADSCs / osteogenic differentiation	Pre-treatment of cells for 1, 2 and 4 days with VPA

In this chapter two different osteogenic media were used. The ‘osteogenic induction medium’ was a combination of basal medium (10% FCS in α-MEM) supplemented with ascorbic acid 2-phosphate, which promotes extracellular matrix formation

(Vater et al. 2011), and dexamethasone, which, although the exact mechanism of action is unknown, is thought to activate osteogenic transcription factors and is an often utilised promoter of osteogenic differentiation (Hildebrandt et al. 2009). The concentrations utilised were based on a review article suggesting that 10 nM of dexamethasone and 100 µM L-Ascorbic acid 2-phosphate were optimal for osteogenic differentiation (Hoemann et al. 2009). In this chapter it was shown that this medium strongly stimulated ALP production in ADSCs, so was used for the early osteogenic induction of ADSCs. The second medium, the 'osteogenic mineralisation medium' is discussed later.

ALP is found in elevated levels in osteoblasts. It is produced in pre-osteoblast cells and thus is an early stage indicator of osteogenic differentiation. Generally an increase in ALP activity is commonly associated with the osteogenic differentiation of stem cells (Boer et al. 2006; Vater et al. 2011). A number of studies show ALP levels to be elevated, in several different cell types, when investigating the effect of HDACis on osteogenic differentiation (Boer et al. 2006; Xu et al. 2013). When investigating ALP expression levels in ADSCs, pre-treatment with 30 µM MI192 (with subsequent osteogenic culture) was increased the ALP staining of ADSCs (Figure 5.1). The higher dose of MI192 (100 µM), did not result in an increase in ALP staining. This high a dose of MI192 is known to have a high cytotoxic effect on the ADSC and resulted in massively reduced cell numbers, as well as no ALP expression.

To quantify ALP activity, the total ALP was normalised to the total DNA content of the same well. The effect of a range of doses of MI192, with two different pre-treatment periods (1 and 2 days), was investigated (Figure 5.2). Due to the cytotoxic effects, longer pre-treatment lengths were not investigated. The normalised ALPSA levels account for the cell loss due to the cytotoxic effect of MI192 and there was an increase over the controls for every dose in both time points. For the two days of treatment there was a dose response, which suggested that 30 µM pre-treatment for two days was the optimal dose and treatment length. This result was confirmed with several experimental repeats. This can also be seen in other experiments in the chapter (e.g. Figure 5.3 B). A two day 30 µM treatment was chosen as the optimal dose for future experiments. Cell numbers in the MI192 pre-treated groups were lower, but still around 70% of the osteogenic controls, so sufficient cells are surviving the treatment.

In the literature, one study demonstrated that the specific knockdown of HDAC3 with siRNAs has been shown to increase different bone marker levels, although not ALP, in cell lines (Schroeder et al. 2004). Therefore, it may be the inhibition of HDAC2 specifically, which is responsible for the huge increase in ALP levels in these cells. That being said, in colon cancer cells the specific silencing of HDAC3, when compared to HDAC1 and HDAC2, increased ALP levels in the cells (Wilson et al. 2006). The reports vary depending on the cell type and the experimental parameters, therefore it could be the combination of inhibition of HDAC2 and HDAC3, or the isoforms individually, which causes this.

To ensure the pre-treatment strategy was the optimal strategy, the treatment of ADSCs for the “whole time” of the experiment was also investigated (Figure 5.3). Lower doses of MI192 were used for the “whole time” treatment, and compared to pre-treatment with the same doses, as well as the optimised 30 µM (and 20 µM, for comparison) dose. The cytotoxic effect of MI192 was seen in the cells treated for the whole 7 days with higher doses of MI192, the total DNA content was very low. Although the cell numbers in the lower doses (2.5 µM – 750 nm) were comparable to the pre-treatment groups. The ALPSA was elevated over the osteogenic controls in the “whole time” MI192 treatment groups, but the 30 µM pre-treatment had the highest ALPSA overall. It was also important to investigate pre-treatment with the lower doses of MI192. However the results show that to see the greatest increased ALPSA, the higher concentrations of MI192 are necessary. A lower dose for a longer time would be better if there was a lower level of cell loss due from the cytotoxic effect; however there was still significant cell death with extended culture with lower MI192 doses. Therefore, the advantages of the increased osteogenic potential with the higher doses, with the caveat of the increased cell death, was investigated in the majority of this thesis.

To investigate if MI192 alone, without any additional osteogenic induction, had any effect on the ALPSA levels in ADSCs, cells were pre-treated for two days with 30 µM and subsequently cultured in basal medium, not osteogenic medium (Figure 5.4). There was only a slight increase in the ALPSA over the positive osteogenic control, and the increase was not significant enough to warrant further investigation. This indicated that MI192 treatment alone is not sufficient; that osteogenic induction is needed.

Different batches of MI192 were available for the project, one synthesised by the author (outlined in Chapter 3: The Chemical Synthesis of MI192) and one provided by a commercial partner. NMR spectroscopy indicated both compounds were pure and chemically identically (NMR data for the commercially provided MI192 not shown). However, to investigate if any differences were present on a biological level (perhaps due to impurities or different rates of degradation of the compounds), the effect of pre-treatment with 30 µM for two days on ALPSA levels of the ADSCs was investigated. While there was a difference in ALPSA, likely due to experimental error or variability due to low number of biological repeats, there was no statistical difference between the ALPSA of the ADSCs pre-treated with the two different batches, and the error bars over lapped.

Maroni et al. utilising a 2 day 1 – 2.5 µM TSA pre-treatment strategy to improve the osteogenic differentiation potential of ADSCs (Maroni et al. 2012). However, when the effect of pre-treatment with TSA on ADSC ALPSA was investigated, there was only a very small increase ($P > 0.05$) in the ALP levels of the ADSCs, compared to the controls (Figure 5.5). This was unexpected, because the ADSCs used by Maroni et al. were primary ADSCs from human donors, similar to those cells used in this thesis. A dose range was utilised, to investigate if higher concentrations of TSA would increase the osteogenic potential of ADSCs; however, in doses 10 times higher than those used in the literature no significant effect was seen. This may be due to the purer nature (they are sorted for stem cell markers) of these cells, or perhaps the increase seen would be comparatively large to the controls if MI192 treatment was not included.

Properties such as the differentiation potential and proliferation of cells can vary depending on the donor from which the cells are sourced. With MSCs, this does not, as often only reported, always correlate to age or gender (Siddappa et al. 2007). Donor variability can cause problems with commercialisation of stem cell related products. For practical reasons, the majority of experiments in this thesis investigate the effects of MI192 on cells from a single donor. This was a representation of how the inhibitor could be utilised in a clinical setting. To investigate donor variability, and to ensure the increase in ALPSA wasn't donor dependent, the effects of MI192 on ALPSA of cells from 4 donors were tested (Figure 5.6). For all four donors, a large, statistically significant ($P \leq 0.001$ to ≤ 0.05)

in ALPSA was seen in cells pre-treated with MI192, over the osteogenic controls, mirroring the trend from previous experiments (Figure 5.2). There was a slight difference between donors in the dose response, which may be because of subtle difference in cells between donors. From this data it can be concluded that the increase in osteogenic potential in ADSCs is not donor dependent. The assumption was made that the results from the one main donor are representative of all ADSCs from all donors (processed in this way). It is worth noting that three of the four donors were female and all were over the age of 45, so this is not totally representative of all possible donors, but these were the donors available from the manufacturers at the time.

For the long term experiments, an ‘osteogenic mineralisation medium’ was utilised, which is a commercial medium from Life Technologies. The exact composition is unknown, but it causes a strong mineralisation of ADSCs, so at least likely contains a mineral source. Firstly, it was tested and compared to the ‘osteogenic induction medium’, to ensure the same effects with MI192 were seen (Figure 5.7). Any difference in ALPSA levels across 4 time points, with both media, was also investigated. The same increase in ALPSA levels with the osteogenic mineralisation medium as with the osteogenic induction medium was seen, although the ALP levels peaked earlier (at day 5 not day 7). The mineralisation medium likely has a quicker effect than the ‘osteogenic induction medium’; it may contain stronger acting osteogenic differentiation inducing compounds, such as BMP2. MI192 having the same effect with the mineralisation medium lead to further, long term, experiments with the osteogenic mineralisation medium.

Gene expression is coordinated by the epigenetic make up of cells, and HDACis are known to affect the osteogenic gene expression of cells (for examples, see (Schroeder et al. 2007; Paino et al. 2014; Cho et al. 2005)). The effect of MI192 pre-treatment on ADSC osteogenic gene expression was investigated. Measuring gene expression levels can provide an indication of multiple different changes to the cell, over multiple time points, in one experiment; indicating how the cells are responding to stimuli. However it is important to note that changes in gene expression are not always representative of what actually happens in the cell, as it only measures transcript levels, not actual proteins produced.

RUNX2 is an early osteogenic transcription factor, which the initially high expression of drops over time in the osteogenic positive controls (Figure 5.8 A). This was expected, as it is an early stage marker, transcript levels should drop over time. In the MI192 pre-treated cells, expression is initially lower than the osteogenic controls, but peaks at day 14 when it is higher than the osteogenic controls. This lag in expression indicates that MI192 actually inhibits *RUNX2* expression initially, with expression at the level of the basal controls at day 3 and day 5. Runx2 protein is known form complexes with HDAC3 (Hesse et al. 2010; Schroeder et al. 2004), and it has been reported that inhibition of HDAC3 (along with HDAC1) with siRNAs in ADSCs activated *RUNX2* expression, across several time points (Maroni et al. 2012). HDAC3 is involved in the mediation of Runx2 protein by zinc finger protein 521 (Zfp521); Zfp521 recruits HDAC3 into a transcriptional repression complex with Runx2 (Hesse et al. 2010). The lag in expression may be evidence of an effect of the HDAC2 inhibition by MI192. HDAC2 may be necessary for stimulation of *RUNX2* expression. Alternatively, the inhibition of HDAC3 may mean that no *RUNX2* transcripts are necessary, as any already present but otherwise occupied Runx2 protein bound to HDAC3 could be released when HDAC3 is inhibited. Therefore the cells don't need to increase *RUNX2* gene expression, whereas in the osteogenic control expression increases in response to the medium.

BMP2 encodes for bone morphogenetic protein 2 (BMP2), and is perhaps the most explored protein in the osteogenic differentiation pathway, as it is widely reported treating cells with BMP2 induces osteogenic differentiation of the cells (Carragee et al. 2011). BMP2 is known to induce osteoblast differentiation through increasing expression of ATF6, a transcription factor that is dependent on Runx2. BMP2-induced osteoblast differentiation mediates ATF6, and in turn regulates expression of further osteogenic differentiation related genes such as *ALP* (Jang et al. 2012). MI192 pre-treatment increase expression of *BMP2* (Figure 5.8 B), at several time points. This increased *BMP2* expression, especially at the early day 3 time point, may in turn result in the observed increases in ALP levels in ADSCs. BMP2 and HDAC proteins are all part of a complicated regulatory network that can result in the osteogenic differentiation of stem cells (Scholl et al. 2012; Jeon et al. 2006). Here, HDAC2 and HDAC3 inhibition lead to an increase in expression of *BMP2*, at least initially.

ALP encodes alkaline phosphatase, and ALP levels have been measured in multiple experiments in this chapter. Increased levels of ALP protein were observed in cells pre-treated with MI192, therefore an increased gene expression was expected. In the M192 pre-treated cells, the ALP expression is much greater than the osteogenic controls at day 5. This increased gene expression likely results in the increased protein levels seen in the ALPSA experiments (for example Figure 5.9 A). *ALP* expression peaks at day 5 in the MI192 pre-treated cells, and expression decreases down to a level of the basal controls after day 7, while in the osteogenic control it continues to increase. This indicates that the cells pre-treated with MI192 initially produce a large amount of ALP, but then stop. This increase may be caused by the spike in BMP2 expression at day 3. The cells pre-treated with MI192 seemingly produce enough ALP protein from this spike in expression and gene expression reduces back down to a near basal level afterwards.

Another gene that shows a spike in cells pre-treated with MI192 treatment is *COL1*. *COL1* is the main gene responsible for formation of type 1 collagen, the primary type of collagen associated with bone cells and an mid-stage marker of osteogenic differentiation (Schroeder & Westendorf 2005). The levels of *COL1* are high, and in the basal culture controls, increase consistently with time, an apparent effect of culturing the cells in the MesenPRO RS™ growth medium (Figure 5.9 B). *COL1* expression peaks at day 7 in both the osteogenic control and the MI192 pre-treated cells, although expression is statistically significantly higher ($P \leq 0.001$) in the MI192 pre-treated cells. The pattern is similar in both the controls and the MI192 pre-treated cells, except for a peak at day 3 in the osteogenic controls over the MI192 pre-treated cells. At the later time points *COL1* expression drops off, although this is compared to the basal control where expression keeps increasing. This lag in expression may be linked to the suppression of *RUNX2* in the MI192 pre-treated cells. The increase in *COL1* expression is similar to findings in the literature, where HDAC inhibition, with VPA and NaB has been found to increase *COL1* expression increase in mouse ADSCs (Xu et al. 2009) and TSA was found to accelerate *COL1* expression in a MC3T3-E1 mouse preosteoblast cell line (Schroeder & Westendorf 2005). However, not all HDACi treatment results in increasing *COL1* expression; the treatment of mice with SAHA was found to down-regulate *COL1* in mouse tibia (McGee-Lawrence et al. 2011). The increase in *COL1* expression in the MI192 pre-treated cells over the osteogenic control is another indicator that MI192 pre-treatment improves the osteogenic differentiation potential of ADSCs.

OCN/BGLAP encodes osteocalcin/bone gamma-carboxyglutamic acid-containing protein, a non-collagenous protein found in bone, often utilised as a later stage marker of osteogenic differentiation (Schroeder & Westendorf 2005). *OCN* expression is initially inhibited by MI192 treatment, to a level below that even of the basal culture cells (Figure 5.10 A). This is likely as a result of the inhibition of *RUNX2* expression, as Runx2 is a known promoter of *OCN* expression (Fu et al. 2014; Vrtačnik et al. 2013). In the MI192 pre-treated cells at day 7 expression of *OCN* increases over the osteogenic control; however, it is only a slight increase and expression is less at day 14 and day 21 in the MI192 pre-treated cells. Importantly, Paino et al. (2013) discovered that the silencing of HDAC2 decreases *OCN* expression in a Saos-2m bone osteosarcoma cell line, making it likely HDAC2 is key for *OCN* expression (Paino et al. 2014). Reports of the importance of HDAC3 with regards to OCN are conflicting; deletion of HDAC3 resulted in no effect on OCN levels *in vivo* (Razidlo et al. 2010; McGee-Lawrence et al. 2013), but *in vitro* with osteoblasts it was found that HDAC3 had a suppressive effect on OCN, believing its deletion of inhibition would result in increased *OCN* expression (Lamour et al. 2007). An increase in *OCN* expression with TSA treatment has been observed in some of the literature (Schroeder & Westendorf 2005; Jin et al. 2013; Hu et al. 2013), although the treatment of mice with SAHA was found to down-regulate *OCN* in mouse tibia (McGee-Lawrence et al. 2011), and treatment of human osteoblasts and human dental pulp stem cells with VPA reduced *OCN* expression (Paino et al. 2014). There are clear differences in HDACis here, likely due to different HDAC isoforms being targeted. Here, it would appear HDAC2 and HDAC3 inhibition combined may negatively affect *OCN* expression. This could just be due to the HDAC2 inhibition. The lack of *OCN* expression may be a problem for the long term differentiation prospects of these MI192 pre-treated cells, as OCN is a key bone protein.

SPP1 encodes osteopontin (OPN), a structural extracellular protein found in osteoblasts, forming part of the organic component of bone. It is found in several other tissues, such as the lung and vasculature, and plays a role in controlling mineralisation, coupling of bone formation and bone resorption (Subramani 2015), although its full function is not completely understood. While being found abundantly in bone, it appears to modulate the formation of hydroxyapatite, preventing crystal growth, ensuring that they grow in the correct locations (Hunter 2013). The addition of exogenous OPN to cells actually inhibited mineralisation (Addison et al. 2007). Here, expression of *SPP1* was consistently down-regulated in

the osteogenic control, and the pre-treatment of ADSCs with MI192 resulted in an even greater down-regulation (Figure 5.10 B). This trend was consistently seen across all time points. The only notable change in the pattern of expression was at day 14 in the osteogenic controls, where there was a peak in *OPN* expression. OPN protein is a target of Runx2, but the increase in *RUNX2* expression in these cells does not seem to correlate to an increase in *SPP1* expression. The down-regulation of *SPP1* may enable the MI192 pre-treated cells to mineralise more freely. In the literature, expression of *SPP1* was also seen to be down-regulated in the tibia of mice treated with SAHA (McGee-Lawrence et al. 2011). In human osteoblast cells, treatment with VPA reduced *SPP1* expression, although in dental pulp stem cells, *SPP1* expression was increased with VPA treatment (Paino et al. 2014).

The effect of MI192 pre-treatment on the mineralisation of ADSCs was next explored, with an Alizarin Red stain for calcium accumulation and a Von Kossa stain for mineral nodule formation (Figure 5.11, Figure 5.12 and Figure 5.13). MI192 pre-treatment resulted in more mineral nodules forming in the cells. Overall calcium accumulation in the cells was lower, although this was not normalised to cell number and may just be as a result of a lower cell number. Indeed, almost all the cells visible had calcium deposition, whereas in the osteogenic control there were areas of negative staining (Figure 5.11). The Von Kossa stain was strongest with MI192 pre-treatment, indicating these cells were forming more functional mineral nodules, and not just accumulating minerals such as calcium and not actually functionalising them or doing anything with them, as may be happening in the osteogenic controls. Typically in the literature, treatment of cells with HDACis increases their mineralisation potential (Xu et al. 2013; Paino et al. 2014), although pre-treatment of ADSCs with TSA has actually been show to decrease mineralisation (Maroni et al. 2012). It was also found that inhibition of HDAC3 (with siRNAs) will increase the speed at which cells mineralise (Schroeder et al. 2004), and has been shown to increase Alizarin Red staining of ADSCs (Maroni et al. 2012). The down-regulation of *SPP1* expression seen above may explain why the mineralisation was greater in the MI192 pre-treated cells, as SPP1 can inhibit the formation of mineral nodules.

Osteogenic differentiation and adipogenic differentiation regulatory machinery is closely linked (Ducy et al. 2000). The effects of MI192 on adipogenic differentiation

were explored, to see if different lineages of differentiation were affected, either positively or negatively, with MI192 treatment.

Accumulation of fat droplets is an indicator of adipogenic differentiation. Staining with Oil Red O for lipid droplets found that pre-treatment with MI192 inhibited the adipogenic differentiation of ADSCs. Staining was strong in the adipogenic controls, but was statistically significantly weakened (when destained) with MI192 treatment. There are reports that HDACi inhibition will promote adipogenic differentiation of cells. Treatment of a 3T3-L1 mouse fibroblast/adipocyte cell line with several HDACis found that adipogenic activity was stimulated (Fajas et al. 2002), and a further study by Yoo at al. (2006) also found that treatment of 3T3-L1 cells with NaB resulted adipogenic differentiation (Yoo et al. 2006). They also found that specifically knocking down HDAC1 also stimulated adipogenesis. Furthermore, Jiang at al. (2013) found that HDAC3 inhibition promoted PPARγ mediated adipogenic differentiation in the same 3T3-L1 cells (Jiang et al. 2013). Peroxisome proliferator activated receptors (PPARs) are nuclear receptor proteins that function as transcription factors regulating the expression of genes, with the gamma (γ) type being a regulator of adipogenic differentiation and metabolic response to the external environment (Lehrke & Lazar 2005). However, the findings in these studies were all with the same cell line. With primary ADSCs, Maroni et al. found that silencing of HDAC3 with siRNAs inhibited *PPARγ* expression (Maroni et al. 2012). The study by Maroni et al. was undertaken with ADSCs, so the most applicable to this study, although they did not explore the effects of the inhibition on the actual adipogenic differentiation of the ADSCs. In this study, it would seem that these findings are in line with those of Maroni et al., and the inhibition of HDAC3 (and HDAC2) inhibits the adipogenic differentiation of these cells. *PPARγ* gene expression in ADSCs undergoing adipogenic differentiation after MI192 pre-treatment was investigated. Also investigated was *ADIPOQ*, which encodes adiponectin, a protein involved in regulating glucose levels and fate storage in the body, which can be used as a later stage marker of adipogenic differentiation (Haberland et al. 2010).

On analysing the adipogenic gene expression changes with MI192 treatment, *PPARγ* and *ADIPOQ* expression was down-regulated. This is in line with the findings of Maroni et al., where *PPARγ* was down-regulated (Maroni et al. 2012). The fact that the findings are different to those found in the 3T3-L1 cells, which may

indicate a difference in the use of species (mouse vs human) or the fact that the 3T3-L1 cells are transformed (Yoo et al. 2006). The creation of the HDAC3-PPARγ complex in the ADSCs, if it has an oppressive effect on adipogenic differentiation, and why the inhibition of HDAC3 appears to down-regulate *PPARγ* expression and not leave the protein free to induce adipogenic differentiation as in the 3T3-L1 cells is unclear from these initial experiments. It is clear; however, that MI192 inhibits adipogenic gene expression.

Chapter 6: The Effects of MI192 on Bone Tissue Engineering using Adipose Derived Stem Cells and Three Dimensional *In Vitro* Models

The aim of this chapter was to investigate the effect of MI192 treatment on the osteogenic differentiation of ADSCs, using scaffolds cast from silk fibroin extracted from Antheraea mylitta silk worms. The objectives were to assess how cells attached and spread on the scaffolds with live/dead cell labelling and to assess the ADSCs ability to lay down extracellular matrix, their ability to mineralise and their formation of proteins known to be important in bone cells through histology and immunohistochemistry.

6.1 Introduction

It was well known that cells cultured in monolayer on tissue culture plastic are forced to act atypically (Baker & Chen 2012; Griffith & Swartz 2006), which therefore can only tell a part of a story. A huge amount of early research into cells behaviour has been undertaken in monolayer; however, this is not representative of how cells are located, and therefore act, *in vivo*. That being said, 2D cell culture systems are still a useful tool in research. They are standardised, still mimic the condition of the body to some degree and are easily used and set up. Naturally, in the body, cells are found in complicated, three dimensional (3D) environments, usually surrounded by cells of many different types, naturally occurring chemicals, signals and constantly changing conditions (Baker & Chen 2012), i.e. not just at a steady temperature of 37 °C, with 5% CO_2 and constantly defined nutrient source (tissue culture medium). When cultured in 2D, the morphology of cells is altered causing an alteration in the cell properties (Baker & Chen 2012; Griffith & Swartz 2006). Perhaps most significantly, cells cultured in 3D culture models are able to interact with other cells much more naturally, not just by touching at the edges. This is a potential issue with 2D culture that has been recognised for decades (Vondermark et al. 1977). A summary of the difference between 2D and 3D culture systems can be seen in Figure 6.1. When

trying to tissue engineer complex 3D tissues, it is important to investigate cell behaviour in 3D.

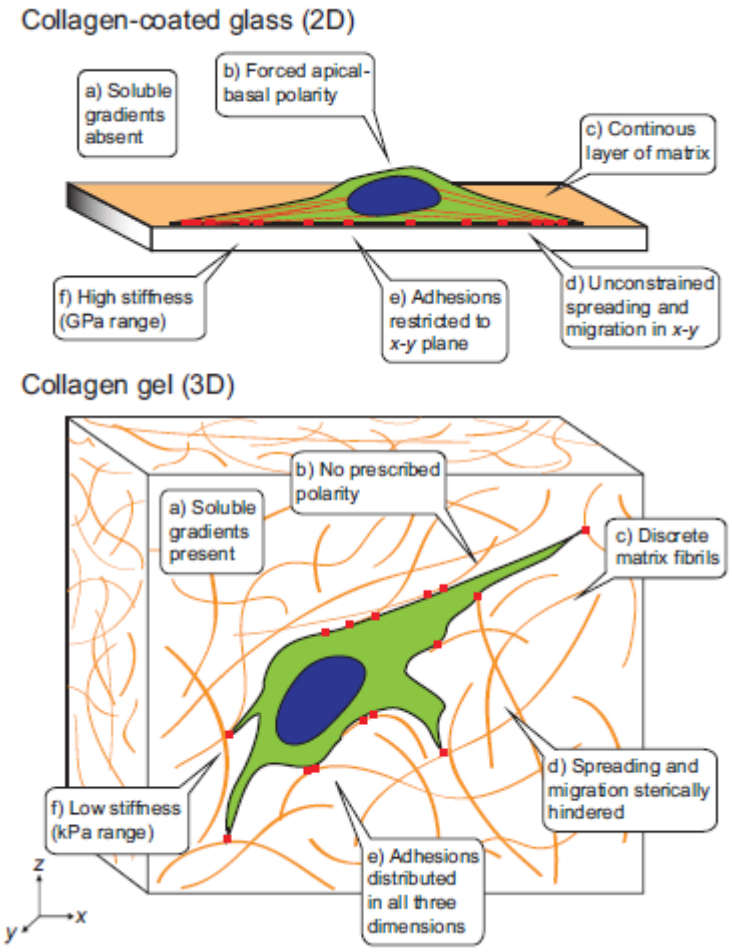

Figure 6.1 – Depictions of cells in 2D and 3D culture systems. An illustration of the difference in cell morphology, and therefore adhesive, topographical, mechanical and soluble cues between 2D and 3D culture systems. Reprinted with permission from (Baker & Chen 2012)**.**

'Scaffolds' form one of the four key pillars of tissue engineering, (Chapter 1:Literature Review, Figure 1.1), providing a 3D template and the microenvironment to support cell growth, extra cellular matrix deposition and tissue formation. 3D culture models utilising scaffolds have been extensively explored for bone tissue engineering (Laino et al. 2006; El-Gendy & Yang 2012; Amini et al. 2012). The goal when utilising these scaffolds is typically to have them integrate into the surrounding bone and heal the

defects, or strengthen weakened bone (Amini et al. 2012; Ericka M. Bueno & Glowacki 2011).

For the purposes for tissue engineering, researchers look to design scaffolds that are biocompatible, economically viable, inductive for the tissue of choice and which support cell growth and differentiation (Ericka M Bueno & Glowacki 2011). To date, many different scaffolds have been utilised in bone tissue engineering, including Bioglass® (W. Lu et al. 2014), peptides (Sfeir et al. 2014) and bioresorbable polymer based scaffolds, such as those based on lactic acid or other copolymers (which have FDA approval in surgical applications and as drug delivery systems (Howard et al. 2002)). Due to the need for a high mechanical strength, in bone tissue, glass-ceramics, such as Apatite-Wollastonite (Dyson et al. 2007), have also been explored.

Regarding utilising HDACis in bone tissue engineering, there has been very little work utilising HDACis in combination with scaffolds. Some researchers jumped straight from 2D *in vitro* validation, to *in vivo* studies, where they investigated bone healing utilising injection of a cell suspension, without any 3D experiments with scaffolds (Xu et al. 2009). Others will utilise scaffolds but implant them *in vivo* without first reporting or undertaking *in vitro* validation, moving directly onto *in vivo* models utilising the scaffolds. For example, Boer et al. (2006) utilised biphasic calcium phosphate ceramic granules as a scaffold to investigate the effect of TSA and NaB on bone formation in a subcutaneous mouse model. However, the results from this were inconclusive, perhaps because the authors missed out the 3D *in vitro* testing, which can be very important step prior pre-clinical and clinical assessments (Boer et al. 2006).

Lee et al. (2011) utilised two different animal models to investigate the *in vivo* osteogenic activity of Largazole: 1) collagen sponge scaffolds doped with Largazole were implanted calvaria bones, and 2) macroporous biphasic calcium phosphate scaffolds were also doped with Largazole in a rabbit calvaria bone defect model. The results showed that Largazole improved osteogenic healing in both models (Lee et al. 2011). In another study, Jung at al. (2010) combined TSA and NaB with calcium sulphate scaffolds during the setting process. These HDACi doped scaffolds were found to have increased osteoinductive capability, improving the osteogenic

differentiation of a murine MC3T3-E1 pre-osteoblast cell line (while simultaneously inhibiting the osteoclastic potential of these cells), unusually with the 3D results validated both *in vitro* and *in vivo* (Jung et al. 2010). These studies are the sum total of the literature surrounding this topic, so there are very few studies to compare results with in this chapter.

Silk scaffolds are a type of scaffold that have shown much promise for multiple areas of tissue engineering, including cartilage (Saha et al. 2013), cardiac (Patra et al. 2012) and nervous tissue engineering (Allmeling et al. 2008). Silk is an abundant natural polymer biomaterial, which can be farmed in large amounts from spiders or silk worms. Silk fibroin protein has been utilised in oral surgeries, wound healing and has FDA approval as a material for ligament and tendon approval (marketed as Serica, by Allergan) (Kundu et al. 2013). As well as being abundant, silk has the advantage of being a biocompatible natural material, which will elicit a low immune response on implantation. Silk is also mechanically robust and biodegradable, at a rate typically useful for implantation. Another beneficial property of silk is that it can be easily cast into shapes, or electro spun, to create scaffolds of a desired shape, size and physical properties. Finally, typically scaffolds formed from silk are porous, allowing good cell ingrowth (Saha et al. 2013; Kundu et al. 2013; Omenetto & Kaplan 2010). Silk scaffolds have been utilised in multiple bone tissue engineering studies. For example, Meinel et al. (2005) demonstrated that they can heal critical sized bone defects in mouse models (Meinel et al. 2005). Scaffolds can be coated, for example with apatite (Zhao et al. 2009) or have growth factors incorporated (Saha et al. 2013), to enhance their osteogenic induction properties.

The majority of studies utilising silk from silk worms investigate silk from the *Bombyx mori* (Bm) silk worm, which is a mulberry silk, (where mulberry refers to the plants the worms eat). Silk produced from Am worms is a non-mulberry silk and the worm is found almost exclusively in the north eastern parts of India. The silk produced from an Am worm has slightly different properties to that of a Bm worm, as can be seen in comparative studies of the two. Reports are conflicting as to which is the more osteoinductive, with S. Saha of Oral Biology, and Miyamoto et al. (2013) finding that Bm is more osteoinductive (Miyamoto et al. 2013; Saha et al. 2013), but Sahu et al. finding Am to be more so (Sahu et al. 2015). Because they were the most

abundantly available from collaborators, and they were found to be osteoinductive in the latest study carried out with them, Am silk scaffolds were used for these studies.

3D scaffolds produced from Indian tropical *Antheraea mylitta* (Am), in the laboratory of Professor S. C. Kundu of the Indian Institute of Technology Kharagpur, were utilised to investigate the aims of this chapter. To fully investigate the potential of these, a number of experimental designs were investigated. A schematic explaining these can be seen in Figure 6.2.

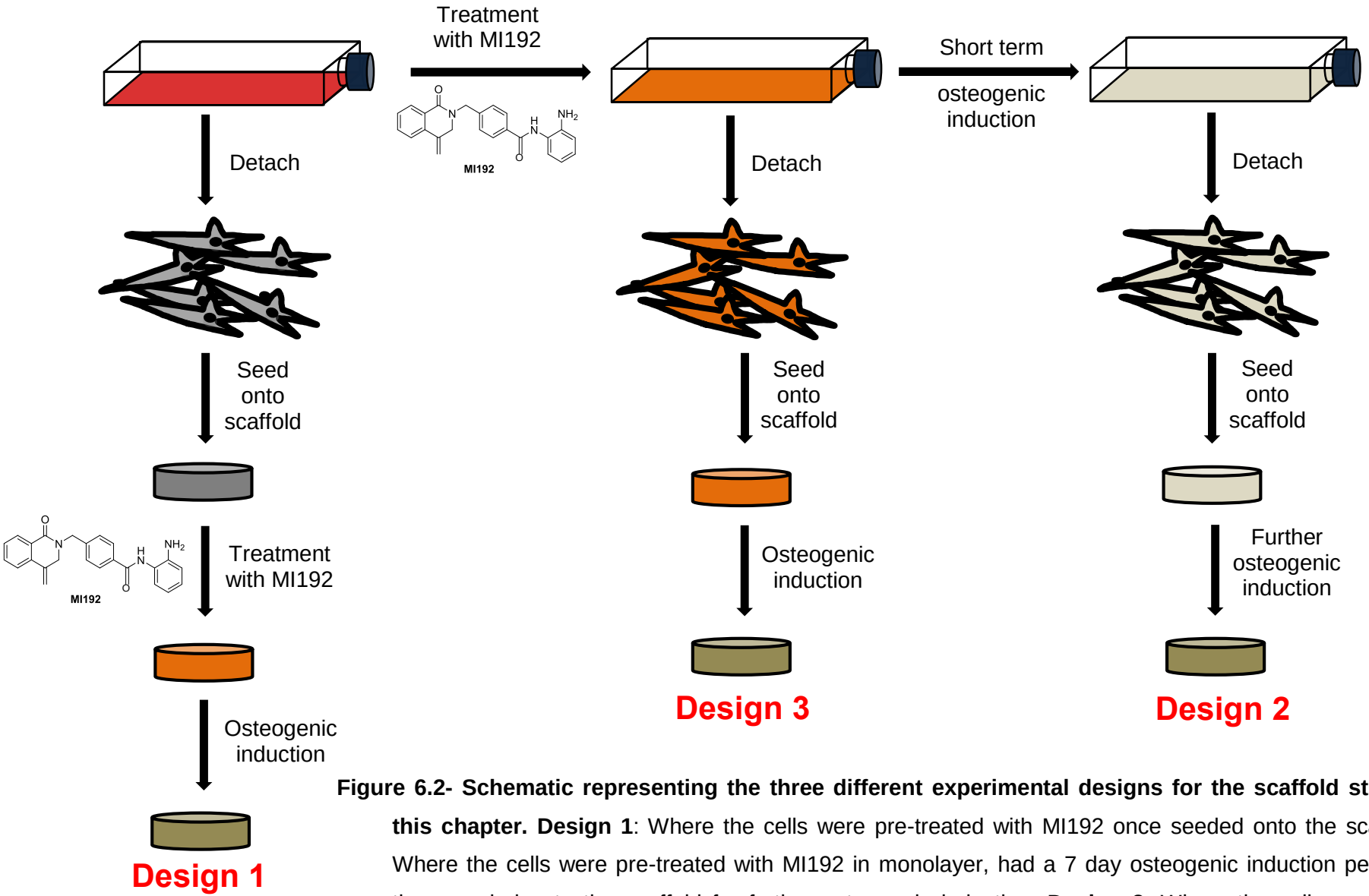

Figure 6.2- Schematic representing the three different experimental designs for the scaffold studies covered in this chapter. Design 1: Where the cells were pre-treated with MI192 once seeded onto the scaffolds. **Design 2**: Where the cells were pre-treated with MI192 in monolayer, had a 7 day osteogenic induction period in monolayer, then seeded onto the scaffold for further osteogenic induction. **Design 3**: Where the cells were pre-treated with MI192 in monolayer and seeded straight onto the scaffold.

6.2 Materials and Methods

Scaffolds used in this chapter were created in the laboratory of Professor S. C. Kundu, of the Indian Institute of Technology (IIT) Kharagpur, as part of a collaborative project between Leeds School of Dentistry and IIT Kharagpur. Scaffold production (6.2.1) was carried out in India, but the scaffold preparation (crosslinking, sterilisation and FCS treatment) was carried out by the author in Leeds (6.2.2).

6.2.1 Silk protein fibroin extraction and 3D scaffold production

Briefly, silk larvae from the Indian tropical *Antheraea mylitta* were obtained from the Tasar Sericulture Farm, West Midnapur, West Bengal State, India. After washing with dH_2O, the glands of *Antheraea mylitta* larvae were dissected and silk protein fibroin was collected by squeezing it out of the glands. The extract was dissolved in 1% (w/v) Sodium dodecyl sulfate (SDS) aqueous solution containing 10 mM Tris (pH 8.0) and 5 mM EDTA. To then remove any traces of solvents, the fibroin solution was extensively dialyzed against dH_2O. This was then cast in moulds (5 mm diameter 2 mm thickness) and lyophilised to obtain 3D silk scaffolds, with a slow pre-cooling step of – 20 °C to obtain scaffolds with uniform and interconnected pores (Saha et al. 2013; Patra et al. 2012). All scaffolds used in this chapter were this size and were produced in this way. They are referred to as ‘Am silk scaffolds’ throughout.

6.2.2 Scaffold preparation before experiments

Prior to cell seeding, dried scaffolds were crosslinked and sterilised in 70 % EtOH for 30 minutes at 37 °C, washed three times with 1x PBS, (30 minutes per wash) and then incubated in 20 % FCS α-MEM over night at 37 °C. Prior to cell seeding the scaffolds were washed twice in plain medium.

6.2.3 Dynamic seeding of cells on 3D silk scaffolds

Cells were dynamically seeded onto scaffolds using an in house dynamic seeding device (Figure 6.3). Briefly, 1.5 mL cell suspension containing the appropriate cell number was placed in a sterile 2 mL Eppendorf tube with a hole pieced in the lid. The sterilised, crosslinked and FCS pre-treated silk scaffold was then placed in each tube,

in the cell suspension. The lid was shut and the hole was covered with a layer of Opsite (Smith & Nephew, Cat. No: 4630), a transparent, adhesive polyurethane film, used in surgeries and wound healing, which allows gas exchange in and out of the tube, while keeping the contents sterile.

The tubes were then placed in the rotating seeding device (Figure 6.3) that was kept in a standard cell culture incubator for the seeding duration. The seeding device turns at a constant rate, of around 10 rotations per minute, thereby increasing the opportunity for cells to come into contact with and seed onto the scaffolds.

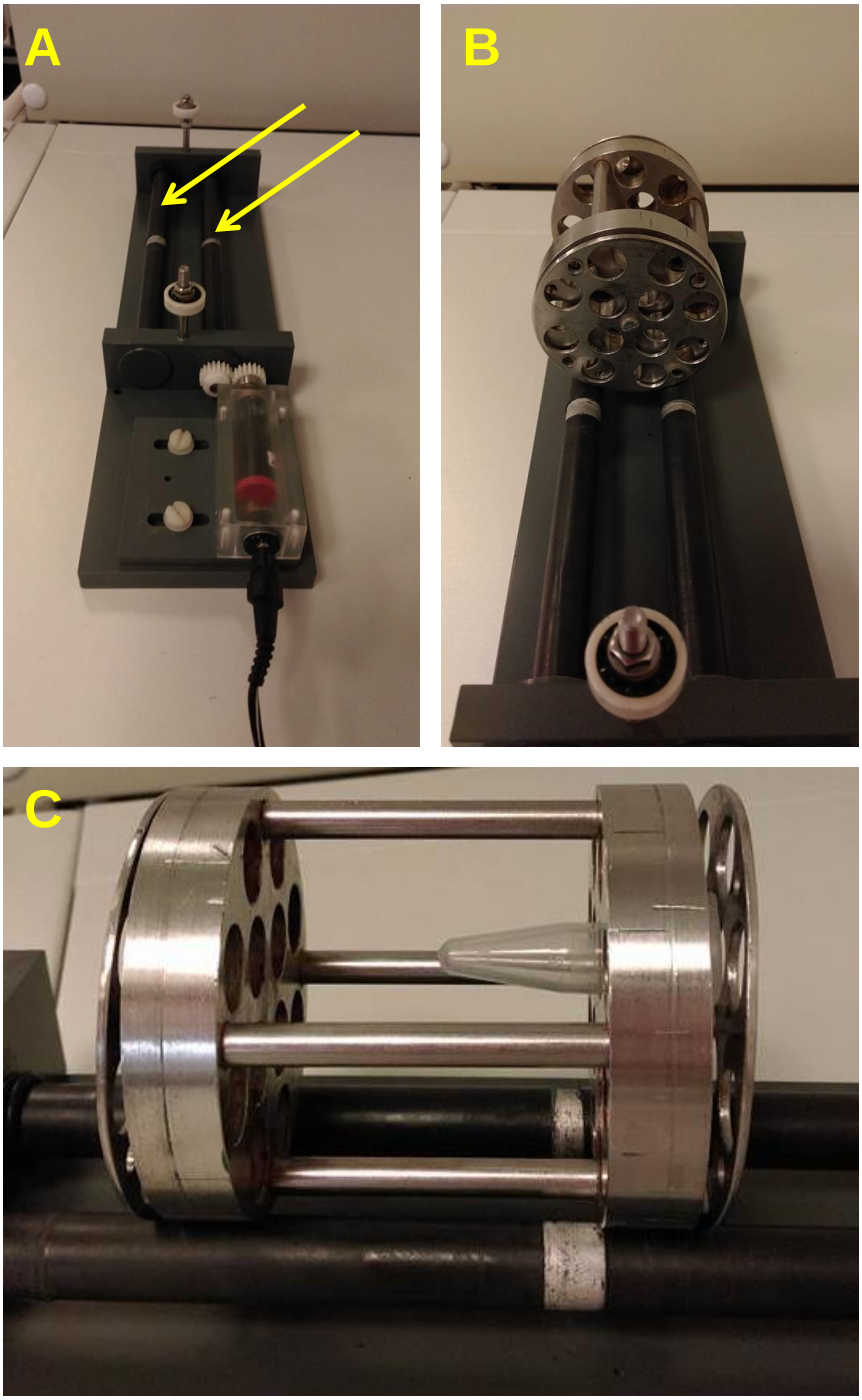

Figure 6.3 – Photographs of the in house dynamic cell seeding device. A – Unloaded device. Arrows indicate the black bars which rotate when the device is turned on, which causes the seeding device to rotate. B – Empty seeding device loaded onto the cell seeder. C – Seeding device with an empty tube in, indicating how tubes sit in the device.

6.2.4 Live and dead cell Labelling

Live/dead cell labelling can be utilised for the *in situ* imaging of cells in culture. Labelling and imaging were carried out with ascetic technique, so culture can be continued after imaging.

CellTracker™ Green CMFDA (5-chloromethylfluorescein diacetate) dye (ThermoFisher Scientific, Cat. no: C7025) can be utilised as a live cell label. The dye can be absorbed freely across cell membranes, reacts with cellular components and is converted to cell-impermeable products. These products emit fluorescence for at least 24 hours and can be passed to daughter cells through several generations, while not being transferred to any adjacent cells, or leaving the cells. CMFDA emits green fluorescence (excitation/emission maxima ~492/517 nm). Ethidium homodimer I (EthD-1, Sigma, 2 mM in DMSO, Cat. no: E1903) dye can be utilised as a dead cell maker. EthD-1 is an intact membrane-impermeable dye, which will only be absorbed into dead cells due to their disrupted membranes. EthD-1 binds to DNA in dead cells and emits red fluorescence (excitation/emission maxima ~528/617 nm).

Scaffolds were immersed for 30 minutes in basal medium containing the dyes prepared according to the manufacturer's instructions. For CFMDA, 10 µL DMSO was added to 1 vial containing 50 µg of CFMDA, which was then diluted in 5 mL of culture medium to a final concentration of 10 µg/mL medium. For EthD-1, 20 µL of the dye (which came prepared by the manufacturer at 2 mM in DMSO) was added to the same 5 mL of culture medium, to a final concentration of 6.8 µg/mL medium. Labelled scaffolds were then washed in basal medium for 30 minutes, before placing in fresh basal medium for imaging.

6.2.5 ADSCs seeded onto 3D silk scaffolds prior to MI192 treatment (Expt 1)

ADSCs were dynamically seeded (1 x 10^5 cells per scaffold), as described above onto Am scaffolds in basal medium for 48 hours. Then, the cell-scaffolds constructs were cultured in basal medium for further 24 hours. The medium was then replaced with MI192 containing medium (30 µM in 1 mL basal medium per scaffold), with untreated control scaffolds. After 48 hours, the scaffolds were carefully washed in 1x

PBS. The medium for the test groups (MI192 pre-treated scaffolds) and the osteogenic positive control group was changed to osteogenic mineralisation medium. The sample size was three for both groups (n=3). The medium was changed every 4-5 days. After 6 weeks of culture, live cells on two of the scaffolds from each group were labelled with CellTracker™ Green CMFDA Dye and the scaffolds were imaged under a Leica DMI6000 B inverted confocal microscope. Following imaging at 6 weeks, the cell density was observed to be too low to stop the experiment, so the scaffolds were cultured for a further 3 weeks. After 9 weeks culture, live cells on the same two scaffolds from each group were labelled with CellTracker™ Green CMFDA Dye and imaged under a Leica DMI6000 B inverted confocal microscope. Scaffolds were then fixed in 10 % NBF for 24 hours, before being paraffin embedded, sectioned and histologically stained with a Van Gieson's stain, to visualise tissue formation.

6.2.6 ADSCs treated with MI192 followed by 7 days of osteogenic induction prior to seeding on 3D silk scaffolds (Expt 2)

ADSCs in T175 tissue culture flasks were washed with 1x PBS and the medium then replaced with medium containing MI192 (10 µM and 30 µM in 25 mL basal medium per flask), with cells in one other flask untreated, as a control. After 48 hours, the flasks were carefully washed in 1x PBS. The medium for the test groups (MI192 pre-treated) and the osteogenic positive control groups was changed to osteogenic mineralisation medium and the negative basal control group was changed to MesenPRO RS™ growth medium. The ADSCs were then cultured for 7 days, with the medium changed at day 3. The ADSCs were detached and then dynamically seeded onto Am silk scaffolds (2.5×10^5 cells per scaffold) for 48 hours, in osteogenic mineralisation or MesenPRO RS™ growth medium as appropriate. The sample size was four for all groups (n=4). After 24 hours of culture, live cells on two of the scaffolds from each group were labelled with CellTracker™ Green CMFDA Dye and the scaffolds were imaged under a Leica DMI6000 B inverted confocal microscope. The scaffolds were then cultured for 6 weeks, with the medium being changed every 4 - 5 days. Then, live cells on two of the scaffolds from each group were labelled with CellTracker™ Green CMFDA Dye and the scaffolds were imaged under a Leica DMI6000 B inverted confocal microscope. Scaffolds were then fixed in 10 % NBF for 24 hours, before being paraffin embedded, sectioned and histologically stained with a Van Gieson's, Picrosirius red and Von Kossa stain, to visualise tissue formation, collagen formation and mineralisation.

6.2.7 ADSCs treated with MI192 prior to seeding on 3D silk scaffolds (Expt 3)

ADSCs in T175 tissue culture flasks were washed with 1x PBS and the medium was then replaced with medium containing MI192 (10 µM and 30 µM in 25 mL basal medium per flask), with untreated control flasks. After 48 hours, the flasks were carefully washed in 1x PBS. The ADSCs were then detached and were dynamically seeded (2.5 x 10^5 cells per scaffold) onto Am silk scaffolds for 48 hours, in MesenPRO RS™ growth medium. After seeding, the scaffolds were then cultured in the same medium for 24 hours. Then live cells on two of the scaffolds from each group were labelled with CellTracker™ Green CMFDA Dye and the scaffolds were imaged under a Leica DMI6000 B inverted confocal microscope. The scaffolds were then placed in culture medium; for the test groups (MI192 pre-treated scaffolds) and the osteogenic positive control groups was osteogenic mineralisation medium and the negative basal control group was changed to MesenPRO RS™ growth medium. The sample size was four for all groups (n=4). The scaffolds were then cultured for 6 weeks, with the medium being changed every 4-5 days. Then, live cells on two of the scaffolds from each group were labelled with CellTracker™ Green CMFDA Dye and the scaffolds were imaged under a Leica DMI6000 B inverted confocal microscope. Scaffolds were then fixed in 10 % NBF for 24 hours. One scaffold from each group was imaged with environmental Scanning Electron Microscopy (SEM), with additional Energy Dispersive X-ray Spectroscopy (EDS) analysis. Scaffolds were then paraffin embedded, sectioned and histologically stained with a Van Gieson's, Picrosirius red and Von Kossa stain, to visualise tissue formation, collagen formation and mineralisation. Sections were also stained with antibodies in immunohistochemical staining protocols for Runx2, Col1 and OCN.

6.2.8 Immunohistochemical staining

EnVision™ Detection Systems Peroxidase/DAB, Rabbit/Mouse (Dako, Cat. no: K406511) and a Thermo Scientific Shandon ® Sequenza Immunostaining Center with coverplates (Thermo Scentific Cat. no: 72110013) were utilised for immunohistochemical staining.

After being taken to water, slides were blocked for peroxidase with the 'Dual Endogenous Enzyme Block' from the EnVision™ kit for 10 minutes. Slides were then washed in a 1x PBS wash box for 5 minutes. For the Ocn and Col1 staining antigen retrieval was performed, where slides were immersed in a 37 ºC, pH 7.8, 0.1% chymotrypsin in 0.1% $CaCl_2$ solution for 20 minutes. Slides were then washed in a 1x PBS wash box for 5 minutes before loading into coverplates and then the Immunostaining Centre. Slides were washed with 1x PBS for 5 minutes to ensure equal reagent flow through the coverplates. The slides were then incubated in normal goats serum (1:5 ratio in 1x PBS, Dako, Cat. no: X090710) for 30 minutes. The primary antibody (Table 6-1) was then applied, for the length of time specified below (Table 6-1). Antibody concentration refers to a dilution in PBS. After incubation with the primary antibody, the slides were washed with 1x PBS for 5 minutes. 2 drops from the bottle 'Labelled Polymer', the secondary antibody, from the EnVision™ kit were then loaded into each slide, and slides incubated at room temperature for 30 minutes. Slides were then washed in 1x PBS 5 minutes before removal from the coverplates. The stain was then developed for 5 – 10 minutes using the 'DAB+ Chromogen' in the provided 'Substrate Buffer', from the EnVision™ kit. Slides were then washed in a running tap water bath for 5 minutes, stained with Harris's Haematoxylin for 30 seconds, washed in a tap water bath for 2 minutes and developed in Scott's tap water for 2 minutes. The slides were then immersed in a running tap water bath for 5 minutes, and two 100 % EtOH baths, for 5 minutes each, and in xylene for 2 minutes before mounting in DPX. The stains were then observed under an Olympus BX50 microscope.

Table 6-1 – Antibodies for immunohistochemical staining and the conditions they were used in

Protein	Abcam Cat. no.	Antigen retrieval?	Concentration	Length of time / temperature of application
Runx2	ab6308	No	1/600	1 hour / room temp
Collagen I	ab6308	Yes	1/100	16 hours / 4 ºC
Ocn	ab13420	Yes	1/400	16 hours / 4 ºC

6.3 Results

6.3.1.1 Assessment of cell viability and growth

Am silk cell-scaffold constructs were labelled with CFMDA and EthD-1 to visualise the viable and dead cells on the 3D silk scaffolds. However, it was discovered that the Am silk scaffolds absorb the EthD-1, causing large background fluorescence, which can be observed in Figure 6.4, where a scaffold has been labelled with both CFMDA and EthD-1. This made imaging of dead cells vary hard. In Figure 6.4 A the scaffold architecture can be seen as dark, not fluorescing, and live cells can be seen. Figure 6.4 B shows the scaffold fluorescing when exposed to the light usually utilised to visualise dead cells labelled with EthD-1 (excitation/emission maxima 528/617). When exposed to the same light, a scaffold not labelled with EthD-1 does not fluoresce, indicating this is not auto-fluorescence of the scaffold, but the scaffold itself somehow taking the label up. Figure 6.4 C shows the two previous images superimposed onto one another, showing that the darkness in the live cell image (Figure 6.4 A) follows the same architecture as the fluorescent image in the dead cell image (Figure 6.4 B). The fact the scaffold absorbs the dye and fluoresces means that imaging of dead cells was difficult, as the scaffold obscures the dead cells, resulting in false positive staining. Therefore, no dead dye was used in the rest of experiments detailed in this thesis.

6.3.2 The effect of MI192 on ADSCs seeded onto 3D silk scaffolds prior to MI192 treatment (Expt 1)

ADSCs were seeded onto Am scaffolds prior to the two days of pre-treatment with MI192, followed by osteogenic induction for 9 weeks.

6.3.2.1 Assessment of cell viability and growth

After 6 weeks of culture fluorescent images showed that viable cells were present on all scaffolds. Cells were quite dispersed and with variable morphologies. The density of viable cells in the osteogenic control scaffolds (Figure 6.5 A + B) was higher than those treated with MI192 (Figure 6.5 C + D). The cell density was too low in all samples to stop the experiment at the planned 6 week end point, so constructs were cultured for a further 3 weeks.

At 9 weeks, viable cells were observed on the scaffolds (Figure 6.6). The cell phenotype was similar in both groups: cells are typically aligned with one and other, although on top of this aligned pattern some randomly orientated cells can be observed (especially visible in Figure 6.6 B). The cell density was higher in both groups compared to the same group at 6 weeks (Figure 6.5). The cell density was similar in all groups and based on this the experiment was stopped and scaffolds were analysed with histology.

6.3.2.2 Histological Analysis

Negative control scaffolds, with no cells on, did not stick to the slides well and nothing was observable, presumably due to a lack of cells to support the scaffold structure or to bind to the slides. However, the scaffold is observed when cells are present, and the scaffold can be distinguished from the cells/tissues with some stains. Typically in histology, Harris' haematoxylin and Eosin staining is utilised as a basic stain to observe tissue formation. However, the Am silk scaffolds strongly stain red with the eosin dye, making it difficult to differentiate between scaffold and cells. Furthermore, ADSCs in these studies did not absorb eosin dye well, and thus overall tissue identification was not good. Therefore, a Van Gieson's stain for connective tissue was utilised, which stains the ADSCs strongly with a pink colour. The scaffold, when visible and not obscured by cells, stains yellow, or a different shade of pink with Van Gieson's stain.

In the osteogenic control scaffolds the tissue density was high in two of three scaffolds, with a lower tissue formation in the third (Figure 6.7 A, B and C). The silk scaffolds stained a yellow colour, thus the newly formed tissue can be distinguished from the scaffolds. In the higher cell density samples, the scaffold architecture is difficult to observe, as it is obscured by the tissue.

In the scaffolds treated with MI192, the staining/cell density was much lower than that of the osteogenic control group (Figure 6.7 D, E and F). Although a thick, strongly stained capsule appears to have formed around the edge all the scaffolds. Cell penetration and growth is low in the MI192 pre-treated groups compared to the osteogenic control group.

Due to the poor tissue formation in the test group (MI192 treatment group), further analysis was not carried out on the samples and alternative experimental designs were explored.

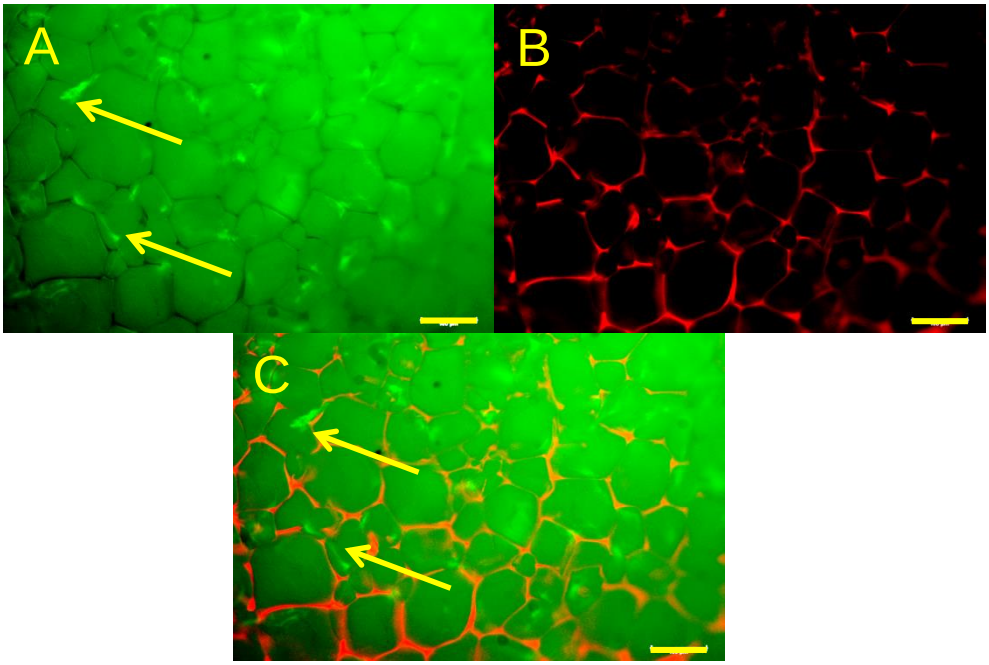

Figure 6.4 – Live/Dead cell dye test. Fluorescent imaging of viable ADSCs (green colour) on Am silk scaffolds labelled with both the live (CFMDA) and the dead (EthD-1) markers 1 day after seeding. **A** – Live marker alone; **B** – dead marker alone; **C** – superimposed images A and B. Scale bars = 100 µM. Yellow arrows indicate live cells growing aligned with the fibres of the scaffold.

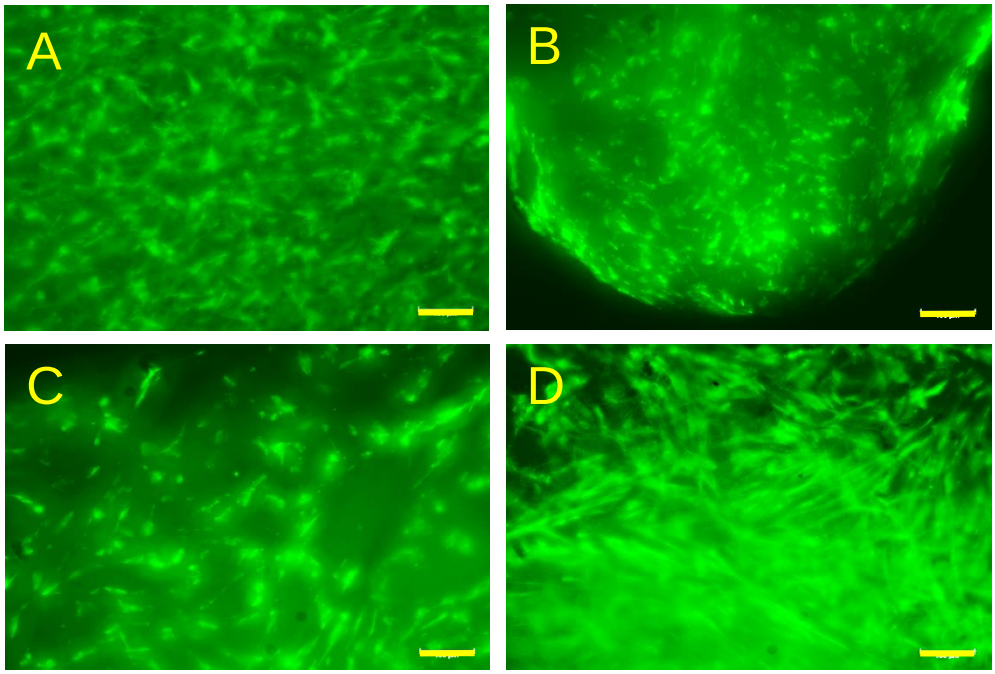

Figure 6.5 - Fluorescent imaging of viable ADSCs (green colour) on Am silk scaffolds 6 weeks after seeding, in Expt 1. **A + B** – Osteogenic control; **C + D** – pre-treated with 30 µM MI192. Scale bars = 100µM.

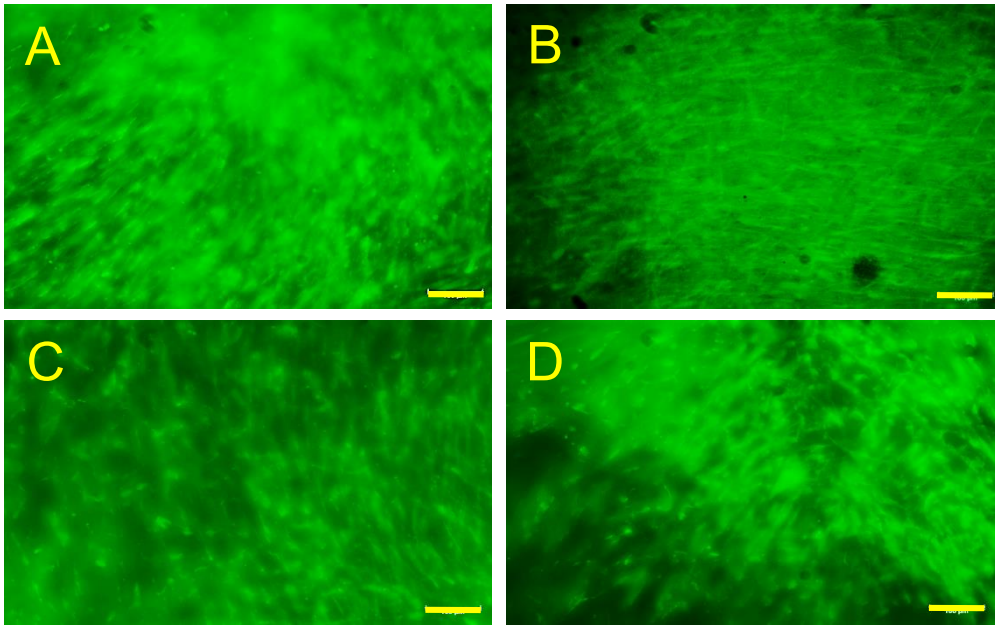

Figure 6.6 - Fluorescent imaging of viable ADSCs (green colour) on Am silk scaffolds 9 weeks after seeding, in Expt 1. **A + B** – Osteogenic control; **C + D** – pre-treated with 30 µM MI192. Scale bars = 100 µM

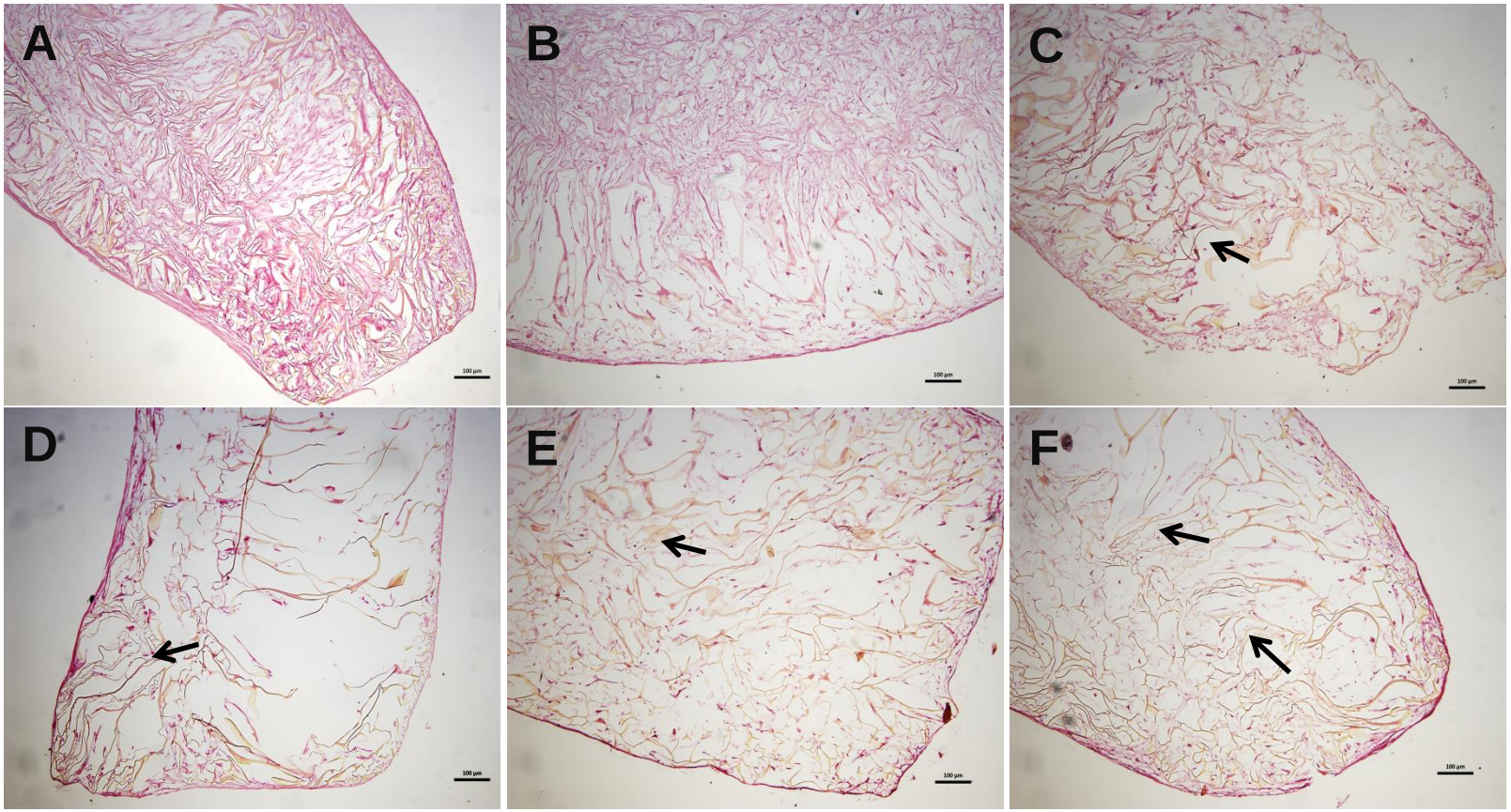

Figure 6.7 – Van Gieson's Stain of sections from ADSC-silk scaffold constructs after 9 weeks of *in vitro* culture (Exp1). A – C – Osteogenic control; **D – F** – Constructs treated with 30 µM MI192. Silk scaffold stained a yellow colour and the tissues were stained a pink colour. Arrows indicate the scaffold architecture. Scale bars = 100 µM.

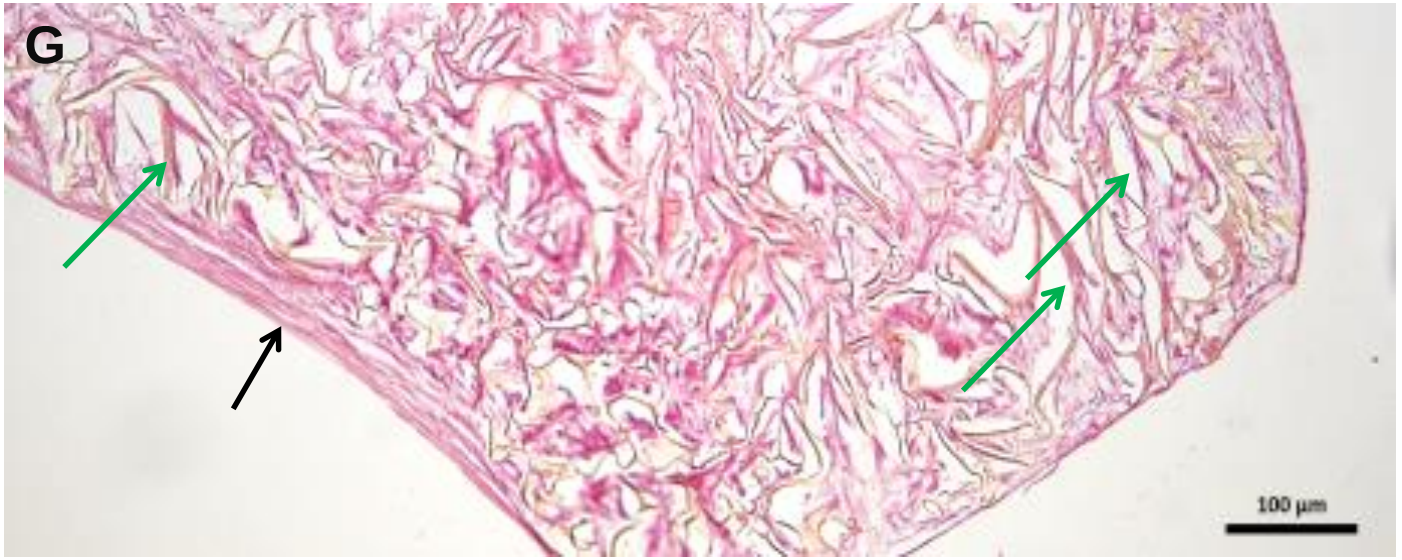

Figure 6.7 G – High magnification image of Figure 6.7 A. The black arrow indicates where layers of cells have formed on the outside of the scaffold. The green arrows show the cell structures growing along the architecture of the scaffold.

6.3.3 The effect of MI192 treatment on ADSCs, which underwent osteogenic induction prior to seeding on 3D silk scaffolds (Expt 2)

After being pre-treated with MI192 (10 µM and 30 µM) for two days, followed by culture in osteogenic medium for 7 days, ADSCs (2.5×10^5 cells per scaffold, 2.5 x higher than Expt 1) were seeded onto the Am scaffolds, followed by osteogenic induction for 6 weeks.

6.3.3.1 Assessment of cell viability and growth

24 hours after seeding live cell imaging of two scaffolds from each group labelled with with CFMDA showed that viable cells had attached to the silk scaffolds in all groups (Figure 6.8). In some scaffolds (Figure 6.8 A, B and E) the cell morphology was rounded, with very few cell processes. Other scaffolds had more expected cell morphology, with cell processes visible (Figure 6.8 C, D and F). This rounded morphology was different to what had been observed in previous experiments (e.g. Figure 6.5). These abnormal morphology cells were apparent in scaffolds across all treatment groups. Overall, the cell density was comparable to, or better than, the cell density after six weeks of culture in Expt 1 (Figure 6.5). The increased seeding density had the desired effect.

After 6 weeks of culture two scaffolds from each group (the same scaffolds as at 24 hours) were labelled for live cells again, to check if the tissue growth was sufficient to end the experiment (Figure 6.9). Viable cells were visible on all scaffolds from all groups labelled. In some scaffolds (Figure 6.9 C and F) the cell density had increased from the 24 hour time point, and there were large areas of confluent cells. However, other scaffolds had a lower cell density, (Figure 6.9 A, B D, E and F). In these lower density scaffolds, the cells had a rounded morphology. This cell density and the rounded morphology was the same as at the 24 hour time point (Figure 6.8).

6.3.3.2 Histological Analysis

There were four scaffolds for each group processed for histology; however, consistent staining could not be observed in two scaffolds of each group. These corresponded to the scaffolds where abnormal cell morphology was observed in the live cell labelling experiments. In these samples, in sections from throughout the whole paraffin block and therefore scaffold, only minimal staining could be observed. Prior to staining, the scaffold could be seen attached to the slide, but as with the negative control scaffolds there was very little staining observed. What could be seen were rounded dots, which was abnormal compared to other samples. Examples of such staining can be seen in Figure 6.10 (Van Gieson's stain, A + B). No collagen fibres could be seen when these were stained with Picrosirius red (Figure 6.10 C) and when stained with a Von Kossa stain (Figure 6.10 D) for mineralisation these dots appeared dark; however, they were not black as in the scaffolds with good cell formation (Figure 6.13), so this is probably not mineralisation.

Those samples which could be stained yielded inconclusive results, and a low sample number means that conclusions could not be drawn. The tissue penetration was good in all scaffolds where staining could be achieved, with strong Van Gieson's staining throughout the scaffolds, in both the osteogenic controls (Figure 6.11 A + B) and the groups with cells pre-treated with MI192 (10 µM - Figure 6.11 C + D and 30 µM - Figure 6.11 E + F).

Picrosirius red staining for collagen indicated strong staining for some samples (Figure 6.12 B, D + F); however, this varied across the groups and the other samples had much weaker staining. Results were inconsistent for this stain.

Mineralisation close to the surface could be observed in all samples (Figure 6.13). The mineralisation was marginally higher in the two pre-treated groups (10 µM - Figure 6.13 C + D and 30 µM - Figure 6.13 E + F), compared to the osteogenic controls (Figure 6.13 A + B) indicating that MI192 pre-treatment had improved the mineralisation capacity of the ADSCs. The mineralisation in the treated samples seemed to occur in large zones, and was less spread around the same than the osteogenic control.

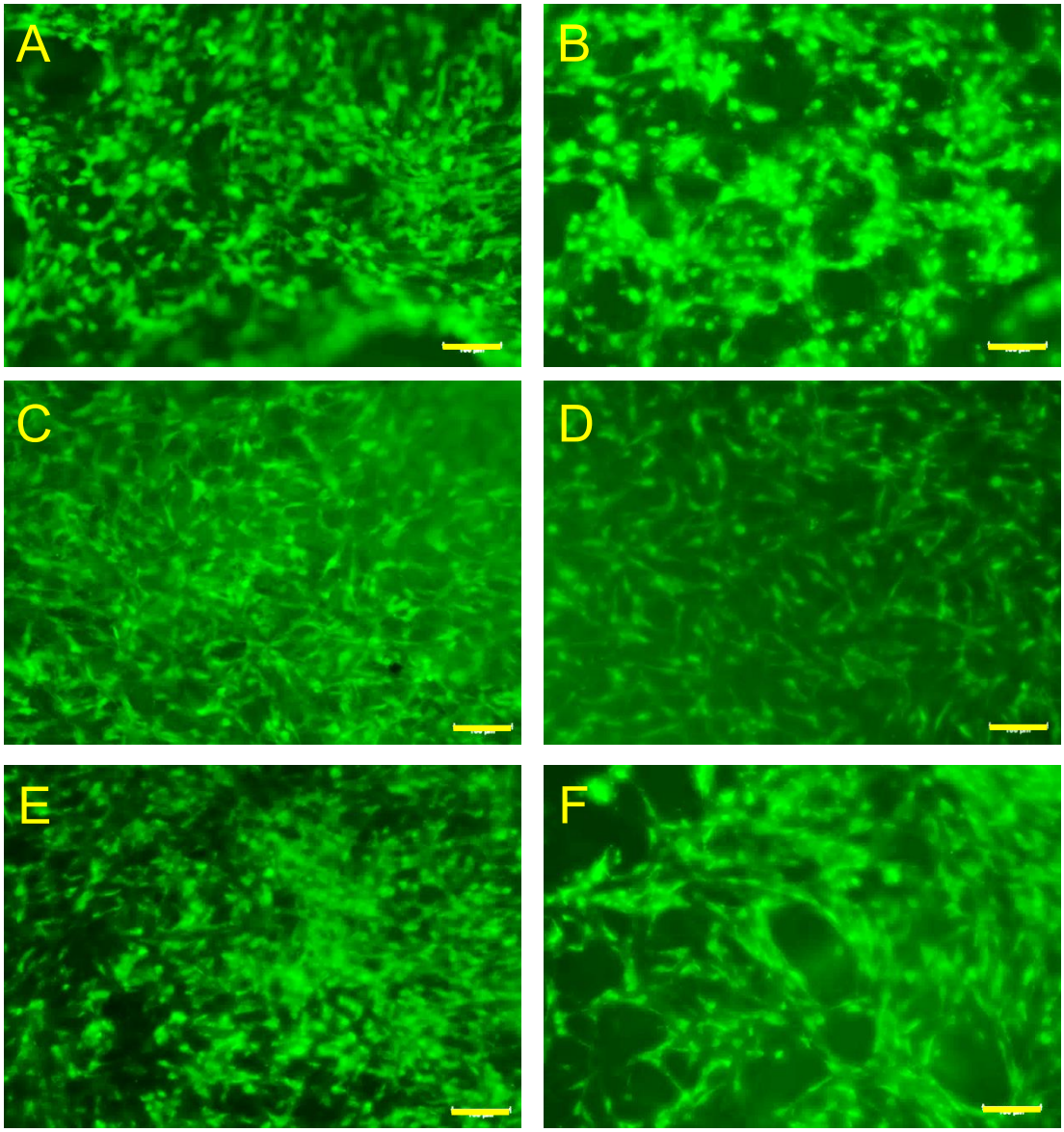

Figure 6.8 - Fluorescent imaging of viable ADSCs (green colour) on Am silk scaffolds 24 hours after seeding, in Expt 2. A + B – osteogenic control; **C + D** – ADSCs pre-treated with 10 µM MI192; **E + F** – ADSCs pre-treated with 30 µM MI192. Scale bars = 100 µM.

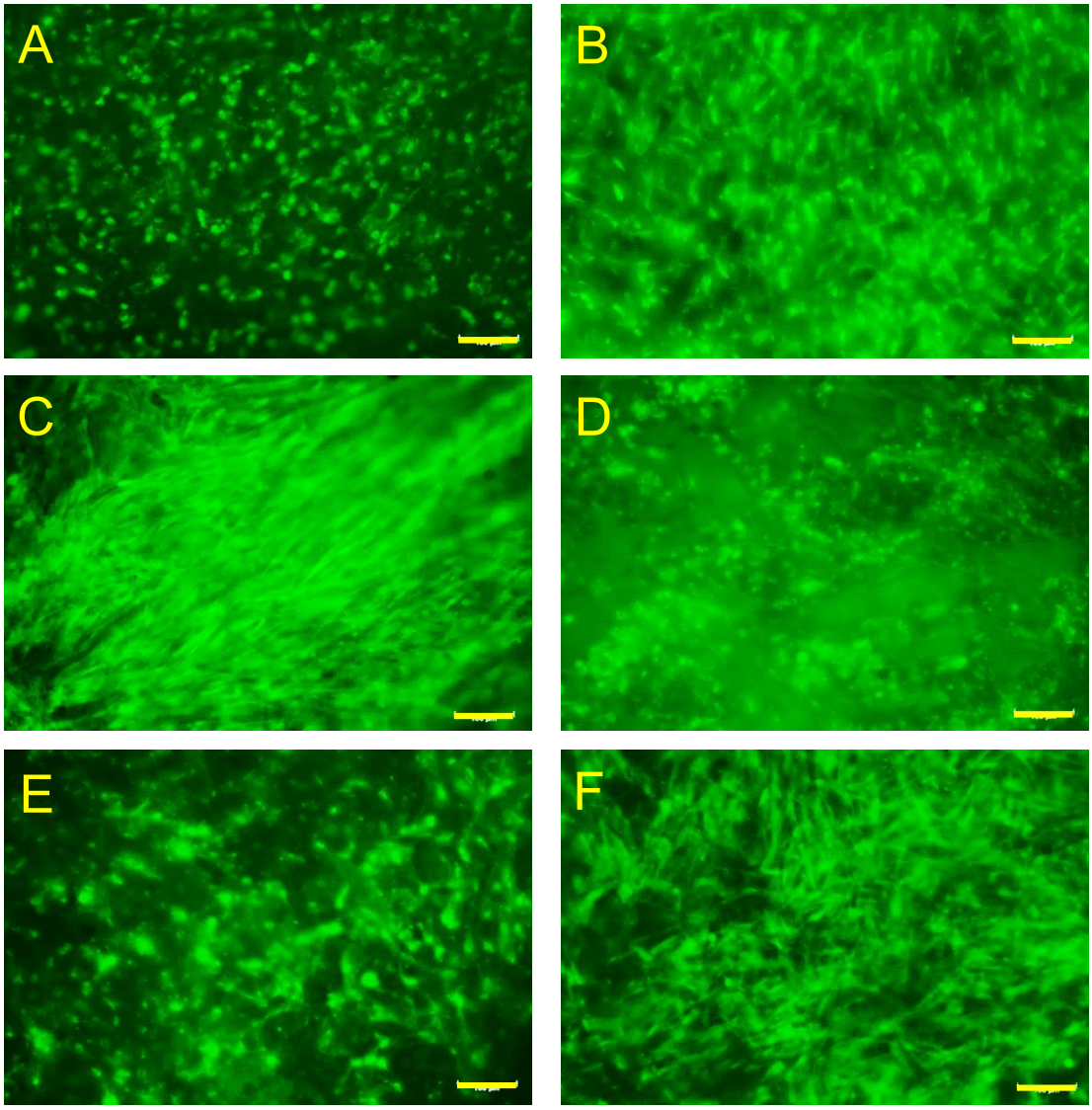

Figure 6.9 - Fluorescent imaging of viable ADSCs (green colour) on Am silk scaffolds 6 weeks after seeding, in Expt 2. A + B – osteogenic control; **C + D** – ADSCs pre-treated with 10 µM MI192; **E + F** – ADSCs pre-treated with 30 µM MI192. Scale bars = 100 µM.

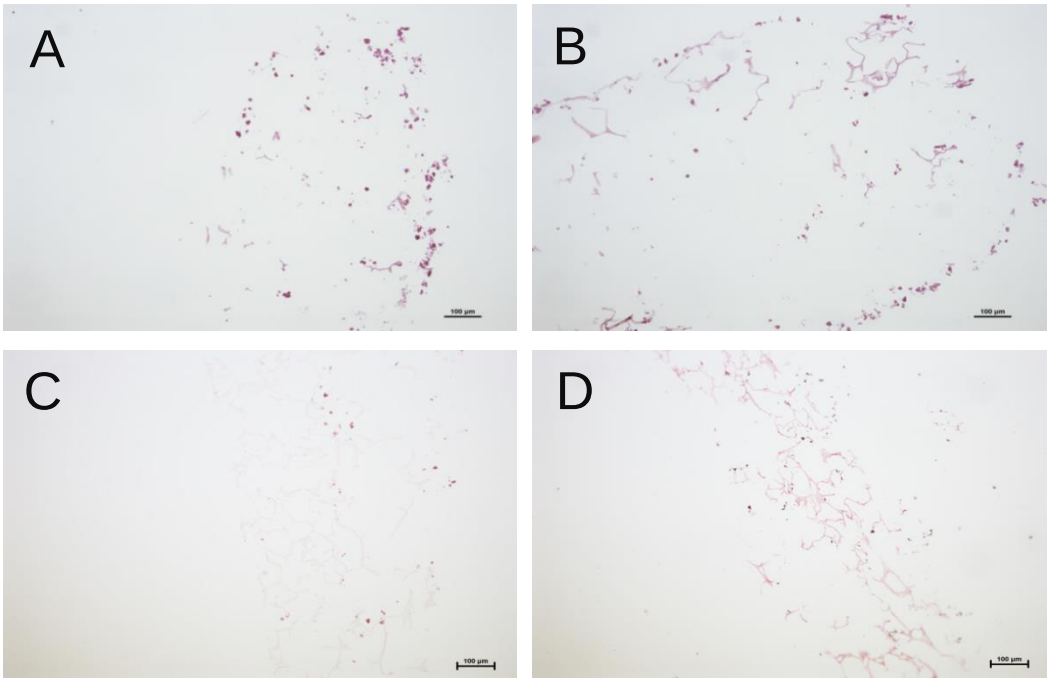

Figure 6.10 - Van Gieson's, Picrosirius red and Von Kossa stain of sections from ADSC-silk scaffold constructs after 6 weeks of *in vitro* culture (Expt 2). Example stains of samples where there was poor tissue formation, where cells and scaffold were not visible. **A** – Van Gieson's stain of osteogenic control; **B** – Van Gieson's stain of ADSCs pre-treated with 10 µM MI192; **C** – Picrosirius red stain Osteogenic control, A; **D** – Von Kossa stain of osteogenic control. Scale bars = 100 µM.

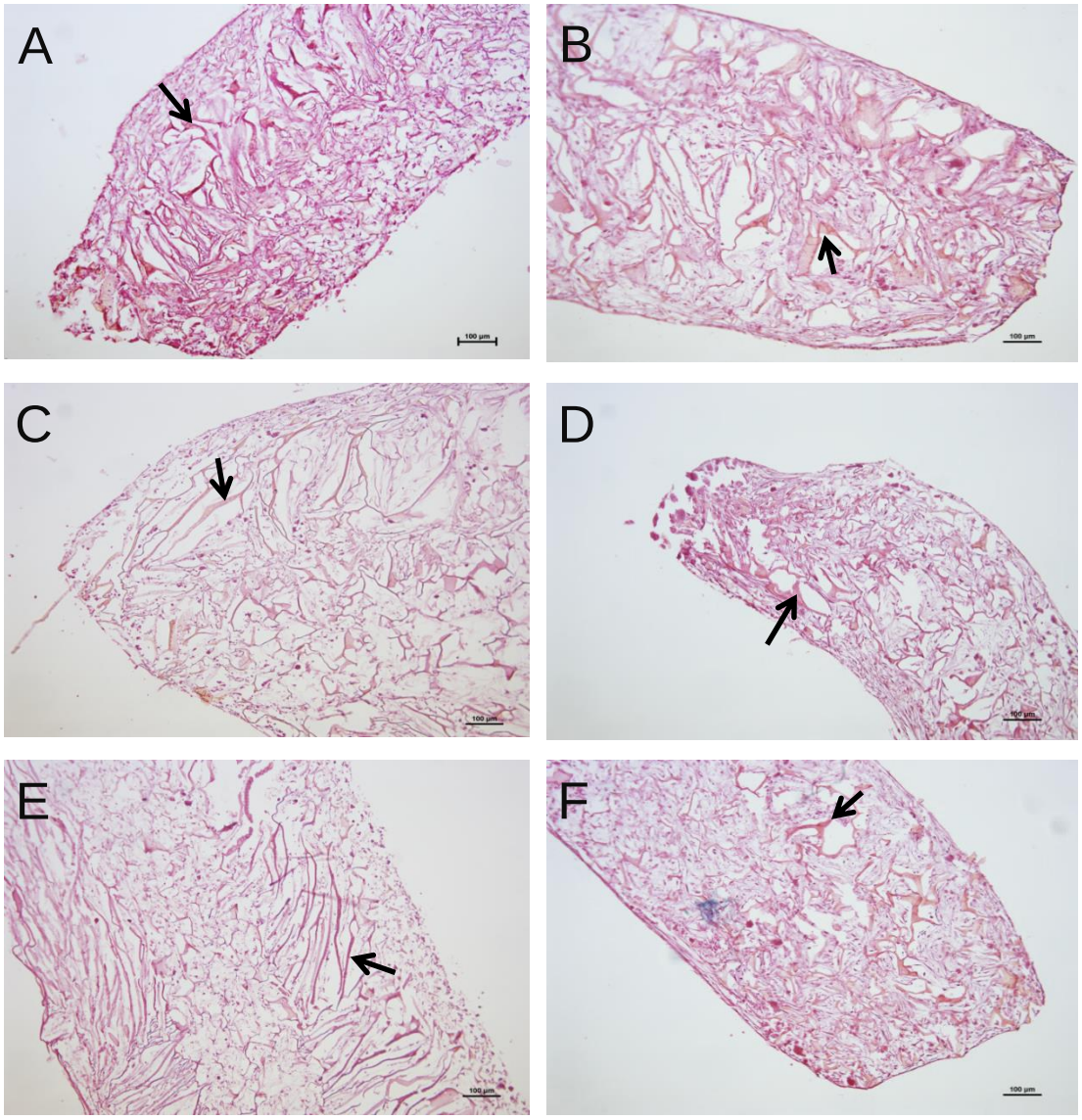

Figure 6.11 - Van Gieson's stain of sections from ADSC-silk scaffold constructs after 6 weeks of *in vitro* culture (Expt 2). A + B – Osteogenic control; **C + D** – ADSCs pre-treated with 10 µM MI192; **E + F** – ADSCs pre-treated with 30 µM MI192. Silk scaffold stained a yellow/pink colour and the tissues were stained a darker pink colour. Arrows indicate the scaffold architecture. Scale bars = 100 µM.

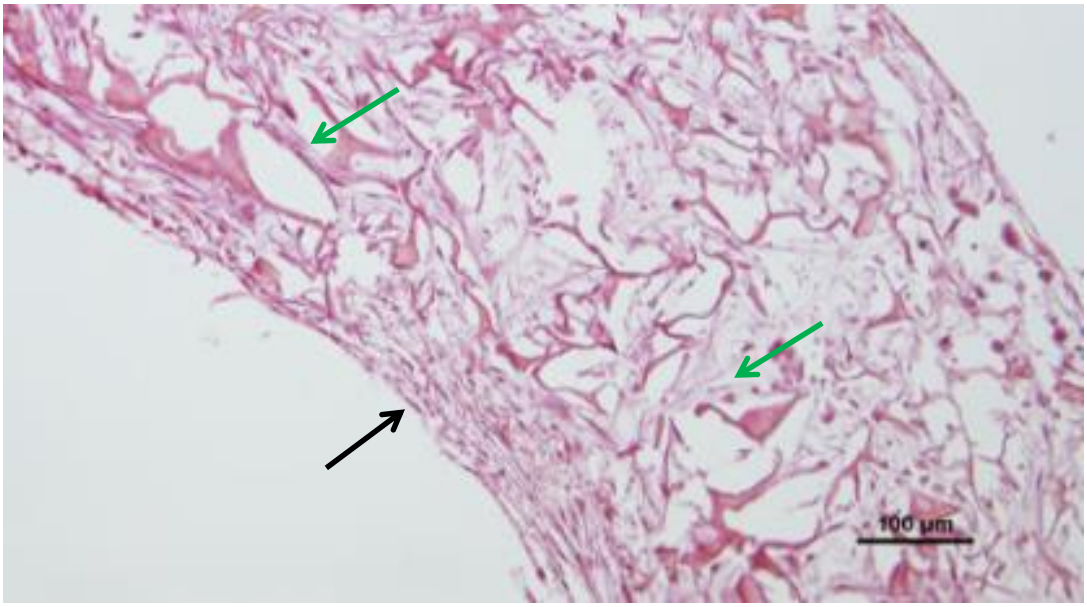

Figure 6.11 G – High magnification image of Figure 6.11 D. The black arrow indicates where layers of cells have formed on the outside of the scaffold. The green arrows show the cell structures growing along the architecture of the scaffold.

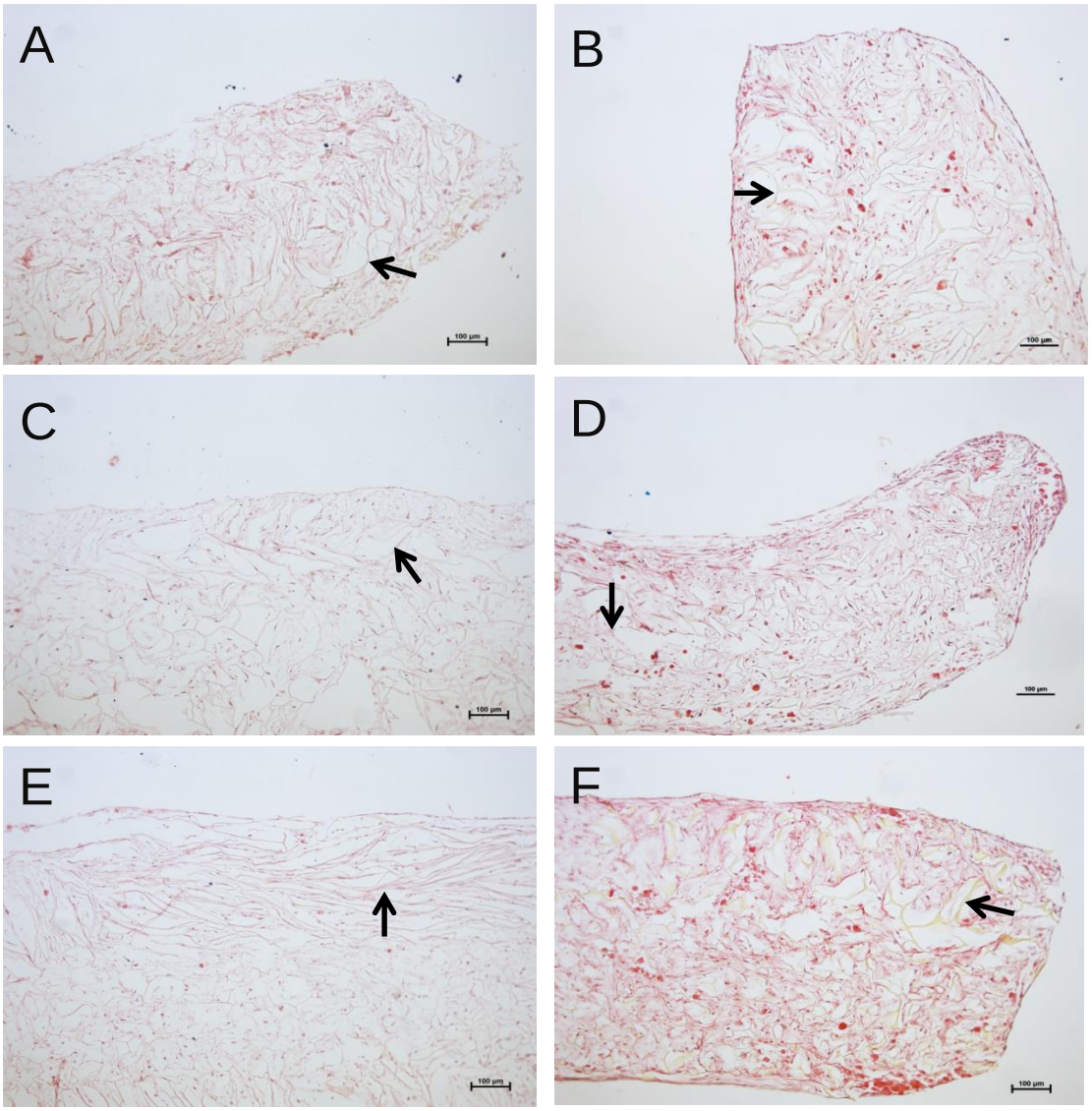

Figure 6.12 – Picrosirius red stain, with Weigert's haematoxylin nuclei counterstain, of sections from ADSC-silk scaffold constructs after 6 weeks of *in vitro* culture (Expt 2). A + B – Osteogenic control; **C + D** – ADSCs pre-treated with 10 µM MI192; **E + F** – ADSCs pre-treated with 30 µM MI192. Silk scaffold stained a yellow/grey colour, the tissues were stained red if collagen was present and the nuclei were stained black. Arrows indicate the scaffold architecture. Scale bars = 100 µM.

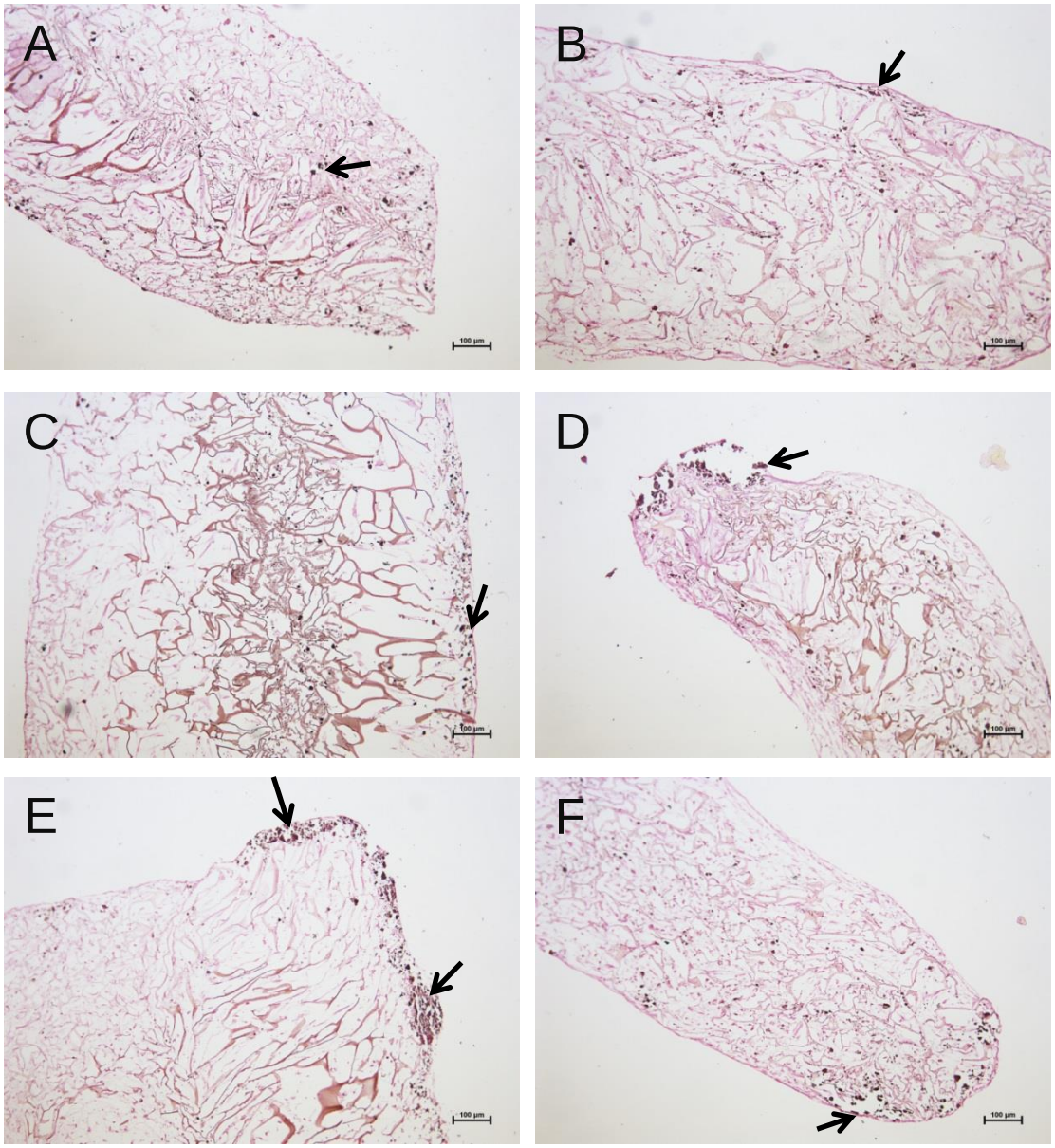

Figure 6.13 – Von Kossa staining, with a weak Van Gieson's counter stain for tissue, of sections from ADSC-silk scaffold constructs after 6 weeks of *in vitro* culture (Expt 2). A + B – Osteogenic control; **C + D** – ADSCs pre-treated with 10 µM MI192; **E + F** – ADSCs pre-treated with 30 µM MI192. Mineral nodules stained black/dark brown, silk scaffold stained a pink/brown colour and the cell tissue stained pink. Arrows indicate strong areas of mineralisation in each scaffold. Scale bars = 100 µM.

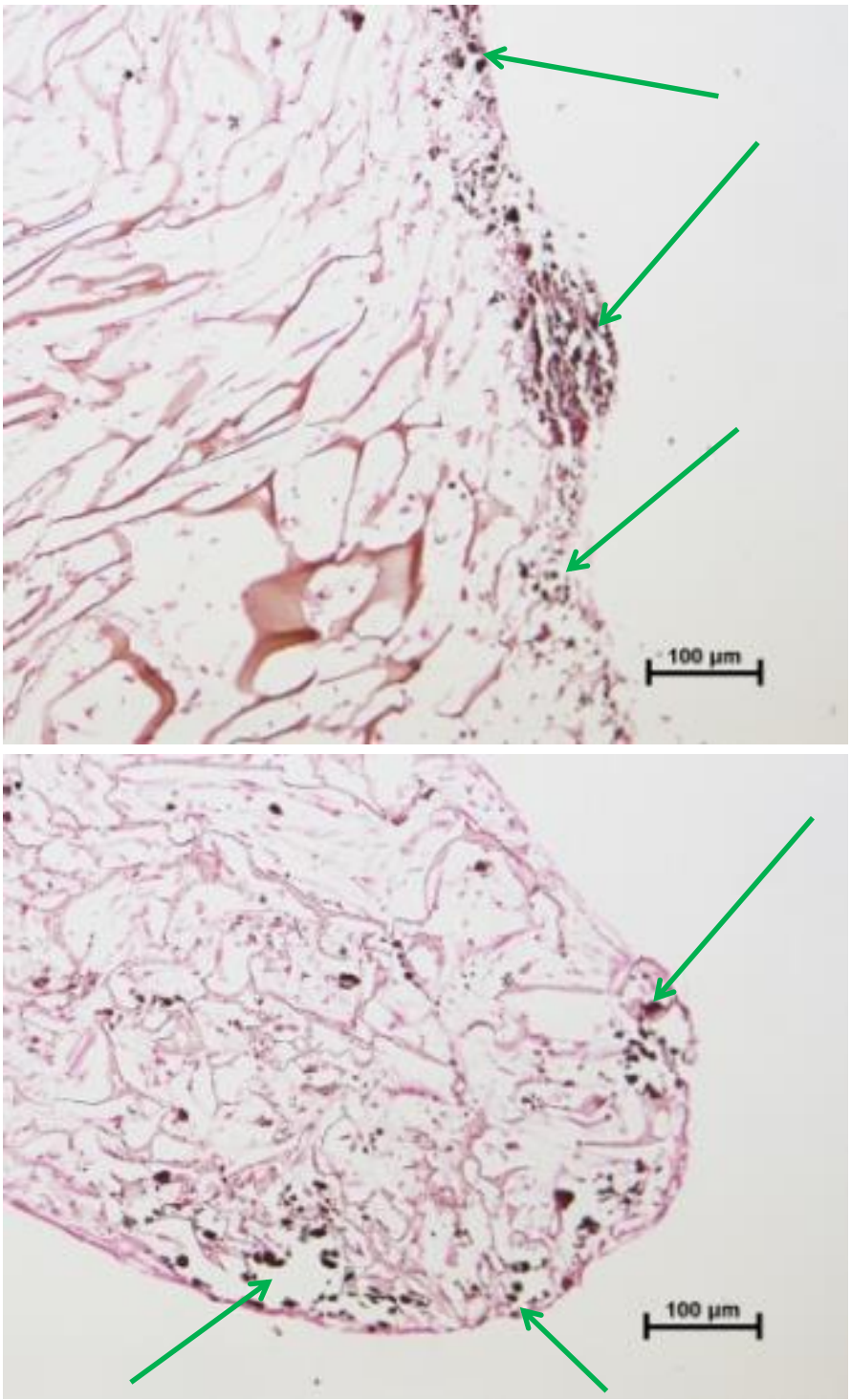

Figure 6.13 G + H – High magnification image of Figure 6.12 E and F, respectively. The green arrows indicate some of the mineralisation.

6.3.4 The effect of MI192 treatment on ADSCs treated with MI192 prior to seeding on 3D silk scaffolds and osteogenic induction (Expt 3)

After being pre-treated with MI192 (10 µM and 30 µM) for two days, ADSCs (2.5 × 10^5 cells per scaffold) were seeded onto the Am scaffolds, followed by osteogenic induction for 6 weeks.

6.3.4.1 Assessment of cell viability and growth

24 hours after seeding, imaging of live cells on two scaffolds from each group showed that viable cells had attached to the surface of the scaffolds in all groups (Figure 6.14). Cells in all groups had a normal morphology, with processes visible, indicating cell attachment and spreading. Cell density was similar across all labelled scaffolds. The density was comparable to, or better than the cell density after 24 hours in experimental design 2 (Figure 6.8). None of the abnormal rounded cell morphology from Expt 2 was observed (Figure 6.10).

After 6 weeks of culture, imaging of live cells on two scaffolds from each group (the same scaffolds as at 24 hours) was undertaken, to check if the tissue growth was sufficient to end the experiment (Figure 6.15). Viable cells were visible on all scaffolds from all groups labelled, with all scaffolds showing large areas of confluent cells. The cell density was comparable across all scaffolds. The morphology of the negative control ADSCs cultured in the basal MesenPRO RS™ growth medium (Figure 6.15 A + B) were more elongated and the cells were more aligned, compared to the cells cultured in the osteogenic mineralisation medium (Figure 6.15 C – H). The cell density had increased from the 24 hour time point.

6.3.4.2 SEM Analysis

One scaffold from each group, along with unseeded negative control scaffolds, was analysed using SEM (Figure 6.16).

The negative control scaffold, with no cells seeded, has a highly porous structure, with no evidence of cells (Figure 6.16 **-**). The cell seeded scaffolds had only minimal scaffold architecture visible (Figure 6.16 A - H), compared to the negative control with no cells, as the pores are covered by cells. Cell processes could be observed in the lower magnification images (Figure 6.16 B, D, F + H). Cell density was highest in the basal MesenPRO RS™ growth medium negative control (Figure 6.16 A + B), where no scaffold is visible through the layer of cells. The other groups all had comparable cell density to each other, with the scaffold visible in places.

The white deposition visible in the samples cultured in osteogenic medium (Figure 6.16 C - H) is mineralisation. This appears white because of the higher molecular weight of the metallic elements compared to the carbon, oxygen and hydrogen, which make up the majority of the organic constituents of the scaffolds. There is no white mineral deposition visible in the basal MesenPRO RS™ growth medium negative control (Figure 6.16 A + B), compared to the osteogenic medium positive control (Figure 6.16 C - H). The highest level of mineralisation can be seen in the 30 µM pre-treated ADSC sample (Figure 6.16 G). This visible mineralisation can be nodule like (Figure 6.16 F) or more spread out (Figure 6.16 H).

The fact this was mineralisation, and not something else such as crystals of the fixative or frozen water on the samples, was confirmed by EDS analysis. Analysis of the minerals present showed the areas that were not white to mainly be carbon (red in Figure 6.17) and the white nodules to be comprised of phosphorus and calcium (green and blue in Figure 6.17). The basal control samples cultured in the MesenPRO RS™ basal growth medium had almost no calcium or phosphorus present (Figure 6.17 B). The mineralisation can be seen on a lower magnification scale (Figure 6.17 C + D) or at a high magnification (Figure 6.17 E, F, G + H).

EDS can also produce quantitative analysis of the minerals present, taken from a low magnification to analyse this on a large area of the scaffold surface area. Histograms showing the elements present can be produced (Figure 6.18), clearly showing a calcium and a phosphorous peak present in the osteogenic control (Figure 6.18 B), and the MI192 pre-treated samples (Figure 6.18 C + D), but not in the MesenPRO RS™ basal growth medium sample (Figure 6.18 A). Quantification of this shows the

global levels of elements present (Table 6-2). The osteogenic control had the highest level of mineralisation, with a total calcium and phosphorus percentage of 20.93%, compared to only 1.09% for the negative, basal, control. The 10 µM pre-treated sample had a combined percentage of 16.93%, and the 30 µM pre-treated sample 19.22 %. This indicates that the overall mineralisation is higher for the osteogenic control than the MI192 pre-treated groups. However, the mineralisation in 30 µM MI192 pre-treatment is very close to that of the osteogenic control.

6.3.4.3 Histological Analysis

Van Gieson's histological staining showed the tissue penetration was high, and cells have penetrated completely every sample (Figure 6.19). The MesenPRO RS™ basal growth medium controls (Figure 6.19 A + B) had more layers of tissue formed around the outside of the scaffold, likely due to the increased proliferation capacity of cells in this medium. This has formed a thick, capsule like, layer of tissue. Cell density is lower at the surface of the other samples (Figure 6.19 C - L). The cell penetration was comparable across all groups. Cell density is similar in all scaffolds in the centre, which indicates that despite increased proliferative capacity of cells in the basal control, there is a maximum cell density in the scaffolds, which is still reached in the slower growing cell groups.

Picrosirius red staining shows that collagen had formed in all samples, although the amount varies between groups (Figure 6.20). The capsule observable in the MesenPRO RS™ basal growth medium controls stains strongly red, indicating a high level of collagen is present. There is very little staining on the cells on the inside of the scaffold (Figure 6.20 A + B). The osteogenic control scaffolds have a several cell deep layer of staining close to the surface, showing the more mature cells located at the surface of the scaffold have laid down more collagen than the potentially less mature cells in the centre of the scaffold (Figure 6.20 C + D). The Picrosirius red staining is higher in the cells pre-treated with 10 µM of MI192 (Figure 6.20 E - H) than the osteogenic controls (Figure 6.20 C + D). The Picrosirius red staining can be observed strongly throughout the whole scaffold, especially in samples E and G. Staining is weaker in the samples with cells pre-treated with 30 µM of MI192 (Figure 6.20 I – L) than the samples with cells pre-treated with 10 µM of MI192, but is comparable to the osteogenic medium controls (Figure 6.20 C + D). The samples

with cells pre-treated with 30 µM of MI192 (Figure 6.20 I – L) also have a strongly stained, thin capsule of cells at the surface.

The Von Kossa's staining for mineralisation showed no staining and thus no mineralisation of the MesenPRO RS™ basal growth medium control sections (Figure 6.21 A + B), compared the other samples that were cultured in osteogenic mineralisation medium (Figure 6.21 C - L). Von Kossa's staining was observed in the osteogenic mineralisation medium controls (Figure 6.21 C + D), showing that the osteogenic mineralisation medium induced mineralisation and the MesenPRO RS™ basal growth medium did not. The Von Kossa's staining was stronger in both of the sample groups with cells pre-treated with MI192 (10 µM of MI192: Figure 6.21 E – H and 30 µM of MI192: Figure 6.21 I – L) than the osteogenic controls (Figure 6.21 C + D). The staining was comparable between the two groups of MI192 pre-treated cell scaffolds. In all groups cultured in osteogenic mineralisation medium, the mineralisation staining was found to be stronger closer to the surface of the constructs, where cells were more mature.

6.3.5 Immunohistochemical staining

Due to the high magnification needed to see staining with the Runx2 and Ocn staining, only one representative image is shown. For the collagen 1 staining, a high and a low magnification image from two different scaffolds are sown.

6.3.5.1 Runx2

Runx2 is a transcription factor, so should primarily only be seen in the nuclei of cells. Much optimisation was necessary to remove non-nuclear background staining. No Runx2 staining can be observed in the MesenPRO RS™ basal growth medium controls. Staining can be observed in the osteogenic control and both MI192 treated groups. Staining was largely the same in all three groups. Staining was located throughout the cells in the scaffold.

6.3.5.2 Col1

Col1 staining mimicked that seen with the Picrosirius red staining for the osteogenic control and the MI192 treated cells. There was a low level of staining seen in the MesenPRO RS™ basal growth medium controls, despite the Picrosirius red staining, perhaps indicating the collagen formed when cells form a capsule like this is another type of collagen (likely type 2). Col1 staining was stronger in the two MI192 treated groups than the osteogenic controls, with the strongest staining visible in the 10 µM group. Staining was located most strongly at the cells on the surface of the scaffolds.

6.3.5.3 Ocn

No Ocn staining can be observed in the MesenPRO RS™ basal growth medium controls. Staining can be observed in the osteogenic control and both MI192 treated groups. Staining was largely the same in all three groups, although there was slightly stronger staining in the 30 µM MI192 group. Staining was located most strongly at the cells on the surface of the scaffolds.

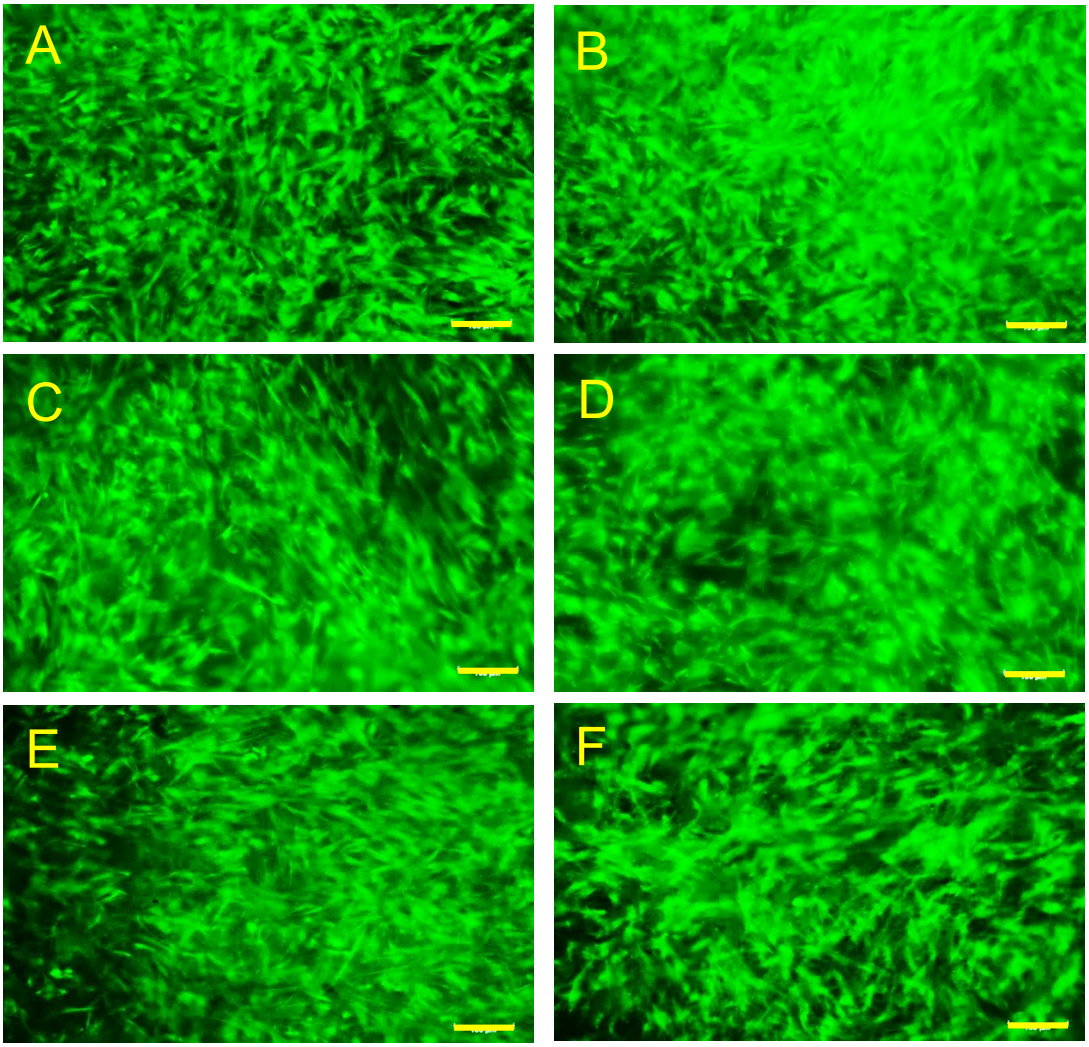

Figure 6.14 – Fluorescent imaging of viable ADSCs (green colour) on Am silk scaffolds 24 hours after seeding, in Exp3. A + B – Untreated ADSCs, seeded onto the scaffolds; **C + D** – ADSCs pre-treated with 10 µM MI192; **E + F** – ADSCs pre-treated with 30 µM MI192. Scale bars = 100 µM.

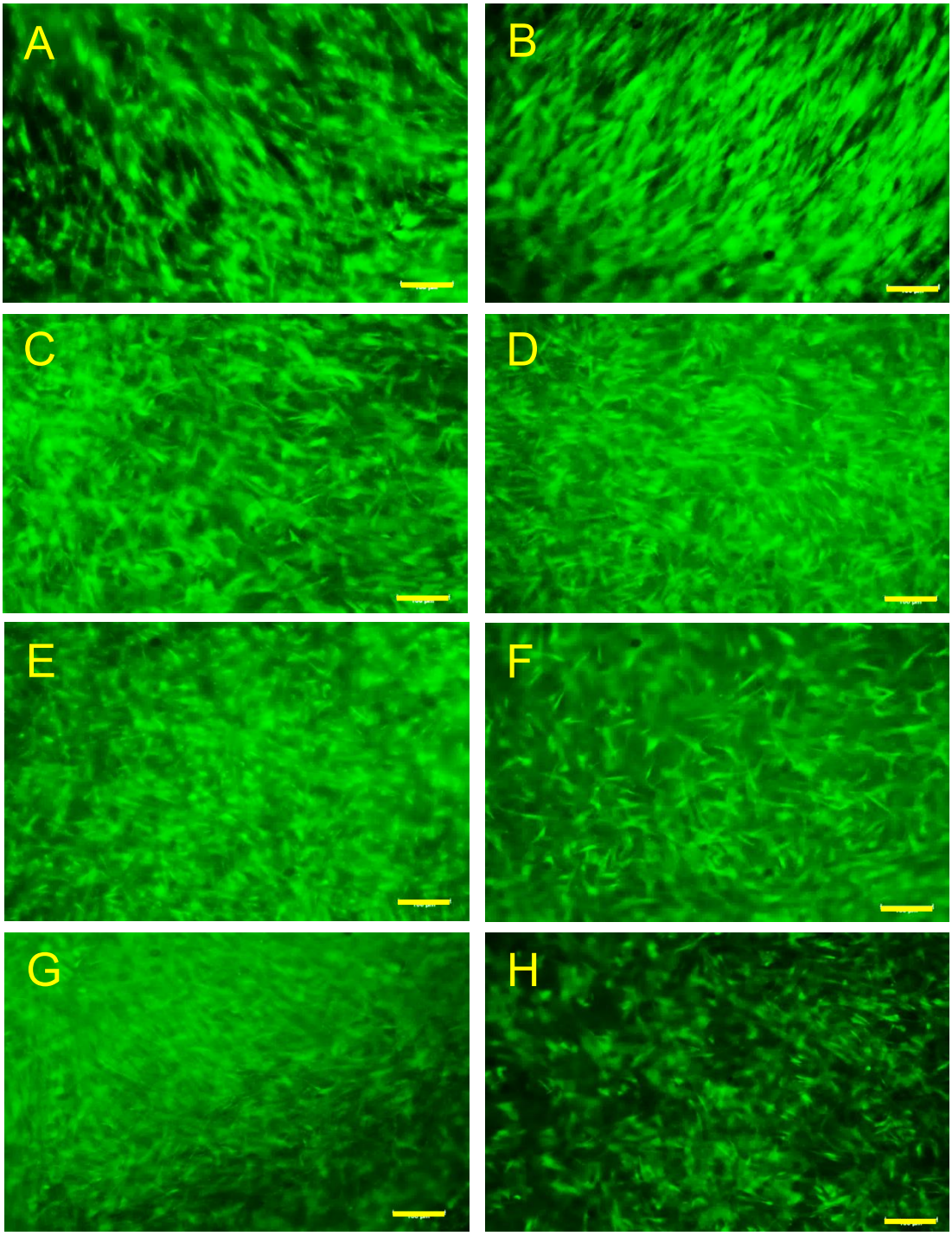

Figure 6.15 – Fluorescent imaging of viable ADSCs (green colour) on Am silk scaffolds 6 weeks after seeding, in Exp3. A + B – basal medium control; **C + D** – osteogenic control; **E + F** – ADSCs pre-treated with 10 µM MI192; G + H – ADSCs pre-treated with 30 µM. Scale bars = 100 µM.

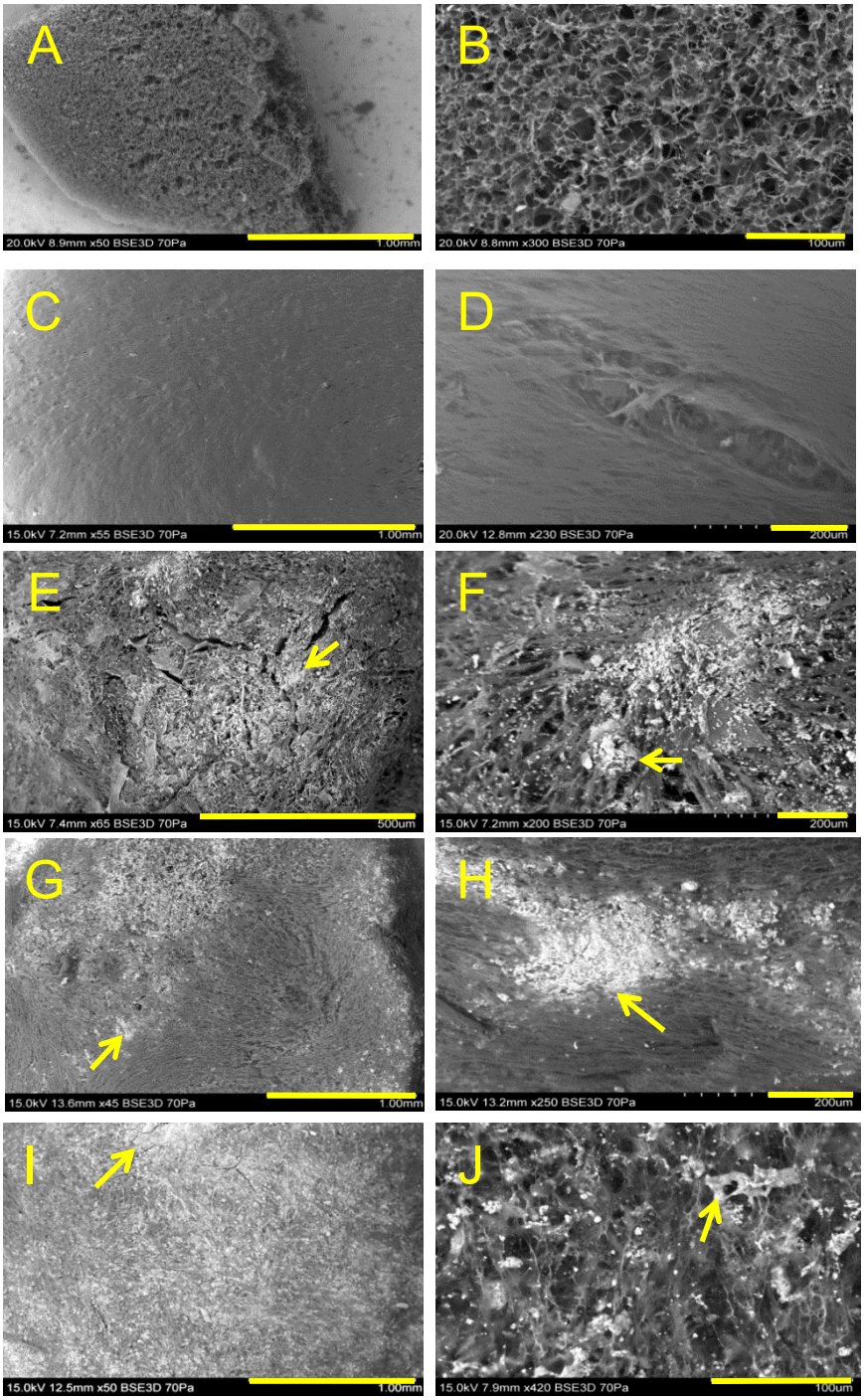

Figure 6.16 - SEM images of ADSCs on Am silk scaffolds 6 weeks after seeding, in Exp3. Low magnification images (scale bars = 1 mm) on the left, high magnification images (scale bars = 100 µm) on the right. **A + B** – Unseeded control scaffolds; **C + D** – basal control; **E + F** – osteogenic control; **G + H** – ADSCs pre-treated with 30 µM MI192; **I + J** – ADSCs pre-treated with 10 µM MI192. Arrows indicate some of the mineralisation. Magnification and scale indicated on the image.

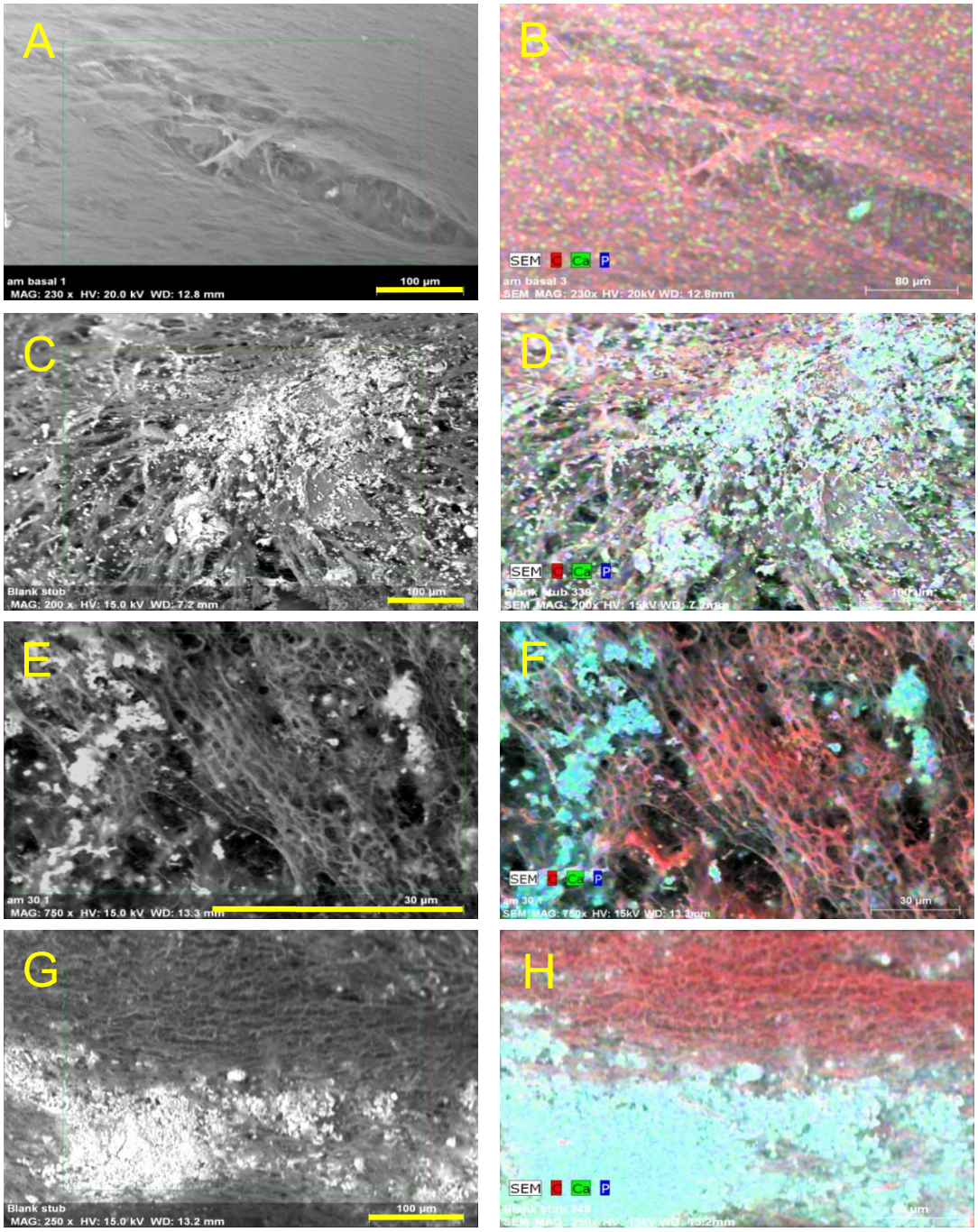

Figure 6.17 - SEM images, with environmental EDS SEM images, of ADSCs on Am silk scaffolds 6 weeks after seeding, Exp3. In EDS images: Red = carbon, green = calcium and blue = phosphorus. **A + B** – basal control; **C + D** – osteogenic control; **E + F** – ADSCs pre-treated with 10 µM MI192; **G + H** – ADSCs pre-treated with 30 µM MI192. Magnification and scale indicated on the image. Magnification bars on left hand imagines = 100 µm, scale of right hand images is the same.

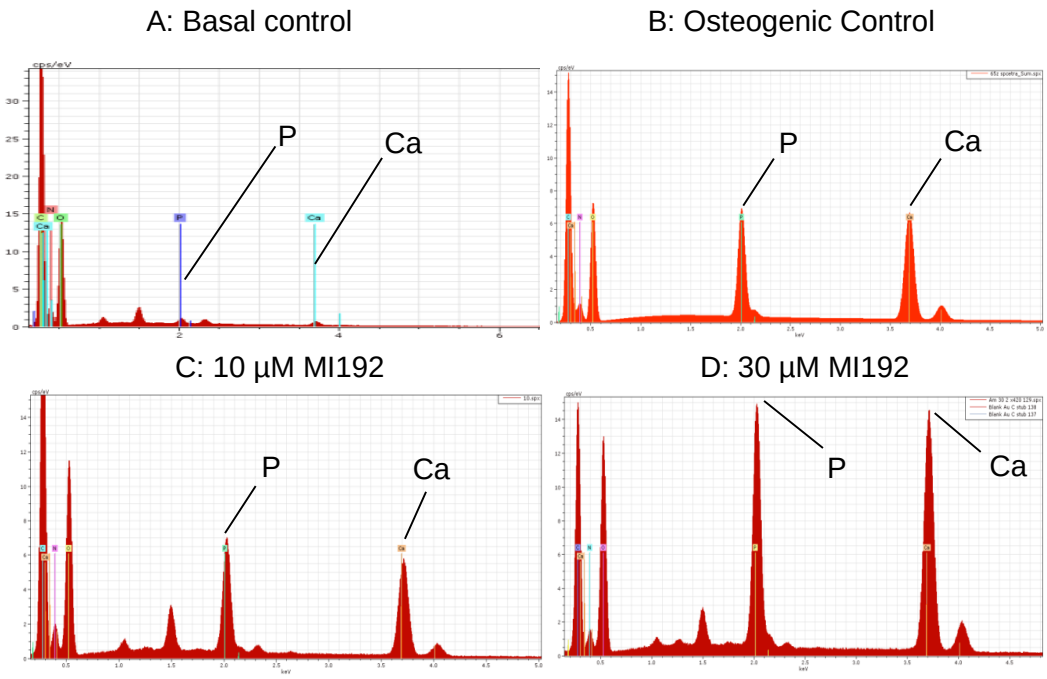

Figure 6.18 – Histograms showing elemental mapping of the elements present in the experimental Design 3 scaffolds. Maps taken at a low magnification to give indication of overall mineralisation levels. Labelled peaks show the Phosphorous and Calcium peaks.

Table 6-2 - Element analysis of Design 3 scaffolds using EDS (% w.t.)

	Carbon %	Nitrogen %	Oxygen %	Phosphorus %	Calcium %	Calcium : phosphorus ratio
Basal control	47.79	13.45	37.67	0.41	0.68	1.66
Osteogenic control	38.13	9.71	31.82	6.42	14.51	2.26
10 µM MI192	37.8	10.08	36.99	4.83	12.1	2.5
30 µM MI192	26.68	8.31	37.29	9.06	10.16	1.12

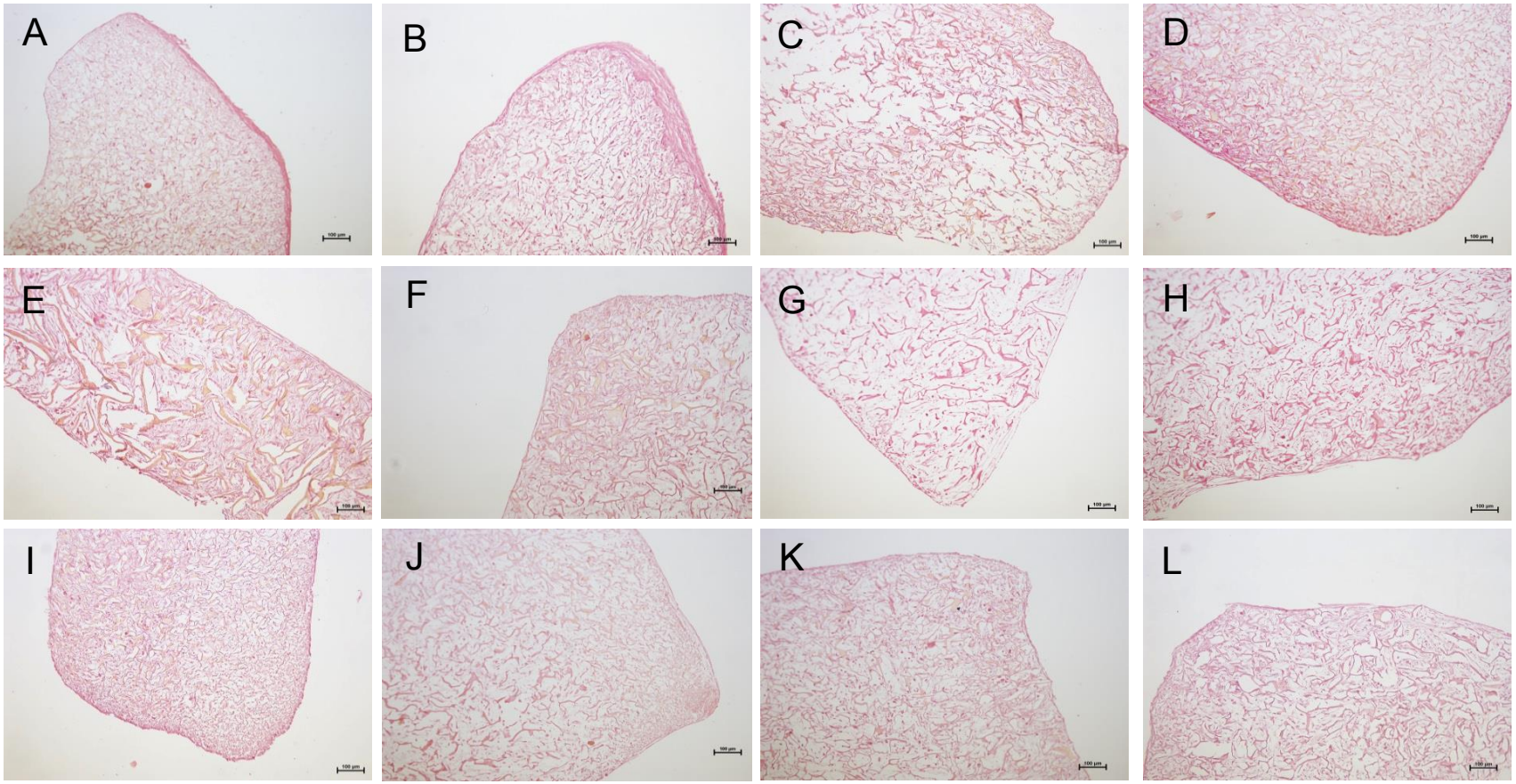

Figure 6.19 – Van Gieson's stain of sections from ADSC-silk scaffold constructs after 6 weeks of *in vitro* culture (Exp3). A + B – basal control; **C + D** – osteogenic control; **E - H** – ADSCs pre-treated with 10 µM MI192; **I - L** – ADSCs pre-treated with 30 µM MI192. Silk scaffold stained a yellow/pink colour and the tissues were stained a darker pink colour. Scale bars = 100 µM.

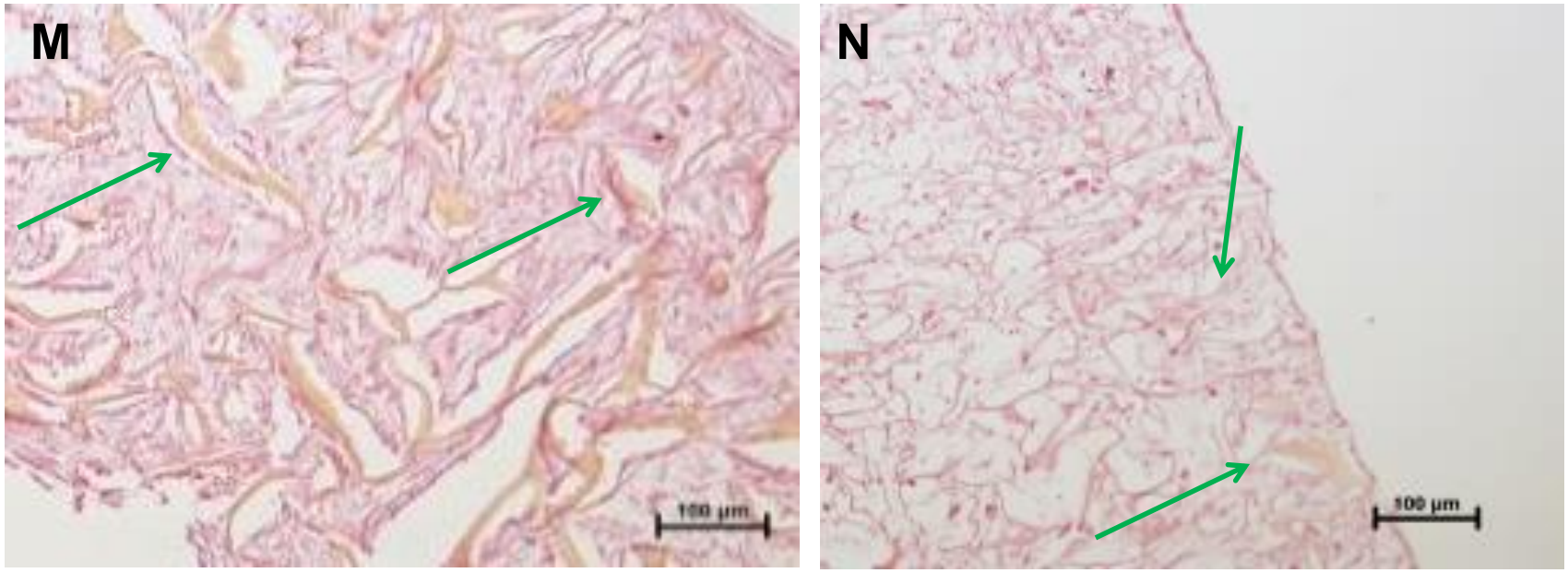

Figure 6.19 M + N – High magnification image of Figure 6.19 E and K, respectively. The green arrows indicate the cells growing along the scaffold.

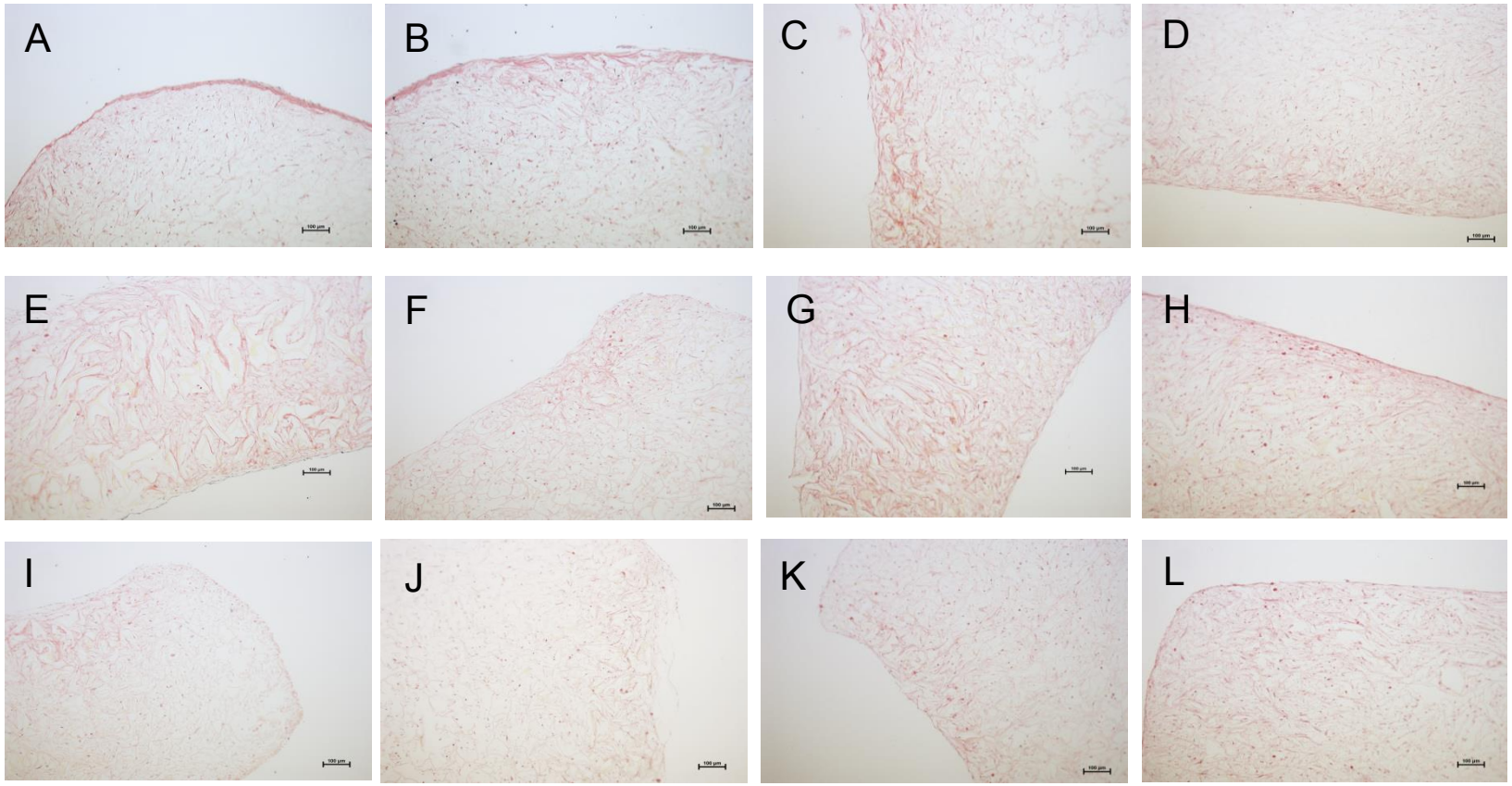

Figure 6.20 – Picrosirius Red stain, with Weigert's haematoxylin nuclei stain, of sections from ADSC-silk scaffold constructs after 6 weeks of *in vitro* culture (Exp3). All samples labelling (**A – L**) same as Figure 6.19. Silk scaffold stained a yellow/grey colour, the tissues were stained red if collagen was present, with the nuclei counterstained black. Scale bars = 100 µM.

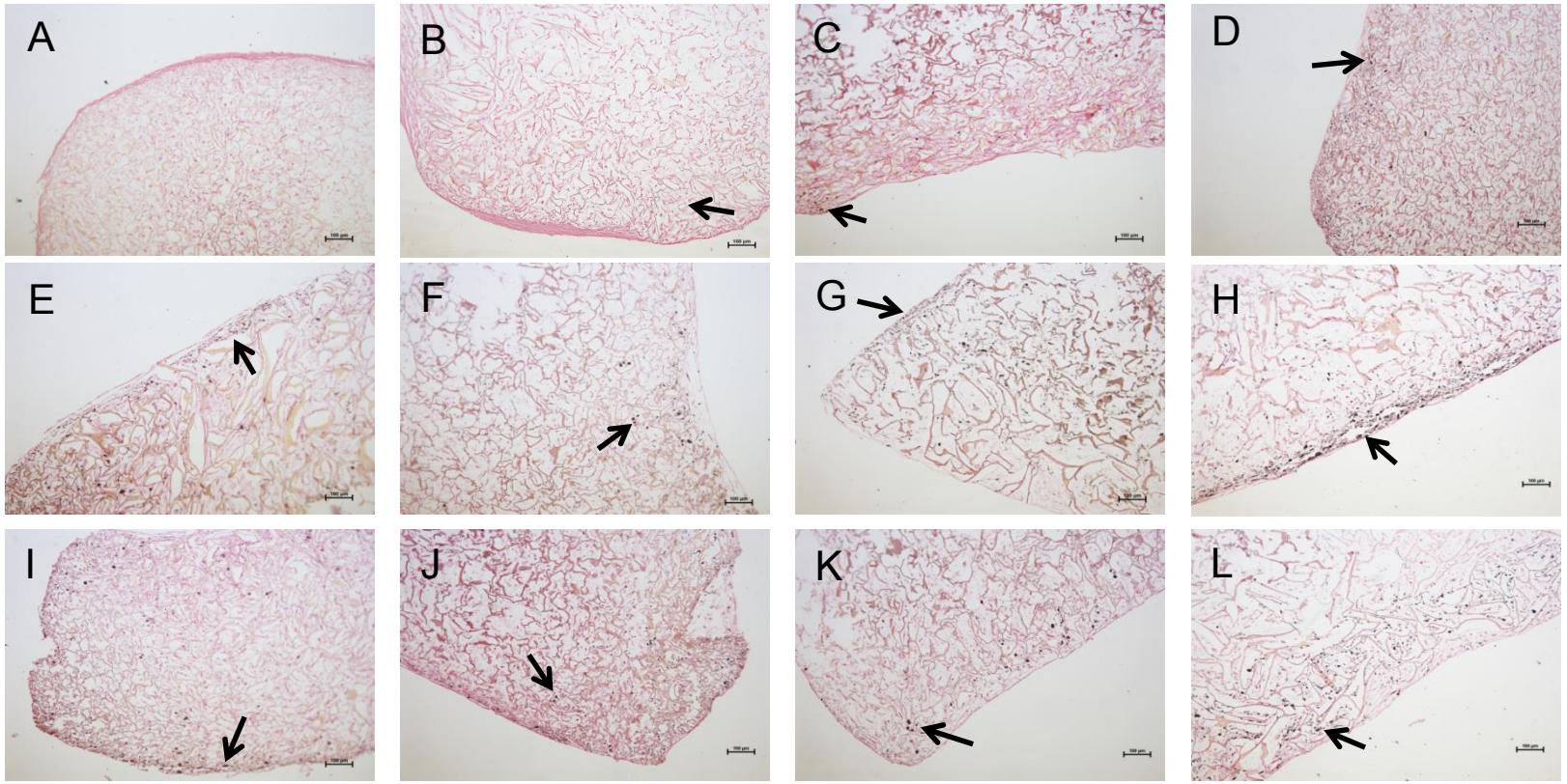

Figure 6.21 – Von Kossa staining, with a weak Van Gieson's counter stain for tissue, of sections from ADSC-silk scaffold constructs after 6 weeks of *in vitro* culture (Exp3). All samples labelling (**A – L**) same as Figure 6.19. Mineral nodules stained black/dark brown, silk scaffold stained a pink/brown colour and the cell tissue stained pink. Arrows indicate some strong areas of mineralisation in each scaffold. Scale bars = 100 µM.

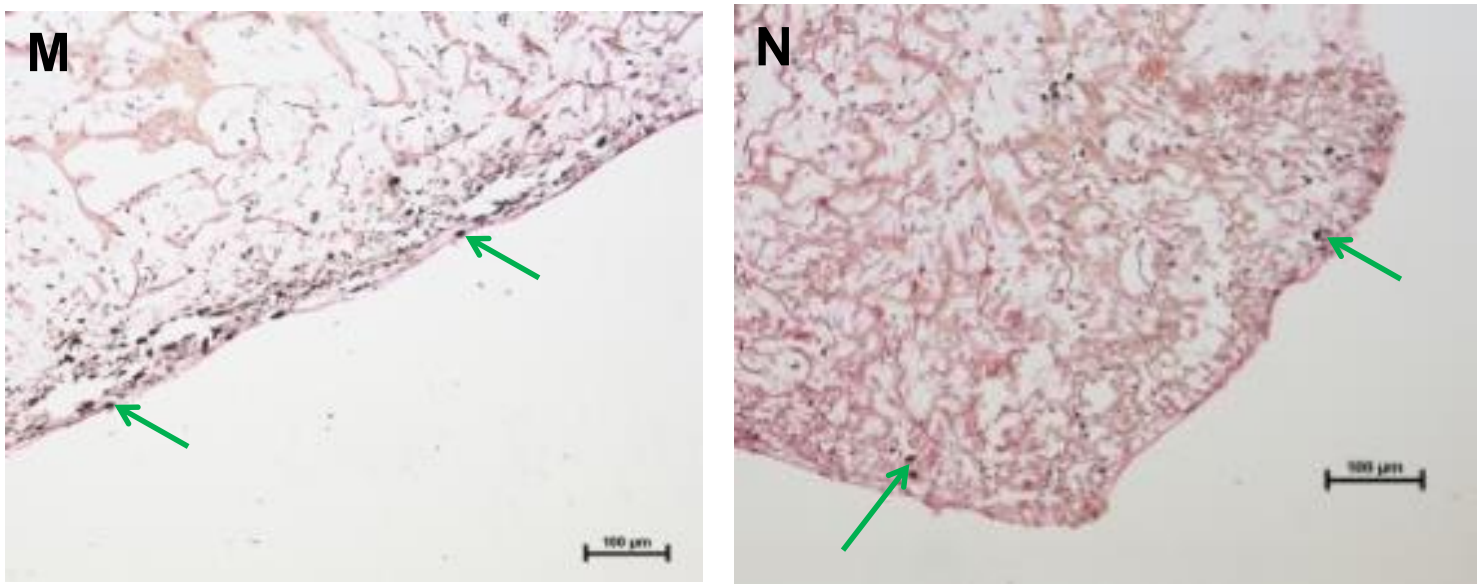

Figure 6.21 M + N – High magnification image of Figure 6.19 H and J, respectively. The green arrows indicate some of the mineralisation.

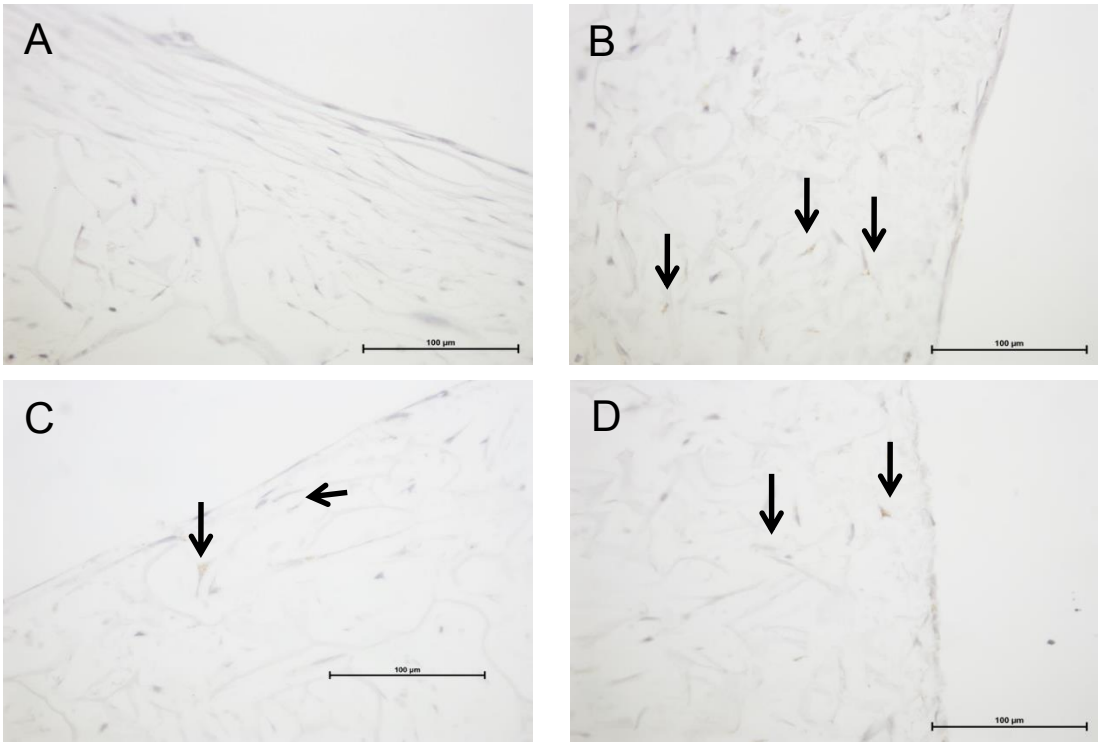

Figure 6.22 – Runx2 immunohistochemistry. Low magnification Runx2 immunohistochemical staining (brown), with a weak Harris haematoxylin counter stain (purple) for tissue, of sections from ADSC-silk scaffold constructs after 6 weeks of *in vitro* culture (Exp3). **A** – basal control; **B** – osteogenic control; **C** – ADSCs pre-treated with 10 µM MI192; **D** – ADSCs pre-treated with 30 µM MI192. Arrows indicate some of the Runx2 staining. Scale bars = 100 µM.

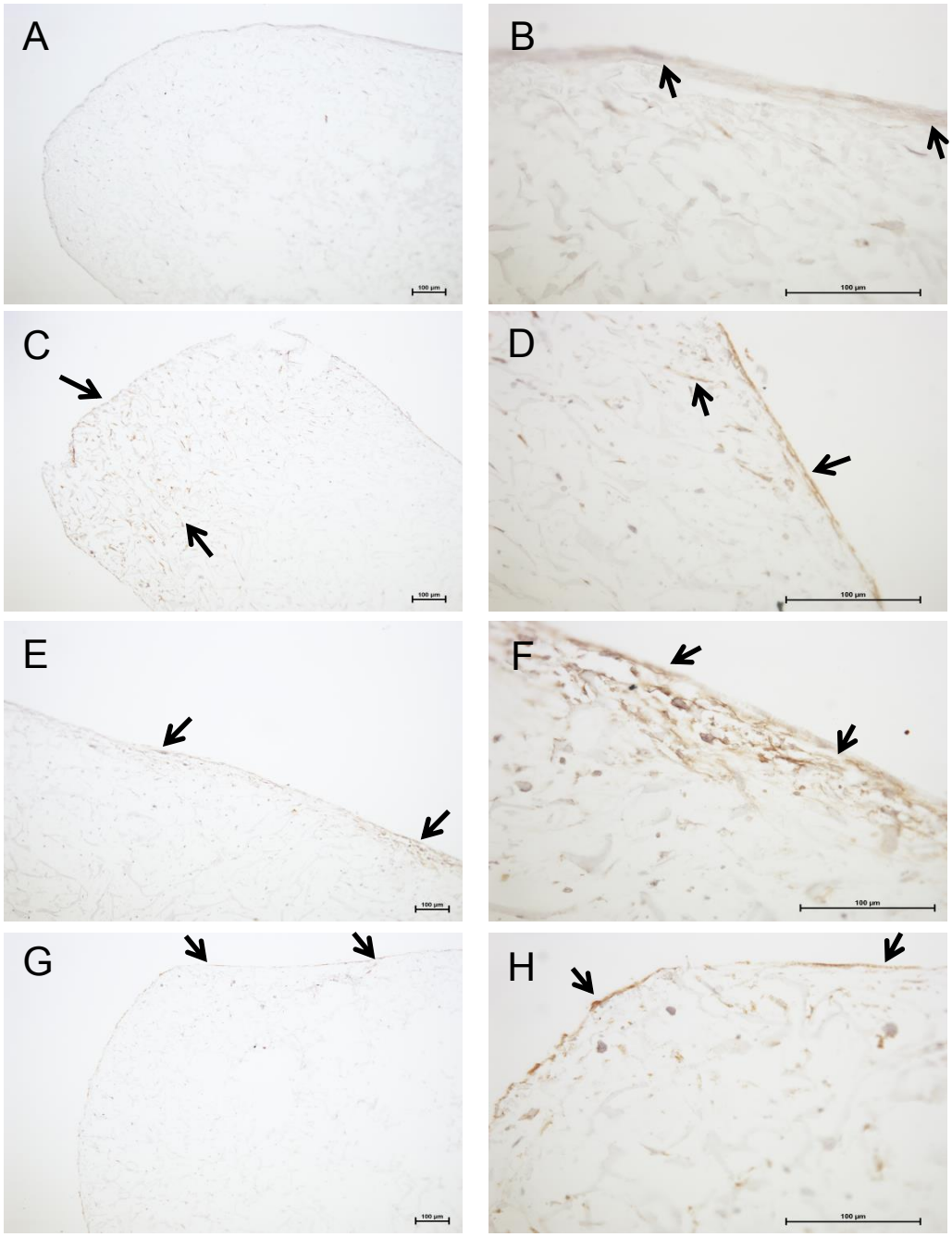

Figure 6.23 – Col1 immunohistochemistry. High and low magnification collagen 1 immunohistochemical staining (brown), with a weak Harris haematoxylin counter stain (purple) for tissue, of sections from ADSC-silk scaffold constructs after 6 weeks of *in vitro* culture (Exp3). **A + B** – basal control; **C + D** – osteogenic control; **E + F** – ADSCs pre-treated with 10 µM MI192; G +**H**– ADSCs pre-treated with 30 µM MI192. Arrows indicate some of the collagen 1 staining. Scale bars = 100 µM.

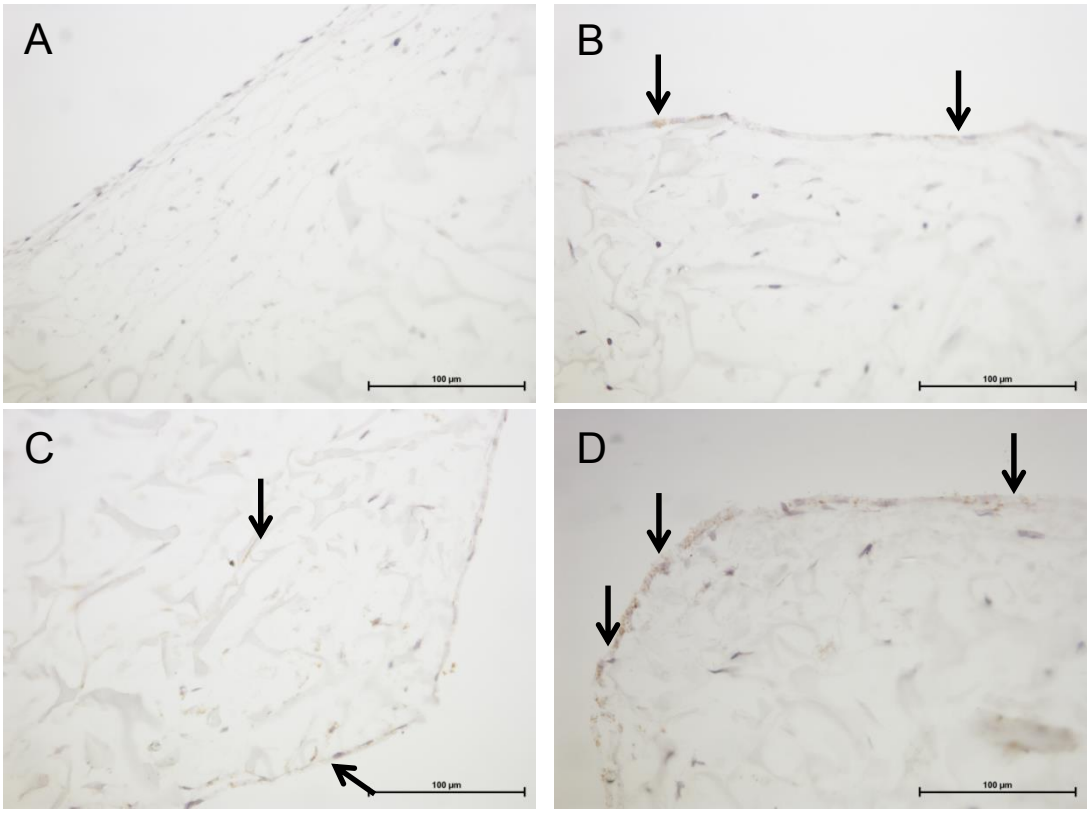

Figure 6.24 – Ocn immunohistochemistry. Low magnification Ocn immunohistochemical staining (brown), with a weak Harris haematoxylin counter stain (purple) for tissue, of sections from ADSC-silk scaffold constructs after 6 weeks of *in vitro* culture (Exp3). **A** – basal control; **B** – osteogenic control; **C** – ADSCs pre-treated with 10 µM MI192; **D** – ADSCs pre-treated with 30 µM MI192 for two days. Arrows indicate Ocn staining. Scale bars = 100 µM**.**

6.4 Discussion

In the previous chapter, the ability of MI192 to improve the osteogenic differentiation of ADSCs in monolayer was demonstrated, whereas in this chapter, this ability was investigated in 3D models. Am silk scaffolds were utilised as a scaffolds and three different experimental designs were explored (Figure 6.2).

It is important to investigate how cells grow in 3D, as this is much more typical of how the cells actually exist and act *in vivo* (Baker & Chen 2012; Griffith & Swartz 2006). Scaffolds are an integral part of bone tissue engineering, essential in guiding the formation of functional bone, providing a 3D environment to support cell attachment, growth (Baker & Chen 2012), and (in the case of stem cells), differentiation into bone forming cells (Amini et al. 2012; Ericka M. Bueno & Glowacki 2011). While *in vivo* models are the most effective way of investigating bone tissue engineering, due to ethical considerations and their financial cost, it is advisable to optimise experimental parameters *in vitro* before moving onto *in vivo* models (Beckmann & Kneuer 2007; Tremoleda et al. 2011).

3D models have been utilised to explore how HDACis can influence bone tissue engineering, although studies are limited and some utilise the scaffolds without addition of cells in *in vivo* models, not *in vitro*. For example, Boer et al. (2006) investigated TSA and NaB with calcium phosphate ceramic granules in a subcutaneous mouse model (Boer et al. 2006). Lee et al. (2011) investigated Largazole with collagen sponge scaffolds and biphasic calcium phosphate scaffolds in rabbit calvaria bone defect models (Lee et al. 2011). The only study with much evidence of *in vitro* work was by Jung at al. (2010), where they investigated TSA with calcium sulphate scaffolds (by doping the scaffolds with the HDACis during the setting phase) both *in vitro* and *in vivo* (Jung et al. 2010). The final two of these three studies showed HDACis to improve bone tissue engineering outcomes.

Am silk scaffolds were chosen due to their biocompatibility, abundance, biodegradability and because their ability to be successfully utilised in bone tissue engineering models have been demonstrated in the department and the literature (Saha et al. 2013; Sahu et al. 2015; Kundu et al. 2013). Due to the lack of

precedent in the literature for HDACis and scaffold studies, the best available scaffolds were chosen, rather than attempting to mimic what had already been done in the literature.

The first experimental design (Expt 1) involved the treatment of the ADSCs with MI192 after they had been seeded onto the scaffold. Live/dead cell labelling is a technique used often to assess the attachment, spreading and viability of cells seeded onto scaffolds, and was used to assess all experimental design scaffolds at various time points (W. Lu et al. 2014; El-Gendy & Yang 2012). Unfortunately this technique did not give an idea of the effects of the MI192 treatment on the cell viability, because the dead marker did not work with these scaffolds (Figure 6.4).

In Expt 1, the initial seeding density was too low (Figure 6.5). In line with the literature, 2.5 x 10^5 cells should have been seeded (Saha et al. 2013), but due to low cell availability at the time, a lower number (1 x 10^5) cells was seeded. Early live cell marking showed that cells had attached and were growing on the scaffold (Figure 6.5), but density was low. This was especially apparent in the MI192 treated scaffolds, where treatment with MI192 had caused a drop in cell numbers. In hindsight, a seeding density optimisation experiment should have been undertaken, and a higher density was likely necessary for the experiment. At 9 weeks it appeared cell density was much higher (Figure 6.6), with at least a confluent layer of cells on every scaffold, so it was believed that sufficient tissue would have formed and the effect of MI192 should still be apparent.

Van Gieson's staining showed tissue formation at the scaffold surface was thicker in the MI192 treated constructs (Figure 6.7 D – E), than the osteogenic control constructs (Figure 6.7 A – C). There was good cell penetration and growth inside the osteogenic controls, but less cell penetration in the MI192 treated constructs. The osteogenic controls had a cell density and capsule formation similar to that seen in a study with these scaffolds carried out previously (Saha et al. 2013). It is know that HDACi treatment halts the cell cycle and cellular proliferation (Zhang & Zhong 2014; Gabrielli et al. 2011; Bhaskara et al. 2009), which has been demonstrated previously with MI192 in the monolayer experiments. So here, the cells treated with MI192 may be less capable of growth and movement on the

scaffold, resulting in the thick cell capsule forming on the outside of the scaffold. Also, this lack of movement is in combination with the cytotoxic effect of MI192 reducing cell numbers. Those cells that had survived may have been capable of laying down more extra cellular matrix, causing the higher density capsule to form. However, the MI192 is clearly having a negative effect on long term tissue formation, either by simply reducing cell numbers, or by also inhibiting cell movement and growth. In further experiments the cells were treated with MI192 before being seeded onto the scaffolds, preventing a bias due to loss of cells. Aside, a higher more optimal cell seeding density was used on the other experiments (2.5 times the cells, 250,000 per scaffold).

In experimental design 2 (Expt 2), the cells were pre-treated with MI192 for two days in monolayer, prior to undergoing osteogenic pre-seeding induction for 7 days before seeding. Cells were then seeded onto the scaffold for further osteogenic induction. This procedure mimicked that carried out in monolayer in Chapter 5: The Effects of MI192 on the Differentiation of Adipose Derived Stem Cells in 2D.

Cell viability and density was checked earlier in Expt 2 than Expt 1, to ensure sufficient cells had been seeded. 24 hours after seeding it appeared that there were sufficient cells seeded onto the scaffold (Figure 6.8), with cell density being similar to at 6 weeks of the previous experiment. However, rounded cell morphology was observed in the cells on some of the scaffolds (Figure 6.8 A, B and E). It was believed that over 6 weeks of culture the cells may spread and behave more typically, so the scaffolds were left and cultured for 6 weeks. When assessed again at 6 weeks (Figure 6.9), the same atypical morphology was observed in the same scaffolds. This was unexpected and not comparable to the previous experiment. To assess more closely what had happened, the scaffolds were processed for histology.

Histology of these scaffolds also yielded atypical results, where no cells with typical morphology could be observed (Figure 6.10). The cells were still seen as viable when labelled with the live cell marker (Figure 6.8 and Figure 6.9); therefore, the roundness is not caused by cell death. It could be a result of the differentiation the cells underwent before seeding, which may cause them to change morphology or

halt proliferation. However, in the scaffolds with the abnormal cell morphology, a range of cell phenotype would be expected if it was down to cell behaviour, and cells seeded from exactly the same batch in the same conditions did not display these properties. It could be a problem with the scaffolds, but these abnormalities were only every observed in this experiment, and the cells on the other half of the scaffolds behaved as expected. The reason for this behaviour remains unknown.

The other scaffolds in the group had the expected cell morphology, comparable to Expt 1 and the literature (Saha et al. 2013), and had cell growth throughout the whole scaffold (Figure 6.11). Staining for collagen with Picrosirius red (Figure 6.12) and mineralisation with Von Kossa (Figure 6.13) gave good results. The collagen formation in the constructs seeded with the MI192 pre-treated cells (Figure 6.12 C – F) was comparable to the osteogenic medium alone controls (Figure 6.12 A + B). The mineralisation was greater in the MI192 pre-treated scaffolds (Figure 6.13 C – F) than the osteogenic medium alone controls (Figure 6.13 A + B). However, due to a low scaffold number (2), conclusions cannot be drawn with full confidence. Rather than repeat the experiment, a third experiment with a simpler experimental design was undertaken.

A third experimental design, where cells were seeded straight after being treated with MI192 in monolayer for 2 days, was the final experimental design to be explored (Expt 3). In this experiment, a basal control scaffold group was also included, where the constructs were cultured in MesenPRO RS™ basal growth expansion medium, to act as a negative control for the osteogenic differentiation groups.

24 hours after seeding, the cell-scaffold constructs showed a high density of viable cells (Figure 6.13), with high and normal cell attachment observed. Cell density was similar across all groups. There was no evidence of the rounded cell morphology, as in Expt 2. When labelled again after 6 weeks of culture the cell density was high in all scaffolds (Figure 6.15). There was a difference in cell morphology in the basal scaffold group (Figure 6.15 A + B), were cells were more elongated, with a more fibroblast like cell morphology. This mimics the results seen in the 2D morphological

analysis of the cells (Chapter 4: The General Effects of MI192 on Adipose Derived Stem Cells Cultured in Monolayer, Figure 4.3 - Figure 4.5).

SEM analysis was carried out on the scaffolds, to further assess cell morphology and as an additional assessment of cell mineralisation. Compared to the highly porous negative control scaffold (Figure 6.15 A + B) cells could clearly be seen on all experimental scaffolds (Figure 6.15 C - J). Likely due to the increased proliferative capacity of the cells in the expansion medium, the highest cell density appeared to be in the basal control scaffolds (Figure 6.15 C + D). Compared to the basal control, mineralisation (the white deposition) could be seen in the osteogenic control (Figure 6.15 E + F), and both of the MI192 treated scaffolds (Figure 6.15 G – J). EDS analysis of this deposition showed this white deposition to comprise of calcium and phosphorous (Figure 6.16), the primary minerals found in bone. When quantified (Table 6-2), minimal mineralisation seen in the basal medium negative control (1.09 %). The highest total mineralisation was seen in the osteogenic control, with 20.93 %, compared to 16.93 % and 19.22 % for the samples with the 10 µM and 30 µM pre-treated cells, respectively. This indicates that the overall mineralisation is higher for the osteogenic control than the MI192 pre-treated groups. The ratio of calcium and phosphorous was also calculated (Table 6-2). The typical calcium/phosphorous ratio in functional bone is between 1.95 and 2.07 (Kourkoumelis et al. 2012). The osteogenic control has a ratio closest to this (2.26) and along with the 10 µM pre-treated sample (with a ratio of 2.5) had a higher level of calcium than typical of bone. The opposite was true for the 30 µM pre-treated sample, where the phosphorous levels were high and therefore the ratio low, at 1.12.

The MI192 treatment has clearly altered how the scaffolds mineralise, and this suggests it may have lowered the mineralisation ability of the cells. However, this was only a pilot study, primarily to check is the mineralisation being observed in the histology was true mineralisation. There was only data from one sample, and the analysis would need to be repeated with multiple samples for a full comparison. This also doesn't analyse mineralisation below the surface of the scaffold. It has been demonstrated in Chapter 5: The Effects of MI192 on the Differentiation of Adipose Derived Stem Cells in 2D (Figure 5.13) that the MI192 may improve the

ability of the cells to form functional mineral nodules. Also, mineralisation below the surface may be different in the MI192 treatment constructs.

Histological analysis of the scaffolds showed good cell growth and penetration in all scaffolds (Figure 6.19). Compared to those scaffolds cultured in osteogenic medium, the basal negative control scaffolds (Figure 6.19 A + B) had tissue forming thickly on the outside of the scaffold, indicating layers of cells growing on top of each other. The cell density in the centre of the basal control was similar to that of all the other scaffolds, so in proliferative promoting medium, the cell density cannot increase past a certain point inside the scaffolds. The osteogenic control (Figure 6.19 C + D) and the scaffolds cultured with MI192 treated cells (Figure 6.19 E – L) had similar cell densities to each other.

The thick layer of cells formed in the basal control scaffolds stained positive for collagen with a Picrosirius red stain (Figure 6.20 A + B). The osteogenic control scaffolds (Figure 6.20 C + D) and the scaffolds seeded with cells pre-treated with 30 µM MI192 (Figure 6.20 I – L) showed a similar level of collagen staining, with the collagen mostly located nearer the surface of the scaffold. The more mature cells are located there, and they have the greatest concentration of any growth factors and osteogenic stimulating supplements from the medium, so this was expected. The scaffolds seeded with cells pre-treated with 10 µM of MI192 (Figure 6.20 E – H) showed high levels of collagen, with two of the scaffolds (Figure 6.20 E + G) showing strong staining throughout the scaffold. This may be an indicator these scaffolds are showing enhanced osteogenic differentiation capability.

In the basal medium negative control scaffolds, the Von Kossa stain for mineralisation was negative (Figure 6.21 A + B), as expected. Mineralisation staining was observed in all of the osteogenic controls (Figure 6.21 C + D) and both groups of scaffolds seeded with MI192 pre-treated cells (Figure 6.21 A – L). The levels of mineralisation were similar in 3 of the 30 µM pre-treated cell scaffolds (Figure 6.21 I – K) to the osteogenic controls, with one showing much higher mineralisation (Figure 6.21 L). The mineralisation, especially deeper into the scaffolds, was higher in the 10 µM pre-treated cell scaffolds (Figure 6.21 E – H), indicating a greater level of mineralisation. 10 µM MI192 may be the preferred dose

for improving the osteogenic differentiation of ADSCs in long term 3D culture models.

Runx2 and Ocn protein can be seen in the osteogenic controls and the MI192 treated groups, but staining is quite weak and is comparable across all three groups grown in osteogenic medium. There was no staining in the basal controls, which is a good indicator staining is not a false positive. However, there's no obvious increase or decrease in production of Ocn or Runx2 with MI192 treatment. Due to the reduction in *OCN* gene expression seen in Chapter 5: The Effects of MI192 on the Differentiation of Adipose Derived Stem Cells in 2D (Figure 5.10), the fact that Ocn protein is present in the MI192 treated cells is an interesting and important result, as this allays concerns that this protein may not be produced in the MI192 treated cells, causing problems in the long term for these experiments. Collagen 1 production is highest in the 10 µM treated cells, indicating that MI192 treatment may be improving the osteogenic differentiation of these cells. The staining in the 30 µM treated cells was weaker, so again 10 µM may be the preferred dose in the long term.

The fact the cell density appears to plateau, not increased even in the proliferative medium, may affect the cells ability to differentiate into bone. The higher density cells found near the scaffold surface may be more suitable for differentiation down an osteogenic lineage, and therefore mineralise more highly and produce more osteogenic proteins. This may be because the cells are more mature, and the cells deeper into the scaffold have grown through after seeding and may differentiate further down an osteogenic lineage with more time. Finally, the cells nearer the surface have a greater access to minerals and growth factors from the culture medium, as they in contact with the medium and the cells in the middle must rely on diffusion of these through the cells closer to the surface.

This study shows that the most suitable model for future studies is Experimental Design 3. MI192 treatment appears to increase the osteogenic differentiation of the ADSCs, especially when looking at the collagen deposition and the mineralisation. The results are better for the 10 µM MI192 dose, and this should be considered in the future work.

Chapter 7: The effect of MI192 treatment on ADSC gene expression

The aim of this chapter was to investigate the effect of MI192 treatment on the gene expression of ADSCs, using 96 gene microfluidic TaqMan® Array cards. The gene expression in ADSCs before and after two days of MI192 treatment were investigated, to explore the potential mechanisms behind the alterations in differentiation potential seen in the ADSCs in previous chapters.

7.1 Introduction

The work in this chapter was carried out in conjunction with Sarah M. Churchman, from Leeds Institute of Rheumatic and Musculoskeletal Medicine, University of Leeds. Cell culture was carried out by the author, RNA extraction was carried out jointly by the author and S. Churchman, qRT-PCR by S. Churchman (observed by the author), data collection and processing was carried out jointly and data analysis and presentation by the author.

In previous work in this thesis, gene expression changes in cells treated with MI192 during osteogenic and adipogenic differentiation culture have been explored; however, what happens to the gene expression immediately after the initial MI192 pre-treatment has not been explored. This could answer questions about the pathways by which MI192 affects differentiation potential of ADSCs, along with potentially opening up other avenues for HDACi and MI192 research in the future.

Custom 384-well, 96 gene microfluidic TaqMan® Array cards can be utilised to investigate a large number of genes from up to 4 samples at one time. The genes on the card were chosen as important in characterising MSCs by Churchmen et al. based on their previous work in characterisation of MSCs (Churchman et al. 2013; Churchman et al. 2012).

7.2 Materials and Methods

7.2.1 MI192 treatment of ADSCs

To account for donor variation, the effect of MI192 treatment on the gene expression of 6 different ADSC batches (4 single donors, and two samples with 6 and 8 donors) was tested. Full donor information can be found in Table 7-1.

Table 7-1 - donor and passage information for the 6 batches of ADSCs

Company (Catalogue number)	Donor/Lot number	Donor(s) age/sex/Tissue Location
Life Technologies (R7788110)	2118	45/female/abdomen
Life Technologies (R7788110)	2117	49/female/abdomen
Life Technologies (R7788110)	2033	63/male/breast and abdomen
Lonza (PT-5006)	407088	46/female/abdomen
Zen Bio (ASC-F)	ASC0046	29-62 (average 50.7)/female/ abdomen, thigh and knee
Zen Bio (ASC-F)	ASC0049	29-51 (average 44)/female/ abdomen, breast, flank, hip, thigh and knee

ADSCs (passage 2) from each donor were seeded in 6 well plates (2.5×10^5 cells/well) and cultured in basal medium. 2.5×10^5 ADSCs from each donor were placed directly into a lysis buffer (Norgen Biotek Corp, Cat. no: 24000) as the untreated controls. After 24 hours of initial culture, the medium was then replaced with MI192 containing medium (30 μM in 1 mL basal medium). After 48 hours induction, the cells were washed twice with 1x PBS and lysed in 500 μL lysis buffer for 20 minutes. Lysates were then stored at – 80 °C until RNA/DNA/Protein isolation.

7.2.2 Isolation of RNA/DNA/Protein

The total RNA, genomic DNA and protein was purified from the samples using Norgen's RNA/DNA/Protein Purification Kit (Norgen Biotek Corp, Cat 24000), following the manufacturer's instructions. For each sample, the total RNA, genomic DNA and proteins were all purified using the same column. Purification is based on spin column chromatography using Norgen's proprietary resin as the separation matrix. Before loading, the samples are washed with detergents and chaotropic denaturants that will inactive RNAses and proteases. Nucleic acids (the RNA and the DNA) are bound to the column, separate from the protein in the eluent. The column was then washed and the RNA eluted, while the DNA remains bound to the column. This was then washed and eluted in a separate solution. After this the proteins can be loaded and purified on the same column, using pH altering methods. RNA was then frozen and stored at - 80 °C. Genomic DNA and protein were stored at - 20 °C in case they were needed for any future/further studies.

7.2.3 Reverse Transcription

Reverse transcription was carried out as described in Chapter 2: General Materials and Methods, 2.7.2 Reverse Transcription.

7.2.4 qRT-PCR

Custom 384-well, 96 gene microfluidic TaqMan® Array Cards were used utilised to compare the gene expression difference between samples treated for 2 days with MI192, and untreated controls.

200 ng of cDNA per port (4 ports/samples per card) was loaded onto a Custom TaqMan Array (format 96a; from Applied Biosystems). The cards are designed to not need technical repeats for samples, as each sample is loaded into a single port for all 96 genes. Genes were selected for the custom card by Sarah Churchman and co-workers to span a wide range of genes related to MSCs. Exon-spanning, '3 most' TaqMan assays were selected for the array when possible. The full gene information can be found in Table 7-2.

Amplification curves were obtained using an Applied Biosystems 7900HD sequence detection system with a 40 cycle standard Taqman protocol. Samples underwent a

10 minute 95 °C pre-incubation step, followed by 45 cycles of 10 seconds at 95 °C, 30 seconds at 60 °C and 1 second at 72 °C. Samples were cooled to 40 °C at the end of the 40 cycles.

Table 7-2 - Assay identification for microfluidic card.

TaqMan assay identification	Gene Symbol	Description
Hs00153936_m1	*ACAN*	Aggrecan, cartilage-specific proteoglycan core protein (CSPCP)
Hs00909449_m1	*ACTA2*	actin, alpha 2, smooth muscle, aorta
Hs00244715_m1	*ACVR1B*	activin A receptor, type IB
Hs00155658_m1	*ACVR2A*	activin A receptor, type IIA
Hs00758162_m1	*ALPL*	alkaline phosphatase
Hs00181613_m1	*ANGPT1*	angiopoietin 1
Hs01101127_m1	*ANGPTL4*	angiopoietin-like 4
Hs03044164_m1	*BAMBI*	BM activin membrane inhibitor homolog
Hs00609452_g1	*BGLAP*	PMF-bone gamma-carboxyglutamate(gla) protein/ osteocalcin
Hs00154192_m1	*BMP2*	bone morphogenetic protein 2
Hs00370078_m1	*BMP4*	bone morphogenetic protein 4
Hs00234930_m1	*BMP5*	bone morphogenetic protein 5
Hs00403062_m1	*BMPER*	BMP binding endothelial regulator
Hs00831730_s1	*BMPR1A*	bone morphogenetic protein receptor, type IA
Hs00156438_m1	*CDH11*	cadherin 11, type 2, OB-cadherin (osteoblast)
Hs00269972_s1	*CEBPA*	CCAAT/enhancer binding protein (C/EBP), alpha
Hs00154382_m1	*CHAD*	chondroadherin

Hs00253550_m1	*CLEC4M*	CD209 molecule,C-type lectin domain family 4, member M
Hs00166657_m1	*COL10A1*	collagen, type X, alpha 1
Hs01076777_m1	*COL1A1*	collagen, type I, alpha 1
Hs01028971_m1	*COL1A2*	collagen, type I, alpha 2
Hs00264051_m1	*COL2A1*	collagen, type II, alpha 1
Hs00164359_m1	*COMP*	cartilage oligomeric matrix protein
Hs00426981_m1	*CSPG4*	chondroitin sulfate proteoglycan 4
Hs00171022_m1	*CXCL12*	chemokine (C-X-C motif) ligand 12/ stromal cell-derived factor 1
Hs00601975_m1	*CXCL2*	chemokine (C-X-C motif) ligand 2
Hs00322497_m1	*DAAM2*	dishevelled associated activator of morphogenesis 2
Hs00178815_m1	*DDR2*	discoidin domain receptor tyrosine kinase 2
Hs00182901_m1	*DVL2*	dishevelled, dsh homolog 2
Hs00358886_m1	*EFNA1*	ephrin-A1
Hs00174752_m1	*EPHB4*	EPH receptor B4
Hs00191912_m1	*EPYC*	epiphycan
Hs00609791_m1	*FABP4*	fatty acid binding protein 4, adipocyte
Hs00170454_m1	*FGF5*	fibroblast growth factor 5
Hs00241111_m1	*FGFR1*	fibroblast growth factor receptor 1
Hs00179829_m1	*FGFR3*	fibroblast growth factor receptor 3
Hs00173503_m1	*FRZB*	frizzled-related protein/ secreted frizzled-related protein 3
Hs00268943_s1	*FZD1*	frizzled homolog 1
Hs00201853_m1	*FZD4*	frizzled homolog 4
Hs00275833_s1	*FZD7*	frizzled homolog 7

Hs00259040_s1	*FZD8*	frizzled homolog 8
Hs00268954_s1	*FZD9*	frizzled homolog 9
Hs99999905_m1	*GAPDH*	glyceraldehyde-3-phosphate dehydrogenase
Hs00231119_m1	*GATA2*	GATA binding protein 2
Hs00167060_m1	*GDF5*	growth differentiation factor 5
Hs01075601_m1	*GHR*	growth hormone receptor
Hs00748445_s1	*GJA1*	gap junction protein, alpha 1, 43kDa/ Connexin 43
Hs00157103_m1	*HAPLN1*	hyaluronan and proteoglycan link protein 1
Hs99999909_m1	*HPRT1*	hypoxanthine phosphoribosyltransferase 1*
Hs99999041_m1	*IFNG*	interferon, gamma,
Hs01005963_m1	*IGF2*	insulin-like growth factor 2 (somatomedin A),INS-IGF2
Hs00181211_m1	*IGFBP3*	insulin-like growth factor binding protein 3
Hs00961622_m1	*IL10*	interleukin 10
Hs00174202_m1	*IL7*	interleukin 7
Hs01070036_m1	*JAG1*	jagged 1
Hs00174492_m1	*LEPR*	leptin receptor
Hs01012571_m1	*LPL*	lipoprotein lipase
Hs00174838_m1	*MCAM*	melanoma cell adhesion molecule/ CD146
Hs00427183_m1	*MSX1*	msh homeobox 1
Hs02379661_g1	*MT2A*	metallothionein 2A
Hs00159522_m1	*MYH9*	myosin, heavy chain 9, non-muscle
Hs02387400_g1	*NANOG*	Nanog homeobox
Hs00707120_s1	*NES*	nestin
Hs00918411_s1	*NGFRAP1*	nerve growth factor receptor (TNFRSF16) associated protein 1

Hs00182120_m1	*NGFR*	nerve growth factor receptor (TNFR superfamily, member 16)/ CD271
Hs00271352_s1	*NOG*	noggin
Hs00192325_m1	*OMD*	osteomodulin
Hs00190682_m1	*PAPSS2*	3'-phosphoadenosine 5'-phosphosulfate synthase 2
Hs00170179_m1	*PCOLCE*	procollagen C-endopeptidase enhancer
Hs00998018_m1	*PDGFRA*	platelet-derived growth factor receptor, alpha polypeptide
Hs00185122_m1	*PDGFRL*	platelet-derived growth factor receptor-like
Hs01370291_g1	*PHOSPHO1*	phosphatase, orphan 1
Hs00999632_g1	*POU5F1*	POU class 5 homeobox 1 (Oct 4)
Hs01115513_m1	*PPARG*	peroxisome proliferator-activated receptor gamma
Hs00160431_m1	*PRELP*	proline/arginine-rich end leucine-rich repeat protein
Hs00231079_m1	*RUNX1*	runt-related transcription factor 1
Hs00231692_m1	*RUNX2*	runt-related transcription factor 2
Hs00173499_m1	*S1PR1*	sphingosine-1-phosphate receptor 1
Hs00610060_m1	*SFRP1*	secreted frizzled-related protein 1
Hs00180066_m1	*SFRP4*	secreted frizzled-related protein 4
Hs00361747_m1	*SORT1*	sortilin 1
Hs01053049_s1	*SOX2*	SRY (sex determining region Y)-box 2
Hs00165814_m1	*SOX9*	SRY (sex determining region Y)-box 9
Hs00541729_m1	*SP7*	Sp7 transcription factor/ osterix
Hs00277762_m1	*SPARC*	secreted protein, acidic, cysteine-rich/ osteonectin
Hs00959010_m1	*SPP1*	osteopontin/ secreted phosphoprotein 1/ bone sialoprotein I

Hs00559661_m1	*TGFBR2*	transforming growth factor, beta receptor II (70/80kDa)
Hs00234257_m1	*TGFBR3*	transforming growth factor, beta receptor III
Hs01113602_m1	*TNFAIP6*	tumor necrosis factor, alpha-induced protein 6
Hs00900360_m1	*TNFRSF11B*	tumor necrosis factor receptor superfamily, member 11b/ osteoprotegerin
Hs00361186_m1	*TWIST1*	twist homolog 1
Hs00382379_m1	*TWIST2*	twist homolog 2
Hs01097550_m1	*UGDH*	UDP-glucose 6-dehydrogenase
Hs00900058_m1	*VEGFA*	vascular endothelial growth factor A
Hs01099206_m1	*VEGFC*	vascular endothelial growth factor C
Hs00183662_m1	*WIF1*	WNT inhibitory factor 1

**HPRT, reference gene.*

7.2.5 Ct Value Calculations

Once all samples had been run, (multiple cards were necessary due to there being a 4 sample limit per card), data from all cards was pooled in RQ Manager Software (Life Technologies) and analysed together in one project file, ensuring equal treatment and relative expression levels for all samples. A threshold was automatically generated by the software. The amplification curves of any flagged values were individually scrutinised in SDS v2.3 software to deduce if the result was genuine amplification or an automatic machine error in the curve detection. Samples were measured against a background standard and a ROX stable fluorescent marker, and flagged values were compared to these. Any questionable results were not included in the final analysis; any genes with consistently flagged results were noted as potentially erroneous results in Table 7-11.

The comparative Ct method ($2^{-\Delta\Delta Ct}$) was utilised to quantify gene expression levels, with the results normalised to the reference gene *HPRT*. Once Ct values for all samples had been generated, the fold difference between untreated and treated

samples was calculated for each donor. An average fold change for each gene was then produced.

Samples where expression had increased from an undetectable/undetermined value to a detected value, or from a value to an undetectable/undetermined value were not included in statistical analysis, as creating false values (e.g. 0 for “undetermined”) can lead to inaccuracies in statistics. Undetermined just means not detected within the confines of this experiment and does not mean that there is no expression, or subsequent change of expression, for the gene.

7.2.6 Statistical Analysis

Fold changes for each gene, indicating up or down regulation (where a positive number is fold up-regulation and a negative number is fold down-regulation), were analysed in GraphPad Prism 5.0 using the non-parametric Wilcoxon paired signed rank test. n = 6. P value equal or below 0.05 was considered statistically significant (*).

7.2.7 Data Presentation

Tables of fold changes have been produced, indicating up or down regulation and if the result is significant. Transcripts were grouped based on their function. Graphs indicating the trend of up-regulation or down-regulation between treated and untreated cells have been produced on a log scale, with indication of if the result was significant. Those genes with potentially erroneous results, or with vast (500 fold plus) variance between donors are analysed separately (Table 7-11). The one gene not determined in either treated or untreated samples was also indicated separately.

For each gene, a graph depicting the fold change for each donor on a logarithmic scale was produced, showing the difference between untreated and MI192 treated ADSCs. The average fold change, standard deviation and the statistical significance (P value) for each gene was also calculated and is in tabular form.

7.3 Results

The 96 transcripts investigated have been grouped into physiologically relevant categories. An increase or decrease in expression with MI192 treatment refers to an increase or decrease of expression compared to the untreated control cells.

7.3.1.1 The effect of MI192 treatment on the expression of Wnt related transcripts in ADSCs

MI192 treatment significantly up-regulated *FRZB*, *SFRP1* and *FZD9* gene expression (15.5 fold, 20.2 fold and 6.7 fold, $P \leq 0.05$) in treated ADSCs (Table 7-3).

In the MI192 treatment groups, the expression levels of *FZD1*, *FZD7* and *FZD8* were down-regulated (3.57 fold, $P > 0.05$; 4.19 fold, $P \leq 0.05$ and 1.32 fold, $P > 0.05$, respectively). Of these, only *FZD7* showed a strong down-regulation between donors, *FZD1* and *FZD8* had a poor level of consistency between donors.

DVL2, *SRFP4*, *FDZ4, NANOG* and *POU5F1* had inconclusive changes in expression, with mixed results between donors (Figure 7.1) and expression changes below 2 fold up and down-regulation (Table 7-3).

Table 7-3 – Fold changes in expression of Wnt related transcripts in ADSCs treated with MI192 for 2 days

Gene	Fold Change	Significance
FRZB	15.51	*
SFRP1	20.23	*
SFRP4	0.12	ns
DAAM2	-15.95	*
DVL2	-1.23	ns
FZD1	-3.57	ns
FZD4	0.88	ns
FZD7	-4.19	*
FZD8	-1.32	ns
FZD9	6.73	*
NANOG	-0.03	ns
POU5F1	0.85	ns

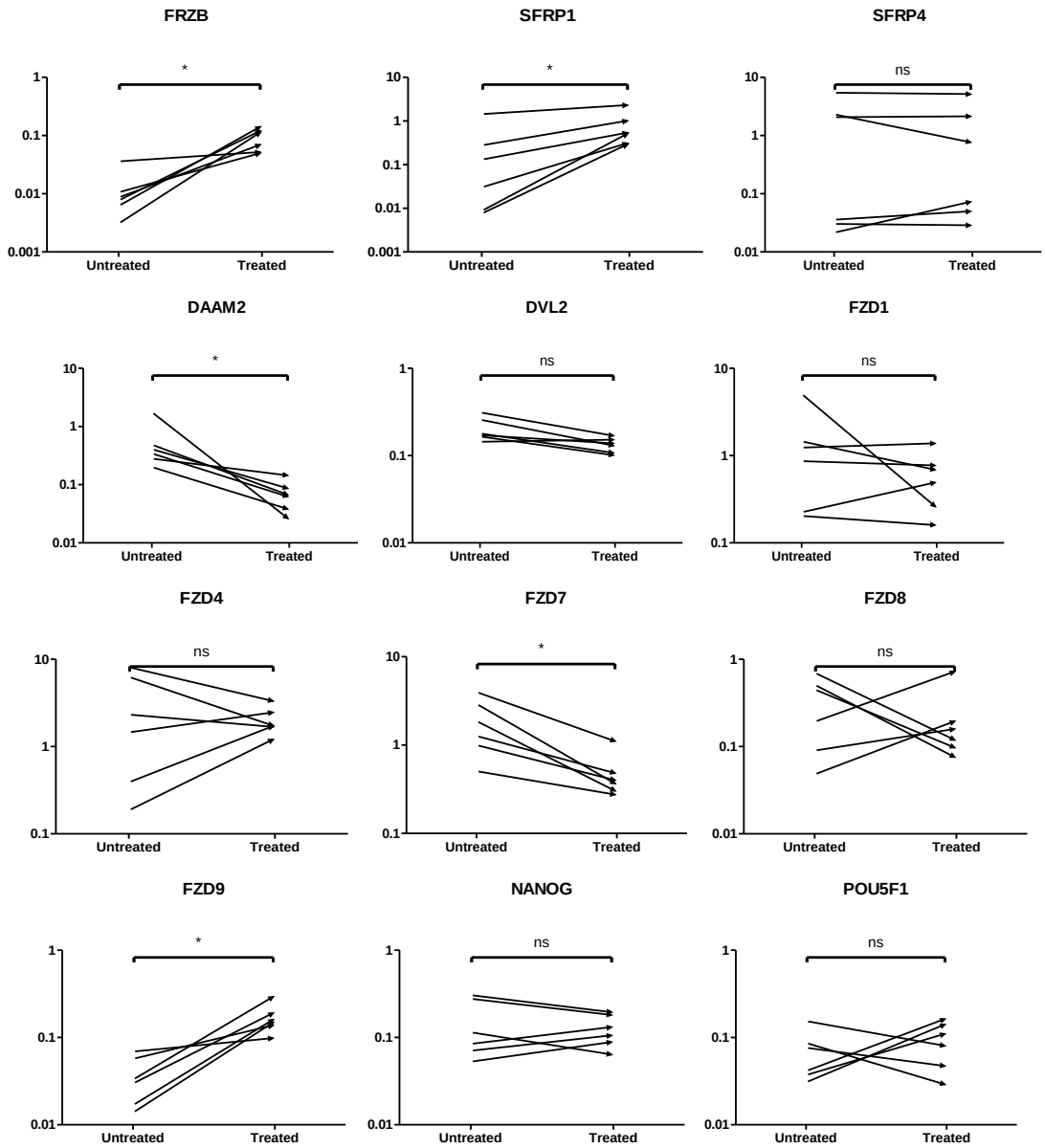

Figure 7.1 - Graphical depictions of gene expression changes between treated and untreated cells in Wnt pathway related transcripts. Graphs on a logarithmic scale and results expressed as fold changes (n=6). * = P ≤ 0.05

7.3.2 The effect of MI192 treatment on the expression of early cartilage and bone related transcripts in ADSCs

BMP2 and *BMP4* transcript levels were significantly up-regulated (32.76 and 12.3 fold, $P \leq 0.05$, both strongly in all donors, Table 7-4 and Figure 7.2) in the MI192 treated ADSCs. *IGF2* was 30.14 fold up-regulated ($P > 0.05$), with 5 out of 6 donors showed up-regulation.

Transcript levels of *BMPER* were down regulated (4.63 fold, although not statistically significantly, $P > 0.05$), with five out of six donors showing down-regulation. *GDF5* was down-regulated 26.05 fold in all donors but not statistically significant ($P > 0.05$). *IGFBP3*, *ACVR1B*, *ACVR2A* and *RUNX2* were all uniformly and statistically significantly down-regulated in all donors (8.05 fold, 3.33 fold, 2.42 fold and 3 fold $P \leq 0.05$). *TWIST1* was down-regulated 10 fold ($P > 0.05$), although it was up-regulated in 2 donors. Finally, *TWIST2* and *DDR2* were down-regulated (10 fold and 18.9 fold $P \leq 0.05$), in all donors.

Results were less conclusive, with varying results between donors, ($P > 0.05$) for *SOX9* (1.48 fold up-regulated), *BMPR1A* (3.55 fold down-regulated), *BMPER* (4.63 fold down-regulated) and *NOG* (0.35 fold up-regulated).

Table 7-4 - Fold changes in expression of early cartilage and bone related transcripts in ADSCs treated with MI192 for 2 days

Gene	Fold Change	Significance
BMP2	32.762	*
BMPR1A	-3.55	ns
BMP4	12.29	*
GDF5	-26.05	ns
BMPER	-4.64	ns
NOG	0.35	ns
SOX9	1.48	ns
IGF2;INS-IGF2	30.14	ns
IGFBP3	-8.05	*
ACVR1B	-3.32	*
ACVR2A	-2.42	*
RUNX2	-3.09	*
TWIST1	-9.97	ns
TWIST2	-10.06	*
DDR2	-18.86	*

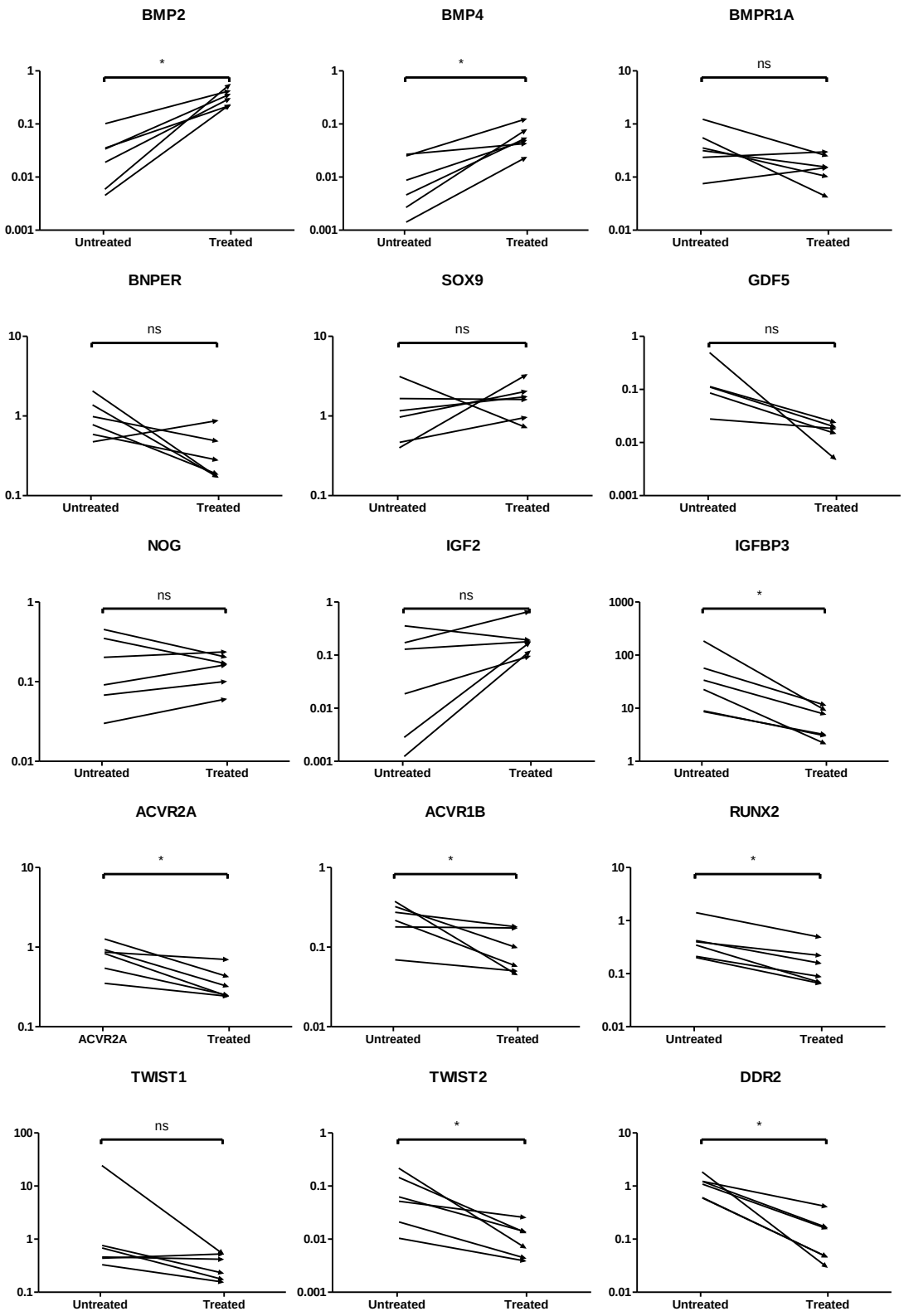

Figure 7.2 - Figure 7.3 - Graphical depictions of gene expression changes between treated and untreated cells in early cartilage and bone related transcripts. Graphs on a logarithmic scale and results expressed as fold changes (n=6). * = P ≤ 0.05

7.3.3 The effect of MI192 treatment on the expression of bone related transcripts in ADSCs

In this study, in MI192 treated ADSCs the transcript levels of *ALPL* and *PMF-BGLAP* had a trend of down-regulation (both ~3.5 fold, P > 0.05) but with mixed results between donors (Table 7-5 and Figure 7.4). *SPP1* and *PHOSPHO1* were both up-regulated strongly, *SPP1* in all donors and *PHOSPHO1* in 5 out of 6 (35 fold, P ≤ 0.05, and 59 fold, P > 0.05, respectively).

SPARC, *TNFRSF11B*, *CDH11*, *COL1A1* and *COL1A2* were all strongly down-regulated in all donors (P ≤ 0.05, 11 fold, 52 fold, 11 fold, 22 fold and 11 fold respectively). *EPHB4* and *TGFBR3* had variable and mixed results between donors, with small, below 2 fold, down-regulation (P > 0.05).

Table 7-5 – Fold changes in expression of markers of osteogenic differentiation in ADSCs treated with MI192 for 2 days

Gene	Fold Change	P Value
ALPL	-3.53	ns
SPARC	-11.71	*
BGLAP;PMF-BGLAP	-3.34	ns
TNFRSF11B	-52.28	*
CDH11	-11.00	*
EPHB4	-1.80	ns
TGFBR3	-0.33	ns
COL1A1	-22.29	*
SPP1	35.31	*
PHOSPHO1	58.59	ns

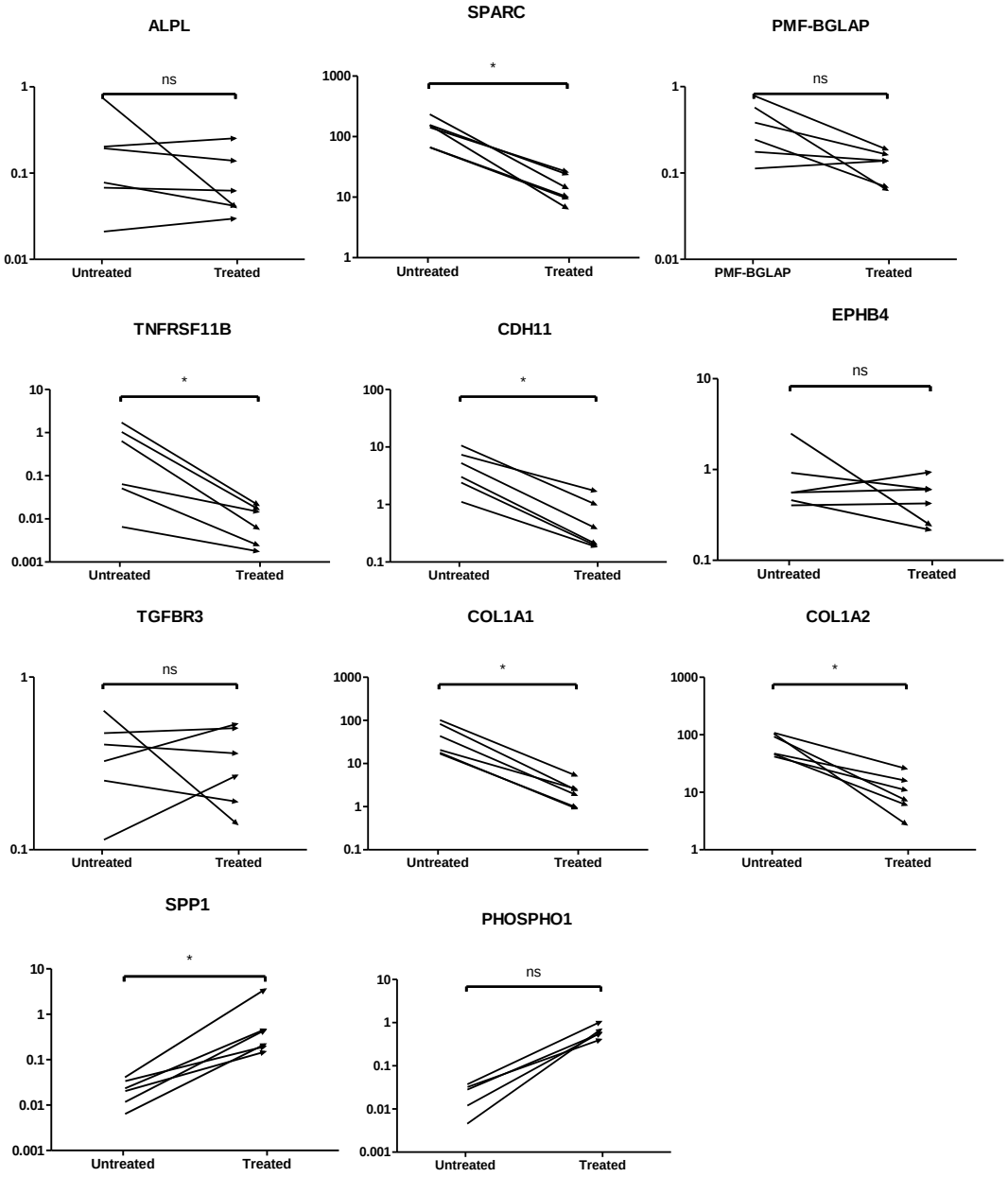

Figure 7.4 - Graphical depictions of gene expression changes between treated and untreated cells in later stage bone related transcripts. Graphs on a logarithmic scale and results expressed as fold changes (n=6). * = $P \leq 0.05$.

7.3.4 The effect of MI192 treatment on the expression of early stage cartilage, and cartilage and bone extracellular matrix related transcripts in ADSCs

TNFAIP6 was statistically significantly ($P \leq 0.05$) up-regulated 7.4 fold, in all 6 donors. *EPYC* was up-regulated 5.3 fold, although not statistically significantly ($P > 0.05$), likely because one donor showed down-regulation.

Expression of *COL2A1* was up-regulated in MI192 pre-treated cells (2.5 fold); however, in 3 donors expression went from an undetected level to a detected level, and the other three donors all had the expression up-regulated, indicating a strong up-regulation. *CHAD* had similar results (8 fold up-regulation overall, $P > 0.05$), with 3 donors showing up-regulation, one down-regulation and two with expression initially undetermined become determined from, therefore with strong indication of up-regulation.

Transcription levels of *PCOLCE*, *PAPSS2*, *UGDH* and *COL10A1* were all down-regulated ($P \leq 0.05$) in MI192 treated cells, (8.1 fold, 6.1 fold, 6.3 fold and 10.36 fold respectively) in all donors (Figure 7.5 and Table 7-6). *HAPL1* was also down-regulated (47.8 fold, $P > 0.05$, with 5 out of 6 donors having down-regulation).

COMP was down-regulated by 0.45 fold, but was not statistically significant ($P > 0.05$), as the expression was actually up-regulated in 2 donors. *ACAN* had mixed and inconclusive results. Results were also mixed for *PRELP*, where 2 donors showed down-regulation, one donor had expression initially undetermined become determined, and up-regulation (45, 18 and 2.27 fold) in 3 donors. Overall it showed an up-regulation of 12.6 fold, although this was not statistically significantly ($P > 0.05$).

Table 7-6 – Fold changes in expression of cartilage and bone extracellular matrix related transcripts in ADSCs treated with MI192 for 2 days

Gene	Fold Change	P Value
PCOLCE	-8.11	*
PAPSS2	-6.07	*
UGDH	-6.32	*
COL10A1	-10.36	*
HAPLN1	-47.83	ns
COMP	-0.45	ns
COL2A1	2.45	ns
TNFAIP6	7.43	*
EPYC	5.31	ns
PRELP	12.55	ns
CHAD	7.97	ns
ACAN	-9.06	ns

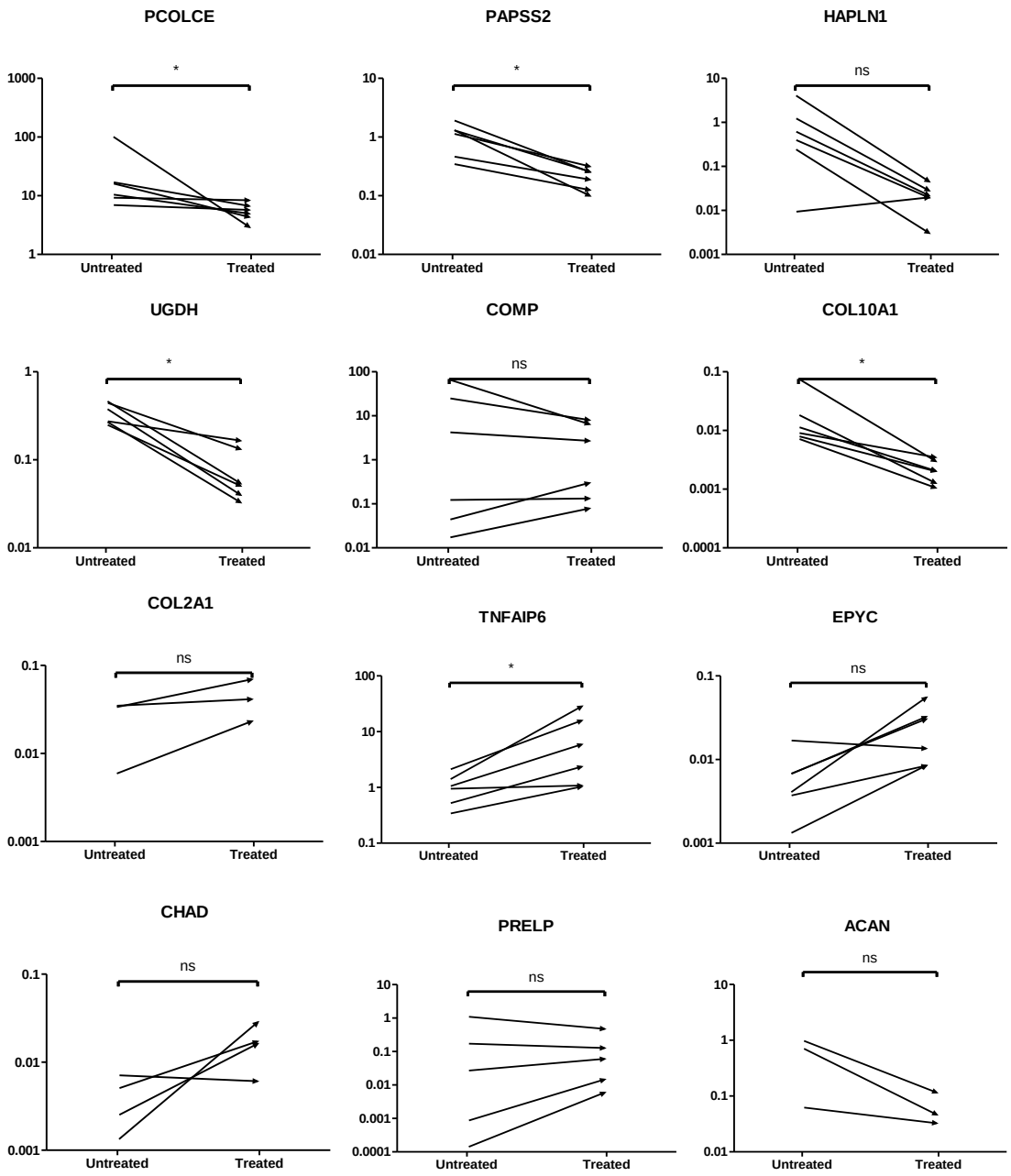

Figure 7.5 - Graphical depictions of gene expression changes between treated and untreated cells in cartilage and bone extracellular matrix related transcripts. Graphs on a logarithmic scale and results expressed as fold changes (n=6). * = $P \leq 0.05$.

7.3.4.1 The effect of MI192 treatment on the expression of adipogenic transcripts in ADSCs

CEBPA expression in MI192 treated cells was statistically significantly up-regulated 6 fold ($P \leq 0.05$) in all 6 donors. *FABP4* expression in MI192 treated cells was up-regulated ($P > 0.05$), with up-regulation in 3 donors (22 fold, 1230 fold and 1817 fold), and from undetermined to determined in 3 donors.

LEPR expression in MI192 treated cells down-regulated 4.2 fold, although not statistically significantly ($P > 0.05$), with up-regulation in 1 of 6 donors. *PPARγ* was down-regulated in MI192 treated cells (Figure 7.6), although this was not statistically significant ($P > 0.05$), as the down-regulation was only 1.1 fold over all, and was actually up-regulated in 2 donors (Table 7-7).

LPL expression in the MI192 treated and untreated ADSCs was flagged as unreliable, and results varied massively between donors. The expression of *TGFBR2* was also variable between donors, so no conclusion could be drawn from that data. *BAMBI* expression in MI192 treated cells was up-regulated 2.7 fold ($P > 0.05$), also with mixed results between donors.

Table 7-7 – Fold changes in expression of adipogenic transcripts in ADSCs treated with MI192 for 2 days

Gene	Fold Change	P Value
PPARG	-1.14	ns
FABP4	1023.56	ns
BAMBI	2.65	ns
CEBPA	6.00	*
LEPR	-4.16	ns
TGFBR2	-0.134	ns

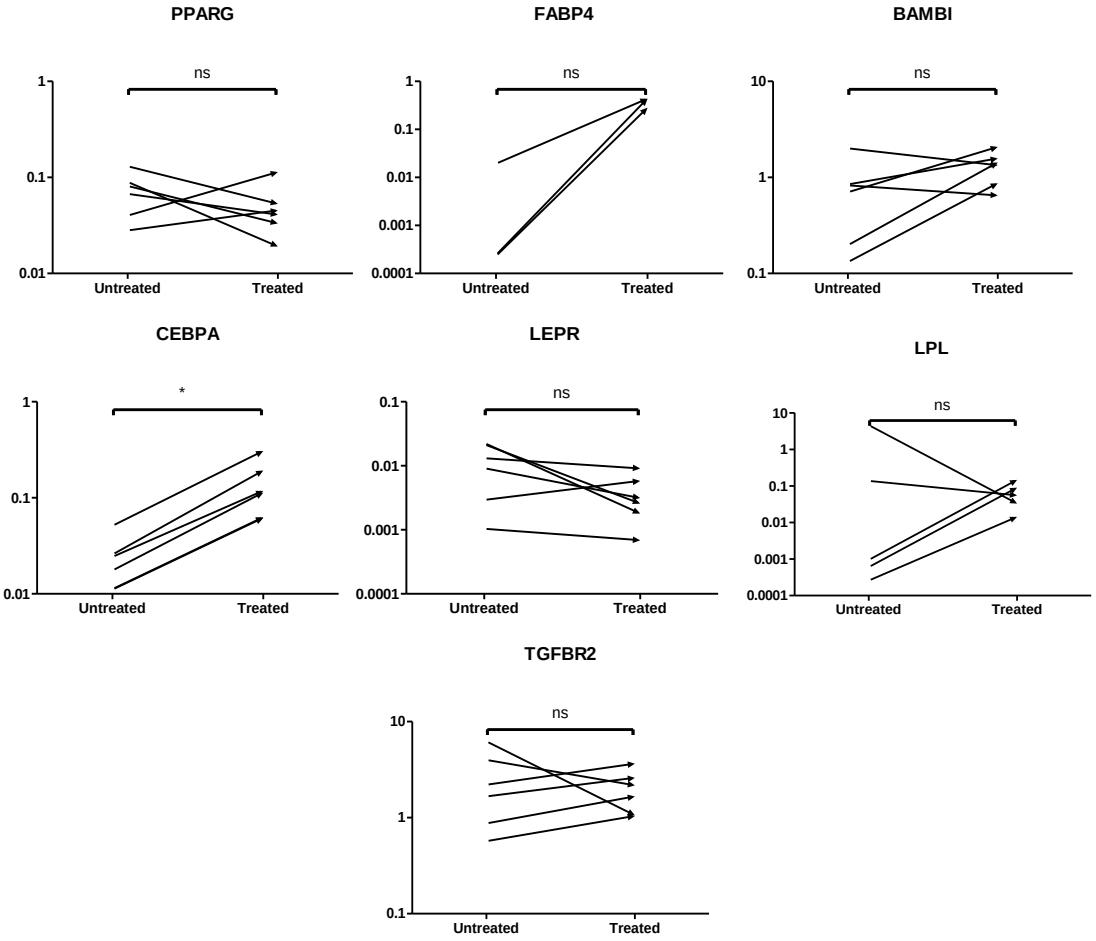

Figure 7.6 - Graphical depictions of gene expression changes between treated and untreated cells in adipogenic transcripts. Graphs on a logarithmic scale and results expressed as fold changes (n=6). * = P ≤ 0.05

7.3.5 The effect of MI192 treatment on the expression of stromal related transcripts in ADSCs

7.3.5.1 Angiogenesis related transcripts

Expression of *ANGPTL4* in MI192 treated cells was up-regulated 29.75 fold ($P \leq 0.05$, Table 7-8) in all 6 donors (Figure 7.7). *VEGFA*, *VEGFC* and *ANGPT1* expression in MI192 treated cells was strongly down-regulated (9.5 fold, 6.6 fold and 10 fold respectively $P \leq 0.05$), in all donors. Expression of *EPHB4* in MI192 treated cells is varied between donors and overall was not significantly ($P > 0.05$) down-regulated (1.8 fold) with MI192 treatment cells (shown previously in Figure 7.4 and Table 7-5).

7.3.5.2 Pericyte related transcripts

MCAM was 4.79 fold up-regulated ($P > 0.05$, Table 7-8) with MI192 treatment, with one donor showing down-regulation (Figure 7.7). *PDGFRL* was 14.5 fold up-regulated in MI192 treated ADSCs, although not significantly ($P > 0.05$), and results were inconclusive as in 3 donors it was actually down-regulated. *CSPG4*, *ANGPT1*, *ACTA2* and *PDGFRA* expression was down-regulated 2.9 fold, 10 fold, 13 fold and 8.53 fold ($P \leq 0.05$, Table 7-8) in MI192 treated ADSCs in all 6 donors.

7.3.5.3 Hematopoietic related transcripts

CXCL2 expression in MI192 treated cells was 86 fold significantly up-regulated, ($P \leq 0.05$), with a strong up-regulation visible in all 6 donors. With MI192 treatment, expression of *GJA1* was statistically significantly ($P \leq 0.05$, Table 7-8) down-regulated (6 fold) in all 6 donors (Figure 7.8). *RUNX1* was down-regulated 4.5 fold ($P > 0.05$), with most donors showing very little change in expression with MI192 treatment. Also minimally altered with MI192 treatment was *JAG1* (up-regulated, 0.35 fold, $P > 0.05$), where results were mixed between donors. *CXCL12*, *GATA2, IL7* and *IL10* all had mixed results between donors, both with fold changes all less than 2 fold, and nothing statistically significantly ($P > 0.05$).

7.3.5.4 Muscle related

ACTA2 and *MSX1* expression in MI192 treated cells was significantly down-regulated 13 fold and 3 fold ($P \leq 0.05$) in all 6 donors.

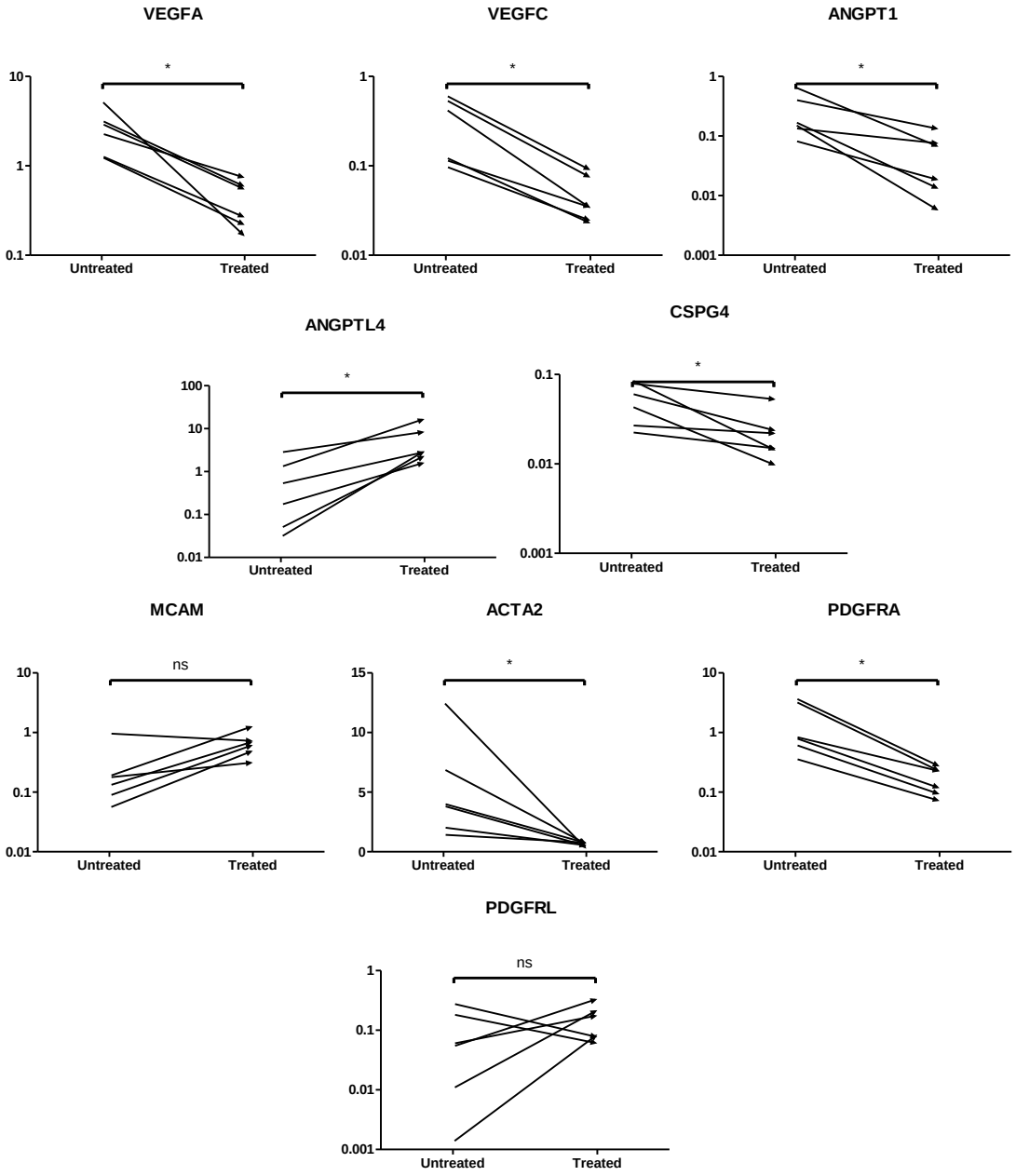

Figure 7.7 - Graphical depictions of gene expression changes between treated and untreated cells in half of the stromal related transcripts. Graphs on a logarithmic scale and results expressed as fold changes (n=6). * = P ≤ 0.05

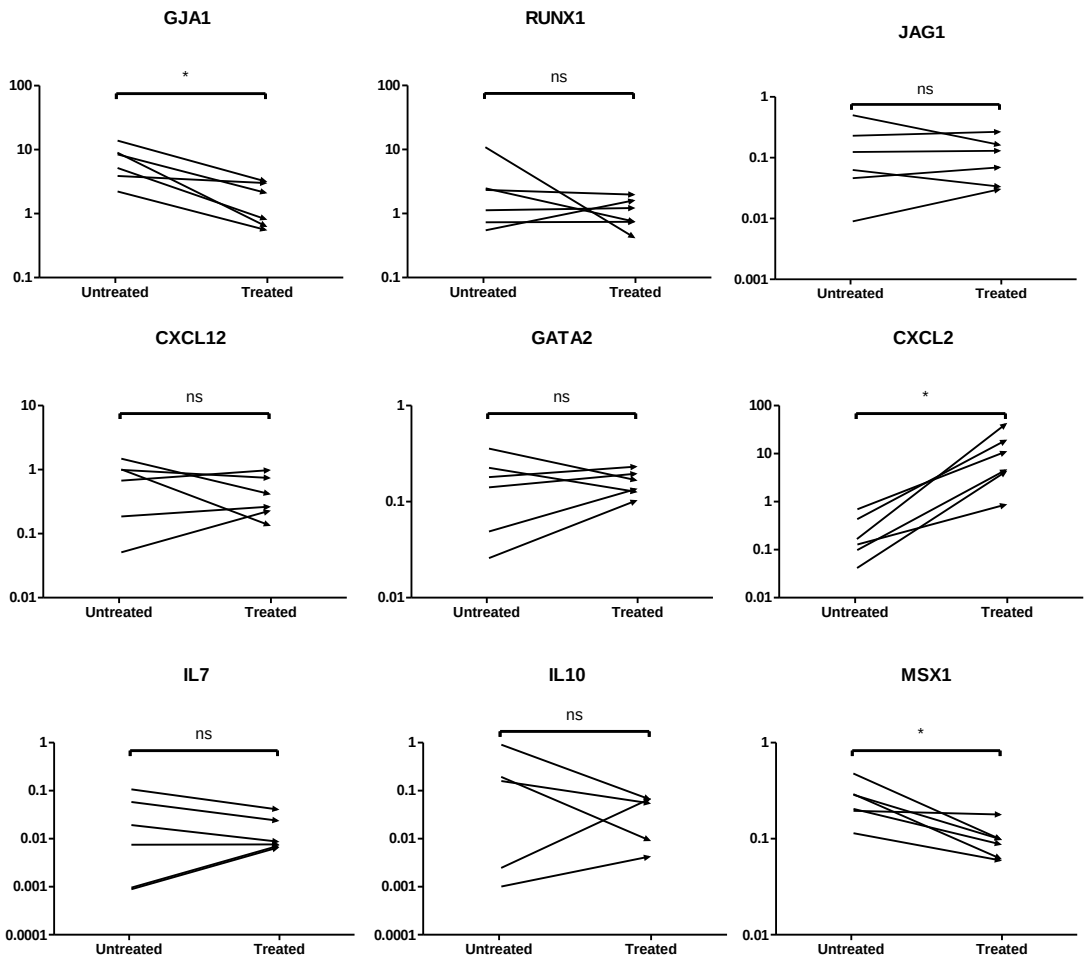

Figure 7.8 - Graphical depictions of gene expression changes between treated and untreated cells in the other half of the stromal related transcripts. Graphs on a logarithmic scale and results expressed as fold changes (n=6). * = $P \leq 0.05$

Table 7-8 – Fold changes in expression of stromal related transcripts in ADSCs treated with MI192 for 2 days

Gene	Fold Change	P Value
VEGFA	-9.54	*
VEGFC	-6.64	*
ANGPT1	-10.04	*
ANGPTL4	29.75	*
CSPG4	-2.92	*
MCAM	4.79	ns
ACTA2	-13.01	*
PDGFRA	-8.53	*
PDGFRL	14.51	ns
GJA1	-5.96	*
RUNX1	-4.50	ns
JAG1	0.35	ns
CXCL12	-0.90	ns
GATA2	0.94	ns
CXCL2	86.19	*
IL7	1.52	ns
IL10	-2.54	ns

7.3.6 The effect of MI192 treatment on the expression of Neural/nerve related transcripts in ADSCs

NGFR expression in MI192 treated was up-regulated 36.8 fold (P > 0.05, Table 7-9), with measurable up-regulation in 5 donors and from undetermined to determined in 1 donor (Figure 7.9). *SORT1* was also strongly up-regulated in all donors (6.63 fold, P ≤ 0.05). *NGFRAP1* and *NES* expression changes were mixed between donors and largely unaffected (0.21 and 0.86 fold down-regulation overall P > 0.05), with MI192 treatment.

Table 7-9 - Fold changes in expression of neural/nerve related transcripts in ADSCs treated with MI192 for 2 days

Gene	Fold Change	P Value
NGFR	36.79	ns
NGFRAP1	-0.21	ns
NES	-0.86	ns
SORT1	6.63	*

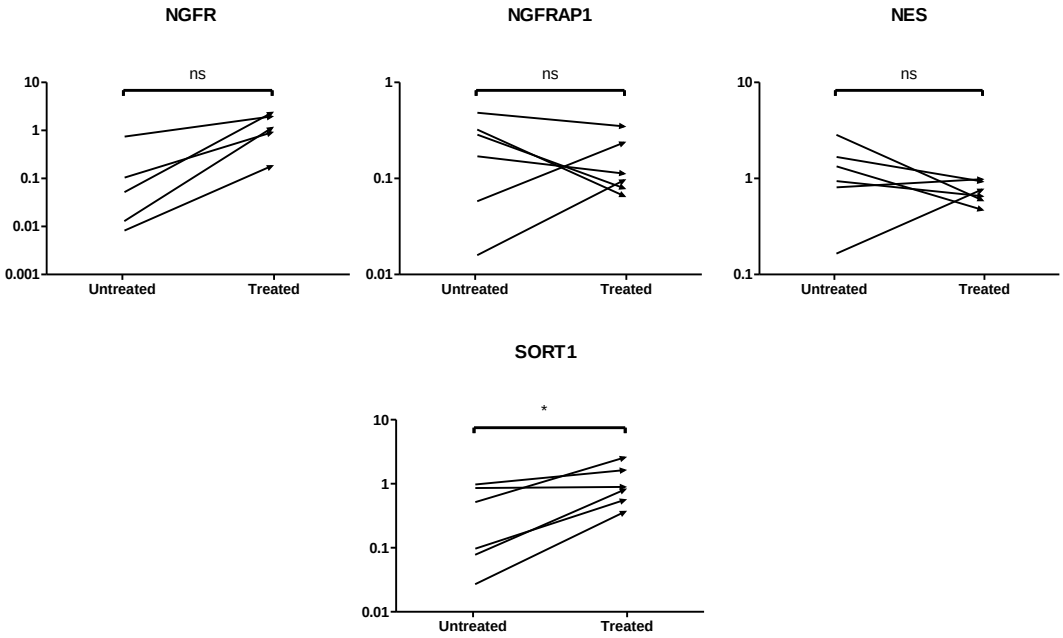

Figure 7.9 - Graphical depictions of gene expression changes between treated and untreated cells in neural/nerve related transcripts. Graphs on a logarithmic scale and results expressed as fold changes (n=6). * = P ≤ 0.05.

7.3.7 The effect of MI192 treatment on the expression of miscellaneous transcripts in ADSCs

FGFR3 was significantly up-regulated 38 fold (P ≤ 0.05), with strong up-regulation in all donors. *MYH9* was slightly down-regulated in 5 donors, although only 1.78 fold in total and not significantly (P > 0.05). Change in expression of *FGFR1*, *FGF5, SOX2* and *GHR* with MI192 treatment were minimal and varied between donors (Figure 7.10).

Table 7-10 – Fold change in expression of miscellaneous transcripts in ADSCs treated with MI192 for 2 days

Gene	Fold Change	P Value
FGFR1	-0.71	ns
FGF5	0.90	ns
FGFR3	38.30	*
SOX2	1.68	ns
GHR	1.34	ns
MYH9	-1.78	ns

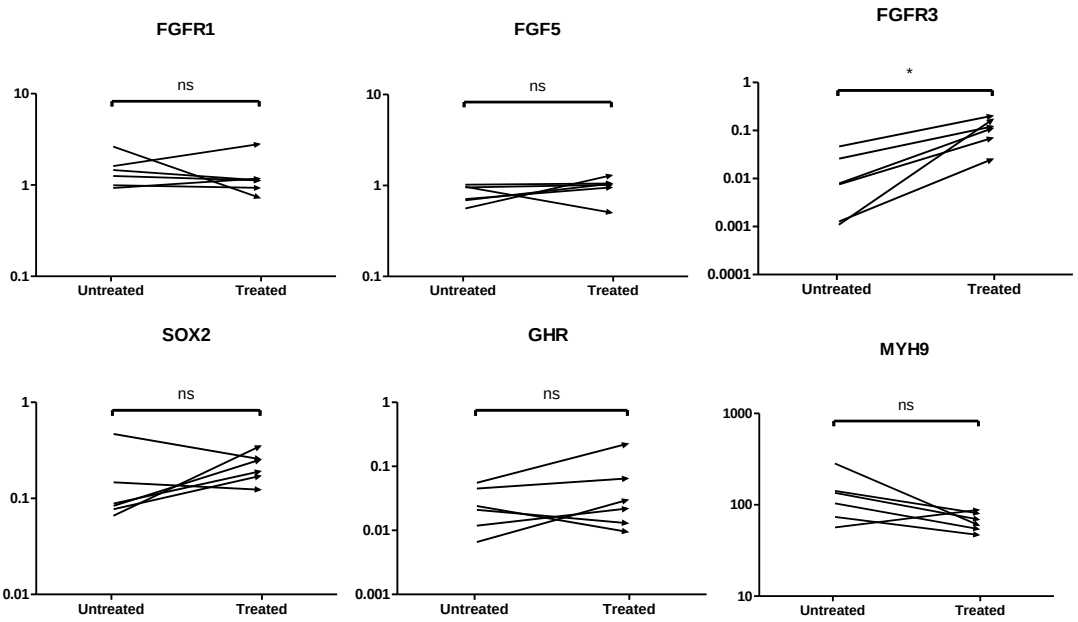

Figure 7.10 - Graphical depictions of gene expression changes between treated and untreated cells in miscellaneous transcripts. Graphs on a logarithmic scale and results expressed as fold changes (n=6). * = P ≤ 0.05.

7.3.8 Genes that were flagged due to potentially erroneous results or non-expression

Some genes (Table 7-11) were flagged by the software as having Ct values that were questionable. The questionable Ct values and thus fold changes often resulting in very, and very variable between donors large fold changes. These were noted as being inconclusive and these results were not analysed further.

Finally, *BMP5* was undetermined in all samples both before and after MI192 treatment, so no conclusions could be drawn other than ADSCs must have a low expression of *BMP5*.

Table 7-11 - Genes that were flagged due to potentially erroneous results. No transcripts were significantly up or down-regulated.

Gene	Fold Change	P Value	Notes
CLEC4M; CD209	14.40	ns	Up-regulated 14.4 fold in one donor, from undetermined to determined in 4 donors and down regulated from determined to undetermined in 1 donor.
LPL	43.39	ns	Very varied expression changes, including up and down regulations. Data not reliable at all.
WIF1	-1655.11	ns	Overall trend of up-regulation, however with one donor with a huge down-regulation, and overall widely variable changes.
SP7	-1317.68	ns	Overall trend of down-regulation, but with widely variable changes and with one donor having no expression in MI192 treated and untreated samples.
OMD	-1307.61	ns	Varied expression changes, including up and down regulations. Down-regulation from determined to undetermined from 3 donors. Overall trend of down-regulation.
IFNG	-448.23	ns	Very varied expression changes, including up and down regulations. Data not reliable at all.

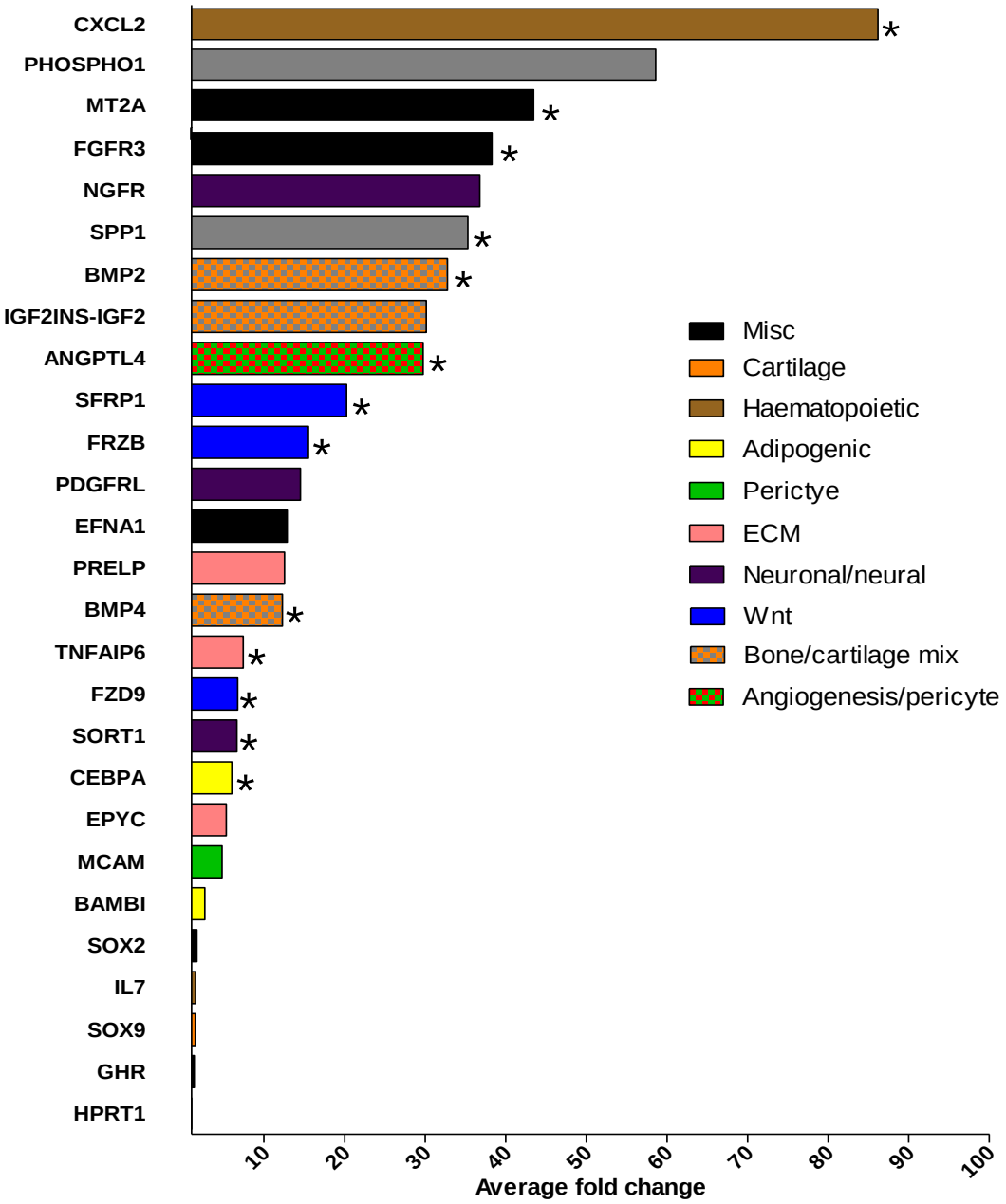

Figure 7.11 – Up-regulated fold changes grouped. Graph indicating the average fold change for every up-regulated transcript with MI192 treatment. HPRT reference gene is set to 1. A number greater than 1 indicates an up-regulation. Statistical significant ($P \leq 0.05$) indicated on the graph with a *. Any gene with a donor number less than 4, or with abnormal amplification curves were removed from the graph.

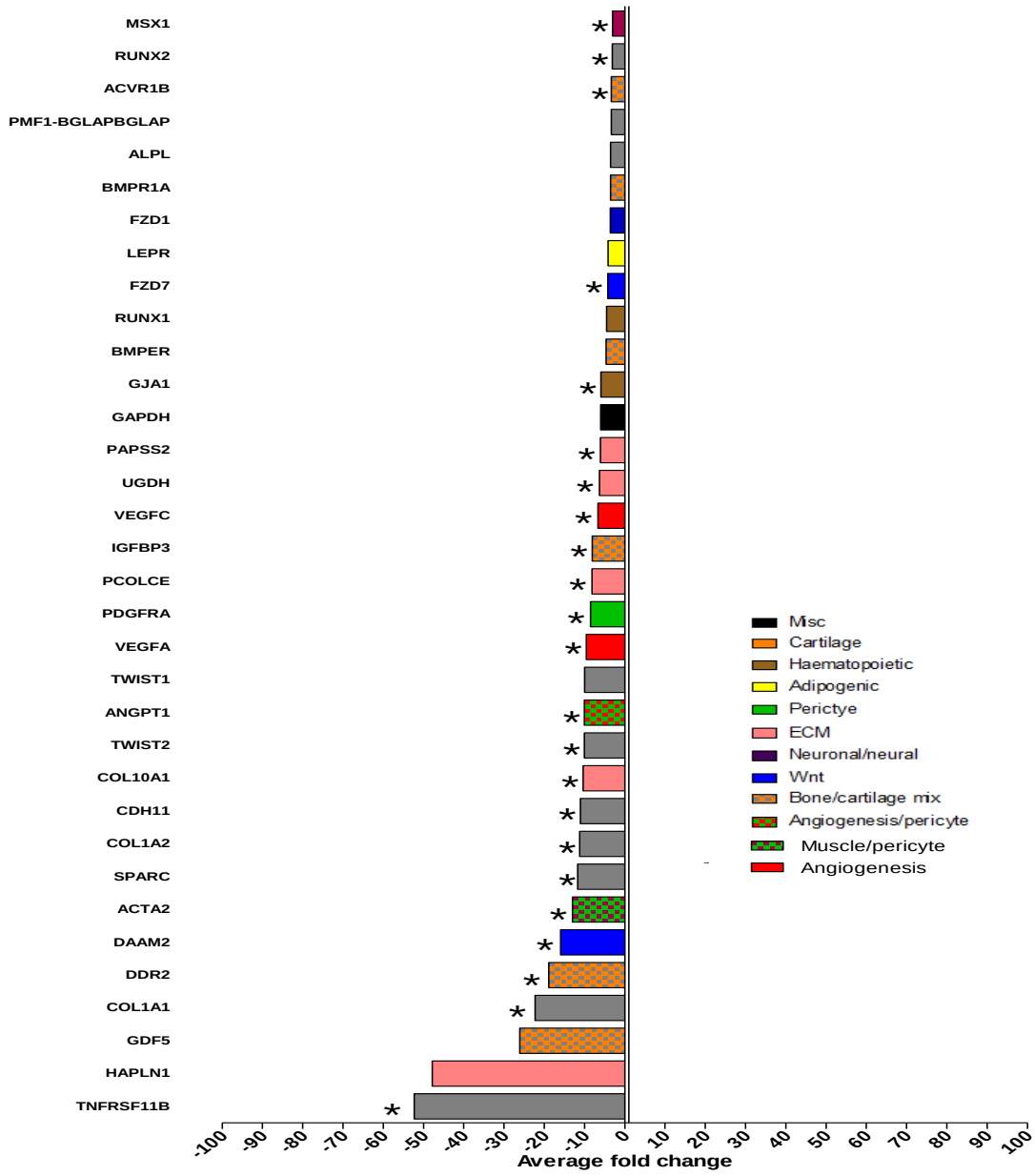

Figure 7.12- Down-regulated fold changes grouped. Graph indicating the average fold change for every down-regulated transcript with MI192 treatment. HPRT reference gene is set to 1. A number less than 1 indicates a down-regulation. Statistical significant ($P \leq 0.05$) indicated on the graph with a *. Any gene with a donor number less than 4, or with abnormal amplification curves were removed from the graph.

7.4 Discussion

Those genes in which a noticeable change with MI192 treatment will be discussed. Where relevant, those where no change was observed will be discussed, otherwise the results won't be discussed for conciseness.

7.4.1 The effect of MI192 treatment on the expression of Wnt related transcripts in ADSCs

MI192 had a strong effect on several transcripts linked to the Wnt/β-catenin pathway. The Wnt/β-catenin pathway is a key pathway in MSC differentiation, with complicated and wide ranging effects. When activated, Wnt ligands combine with frizzled receptors and co-receptors, such as lipoprotein receptors, to facilitate β-catenin accumulation. This inhibits glycogen synthase kinase-3β (GSKβ3), and the β-catenin enters the nucleus, regulating many proteins and subsequent pathways. Related to this investigation, Wnt signalling is an upstream activator of *BMP2* expression in osteoblasts, and the cross talk that occurs between Wnt and BMP2 signalling is essential for both osteogenic differentiation and skeletal maintenance. Increasing Wnt signalling causes MSCs to begin to differentiate into osteoblasts, and continued signalling triggers these pre-osteoblast cells to develop into mature osteoblasts, leading to ALP activation and mineralisation, which also needs Wnt and BMP signalling (Zhang et al. 2013; Enomoto-Iwamoto et al. 2002). It is known that some osteogenic differentiation altering methods, such as mechanical loading, affect the Wnt pathway, one way or another (Vrtačnik et al. 2013). Interestingly, activated Wnt signalling can also result in both the degradation of adult cartilage, the chondrogenic differentiation of MSCs and inhibition can cause the apoptosis of adult chondrocytes. In addition to this, Wnt signalling maintains the undifferentiated states of human and mouse ESCs (Sato et al. 2004). Furthermore, Wnt/β-catenin signalling is known to enhance neuronal differentiation (Yu et al. 2013).

Burba et al. (2011) found VPA to treatment of $CD34^+$ HSCs up-regulated the expression of Wnt pathway transcripts *WNT1* and *FZD1*. They suggested that this could be a sign of the enhanced self-renewal, as these pathways are a key regulator of stem cells in the stem cell niche (Burba et al. 2011).

7.4.1.1 The effect of MI192 treatment on the expression of Wnt modulating *FRZB*, *SFRP1*, *SRFP4*, *DAAM2* and *DVL2* transcripts

FRZB, which was up-regulated with MI192 treatment, encodes for a Wnt modulating protein key to bone and cartilage development, regulating skeletalgenesis, long bone formation and chondrocyte maturation. It is thought that the increased levels of this are linked to an increase in chondrogenic differentiation (Thysen et al. 2015).

Secreted frizzled-related proteins (SFRPs) act as modulators of Wnt signalling. There was a large up-regulation of *SFRP1* and a very small down-regulation of *SRFP4*. *SFRP1* is a Wnt transcript, which modulates the Wnt pathway linked to bone, cartilage and osteoblast differentiation and inhibition of osteoclasts (Thysen et al. 2015). SFRP4 is a member of the SFRP family that contains a cysteine-rich domain homologous to the putative Wnt-binding site of frizzled proteins. The expression of *SFRP4* in ventricular myocardium correlates with apoptosis related gene expression. SFRP4 is a Wnt pathway antagonist, inhibiting the pathway, while lowering BMP2 levels (Wagner et al. 2005).

Up-regulation of *FRZB* and *SFRP1*, combined with down-regulation of SFRP4, may (partially at least) explain the pathway by which MI192 improves osteogenic differentiation potential of ADSCs. FRZB and SFRP1 are involved in chondrogenic and osteogenic Wnt related pathways. An increase in the transcript levels of *SRFP1* indicates an increase in Wnt signalling potential. Also, the decreased levels of SRFP4 and increased levels of FRZD proteins are associated with undifferentiated MSCs. Down-regulation of the antagonist *SFRP4* allows for increase Wnt signalling in the cells (Wagner et al. 2005; Thysen et al. 2015).

DAAM2 encodes dishevelled associated activator of morphogenesis 2 protein, which is known to amplify Wnt signalling. It is possibly related to spinal cord development and general cell actin cytoskeleton function (Lee et al. 2015), and the strong down-regulation of this indicates the MI192 treated cells are not being amplified for this.

7.4.1.2 The effect of MI192 pre-treatment on the expression of Wnt receptor transcripts *FZD1*, *FZD4*, *FZD7*, *FZD8* and *FZD9*

FZD1, *FZD4*, *FZD7*, *FZD8* and *FZD9* are all transcripts for Wnt receptors, and their individual functions are not very well understood. They act as part of the Wnt/β-catenin pathway (Burba et al. 2011; Reya et al. 2001).

FZD7 was down-regulated with MI192 treatment, and *FZD9* up-regulated, which may give more insight into which receptors are involved in these Wnt signalling pathways. In the literature, for example, *FZD1* is up-regulated in HSCs treated with VPA (Burba et al. 2011). Here, only *FZD9* expression is up-regulated with MI192 treatment, perhaps indicating it the key receptor of these in the Wnt pathway when activated by HDAC2 and HDAC3 inhibition, or by the other Wnt related proteins potentially increased with MI192 treatment. For the other receptors (*FZD1*, *FZD8* and *FZD4*) the responses to MI192 treatment were mixed between donors.

7.4.1.3 The effect of MI192 treatment on the expression of Wnt Targets *NANOG*, *POU5F1*, and SOX2

NANOG and *POU5F1* encode proteins (Nanog homeobox and POU domain, class 5, transcription factor 1, also known as Oct-4, octamer-binding transcription factor 4)). They are transcription factors related to the pluripotency of ESCs and are two of the four famous key factors utilised in generation of pluripotent stem cells from adult cell sources (Takahashi et al. 2007). They are key Wnt targets and can be utilised as markers for undifferentiated cells, and are essential for maintaining the self-renewing undifferentiated state. NANOG acts to bind SMADs, regulators of BMP, blocking BMP function and preventing mesoderm differentiation (Gaarenstroom & Hill 2014). In this study, both *NANOG* and *POU5F1* transcript levels are almost unchanged in the MI192 treated cells ($P > 0.05$). It has been suggested in the literature that treatment with HDACis (here TSA and VPA) decreases the levels of NANOG and POU5F1 in cell lines of malignant testicular germ cell tumour cells (Schweyer 2013). However, here there is a lack of change in *NANOG* and *POU5F1* expression with HDAC inhibition. *SOX2* encodes Sox2, a transcription factor that is essential for maintaining self-renewal, or pluripotency, of undifferentiated ESCs. This was also unchanged with MI192 treatment.

This blanket lack of change in these transcripts indicates that the pluripotency, or ESC like capacity, of the ADSCs cells is maintained, and certainly not decreased, with MI192 treatment.

7.4.2 The effect of MI192 treatment on the expression of early cartilage and bone related transcripts in ADSCs

Markers linked to the early stages of bone and cartilage differentiation have been grouped together. The change in expression of these genes may account for why pre-treatment of ADSCs with MI192 leads to an increased sensitivity to osteogenic differentiation protocols.

7.4.2.1 *BMP2*, *BMPR1a*, *BMP4*, *BMPER*, *NOG* and *GDF5*

A key finding from this study was finding that fact *BMP2* was significantly up-regulated with MI192 treatment. *BMP2* encodes for bone morphogenetic protein 2 (BMP2), and is perhaps the most explored protein in the osteogenic differentiation pathway, due to investigations into its potential clinical application (Carragee et al. 2011). BMP2 binds to BMPR1a and 1b, but also interacts with many targets, especially in osteogenic differentiation linked signalling pathways (Jang et al. 2012). Unfortunately *BMPR1B* was not on the card, but the expression of *BMPR1A* was found to be slightly down-regulated. The BMP2 pathway crosstalks with the aforementioned Wnt pathway, and it is believed Wnt signalling is an upstream regulator of BMP signalling (Zhang et al. 2013). Despite its bone-related name, BMP2 acts in many pathways, such as cardiac differentiation (van Wijk et al. 2007), and not just in osteogenic differentiation pathways. Here, the BMP2 pathway seems to be up-regulated with MI192 treatment.

BMP4 is responsible for early chondrogenesis, and can induce MSCs down a chondrogenic lineage (Karamboulas et al. 2006; Hatakeyama et al. 2004). *BMP4* was up-regulated in MI192 treated ADSCs, and this is similar to findings in the literature, where TSA treated P19 embryonic carcinoma cell line cells showed increased levels of *BMP4* (Karamboulas et al. 2006). *BMPER* encodes BMP binding endothelial regulator (BMPER), which is a BMP4 inhibiting protein (Moser et al. 2003). *BMPER* was down-regulated with MI192 treatment. *NOG* encodes for

Noggin, another BMP pathway inhibiting protein (Zhang et al. 2013), which was unaffected with MI192 treatment.

BMP2 and *BMP4* encode proteins key to the promotion of osteogenic differentiation of stem cells. The observed increase of Wnt signalling in the MI192 treated cells may account for their elevated transcription, as increased Wnt signalling in cells is known to lead to an increase in *BMP2* and *BMP4* levels (Zhang et al. 2013). The fact *BMP2* and *BMP4* are significantly up-regulated with MI192 treatment, with *BMPER* encoding an inhibitor for these pathways, significantly down-regulated is very interesting.

Finally, *GDF5* encodes growth/differentiation factor-5, a member of the TGF-β super family, is responsible for later stage chondrogenesis (following on from BMP4 in the pathway), and promotes chondroprogenitor cell aggregation (Hatakeyama et al. 2004). *GDF5* was down-regulated in all donors, so the fact this was not significant is unusual, and there is a definite trend of down-regulation. GDF5 is involved downstream in chondrogenic differentiation to BMP4, indicating that MI192 treatment might be inducing the earlier stages of chondrogenic differentiation.

7.4.2.2 *IGF2* and *IGFBP3*

IGF2 and IGFBP3 may also be linked to osteogenic differentiation. MI192 treatment had the opposite effect on these transcripts, largely up-regulating *IGF2* but down-regulating *IGFBP3*. *IGF2* encodes insulin-like growth factor 2, which is thought to trigger osteogenic differentiation in MSCs and ESCs (Ding et al. 2015; Kang et al. 2012). Insulin-like growth factor-binding protein 3 (IGFBP3) is a binder and a blocker of BMP2 and BMP4 (Zhong et al. 2011), and is thought to regulate and inhibit bone formation (Silha et al. 2003). An increase in *IGF2* and a decrease in *IGFBP3* with MI192 treatment may help account for the increased osteogenic potential of these cells. The down-regulation of *IGFBP3* fits the picture with the up-regulation of BMP2 and BMP4.

7.4.2.3 *ACVR1B* and *ACVR2A*

ACVR1B encodes activin receptor type-1B, a growth factor part of the transforming growth factor-beta (TGF-beta) superfamily of structurally related signalling proteins.

ACVR1B can bind to activin receptor type-2A, a receptor type protein encoded by *ACVR2A*. Both of these were statistically significantly ($P \leq 0.05$) down-regulated with MI192 treatment. They transmit signals to receptor-regulated SMAD2 and SMAD3, resulting in the transcription of genes that function as inhibitory regulators of proliferation. This acts differently to BMP signalling, which through other receptors such as BMPR1a, transmit their signals through SMAD1, SMAD5 and SMAD8, initiating osteogenic differentiation. These two signalling pathways have compete for binding of a co-SMAD, SMAD4, interfering in signalling with each other. Inhibition of SMAD2/3 activates SMAD1/5/8 signalling, and therefore increasing osteogenic differentiation. It is believed that it is the targeting and inhibition of ACVR1B by microRNA miRNA-210, which results in the improved osteogenic differentiation seen when this mRNA is utilised (Mizuno et al. 2009; Maeda et al. 2004). Here MI192 treatment results in the down-regulation of *ACVR1B* and *ACVR2A*, which may act in the same way as miRNA-210, inhibiting the TGF-β/activin signalling pathway, resulting in more SMAD4 being available to take part in BMP signalling pathways, in turn, resulting in increased osteogenic differentiation. Alternatively, the up-regulation of *BMP2* and *BMP4* may be accounting for the increase in these transcripts. Either way this is part of an overall explanation for the increased osteogenic differentiation potential observed with MI192 treatment.

7.4.2.4 *RUNX2*, *TWIST1*, *TWIST2* and *DDR2*

Runx2, encoded by *RUNX2*, is the key bone transcription factor, activated by Wnt and BMP signalling, known to form a complex with HDAC3 (Schroeder et al. 2004). Here, inhibition of *RUNX2* expression was demonstrated with MI192 treatment. *RUNX2* expression was also investigated in Chapter 5: 5.3.4, where the inhibition of *RUNX2* at an early stage was also seen, the reasons for this were extensively discussed.

TWIST1 and *TWIST2* encode for twist transcription factor proteins, which are antagonists of Runx2 (Bialek et al. 2004). *TWIST2* is clearly down-regulated with MI192 treatment, while *TWIST1* is down-regulated in 4 of 6 donors, so there is a trend of down-regulation, but it is inconclusive. The up-regulation of these two genes with MI192 treatment could have accounted for the down-regulation of *RUNX2*; however, this is clearly not the case here. It may be that this whole pathway is down-regulated with HDAC2/HDAC3 inhibition. TWIST-1 and TWST-2

proteins transiently inhibit Runx2 proteins during osteogenic differentiation, and their inhibition is necessary for osteoblast differentiation to take place (Bialek et al. 2004). A down-regulation of these genes does indicate an increased osteogenic differentiation potential, and it may be that this down-regulation allows a later increase in the Runx2 levels and osteogenic differentiation potential of the MI192 treated cells.

DDR2 encodes discoidin domain-containing receptor 2, a receptor tyrosine kinase (RTK) linked to bone, a key osteoblast regulator. It is a cell surface receptor, with fibrillar collagen as a ligand, which regulates cell differentiation, cell migration, cell proliferation and remodelling of the extracellular matrix. It is required for normal bone and cartilage development and regulates osteoblast differentiation and chondrocyte maturation via the activation of Runx2 (Y. Zhang et al. 2011). Increased levels of DDR2 protein leads to an increase of Runx2 activity, and in the MI192 treated ADSCs, *DDR2* expression is significantly down-regulated, which would be expected given the down-regulation of Runx2.

The decrease in the expression of *RUNX2* and Runx2 antagonist *TWIST1* and *TWIST2*, along with the down-regulation of *DDR2* that can activate Runx2, indicates that this pathway is not being engaged when the cells are inhibited with MI192. This gives some clues as to the pathway by which HDAC3/2 inhibition is improving the osteogenic differentiation of these cells, likely through BMP2 and BMP4 and not through GDF5 or direct activation of Runx2. The activation of the BMP and Wnt pathways may later lead to a later than 2 day increase in *RUNX2*, and other osteogenic transcripts.

7.4.2.5 Chondrogenic transcription factors – *SOX9*, *RUNX2* and *DDR2*

Chondrogenic transcription factor Sox9 is expressed by proliferative, but not hypertrophic, chondrocytes. It is used as a marker of early chondrogenic differentiation of MSCs, and forced over expression induces chondrogenesis in MSCs (Tsuchiya et al. 2003). Sox9 induces expression of components of cartilage matrix such as collagen type II (Lefebvre & Smits 2005). However here, expression of *SOX9* varied between donors and results were inconclusive.

The aforementioned down-regulated transcription factor Runx2 is also an important transcription factor in cartilage development. In hypertrophic cartilage Runx2 activates hypertrophic chondrocyte genes, such as *COL10A1*, which encodes collagen type X. Runx2 and Sox9 interact, and Runx2 is repressed by Sox9 (Zhou et al. 2006). Another marker of early chondrogenic differentiation mentioned earlier is DDR2 protein, which regulates chondrocyte maturation via the activation of Runx2 (Y. Zhang et al. 2011). *DDR2* expression was down-regulated in the MI192 treated cells, in line with the reduction also seen in *RUNX2*.

7.4.2.6 The Wnt/β-catenin pathway

In MI192 treated cells secreted Wnt pathway antagonist Frzb-1 (*FRZB*) is up-regulated 15.5 fold. Frzb-1 is expressed by prehypertrophic chondrocytes and is likely to act as an endogenous modulator of Wnt's effects on chondrocyte maturation (Enomoto-Iwamoto et al. 2002). It is a modulator of the Wnt pathway and over expression will inhibit the Wnt pathway, preventing chondrocyte maturation and processes such as endochondral ossification. Up-regulation of this gene indicates that these MI192 treated cells may be becoming less mature cartilage cell like, and more cartilage progenitor cell like, an early chondrocyte cell type (Mackie et al. 2008).

7.4.3 The effect of MI192 treatment on the expression of later stage bone related transcripts in ADSCs

The increase in the osteogenic differentiation potential of the ADSCs treated with MI192 for two days is known and proven in previous chapters. This may be as a result of the up-regulation of some of the transcripts affected by MI192 pre-treatment explored with this experiment. The up-regulation of several early markers of osteogenic differentiation has been seen, so later markers of bone differentiation, key to osteoblastic differentiation and those involved in biomineralisation, have been grouped together for discussion.

7.4.3.1 The down-regulated later stage markers of osteogenic differentiation - *ALPL*, *SPARC*, *PMF-BGLAP*, *TNFRSF11B*, *CDH11*, *COL1A1* and *COL1A2*

The majority of the later stage markers of osteogenic differentiation investigated were down-regulated with MI192 treatment of ADSCs, compared to control cells untreated with MI192.

ALPL is the gene responsible for alkaline phosphatase, a key enzyme to cell mineralisation and discussed at length in Chapter 5: 5.3.4. The initial down-regulation of *ALPL* is likely as a result of the down-regulation of other osteogenic markers, such as *RUNX2*, and is in line with the previous results, where *ALP* was also down-regulated at an early time point after MI192 treatment. Also explored in Chapter 5: 5.3.4 was *PMF-BLGAP* (encoding for BGLALP/Osteocalcin/OCN). In this study it was down-regulated 3.5 fold (although not statistically significant, there was a down regulation in 5 of the 6 donors), which is also in line with the data on early expression of *PMF-BLGAP* in ADSCs, where MI192 treatment lead to a drop in *PMF-BLGAP* expression.

Collagen production is another sign of the medium to late stages of osteogenic differentiation, with collagen being a key organic structural component of bone (Junqueira et al. 1979; Donald L. Bartel et al. 2006; Pocock & Richards 2006). In this study, the transcript levels of *COL1A1* and *COL1A2* were down-regulated highly in the MI192 treated cells, (22 and 11 fold respectively, $P \leq 0.05$). This matches the results from Chapter 5: 5.3.4, where the expression of *COL1A1* was found to be down-regulated at the early (day 3) time point of the MI192 treated cells. That study found it was down-regulated below even the basal control. The combined results of these two studies indicate that MI192 treatment inhibits genes linked to collagen formation.

Other later stage markers of osteogenic differentiation in MSCs on the card were proteins found in mature osteoblasts, including *SPARC* (encoding for Osteonectin/ON), *TNFRSF11B* (encoding for OPG/Osteoprotegrin) and *CDH11* (encoding Cadherin-11). They were all statistically significantly ($P \leq 0.05$) down-regulated by MI192 pre-treatment.

The decrease in these genes related to the later stage markers of osteogenic differentiation, along with the increase in so many earlier stage markers of osteogenic differentiation, may indicate that the cells are becoming more primed and with a greater osteogenic potential, rather than actually starting down the osteogenic differentiation potential process itself. After all, this is after only two days of treatment, the later stages of differentiation should not be expressed prematurely. Previous work (in Chapter 5: 5.3.4) suggests that, ADSCs still need osteogenic medium/stimulus to begin osteogenic differentiation; treatment with MI192 alone does not result in osteogenic differentiation. These results provide an explanation of that.

7.4.3.2 The up-regulated later stage markers of osteogenic differentiation - *SPP1*, *PHOSPHO1*

Not all later stage markers of osteogenic differentiation were down-regulated; *SPP1* and *PHOSPHO1* were both found to be up-regulated with MI192 treatment.

SPP1 encodes osteopontin (OPN), which is found in osteoblasts and is an extracellular structural protein forming part of the organic component of bone. In this study, the expression was convincingly up-regulated in 6 donors with MI192 treatment. The results are conflicting, as previously, in Chapter 5: 5.3.4, the expression of *SPP1* was down-regulated with MI192 treatment (across all time points). A full discussion of the role of osteopontin, especially with regards to mineralisation, was undertaken there. The differences in these results may arise due to the additional growth in osteogenic medium the cells underwent in the other study. The initial increase of *SPP1* expression may indicate an un-readiness of the cells to mineralise yet, preventing mineralisation and fitting the picture of the cells become more osteo-progenitor like, and less like more mature osteogenic cells.

Furthermore, expression of *PHOSPHO1*, encoding phosphoethanolamine/ phosphocholine phosphatase, a protein that plays a role in inorganic phosphate cell formation was up-regulated with MI192 treatment. Since the expression of *SPP1* and *PHOSPHO1* are linked, and PHOSPHO1 is regulated by OPN, so if one is up-regulated, so should the other be (Yadav et al. 2014). These mineralisation linked genes are up-regulated earlier than others mineralisation genes in the MI192

treated cells, which may indicate the pathway by which ADSCs display an increased mineralisation potential when treated with MI192.

7.4.4 The effect of MI192 treatment on the expression of cartilage and bone extracellular matrix formation related transcripts in ADSCs

The effect of MI192 on the expression genes related to the extracellular matrix formed in bone and cartilage (although also many other tissues) was investigated.

7.4.4.1 Down-regulated extracellular matrix (ECM) related transcripts – *PCOLCE*, *PAPSS2*, *HAPL1*, *UGDH* and *COL10A*

PCOLCE encodes procollagen C-endopeptidase enhancer 1, a pre-collagen protein is involved in collagen formation (Bourhis et al. 2013), down-regulated by MI192 pre-treatment. Similarly, *PAPSS2* was also down-regulated, which encodes a sulfation protein, with wide reaching roles, known to be a key extracellular matrix protein linked to osteochondral tissue formation. It was reported that silencing of *PAPSS2* expression significantly decreased ALP activity and mineralization, inhibiting *OPN* and *COL1* expression, while over expression lead to osteoblast development and mineralisation in osteoclast like cells (Wang et al. 2012). Another gene down-regulated with MI192 treatment was *HAPL1*, which encodes hyaluronan binding link protein, a cartilage proteoglycan link protein key to cartilage and bone structure (Mundlos et al. 1991). UDP-glucose 6-dehydrogenase (*UGDH*), another extracellular matrix linked gene, was down-regulated 6.3 fold in MI192 treated cells. UGDH is an enzyme key in GAG formation, known to enhance chondrogenesis in models of cartilage formation (C. E. Clarkin et al. 2011; Claire E. Clarkin et al. 2011). Finally, *COL10A1* which encodes for collagen, type X was statistically significantly down-regulated in the MI192 treated cells. Type X collagen is key in endochondral ossification, in new bone formation (Shen 2005). DDR2 acts as a receptor for type X Collagen (Leitinger & Kwan 2006), and the down-regulation of *DDR2* was mentioned earlier; their combined down-regulation is likely linked.

7.4.4.2 Up-regulated extracellular matrix (ECM) related transcripts – *COL2*, *TNFAIP6*, *EPYC*, *CHAD* and *PRELP*

Collagen 2, encoded by *COL2*, is the key collagenous component of cartilage (Kessler & Grande 2008), and was strongly up-regulated with MI192 treatment. Collagen 1 gene expression levels are down-regulated in the MI192 treated cells, so the cells are being primed for collagen II and not collagen I formation. This could indicate that these cells are stimulated to undergo an endochondral ossification type pathway (Chen et al. 2012), although without the initial involvement of the down-regulated of type X collagen.

TNFAIP6 and *EPYC* were also, although not strongly, up-regulated with MI192 treatment. TNFAIP6 encodes tumour necrosis factor alpha induced protein 6, which is related to binding of hyaluronan and protects against cartilage matrix destruction (Blundell et al. 2003). *EPYC*, which was up-regulated although not significantly, encodes epiphycan, a proteoglycan that regulates fibrillogenesis, playing a role in ECM formation of bone and cartilage (Kurita et al. 1996; Wang et al. 2009). *CHAD* encodes chondroadherin protein, which is known to mediate adhesion of isolated cells, and may be central for maintaining the adult chondrocyte phenotype and cartilage homeostasis (Haglund et al. 2011). MI192 treatment also resulted in up-regulation of *CHAD* expression in ADSCs. *PRELP* encodes proline arginine-rich end leucine-rich repeat protein, which is found in connective tissue extracellular matrix. It binds collagen type I and type II and the basement membrane heparan sulfate proteoglycan perlecan (Bengtsson et al. 2002). When gene expression in tissues was analysed, there were high levels of this gene found in adult cartilage and low levels in juvenile cartilage, so it can be utilised as a late stage marker of chondrogenesis (Grover et al. 1996). *PRELP* was also up-regulated (although not a completely true picture only in 4 of 6 donors).

The up-regulation of these specific ECM related genes could indicate by which pathways the early stage osteogenic/endochondral ossification related transcripts act. They may be as a direct result of MI192 treatment (i.e. HDAC2 or HDAC3 inhibition).

7.4.5 The effect of MI192 treatment on the expression of adipogenic transcripts in ADSCs

Adipogenic differentiation was always thought of as the classical opposite of osteogenic differentiation; however, some genes control aspects of both (Ducy et al. 2000). It has been proven in Chapter 5: 5.3.7 that MI192 pre-treatment strongly inhibits future adipogenic differentiation. In this chapter, the results aim to answer the question of the how the adipogenic related genes were initially affected when the cells were treated with MI192.

7.4.5.1 *PPARγ*, *FABP4, CEBPA* and *LEPR*

The expression of *PPARγ* was found to be down-regulated in Chapter 5: 5.3.7, even with cultured in medium containing a PPARγ activator, where its function as an adipogenic transcription factor was discussed extensively. Unfortunately the results from this study were inconclusive regarding *PPARγ*, which was due to the varied response across different donors.

FABP4 is another adipogenic related transcript, coding for fatty acid binding protein, and used as a marker of late stage adipogenic differentiation. It is PPARγ responsive and in the literature HDAC3 inhibition was found to increase levels of *FABP4* expression (Jiang et al. 2013). In this study *FABP4* expression in MI192 treated cells was up-regulated; however, the results were not statistically significant ($P > 0.05$), likely due to only 3 donors having been analysed. However, the trend of up-regulation is still clear. However, a study by Catalioto et al. found that HDAC inhibition by MS-275, SAHA and VPA (Catalioto et al. 2009), strongly reduced *FAB4* levels in human white preadipocytes, opposite to the results of treatment with MI192. CD271+ sorted cells were also found to have high levels of FABP4 expression, indicating a steady-state engagement with adipogenesis, which may be the same with the MI192 treated cells (Churchman et al. 2012). The links between CD271+ cells and MI192 treated cells are discussed at length later (in 7.4.8).

CEBPA, encodes for CCAAT/enhancer-binding protein alpha, a protein involved in body weight homeostasis, with increased levels found in adipogenic differentiation of MSCs (Sekiya et al. 2004). *CEBPA* was strongly up-regulated with MI192 treatment.

LEPR, which was down-regulated with MI192 treatment, encodes leptin receptor. Leptin is a small polypeptide hormone secreted primarily by adipocytes, which is involved in control of body weight, and is linked to obesity. However, it also is an important regulator of bone mass, and controls the balance between bone and fat in the bone marrow (Ducy et al. 2000), although this can be time frame dependent (Gordeladze et al. 2002). The down-regulation of *LEPR* in MI192 treated cells may indicate a reduction in cells in susceptibility to Leptin. This may result in a reduction of the osteogenic differentiation potential of these cells, as leptin is known to increase bone formation, while it is also associated with adipogenic lineages.

The results from several of the genes (*BAMBI*, *PPARγ*, *LPL* and *TGFBR2*) were also inconclusive, so the complete effect of MI192 on the adipogenic potential of these cells remains unclear. Although with the increases in *FABP4* and *CEBPA* expression, along with the decrease in *LEPR* would suggest an overall increase in adipogenic differentiation potential of these cells. This does not really explain why when pre-treated with MI192 and then cultured in adipogenic medium there is a large decrease in adipogenic differentiation of these cells.

7.4.6 The effect of MI192 treatment on the expression of stromal related transcripts in ADSCs

The effect of MI192 on some markers connected with muscle, connective, blood and bone marrow like tissue in ADSCs was also measured.

7.4.6.1 Angiogenesis transcription factors – VEGFA, VEGFC and ANGPT1

Both *VEGFA* and *VEGFC* (vascular endothelial growth factors A and C) are part of the VEGF family, and are down-regulated with MI192 treatment. This family of transcription factors encode proteins that control a large number of processes, including angiogenesis, vasculogenesis and endothelial cell growth (Gerber et al. 1999). VEGFA and VEGFC proteins also act as are promoters of cell migration, inhibitors of apoptosis and are important in the later stages of cartilage formation, as well as for vasculature growth in bone (Zelzer et al. 2004; Kozhemyakina et al. 2015). VEGFA is produced in osteoblasts in response to BMP2, BMP4 and BMP6 signalling and is key to angiogenesis of bone (Deckers et al. 2002). However, here

it seems the elevated levels of *BMP2* and *BMP4* have not resulted in elevated levels of *VEGFA* (levels were down with MI192 treatment). This may be because the cells have not had time to response to these increases yet. Another transcription factor down-regulated with MI192 treatment is *ANGPT1*, which encodes Angiopoietin-1. Angiopoietin-1 belongs to the angiotrophic family, and is key to vasculature maturation, through pericyte recruitment, as well we being involved in the second stage of angiogenesis (Kosacka et al. 2006; Thurston 2003).

Strongly up-regulated on treatment with MI192 treatment, and also from the angiotrophic family *ANGPTL4*. This encodes for angiopoietin-like 4, a protein expressed highly in adipose tissue, liver, and placenta, repressed by leptin and activated by ligands of peroxisome-activated receptors (e.g. PPARγ) (Ge et al. 2005). It has actually been found to inhibit angiogenesis in *in vitro* models (Okochi-Takada et al. 2014).

The down-regulation of *ANGPT1*, *VEGFA* and *VEGFC*, along with the up-regulation of *ANGPTL4*, indicates treatment with the MI192 may inhibit angiogenesis, which could have effects on the formation of tissue such as bone in the long term. If MI192 was considered for long term use, or even with the pre-treatment of cells for bone formation, the effect on the ability of the bone to vascularise would need to be investigated.

7.4.6.2 Pericyte transcripts - *CSPG4*, *MCAM*, *ANGPT1*, *ACTA2*, *PDGFRA* and *PDGFRL*

Pericytes are the cells that wrap around the endothelial cells of capillaries and vasculature. *CSPG4* (chondroitin sulfate proteoglycan 4), *ANGPT1* (encoding angiopoietin-1), *ACTA2* (encoding for smooth muscle actin), and *PDGFRA* (encoding for alpha-type platelet-derived growth factor receptor) were all down-regulated (Churchman et al. 2012). The majority of the pericyte markers identified by Churchman et al. were down-regulated, statistically significantly ($P \leq 0.05$) after treatment with MI192. The exceptions were *PDGFRL*, encoding platelet-derived growth factor receptor-like, which had inconclusive results and *MCAM*, which was up-regulated, although not statistically significantly (It was up-regulated in 5 of 6 donors, $P > 0.05$)

Apart from the increase in *MCAM*, the down-regulation of all of these markers indicates the cells are becoming less pericyte like. MCAM is highly expressed in blood vessels, smooth muscles and pericytes, although its function is not well understood and is a commonly used marker of multipotent mesenchymal stromal cells. MCAM is also known as CD146 and the expression of this was found to be increased on ADSCs treated with MI192 for two days in Chapter 4: 4.3.7. These results complement each other. This increase in surface marker can be accounted for by this increase in gene expression. MCAM is thought to be involved in interactions of MSCs and other cells with endothelial cells (Robey 2011; Covas et al. 2008). The up-regulation of this is interesting and may be indicative of these cells becoming more multipotent and less committed to a lineage, such as the pericytes lineage.

7.4.6.3 Hematopoietic stem cell (HSC) related transcripts - *GJA1*, *RUNX1*, *JAG1*, *CXCL12* and *GATA2*

GJA1 encodes gap junction protein alpha 1, which is also known as connexin 43 (Cx43). This protein is found in high levels in osteoblasts, a population of osteo-progenitor cells and HSCs, and is key to the communication of these cells, especially homing of cells, in the bone marrow niche (Gonzalez-Nieto et al. 2012). The down-regulation of *GJA1* with MI192 treatment may indicate the cells becoming less mature, as they are key to the maturation of several tissue types such as the blood (Montecino-Rodriguez et al. 2000).

Also down-regulated, *RUNX1* encodes Runx1, a transcription factor that regulates the differentiation of HSCs into mature blood cells, and is widely expressed in mature hematopoietic cells, so is possible required for HSC maturation (Huang et al. 2008). A down-regulation of this may indicate an increasing naivety and more stem cell like profile being adopted by the MI192 treated cells, becoming less adult regarding hematopoietic lineages. However, conclusions cannot be fully drawn as this trend is only strongly observed in one donor, and several remain unchanged.

Changes in *JAG1*, *CXCL12* and *GATA2* expression with MI192 treatment were minimal and inconclusive. GATA2 encodes GATA binding protein 2, a transcription factor that is expressed in hematopoietic progenitors, and also in ESCs. Interestingly, research has shown that HDAC3 associates with GATA2, repressing

GATA2 transcription (Ozawa et al. 2001). Inhibiting HDAC2 and HDAC3, with MI192, at least in the short term, appears to have had had no effect on the expression of *GATA2* in the ADSCs.

The down-regulation of *RUNX1* and *GJA1* may indicate movement away from hematopoietic cell type, although related genes *JAG1*, *CXCL12* and *GATA2* are relatively unaffected.

7.4.6.4 *CXCL12 and CXCL2*

CXCL2 is a human chemokine that is known to bind the CXCR2 receptor and is involved in the mobilisation of human hematopoietic stem and progenitor cells (Pelus et al. 2002). Chemokine receptors such as these can be activated in peripheral blood stem cell transplants. There has been studies showing that HDACis can promote the self-renewal of hematopoietic stem cells This study has shown that with MI192 treatment *CXCL12* expression is unaffected. However, the expression of *CXCL2* with MI192 treatment was massively increased, 86 fold (statistically significantly, $P \leq 0.05$); it was the largest increase in expression seen in all genes investigated. The huge increase in *CXCL2* expression is an interesting result regarding HSCs. HDACis are known to increase the mobilisation/self-renewal of human HSCs, and it may be that they act to increase the expression of *CXCL2*, as MI192 does in these ADSCs.

7.4.6.5 Muscle differentiation cell related transcripts - *ACTA2*, *DVL2* and *MSX1*

ACTA2 encodes smooth muscle actin, which can be used as a myofibroblast differentiation marker and is found in linked to muscle, liver and stromal lineages (Ozgurll et al. 1990). *ACTA2* expression down-regulated strongly with MI192 treatment, indicating the cells are not moving down a muscle lineage. However, conversely, the Wnt regulator *DVL2*, discussed earlier, inhibits myogenesis (Yamaguchi et al. 2012), and was slightly down-regulated in most samples that might have indicated a readiness for muscle formation, although conflicting with the down-regulation of *ACTA2*.

The muscle segment homeobox gene (*MSX1*) encodes for a protein essential for cell proliferation and differentiation of several cell types, and is key in normal tooth, limb development and craniofacial bone development (Vastardis et al. 1996). When knocked down (with a siRNA) in mouse dental MSCs, down-regulated *MSX1* expression could promote the expression of *ALP*, *COL1A1*, *OCN*, *RUNX2*, *DSPP*, and *DMP1*, and increase ALP activity and mineralised nodule formation (Feng et al. 2013). MSX1 is known to be essential for BMP4 induction in embryonic mouse models of tooth development (Chen et al. 1996). *MSX1* was down-regulated in the MI192 treated cells, although interestingly, this down-regulation has not had a negative effect on BMP4 transcription levels (which has a large up-regulation in the MI192 treated cells). This down-regulation is especially interesting, when considering that the knockdown of this can improve the osteogenic differentiation of mouse dental MSCs (Feng et al. 2013). This may, at least in part, account for the increased osteogenic potential of the ADSCs on treatment with MI192.

7.4.7 The effect of MI192 treatment on the expression of Neural/nerve related transcripts in ADSCs

7.4.7.1 *NGFR*, *NGFRAP1*, *ANGPT1* and *NES*

Low-Affinity Nerve Growth Factor Receptor (CD271/p75 neurotrophin receptor/p^{75NTR}), encoded by the *NGFR* gene, was strongly up-regulated with MI192 treatment. NGFR, as well as potentially being a useful stem cell marker (for a specific discussion of this see ahead to 7.4.8) is a receptor involved in mediating survival and cell death in the neurons (Barrett & Bartlett 1994), depending on the developmental stage, expressed in situations such as injury to the nervous system (Ibáñez & Simi 2012). *NGFRAP1*, nerve growth factor receptor associated protein 1 (NADE), was unaffected by MI192 treatment. The up-regulation of the receptor but not one of proteins known to interact with the receptor is interesting, perhaps indicating another, alternative role of NGFR, discussed in the next section.

Previously mentioned down-regulated gene *ANGPT1*, encoding Ang-1 of the angiotrophic family, is involved in the activation of nerve growth factor receptor. A down-regulation of this indicates an inhibition of any neurite growth, a shift away from any nervous system role of the MI192 treated cells (Kosacka et al. 2006). *NES* encodes Nestin, a filament protein that is found in the peripheral and central nervous system, which can be used as a marker of neural stem cells, was

unaffected by MI192 treatment (Michalczyk & Ziman 2005; Cattaneo & McKay 1990).

Based on these results, MI192 treated ADSCs don't appear to be being induced to play a role in nervous or neural systems. However, the up-regulation of NGFR may indicate differently, although it is also a marker of MSCs, and is not only linked to the nervous/neural systems.

7.4.7.2 *SORT1*

SORT1 encodes for a neurotensin receptor involved in the neurotensin-induced migration of human microglia, especially found in inflammatory responses of the brain (Martin et al. 2003). *SORT1* expression was found to be 6 fold, statistically significantly ($P \leq 0.05$) up-regulated in the MI192 treated ADSCs.

7.4.8 The effect of MI192 treatment on the expression of *NGFR* (CD271) in ADSCs and a comparison of the transcription profile to CD271+ cells

The aforementioned *NGFR* encodes a protein also known as CD271, a potentially useful stem cell marker. CD271 sorting has been suggested as a method of isolating clinically useful pure populations MSCs, with excellent differentiation potential, especially down an osteogenic lineage (Cuthbert et al. 2015). As mentioned in the previous section, this was up-regulated with MI192 treatment.

CD271 positive cells sorted from bone marrow were found by Churchman et al. to have a transcriptional profile comparable to bone marrow MSCs, with regards to the potential to commit to multiple fates (including osteogenic, adipogenic, pericytic, and haematopoietic). CD271 is down-regulated in MSCs that have been expanded in tissue culture and has low expression in hematopoietic-lineage cells.

Positive sorting for CD271 in combination with negative sorting for PDGFRA has been suggested as a method of isolating a close to pure population of human MSCs with multi-function potential (Li et al. 2014). MI192 treatment results in an up-regulation of *CD271* and a down-regulation of *PDGFRA* (8.5 fold, statistically

significantly, P ≤ 0.05) so in a way is acting as in the sorting work by Li et al., increasing the percentage of cells with a stromal stem/progenitor cell like properties, similar to the pure cells in the adult human bone marrow. It is worth noting that Churchman et al. found expression of *PDGFRA* to be higher in the CD271+ cells isolated from bone marrow than hematopoietic-lineage cells (Churchman et al. 2012), different to the MI192 treated cells, so the population of cells created by the MI192 pre-treatment is different to the just CD271+ cells (Churchman et al. 2012).

When compared to cultured MSCs, CD271+ cells expressed certain transcriptional activities differently, perhaps most notable Wnt-related genes *FRZB* and *WIF1*. The MI192 pre-treated cells in this study showed *FRZB* to be up-regulated 15.5 fold (P ≤ 0.05). WIF1 was up-regulated very highly in two donors (161 fold and 554 fold), slightly in one donor (2.5 fold), from not determined to determined in 2 donors and in one donor it was down-regulated (7337 fold). This has skewed the average results in favour of down-regulated, despite an overall trend of up-regulation. *SFRP1* and *SRFP4* were also found to be highly up-regulated in the CD271+ cells. Comparatively, in the MI192 pre-treated cells *SFRP1* was up-regulated, while *SRFP4* was not affected. This transcriptional picture fits that of the CD271+ cells, where the cells are more Wnt active, and ready for Wnt pathway activation and regulation.

Other genes with increased transcriptional activity in CD271 sorted cells include an increased pericyte-like transcription profile. However, in contrast to the CD271 sorted cells, the MI192 pre-treated cells have only *MCAM* expression increased, with other pericytes related genes such as *ANGPT1*, *ACTA2* and *PDGFRA* being down-regulated.

CD271+ cells also had a higher expression of haematopoiesis-supporting cytokines CXCL12 and IL7, whereas the expression was up and down-regulated in different donors on MI192 treatment, with no real conclusion to be drawn about these transcripts. Expression in CD271+ cells of adipogenic transcripts *PPARG*, *LPL*, and *FABP4* was increased and osteogenic transcripts *SP7*, *SPARC*, *SPP1* and *BGLAP-OCN* indicating a steady stage engagement with adipogenic and osteogenesis. In the MI192 treated cells, results for *PPARG* and *LPL* were inconclusive, while

FABP4 was up-regulated. *SP7* and *BGLAP* were down-regulated, although not consistently between donors or significantly, while *SPARC* and *SPP1* were up-regulated. So the transcription profile of the MI192 treated cells is similar to the CD271+ cells; however the expression of some genes in the M192 treated cells drops when it would be expected to rise if the selection was making them more CD271+ cell like. Another example of this is in that expression of *NANOG* and *POU5F1* were higher in CD271 cells, whereas in the MI192 treated cells the expression of these was virtually unchanged with treatment.

One key point in the Churchmen et al. CD271 study was that to the author's knowledge, no native MSCs with a higher expression of *BMP2*, and *IGF2* over cultured MSCs had been found. They believe this makes CD271+ sorted cells a strong potential candidate for injectable stem cell therapies for bone healing. Interestingly, the MI192 cells show increased expression of *BMP2* and *IGF2* over the untreated counterparts, making them a similarly improved cell population for that purpose.

7.4.9 The effect of MI192 treatment on the expression of miscellaneous transcripts in ADSCs

The card contained three fibroblast growth factor related genes; *FGFR1*, encoding fibroblast growth factor receptor 1 and *FGF5*, encoding fibroblast growth factor 5 were both unaffected by MI192 treatment, and *FGFR3* was strongly up-regulated with treatment.

FGF5 is involved in many cellular processes, including embryonic development and cell growth (Haub & Goldfarb 1991), and is not highly expressed in adult tissue, it is primarily expressed during embryonic development and in the nervous system (Allerstorfer et al. 2008). FGF5 signals are predominantly target for FGFR1 (Ornitz et al. 1996), so it is unsurprising that if one of these was unaffected by MI192 treatment, the same was seen in the other.

FGFR3 is crucial to bone and cartilage development, and mutations in this gene lead to a range of short-limb dwarfism in humans, along with other skeletal conditions such as Muenke and Crouzon syndromes. FGFR3 plays a number of

roles endochondral ossification, it initially enhances proliferation of immature chondrocytes (Iwata et al. 2000); however, at a later stage acts to inhibit chondrocyte proliferation and differentiation (Naski et al. 1998). Therefore, an increase in *FGFR3* expression must be looked at within the context of other genes. Here the increase of *FGFR3* may help these cells to advance on an endochondral ossification type pathway of osteogenic differentiation. Interestingly, FGFR3 is known to down-regulated BMP4 expression (Naski et al. 1998); however, *BMP4* is also up-regulated in the MI192 treated cells.

7.4.10 Discussion summary

The increased osteogenic differentiation potential of these cells has been proven, in several models, so the effect of MI192 on many genes was explored in an effort to explain this, along with other effects such as increased stem cell markers and a decrease in adipogenic differentiation potential of the cells.

Some key Wnt transcripts, *FRZB* and *SFRP1* were up-regulated, along with the down-regulation of *SFRP4*. Also up-regulated were *BMP2* and *BMP4*, and BMP pathway inhibitor *BMPER* was down-regulated. The BMP and Wnt pathway are interconnected, and it appears that the treatment for two days with MI192 increases the activation of these pathways, perhaps explaining the increase osteogenic differentiation potential of these cells. The increased osteogenic potential may also be mediated by the IGF pathways, as the up-regulation of *IGF2* and down-regulation of *IGFBP3* also indicates a priming for osteogenic differentiation (Zhong et al. 2011; Silha et al. 2003; Ding et al. 2015; Kang et al. 2012). The down-regulation of *ACVR1B* and *ACVR2A*, which can compete with BMP signalling to inhibit osteogenic differentiation, also contributes to overall picture of increased BMP signalling (Mizuno et al. 2009; Maeda et al. 2004). Also down-regulated with MI192 treatment, with down-regulation linked to improved osteogenic differentiation in the literature (Feng et al. 2013), was MSX1.

Most later markers of osteogenic differentiation, for example *ALPL*, *SPARC*, *PMF-BGLAP*, *COL1A1* and *COL1A2* were down-regulated. The treatment of cells with MI192 alone does not increase the osteogenic differentiation of the ADSCs, it appears to only increase the potential; osteogenic stimulation is also required. The cells appear to be being primed for osteogenic differentiation, they are not

beginning the osteogenic differentiation process with MI192 treatment. Runx2 is an early stage bone transcription factor and its up-regulation was expected, given the increased osteogenic potential of these cells. However, this was not the case, which mirrored the results seen in Chapter 5: 5.3.4. This may also require osteogenic stimulus, and/or time for the effects of the BMP/Wnt pathways to kick in. Although, of the osteogenic transcripts, mineralisation linked genes *SPP1* and *PHOSPHO1* were up-regulated. An increase in *SPP1* actually also indicates that the cells are becoming more mature, as *SPP1* controls and prevents mineralisation.

No direct increase in chondrogenic potential was seen with MI192 treatment of ADSCs (there was no increase in *SOX9* expression, and *DDR2* and *RUNX2* down-regulated). However, some genes perhaps linked to endochondral ossification such as *FRZB*, *COL2*, *CHAD* and *FGFR3*, were up-regulated, so the cells may be being primed to form tissue in the areas where bone and cartilage interact, or just bone formation via an endochondral ossification pathway. Associated closely with cartilage formation, but often all types of extracellular matrix formation in other tissues, the up-regulation of some specific ECM related genes (COL2, *TNFAIP6*, *EPYC*, *CHAD* and *PRELP*) was also discovered. These genes may be as a result of the increase of the early stage transcription factors linked to bone and endochondral ossification, or as a direct result of the MI192 treatment.

Moving on from bone and cartilage, a key question in this experiment was what effect would MI192 treatment have on adipogenic gene expression. The results for these genes were mostly unclear, with mixed results with donors. However, there was an increase in *FABP4* and *CEBPA* expression, and a decrease in *LEPR* expression, indicating a trend to increased adipogenic differentiation of the MI192 treated cells. However, this doesn't match the results from Chapter 5: 5.3.6. *FABP4* is also linked to control of bone formation. The reason for the decrease in adipogenic potential of the MI192 pre-treated ADSCs remains unanswered from this specific study.

As bone is a vascularised tissue, angiogenesis may be key in new bone formation. However, it was concluded that MI192 treatment decreased the angiogenic potential of these cells, which may have long term consequences. This may be important to investigate in the future. Also decreased were most pericyte related

markers, meaning MI192 treatment does not seem to improve the stromal tissue like properties of these cells. The treatment of ADSCs with MI192 didn't appear to increase the neural/nervous or muscle differentiation potential of these cells, although only a small number of genes in these areas were investigated.

The expression of two genes encoding for stem cell markers, *NGFR* (CD271) and *MCAM* (CD146) were up-regulated. The increased expression of CD146 was already seen in Chapter 4:4.3.7, and may indicate an increase in the stem cell-like potential of these cells. CD271 expression was not measured, but this has also been linked with stem cell like properties of cells. While individual groups of gene expression may be affected with MI192, there may be an increase in the stem cell like properties of the cells when treated with MI192. *NANOG*, *SOX2* and *POU5F1* was not altered with MI192, so the treated cells may have properties closely linked to adult stem cells, such as bone marrow MSCs or HSCs, not ESCs that these are markers of. *RUNX1* and *GJA1* are hematopoietic markers, and they were down-regulated with MI192 treatment, so the cell may be forming more immature cell versions. Another HSC marker, *CXCL2* is known to mobilise HSCs and this may account for the massive increase in expression of *CXCL2* with MI192 treatment, as HDACis are known to increase mobilisation of HSCs. Overall, MI192 treatment clearly has an effect on HSC like properties of the ADSCs, perhaps making them more transcriptionally similar. Further investigation of this effect may yield interesting results.

Chapter 8: General Discussion, Conclusions and Future Work

This final chapter includes a general discussion of the findings of the thesis, placing them in context of the literature, summarising the results from each chapter and linking them together. Following that, the conclusions of the study are collated, and finally, potential future work for the study is outlined.

8.1 General Discussion

Researchers can approach the huge clinical demand for generating organs and tissues with a 'from scratch' tissue engineering approach, combining the key elements of cells, scaffolds, environmental stimuli and chemical cues (Naderi et al. 2011; Payne 2013). The cells utilised are typically stem cells, and poor control of how these differentiate into tissue specific cells is a key limitation of the field. More specifically, currently bone tissue engineering is a key target for researchers, largely because of the huge clinical need, and limitations of current technologies in practice. Although many advances have been made in recent years, there is still much work to be done to successfully bring bone tissue engineering to the clinic (Amini et al. 2012).

As discussed extensively in the literature review, it has been highlighted that HDACis can have an effect on stem cell differentiation potential (Tollervey & Lunyak 2012; Kretsovali et al. 2012b; Maroni et al. 2012). There is the potential to harness this, utilising HDACis, to control stem cell fate to assist in the formation of functional tissue and organs in tissue engineering. This study sits alongside those where the potential of a HDACi to improve the osteogenic differentiation of cells is demonstrated. For example, this has been demonstrated with TSA (Hu et al. 2014; Hu et al. 2013), NaB (Xu et al. 2009) and MS-275 (Kim et al. 2012; H.-N. Kim et al. 2011). The most relevant comparisons are to those where HDACis, such as VPA and TSA have been shown to improve the osteogenic differentiation of specifically ADSCs (Xu et al. 2009; Kurihara & Suzuki 2014; Maroni et al. 2012).

The design of next generation, isoform specific HDACis, provides researchers with a whole new set of tools to investigate the effect of HDACis on stem cell differentiation. MI192 was designed to be a Class 1 specific HDACi, and was found to be specific for HDAC2 and HDAC3 (Boissinot et al. 2012). It is believed to be the only HDACi of its kind, and no evidence of studies can be found where the effects of inhibiting HDAC2 and HDAC3 together in stem cells is explored. MI192 has so far only been explored as an anti-cancer agent, and in rheumatoid arthritis research (Boissinot et al. 2012; Gillespie et al. 2012).

To date, the vast majority of studies with regards to stem cells have only investigated HDAC2 and HDAC3 individually (Schroeder & Westendorf 2005; Schroeder et al. 2004; Razidlo et al. 2010; McGee-Lawrence et al. 2013; Hesse et al. 2010; Lamour et al. 2007; Choo et al. 2009; Shen et al. 2002; Paino et al. 2014). The most similar studies to this, exploring inhibitors in bone tissue engineering, are with MS-275, which is believed to inhibit HDAC1, HDAC2 and HDAC3 (although reports of the exact isoform specificity are conflicting (Bradner et al. 2010; H.-N. Kim et al. 2011)) where MS-275 was found to improve the differentiation of osteoblasts (Kim et al. 2012; H.-N. Kim et al. 2011). The results with MI192 were similar to these studies, providing further evidence that inhibiting Class 1 HDAC isoforms is a valuable tool for bone tissue engineering.

Furthermore, this study explores new ground by investigating the effect of HDACis on the osteogenic differentiation of ADSCs in 3D. To date, studies in this fields have been limited, with only a few examples (Boer et al. 2006; Lee et al. 2011; Jung et al. 2010). Finally, there has also never been such a comprehensive exploration of the effect of a HDACi on the gene expression profile of cells. The effect on gene expression of ADSCs by MI192 was extensively explored (Chapter 7: The effect of MI192 treatment on ADSC gene expression), which yielded some very interesting results, opening avenues for exploration of both MI192 and the specific inhibition of HDAC2 and HDAC3 isoforms in the future. The specifics of what were achieved in this study will be discussed, within the context of the literature.

In this study, MI192 was synthesised and characterised using NMR spectroscopy. The final step of the MI192 synthesis involves a relatively dangerous and difficult to perform step using allene gas, and improvements to the synthesis route were limited

by the cost and the availability of this gas, and if the scale up of MI192 was ever sought this may need to be addressed with an alternative reaction route.

Just before this study was begun, a commercial partnership with Cancer Research Technologies was established by Professor Ron Grigg, attempting to commercialise MI192 for the use in cancer medicaments. There is a patent application on-going, with the intention of filing further patents for further medical use claims in the future, if anything else was discovered (such as may result from this study). Consequently, the scale up of MI192 has likely been explored by Cancer Research Technologies, especially as since then MI192 has become available commercially through Abcam (Abcam Cat. no: ab146817). If the scale up of MI192 was necessary in the future, speaking to the commercial partners already in place would be the best course of action, as they may have circumnavigated the need for allene gas. Alternatively, while it is expensive at £360 for 5 mg, MI192 could just be purchased commercially. 5 mg is a large amount of inhibitor at the small doses that these studies are carried out at.

It was discovered that MI192 clearly had a cytotoxic effect on cells, as well as decreasing cell viability. This effect is undesirable, but does not totally prevent use if used in the right way or for a short enough length of time. This lead to the pre-treatment strategy being adopted, which minimises (although does not totally eliminate) the negative effects of inhibitor, while still being able to explore the effects of MI192 on the differentiation potential of the cells. The basis for this strategy was found in the literature (see a summary in Table 5-4) (Xu et al. 2009; Cho et al. 2005; Maroni et al. 2012). MI192 was also shown to inhibit the HDAC activity of ADSCs, although the study undertaken was limited and the effect of this was not explored further due to the expensive assay kit and limited test values. It was thought enough for this study to assume that the HDAC inhibitory effect was taking place.

It was also found that MI192 halted the cell cycle of ADSCs, at least to some degree, in the G2/M phase. The cell cycle is essential to normal cell function, and controls cell proliferation (Majdzadeh et al. 2008; Jiang & Hsieh 2014). It is well known in the literature that the HDAC enzymes are key to normal cell cycle function, with HDAC3 especially key to cells progressing past the G2/M checkpoint in the cell cycle (McGee-Lawrence et al. 2011; Petruccelli et al. 2011). As MI192 inhibits HDAC3, it

would follow that this is the mechanism by which MI192 is halting the cell cycle of the ADSCs. This cell cycle halting effect may be linked to the cytotoxic effect of the MI192, as cells are unable to repair any DNA damage as a result of treatment at this checkpoint, which may result in apoptosis. The study was limited because there was a high standard deviation for the later time point samples, and further time points and doses of MI192 could have been explored. It would be interesting to explore if proteins, such as the cyclin-dependent kinase inhibitors (CKIs) p21CIP1 and p27KIP1 (Park et al. 2011), linked to the cell cycle are also affected, and establish the full link between the HDAC inhibition and the cell cycle halting effect. The halting of the cell cycle is likely responsible for a decrease in cellular proliferation, and thus lower cell migration seen in MI192 treated cells through scaffolds in Chapter 6:.

Also investigated was the effect of MI192 on stem cell markers. The results from this were especially interesting, because there are no studies of its kind in the literature, with only the pluripotency markers explored with HDACi treatment (Y. Kim et al. 2013). With MI192 treatment there was a rise in expression of CD34 and CD146, with a decrease in expression of CD29, CD44, CD73, CD105 and CD166. There was no change in the expression of CD45 and CD90. This study was limited in that it only analysed a small number of markers, but it provided an interesting result none the less. When the 96 different gene expression changes were measured in Chapter 7:, the expression of MCAM, which encodes for CD146, was found to be up-regulated with MI192 treatment. The results from the different experiments were consistent. The only other stem cell marker related gene tested in the panel was *NGFR*, or CD271. This was also found to be up-regulated with MI192 treatment.

This study found that pre-treating ADSCs with MI192 improved the osteogenic differentiation potential of ADSCs, while also decreasing the cell's adipogenic differentiation potential. MI192 was found to elevate ALPSA in cells, especially when the cells were pre-treated for two days. A 30 µM dose for two days of treatment was found to be the optimal pre-treatment strategy, with a good balance between cell death and increased ALP levels. Measurement of ALPSA was also utilised to show that there was no difference in MI92 pre-treatment on 4 different ADSC donors, that the effect was seen with two different types of osteogenic induction media, that the effect was seen across multiple time points and that there was no difference in effect with two different batches of MI192. The effect of pre-treatment with TSA was also investigated and compared to MI192, as it was found in the literature that pre-

treatment with TSA would increase the osteogenic differentiation of ADSCs (Maroni et al. 2012), but was found to have a much smaller effect on ADSCs ALP levels compared to MI192. It was also demonstrated that MI192 treatment alone, without osteogenic induction, did not increase ALP levels; at least some osteogenic induction is needed.

MI192 pre-treatment increased expression of *RUNX2*, *BMP2*, *ALP* and *COL1* over osteogenic controls at certain time points, although expression often peaked and was lower than controls at other time points. There was an initial, at day 3, increase in *BMP2* expression, which is followed by a spike in *ALP* expression at day 5, *COL1* at day 7, and *RUNX2* expression at days 7 and day 14. It appears that the initial increase in *BMP2* expression may be responsible for this. Interestingly, the MI192 pre-treatment was found to reduce the expression of *OCN/BGLAP* (responsible for osteocalcin production) in the ADSCs, which may result in problems in long term osteogenic differentiation studies. The decrease in *SPP1/OPN* expression (responsible for osteopontin production) was also interesting, as there was a significant down-regulation of the gene in both the osteogenic control and the MI192 pre-treated cells, but the down-regulation was greater in the MI192 pre-treated cells.

The expression of these changes was also investigated when the effect of MI192 treatment on gene expression changes, without osteogenic differentiation was explored in Chapter 7:. In that study, there was a large increase in the expression of *BMP2,* while *COL1* and *RUNX2* expression were both down-regulated with MI192 treatment. This matches the data seen in Chapter 5:, where at day 3 the expression pattern was similar. The results for *OCN* and *ALP* were inconclusive, with mixed results between donors (although there was an overall trend of down-regulation, matching the decrease in expression at day 3 seen in this experiment). The only conflicting result was with *SPP1*, where expression was increased with MI192 treatment before osteogenic induction, but was found to be decreased throughout the experiment here. The effect of the osteogenic medium has clearly had a strong effect on the expression of *SPP1* in these cells. Also investigated before MI192 induction were Wnt related genes, and other genes related or down-stream of *BMP2*. In hindsight, it may have been useful to investigate genes such as these during the differentiation process..

Importantly there was an increase in functional mineralisation in the MI192 pre-treated cells seen with a Von Kossa stain. This study was limited in that it only investigates the mineralisation at one, quite late time point. It would have been interesting to investigate the mineralisation over time, with earlier time points. MI192 may have also resulted in the quicker mineralisation of the ADSCs. This may have been due to the decrease in *SPP1* expression and this Opn formation, allowing more free and less controlled mineralisation.

A decrease in adipogenic differentiation potential was seen in the cells pre-treated with MI192. With adipogenic differentiation induction, the lipid accumulation and adipogenic gene expression was seen to be greatly decreased in the cells pre-treated with MI192. The inhibition of HDAC2 and HDAC3 in combination appears to have a negative effect on the adipogenic differentiation potential of the ADSCs. This is countered with a large increase in the osteogenic differentiation potential of these cells. This was in contrast to reports that HDAC inhibition would promote the adipogenic differentiation of cells, (Yoo et al. 2006) (Jiang et al. 2013), although these were with a 3T3-L1 mouse fibroblast/adipocyte cell line. The most relevant study found that HDAC3 inhibition inhibited *PPARγ* expression in ADSCs (Maroni et al. 2012), so the findings of this study corroborate the findings of Maroni et al. The addition of a HDAC2 inhibitory effect does not seem to have an impact on the adipogenic differentiation of the ADSCs. This adipogenic inhibitory effect must be considered when using MI192, as it could be a detrimental side effect of using the compound in a physiological setting. These results were actually in contrast with the results seen in Chapter 7:, where the adipogenic potential was seen to increase. This only goes to highlight how changes in gene expression cannot be used in isolation to draw conclusions.

The effect of MI192 on ADSCs was also investigated in a number of 3D culture models. Three different experimental designs were investigated, so the best design could be found for any future work. While all three were not carried out at the same time, so they are not a direct comparison, the conclusions are clear. The strategy with the best outcome was experimental design 3, where cells were pre-treated for two days in 2D before seeding, in equal numbers, onto the scaffolds. In hindsight this is much more informative of the effects of MI192 on the differentiation potential of the cells than experimental design 1, as this allows for a fairer test with the cell numbers (at least at the time of seeding) being equal.

The treatment with MI92 was shown to increase the mineralisation of the ADSCs, and increase collagen production in 3D. The mineralisation and collagen production was highest in the scaffolds seeded with the 10 µM MI192 pre-treated cells, not those pre-treated with 30 µM of MI192 which was expected due to the results seen in the 2D studies. This may be a sign that in the long term a lower than initially optimal dose of MI192 may be the best. These results matched those found in monolayer (Chapter 5:); there was an increase in *COL1* expression found in cells pre-treated with MI192, and the Von Kossa and Alizarin Red staining indicated that mineralisation potential was increased with MI192 treatment.

MI192 treatment didn't lower or raise levels of bone proteins Ocn and Runx2 over osteogenic controls, despite the indication from monolayer gene expression quantification. However, collagen 1 levels were increased in the MI192 treated cells, which matched the increased Sirius red for collagen staining seen, and the increase in *COL1* expression (Chapter 5:). These results combined with the increase in mineralisation and collagen staining indicates promising results for the utilisation of MI192 to improve bone tissue engineering in long term 3D models.

Exploring the gene expression changes without any osteogenic induction yielded some interesting results. The BMP and Wnt pathway are interconnected, and key genes related to increase in the activity of these pathways were up and down-regulated (*BMP2*, *BMP4*, *FRZB* and *SFRP1*, as well as the down-regulation of *SFRP4*, *ACVR1B* and *ACVR2A*) (Zhang et al. 2013; Enomoto-Iwamoto et al. 2002; Mizuno et al. 2009; Maeda et al. 2004). It was found that that the treatment for two days with MI192 increases the activation of these pathways, which may in turn account for a down-stream increase in osteogenic differentiation pathways. Furthermore, up-regulated of *IGF2* and down-regulation of *IGFBP3* and *MSX1* also indicates a priming for osteogenic differentiation (Ding et al. 2015; Kang et al. 2012; Zhong et al. 2011; Feng et al. 2013). A large proportion of genes linked to endochondral ossification were also up-regulated (e.g. *FRZB*, *COL2*, *CHAD* and *FGFR3*), which may also aid in the general increased osteogenic potential of the cells.

Many of the later stage osteogenic differentiation marker genes, such as *ALP*, *SPARC*, *PMF-BGLAP*, *COL1A1* and *COL1A2* were down-regulated, highlighting the

already demonstrated need for osteogenic induction; MI192 treatment alone is not enough to induce osteogenic differentiation in these cells.

8.1.1 Summary

The aim of this study was to investigate the effect of MI192 on ADSC behaviour. The study has investigated a wide range of effects of the HDAC2 and HDAC3 specific HDACi MI192 on ADSCs, including how it affects cell viability, the cell cycle, stem cell markers and gene expression. MI192 was found to be cytotoxic and affect cell viability in doses as low as 10 µM. Treatment with MI192 also halted the cells in the G2/M phase of the cell cycle and altered the expression of stem cell markers on the ADSCs. The second part of the aim was to investigate this with regards to bone tissue engineering. MI192 was found to improve the osteogenic differentiation of the ADSCs, in several 2D and a 3D model of differentiation. The opposite was found with regards to adipogenic differentiation, MI192 treatment greatly reduced the adipogenic potential of the cells. Due to the cytotoxic and cell viability reducing effects of MI192, a pre-treatment strategy was employed, where cells are typically only exposed to MI192 for 2 days. Cells pre-treated with MI192 were found to have improved osteogenic differentiation seen with increased ALP expression, osteogenic gene expression and mineralisation in 2D. Effects were similar in 3D, with an increase in collagen production and mineralisation in constructs seeded with cells pre-treated with MI192 observed.

The mechanism by which MI192 improves the osteogenic differentiation potential of the cells was investigated. The increase in CD34 and CD146 stem cell markers indicates that the cells are taking on a new profile. Halting the cell in the G2/M phase may be part of the priming effect that MI192 is having on the cells, as cells that are undergoing differentiation are not proliferating. This may also account for a decrease in proliferation and the cytotoxic effect seen with MI192 treatment. The gene expression studies indicate that before osteogenic induction, some key Wnt related genes, as well as other key osteogenic genes such as *BMP2* were up-regulated. These are key osteogenic transcripts and the proteins these encode for are likely responsible for the increase in osteogenic differentiation potential of the cells. However, it was demonstrated that osteogenic induction is needed to see the cells actually differentiate down an osteogenic lineage. During differentiation there is a spike (a higher expression than the osteogenic control) in *BMP2* expression seen initially at day 3, followed by spikes in *ALP*, *COL1* and *RUNX2* expression. All of

these are classic genes in osteogenic differentiation and spikes in these clearly result in the increased differentiation potential seen by the MI192 pre-treatment. The down-regulation of *SPP1* may account for the increased mineralisation potential of the cells. Mechanistically speaking this combined goes someway to explaining why MI192 has the effects seen on ADSCs.

Summary of key conclusions:

- MI192 had a cytotoxic and cell viability reducing effect on ADSCs.
- MI192 inhibited the HDAC activity of ADSCs.
- MI192 halted the cell cycle in the G2/M phase.
- MI192 altered stem cell markers expressed on cells, with a rise in expression of CD34 and CD146, a decrease in expression of CD29, CD44, CD73, CD105, CD166 and no change in the expression of CD45 and CD90.
- MI192 pre-treatment increased the ALP expression of ADSCs.
- MI192 pre-treatment altered the osteogenic gene expression patterns of ADSCs, with increases in *RUNX2*, *BMP2*, *ALP* and *COL1* and decreases in *OCN/BGLAP* and *SPP1* expression over osteogenic controls.
- MI192 pre-treatment increased the mineralisation of ADSCs, increasing calcium accumulation and mineral nodule formation.
- MI192 pre-treatment reduced the adipogenic potential of ADSCs, reducing lipid droplet accumulation and adipogenic gene expression.
- MI192 pre-treatment of cells for 2 days prior to seeding on Am silk scaffolds increased the osteogenic differentiation of ADSCs in long term (6 week) 3D tissue culture models of osteogenic differentiation.
- M192 treatment of cells altered the transcriptional profile of the cells, with some key early osteogenic pathway related genes being increased.

8.2 Conclusion

Pre-treatment of ADSCs with the HDAC2 and HDAC3 specific HDAC inhibitor MI192 was found to increase the osteogenic differentiation potential and decrease the adipogenic differentiation potential of ADSCs. This was while having a cytotoxic and viability decreasing effect on ADSCs, along with altering expression of stem cell markers and halting the cell cycle in the G2/M phase. MI192 pre-treatment was also found to increase the osteogenic differentiation of ADSCs in 3D culture models utilising Am silk scaffolds. Finally, MI192 treatment of ADSCs for two days was found to alter the gene expression profile of ADSC, with some key early osteogenic pathway related genes being increased.

8.3 Future Work

An alternative synthetic route for M192 may be worth exploring to allow the scale up of MI192. This may be necessary if any large scale studies were undertaken in the future. Cancer Research Technologies, the commercial partner who provided a sample for the comparison of MI192 batches experiment, have synthesised MI192 in their laboratories, and may have alternative routes accessible to save time and resources.

In terms of improving upon experiments already undertaken; the effect of MI192 on the HDAC activity of the ADSCs could be explored with a greater dose response and with more time points, to investigate fully how and how quickly MI192 acts on the ADSCs; cell sorting to isolate the potentially formed subpopulation of cells and comparison to the other population of the MI192 treated cells, and untreated cells would be interesting; assessing the marker expression of more stem cell markers on the treated cells would give a better picture of the cells after MI192 treatment; further experiments investigating the mineralisation would be useful for drawing full conclusions, longer and shorter time points would provide a better picture; and finally, further assessment of the 3D studies, with longer time points and more conclusive immunohistochemical studies would be interesting.

Further experiments could include work with siRNAs. siRNAs are another tool utilised by researchers to target specific HDAC isoforms and can knock down specific genes,

thereby affecting enzyme levels in the cell. However, siRNAs only degrade mRNAs, preventing the formation of new proteins, so don't inhibit the already formed proteins in the cells. These have been utilised to knock down HDAC1 and HDAC3 in combination in ADSCs, which improved the osteogenic potential of the cells (Maroni et al. 2012). No studies have investigated the effect of knocking both HDAC2 and HDAC3 down with siRNAs, except with relation to the cell cycle (Ye et al. 2013). An interesting future study would be to explore the knock down of HDAC2 and HDAC3, with siRNAs, and to see if it has the same effect on ADSCs as treatment with MI192. This may help explain the mechanism behind the improvement to osteogenic differentiation seen with MI192 treatment.

To best explore the effect of a compound such as MI192 on the differentiation of cells is in an *in vivo* model. *In vivo* models have been used to investigate how HDACis effect cells *in vivo* in a limited number of studies, there are definite gaps in the knowledge in the literature. The scaffolds from experimental design 3 in the 3D chapter could be implanted in *in vivo* models to investigate how the cells react under more realistic physiological conditions than *in vitro* culture conditions. The scaffolds could be implanted in a diffusion chamber, which separates the scaffold from the host tissue and cells, but still provides a physiological relevant model better than a tissue culture incubator, as growth factors, minerals, nutrients etc are able to diffuse into the chamber (W. Lu et al. 2014; Yang et al. 2003). Subcutaneous implantation model could also be used, where the scaffolds are in contact with host cells as well. Alternatively, or after conclusions are drawn from a diffusion chamber model, scaffolds can be implanted in a defect models (such as those utilised by Lee et al, where Largazole demonstrated bone-forming activity in mouse calvaria defect models (Boer et al. 2006)). These provide a model of bone healing, investigating if the scaffolds aid bone healing. If the constructs with cells pre-treated with MI192 provided a better healing of a bone defect, the conclusion that MI192 improves the osteogenic differentiation of ADSCs would be more concrete. An alternative model to investigate the effect of MI192 on bone healing would be to implant scaffolds soaked in MI192 medium, with no cells seeded, into defects. This would indicate if MI192 could be incorporated in simpler models of bone healing and just aid the host cells in the process.

With regards to the more general effects of MI192 on ADSCs, there could be more exploration of the apoptotic effects of MI192. How the cells are dying and if this could

be prevented could be explored. The levels of stress markers, cytokines or DNA fragmentation in the cells could be measured to indicate pathways by which this is happening. Comparison of different morphological, biochemical, and cell-cell interaction changes can indicate if the cells are dying from apoptosis, autophagy or necrosis (Krysko et al 2008).

Furthermore, the cells which detached on MI192 treatment were assumed to be apoptotic dead cells and were never investigated. There was no guarantee that these cells were in fact dead, and MI192 may merely have affected their adhesion properties. Further characterisation of these cells, to either confirm cell death or attachment, should be carried out.

The effect of MI192 on the angiogenic potential of these cells has not been explored, and it would be interesting to link this to the results from the effect of MI192 on the stem cell markers. This may be best undertaken *in vivo.* Sorting for certain markers after MI192 treatment could lead to the isolation of an interesting subpopulation of cells, perhaps with increased osteogenic differentiation potential.

While the effect of MI192 was explored on osteogenic and adipogenic differentiation, the third part of the classical trilineage test of differentiation is chondrogenic differentiation. Chondrogenic differentiation and osteogenic differentiation are closely linked in the body, as can be seen in processes such as endochondral ossification. It was demonstrated that with MI192 treatment came an increase in expression of genes such as Wnt pathway promoters and BMP4, so MI192 may increase chondrogenic differentiation of the ADSCs. This could be explored through pellet culture or scaffold studies. Furthermore, only ADSCs were explored in this study. While they are an abundant and very promising source of MSCs for use in the clinic, there are alternative benefits to utilising bone marrow MSCs. They are more commercially explored and more studies have been undertaken with them, giving a wider knowledge base. The effect of MI192 on those, or other MSCs (with their own plethora of advantages and disadvantages) would be very interesting.

The work in this study was only carried out on ADSCs. As discussed extensively in the Introduction, ADSCs are a useful and plentiful source of MSCs. However, they only represent one source of stem cells. For future commercialisation, it may be

useful to explore alternative sources of stem cells. ADSCs are most comparable to other MSCs such as bone marrow MSCs (Wagner et al. 2005). Therefore, it would be useful from a translational perspective to compare the effects of MI192 on bone marrow MSCs to ADSCs, especially to see if the same increased osteogenic differentiation potential was observed. If the results could be translated into all types of MSCs, or even other sources of stem cells, then the potential usefulness of MI192 would be greatly increased. Bone marrow MSCs are the best characterised and commercialised MSCs, so a compatibility with those cells would be a great advantage in commercialisation of MI192.

Finally, the actual commercialisation of MI192 need to be explored. Based on the results obtained in this study, MI192 could be utilised as part of a pre-treatment strategy to improve the osteogenic potential of ADSCs (or maybe all MSCs) *in vitro*. It could be sold in medium as part of a media package, where a pre-treatment medium is used with the cells prior to full differentiation. Or further work with lower doses may indicate it could be included as a component of medium for use with the cells the 'whole time'. Alternatively, it could be sold as a supplement in powder form and researchers optimise their own treatment strategies with.

Further, ADSCs treated (or "primed") with MI192 could be sold as a cell source capable of osteogenic differentiation. The cells could be treated with MI192, frozen, packaged and sold ready for use. If the cells were not grown in any osteogenic medium, and only primed, then researchers/clinicians could tailor differentiation protocols to suit their needs. Presently, this research has focused on osteogenic differentiation, and there looks to be potential to utilise them with scaffolds. If this work was to be continued, such scaffolds could be implanted in bone defects, such as those created when fractures are too large to heal alone (critical-size defects). This would work best for hard bone, but could potentially be applied in reconstruction of craniofacial bone. Standardisation of protocols and full characterisation of the treated cells would be key if this was the case, to meet regulatory standards.

Without further work, nothing can be concluded about its potential usefulness in other scenarios, such as incorporation in scaffolds. Intellectual property on the compound is owned by the Grigg group, and a patent application is pending for MI192 for in cancer treatment. Further patent applications could be filed with second medical use

type claims, where the patent claimed the compound for use as a tool for improving the osteogenic differentiation of stem cells.

Bibliography

Addison, W.N. et al., 2007. Pyrophosphate Inhibits Mineralization of Osteoblast Cultures by Binding to Mineral, Up-regulating Osteopontin, and Inhibiting Alkaline Phosphatase Activity. *Journal of Biological Chemistry*, 282(21), pp.15872–15883.

Agis-Balboa, R.C. et al., 2013. Loss of HDAC5 impairs memory function: implications for Alzheimer's disease. *Journal of Alzheimer's disease : JAD*, 33(1), pp.35–44.

Agudelo, M., Yoo, C. & Nair, M.P., 2012. Alcohol-induced serotonergic modulation: The role of histone deacetylases. *Alcohol*, 46(7), pp.635–42.

Akhtar, M.W. et al., 2009. Histone deacetylases 1 and 2 form a developmental switch that controls excitatory synapse maturation and function. *The Journal of neuroscience : the official journal of the Society for Neuroscience*, 29(25), pp.8288–97.

Allerstorfer, S. et al., 2008. FGF5 as an oncogenic factor in human glioblastoma multiforme: autocrine and paracrine activities. *Oncogene*, 27(30), pp.4180–4190.

Allmeling, C. et al., 2008. Spider silk fibres in artificial nerve constructs promote peripheral nerve regeneration. *Cell proliferation*, 41(3), pp.408–20.

Amini, A.R., Laurencin, C.T. & Nukavarapu, S.P., 2012. Bone tissue engineering: recent advances and challenges. *Critical reviews in biomedical engineering*, 40(5), pp.363–408.

Atadja, P. et al., 2004. Selective Growth Inhibition of Tumor Cells by a Novel Histone Deacetylase Inhibitor, NVP-LAQ824. *Cancer Research*, 64(2), pp.689–695.

Atala, A. et al., 2006. Tissue-engineered autologous bladders for patients needing cystoplasty. *Lancet*, 367(9518), pp.1241–6.

Avrahami, D. & Kaestner, K.H., 2012. Epigenetic regulation of pancreas development and function. *Seminars in cell & developmental biology*, 23(6), pp.693–700.

Baboolal, T.G. et al., 2014. Intrinsic multipotential mesenchymal stromal cell activity in gelatinous Heberden's nodes in osteoarthritis at clinical presentation. *Arthritis research & therapy*, 16(3), pp.1–10.

Baer, P.C. & Geiger, H., 2012. Adipose-Derived Mesenchymal Stromal/Stem Cells: Tissue Localization, Characterization, and Heterogeneity. *Stem Cells International*, 2012, pp.1–11.

Bai, S. et al., 2005. DNA Methyltransferase 3b Regulates Nerve Growth Factor-Induced Differentiation of PC12 Cells by Recruiting Histone Deacetylase 2. *Molecular and cellular biology*, 25(2), pp.751–766.

Baker, B.M. & Chen, C.S., 2012. Deconstructing the third dimension - how 3D culture microenvironments alter cellular cues. *Journal of Cell Science*, 125(13), pp.3015–3024.

Balasubramanian, A. et al., 2014. Fam65b is important for formation of the HDAC6-dysferlin protein complex during myogenic cell differentiation. *The FASEB Journal*, 28(7), pp.2955–2969.

Balasubramanian, S., Verner, E. & Buggy, J.J., 2009. Isoform-specific histone deacetylase inhibitors: the next step? *Cancer letters*, 280(2), pp.211–21.

De Bari, C. et al., 2001. Multipotent mesenchymal stem cells from adult human synovial membrane. *Arthritis and rheumatism*, 44(8), pp.1928–1942.

Barrett, G.L. & Bartlett, P.F., 1994. The p75 nerve growth factor receptor mediates survival or death depending on the stage of sensory neuron development. *Proceedings of the National Academy of Sciences of the United States of America*, 91(14), pp.6501–6505.

Bartel, D.L., Davy, D.T. & Keaveny, T.M., 2006. *Orthopaedic Biomechanics: Mechanics and Design in Musculoskeletal Systems*, Prentice Hall.

Bartel, D.L., Davy, D.T. & Keaveny, T.M., 2006. *Orthopaedic Biomechanics: Mechanics and Design in Musculoskeletal Systems*, Pearson Education.

Barton, K.M. et al., 2014. Selective HDAC Inhibition for the Disruption of Latent HIV-1 Infection. *PloS one*, 9(8), p.e102684.

Battula, V.L. et al., 2009. Isolation of functionally distinct mesenchymal stem cell subsets using antibodies against CD56, CD271, and mesenchymal stem cell antigen-1. *Haematologica*, 94(2), pp.173–184.

Beckmann, N. & Kneuer, R., 2007. In vivo mouse imaging and spectroscopy in drug discovery. *NMR in Biomedicine*, 20, pp.154–185.

Bengtsson, E. et al., 2002. The leucine-rich repeat protein PRELP binds perlecan and collagens and may function as a basement membrane anchor. *Journal of Biological Chemistry*, 277(17), pp.15061–15068.

Di Bernardo, G. et al., 2009. Histone deacetylase inhibitors promote apoptosis and senescence in human mesenchymal stem cells. *Stem cells and development*, 18(4), pp.573–81.

Bertino, E.M. & Otterson, G.A., 2011. Romidepsin: a novel histone deacetylase inhibitor for cancer. *Expert opinion on investigational drugs*, 20(8), pp.1151–8.

Bertrand, P., 2010. Inside HDAC with HDAC inhibitors. *European journal of medicinal chemistry*, 45(6), pp.2095–116.

Bhaskara, S. et al., 2009. Deletion of Histone Deacetylase 3 reveals critical roles in S-phase progression and DNA damage control. *Molecular Cell*, 30(1), pp.61–72.

Bhavsar, P., Ahmad, T. & Adcock, I.M., 2008. The role of histone deacetylases in asthma and allergic diseases. *The Journal of allergy and clinical immunology*, 121(3), pp.580–4.

Bialek, P. et al., 2004. A Twist Code Determines the Onset of Osteoblast Differentiation Bone Disease Program of Texas. *Developmental cell*, 6, pp.423–435.

Bianco, P., Robey, P.G. & Simmons, P.J., 2009. Mesenchymal stem cells: revisiting history, concepts, and assays. *Cell Stem Cell*, 2(4), pp.313–319.

Bieliauskas, A. V. & Pflum, M.K.H., 2009. Isoform-selective histone deacetylase inhibitors. *Chemical Society Reviews*, 37(7), pp.1402–1413.

Bird, A., 2007. Perceptions of epigenetics. *Nature*, 447(7143), pp.396–8.

Blundell, C.D. et al., 2003. The link module from ovulation- and inflammation-associated protein TSG-6 changes conformation on hyaluronan binding. *The Journal of biological chemistry*, 278(49), pp.49261–49270.

Bode, K.A. & Dalpke, A.H., 2011. HDAC inhibitors block innate immunity. *Blood*, 117(4), pp.1102–3.

Boer, J., Licht, R. & Bongers, M., 2006. Inhibition of histone acetylation as a tool in bone tissue engineering. *Tissue Engineering*, 12(10), pp.2927–2937.

Boissinot, M. et al., 2012. Induction of differentiation and apoptosis in leukaemic cell lines by the novel benzamide family histone deacetylase 2 and 3 inhibitor MI-192. *Leukemia research*, 36(10), pp.1304–10.

Bolger, T. et al., 2007. The neurodegenerative disease protein ataxin-1 antagonizes the neuronal survival function of myocyte enhancer factor-2. *The Journal of biological chemistry*, 282(40), pp.29186–92.

Bolger, T. & Yao, T.-P., 2005. Intracellular trafficking of histone deacetylase 4 regulates neuronal cell death. *The Journal of neuroscience : the official journal of the Society for Neuroscience*, 25(41), pp.9544–53.

Bose, P., Dai, Y. & Grant, S., 2014. Histone deacetylase inhibitor (HDACI) mechanisms of action: Emerging insights. *Pharmacology and Therapeutics*, 143(3), pp.323–336.

Bourhis, J.-M. et al., 2013. Procollagen C-proteinase enhancer grasps the stalk of the C-propeptide trimer to boost collagen precursor maturation. *Proceedings of the National Academy of Sciences of the United States of America*, 110(16), pp.6394–9.

Boyault, C. et al., 2007. HDAC6 controls major cell response pathways to cytotoxic accumulation of protein aggregates. *Genes & Development*, 21(17), pp.2172–2181.

Bradner, J.E. et al., 2010. Chemical phylogenetics of histone deacetylases. *Nature chemical biology*, 6(3), pp.238–243.

Brodská, B. & Holoubek, A., 2011. Generation of reactive oxygen species during apoptosis induced by DNA-damaging agents and/or histone deacetylase inhibitors. *Oxidative medicine and cellular longevity*, 2011(25352), p.7.

Brodska, B., Otevrelova, P. & Kalousek, I., 2009. Variations in c-Myc and p21WAF1 expression protect normal peripheral blood lymphocytes against BimEL-mediated cell death. *Cell Biochemistry and Function*, 27(December 2008), pp.167–175.

Buchwald, M., Krämer, O.H. & Heinzel, T., 2009. HDACi - targets beyond chromatin. *Cancer letters*, 280(2), pp.160–7.

Buckland, J., 2011. Rheumatoid arthritis: HDAC and HDACi: pathogenetic and mechanistic insights. *Nature reviews. Rheumatology*, 7(12), p.682.

Bueno, E.M. & Glowacki, J., 2011. *Biologic Foundations for Skeletal Tissue Engineering*, Morgan & Claypool Publishers - Technology & Engineering.

Bueno, E.M. & Glowacki, J., 2011. *Biologic Foundations for Skeletal Tissue Engineering*, Morgan & Claypool Publishers.

Burba et al., 2011. Histone deacetylase inhibition enhances self renewal and cardioprotection by human cord blood-derived CD34 cells. *Cancer research*, 6(7).

Burdge, G.C., Hoile, S.P. & Lillycrop, K.A., 2012. Epigenetics: are there implications for personalised nutrition? *Current opinion in clinical nutrition and metabolic care*, 15(5), pp.442–7.

Burgess, A. et al., 2004. Histone deacetylase inhibitors specifically kill nonproliferating tumour cells. *Oncogene*, 23(40), pp.6693–701.

Cantley, M.D. et al., 2012. Histone deacetylase inhibitors as suppressors of bone destruction in inflammatory diseases. *The Journal of pharmacy and pharmacology*, 64(6), pp.763–74.

Cantley, M.D. et al., 2011. Inhibitors of histone deacetylases in class I and class II suppress human osteoclasts in vitro. *Journal of cellular physiology*, 226(12), pp.3233–41.

Carragee, E.J., Hurwitz, E.L. & Weiner, B.K., 2011. A critical review of recombinant human bone morphogenetic protein-2 trials in spinal surgery: emerging safety concerns and lessons learned. *The spine journal : official journal of the North American Spine Society*, 11(6), pp.471–91.

Catalioto, R.-M., Maggi, C.A. & Giuliani, S., 2009. Chemically distinct HDAC inhibitors prevent adipose conversion of subcutaneous human white preadipocytes at an early stage of the differentiation program. *Experimental cell research*, 315(19), pp.3267–80.

Cattaneo, E. & McKay, R., 1990. Proliferation and differentiation of neuronal stem cells requlated by nerve growth factor. *Nature*, 347, pp.762–765.

Chang, S. et al., 2006. Histone deacetylase 7 maintains vascular integrity by repressing matrix metalloproteinase 10. *Cell*, 126(2), pp.321–34.

Chang, S. & McKinsey, T., 2004. Histone Deacetylases 5 and 9 Govern Responsiveness of the Heart to a Subset of Stress Signals and Play Redundant Roles in Heart Development. *Molecular and cellular biology*, 24(19), pp.8467–8476.

Chawla, S. et al., 2003. Neuronal activity-dependent nucleocytoplasmic shuttling of HDAC4 and HDAC5. *Journal of Neurochemistry*, 85(1), pp.151–159.

Chen, B. & Cepko, C.L., 2009. HDAC4 Regulates Neuronal Survival in Normal and Diseased Retinas. *Science*, 323(January), pp.256–259.

Chen, G., Deng, C. & Li, Y.P., 2012. TGF-?? and BMP signaling in osteoblast differentiation and bone formation. *International Journal of Biological Sciences*, 8(2), pp.272–288.

Chen, Y. et al., 2011. HDAC-mediated deacetylation of NF-κB is critical for Schwann cell myelination. *Nature neuroscience*, 14(4), pp.437–41.

Chen, Y. et al., 2004. Histone acetylation regulates p21 WAF1 expression in human colon cancer cell lines. *World Journal of Gastroenterology*, 10(18), pp.2643–2646.

Chen, Y. et al., 1996. Msx1 controls inductive signaling in mammalian tooth morphogenesis. *Development*, 122(10), pp.3035–3044.

Chiechio, S. et al., 2009. Epigenetic Modulation of mGlu2 Receptors by Histone Deacetylase Inhibitors in the Treatment of Inflammatory Pain. *Molecular Pharmacology*, 75(5), pp.1014–1020.

Cho, H.H. et al., 2005. Induction of osteogenic differentiation of human mesenchymal stem cells by histone deacetylase inhibitors. *Journal of cellular biochemistry*, 96(3), pp.533–42.

Choi, S. & Reddy, P., 2011. HDAC inhibition and graft versus host disease. *Molecular medicine*, 17(5-6), pp.404–16.

Choo, M., Yeo, H. & Zayzafoon, M., 2009. NFATc1 mediates HDAC-dependent transcriptional repression of osteocalcin expression during osteoblast differentiation. *Bone*, 45(3), pp.579–589.

Choudhary, C. et al., 2009. Lysine acetylation targets protein complexes and co-regulates major cellular functions. *Science*, 325(5942), pp.834–40.

Christensen, D.P. et al., 2011. Histone deacetylase (HDAC) inhibition as a novel treatment for diabetes mellitus. *Molecular medicine*, 17(5-6), pp.378–90.

Churchman, S.M. et al., 2012. Transcriptional profile of native CD271+ multipotential stromal cells: Evidence for multiple fates, with prominent

osteogenic and wnt pathway signaling activity. *Arthritis and Rheumatism*, 64(8), pp.2632–2643.

Churchman, S.M. et al., 2013. Yield optimisation and molecular characterisation of uncultured CD271+ mesenchymal stem cells in the reamer irrigator aspirator waste bag. *European Cells and Materials*, 26, pp.252–262.

Clarkin, C.E. et al., 2011. Reduced chondrogenic matrix accumulation by 4-methylumbelliferone reveals the potential for selective targeting of UDP-glucose dehydrogenase. *Matrix Biology*, 30(3), pp.163–168.

Clarkin, C.E. et al., 2011. Regulation of UDP-glucose dehydrogenase is sufficient to modulate hyaluronan production and release, control sulfated GAG synthesis, and promote chondrogenesis. *Journal of Cellular Physiology*, 226(3), pp.749–761.

Colgan, S.P. et al., 2006. Physiological roles for ecto-50-nucleotidase (CD73). *Purinergic Signalling*, 2(2), pp.351–360.

Colnot, C., 2011. Cell Sources for Bone Tissue Engineering: Insights from Basic Science. *Tissue Engineering Part B: Reviews*, 17(6), pp.449–457.

Corminboeuf, C. et al., 2006. Unexpected deacetylation mechanism suggested by a density functional theory QM/MM study of histone-deacetylase-like protein. *Journal of the American Chemical Society*, 128(14), pp.4530–1.

Covas, D.T. et al., 2008. Multipotent mesenchymal stromal cells obtained from diverse human tissues share functional properties and gene-expression profile with CD146 + perivascular cells and fibroblasts. *Experimental Hematology*, 36(5), pp.642–654.

Cuthbert, R.J. et al., 2015. Examining the Feasibility of Clinical Grade CD271+ Enrichment of Mesenchymal Stromal Cells for Bone Regeneration. *Plos One*, 10(3), pp.1–17.

d'Ydewalle, C., Bogaert, E. & Van Den Bosch, L., 2012. HDAC6 at the Intersection of Neuroprotection and Neurodegeneration. *Traffic*, 13(6), pp.771–9.

Dai, J. et al., 2012. The effect of co-culturing costal chondrocytes and dental pulp stem cells combined with exogenous FGF9 protein on chondrogenesis and ossification in engineered cartilage. *Biomaterials*, 33(31), pp.7699–711.

Davis, T. et al., 2000. Histone Deacetylase Inhibitors Decrease Proliferation and Modulate Cell Cycle Gene Expression in Normal Mammary Epithelial Cells. *Clinical Cancer Research*, 6, pp.4334–4342.

Deckers, M.M.L. et al., 2002. Bone Morphogenetic Proteins Stimulate Angiogenesis through Osteoblast-Derived Vascular Endothelial Growth Factor A. *Endocrinology*, 143(4), pp.1545–1553.

Dell'Aversana, C., Lepore, I. & Altucci, L., 2012. HDAC modulation and cell death in the clinic. *Experimental cell research*, 318(11), pp.1229–44.

Denk, F. & McMahon, S.B., 2012. Chronic pain: emerging evidence for the involvement of epigenetics. *Neuron*, 73(3), pp.435–44.

Dequiedt, F. et al., 2003. HDAC7, a Thymus-Specific Class II Histone Deacetylase, Regulates Nur77 Transcription and TCR-Mediated Apoptosis. *Immunity*, 18(5), pp.687–698.

Deschamps, N. et al., 2015. How the flexibility of human histone deacetylases influences ligand binding: an overview. *Drug Discovery Today*, 20(6).

Dhalluin, C. et al., 1999. Structure and ligand of a histone acetyltransferase bromodomain. *Nature*, 399(June), pp.491–496.

Dinarello, C.A., Fossati, G. & Mascagni, P., 2011. Histone deacetylase inhibitors for treating a spectrum of diseases not related to cancer. *Molecular medicine*, 17(5-6), pp.333–52.

Ding, W. et al., 2015. miR-30e targets IGF2-regulated osteogenesis in bone marrow-derived mesenchymal stem cells, aortic smooth muscle cells, and ApoE-/- mice. *Cardiovascular Research*, 106(1), pp.131–142.

Dokmanovic, M. et al., 2007. Histone deacetylase inhibitors selectively suppress expression of HDAC7. *Molecular cancer therapeutics*, 6(9), pp.2525–34.

Dowling, M., Voong, K.R. & Keutmann, M.K., 2005. Mitotic Spindle Checkpoint Inactivation by Trichostatin A Defines a Mechanism for Increasing Cancer Cell Killing. *Cancer Biology & Therapy*, 4(2), pp.197–206.

Dragoo, J.L. et al., 2003. Tissue-engineered cartilage and bone using stem cells from human infrapatellar fat pads. *The Journal of bone and joint surgery. British volume*, 85(5), pp.740–747.

Drummond-Barbosa, D., 2008. Stem Cells, Their Niches and the Systemic Environment: An Aging Network. *Genetics*, 180(4), pp.1787–1797.

Ducy, P. et al., 2000. Leptin inhibits bone formation through a hypothalamic relay: a central control of bone mass. *Cell*, 100(2), pp.197–207.

Dudakovic, A. et al., 2015. Histone Deacetylase Inhibition Destabilizes the Multi-Potent State of Uncommitted Adipose-Derived Mesenchymal Stromal Cells. *Journal of Cellular Physiology*, 230(1), pp.52–62.

Duff, S.E. et al., 2003. CD105 is important for angiogenesis: evidence and potential applications. *The FASEB journal : official publication of the Federation of American Societies for Experimental Biology*, 17(9), pp.984–992.

Duncan, H.F. et al., 2011. HDACi: cellular effects, opportunities for restorative dentistry. *Journal of dental research*, 90(12), pp.1377–88.

Duncan, H.F. et al., 2012. Histone deacetylase inhibitors induced differentiation and accelerated mineralization of pulp-derived cells. *Journal of endodontics*, 38(3), pp.339–45.

Dyson, J. a et al., 2007. Development of custom-built bone scaffolds using mesenchymal stem cells and apatite-wollastonite glass-ceramics. *Tissue engineering*, 13(12), pp.2891–901.

Eberharter, A. & Becker, P.B., 2002. Histone acetylation: a switch between repressive and permissive chromatin. Second in review series on chromatin dynamics. *EMBO reports*, 3(3), pp.224–9.

Elboray, E.E., Gao, C. & Grigg, R., 2012. Skeletal diversity via Pd (0) catalysed three-component cascades of allene and halides or tri fl ates with protected hydroxylamines and formamide. *Tetrahedron*, 68(14), pp.3103–3111.

El-Gendy, R. & Yang, X., 2012. Osteogenic Differentiation of Human Dental Pulp Stromal Cells on 45S5 Bioglass® Based Scaffolds In Vitro and In Vivo. *Tissue Engineering: Part A*, 19(5+6), pp.707–715.

Elizalde, C. et al., 2012. Histone deacetylase 3 modulates the expansion of human hematopoietic stem cells. *Stem cells and development*, 21(14), pp.2581–91.

Enomoto-Iwamoto, M. et al., 2002. The Wnt antagonist Frzb-1 regulates chondrocyte maturation and long bone development during limb skeletogenesis. *Developmental biology*, 251(1), pp.142–156.

Eot-Houllier, G. et al., 2009. Histone deacetylase inhibitors and genomic instability. *Cancer letters*, 274(2), pp.169–76.

Erickson, G.R. et al., 2002. Chondrogenic potential of adipose tissue-derived stromal cells in vitro and in vivo. *Biochemical and biophysical research communications*, 290(2), pp.763–769.

Evans, C., 2011. Barriers to the clinical translation of orthopedic tissue engineering. *Tissue Engineering Part B: Reviews*, 17(6), pp.437–441.

Fajas, L. et al., 2002. The retinoblastoma-histone deacetylase 3 complex inhibits PPARgamma and adipocyte differentiation. *Developmental cell*, 3(6), pp.903–910.

Fan, X. et al., 2004. Regulation of RANKL promoter activity is associated with histone remodeling in murine bone stromal cells. *Journal of cellular biochemistry*, 93(4), pp.807–18.

Feng, D. et al., 2011. A circadian rhythm orchestrated by histone deacetylase 3 controls hepatic lipid metabolism. *Science*, 331(March), pp.1315–1320.

Feng, X. et al., 2013. Msx1 regulates proliferation and differentiation of mouse dental mesenchymal cells in culture. *European journal of oral sciences*, 121(5), pp.412–20.

Filippakopoulos, P. & Knapp, S., 2012. The bromodomain interaction module. *FEBS letters*, 586(17), pp.2692–704.

Fink, S.L. et al., 2005. Apoptosis, Pyroptosis, and Necrosis: Mechanistic Description of Dead and Dying Eukaryotic Cells. *Infection and Immunity*, 73(4), pp.1907–1916.

Finnin, M.S. et al., 1999. Structures of a histone deacetylase homologue bound to the TSA and SAHA inhibitors. *Letters to Nature*, 401(July), pp.188–193.

Frew, A.J., Johnstone, R.W. & Bolden, J.E., 2009. Enhancing the apoptotic and therapeutic effects of HDAC inhibitors. *Cancer letters*, 280(2), pp.125–33.

Fu, Y. et al., 2014. Histone deacetylase 8 suppresses osteogenic differentiation of bone marrow stromal cells by inhibiting histone H3K9 acetylation and RUNX2 activity. *International Journal of Biochemistry and Cell Biology*, 54, pp.68–77.

Gaarenstroom, T. & Hill, C.S., 2014. TGF-β signaling to chromatin: How Smads regulate transcription during self-renewal and differentiation. *Seminars in cell & developmental biology*, 32(August), pp.107–118.

Gabrielli, B., Chia, K. & Warrener, R., 2011. Finally, how histone deacetylase inhibitors disrupt mitosis! *Cell Cycle*, 10(16), pp.2658–2661.

Gao, L. et al., 2002. Cloning and functional characterization of HDAC11, a novel member of the human histone deacetylase family. *The Journal of biological chemistry*, 277(28), pp.25748–55.

Ge, H. et al., 2005. Differential regulation and properties of angiopoietin-like proteins 3 and 4. *Journal of lipid research*, 46(7), pp.1484–1490.

Gerber, H.P. et al., 1999. VEGF is required for growth and survival in neonatal mice. *Development*, 126(6), pp.1149–1159.

Gilbert, S., 2000. Osteogenesis: The Development of Bones. In *Developmental Biology*. Sinauer Associates.

Gillespie, J. et al., 2012. Histone deacetylases are dysregulated in rheumatoid arthritis and a novel histone deacetylase 3-selective inhibitor reduces interleukin-6 production by peripheral blood mononuclear cells from rheumatoid arthritis patients. *Arthritis and rheumatism*, 64(2), pp.418–22.

Glenisson, W., Castronovo, V. & Waltregny, D., 2007. Histone deacetylase 4 is required for TGFβ1 -induced myofibroblastic differentiation. *Biochimica et Biophysica Acta*, 1773(10), pp.1572–1582.

Golipoor, Z. et al., 2010. Differentiation of Adipose-derived Stem Cells into Schwann Cell Phenotype in Comparison with Bone Marrow Stem Cells. *Iranian Journal of Basic Medical Sciences*, 13(3), pp.76–84.

Gonzalez-Nieto, D. et al., 2012. Connexin-43 in the osteogenic BM niche regulates its cellular composition and the bidirectional traffic of hematopoietic stem cells and progenitors. *Blood*, 119(22), pp.5144–5154.

Gordeladze, J.O. et al., 2002. Leptin stimulates human osteoblastic cell proliferation, de novo collagen synthesis, and mineralization: Impact on differentiation markers, apoptosis, and osteoclastic signaling. *Journal of Cellular Biochemistry*, 85(4), pp.825–836.

Göttlicher, M. et al., 2001. Valproic acid defines a novel class of HDAC inhibitors inducing differentiation of transformed cells. *The EMBO journal*, 20(24), pp.6969–78.

Gradilone, S. a. et al., 2014. HDAC6 Is Overexpressed in Cystic Cholangiocytes and Its Inhibition Reduces Cystogenesis. *The American Journal of Pathology*, 184(3), pp.600–608.

Grafi, G. & Avivi, Y., 2004. Stem cells: a lesson from dedifferentiation. *Trends in biotechnology*, 22(8), pp.388–9.

Grausenburger, R. et al., 2010. Conditional deletion of histone deacetylase 1 in T cells leads to enhanced airway inflammation and increased Th2 cytokine production. *Journal of immunology*, 185(6), pp.3489–97.

Gregoretti, I. V, Lee, Y.-M. & Goodson, H. V, 2004. Molecular evolution of the histone deacetylase family: functional implications of phylogenetic analysis. *Journal of molecular biology*, 338(1), pp.17–31.

Griffith, L.G. & Swartz, M. a., 2006. Capturing complex 3D tissue physiology in vitro. *Nature Reviews Molecular Cell Biology*, 7(3), pp.211–224.

Gronthos, S. et al., 2000. Postnatal human dental pulp stem cells (DPSCs) in vitro and in vivo. *Proceedings of the National Academy of Sciences (PNAS)*, 97(25), pp.13625–13630.

Gronthos, S. et al., 2002. Stem Cell Properties of Human Dental Pulp Stem Cells. *Journal of dental research*, 81(8), pp.531–535.

Grover, J. et al., 1996. The gene organization, chromosome location, and expression of a 55-kDa matrix protein (PRELP) of human articular cartilage. *Genomics*, 38(2), pp.109–117.

Grunstein, M., 1997. Histone acetylation in chromatin structure and transcription. *Nature*, 389(6649), pp.349–52.

Guan, J.-S. et al., 2009. HDAC2 negatively regulates memory formation and synaptic plasticity. *Nature*, 459(7243), pp.55–60.

Gui, C. et al., 2003. Histone deacetylase (HDAC) inhibitor activation of p21WAF1 involves changes in promoter-associated proteins , including HDAC1. *Proceedings of the National Academy of Sciences of the United States of America*, 101(5), pp.1241–1246.

Gum, J.R. et al., 1997. Effects of Sodium Butyrate on Human Colonic Adenocarcinoma Cells. *The Journal of biological chemistry*, 262(3), pp.1092–1097.

Haberland, M. et al., 2009. Epigenetic control of skull morphogenesis by histone deacetylase 8. *Genes & development*, 23, pp.1625–1630.

Haberland, M. et al., 2010. Redundant control of adipogenesis by histone deacetylases 1 and 2. *The Journal of biological chemistry*, 285(19), pp.14663–70.

Haglund, L. et al., 2011. Identification and characterization of the integrin α 2β1 binding motif in chondroadherin mediating cell attachment. *Journal of Biological Chemistry*, 286(5), pp.3925–3934.

Hahnen, E. et al., 2008. Histone deacetylase inhibitors: possible implications for neurodegenerative disorders. *Expert opinion on investigational drugs*, 17(2), pp.169–84.

Halvorsen, Y.D. et al., 2001. Extracellular matrix mineralization and osteoblast gene expression by human adipose tissue-derived stromal cells. *Tissue engineering*, 7(6), pp.729–741.

Hatakeyama, Y., Tuan, R.S. & Shum, L., 2004. Distinct functions of BMP4 and GDF5 in the regulation of chondrogenesis. *Journal of Cellular Biochemistry*, 91(6), pp.1204–1217.

Haub, O. & Goldfarb, M., 1991. Expression of the fibroblast growth factor-5 gene in the mouse embryo. *Development*, 112(2), pp.397–406.

Hesse, E. et al., 2010. Zfp521 controls bone mass by HDAC3-dependent attenuation of Runx2 activity. *The Journal of cell biology*, 191(7), pp.1271–83.

Hildebrandt, C., Büth, H. & Thielecke, H., 2009. Influence of cell culture media conditions on the osteogenic differentiation of cord blood-derived mesenchymal stem cells. *Annals of anatomy = Anatomischer Anzeiger : official organ of the Anatomische Gesellschaft*, 191(1), pp.23–32.

Hillemacher, T. et al., 2008. Global DNA methylation is influenced by smoking behaviour. *European neuropsychopharmacology : the journal of the European College of Neuropsychopharmacology*, 18(4), pp.295–8.

Hochedlinger, K. & Plath, K., 2009. Epigenetic reprogramming and induced pluripotency. *Development*, 136(4), pp.509–23.

Hoemann, C.D., El-Gabalawy, H. & McKee, M.D., 2009. In vitro osteogenesis assays: influence of the primary cell source on alkaline phosphatase activity and mineralization. *Pathologie-biologie*, 57(4), pp.318–23.

Hondele, M. & Ladurner, A.G., 2011. The chaperone-histone partnership: for the greater good of histone traffic and chromatin plasticity. *Current opinion in structural biology*, 21(6), pp.698–708.

Hong, S. et al., 2009. A novel domain in histone deacetylase 1 and 2 mediates repression of cartilage-specific genes in human chondrocytes. *FASEB journal : official publication of the Federation of American Societies for Experimental Biology*, 23(10), pp.3539–52.

Hooker, J.M. et al., 2010. Histone deacetylase inhibitor, MS-275, exhibits poor brain penetration: PK studies of [C]MS-275 using Positron Emission Tomography. *ACS chemical neuroscience*, 1(1), pp.65–73.

Howard, D. et al., 2002. Immunoselection and adenoviral genetic modulation of human osteoprogenitors: In vivo bone formation on PLA scaffold. *Biochemical and Biophysical Research Communications*, 299(2), pp.208–215.

Hsieh, J. et al., 2004. Histone deacetylase inhibition-mediated neuronal differentiation of multipotent adult neural progenitor cells. *Proceedings of the National Academy of Sciences of the United States of America*, 101(47), pp.16659–64.

Hu, X. et al., 2014. Histone deacetylase inhibitor sodium butyrate promotes the osteogenic differentiation of rat adipose-derived stem cells. *Development, growth & differentiation*, 56(3), pp.206–213.

Hu, X. et al., 2013. Histone deacetylase inhibitor trichostatin A promotes the osteogenic differentiation of rat adipose-derived stem cells by altering the epigenetic modifications on Runx2 promoter in a BMP signaling-dependent manner. *Stem cells and development*, 22(2), pp.248–55.

Huang, G. et al., 2008. PU.1 is a major downstream target of AML1 (RUNX1) in adult mouse hematopoiesis. *Nature genetics*, 40(1), pp.51–60.

Huang, S. et al., 2012. Upregulation of miR-22 promotes osteogenic differentiation and inhibits adipogenic differentiation of human adipose tissue-derived mesenchymal stem cells by repressing HDAC6 protein expression. *Stem cells and development*, 21(13), pp.2531–40.

Humphrey, G.W. et al., 2008. Complementary roles for histone deacetylases 1, 2, and 3 in differentiation of pluripotent stem cells. *Differentiation; research in biological diversity*, 76(4), pp.348–56.

Hunter, G.K., 2013. Role of osteopontin in modulation of hydroxyapatite formation. *Calcified Tissue International*, 93, pp.348–354.

Hynes, R.O., 1992. Integrins: versatility, modulation, and signaling in cell adhesion. *Cell*, 69(1), pp.11–25.

Ibáñez, C.F. & Simi, A., 2012. P75 neurotrophin receptor signaling in nervous system injury and degeneration: paradox and opportunity. *Trends in Neurosciences*, 35(7), pp.431–440.

Ishii, S. et al., 2008. Histone deacetylase 3 localizes to the mitotic spindle and is required for kinetochore-microtubule attachment. *Proceedings of the National Academy of Sciences of the United States of America*, 105(11), pp.4179–4184.

Iwami, K. & Moriyama, T., 1993. Effects of short chain fatty acid, sodium butyrate, on osteoblastic cells and osteoclastic cells. *International Journal of Biochemistry*, 25(11), pp.1631–1635.

Iwata, T. et al., 2000. A neonatal lethal mutation in FGFR3 uncouples proliferation and differentiation of growth plate chondrocytes in embryos. *Human molecular genetics*, 9(11), pp.1603–1613.

Jackson, L.N. & Evers, B.M., 2009. Regulation of proliferation, apoptosis and cell cycle in gastrointestinal disorders. *Current opinion in pharmacology*, 9(6), pp.708–14.

Jacob, C. et al., 2011. HDAC1 and HDAC2 control the transcriptional program of myelination and the survival of Schwann cells. *Nature neuroscience*, 14(4), pp.429–36.

Jacobs, S.A. et al., 2013. Immunological characteristics of human mesenchymal stem cells and multipotent adult progenitor cells. *Immunology and cell biology*, 91(1), pp.32–9.

Jang, W.G. et al., 2012. BMP2 protein regulates osteocalcin expression via Runx2-mediated Atf6 gene transcription. *Journal of Biological Chemistry*, 287(2), pp.905–915.

Jawerka, M. et al., 2010. The specific role of histone deacetylase 2 in adult neurogenesis. *Neuron glia biology*, 6(2), pp.93–107.

Jeon, E.-J. et al., 2006. Bone morphogenetic protein-2 stimulates Runx2 acetylation. *The Journal of biological chemistry*, 281(24), pp.16502–11.

Ji, H. et al., 2010. A comprehensive methylome map of lineage commitment from hematopoietic progenitors. *Nature*, 467(7313), pp.338–342.

Jiang, X. et al., 2013. Inhibition of HDAC3 promotes ligand-independent PPARγ activation 1 by protein 2 acetylation. *J Mol Endocrinol*, 2014(October), pp.1–30.

Jiang, Y. & Hsieh, J., 2014. HDAC3 controls gap 2/mitosis progression in adult neural stem/progenitor cells by regulating CDK1 levels. *Proceedings of the National Academy of Sciences of the United States of America*, 111(37), pp.13541–6.

Jin, H. et al., 2013. HDAC Inhibitor Trichostatin A Promotes Proliferation and Odontoblast Differentiation of Human Dental Pulp Stem Cells. *Tissue Engineering Part A*, 19(5+6), pp.613–624.

Johnstone, R.W., 2002. Histone-deacetylase inhibitors: novel drugs for the treatment of cancer. *Nature reviews. Drug discovery*, 1(4), pp.287–99.

Jones, E. & Yang, X., 2011. Mesenchymal stem cells and bone regeneration: current status. *Injury*, 42(6), pp.562–8.

Jones, P., 2012. Development of second generation epigenetic agents. *Med. Chem. Commun.*, 3(2), p.135.

Jung, H.-M. et al., 2010. Modulation of the resorption and osteoconductivity of alpha-calcium sulfate by histone deacetylase inhibitors. *Biomaterials*, 31(1), pp.29–37.

Junqueira, L.C., Bignolas, G. & Brentani, R.R., 1979. Picrosirius staining plus polarization microscopy, a specific method for collagen detection in tissue sections. *The Histochemical journal*, 11(4), pp.447–55.

Kamiński, Z.J. et al., 2005. N-Triazinylammonium Tetrafluoroborates. A New Generation of Efficient Coupling Reagents Useful for Peptide Synthesis. *Journal of the American Chemical Society*, 127(48), pp.16912–16920.

Kang, H. et al., 2012. Insulin-Like Growth Factor 2 Promotes Osteogenic Cell Differentiation in the Parthenogenetic Murine Embryonic Stem Cells. *Tissue Engineering Part A*, 18(3-4), pp.331–341.

Kang, J.S. et al., 2005. Repression of Runx2 function by TGF-beta through recruitment of class II histone deacetylases by Smad3. *The EMBO journal*, 24(14), pp.2543–55.

Kao, H.-Y. et al., 2002. Isolation and characterization of mammalian HDAC10, a novel histone deacetylase. *The Journal of biological chemistry*, 277(1), pp.187–93.

Karamboulas, C. et al., 2006. HDAC activity regulates entry of mesoderm cells into the cardiac muscle lineage. *Journal of cell science*, 119(Pt 20), pp.4305–14.

Keller, G., 2005. Embryonic stem cell differentiation : emergence of a new era in biology and medicine. *Genes & development*, 19, pp.1129–1155.

Kelly, W.K. et al., 2003. Phase I Clinical Trial of Histone Deacetylase Inhibitor : Suberoylanilide Hydroxamic Acid Administered Intravenously Phase I Clinical Trial of Histone Deacetylase Inhibitor : Administered Intravenously 1. *Clinical Cancer Research*, 9(10), pp.3578–3588.

Kessler, M.W. & Grande, D. a, 2008. Tissue engineering and cartilage. *Organogenesis*, 4(1), pp.28–32.

Khan, N. et al., 2008. Determination of the class and isoform selectivity of small-molecule histone deacetylase inhibitors. *The Biochemical journal*, 409(2), pp.581–9.

Kim, D. et al., 2008. Deregulation of HDAC1 by p25/Cdk5 in neurotoxicity. *Neuron*, 60(5), pp.803–817.

Kim, H.-N. et al., 2011. Histone deacetylase inhibitor MS-275 stimulates bone formation in part by enhancing Dhx36-mediated TNAP transcription. *Journal of bone and mineral research*, 26(9), pp.2161–73.

Kim, H.-N. et al., 2012. MS-275, a benzamide histone deacetylase inhibitor, prevents osteoclastogenesis by down-regulating c-Fos expression and suppresses bone loss in mice. *European journal of pharmacology*, 691(1-3), pp.69–76.

Kim, J.H. et al., 2011. RANKL induces NFATc1 acetylation and stability via histone acetyltransferases during osteoclast differentiation. *The Biochemical journal*, 436(2), pp.253–62.

Kim, K.-I., Park, S. & Im, G.-I., 2014. Osteogenic differentiation and angiogenesis with cocultured adipose-derived stromal cells and bone marrow stromal cells. *Biomaterials*, 35(17), pp.4792–804.

Kim, M.-S. et al., 2008. Protein kinase D1 stimulates MEF2 activity in skeletal muscle and enhances muscle performance. *Molecular and cellular biology*, 28(11), pp.3600–9.

Kim, T.-I. et al., 2013. Analysis of histone deacetylase inhibitor-induced responses in human periodontal ligament fibroblasts. *Biotechnology letters*, 35(1), pp.129–33.

Kim, Y. et al., 2013. Enhancement of Transgene Expression by HDAC Inhibitors in Mouse Embryonic Stem Cells. *Development & Reproduction*, 17(4), pp.379–387.

Kinugasa, F. et al., 2008. Effect of a new immunosuppressant histon deacetylase (HDAC) inhibitor FR276457 in a rat cardiac transplant model. *Biological & pharmaceutical bulletin*, 31(9), pp.1723–6.

Kisselbach, L. et al., 2009. CD90 expression on human primary cells and elimination of contaminating fibroblasts from cell cultures. *Cytotechnology*, 59(1), pp.31–44.

Knutson, S.K. et al., 2008. Liver-specific deletion of histone deacetylase 3 disrupts metabolic transcriptional networks. *The EMBO journal*, 27(7), pp.1017–28.

Kosacka, J. et al., 2006. Adipocyte-Derived Angiopoietin-1 Supports Neurite Outgrowth and Synaptogenesis of Sensory Neurons. *Journal of neuroscience research*, 83, pp.1160–1169.

Kourkoumelis, N., Balatsoukas, I. & Tzaphlidou, M., 2012. Ca/P concentration ratio at different sites of normal and osteoporotic rabbit bones evaluated by Auger and energy dispersive X-ray spectroscopy. *Journal of Biological Physics*, 38(2), pp.279–291.

Kozhemyakina, E., Lassar, A.B. & Zelzer, E., 2015. A pathway to bone: signaling molecules and transcription factors involved in chondrocyte development and maturation. *Development (Cambridge, England)*, 142(5), pp.817–831.

Kretsovali, A., Hadjimichael, C. & Charmpilas, N., 2012a. Histone deacetylase inhibitors in cell pluripotency, differentiation, and reprogramming. *Stem Cells International*, 2012, p.10.

Kretsovali, A., Hadjimichael, C. & Charmpilas, N., 2012b. Histone deacetylase inhibitors in cell pluripotency, differentiation, and reprogramming. *Stem cells international*, 2012, p.184154.

Krysko, DV, Vanden Berghe ,T, Parthoens, E, D'Herde, K, Vandenabeele, P, Methods for distinguishing apoptotic from necrotic cells and measuring their clearance .*Methods Enzymo*l. 2008; 442:307-41.

Kundu, B. et al., 2013. Silk fibroin biomaterials for tissue regenerations. *Advanced Drug Delivery Reviews*, 65(4), pp.457–470.

Kurihara, Y. & Suzuki, T., 2014. Valproic Acid, a Histone Deacetylase Inhibitor, Decreases Proliferation of and Induces Specific Neurogenic Differentiation of Canine Adipose Tissue-Derived Stem. *The Journal of Veterinary Medical Science*, 76(1), pp.15–23.

Kurinna, S. & Barton, M.C., 2011. Cascades of transcription regulation during liver regeneration. *The international journal of biochemistry & cell biology*, 43(2), pp.189–97.

Kurita, K. et al., 1996. Occurrence of PG-Lb, a leucine-rich small chondroitin/dermatan sulphate proteoglycan in mammalian epiphyseal cartilage: molecular cloning and sequence analysis of the mouse cDNA. *The Biochemical journal*, 318(3), pp.909–914.

Kuzelová, K. et al., 2010. Suberoylanilide hydroxamic acid (SAHA) at subtoxic concentrations increases the adhesivity of human leukemic cells to fibronectin. *Journal of cellular biochemistry*, 109(1), pp.184–95.

Kwon, S., Zhang, Y. & Matthias, P., 2007. The deacetylase HDAC6 is an essential component of stress granules and plays a critical role in the cellular response to stress Inauguraldissertation. *Genes & development*, 21, pp.3381–3394.

Lagger, G. et al., 2002. Essential function of histone deacetylase 1 in proliferation control and CDK inhibitor repression. *The EMBO journal*, 21(11), pp.2672–81.

Lai, I.-L. et al., 2010. Histone deacetylase 10 relieves repression on the melanogenic program by maintaining the deacetylation status of repressors. *The Journal of biological chemistry*, 285(10), pp.7187–96.

Laino, G. et al., 2006. An approachable human adult stem cell source for hard-tissue engineering. *Journal of cellular physiology*, 206(3), pp.693–701.

Lamour, V., Detry, C. & Sanchez, C., 2007. Runx2-and histone deacetylase 3-mediated repression is relieved in differentiating human osteoblast cells to allow high bone sialoprotein expression. *J. Biol. Chem.*, 282(50), pp.36240–9.

Leboeuf, M. et al., 2010. Hdac1 and Hdac2 act redundantly to control p63 and p53 functions in epidermal progenitor cells. *Developmental Cell*, 19(6), pp.807–818.

Lee, H.K. et al., 2015. Daam2-PIP5K Is a Regulatory Pathway for Wnt Signaling and Therapeutic Target for Remyelination in the CNS. *Neuron*, 85(6), pp.1227–1243.

Lee, H.W. et al., 2006. Histone deacetylase 1-mediated histone modification regulates osteoblast differentiation. *Molecular endocrinology*, 20(10), pp.2432–43.

Lee, J.H. et al., 2010. Histone deacetylase inhibitor induces DNA damage, which normal but not transformed cells can repair. *Proceedings of the National Academy of Sciences of the United States of America*, 107(33), pp.14639–44.

Lee, J.H. & Kemp, D.M., 2006. Human adipose-derived stem cells display myogenic potential and perturbed function in hypoxic conditions. *Biochemical and Biophysical Research Communications*, 341(3), pp.882–888.

Lee, J.-Y. et al., 2010. HDAC6 controls autophagosome maturation essential for ubiquitin-selective quality-control autophagy. *The EMBO journal*, 29(5), pp.969–80.

Lee, S. et al., 2009. Histone deacetylase inhibitors decrease proliferation potential and multilineage differentiation capability of human mesenchymal stem cells. *Cell proliferation*, 42(6), pp.711–20.

Lee, S.-U. et al., 2011. In vitro and in vivo osteogenic activity of largazole. *ACS Med. Chem. Lett.*, 2, pp.248–251.

Lee, T., Lin, M. & Chang, N., 2007. Inhibition of histone deacetylase on ventricular remodeling in infarcted rats. *American Journal of Physiology*, 293(2), pp.968–977.

Lefebvre, V. & Smits, P., 2005. Transcriptional control of chondrocyte fate and differentiation. *Birth Defects Research Part C - Embryo Today: Reviews*, 75(3), pp.200–212.

Lehrke, M. & Lazar, M., 2005. The many faces of PPARg. *Cell*, 123(6), pp.993–999.

Leitinger, B. & Kwan, A.P.L., 2006. The discoidin domain receptor DDR2 is a receptor for type X collagen. *Matrix Biology*, 25(6), pp.355–364.

Levi, B. & Longaker, M.T., 2011. Concise review: adipose-derived stromal cells for skeletal regenerative medicine. *Stem cells*, 29(4), pp.576–82.

Li, H. et al., 2012. Expression of acetylated histone 3 in the spinal cord and the effect of morphine on inflammatory pain in. *Neural regeneration research*, 7(7), pp.517–522.

Li, H. et al., 2014. Low/Negative Expression of PDGFR-α Identifies the Candidate Primary Mesenchymal Stromal Cells in Adult Human Bone Marrow. *Stem Cell Reports*, 3(6), pp.965–974.

Liang, G. et al., 2010. Butyrate promotes induced pluripotent stem cell generation. *The Journal of biological chemistry*, 285(33), pp.25516–21.

Lindner, U. et al., 2010. Mesenchymal stem or stromal cells: Toward a better understanding of their biology? *Transfusion Medicine and Hemotherapy*, 37(2), pp.75–83.

Liu, H. et al., 2008. Developmental expression of histone deacetylase 11 in the murine brain. *Journal of Neuroscience Research*, 86(3), pp.537–543.

Liu, W. et al., 2012. HDAC6 regulates epidermal growth factor receptor (EGFR) endocytic trafficking and degradation in renal epithelial cells. *PloS one*, 7(11), p.e49418.

Liu, Y., Lim, J. & Teoh, S.-H., 2013. Review: Development of clinically relevant scaffolds for vascularised bone tissue engineering. *Biotechnology Advances*, 31(5), pp.688–705.

Lu, D.-F. et al., 2014. Knockdown of the HDAC1 Promotes the Directed Differentiation of Bone Mesenchymal Stem Cells into Cardiomyocytes. *PloS one*, 9(3), p.e92179.

Lu, W. et al., 2014. Bone tissue engineering by using a combination of polymer/Bioglass composites with human adipose-derived stem cells. *Cell and tissue research*, 356(1), pp.97–107.

Luger, K. et al., 1997. Crystal structure of the nucleosome core particle at 2 . 8 A° resolution. *Nature*, 389(6648), pp.251–260.

Lv, F. et al., 2014. Concise Review : The Surface Markers and Identity of Human Mesenchymal Stem Cells. *Stem Cells*, 32, pp.1408–1419.

MacDonald, J.L. & Roskams, A.J., 2008. Histone deacetylases 1 and 2 are expressed at distinct stages of neuro-glial development. *Developmental Dynamics*, 237(8), pp.2256–67.

Mackie, E.J. et al., 2008. Endochondral ossification: How cartilage is converted into bone in the developing skeleton. *International Journal of Biochemistry and Cell Biology*, 40(1), pp.46–62.

Madsen, A.S. & Olsen, C.A., 2012. Profiling of substrates for zinc-dependent lysine deacylase enzymes: HDAC3 exhibits decrotonylase activity in vitro. *Angewandte Chemie*, 51(36), pp.9083–7.

Maeda, S. et al., 2004. Endogenous TGF-beta signaling suppresses maturation of osteoblastic mesenchymal cells. *The EMBO journal*, 23(3), pp.552–563.

Majdzadeh, N. et al., 2008. HDAC4 inhibits cell cycle progression and protects neurons from cell death. *Developmental Neurobiology*, 68(8), pp.1076–1092.

Marks, P. & Breslow, R., 2007. Dimethyl sulfoxide to vorinostat: development of this histone deacetylase inhibitor as an anticancer drug. *Nature biotechnology*, 25(1), pp.84–90.

Maroni, P. et al., 2012. Chemical and genetic blockade of HDACs enhances osteogenic differentiation of human adipose tissue-derived stem cells by oppositely affecting osteogenic and adipogenic transcription factors. *Biochemical and biophysical research communications*, 428(2), pp.271–7.

Martin, S., Vincent, J.-P. & Mazella, J., 2003. Involvement of the neurotensin receptor-3 in the neurotensin-induced migration of human microglia. *The Journal of neuroscience*, 23(4), pp.1198–1205.

Martínez-Balbás, M.A. et al., 2000. Regulation of E2F1 activity by acetylation. *The EMBO journal*, 19(4), pp.662–71.

Mayani, H. & Lansdorp, P., 1994. Thy-1 Expression is linked to functional properties of primitive hematopoietic progenitor cells from human umbilical cord blood. *Blood*, 83(9), pp.2410–2417.

McGee-Lawrence, M.E. et al., 2013. Histone deacetylase 3 is required for maintenance of bone mass during aging. *Bone*, 52(1), pp.296–307.

McGee-Lawrence, M.E. et al., 2011. Suberoylanilide hydroxamic acid (SAHA; vorinostat) causes bone loss by inhibiting immature osteoblasts. *Bone*, 48(5), pp.1117–26.

McKinsey, T.A., 2011. Isoform-selective HDAC inhibitors: closing in on translational medicine for the heart. *Journal of molecular and cellular cardiology*, 51(4), pp.491–6.

Mckinsey, T.A. et al., 2000. Signal-dependent nuclear export of a histone deacetylase regulates muscle differentiation. *Letters to Nature*, 408(November), pp.106–111.

McMahon, R.E. et al., 2013. Development of nanomaterials for bone repair and regeneration. *Journal of Biomedical Materials Research Part B: Applied Biomaterials*, 101B(2), pp.387–397.

McQuown, S.C. et al., 2011. HDAC3 is a critical negative regulator of long-term memory formation. *The Journal of neuroscience*, 31(2), pp.764–74.

Meinel, L. et al., 2005. Silk implants for the healing of critical size bone defects. *Bone*, 37(5), pp.688–698.

Méjat, A. et al., 2005. Histone deacetylase 9 couples neuronal activity to muscle chromatin acetylation and gene expression. *Nature neuroscience*, 8(3), pp.313–21.

Michalczyk, K. & Ziman, M., 2005. Nestin structure and predicted function in cellular cytoskeletal organisation. *Histology and Histopathology*, 20(2), pp.665–671.

Mikkelsen, T.S. et al., 2007. Genome-wide maps of chromatin state in pluripotent and lineage-committed cells. *Nature*, 448(7153), pp.553–60.

Miller, K.M. et al., 2010. Human HDAC1 and HDAC2 function in the DNA-damage response to promote DNA nonhomologous end-joining. *Nature structural & molecular biology*, 17(9), pp.1144–51.

Minárovits, J., 2009. Microbe-induced epigenetic alterations in host cells: the coming era of patho-epigenetics of microbial infections. A review. *Acta microbiologica et immunologica Hungarica*, 56(1), pp.1–19.

Mitchell, J.B. et al., 2006. Immunophenotype of Human Adipose-Derived Cells: Temporal Changes in Stromal-Associated and Stem Cell-Associated Markers. *Stem Cells*, 24(2), pp.376–385.

Miyamoto, S. et al., 2013. Bombyx mori silk fibroin scaffolds for bone regeneration studied by bone differentiation experiment. *Journal of Bioscience and Bioengineering*, 115(5), pp.575–578.

Mizuno, Y. et al., 2009. miR-210 promotes osteoblastic differentiation through inhibition of AcvR1b. *FEBS Letters*, 583(13), pp.2263–2268.

Montecino, M. et al., 1999. Chromatin hyperacetylation abrogates vitamin D-mediated transcriptional upregulation of the tissue-specific osteocalcin gene in vivo. *Biochemistry*, 38(4), pp.1338–45.

Montecino-Rodriguez, E., Leathers, H. & Dorshkind, K., 2000. Expression of connexin 43 (Cx43) is critical for normal hematopoiesis. *Blood*, 96(3), pp.917–924.

Montgomery, R.L. et al., 2009. Histone deacetylases 1 and 2 control the progression of neural precursors to neurons during brain development. *Proceedings of the National Academy of Sciences of the United States of America*, 106(19), pp.7876–81.

Montgomery, R.L. et al., 2007. Histone deacetylases 1 and 2 redundantly regulate cardiac morphogenesis , growth , and contractility. *Genes & development*, 21, pp.1790–1802.

Montgomery, R.L. et al., 2008. Maintenance of cardiac energy metabolism by histone deacetylase 3 in mice. *The Journal of clinical investigation*, 118(11), pp.3588–97.

Moore, K.A. & Lemischka, I.R., 2006. Stem cells and their niches. *Science*, 311(5769), pp.1880–1885.

Moresi, V. et al., 2012. Histone deacetylases 1 and 2 regulate autophagy flux and skeletal muscle homeostasis in mice. *Proceedings of the National Academy of Sciences of the United States of America*, 109(5), pp.1649–54.

Morris, G.M. et al., 1998. Automated Docking Using a Lamarckian Genetic Algorithm and an Empirical Binding Free Energy Function. *Journal of Computational Chemistry*, 19(14), pp.1639–1662.

Moser, M. et al., 2003. BMPER, a Novel Endothelial Cell Precursor-Derived Protein, Antagonizes Bone Morphogenetic Protein Signaling and Endothelial Cell Differentiation. *Molecular and cellular biology*, 23(16), pp.5664–5679.

Mundlos, S. et al., 1991. Distribution of Cartilage Proteoglycan (Aggrecan) Core Protein and Link Protein Gene Expression during Human Skeletal Development. *Matrix*, 11(5), pp.339–346.

Naderi, H., Matin, M.M. & Bahrami, A.R., 2011. Review paper: critical issues in tissue engineering: biomaterials, cell sources, angiogenesis, and drug delivery systems. *Journal of biomaterials applications*, 26(4), pp.383–417.

Naguib, M., Bie, B. & Ting, A.H., 2012. Fundamental concepts of epigenetics for consideration in anesthesiology. *Current opinion in anaesthesiology*, 25(4), pp.434–43.

Nair, S.B. et al., 2012. Computational identification of novel histone deacetylase inhibitors by docking based QSAR. *Computers in biology and medicine*, 42(6), pp.697–705.

Nakamura, T. et al., 2005. Inhibition of histone deacetylase suppresses osteoclastogenesis and bone destruction by inducing IFN-beta production. *Journal of immunology*, 175(9), pp.5809–5816.

Naski, M.C. et al., 1998. Repression of hedgehog signaling and BMP4 expression in growth plate cartilage by fibroblast growth factor receptor 3. *Development*, 125, pp.4977–88.

Nebbioso, A. et al., 2012. Trials with “epigenetic” drugs: an update. *Molecular oncology*, 6(6), pp.657–82.

Nebbioso, A. et al., 2005. Tumor-selective action of HDAC inhibitors involves TRAIL induction in acute myeloid leukemia cells. *Nature medicine*, 11(1), pp.77–84.

New, M., Olzscha, H. & La Thangue, N.B., 2012. HDAC inhibitor-based therapies: can we interpret the code? *Molecular oncology*, 6(6), pp.637–56.

Ni, X., Li, L. & Pan, G., 2015. HDAC inhibitor-induced drug resistance involving ATP-binding cassette transporters (Review). *Oncology letters*, 9(2), pp.515–521.

Nielsen, J.S. & McNagny, K.M., 2008. Novel functions of the CD34 family. *Journal of cell science*, 121(Pt 22), pp.3683–3692.

Niki, T. et al., 1999. A histone deacetylase inhibitor, trichostatin A, suppresses myofibroblastic differentiation of rat hepatic stellate cells in primary culture. *Hepatology*, 29(3), pp.858–67.

Nissen-Meyer, L.S.H. et al., 2007. Levetiracetam, phenytoin, and valproate act differently on rat bone mass, structure, and metabolism. *Epilepsia*, 48(10), pp.1850–60.

Oehme, I. et al., 2013. Histone deacetylase 10 promotes autophagy-mediated cell survival. *Proceedings of the National Academy of Sciences of the United States of America*, 110(28), pp.E2592–601.

Ogu, C.C. & Maxa, J.L., 2000. Drug interactions due to cytochrome P450. *Baylor University Medical Center Proceedings*, 13(4), pp.421–423.

Ohtani, K. & Dimmeler, S., 2011. Epigenetic regulation of cardiovascular differentiation. *Cardiovascular research*, 90(3), pp.404–12.

Okochi-Takada, E. et al., 2014. ANGPTL4 is a secreted tumor suppressor that inhibits angiogenesis. *Oncogene*, 33(17), pp.2273–8.

Omenetto, F.G. & Kaplan, D.L., 2010. New opportunities for an ancient material. *Science*, 329(5991), pp.528–531.

Orlando, G. et al., 2011. Regenerative medicine and organ transplantation: past, present, and future. *Transplantation*, 91(12), pp.1310–7.

Ornitz, D.M. et al., 1996. Receptor specificity of the fibroblast growth factor family. *The Journal of biological chemistry*, 271(25), pp.15292–15297.

Ortiz, L. a et al., 2003. Mesenchymal stem cell engraftment in lung is enhanced in response to bleomycin exposure and ameliorates its fibrotic effects. *Proceedings of the National Academy of Sciences of the United States of America*, 100(14), pp.8407–8411.

Ozawa, Y. et al., 2001. Histone deacetylase 3 associates with and represses the transcription factor GATA-2. *Blood*, 98(7), pp.2116–2123.

Ozgurll, K. et al., 1990. Structure of the Human Smooth Muscle Actin Gene. *The Journal of biological chemistry*, 265(3), pp.1683–1687.

Paino, F. et al., 2014. Histone deacetylase inhibition with valproic acid downregulates osteocalcin gene expression in human dental pulp stem cells and osteoblasts: Evidence for HDAC2 involvement. *Stem Cells*, 32(1), pp.279–289.

Pang, M. et al., 2011. Histone deacetylase 1/2 mediates proliferation of renal interstitial fibroblasts and expression of cell cycle proteins. *Journal of Cellular Biochemistry*, 112(8), pp.2138–2148.

Park, I.H. et al., 2008. Reprogramming of human somatic cells to pluripotency with defined factors. *Nature*, 451(7175), pp.141–6.

Park, S.-S. et al., 2011. Esculetin inhibits cell proliferation through the Ras/ERK1/2 pathway in human colon cancer cells. *Oncology reports*, 25(1), pp.223–230.

Patra, C. et al., 2012. Silk protein fibroin from Antheraea mylitta for cardiac tissue engineering. *Biomaterials*, 33(9), pp.2673–2680.

Payne, C.S., 2013. Expenditure on healthcare in the UK : 2011. *Office for National Statistics*, (May), pp.1–14.

Pelus, L.M. et al., 2002. Peripheral blood stem cell mobilization A role for CXC chemokines. *Critical Reviews in Oncology/Hematology*, 43(3), pp.257–275.

Petruccelli, L. et al., 2011. Vorinostat induces reactive oxygen species and dna damage in acute myeloid leukemia cells. *PLoS ONE*, 6(6), p.e20987.

Pham, L. et al., 2011. HDAC3 and HDAC7 have opposite effects on osteoclast differentiation. *The Journal of biological chemistry*, 286(14), pp.12056–65.

Phiel, C.J. et al., 2001. Histone deacetylase is a direct target of valproic acid, a potent anticonvulsant, mood stabilizer, and teratogen. *The Journal of biological chemistry*, 276(39), pp.36734–41.

Planat-Benard, V. et al., 2004. Plasticity of human adipose lineage cells toward endothelial cells: physiological and therapeutic perspectives. *Circulation*, 109(5), pp.656–663.

Pocock, G. & Richards, C.D., 2006. *Human Physiology: The Basis of Medicine* Third., Oxford: OXFORD UNIV PRESS.

Ponta, H., Sherman, L. & Herrlich, P., 2003. CD44: from adhesion molecules to signalling regulators. *Nature reviews. Molecular cell biology*, 4(1), pp.33–45.

Pontiki, E. & Hadjipavlou-Litina, D., 2011. Histone deacetylase inhibitors (HDACIs). Structure—activity relationships: history and new QSAR perspectives. *Medicinal Research Reviews*, 32(1), pp.1–165.

Pratap, J. et al., 2010. The histone deacetylase inhibitor, vorinostat, reduces tumor growth at the metastatic bone site and associated osteolysis, but promotes normal bone loss. *Molecular cancer therapeutics*, 9(12), pp.3210–20.

Preynat-Seauve, O. & Krause, K.-H., 2011. Stem cell sources for regenerative medicine: the immunological point of view. *Seminars in immunopathology*, 33(6), pp.519–24.

Prince, H. & Bishton, M., 2009. Panobinostat (LBH589): a novel pan-deacetylase inhibitor with activity in T cell lymphoma. *Hematology Meeting Reports*, 3(1), pp.33–38.

Purrucker, J.C. et al., 2010. HDAC inhibition radiosensitizes human normal tissue cells and reduces DNA double-strand break repair capacity. *Oncology Reports*, 23(1), pp.263–269.

Qiu, L. et al., 1999. Anti-tumour activity in vitro and in vivo of selective differentiating agents containing hydroxamate. *British Journal of Cancer*, 80(8), pp.1252–1258.

Qiu, L. et al., 2000. Histone deacetylase inhibitors trigger a G2 checkpoint in normal cells that is defective in tumor cells. *Molecular biology of the cell*, 11(6), pp.2069–83.

Ragni, E. et al., 2013. What is beyond a qRT-PCR study on mesenchymal stem cell differentiation properties: how to choose the most reliable housekeeping genes. *Journal of Cellular and Molecular Medicine*, 17(1), pp.168–180.

Rahman, M.M. et al., 2003. Two histone deacetylase inhibitors, trichostatin A and sodium butyrate, suppress differentiation into osteoclasts but not into macrophages. *Blood*, 101(9), pp.3451–9.

Ramalho-Santos, M. et al., 2002. “Stemness”: transcriptional profiling of embryonic and adult stem cells. *Science*, 298(5593), pp.597–600.

Razidlo, D.F. et al., 2010. Histone deacetylase 3 depletion in osteo/chondroprogenitor cells decreases bone density and increases marrow fat. *PloS one*, 5(7), p.e11492.

Reddy, P. et al., 2004. Histone deacetylase inhibitor suberoylanilide hydroxamic acid reduces acute graft-versus-host disease and preserves graft-versus-leukemia effect. *Proceedings of the National Academy of Sciences of the United States of America*, 101(11), pp.3921–6.

Reichert, N., Choukrallah, M.-A. & Matthias, P., 2012. Multiple roles of class I HDACs in proliferation, differentiation, and development. *Cellular and molecular life sciences : CMLS*, 69(13), pp.2173–87.

Reya, T. et al., 2001. Stem cells, cancer, and cancer stem cells. *Nature*, 414(6859), pp.105–11.

Richardson, P. et al., 2008. Phase I trial of oral vorinostat (suberoylanilide hydroxamic acid, SAHA) in patients with advanced multiple myeloma. *Leukemia & lymphoma*, 49(3), pp.502–7.

Riss, T.L. et al., 2004. Cell Viability Assays Assay Guidance Manual. In *Assay Guidance Manual*. pp. 1–23.

Rivieccio, M.A. et al., 2009. HDAC6 is a target for protection and regeneration following injury in the nervous system. *Proceedings of the National Academy of Sciences of the United States of America*, 106(46), pp.19599–604.

Robert, T. et al., 2011. HDACs link the DNA damage response, processing of double-strand breaks and autophagy. *Nature*, 471(7336), pp.74–79.

Robey, P.G., 2011. Cell sources for bone regeneration: the good, the bad, and the ugly (but promising). *Tissue engineering. Part B, Reviews*, 17(6), pp.423–30.

Ropero, S. & Esteller, M., 2007. The role of histone deacetylases (HDACs) in human cancer. *Molecular oncology*, 1(1), pp.19–25.

Rosato, R.R. et al., 2003. The Histone Deacetylase Inhibitor MS-275 Promotes Differentiation or Apoptosis in Human Leukemia Cells through a Process Regulated by Generation of Reactive Oxygen Species and Induction of p21CIP1/WAF11. *Cancer Research*, 63, pp.3637–3645.

Rubie, C. et al., 2005. Housekeeping gene variability in normal and cancerous colorectal, pancreatic, esophageal, gastric and hepatic tissues. *Molecular and cellular probes*, 19(2), pp.101–9.

Ruefli, A.A. et al., 2001. The histone deacetylase inhibitor and chemotherapeutic agent suberoylanilide hydroxamic acid (SAHA) induces a cell-death pathway characterized by cleavage of Bid and production of reactive oxygen species. *Proceedings of the National Academy of Sciences of the United States of America*, 98(19), pp.10833–8.

De Ruijter, A.J.M. et al., 2003. Histone deacetylases (HDACs): characterization of the classical HDAC family. *The Biochemical journal*, 370(Pt 3), pp.737–49.

Sadoul, K. et al., 2015. HDAC6 controls the kinetics of platelet activation. *Platelets and Thrombopoiesis*, 120(20), pp.4215–4219.

Sadoul, K. et al., 2008. Regulation of protein turnover by acetyltransferases and deacetylases. *Biochimie*, 90(2), pp.306–12.

Saha, S. et al., 2013. Osteochondral tissue engineering in vivo: a comparative study using layered silk fibroin scaffolds from mulberry and nonmulberry silkworms. *PloS one*, 8(11), p.e80004.

Sahu, N. et al., 2015. Nonmulberry Silk Fibroin Scaffold Shows Superior Osteoconductivity Than Mulberry Silk Fibroin in Calvarial Bone Regeneration. *Adv Healthc Mater.*, 4(11), pp.1709–21.

Sato, N. et al., 2004. Maintenance of pluripotency in human and mouse embryonic stem cells through activation of Wnt signaling by a pharmacological GSK-3-specific inhibitor. *Nature medicine*, 10(1), pp.55–63.

Schildberg, F.A. et al., 2010. Improved transplantation outcome by epigenetic changes. *Transplant immunology*, 23(3), pp.104–10.

Scholl, C. et al., 2012. Distinct and overlapping gene regulatory networks in BMP- and HDAC-controlled cell fate determination in the embryonic forebrain. *BMC genomics*, 13, p.298.

Schroeder, T.M. et al., 2007. Gene profile analysis of osteoblast genes differentially regulated by histone deacetylase inhibitors. *BMC genomics*, 8, p.362.

Schroeder, T.M. et al., 2004. Histone deacetylase 3 interacts with runx2 to repress the osteocalcin promoter and regulate osteoblast differentiation. *The Journal of biological chemistry*, 279(40), pp.41998–2007.

Schroeder, T.M. & Westendorf, J.J., 2005. Histone deacetylase inhibitors promote osteoblast maturation. *Journal of bone and mineral research : the official journal of the American Society for Bone and Mineral Research*, 20(12), pp.2254–63.

Schweyer, S., 2013. Phytoestrogens regulate the proliferation and expression of stem cell factors in cell lines of malignant testicular germ cell tumors. *International Journal of Oncology*, (10), pp.1385–1394.

Sebaugh, J.L., 2011. Guidelines for accurate EC50/IC50 estimation. *Pharmaceutical Statistics*, 10(2), pp.128–134.

Sekiya, I. et al., 2004. Adipogenic differentiation of human adult stem cells from bone marrow stroma (MSCs). *Journal of bone and mineral research : the official journal of the American Society for Bone and Mineral Research*, 19(2), pp.256–264.

Senese, S. et al., 2007. Role for histone deacetylase 1 in human tumor cell proliferation. *Molecular and cellular biology*, 27(13), pp.4784–95.

Senn, S.M. et al., 2010. Adverse effects of valproate on bone: defining a model to investigate the pathophysiology. *Epilepsia*, 51(6), pp.984–93.

Sera, Y. et al., 2010. Hematopoietic Stem Cell Origin of Adipocytes. *Experimental Hematology*, 37(9), pp.1108–1120.

Sfeir, C. et al., 2014. Synthesis of bone-like nanocomposites using multiphosphorylated peptides. *Acta Biomaterialia*, 10(5), pp.2241–2249.

Shahbazian, M.D. & Grunstein, M., 2007. Functions of site-specific histone acetylation and deacetylation. *Annual review of biochemistry*, 76, pp.75–100.

Shakespear, M.R. et al., 2013. Histone deacetylase 7 promotes Toll-like receptor 4-dependent proinflammatory gene expression in macrophages. *The Journal of biological chemistry*, 288(35), pp.25362–74.

Shakespear, M.R. et al., 2011. Histone deacetylases as regulators of inflammation and immunity. *Trends in immunology*, 32(7), pp.335–43.

Shao, Y. et al., 2004. Apoptotic and autophagic cell death induced by histone deacetylase inhibitors. *Proceedings of the National Academy of Sciences of the United States of America*, 101(52), pp.18030–5.

Shen, G., 2005. The role of type X collagen in facilitating and regulating endochondral ossification of articular cartilage. *Orthodontics and Craniofacial Research*, 8(1), pp.11–17.

Shen, J. et al., 2002. Histone acetylation in vivo at the osteocalcin locus is functionally linked to vitamin D-dependent, bone tissue-specific transcription. *The Journal of biological chemistry*, 277(23), pp.20284–92.

Siddappa, R. et al., 2007. Donor variation and loss of multipotency during in vitro expansion of human mesenchymal stem cells for bone tissue engineering. *Journal of orthopaedic research*, 25(8), pp.1029–1041.

Silha, J. V et al., 2003. Perturbations in bone formation and resorption in insulin-like growth factor binding protein-3 transgenic mice. *Journal of bone and mineral research : the official journal of the American Society for Bone and Mineral Research*, 18(10), pp.1834–1841.

Silvestri, L. et al., 2012. Histone deacetylase inhibitors: structure-based modeling and isoform-selectivity prediction. *Journal of chemical information and modeling*, 52(8), pp.2215–35.

Silveyra, P. & Floros, J., 2012. Air pollution and epigenetics: effects on SP-A and innate host defence in the lung. *Swiss medical weekly*, 142, p.w13579.

Snykers, S. et al., 2009. In vitro differentiation of embryonic and adult stem cells into hepatocytes: state of the art. *Stem cells*, 27(3), pp.577–605.

Somoza, J.R. et al., 2004. Structural snapshots of human HDAC8 provide insights into the class I histone deacetylases. *Structure*, 12(7), pp.1325–34.

Spange, S. et al., 2009. Acetylation of non-histone proteins modulates cellular signalling at multiple levels. *The international journal of biochemistry & cell biology*, 41(1), pp.185–98.

Spivakov, M. & Fisher, A.G., 2007. Epigenetic signatures of stem-cell identity. *Nature reviews. Genetics*, 8(4), pp.263–71.

Stancheva, I., 2011. Revisiting heterochromatin in embryonic stem cells. *PLoS genetics*, 7(6), p.e1002093.

Steinmann, J. et al., 2009. Phenylbutyrate induces antimicrobial peptide expression. *Antimicrobial agents and chemotherapy*, 53(12), pp.5127–33.

Sternson, S.M. et al., 2001. Synthesis of 7200 Small Molecules Based on a Substructural Analysis of the Histone Deacetylase Inhibitors Trichostatin and Trapoxin. *Organic Letters*, 3(26), pp.4239–4242.

Subramani, V., 2015. OPN –Revisited. *Journal of Clinical and Diagnostic Research*, 9(ii), pp.10–13.

Suga, H. et al., 2009. Functional Implications of CD34 Expression in Human Adipose–Derived Stem/Progenitor Cells. *Stem Cells and Development*, 18(8), pp.1201–1210.

Sun, G. et al., 2007. Orphan nuclear receptor TLX recruits histone deacetylases to repress transcription and regulate neural stem cell proliferation. *Proceedings of the National Academy of Sciences of the United States of America*, 104(39), pp.15282–7.

Swart, G.W.M., 2002. Activated leukocyte cell adhesion molecule (CD166/ALCAM): developmental and mechanistic aspects of cell clustering and cell migration. *European journal of cell biology*, 81(6), pp.313–321.

Tait, S.W.G., Ichim, G. & Green, D.R., 2014. Die another way - non-apoptotic mechanisms of cell death. *Journal of cell science*, 127(Pt 10), pp.2135–44.

Takada, Y. et al., 2006. Suberoylanilide hydroxamic acid potentiates apoptosis, inhibits invasion, and abolishes osteoclastogenesis by suppressing nuclear factor-kappaB activation. *The Journal of biological chemistry*, 281(9), pp.5612–22.

Takahashi, K. et al., 2007. Induction of pluripotent stem cells from adult human fibroblasts by defined factors. *Cell*, 131(5), pp.861–72.

Tang, H. et al., 2009. Novel inhibitors of human histone deacetylase (HDAC) identified by QSAR modeling of known inhibitors, virtual screening, and experimental validation. *Journal of chemical information and modeling*, 49(2), pp.461–76.

Teven, C.M. et al., 2011. Epigenetic regulation of mesenchymal stem cells: a focus on osteogenic and adipogenic differentiation. *Stem cells international*, 2011, p.201371.

Thurston, G., 2003. Role of Angiopoietins and Tie receptor tyrosine kinases in angiogenesis and lymphangiogenesis. *Cell and Tissue Research*, 314(1), pp.61–68.

Thysen, S., Luyten, F.P. & Lories, R.J., 2015. Loss of Frzb and Sfrp1 differentially affects joint homeostasis in instability-induced osteoarthritis. *Osteoarthritis and Cartilage*, 23(2), pp.275–279.

Tollervey, J.R. & Lunyak, V. V, 2012. Epigenetics: Judge, jury and executioner of stem cell fate. *Epigenetics*, 7(8), pp.823–40.

Tomlinson, M.J. et al., 2015. Tissue non-specific alkaline phosphatase production by human dental pulp stromal cells is enhanced by high density cell culture. *Cell and Tissue Research*, pp.529–540.

Tremoleda, J.L. et al., 2011. Imaging technologies for preclinical models of bone and joint disorders. *EJNMMI research*, 1(1), p.11.

Trivedi, C.M. et al., 2007. HDAC2 regulates the cardiac hypertrophic response by modulating Gsk3 beta activity. *Nature medicine*, 13(3), pp.324–31.

Trivedi, C.M. et al., 2008. Transgenic overexpression of Hdac3 in the heart produces increased postnatal cardiac myocyte proliferation but does not induce hypertrophy. *The Journal of biological chemistry*, 283(39), pp.26484–9.

Trowbridge, I.S. & Thomas, M.L., 1994. CD45: an emerging role as a protein tyrosine phosphatase required for lymphocyte activation and development. *Annual review of immunology*, 12, pp.85–116.

Tsaniras, S.C. et al., 2014. Licensing of DNA replication, cancer, pluripotency and differentiation: an interlinked world? *Seminars in cell & developmental biology*, 30(June), pp.174–180.

Tsuchiya, H. et al., 2003. Chondrogenesis enhanced by overexpression of sox9 gene in mouse bone marrow-derived mesenchymal stem cells. *Biochemical and Biophysical Research Communications*, 301(2), pp.338–343.

Tsuji, N. et al., 1976. A new antifungal antibiotic, trichostatin. *The Journal of antibiotics*, 29(1), pp.1–6.

Turnpenny, L. et al., 2006. Evaluating human embryonic germ cells: concord and conflict as pluripotent stem cells. *Stem Cells*, 24(2), pp.212–20.

U.S. Food and Drug Administration, FDA approves Farydak for treatment of multiple myeloma. *FDA News Release*. Available at: http://www.fda.gov/NewsEvents/Newsroom/PressAnnouncements/ucm435296.htm.

Uciechowska, U., Sippl, W. & Jung, M., 2009. NAA+-Dependent Histone Deacetylases (Sirtuins) as Novel Therapeutic Targets. *Medicinal Research Reviews*, 30(6), pp.861–889.

Ungerstedt, J.S. et al., 2005. Role of thioredoxin in the response of normal and transformed cells to histone deacetylase inhibitors. *Proceedings of the National Academy of Sciences of the United States of America*, 102(3), pp.673–8.

Vannini, A. et al., 2004. Crystal structure of a eukaryotic zinc-dependent histone deacetylase, human HDAC8, complexed with a hydroxamic acid inhibitor. *Proceedings of the National Academy of Sciences of the United States of America*, 101(42), pp.15064–9.

Vanommeslaeghe, K., Loverix, S., et al., 2005. DFT-based ranking of zinc-binding groups in histone deacetylase inhibitors. *Bioorganic & medicinal chemistry*, 13(21), pp.6070–82.

Vanommeslaeghe, K., De Proft, F., et al., 2005. Theoretical study revealing the functioning of a novel combination of catalytic motifs in histone deacetylase. *Bioorganic & medicinal chemistry*, 13(12), pp.3987–92.

Vastardis, H. et al., 1996. A human MSX1 homeodomain missense mutation causes selective tooth agenesis. *Nature genetics*, 13(4), pp.417–421.

Vater, C., Kasten, P. & Stiehler, M., 2011. Culture media for the differentiation of mesenchymal stromal cells. *Acta biomaterialia*, 7(2), pp.463–77.

Vega, R.B. et al., 2004. Histone deacetylase 4 controls chondrocyte hypertrophy during skeletogenesis. *Cell*, 119(4), pp.555–66.

Verdin, E., Dequiedt, F. & Kasler, H.G., 2003. Class II histone deacetylases: versatile regulators. *Trends in genetics : TIG*, 19(5), pp.286–93.

Verreault, A., 2000. De novo nucleosome assembly: new pieces in an old puzzle. *Genes & development*, 145, pp.1430–1438.

Villagra, A. et al., 2008. The histone deacetylase HDAC11 regulates the expression of interleukin 10 and immune tolerance. *Nature Immunology*, 10, pp.92–100.

Vondermark, K. et al., 1977. Relationship between cell shape and type of collagen synthesised as chondrocytes lose their cartilage phenotype in culture. *Nature*, 267, pp.531–532.

Vrtačnik, P., Marc, J. & Ostanek, B., 2013. Epigenetic mechanisms in bone. *Clinical chemistry and laboratory medicine*, 52(5), pp.1–20.

Vunjak-Novakovic, G. et al., 2010. Challenges in cardiac tissue engineering. *Tissue engineering. Part B, Reviews*, 16(2), pp.169–87.

Wagner, F.F. et al., 2013. Small molecule inhibitors of zinc-dependent histone deacetylases. *Neurotherapeutics*, 10(4), pp.589–604.

Wagner, W. et al., 2005. Comparative characteristics of mesenchymal stem cells from human bone marrow, adipose tissue, and umbilical cord blood. *Experimental Hematology*, 33(11), pp.1402–1416.

Wang, D., 2009. Computational Studies on the Histone Deacetylases and the Design of Selective Histone Deacetylase Inhibitors. *Current Topics in Medicinal Chemistry*, 9(3), pp.241–256.

Wang, L.D. & Wagers, A.J., 2011. Dynamic niches in the origination and differentiation of haematopoietic stem cells. *Nature Reviews Molecular Cell Biology*, 12(10), pp.643–655.

Wang, P. et al., 2009. An evaluation of OPTC and EPYC as candidate genes for high myopia. *Molecular vision*, 15(October), pp.2045–2049.

Wang, W. et al., 2012. PAPSS2 promotes alkaline phosphates activity and mineralization of osteoblastic MC3T3-E1 cells by crosstalk and smads signal pathways. *PLoS ONE*, 7(8), pp.1–9.

Wermuth, C.G. et al., 1998. Glossary of terms used in medicinal chemistry. *Pure and Applied Chemistry*, 70(5), pp.1129–1143.

West, A.C. & Johnstone, R.W., 2014. New and emerging HDAC inhibitors for cancer treatment. *J Clin Invest.*, 124(1), pp.30–39.

Van Wijk, B., Moorman, A.F.M. & van den Hoff, M.J.B., 2007. Role of bone morphogenetic proteins in cardiac differentiation. *Cardiovascular research*, 74(2), pp.244–255.

Wilson, A.J. et al., 2006. Histone deacetylase 3 (HDAC3) and other class I HDACs regulate colon cell maturation and p21 expression and are deregulated in

human colon cancer. *The Journal of biological chemistry*, 281(19), pp.13548–58.

Wilson, J.M., 2009. Medicine. A history lesson for stem cells. *Science*, 324(5928), pp.727–728.

Wilting, R.H. et al., 2010. Overlapping functions of Hdac1 and Hdac2 in cell cycle regulation and haematopoiesis. *The EMBO journal*, 29(15), pp.2586–97.

Witt, O. et al., 2009. HDAC family: What are the cancer relevant targets? *Cancer letters*, 277(1), pp.8–21.

Xiadou Wang et al., 2010. *Fundamental Biomechanics in Bone Tissue Engineering*, Morgan and Claypool Publishers.

Xiang, Y., Hou, Z. & Zhang, Z., 2012. Pharmacophore and QSAR studies to design novel histone deacetylase 2 inhibitors. *Chemical biology & drug design*, 79(5), pp.760–70.

Xu, S. et al., 2013. Effect of the HDAC inhibitor vorinostat on the osteogenic differentiation of mesenchymal stem cells in vitro and bone formation in vivo. *Acta pharmacologica Sinica*, 34(5), pp.699–709.

Xu, W.S. et al., 2005. Induction of polyploidy by histone deacetylase inhibitor: a pathway for antitumor effects. *Cancer research*, 65(17), pp.7832–9.

Xu, W.S., Parmigiani, R.B. & Marks, P.A., 2007. Histone deacetylase inhibitors: molecular mechanisms of action. *Oncogene*, 26(37), pp.5541–52.

Xu, Y. et al., 2009. Inhibition of histone deacetylase activity in reduced oxygen environment enhances the osteogenesis of mouse adipose-derived stromal cells. *Tissue engineering. Part A*, 15(12), pp.3697–707.

Yadav, M.C. et al., 2014. Ablation of Osteopontin Improves the Skeletal Phenotype of Phospho1(-/-) Mice. *Journal of bone and mineral research*, 29(11), pp.1–32.

Yamaguchi, T. et al., 2010. Histone deacetylases 1 and 2 act in concert to promote the G1-to-S progression. *Genes & development*, 24(5), pp.455–69.

Yamaguchi, Y., Naiki, T. & Irie, K., 2012. Stau1 regulates Dvl2 expression during myoblast differentiation. *Biochemical and Biophysical Research Communications*, 417(1), pp.427–432.

Yang, W.-M. et al., 1997. Isolation and Characterization of cDNAs Corresponding to an Additional Member of the Human Histone Deacetylase Gene Family. *Journal of Biological Chemistry*, 272(44), pp.28001–28007.

Yang, X. et al., 2003. Induction of human osteoprogenitor chemotaxis, proliferation, differentiation, and bone formation by osteoblast stimulating factor-1/pleiotrophin: osteoconductive biomimetic scaffolds for tissue engineering. *Journal of bone and mineral research*, 18(1), pp.47–57.

Ye, F. et al., 2009. HDAC1 and HDAC2 regulate oligodendrocyte differentiation by disrupting the beta-catenin-TCF interaction. *Nature neuroscience*, 12(7), pp.829–38.

Ye, Y. et al., 2013. PI(4,5)P2 5-phosphatase A regulates PI3K/Akt signalling and has a tumour suppressive role in human melanoma. *Nature communications*, 4, p.1508.

Yi, T. & Baek, J., 2007. Trichostatin A-mediated upregulation of p21 osteoclast apoptosis. *Experimental and Molecular Medicine*, 39(2), pp.213–221.

Yoo, E.J. et al., 2006. Down-regulation of histone deacetylases stimulates adipocyte differentiation. *The Journal of biological chemistry*, 281(10), pp.6608–15.

Yu, Q. et al., 2013. Wnt/β-catenin signaling regulates neuronal differentiation of mesenchymal stem cells. *Biochemical and Biophysical Research Communications*, 439(2), pp.297–302.

Zaidi, S.K. et al., 2010. Architectural epigenetics: mitotic retention of mammalian transcriptional regulatory information. *Molecular and cellular biology*, 30(20), pp.4758–4766.

Zammit, P.S. & Beauchamp, J.R., 2001. The skeletal muscle satellite cell: stem cell or son of stem cell? *Differentiation*, 68(4-5), pp.193–204.

Zelzer, E. et al., 2004. VEGFA is necessary for chondrocyte survival during bone development. *Development*, 131(9), pp.2161–2171.

Zhang, D. et al., 2014. Activation of histone deacetylase-6 induces contractile dysfunction through derailment of α-tubulin proteostasis in experimental and human atrial fibrillation. *Circulation*, 129(3), pp.346–58.

Zhang, J. & Zhong, Q., 2014. Histone deacetylase inhibitors and cell death. *Cellular and molecular life sciences : CMLS*, 71(20), pp.3885–901.

Zhang, L. et al., 2012. Inhibition of Histone Deacetylase-induced Myocardial Repair Is Mediated by c-kit in Infarcted Hearts. *The Journal of biological chemistry*, 287(47), pp.39338–48.

Zhang, R. et al., 2013. Wnt/β-catenin signaling activates bone morphogenetic protein 2 expression in osteoblasts. *Bone*, 52(1), pp.145–156.

Zhang, X. et al., 2010. FK228 induces mitotic catastrophe in A549 cells by mistargeting chromosomal passenger complex localization through changing centromeric H3K9 hypoacetylation. *Acta Biochimica et Biophysica Sinic*, 42(10), pp.677–687.

Zhang, Y. et al., 2011. An essential role of discoidin domain receptor 2 (DDR2) in osteoblast differentiation and chondrocyte maturation via modulation of Runx2 activation. *Journal of Bone and Mineral Research*, 26(3), pp.604–617.

Zhang, Y. et al., 2008. Mice lacking histone deacetylase 6 have hyperacetylated tubulin but are viable and develop normally. *Molecular and cellular biology*, 28(5), pp.1688–701.

Zhang, Z. et al., 2011. Epigenetic suppression of GAD65 expression mediates persistent pain. *Nature medicine*, 17(11), pp.1448–55.

Zhao, J. et al., 2009. Apatite-coated silk fibroin scaffolds to healing mandibular border defects in canines. *Bone*, 45(3), pp.517–527.

Zhao, L.-R. et al., 2002. Human bone marrow stem cells exhibit neural phenotypes and ameliorate neurological deficits after grafting into the ischemic brain of rats. *Experimental neurology*, 174(1), pp.11–20.

Zhao, X. et al., 2001. The modular nature of histone deacetylase HDAC4 confers phosphorylation-dependent intracellular trafficking. *The Journal of biological chemistry*, 276(37), pp.35042–8.

Zheng, B. et al., 2006. Mouse adipose-derived stem cells undergo multilineage differentiation in vitro but primarily osteogenic and chondrogenic differentiation in vivo. *Tissue engineering*, 12(7), pp.1891–1901.

Zhong, Y. et al., 2011. IGF binding protein 3 exerts its ligand-independent action by antagonizing BMP in zebrafish embryos. *Journal of cell science*, 124(Pt 11), pp.1925–1935.

Zhou, G. et al., 2006. Dominance of SOX9 function over RUNX2 during skeletogenesis. *Proceedings of the National Academy of Sciences of the United States of America*, 103(50), pp.19004–19009.

Zhou, X. et al., 2001. Cloning and characterization of a histone deacetylase, HDAC9. *Proceedings of the National Academy of Sciences of the United States of America*, 98(19), pp.10572–7.

Zhu, Y. et al., 2010. Investigation on the isoform selectivity of histone deacetylase inhibitors using chemical feature based pharmacophore and docking approaches. *European Journal of Medicinal Chemistry*, 45(5), pp.1777–1791.

Zuk, P.A. et al., 2002. Human Adipose Tissue Is a Source of Multipotent Stem Cells. *Molecular Biology of the Cell*, 13(December), pp.4279–4295.

Zuk, P.A. et al., 2001. Multilineage Cells from Human Adipose Tissue : Implications for Cell-Based Therapies. *Tissue engineering*, 7(2), pp.211–228.

Zupkovitz, G. et al., 2010. The cyclin-dependent kinase inhibitor p21 is a crucial target for histone deacetylase 1 as a regulator of cellular proliferation. *Molecular and cellular biology*, 30(5), pp.1171–81.

List of Abbreviations

2D	Two dimensional
3D	Three dimensional
α-MEM	Alpha minimal essential medium
ADSCs	Adipose derived stem cells
ALP	Alkaline phosphatase
ALPSA	Alkaline phosphatase specific activity
aq.	Aqueous
Boc	*tert*-butyl carbamate
br	Broad
δ	Chemical shift
CD	Cluster of differentiation
cDNA	Complementary DNA
CFMDA	5-chloromethylfluorescein diacetate
Ct	Threshold cycle value (for PCR)
d	Doublet
dH_2O	Distilled Water
dd	Double doublet
Et_2O	Diethyl ether
DMF	Dimethylformamide
DMSO	Dimethyl sulfoxide
DNA	Deoxyribonucleic acid
DPX	p-xylene-bis (N-pyridinium bromide)
EDS	Energy-dispersive X-ray spectroscopy
EDTA	Ethylenediaminetetraacetic acid
EthD-1	Ethidium Homodimer-1
EtOAc	Ethyl acetate

EtOH	Ethanol
eq.	Equivalents
FACs	Fluorescence-activated cell sorting
FCS	Fetal calf serum
H+E	Harris' haematoxylin and Eosin histological staining
HATs	Histone acetyltransferases
hBMCs	Human bone marrow stem cells
HCl	Hydrochloric acid
HDAC	Histone deacetylase
HDACi	Histone deacetylase inhibitor
H_2O	Water
HSCs	Haematopoietic stem cells
IC_{50}	Half maximal inhibitory concentration
ITS –G	Insulin-Transferrin-Selenium
L	Litre
LCA	Leukocyte Common Antigen
LCAM	Leukocyte Cell Adhesion Molecule
L-G	L-glutamine
m	Multiplet
MCAM	Melanoma Cell Adhesion Molecule
MHz	Megahertz
Mol/M	Moles
mRNA	Messenger RNA
MSCs	Mesenchymal stem cells
n	Normal
NaB	Sodium butyrate (HDACi)
NBF	Neutral buffered formalin
NMR	Nuclear magnetic resonance
OCN	Osteocalcin

OPN	Osteopontin
PBS	Phosphate buffered saline
PCR	Polymerase chain reaction
P/S	Penicillin-strepto-mycin
PI	Propidium iodide
qRT-PCR	Quantitative real-time polymerase chain reaction
RNA	Ribonucleic acid
RPM	Revolutions per minute
s	Singlet
SAHA	Suberoylnilide hydroxamic acid
SDS	Sodium dodecyl sulfate
SEM	Scanning electron microscopy
t	Triplet
T/E	0.25% Trypsin/EDTA (Ethylenediaminetetraacetic acid)
tert or t	Tertiary
TFA	Trifluoroacetic acid
TGF	Transforming growth factor
THF	Tetrahydrofuran
TSA	Trichostatin A
U.V.	Ultraviolet
VPA	Valproic Acid

Appendix A
Supplementary Lab Data

A.1 - NMR Spectra

Full NMR spectra for the compounds synthesised in Chapter 3: The Chemical Synthesis of MI192 follows. The peaks are described in 3.3: Results.

Figure A.1 - NMR spectrum for compound 1 (4-(4,6-Dimethoxy-1,3,5-triazin-2-yl)-4-methylmorpholinium tetrafluoroborate.

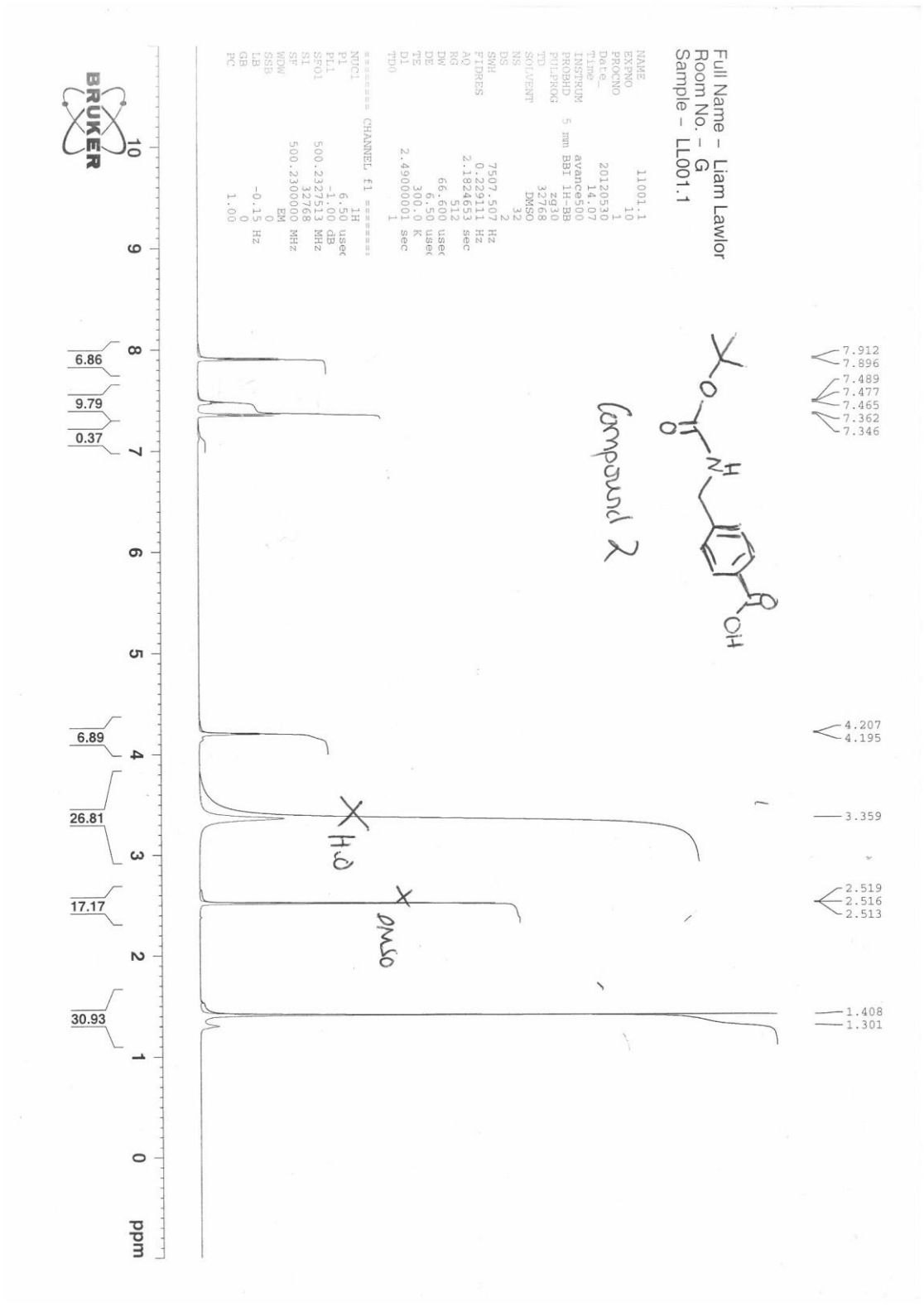

Figure A.2 - NMR spectrum for compound 2 (((Tert-butoxycarbonylamino)methyl)benzoic acid).

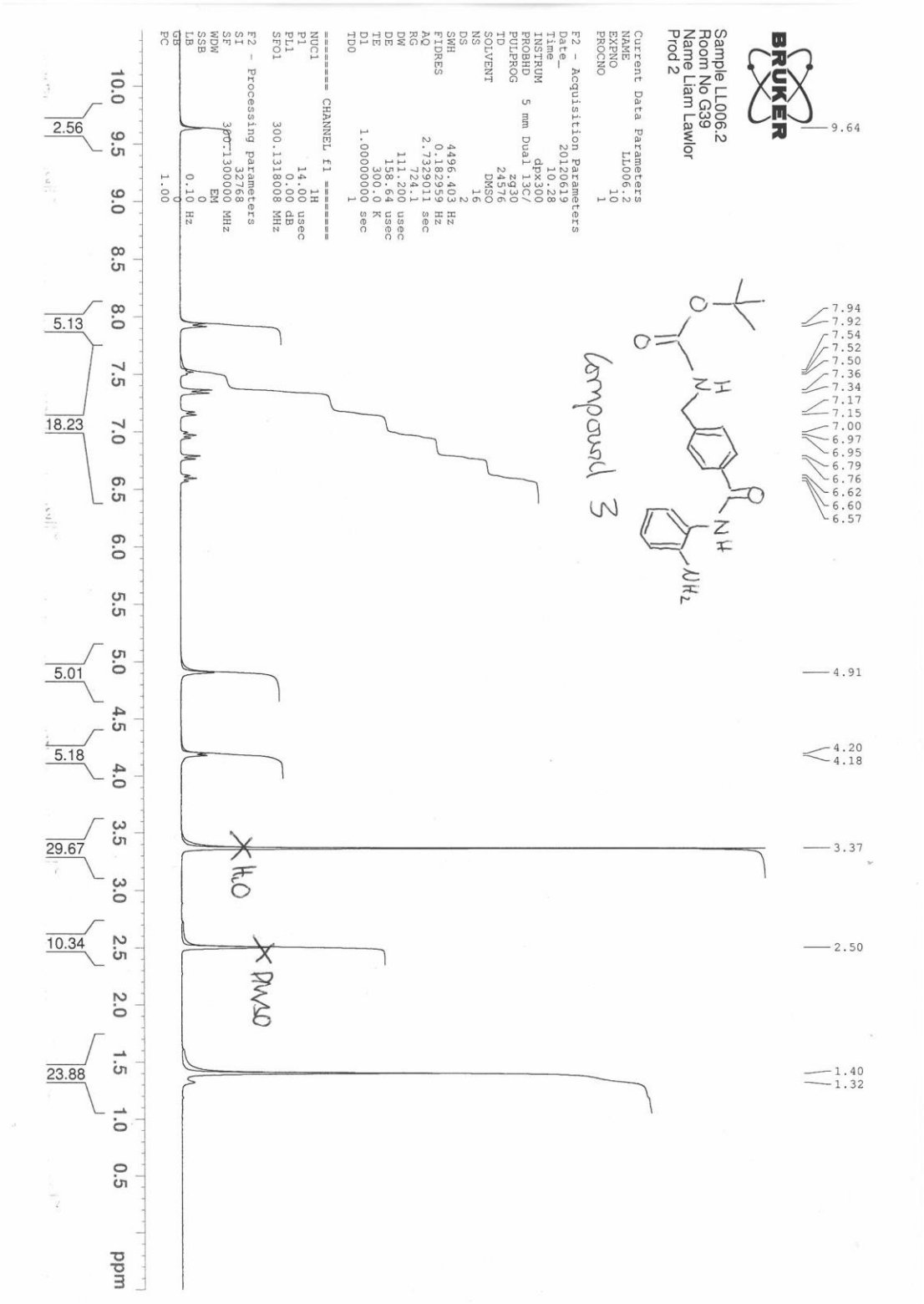

Figure A.3 - NMR spectrum for compound 3 (*tert*-Butyl 4-(2-aminophenylcarbamoyl)benzylcarbamate).

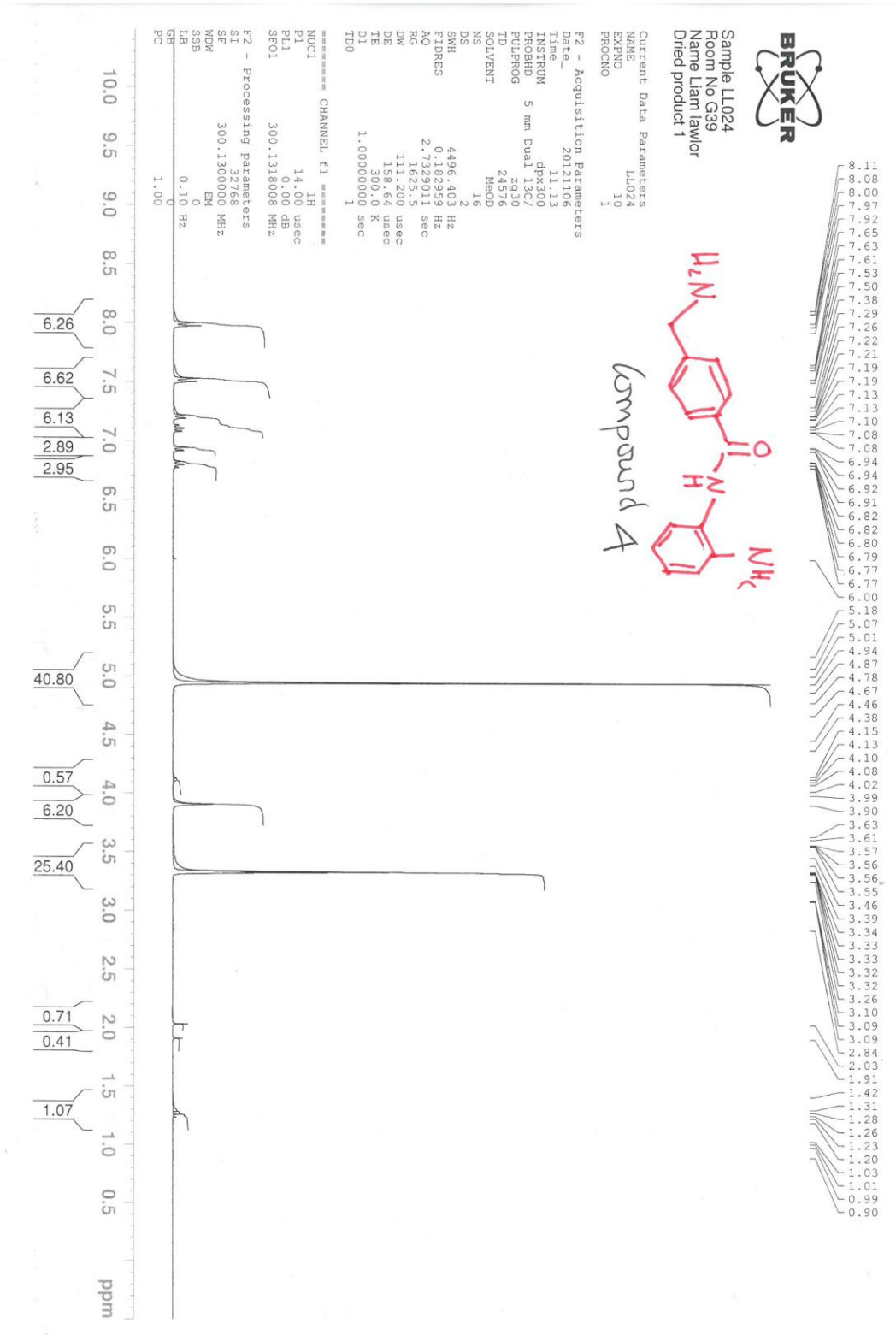

Figure A.4 - NMR spectrum for compound 4 (4-(Aminomethyl)-N-(2-aminophenyl)benzamide).

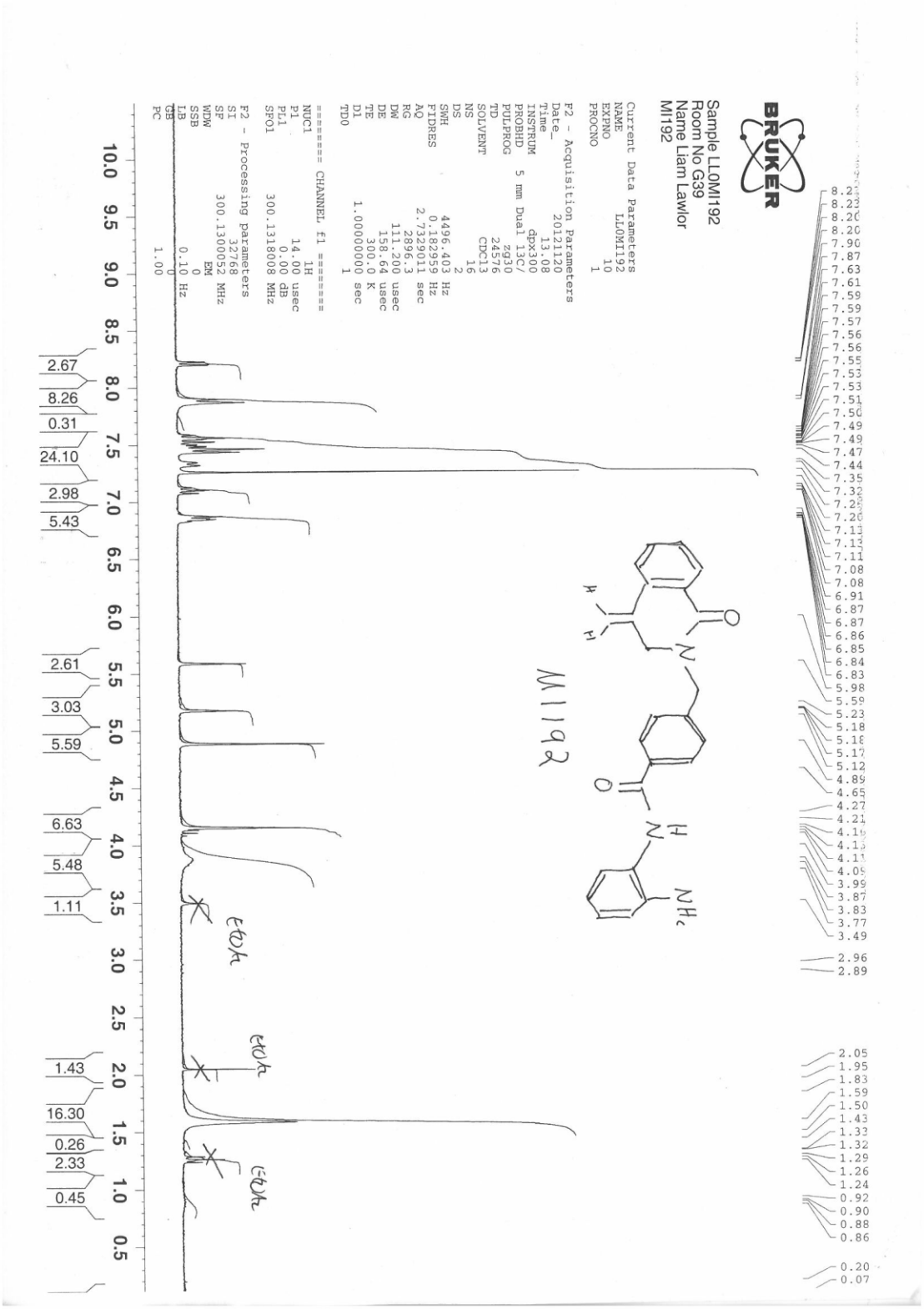

Figure A.5 – NMR spectrum for MI192.

A2 - Confirmation of tri-linage differentiation potential of ADSCs

The ADSCs were capable of mineralised nodule formation, indicating osteogenic differentiation, after 28 days growth in osteogenic induction medium, with calcium mineralisation stained red by Alizarin Red staining (Figure A.6 A). The mineralisation stain was much stronger than in the negative basal control, where no staining was observed.

The ADSCs were capable of lipid droplet accumulation, indicating adipogenic differentiation, after 14 days growth in adipogenic induction medium (Figure A.6 B). The lipid droplet stain was much stronger than in the negative basal control, where no staining was observed.

The ASCSs were also capable of producing Glycosaminoglycans (GAGs) (stained blue with an Alcian blue stain) and a collagenous capsule around a pellet (stained red with a Sirius red stain), indicating chondrogenic differentiation, after 21 days growth in a pellet culture model in chondrogenic induction medium (Figure A.6 C). The collagen and GAG staining was much stronger than in the negative basal control, where weak staining was observed.

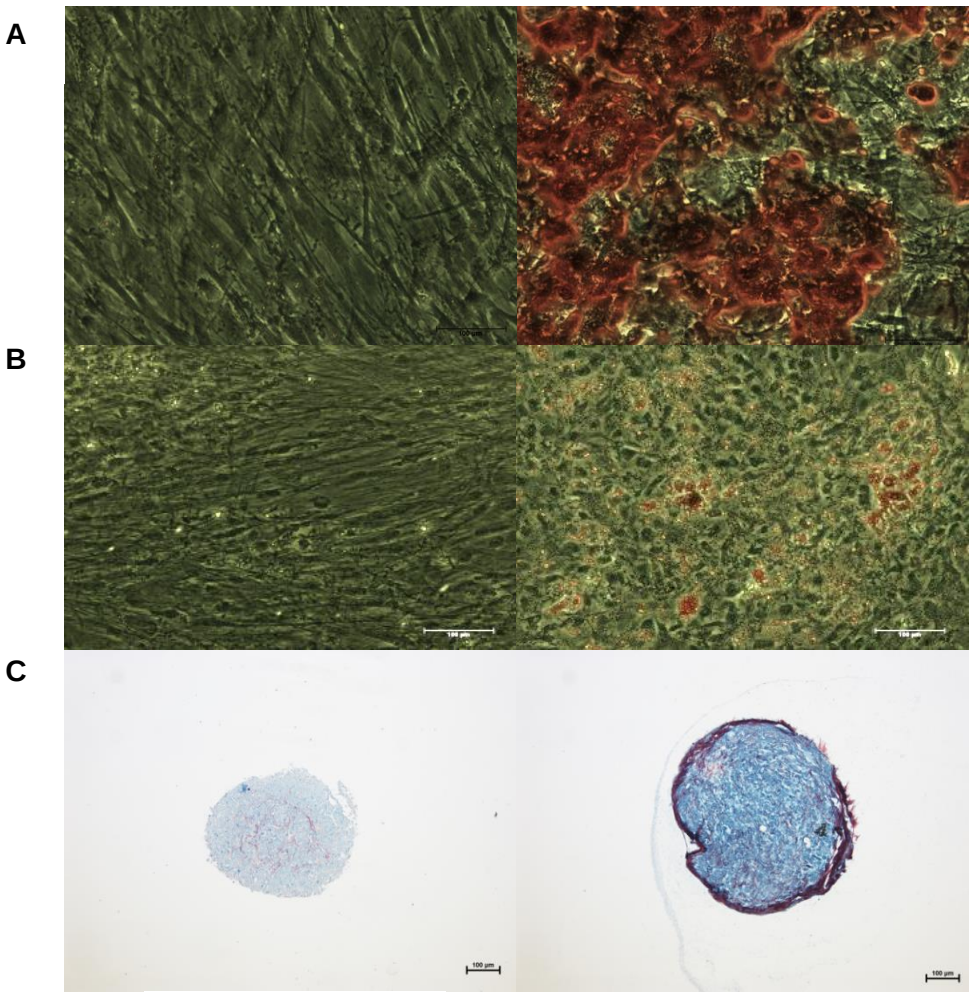

Figure A.6 – Confirmation of tri-lineage differentiation potential of ADSCs. A: Osteogenic differentiation: ADSCs capable of mineralisation after 28 days growth in osteogenic induction medium, stained red for calcium by Alizarin Red staining; **B**: Adipogenic differentiation: ADSCs capable of lipid droplet formation after 14 days growth in adipogenic induction medium, stained red for lipid droplets by oil red O staining; **C**: Chondrogenic differentiation: ADSCs capable of forming cartilage like pellets after 21 days growth in a pellet model and chondrogenic induction medium, stained blue for GAGs by Alcian Blue staining and red for collagen by Sirius Red staining. Scale bars = 100 μM.

A3 - Investigation of the effect off 1% – 0.01% DMSO has on ADSC cell number and viability

To ensure that MI192 dissolved, a stock solution was first made up with DMSO, which was then further diluted in culture medium, resulting in cells being exposed to potentially harmful DMSO. A summary of the equivalent DMSO percentages cells would be exposed to with the relevant doses of MI192 can be seen in Table A 0-1. To investigate the effect DMSO has on ADSCs, ADSCs were cultured with a relevant range of DMSO concentrations and the effect investigated.

PicroGreen® was used to assess the effect on total cell number DMSO had on ADSCs (Figure A.7). Total DNA content at a range of DMSO concentrations, across three days, was compared to a basal, untreated, negative control. These dose ranges and times cover every dose in this thesis. After one day of treatment with a range of DMSO concentrations, DNA content similar was the same as the negative basal control. At day 2 and day 3 the 1% DMSO dose showed a reduced cell number, presumably DMSO was having a cytotoxic effect on the cells. All other doses (0.5% - 0.01%) showed a total DNA content similar to the negative basal control.

The cell viability was investigated after 2 days of culture with DMSO (the most common dose length for experiments in this thesis) with the CellGlo® ATP measuring cell viability assay (Figure A.8). Cell viability was found to be in the range of the negative basal control at all concentrations of DMSO. This was not normalised to cell number, but the cell numbers should be the same across the groups according to the PicoGreen® results (Figure A.7), except the 1% DMSO group, which would only be increased by normalisation to cell number, bringing it closer to the negative basal control.

Table A 0-1 - The equivalent DMSO percentage which cells will be exposed to when dosed with MI192

MI192 dose	Equivalent DMSO %
100 µM	1 %
50 µM	0.5 %
40 µM	0.4 %
30 µM	0.3 %
20 µM	0.2 %
10 µM	0.1 %
1µM	0.01 %

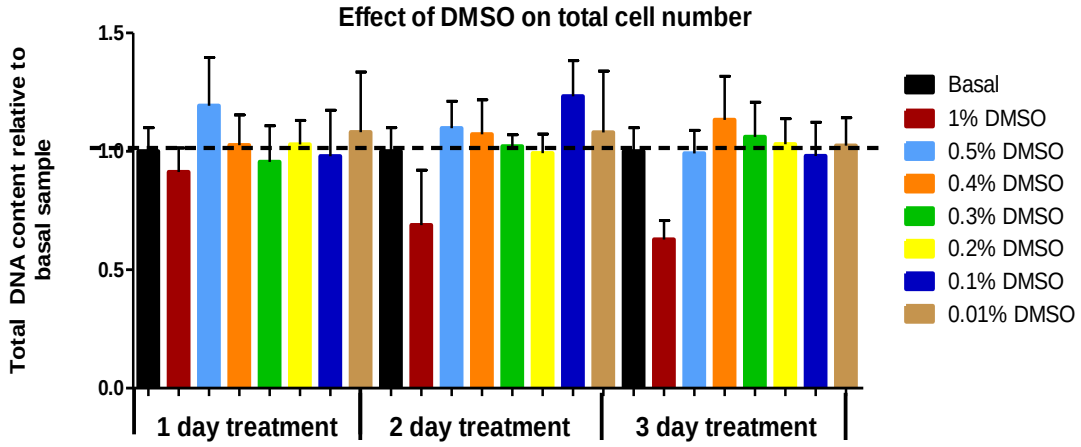

Figure A.7- DMSO effect on cell numbers. Quant-iT™ PicoGreen® analysis of ADSCs treated for 1 day, 2 days and 3 days with a range of concentrations of DMSO (1% - 0.01%), normalised to a 0% basal sample for each time point. Results expressed as mean ± SD (n=3). Dotted line represents the negative, basal control normalised to 1.

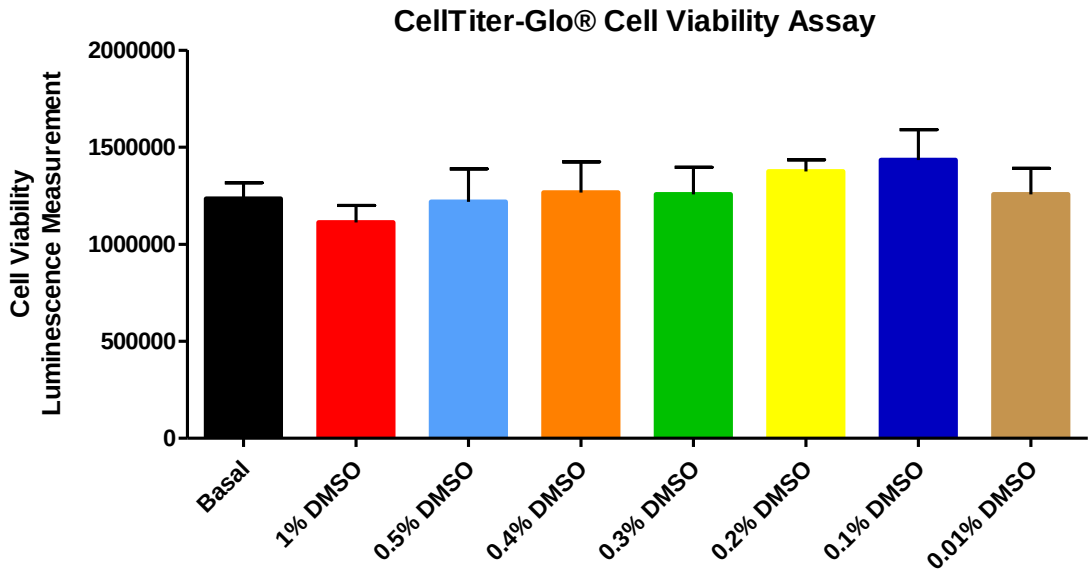

Figure A.8 - CellTiter-Glo® analysis of ADSCs treated with a range of concentrations of DMSO (1% - 0.01%) for 2 days. Results expressed as mean ± SD (n=3).

A4 - Effect of MI192 on ADSC Stem Cell Markers: FACs plots and autofluorescence comparison histograms

The expression of 9 commonly used stem cell markers (see Table 4-1 for full details) was investigated in ADSCs treated with MI192 (30 µM for 2 days), compared to untreated basal medium controls. Markers were assessed as a group of three (CD29/CD73/CD90) and three groups of two (CD34/CD45, CD44/CD166 and CD146/CD105).

Representative dot plots of the events (after gating for intact cells) were produced for the groups of markers for both the untreated (Figure A.9) and the MI192 treated ADSCs (Figure A.10). Also shown are histograms showing the expression of the marker compared to the autofluorescence of the cells, for both untreated (Figure A.8) and the MI192 treated ADSCs (Figure A.9). This was to account autofluorescence when analysing the markers, and to ensure there was no overlap with the expressing populations. Any differences in peak size/areas is due to variations in the event counts.

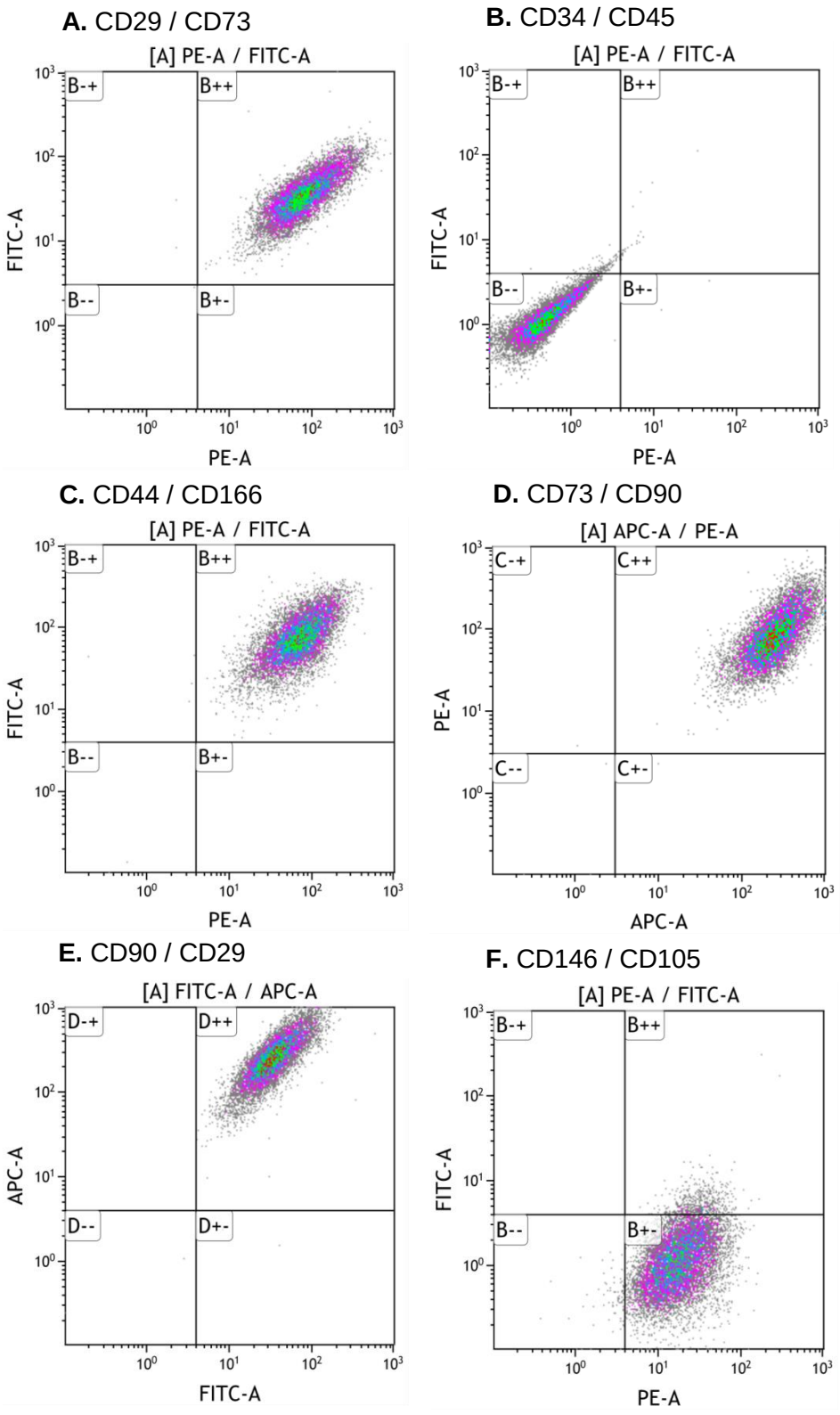

Figure A.9 – Representative FACs plots showing flow cytometric analysis of stem cell markers in untreated ADSCs. A – CD29/CD73; B – CD34/CD45; C – CD44/CD166; D – CD73/CD90; E – CD90/CD29 and F – CD146/CD105. Markers plotted in pairs, with the first marker listed on the Y Axis.

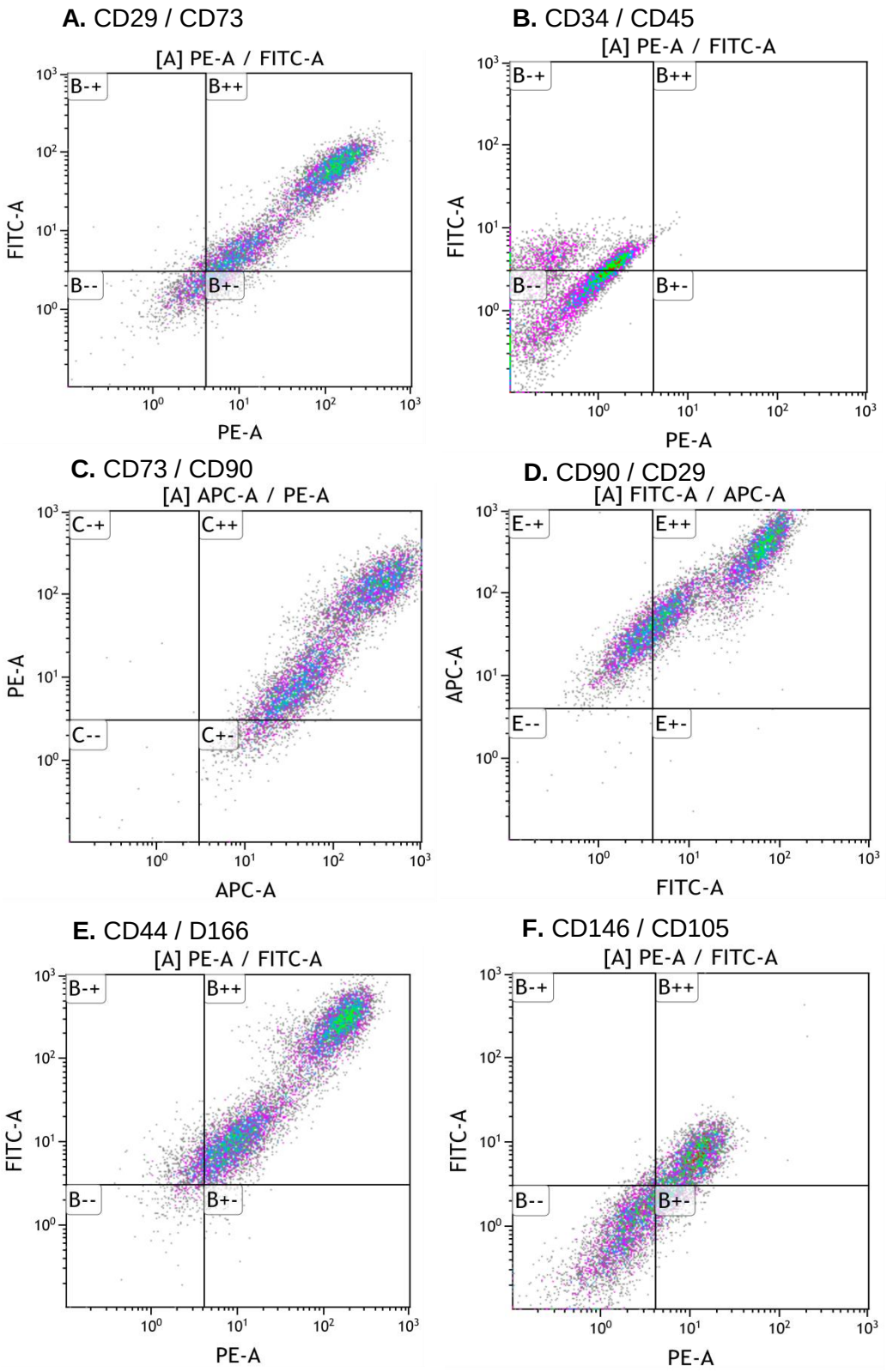

Figure A.1010 - Representative FACs plots showing flow cytometric analysis of stem cell markers in MI192 treated ADSCs. A – CD29/CD73; B – CD34/CD45; C – CD44/CD166; D – CD73/CD90; E – CD90/CD29; F – CD146/CD105. Markers plotted in pairs, with the first marker listed on the Y Axis.

I

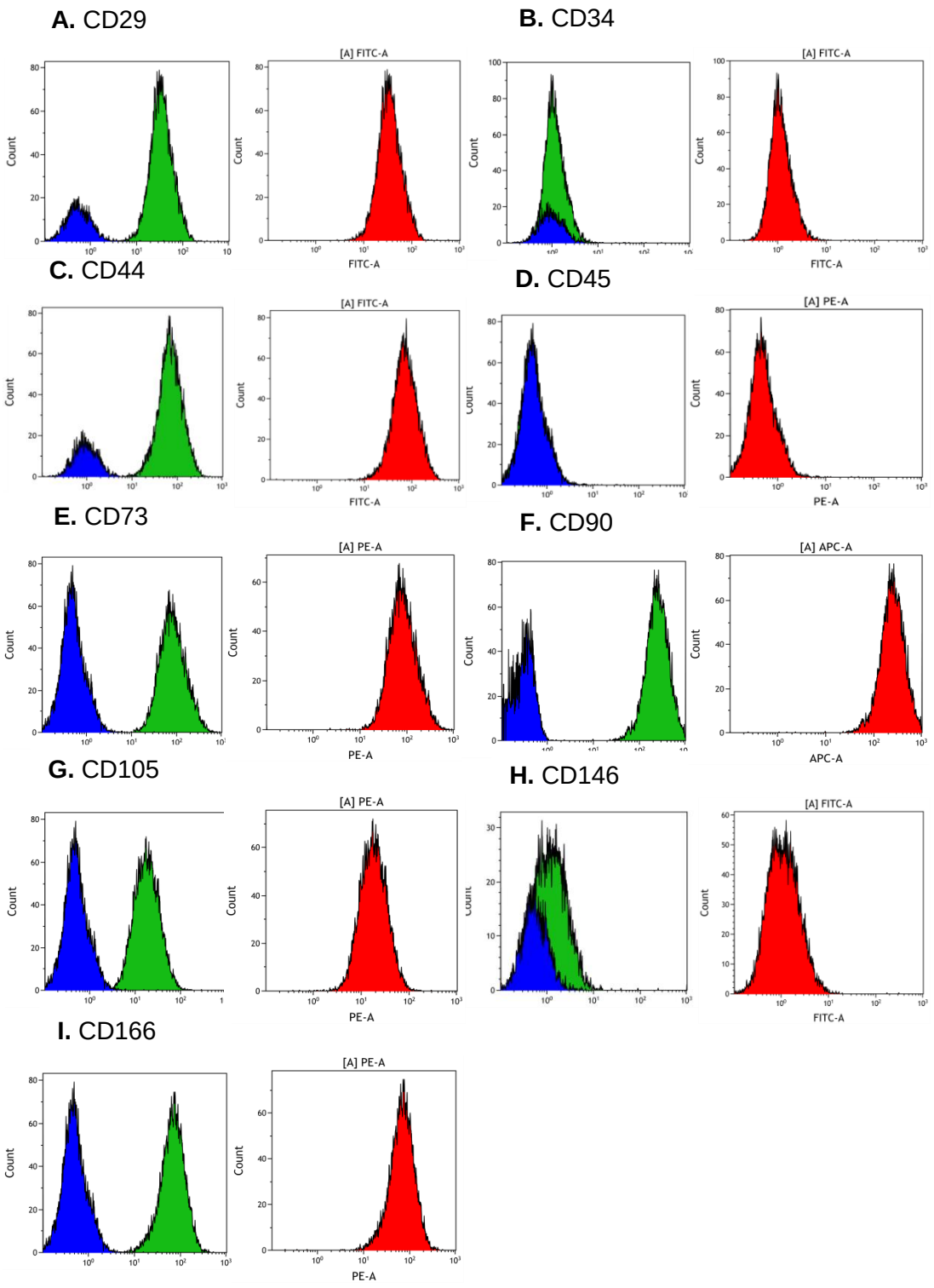

Figure A.111 - Representative histograms showing flow cytometric analysis of stem cell markers in untreated ADSCs. A – CD29, B – CD34, C – CD44, D – CD45, E – CD73, F – CD90, G – CD105, H – CD146, I – CD166. Histograms showing count for each marker (green colour) compared to a negative control (blue colour) and for each marker alone (red).

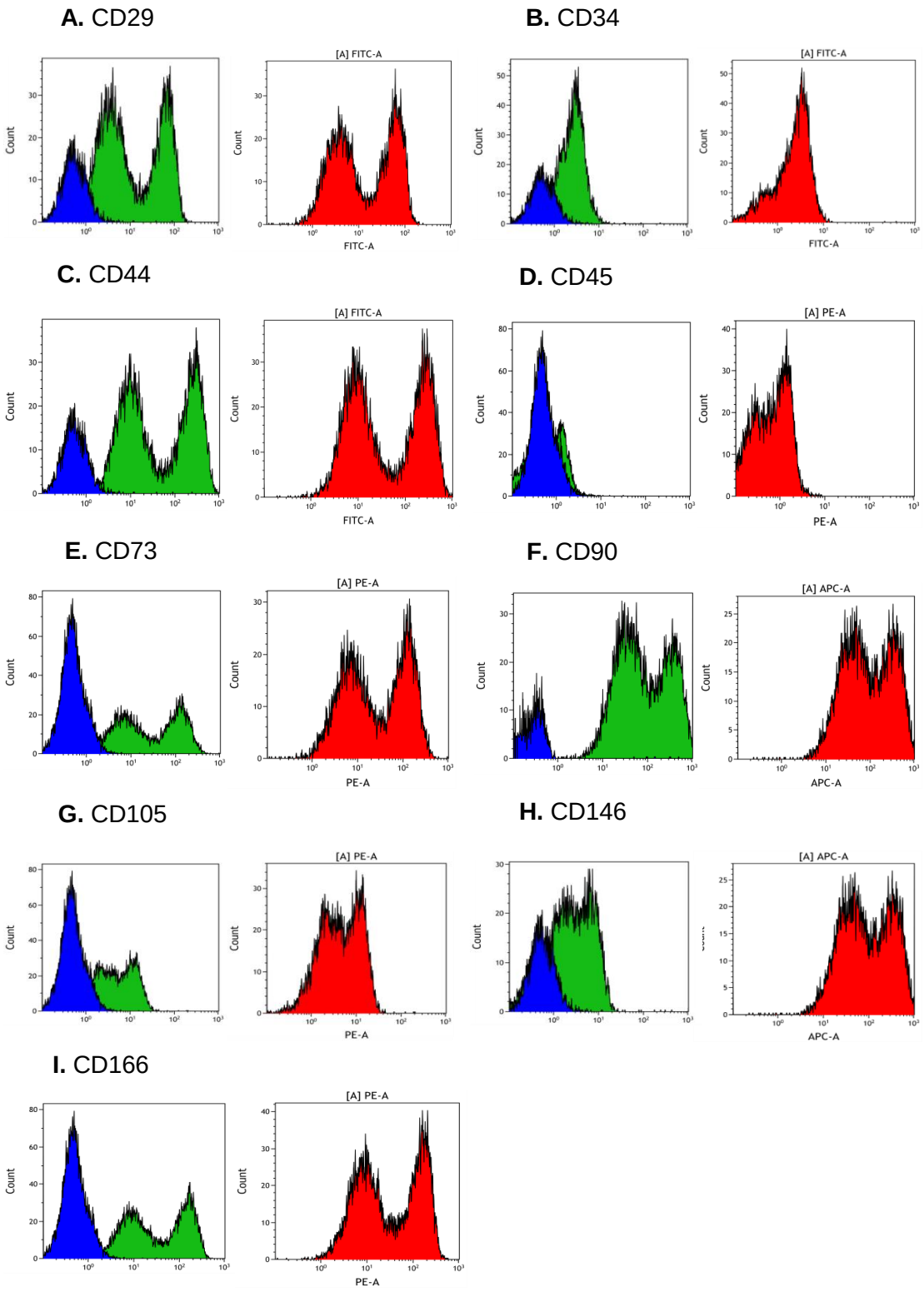

Figure A.12 - Representative histograms showing flow cytometric analysis of stem cell markers in MI192 treated ADSCs. A – CD29, B – CD34, C – CD44, D – CD45, E – CD73, F – CD90, G – CD105, H – CD146, I – CD166. Histograms showing count for each marker (green colour) compared to a negative control (blue colour) and for each marker alone (red).

A5 – qRT-PCR choice of housekeeping gene and standard curves

A5.1 - Choice of Housekeeping Gene for qRT-PCR Assays

For all qRT-PCR experiments, it is standard practice to use a housekeeping to normalise the expression of target genes. An endogenous control housekeeping gene should expressed at a constant level in the samples, and is essential to act as a reference to reduce possible errors (Rubie et al. 2005; Ragni et al. 2013).

The more stable the housekeeping gene, the better for determining the change in expression of other genes. *GAPDH* is a commonly used housekeeping gene; however, there is an argument there are even more stable genes available. Previous work in the department, and a journal article on the topic (Ragni et al. 2013), suggested that *YWHAZ* may be a more stable gene, especially for differentiation protocols.

A comparative study between Glyceraldehyde-3-phosphate dehydrogenase (*GAPDH*) and Tyrosine 3-Monooxygenase/Tryptophan 5-Monooxygenase Activation Protein (*YWHAZ*) was undertaken to determine the most stable housekeeping gene. For four different conditions from the adipogenic differentiation experiment outlined 5.3.7: Assessment of the effect of MI192 pre-treatment on the adipogenic gene expression of ADSCs in Chapter 5: The Effects of MI192 on the Differentiation of Adipose Derived Stem Cells in 2D. The expression of the two genes was calculated, in biological triplicate and with three technical repeats for a total of n = 18 for each condition. Graphs of the mean ± SE was plotted (Figure A.13) and the statistical significance was determined by Kruskal-Wallis 1 way ANOVA test, using Graphpad Version 5 of variance between the Ct values. Calculated was a p value of 0.0016 for *YWHAZ* (**, $P \leq 0.01$) and 0.0005 for *GAPDH* (***, $P \leq 0.001$) The lower variance with the *YWHAZ* housekeeping gene between samples resulted in this being selected for all qRT-PCR experiments.

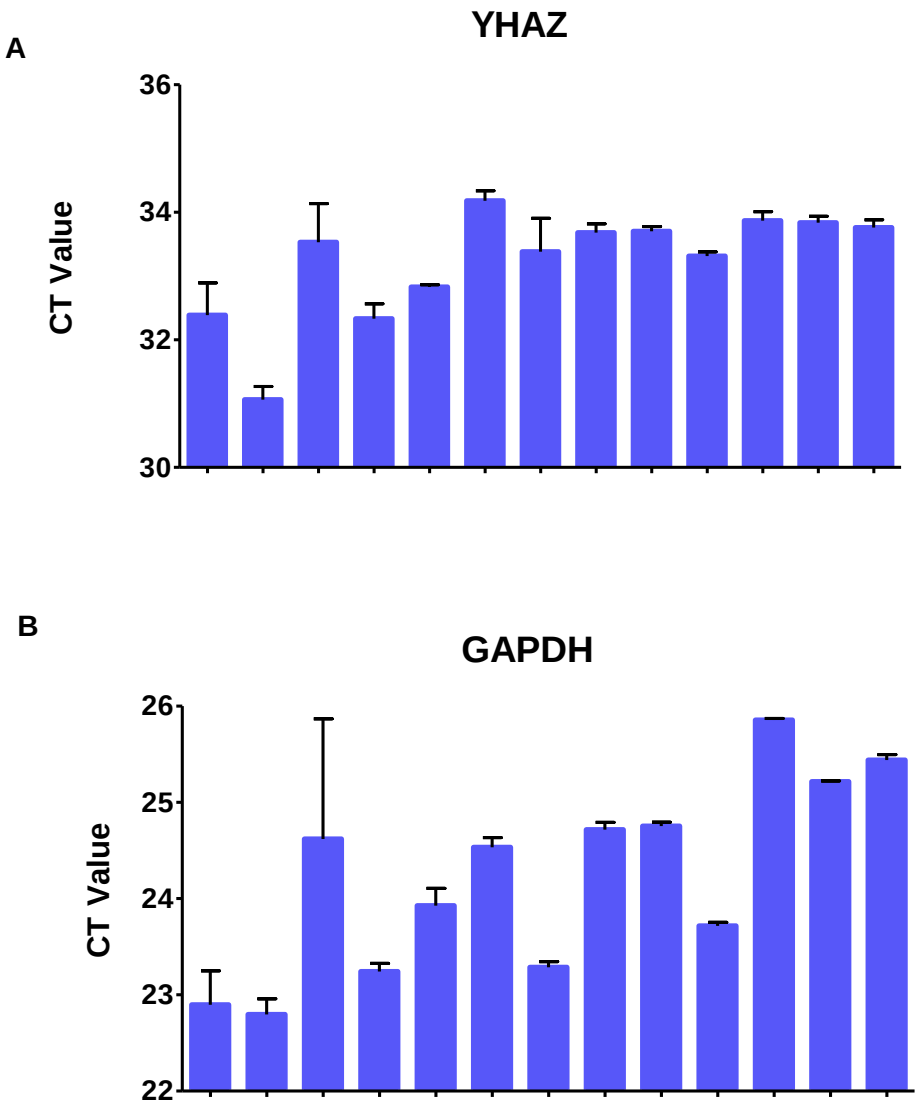

Figure A.12 – Housekeeping gene comparison. CT values for expression of *YWHAZ* (**A**) and *GAPDH* (**B**) derived from 13 samples, in triplicate, from the adipogenic differentiation experiment (5.3.7: Assessment of the effect of MI192 pre-treatment on the adipogenic gene expression of ADSCs)

A5.2 - Standard Curves for qRT-PCR Assays

qRT-PCR was performed using TaqMan gene expression assays (Life Technologies) and the full list of genes and assays can be found in 4.2: Materials and Methods for Chapter 4: The General Effects of MI192 on Adipose Derived Stem Cells Cultured in Monolayer. Optimal cDNA concentration for assays, and probe efficiency was investigated by plotting standard curves for each probe using known cDNA concentrations, from a day 0 sample of cells, against generated Ct values for reactions where all other variables (water, master mix and probe used) all stayed the same. Standard curves allow the user to check that the primer/probe sets are running efficiently. Serial dilutions of cDNA were run with each primer/probe set to produce the standard curves. No template controls were also run to check for unwanted reactions. All reactions were run in triplicate and the average Ct value for each Log_{10} concentration of cDNA was plotted, to give the standard curve (Figure A.14).

Probe efficiency for all genes of interest was satisfactory, as all lines had an R^2 value of 0.97 or over. *ADIPOQ* was the exception, as no Ct value was generated for any concentration of cDNA. However, with samples which had undergone adipogenic expression, transcripts could be detected, and the probe worked well within the context of the experiment, so it was used and assumed to be efficient as all of the other Taqman probes were.

A reaction of 5 ng of cDNA was deemed to be acceptable, allowing changes of gene expression to be observed while using a lower amount of RNA from samples with a low RNA yield.

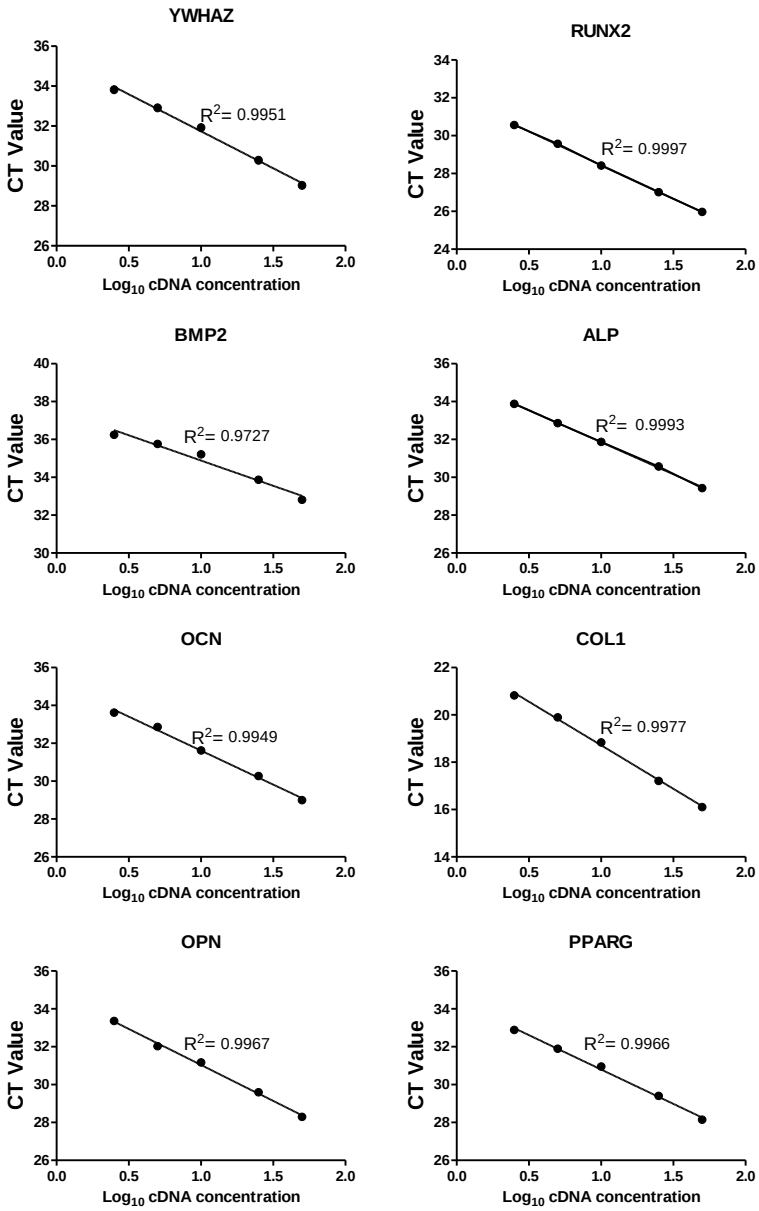

Figure A.14 – Standard curves. Generated from serial dilutions of a day 0 P5 untreated/differentiated ADSC sample, for the amplification of target genes (*RUNX2*, *BMP2*, *ALP*, *OCN*, *COL1*, *OPN* and *PPARG*) and *YWHAZ* housekeeping gene.

Appendix B
List of conference presentations and publications

B.1 Oral Presentations

- The Effect of a Novel HDACi on Osteogenic and Adipogenic Differentiation of Human Adipose Derived Stem Cells. *CDT/DTC Joint Conference, 10th July 2015*.
- The Effect of a Novel HDACi on Osteogenic and Adipogenic Differentiation of Human Adipose Derived Stem Cells. *Leeds School of Dentistry postgraduate research day, 8th July 2015*. (First place – oral presentation awarded)
- A NOVEL HDACI CAN IMPROVE OSTEOGENIC DIFFERENTIATION OF HUMAN ADIPOSE DERIVED STEM CELLS. Biomaterials & Tissue Engineering Group 16th Annual White Rose Work in Progress Meeting (BITEG), 22nd December 2014.
- A novel HDACi can improve osteogenic differentiation of human adipose derived stem cells. *Leeds School of Dentistry postgraduate research day, 9th July 2014*.

B.2 Poster Presentations

- The Effect of a Novel HDACi on Osteogenic Differentiation of Human Adipose Derived Stem Cells. Small-molecule potentiation and differentiation of stem cells: a growth area? *Royal Society of Chemistry Symposium*, 20 April 2015.
- A novel HDACi can improve osteogenic differentiation of human adipose derived stem cells. *Tissue & Cell Engineering Society (TCES) annual conference, July 2nd - 4th July 2014*
- A novel HDACi can improve osteogenic differentiation of human adipose derived stem cells. *CDT/DTC Joint Conference, 11th July 2014.*
- THE EFFECT OF HDAC INHIBITORS ON HUMAN DENTAL PULP STROMAL CELLS FOR CHONDROGENESIS IN VITRO *Biomaterials & Tissue Engineering Group 15th Annual White Rose Work in Progress Meeting (BITEG)*, 19th December 2013.

- The effect of HDAC inhibitors on stem cell behaviour. *Leeds School of Dentistry postgraduate research day*, 9th July 2014.
- The effect of HDAC inhibitors on stem cell behaviour – the potential of using HDACis for bone tissue engineering. *CDT/DTC Joint Conference, 12th July 2013*.
- The effect of HDAC inhibitors on stem cell behaviour. *Leeds School of Dentistry postgraduate research day*, 9th July 2013.
- The effect of HDAC inhibitors on stem cell behaviour – the potential of using HDIs for bone tissue engineering. *CDT/DTC Joint Conference, 20th July 2012*.

B.3 Book Chapter

Lawlor, L., Grigg, R. and Yang, X. 2014 In Vivo Imaging of Bone. In: *In Vivo Imaging: New Research*. eBook: Nova Science Publishers Inc. ISBN-10: 1629486337

Appendix C

Rights Permissions for Figures from Journal Articles

Rights for reuse in a thesis were obtained for the images seen in Figure 1.1, 1.2, 1.4, 1.8 and 6.1. Details below.

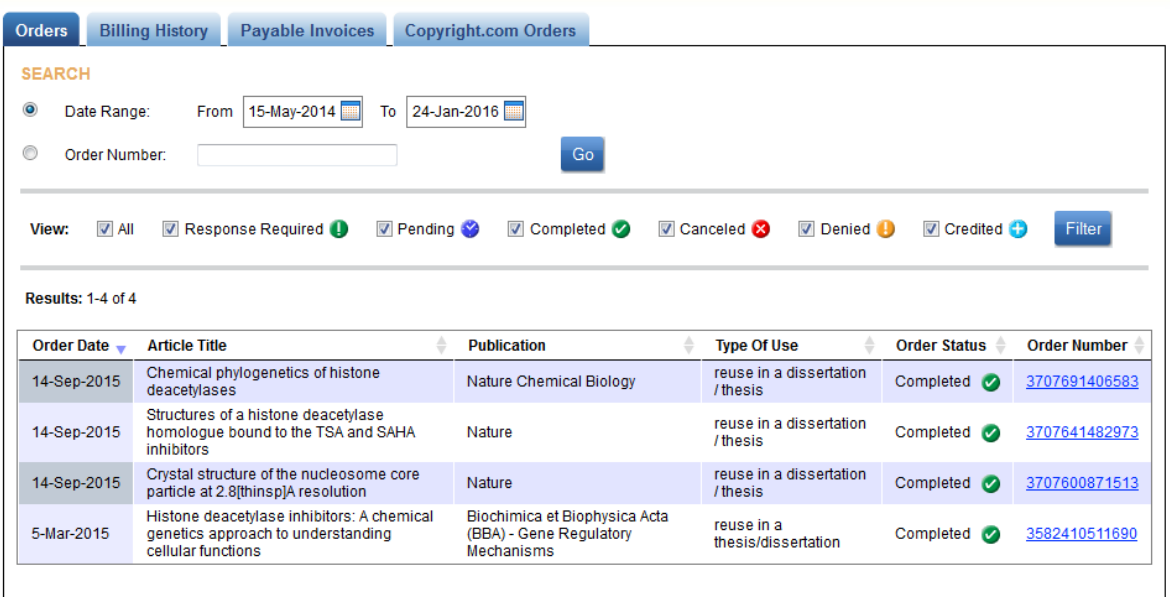

Orders | Billing History | Payable Invoices | Copyright.com Orders

SEARCH

Date Range: From 15-May-2014 To 24-Jan-2016

Order Number: Go

View: All | Response Required | Pending | Completed | Canceled | Denied | Credited | Filter

Results: 1-4 of 4

Order Date	Article Title	Publication	Type Of Use	Order Status	Order Number
14-Sep-2015	Chemical phylogenetics of histone deacetylases	Nature Chemical Biology	reuse in a dissertation / thesis	Completed	3707691406583
14-Sep-2015	Structures of a histone deacetylase homologue bound to the TSA and SAHA inhibitors	Nature	reuse in a dissertation / thesis	Completed	3707641482973
14-Sep-2015	Crystal structure of the nucleosome core particle at 2.8[thinsp]A resolution	Nature	reuse in a dissertation / thesis	Completed	3707600871513
5-Mar-2015	Histone deacetylase inhibitors: A chemical genetics approach to understanding cellular functions	Biochimica et Biophysica Acta (BBA) - Gene Regulatory Mechanisms	reuse in a thesis/dissertation	Completed	3582410511690

This is not an invoice

Order Details

Journal of cell science

Billing Status: **N/A**

Order detail ID: 68433957

ISSN: 0021-9533

Publication Type: Journal

Volume:

Issue:

Start page:

Publisher: Company of Biologists Ltd.

Author/Editor: COMPANY OF BIOLOGISTS

Permission Status: Granted

Permission type: Republish or display content

Type of use: Republish in a thesis/dissertation

Order License Id: 3715531072468

View details

Note: This item was invoiced separately through our **RightsLink service.** More info

$ 0.00